The Glorious Cross

Structural, Dynamics and Fluid Analysis

1-Aug-2021

Table of Contents

I. Building Codes & Standards: 4

A. Pressure, Temperature & Air Density: 7

B. Velocity & Altitude: 11

C. Base Loading, Hand Calculations: 22

II. Structure, Panels/Skin: 23

A. Panel Structure, Rivets: 26

B. Panel Structure, Rivet w/Fine-mesh: 30

C. Structure, Proper Rivet Instillation: 37

D. Structure, Classic Mechanics Bending: 37

III. Structure, Six-Segments: 43

A. Structure, Six-Segments, Rough-mesh: 49

B. Structure, Six-Segments, Fine-mesh: 54

C. Structure, CFD Transient Analysis: 70

D. Structure, Fine-mesh, 24[in] Cross-ribbing: 73

IV. Structure, Twelve-Segments: 86

A. Arm, All Twelve-Segments: 88

B. Segment – 12th, Endcap: 93

C. Segment – 11th: 99

D. Segment – 10th: 103

E. Segment – 9th: 105

F. Segment – 8th: 107

G. Segment – 7th: 110

H. Segment – 6: 112

I. Segment – 5: 114

J. Segment – 4th: 116
K. Segment – 3rd: 118
L. Segment – 2nd: 120
M. Segment – 1st: 122
N. Vibration Model: 128
V. Wind Loadings: 131
A. The arms of the Glorious Cross: 131
B. The Head of the Glorious Cross 140
C. The Intersection of the Glorious Cross: 143
D. Middle of Main Member of the Glorious Cross: 148
E. Mid-Lower I, @ 290[m] 153
F. Mid-Lower II, ... 158
G. Mid-Lower III, The Base 162
VI. Design of Arm: 170
A. 12th Segment, Endcap, for Design: 172
B. 11th Segment for Design: 175
C. 10th Segment for Design: 177
D. 9th Segment for Design: 179
E. 8th Segment for Design: 181
F. 7th Segment for Design: 182
G. 6th Segment for Design: 190
H. 5th Segment for Design 192
I. 4th Segment for Design 194
J. 3rd Segment for Design 196
K. 2nd Segment for Design 198
L. 1st Segment for Design 200
M. Natural Frequency: 202
VII. Fixing the Arm to the Main Structure: 203
A. Connection Beams: 203
B. Main/Body Structure: 212
C. Coupling of Arm to Main Body: 222
D. Panels for Arm to Main Body 254

VIII. Foundation:.... 272
A. Foundation Array/s:.... 274
B. The (x16) Foundation Array: 281
C. Foundation Model Accuracy:.... 284
D. Supporting Structure Lay-out Defined:.... 288
E. Base Segments: 292
F. Base Radial Panel: 294
G. Foundation on Bedrock:.... 301
IX. Prints & Summary: 319

The Glorious Cross

Structural, Dynamics and Fluid Analysis

As of 20201009

I. Building Codes & Standards:

Location of the Glorious Cross: Dozule, France

The European standard detailing structure loadings are found in EN 1991.1-4 for wind loading and EN 1998-4 for seismic loading. The seismic map notes that Dozule France is located in an insignificant seismic zone and as such, seismic conditions are negligible. EN 1991-4 states that it is applicable for structures no greater than 200[m]. The appropriate architecture of the Glorious Cross was determined by factoring in its location and the local weather patterns.

Figure 1: Southern Normandy France

Figure 2: Location of Glorious Cross w/r Dozule

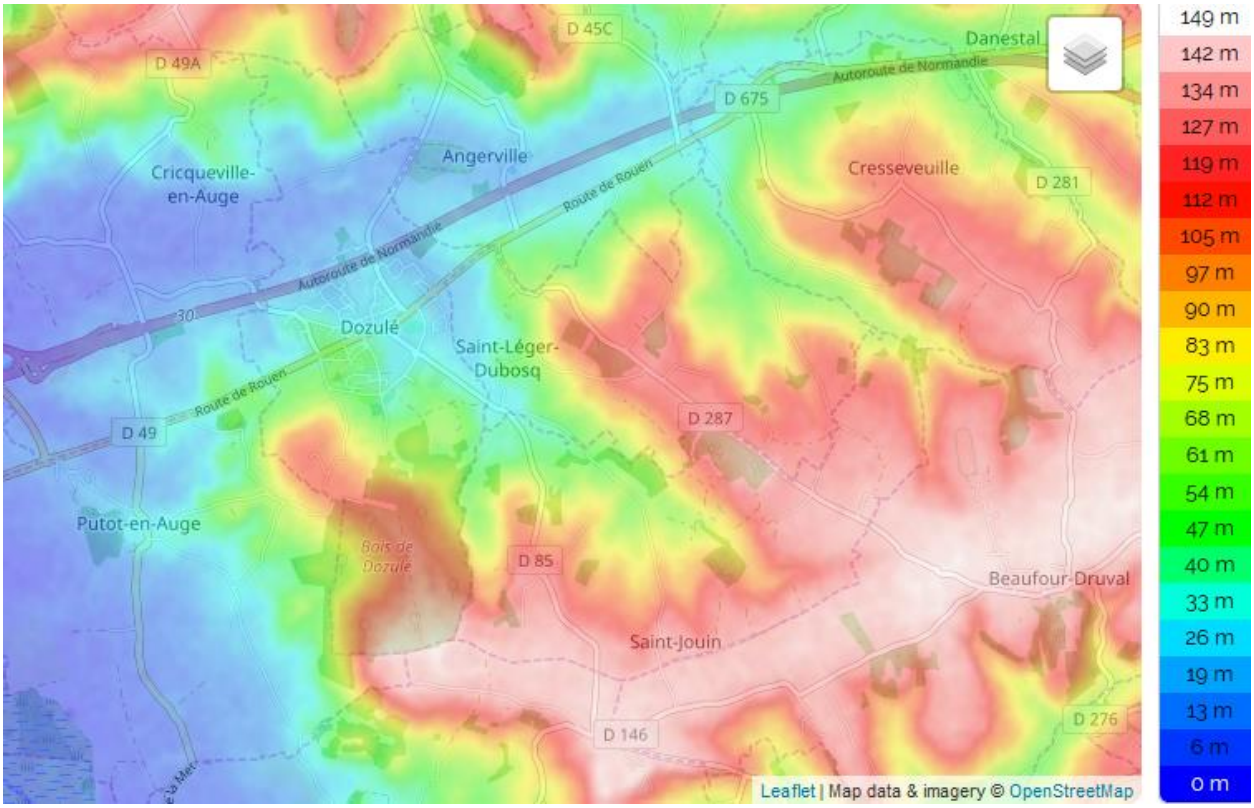

Figure 3: Elevation Map-I of Dozule, France

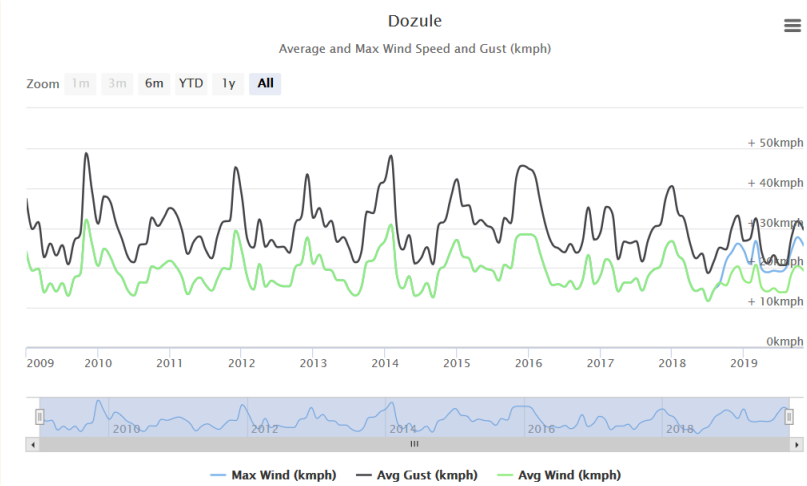

Figure 4: Dozule Wind Speed

Note: The CFD wind speed of 38.7[m/s] at a height of 5[m] is equivalent to 139[km/hr].

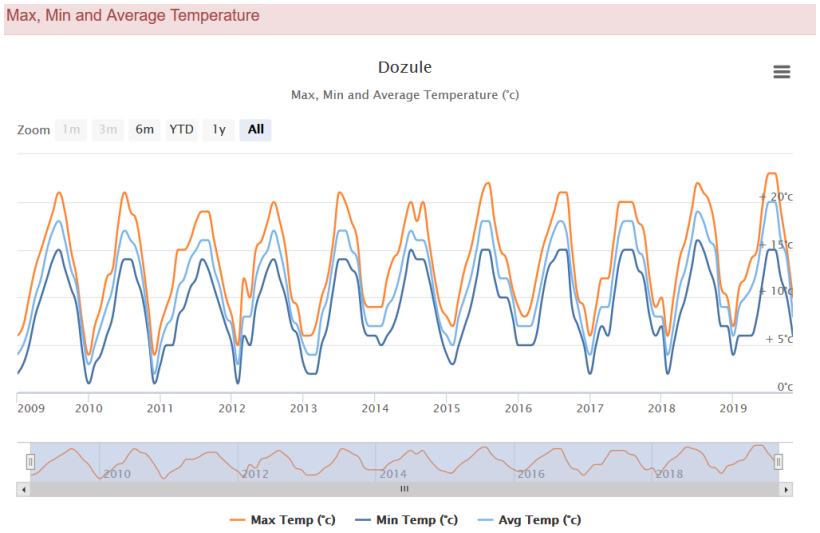

Figure 5: Dozule Temperature

Figure 1 shows a general location of Dozule France, with respect to Caen France. The shortest distance from the boundary of Dozule to the nearest ocean (or like) shore is greater than 6[km].

The region is known as Base-Normandie, Southern Normandie. The district is Lisieux with an area code of 14229 and a zip code of 14430. The township has an area of 5.23[km2] with a minimum altitude of 8[m] and a maximum altitude of 139[m]: It's average altitude is 74[m]. The altitude of city hall is 30[m] and is located at 49.233[ºNorth] latitude and 0.042[ºWest] Longitude. Figure 3 shows the elevation at the location of the Glorious cross is about 120[m].

A. Pressure, Temperature & Air Density:

Though historical weather patterns for Dozule France are difficult to obtain, nearby cities such as Deauville/St-Gatien and Clube de Voile & Pagaie Franceville are readily available. The historical high temperatures are 39[°C] or 102[°F] the lows are -2[°C] or 28[°F].

The average temperature (between highs and lows) is about 18[°C] or 65[°F]. For purposes of fractional simplicity an average temperature of 15[°C] or 59[°F]. Since the Glorious Cross stands 738[m] high, the temperature at its top will be less than the temperature at its base.

In the atmosphere:

Eq - 1: Pressure variance with Height

$$dP = -(\rho)(g)(dh)$$

Eq - 2: Density

$$\rho = \frac{(mw)(P)}{(R)(T)}$$

Where:
(P) is Pressure
(ρ) is density in mass per volume
(g) is gravity
(h) is height
(mw) is molecular weight
(R) is the molar gas constant
(T) is the absolute temperature

Combining the equations and solving for the pressure:
Eq - 3: Air-Pressure w/r Density

$$P_h = P_o e^{-\frac{(mw)(g)(h)}{(R)(T)}}$$

Since the Glorious cross is atop a hill that is about 120[m] high, the standard pressure at the site will be 99,892[Pa] or 29.5["Hg]; utilizing the standard equation from National Oceanic and Atmospheric Administration, NOAA, for dry air.

Taking the weather patterns into account the standard temperature will be defined as 15[C] with a relative humidity of 55%. The molecular weight of air at these conditions is 28.80[kg/kmol] with a density of 1.20[kg/m3].

Solving Eq - 3 for temperature:
Eq - 4: Temperature w/r Pressure, Density and Altitude

$$T = -\frac{(mw)(g)(h)}{(R)\left(Ln\left(\frac{P_h}{P_o}\right)\right)}$$

Thus, the top of the Glorious Cross will be 2.40[°C] or 4.32[°F] cooler than at its foot. As expected, equation (4) is relatively linear and temperatures may be estimated as decreasing 3.51[°C/[km]] or 8.92[°F/5000[ft]].

This leads to defining the standards for the construction of the Glorious Cross will be as follows:
Temperature: 15[°C] or 59[°F]
Temperature - Maximum: 43[°C] or 110[°F]
Temperature - Minimum: -5[°C] or 23[°F]
Temperature - Δ: 30[°C] or 54[°F] (the maximum change in temperature)

Pressure of atmosphere at the base of the Glorious Cross: 99,892[Pa] or 29.50["Hg] @ 120[m]
Pressure of atmosphere of the Glorious Cross: 95,587[Pa] or 28.23["Hg] @ 489[m]

The standard air density is at 55% RH (Relative Humidity): 1.200[kg/m3]

The standard molecular weight is 28.80[kg/kmol]

Note that the nominal material manufacturing dimensions will be derived from a base temperature of 12[°C] or 54[°F].

Per EN 1991-4, since the structure is not standard the roughness factor Cr(z) will be accessed during the calculations. The map, Figure 6, shows a basic velocity of 24[m/s] at an altitude of 34.74[m].

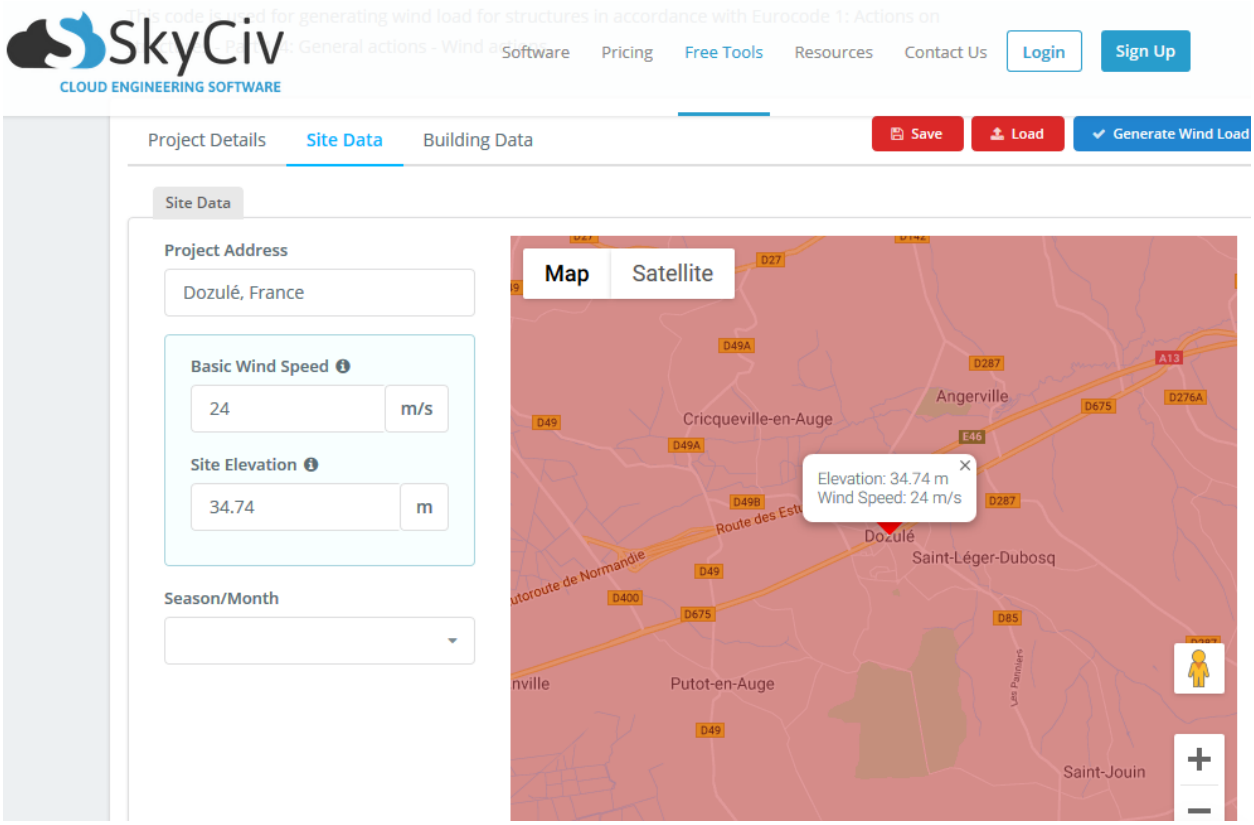

Figure 6: Dozule Vb (Basic Velocity)

Eurocode 1 **Wind Peak Velocity Pressure - UK National Annex**

Description: Calculation of peak velocity pressure qp depending on the basic wind velocity from UK National Annex wind map, and the site distance from shoreline and town boundary. The wind action on the structure (forces and pressures) can be derived from the peak velocity pressure. Calculation according to the UK National Annex.

According to: EN 1991-1-4:2005+A1:2010 Section 4 & UK National Annex to BS EN 1991-1-4:2005+A1:2010

Supported National Annexes: United Kingdom National Annex

Input | Results | Notes | Details

Save | Load | Print-PDF | All Calculations

Rate this calculation: ★★★★★ | Share | Share

Input

Calculation method for the wind action	=	Roughness factor Cr(z)		Calculation of the wind action using the exposure factor $c_e(z)$ is permitted except for the cases where orography is significant ($c_0 > 1.0$) and the total height above ground is $z > 50$ m. The calculation of the wind action using the roughness factor $c_r(z)$ is general and may be applied for all cases.
Fundamental basic wind velocity (before the altitude correction is applied)	$v_{b,map}$ =	24	m/s	The appropriate value for the examined location is determined on the map given in Figure NA.1 of UK National Annex to EN1991-1-4 (reproduced below).

Hint: Calculate basic wind velocity $v_{b,map}$ from OS datum coordinates (UK National grid): $v_{b,map}$

Map of fundamental basic wind velocity Vb,map according to UK National Annex to EN1991-1-4

Map of fundamental basic wind velocity $v_{b,map}$ reproduced from Figure NA.1 of UK National Annex to EN1991-1-4 (click for larger view)

Altitude of the site above mean sea level	A =	120	m	The altitude correction factor c_{alt} is determined from the altitude A. Larger value of altitude A give more unfavorable results. Where there is significant orography ($c_0(z) > 1.0$), as defined in Figure NA.2 of UK National Annex, altitude A should be taken as the altitude of the upwind base of the orographic feature along the wind direction considered.

Figure 7: Wind Loading Calculation 1

Height above ground at which peak velocity pressure is calculated (reference height)	z =	200	m	The appropriate reference height depending on the type of the structure is given in EN1991-1-4 Section 7. For calculation of overall wind force in buildings it is generally equal to the height of the building, measured to the top, which may be a ridge or a parapet.
Displacement height for buildings in town	h_{dis} =	0	m	For buildings not in town $h_{dis} = 0$. The displacement height considers the favorable effect of lifting of the wind profile when upwind town terrain exists The appropriate value is specified in EN1991-1-4 §A.5. Please verify that h_{dis} is not greater than 0.4h, where h is the building height above ground. Conservatively $h_{dis} = 0$ may be considered for all cases.
Orography factor at reference height z	$c_0(z)$ =	1		Orography factor larger than 1.0 may be applicable over isolated hills and escarpments. See EN1991-1-4 §4.3.3 and §A.3 for more details.
Season factor	c_{season} =	1		According to Table NA.2 of UK National Annex to EN1991-1-4. In general $c_{season} = 1.0$ is applicable for permanent structures that exist for the whole year. For structures that are loaded by the wind only for specific periods of the year a smaller value $c_{season} < 1.0$ may be applicable.

Finished

Results

Wind peak velocity pressure	$q_p(z) = 1.732$ kN/m^2	Wind pressure corresponding to the wind peak velocity

Figure 8: Wind Loading Final Calculation

Table 1: Pressure to Velocity

"z" Height of Structure [m]	Pressure [kPa]	Pressure [Pa]	[m/s]
5	0.919	919	38.72
10	1.122	1,122	42.78
20	1.33	1,330	46.58
30	1.436	1,436	48.40
40	1.51	1,510	49.63
50	1.564	1,564	50.51
60	1.591	1,591	50.95
70	1.611	1,611	51.26
80	1.627	1,627	51.52
90	1.64	1,640	51.72
100	1.652	1,652	51.91
110	1.663	1,663	52.09
120	1.672	1,672	52.23
130	1.681	1,681	52.37
140	1.689	1,689	52.49
150	1.697	1,697	52.62
160	1.704	1,704	52.72
170	1.712	1,712	52.85
180	1.719	1,719	52.96
185	1.722	1,722	53.00
190	1.725	1,725	53.05
195	1.729	1,729	53.11
200	1.732	1,732	53.15

B. Velocity & Altitude:

Table 1 depicts the conversion of the calculated pressure to average stream velocity. The website "eurocodeapplied.com" used a density of 1.226[kg/m3] for their calculations.

The power wind law is sufficient to obtain the wind gradient:

Eq - 5: Wind Speed w/r Altitude

$$V_h = V_o \left(\frac{h}{h_o}\right)^{\beta}$$

Where:
V_h is the velocity at height "h"
V_o is the velocity at height "h_o"
h is the height
h_o is the height at the origin
β is the Hellmann exponent

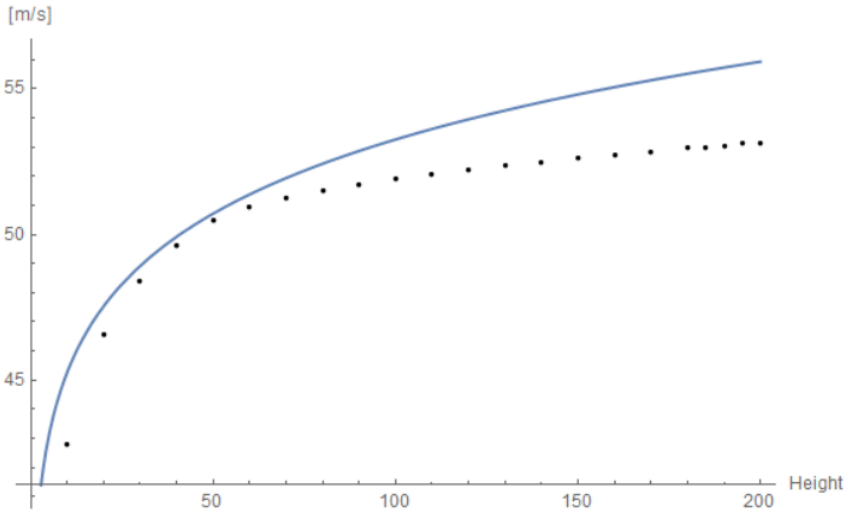

Figure 9: Peak Velocity (vs) Height to 200[m]

Note: Dots are per code, the line is Eq - 6.

Eq - 6: Velocity w/r Altitude at Location

$$V_h = 38.491(h)^{0.070522}$$

Where: "h" is [m]

Eq - 7: Velocity variant of Eq - 6

$$V_h = 62.65\left(\frac{h}{1000}\right)^{0.070522}$$

Above 150[m] the equation overestimates the velocity by about 5[%].

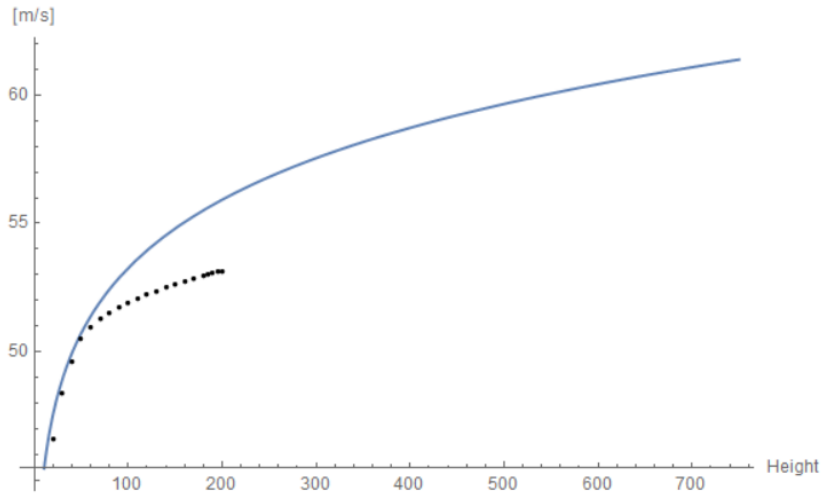

Figure 10: Peak Velocity (vs) Height to 750[m]

Adding 5[%] to the base-curve, at an altitude of 738[m] above ground level the peak velocity is 61.323[m/s] or 137.17[mph].

Considering the maximum height, the maximum temperature differential should be examined. The inner structure will be made of steel, covered with aluminum.

The thermal expansion rate of 6061-T6 aluminum is $23.8(10^{-6})$[1/K] or $13.2(10^{-6})$[1/R].
The thermal expansion rate of standard steels is $11.7(10^{-6})$[1/K] or $6.5(10^{-6})$[1/R].

The aluminum skin will expand about twice as much as its steel support structure. With a maximum dT of 30[°C] or 54[°F] the Glorious Cross will grow about 21[in] or 0.527[m] and the peak velocities increase to 61.326[m/s] or 137.18[mph].

Since the face area is directly related to the forces acting upon the Glorious Cross, a factor of (1/40) will be chosen for its basic width. Note, that on a hot day, the width of the Glorious Cross will increase by 0.52[in] or 13[mm].

Table 2: Overall Dimensions

Overall Dimensions		
Height - Total	738	[m]
	2,421	[ft]
	29,055	[in]
Length/Width - Total - (Arms)	246	[m]
	807	[ft]
	9,685	[in]

Length (One Arm), from Center	123	[m]
	404	[ft]
	4,843	[in]
Length of Flat(portion of Arm - radii – base/width)	4,371	[in]
Length of Flat Arm w/o Radius	2,185	[in]
Width Factor	40	[-]
Actual Width (Constant)	18.450	[m]
	60.53	[ft]
	726	[in]

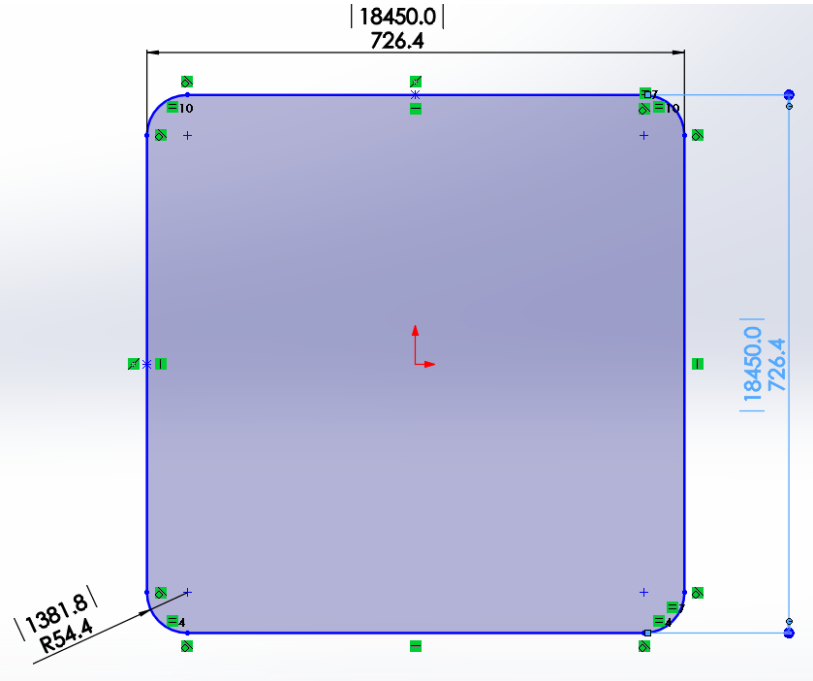

Figure 11: Main Body Cross-section {[in] & |mm|}

CFD analyses were performed with respect to Figure 10 and an air density of 1.226[kg/m3] with a roughness of 3[mm] (3000µm); akin to riveted steel.

Table 3: Wind Velocity w/r Height for CFD

Simulation Wind		
"z" Height of Structure [m]	Peak Velocity [m/s]	Peak Velocity [mph]

0.00	0.00	0.00
10.00	45.28	101.28
25.00	48.30	108.04
50.00	50.72	113.46
75.00	52.19	116.75
100.00	53.26	119.14
150.00	54.81	122.60
200.00	55.93	125.11
236.78	56.60	126.61
246.00	56.75	126.95
255.23	56.90	127.28
300.00	57.55	128.74
350.00	58.18	130.14
400.00	58.73	131.38
450.00	59.22	132.47
500.00	59.66	133.46
550.00	60.06	134.36
600.00	60.43	135.19
650.00	60.78	135.95
700.00	61.09	136.66
738.00	61.323	137.18
738.53	61.33	137.18

Since the pressure is related to the square of the velocity the velocity w/r height equation may be used determine the loading curve over most of the Glorious Cross:

Eq - 8: Pressure at Altitude, Base Equation

$$dP_h = C_d \frac{\rho}{2} V^2 = C_d \frac{\rho}{2} 3925 \left(\frac{h}{1000}\right)^{0.141044}$$

Eq - 9: Force of Action, Base Equation

$$F(y) = \left(6.2 \frac{\rho}{2} V^2\right) A_p = C_2 \left(\frac{y}{1000}\right)^{0.141044}$$

$$F(y) = \left(6.2 \frac{\rho}{2} V^2\right)(w)(y) = \left(6.2 \frac{\rho}{2}\right)(w)(y) 3925 \left(\frac{y}{1000}\right)^{0.141044}$$

Where:
C_d is the drag coefficient: [-]
ρ is the density of air, here it is 1.226[kg/m3]
V is the velocity
A_p is the projected area
y is the altitude in [m]
1000 is an altitude unit in [m]: Note, [y/1000] = [-] (dimensionless)

Eq - 10: Drag Force on Body

$$F_D(738) = \left(6.2\frac{1.226}{2}61.323^2\right)92.25 = C_2\left(\frac{738}{1000}\right)^{0.141044}$$

Eq - 11: Drag Force as a Function of Altitude (y)

$$d\big(F(y)\big) = \left(C_d\frac{\rho}{2}V^2\right)dA_p = \left(C_d\frac{\rho}{2}V^2\right)\left(\frac{y}{1000}\right)^{0.141044}Wdy$$

Where:
W is the projected width of the body; here it is 18.45[m]

Where the C_d = 6.2:

$$F_{Drag(Axial)} = (91045H^{1.1410})$$

$$F_{Drag(Axial)} = (1.71 \times 10^8)[N]$$

$$F_{L(Lateral)} = (8517H^{1.1410})$$

$$F_{L(Lateral)} = (1.5954 \times 10^7)[N]$$

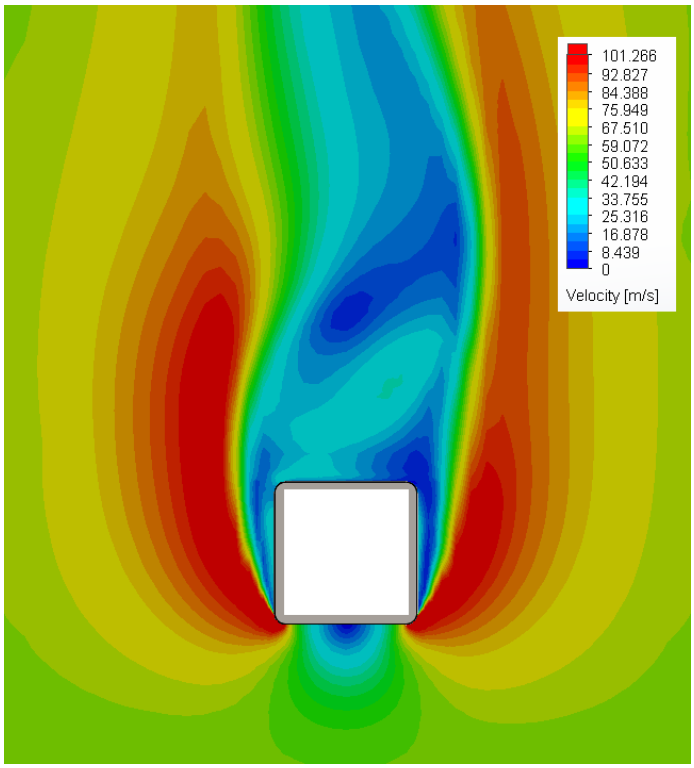

Figure 12: Wind 61[m/s]

Figure 13: Pressure on Flat-face, Perpendicular to Flow

In Figure 13 note that the flat panels experience a lifting force as it/they near the corner radii.

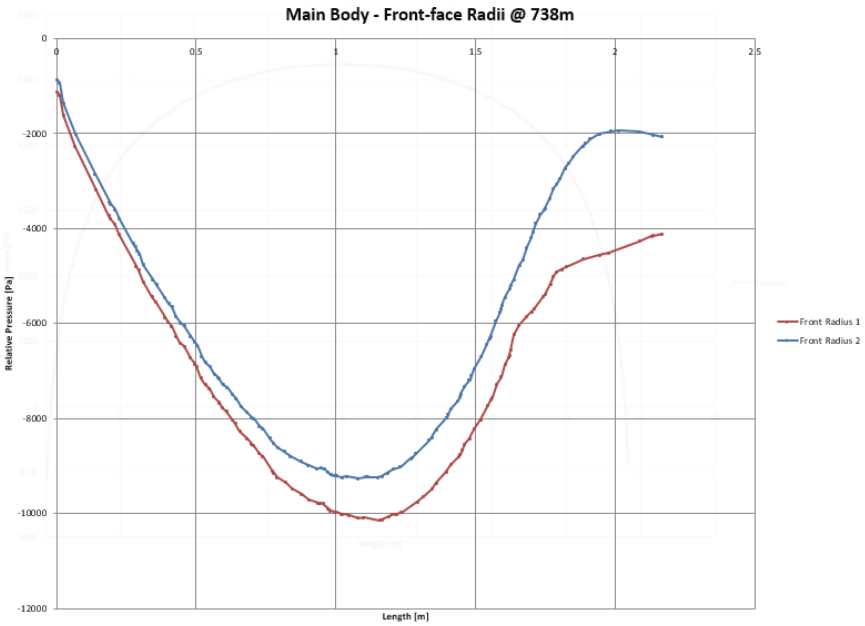

Figure 14: Front-face Radii

In Figure 14 note that the "front" (the face that faces the wind/flow) experiences a lifting or suction force; pulling the panel away from the body.

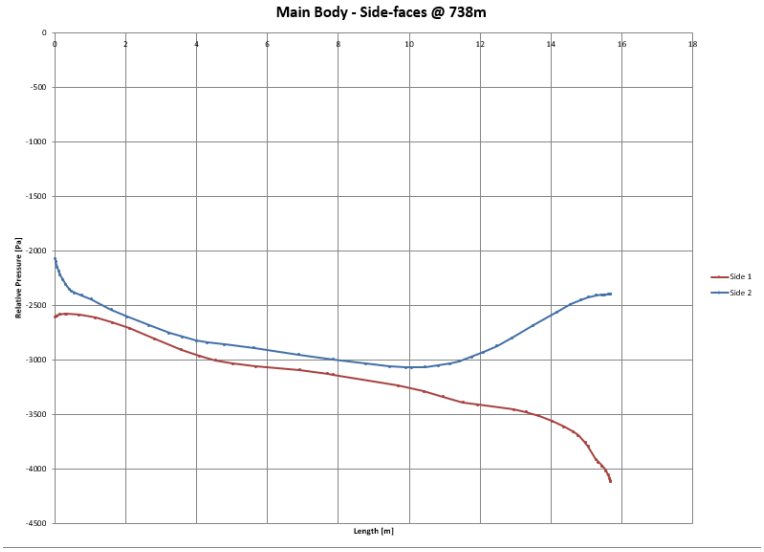

Figure 15: Side-faces

In Figure 15 note that they are, for the most part, being pulled or sucked away from the main-body.

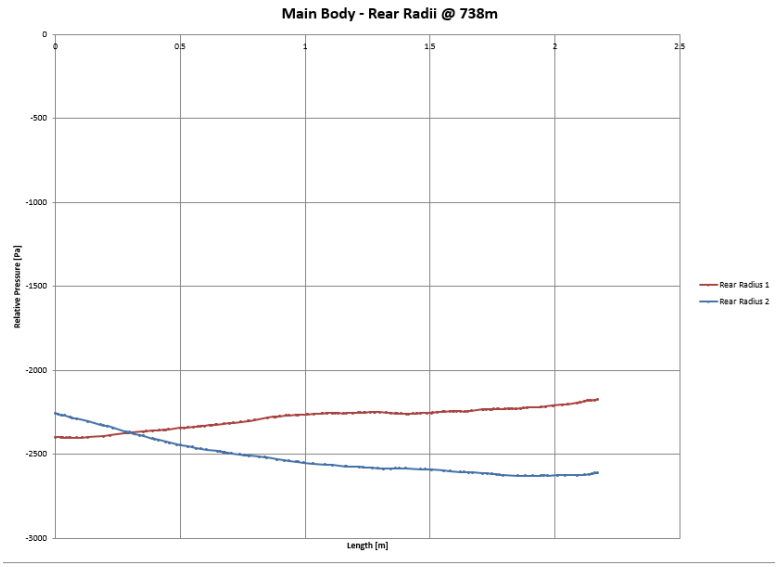

Figure 16: Rear Radii

In Figure 16 it is seen that the radii opposite the flow are being sucked off of the main body.

Figure 17: Front & Rear Faces

Figure 17 shows the impingement (front) face and the opposite (rear) face. The front face is being driven into the body while the rear face is being pulled-off.

The maximum pressure experienced in the center of the structure, the front face, is 5,235[Pa], 0.76[psi] or 21["w.c.]; over the center distance of 40[in] the pressure remains relatively constant.

The minimum vacuum pressure on the front radii is 10,145[Pa], 1.472[psi] or 40.73["w.c.].

CFD verifies that at the three end-caps (the top and both arm-ends) a vacuum is generated, relieving the structural stresses so this factor will be ignored.

Eq - 12: Overall Wind Velocity

$$WindV_{Axial}(y) = 62.6502\left(\frac{y}{1000}\right)^{0.070522}$$

Eq - 13: Overall Axial Body Force

$$F_{Axial}(y) = 6.12\left(\frac{1}{2}1.226\right)\left(WindV_{Axial}(y)\right)^2(18.45)(dy)$$

Eq - 14: Lateral Coefficient of Drag (90[deg] to Front-face) w/r Altitude

$$C_{lat}(y) = (-2.193x10^{-6})y^2 + (397.65x10^{-6})y + 1.49$$

Eq - 15: Overall Lateral Body Force

$$F_{Lateral}(y) = \left(C_{lat}(y)\right)\left(\frac{1}{2}1.226\right)\left(WindV_{Axial}(y)\right)^2(18.45)(dy)$$

Table 4: CFD Results, Drag Coefficients

Height [m]	Velocity [m/s]	F(wind) Axial-Dynamic [N]	Force Axial [N]	Force Lateral [N]	Cd Axial [-]	Cl Lateral [-]
738.00	61.32	212,654	1,279,500	120,100	6.02	0.56
624.23	60.60	207,690	1,246,700	190,970	6.00	0.92
200.00	55.93	176,895	1,025,200	257,920	5.80	1.46

The axial loading remains relatively constant, here-in the value was take as 6.12[-]. The lateral loading coefficient varied slightly:

At top of arm, the altitude is 624.225[m]:

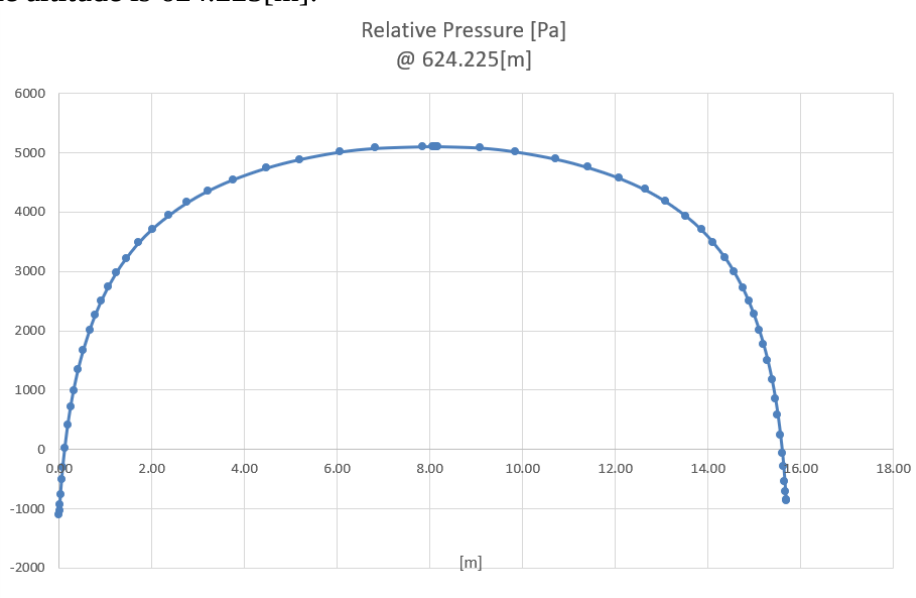

Figure 18: Relative Front Panel Pressure on Arm/s

The relative pressure shown in Figure 18 is the design pressure of the arm structure. The negative pressure is due to the vacuum produced by the corner radii.

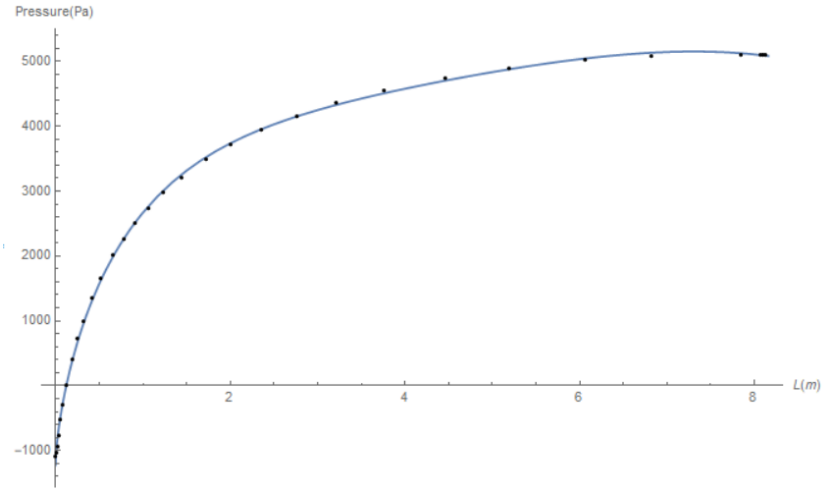

Figure 19: Panel Pressure - Half of Front-face

Eq - 16: Panel Pressure over Half of Front-face, [Pa]

$$dP(x) = -1224 + 2127\left(\sqrt{x}\right) + 5702(x) - 5744\left(x^{\frac{3}{2}}\right) + 2076(x^2) - 266\left(x^{\frac{5}{2}}\right)$$

Adding 1224[Pa] to Eq - 16 would add a safety factor to the following equations:

Eq - 17: Non-negative, Panel Pressure over Half of Front-face, [Pa]

$$dP(x) = 2127\left(\sqrt{x}\right) + 5702(x) - 5744\left(x^{\frac{3}{2}}\right) + 2076(x^2) - 266\left(x^{\frac{5}{2}}\right)$$

Conditions for body forces:

- Factor of safety of no less than 13[%]
- Arm calculations are performed at a constant altitude of 624.225[m]
- The arm calculations include an added safety margin when it intersects with the main body

C. Base Loading, Hand Calculations:

Table 5: Overall Loading

- Both arms:
  - 55.0[MN] or 12,364,000[Lbf]
  - Center (cg) is located at y = 615[m] or 24,213[in]
  - Lateral Load (downward, or Fy, force) 8.42[MN] or 1,894,000[Lbf]
- Main Body:
  - 168.3[MN] or 37,845,000[Lbf]
  - Center (cg) is located at y = 393[m] or 15,485[in]
  - Lateral Load (shear, or Fx, force) 34.35[MN] or 7,722,000[Lbf]
- At Body-base:
  - Mx(overall) = 100.03[GN-m] or $73.782(10)^9$[Lbf-ft]
  - Mz(overall) = 12.545[GN-m] or $9.253(10)^9$[Lbf-ft]

Utilizing Eq - 17 the panel structure may be determined where the panel width & length are defined to be 47.25[in].

*Eq - 18: Non-negative, Panel Loading over **Half** of Front-face, [N/m]*

$$W_o(x) = \left(2127\left(\sqrt{x}\right) + 5702(x) - 5744\left(x^{\frac{3}{2}}\right) + 2076(x^2) - 266\left(x^{\frac{5}{2}}\right)\right)\left(\frac{25.4}{1000}47.25\right)\left[\frac{N}{m}\right]$$

The integration of Eq - 18 between 0 and 7.8432 (half = 15.6864/2[m]) the shear loading may be found. The double integration of Eq - 18 will define the moment over a body face and its quadruple integral will define its deflection; as taught in introductory mechanics.

*Eq - 19: Non-negative, Panel Moment over **Half** of Front-face, [Nm]*

$$M_{Body\ Panels}(x) = \left(-144122 + 50151(x) - 680.6\left(x^{\frac{5}{2}}\right) - 1140.6(x^3) + 787.9\left(x^{\frac{7}{2}}\right) - 207.6(x^4) + 20.2745\left(x^{\frac{9}{2}}\right)\right)[Nm]$$

The moment on the front face is zero at 3.357[m] from the corner radius. The maximum moment is -144,122[Nm]; again, found at the corner radius. Since the panel thickness of (1/16)" cannot withstand this moment, an interior structure must be designed.

After some calculations it is found that a bending resistant structure about 32" long will sufficiently resist the maximum wind loadings presented in Eq - 19; with a maximum deflection of 1.54[in].

*Eq - 20: Deflection of Panels, over **Half** of Front-face, [m]*

$$\delta_{Body\ Panels}(x) = \frac{x^2}{EI}\left(-72061 + 8358(x) - 43.216\left(x^{\frac{5}{2}}\right) - 57.031(x^3) + 31.834\left(x^{\frac{7}{2}}\right) - 6.91983(x^4) + 0.56712\left(x^{\frac{9}{2}}\right)\right)[m]$$

II. Structure, Panels/Skin:

To construct the Glorious Cross various manufacturing methods were considered:

- Solid shell:
  - Negatives: Extensive welding, heavy and very difficult to construct
  - Positives: One unit
- Supported shell:
  - Negatives: A shell requires support
  - The arms would be supported much like aircraft wings
  - Positives: Light weight, relatively easy to construct with current manufacturing techniques

After considering various manufacturing methods, the riveting of the panels was chosen as an effective and efficient method of construction. The ribbing/supporting structure would be constructed with (1/8)" thick members due to the maximum rivet size/s. Though custom rivets are possible, to keep costs down (3/8)" rivets were chosen: Because they are the largest, readily available rivets on the market. The maximum single member working thickens for a (3/8)-[in] rivet is (1/8)-[in].

A (1/4)" reinforcement thickness was considered due to its higher inertial value:

- (1/4)" sheets are difficult to work-with
- The (1/4)" sheet would require a minimum bend of 3.5:1 (vs) 2.5:1 for a (1/8)" panel
- The (3/4)" rivet could be spaced several inches apart and the "weld" construction of the rivets would not apply (noting that riveted constructions are as good (and better than) a weld).
- Riveting with (3/4)" rivets would take a long time and require special equipment

Various simulations with respect to panel thicknesses were performed. The (1/16)" main panel was chosen because it's easy to work with and it's not too thin. Though under maximum wind pressure a

thinner panel would perform the rivet-hole stress would be considerably higher and noticeable permanent deformations may arise.

Recalling Figure 13, the maximum relative pressure is 5,235[Pa] or 0.76[psi]: Adding an additional 3% for computational error the $dP_{Panel\text{-}Max}$ = 0.7821[psi] or 5,392[Pa]; yielding a factor of safety (w/r panel) of at least 16[%].

It was found that the (3/8)" rivet could be spaced about 2" apart. To maintain a weldability classification, 28[-] rivets per side were used with a spacing of 1.680[in].

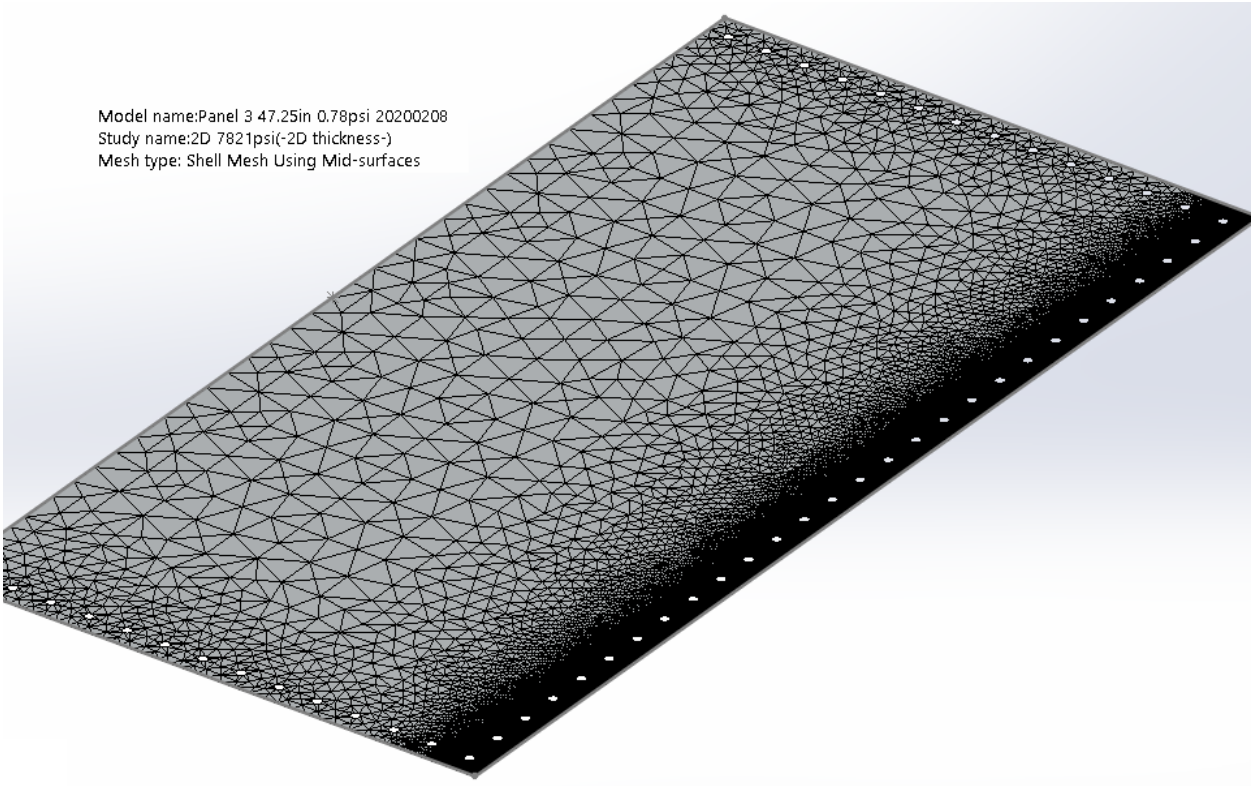

Figure 20: Panel FEA 28 Rivets, 47.25[in] with 0.7821[psi]

The panel ratio of (length/thickness) >>10 therefore a 2-D simplification was applied. Since the panel is symmetrical a half-panel simplification was applied (in the direction shown). The (1/16)" panel deflection, under 0.78[psi] is much greater than (1/4)*Thickness; therefore a "large displacement" analysis was performed. The mesh size around critical holes were (1/16)/3 = 0.02[in] with a growth rate of 20[%].

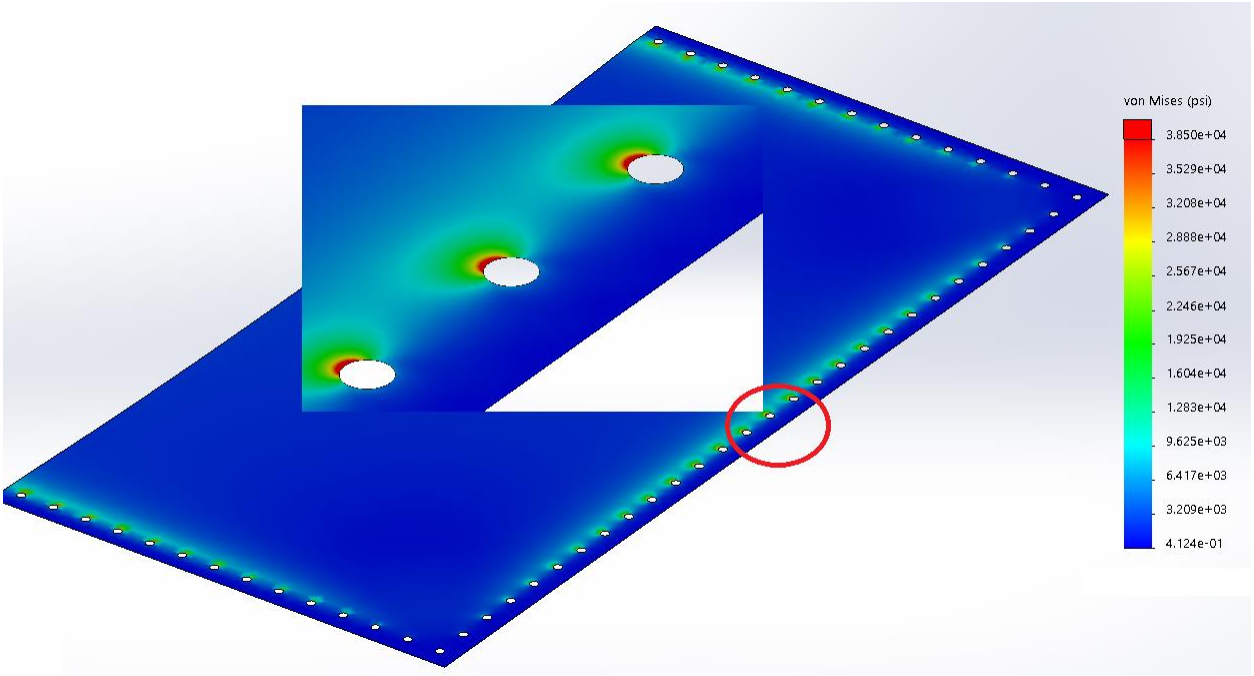

Figure 21: 47.25[in] Panel w/28 Rivets, Overall Stress - [psi]

As seen in Figure 21, minor yielding would occur.

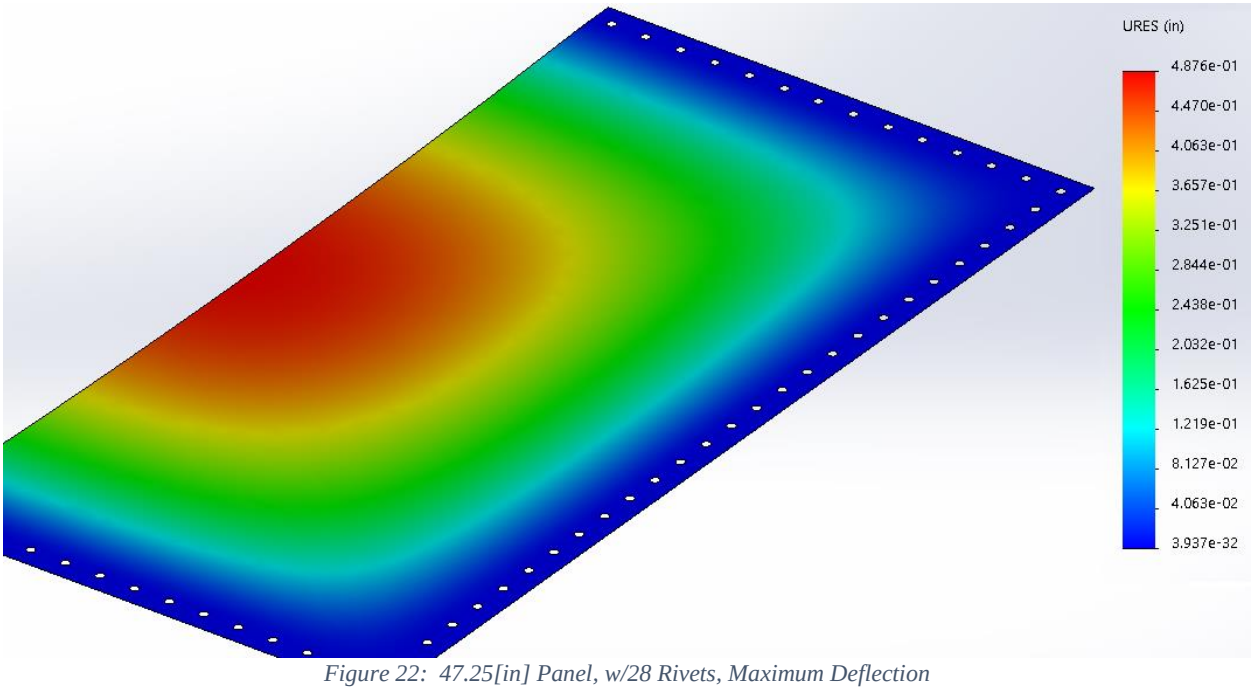

Figure 22: 47.25[in] Panel, w/28 Rivets, Maximum Deflection

The maximum deflection for the 47.25[in] x (1/16)[in] panel under 0.7821[psi] is 0.49[in] or 12.4[mm].

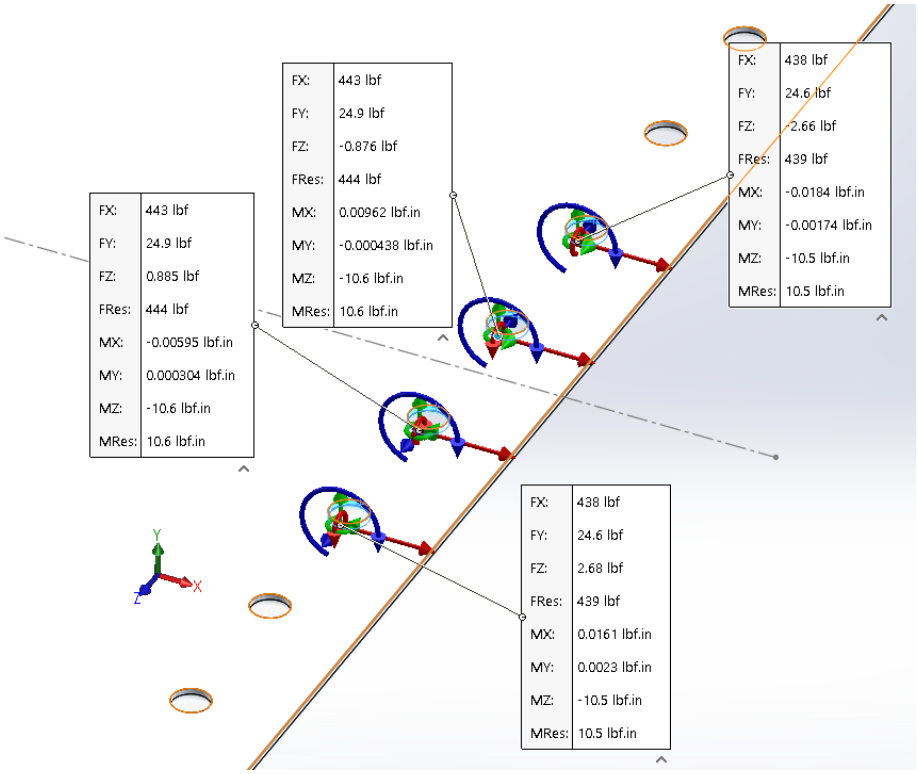

Figure 23: 28 Rivet Maximum Loading

A. Panel Structure, Rivets:

As seen in Figure 23, the maximum shear loading is 443[Lbf]. Adding another 9[%] factor of safety to this value (25[%] overall) the rivet shear load is defined as 483[Lbf] or 2,148[N]. The (3/8)" rivet depicted in Figure 24, will maintain a factor of safety of about 2[-] under worst-case conditions.

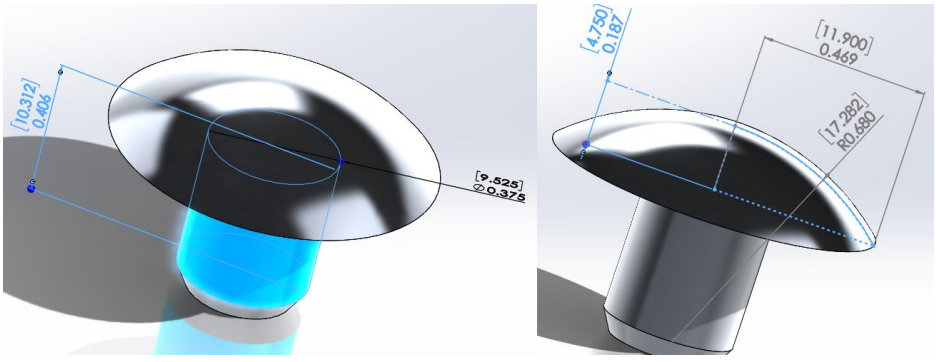

Figure 24: Brazier Head Panel Rivet, (3/8)" x 0.406 w/ 30[deg] x 0.06[in] Chamfer

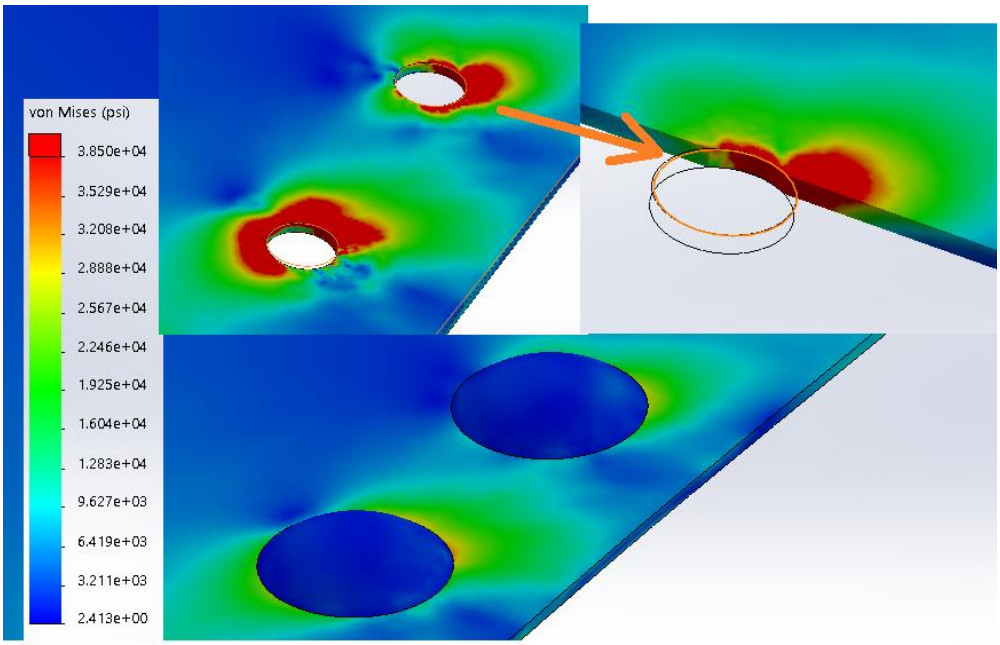

Figure 25: Maximum Stress due to 28 Rivets per Side

Figure 25, shows that about 0.1[in] of permanent deformation would ensue with 28 rivets per side; under maximum loading conditions. However, due to calculation and model irregularities the acutual the permanent deformation zone is over exaggerated.

The model does show that the interaction or action of incidence zone is greater than 95[deg]; which is equivelant to a land-area of (0.320)*(1/16) = 0.02[in2]. Therefore, the maximum stress is near 24,150[psi]; which exists on the (1/16)" panel. The analysis shows that the system will survive thousands of cycles under maximum design conditions.

Since the stresses were relatively small with 28 rivets per side at maximum design conditions, 24 rivets per side will now be considered.

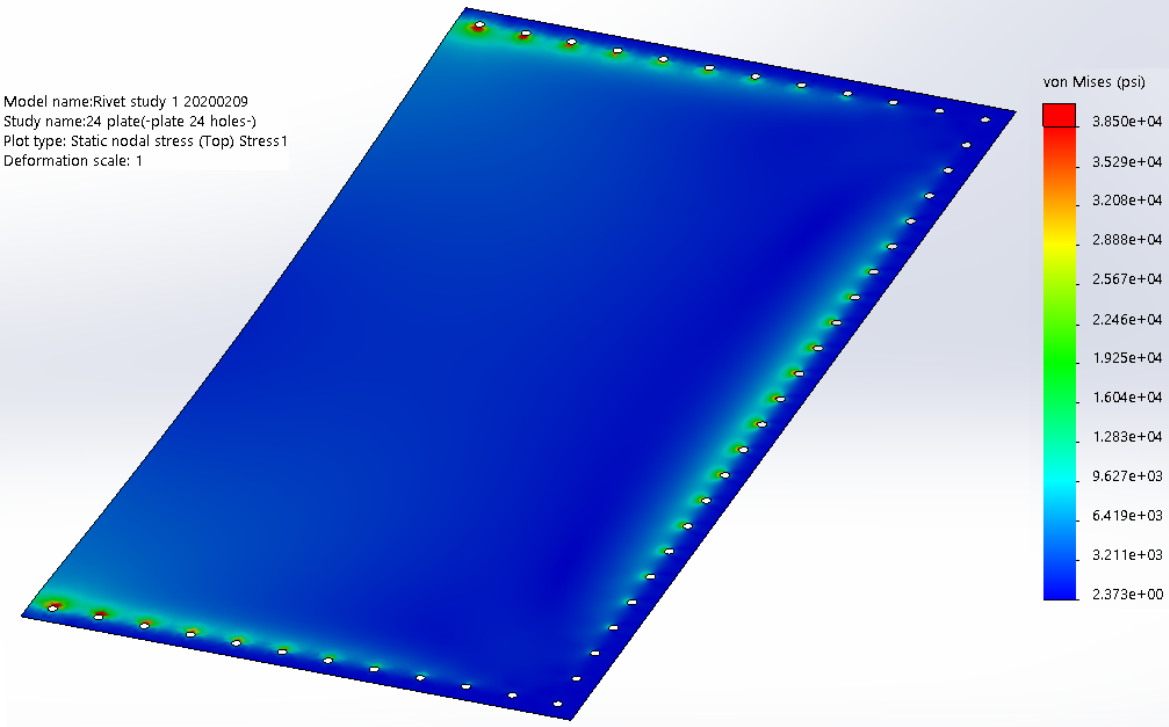

Figure 26: 24 Rivets, Stress

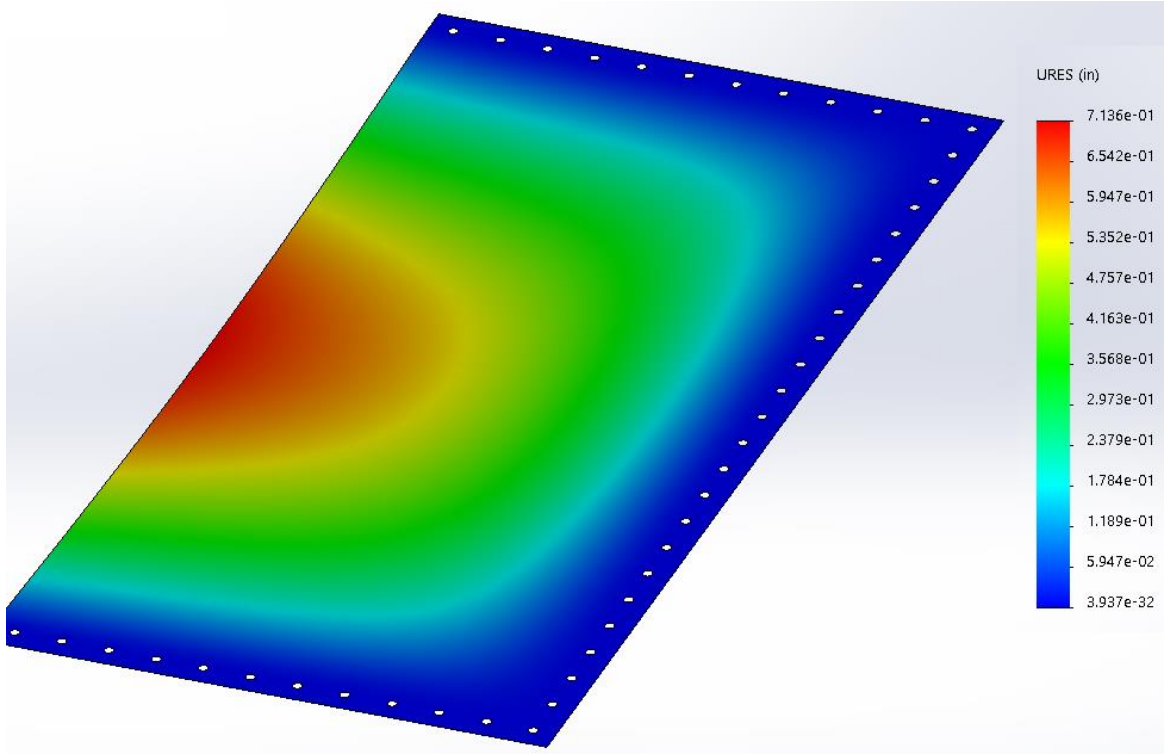

Figure 27: 24 Rivets, Deflection

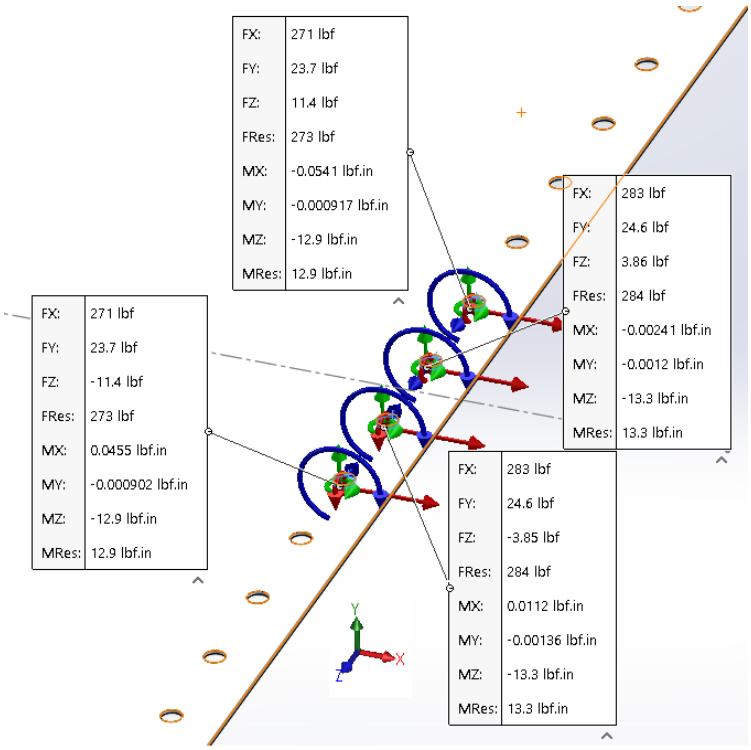

Figure 28: 24 Rivets, Maximum Rivet Loading

The design with 28 holes there is a 1.1[%] force variance between the center holes with a maximum shear load of 483[Lbf] and a deflection of about 0.5[in]. The design with 24 holes there is a 4.4[%] force variance between the center holes with a maximum shear load of 306[Lbf] and a deflection of about 0.72[in].

Now to consider a fully welded panel:

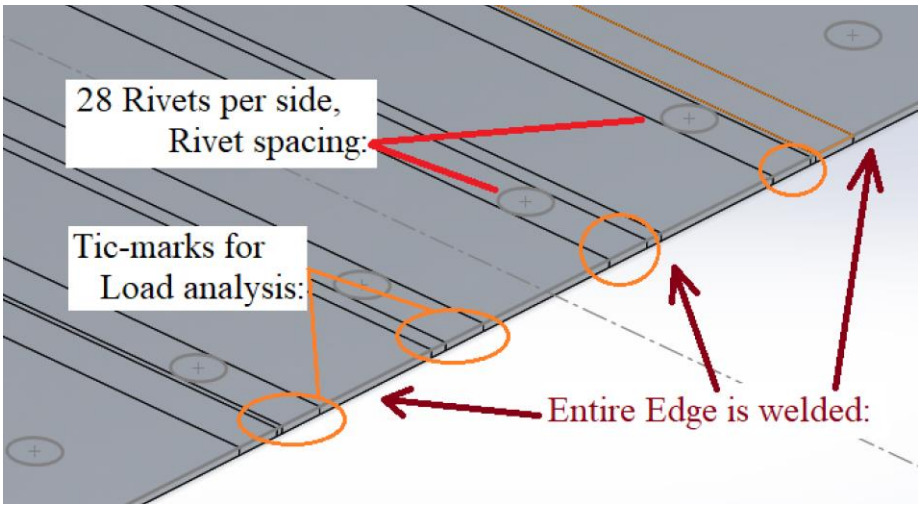

Figure 29: All Sides Full-welded Panel

B. Panel Structure, Rivet w/Fine-mesh:

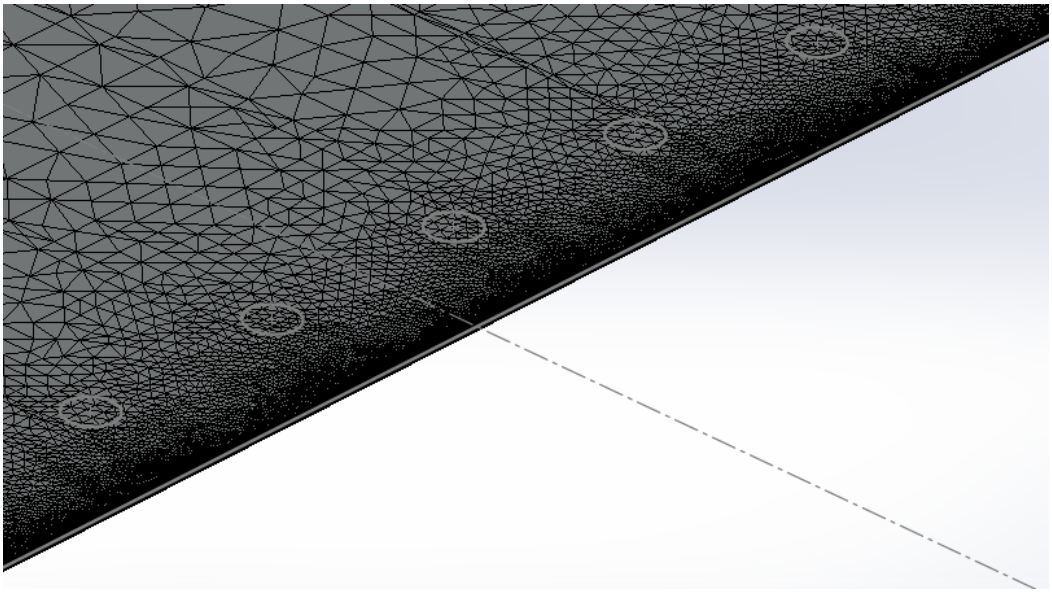

Figure 30: Full-weld, Same Mesh Size 0.0125" with 1.2% Growth

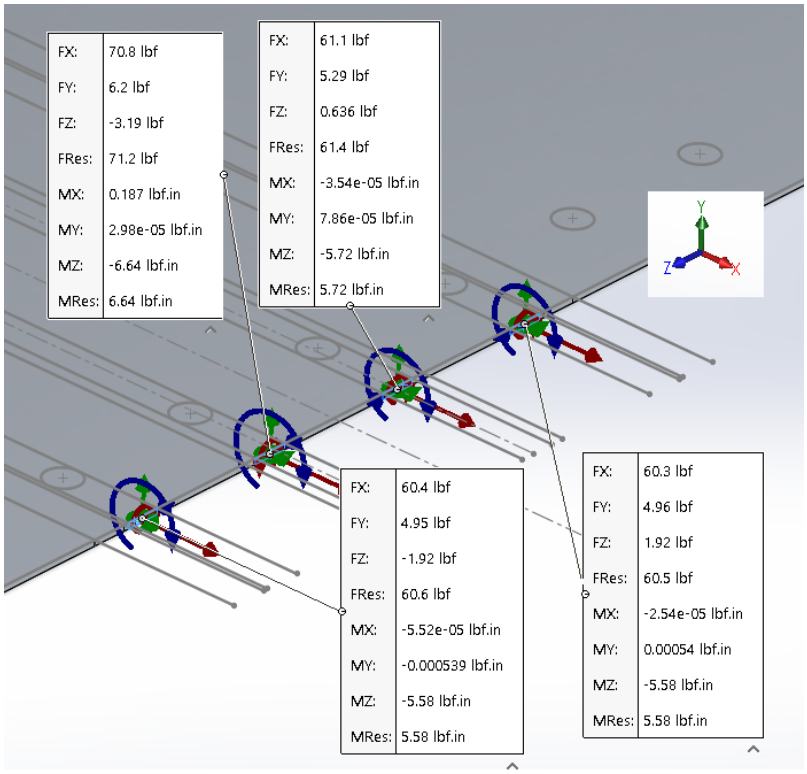

Figure 31: Welded Joint Force Variance

As seen in Figure 31, a welded joint over the same distance has an average force variance over 8[%].

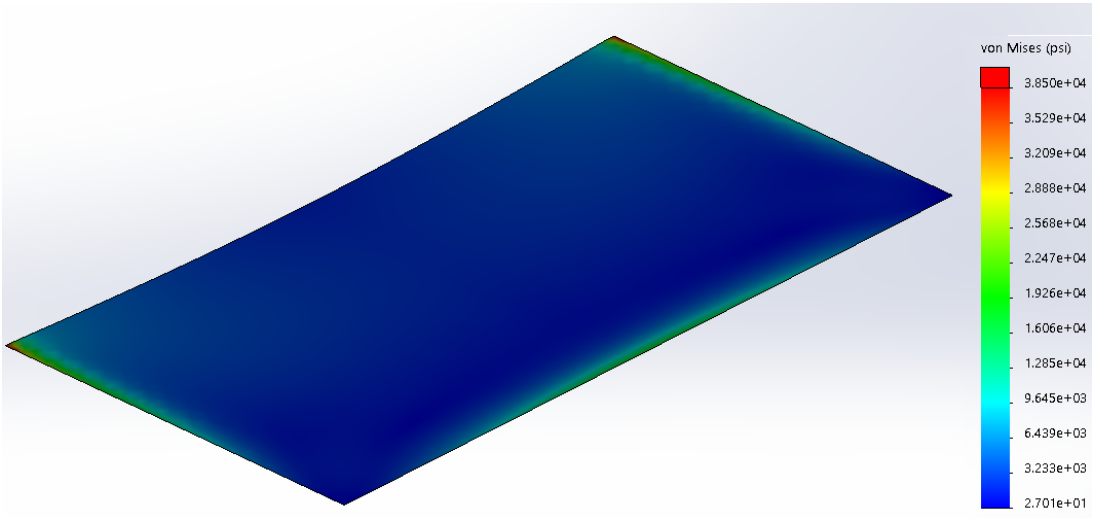

Figure 32: Welded Joint Panel Stress

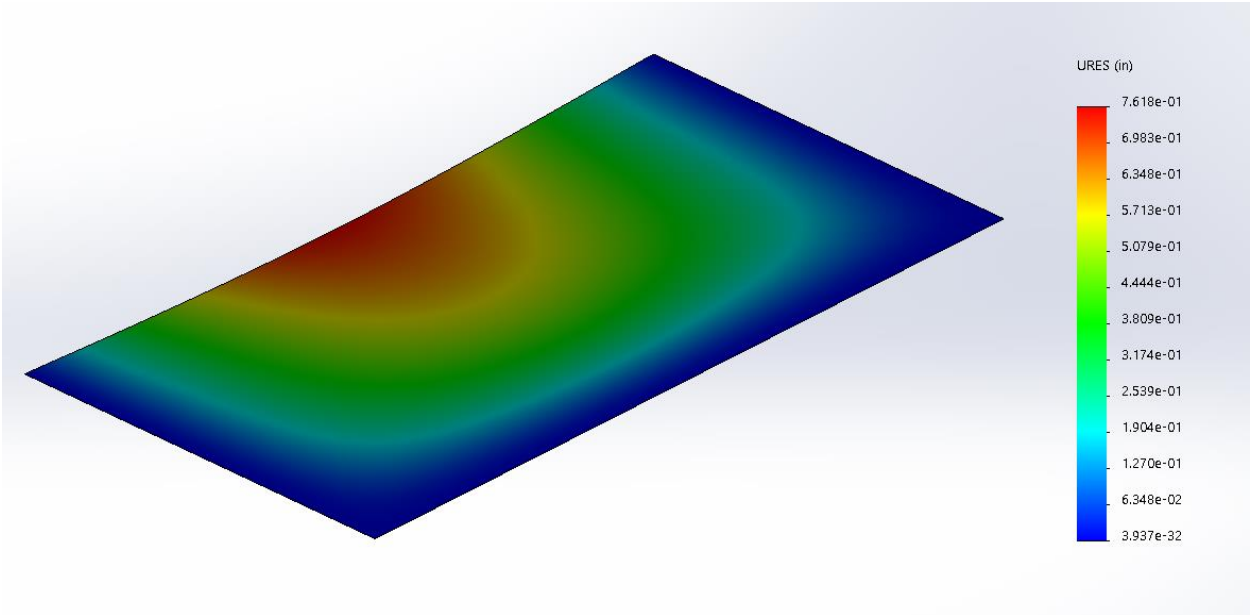

Figure 33: Full-weld Panel Deflection

The final point to consider is the strain. As seen in Figure 34, the strain is inconsequential.

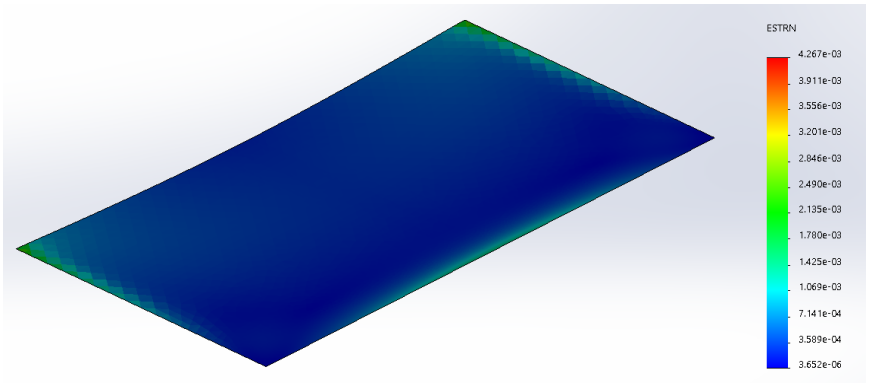

Figure 34: Full-weld Panel, Strain

As seen in Figure 33, the deflection is similar to that in Figure 27, where there were 24 rivets per side. Noting that the average force variance between over about 1.7" is more than 4.4[%] and the deflections between the welded panel and the 24-rivet panel are very similar, 24 rivets per side are to be taken as a welded joint.

Rivets with a 1.97" spacing produce relatively low stresses; as seen in Figure 35.

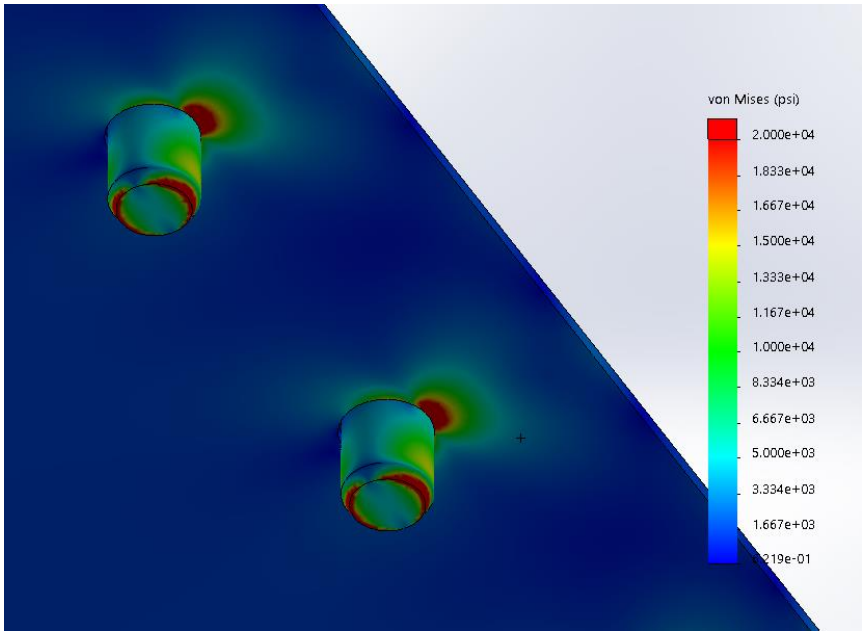

Figure 35: Rivet Stress with 24-rivet Spacing (~1.97")

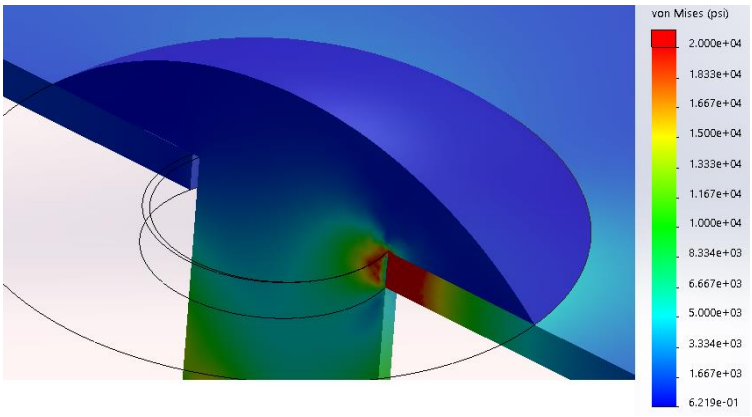

Figure 36: Rivet Stress with 1.97" Spacing

Adding a safety factor of 5[%], the average rivet loading in the simulation was 297[Lbf]. The stresses are such that the (1/16)" plate and the rivet/s will survive indefinitely, under maximum loading, with only minor deformation/s. Deformations near the rivet/s are on the order of 0.002[in] or 0.05[mm].

The radiused corners are constructed in a similar fashion:

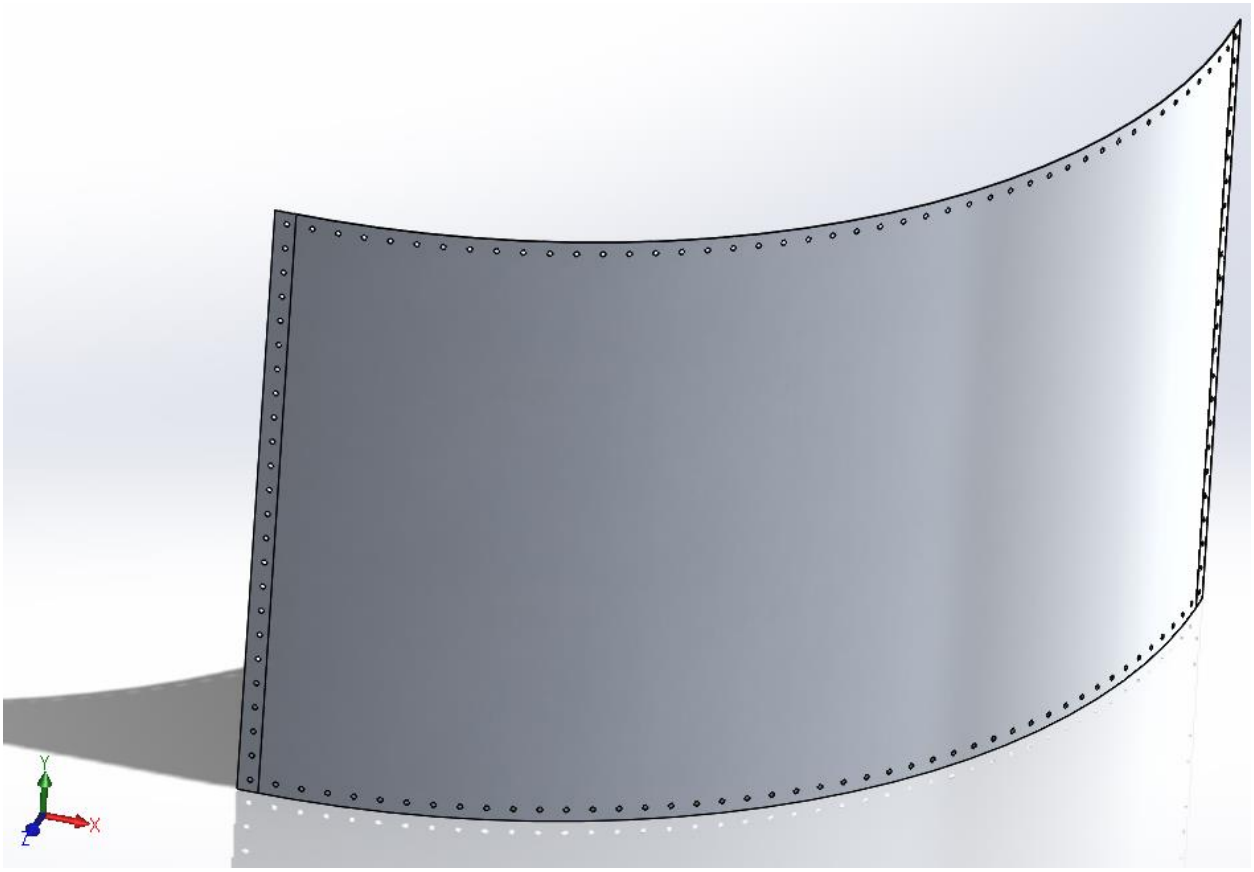

Figure 37: Base-radiused Panel, 54.4"

The radiused panel height is 47.25[in] with an outer radius of 54.4[in]. Each end has a 1.601[in] flat with a total outer-surface length of 88.752 [in]. The straight side has 24 rivets with an average separation of 1.972[in]; and the radius is traversed with 46 rivets with an average spacing of 1.929[in].

As noted earlier, Figure 14, shows the maximum pressure on the radiused panel is -1.471[psi] and this is about 47[%] above the average vacuum pressure; pulling the radiused panel away from the structure. To simplify the FEA modeling, the entire panel will be exposed to a vacuum of 1.472[psi]; with a similar pattern used with the flat panel analysis.

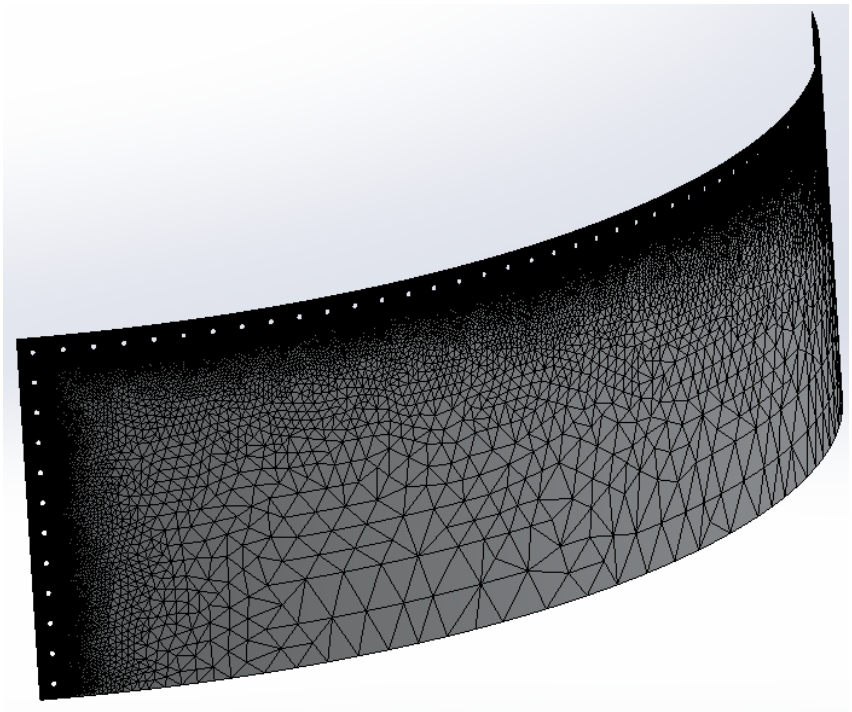

Figure 38: Radiused Panel, 54.4[in], Fine Mesh

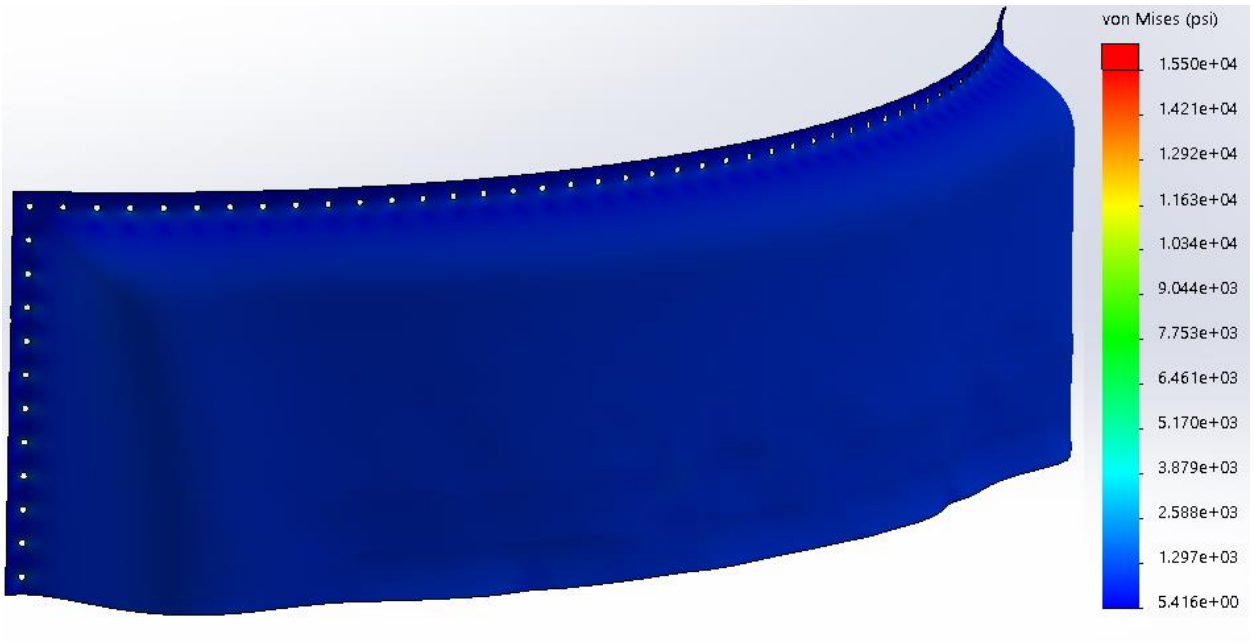

Figure 39: 54.4[in] Radiused Panel Stress

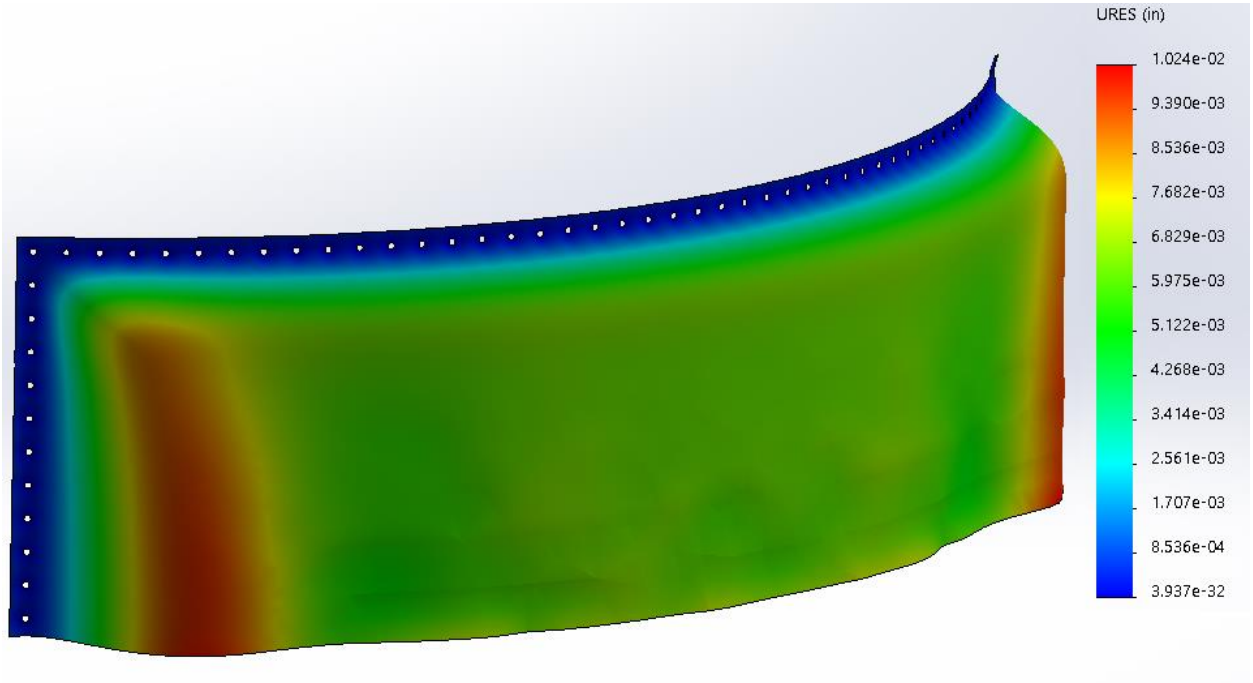

Figure 40: 54.4[in] Radiused Panel Deflection

As seen in Figure 39 and Figure 40, the stresses are insignificant and the deflections are less than 0.011[in] or 0.26[mm].

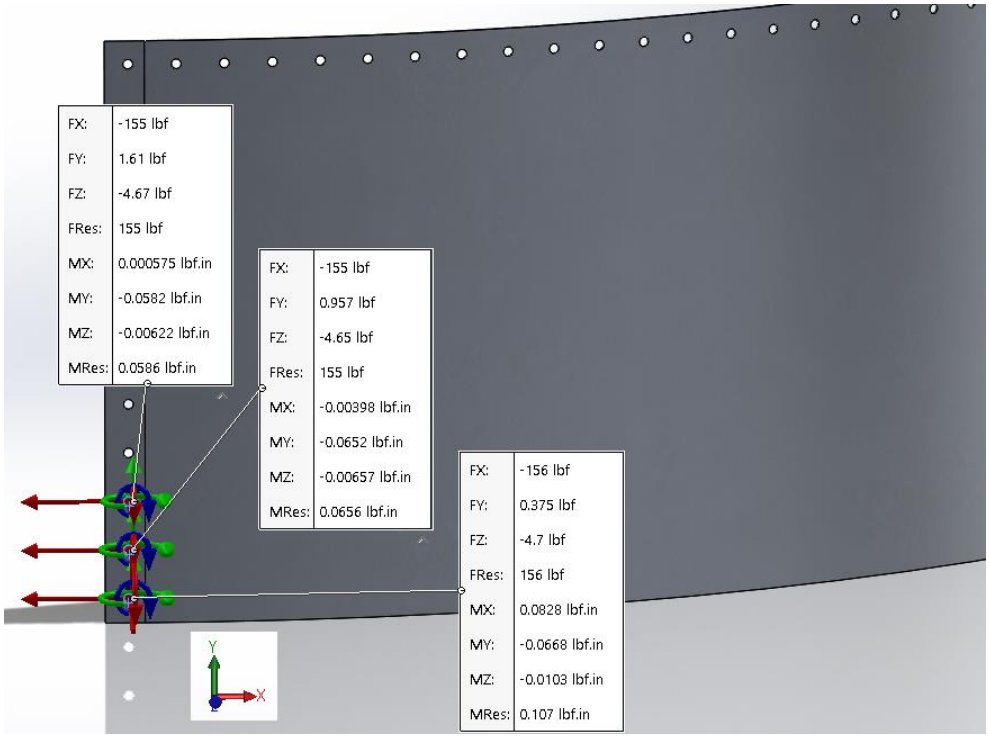

Figure 41: Panel Pull-out Force, Maximum

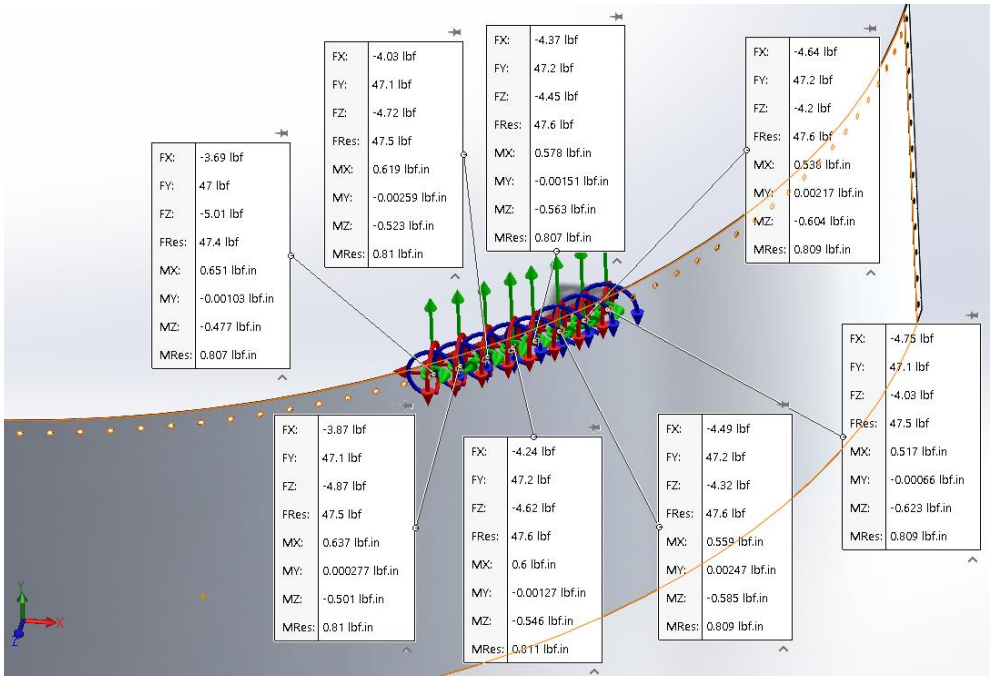

Figure 42: Panel Pull-out Force, 54.4[in] Radius

Noting again, that the values represented in Figure 41 and Figure 42 are with a loading that is 47[%] higher than average. The minimum thickness on a rivet head or the riveted/deformed bottom must be greater than 0.04[in] or 1[mm] for the rivet to hold its position.

C. Structure, Proper Rivet Instillation:

Taking a step back, this is a good time for a short examination of FEA verses classical mechanics.

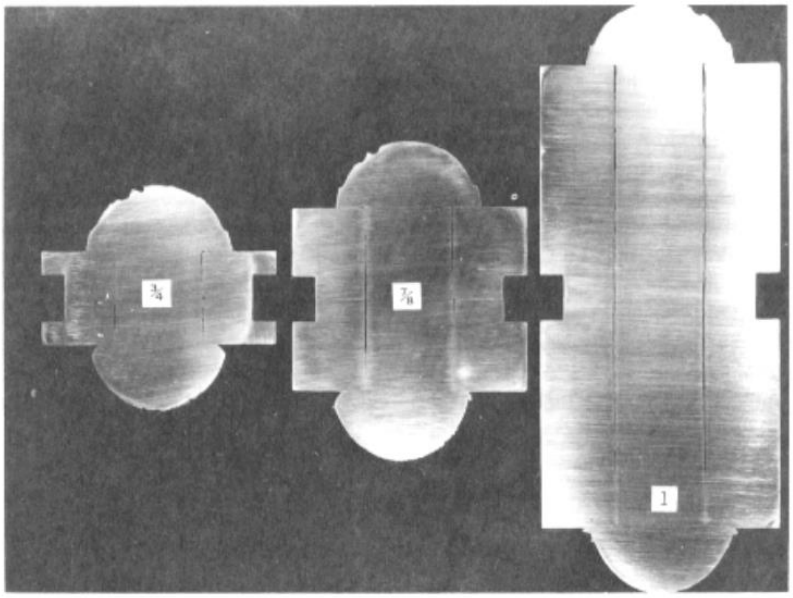

Fig 3.1. Sawed Sections of driven rivets. (Courtesy of University of Illinois.)

Figure 43: Properly Installed Rivets

The "Fig 3.1" from the University of Illinois was referenced from AISC, the American Institute of Steel Construction Incorporated. Figure 43 shows that "In addition to forming the head, the diameter of the rivet is increased, resulting in a decreased hole clearance." Proper guidelines may be taken from Chapter 3, "Rivets" in the "Guide to Design Criteria for Bolted and Riveted Joints" by G. Kulak, J. Fisher and J. Struik. In short, the adjoining plates to either rivet head/end should meld nicely with their respective holes (zero gap).

D. Structure, Classic Mechanics Bending:

The classical mechanics of a cantilevered arm may be found in any mechanical engineering book.

Eq - 21: Classical Mechanics, Cantilevered Beam

$$\sigma_{Max}(x) = \frac{M_{Max}(x)}{S} = \frac{M_{Max}(x)}{\frac{I}{c}}$$

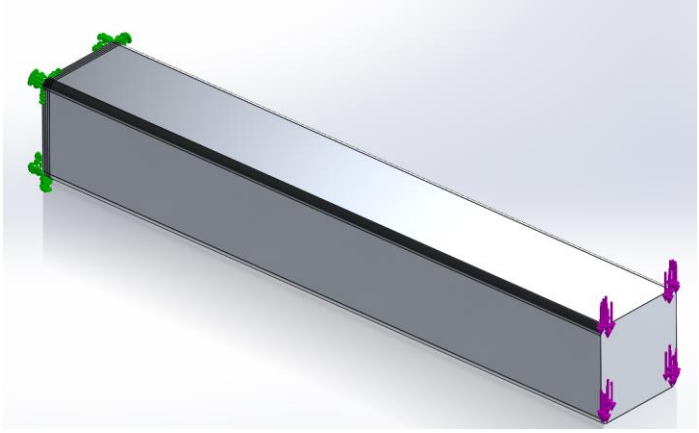

Figure 44: Proportional Cantilevered Beam

Appling a load to the end of this simple beam would give a maximum moment at the base of (Force)*(Length) = (50000[Lbf](80[in]). The simple beam in Figure 44 is proportionally the same as the arm for the Glorious Cross. The maximum stress should be 14,080[psi].

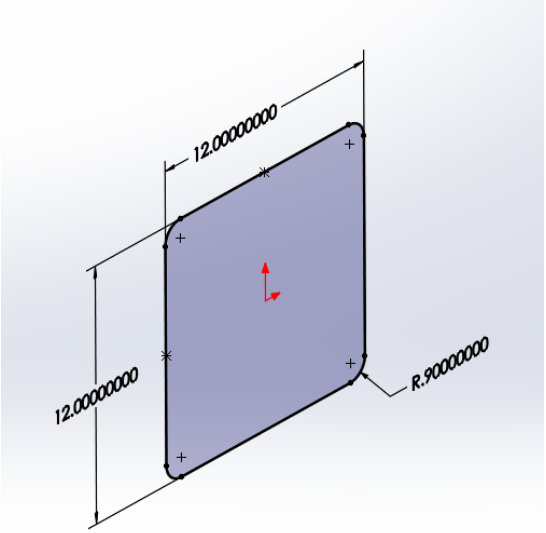

Figure 45: Simplified Beam x-Section

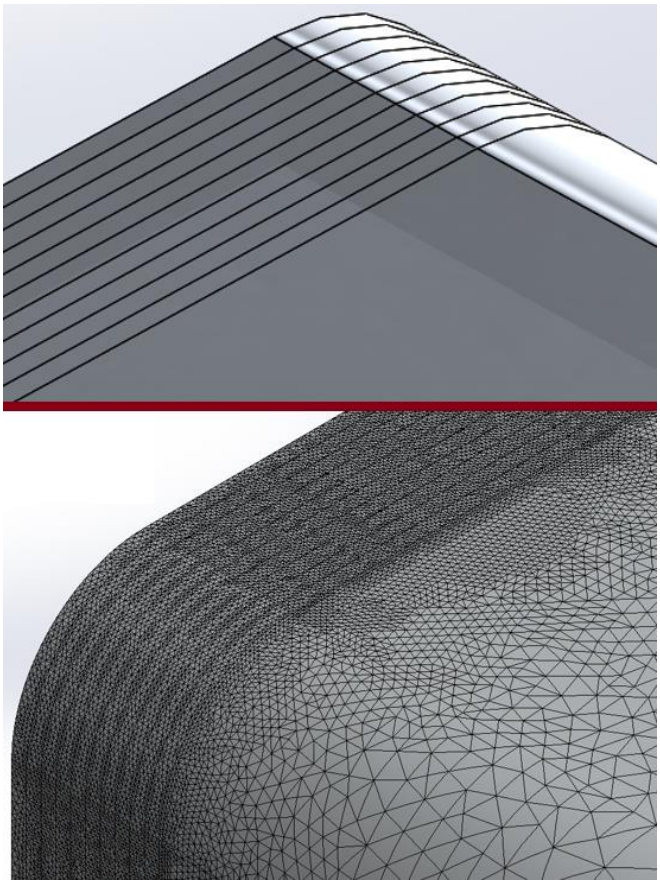

Figure 46: Modeling for Comparison, (1/10)" marks

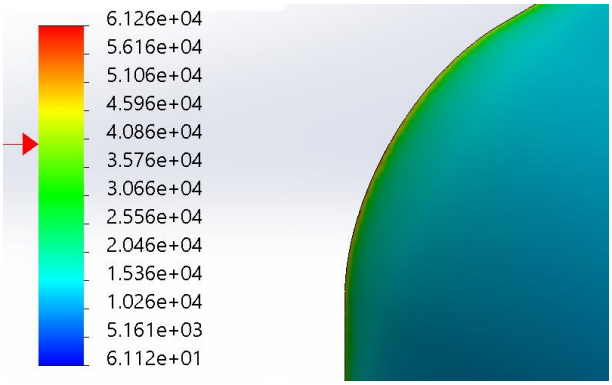

Figure 47: FEA Analysis Maximum Stress, Simple Beam

The FEA shows a maximum stress of 61,260[psi] which is (x4) greater than the expected 14,080[psi]; calculated with classical mechanics equation Eq - 21. Examining the stresses at each $(1/10)^{th}$-line the theoretical stress was found at 0.2[in] from the edge; 14,470[psi] (+3[%]). The high stress of 61,260[psi] is due to the 90[deg] interface: It can be shown that at 90[deg] interfaces in FEA's, the stresses will tend towards infinity. Thus, the stress comparisons will be made at 0.2[in] from the 90[deg] interface for this comparison.

Now a lateral load was applied to the model: Fy = -50,000[Lbf] and Fz = -25,000[Lbf], both applied to the end of the beam. The maximum stress from Fy should be 14,080[psi] and the maximum stress for Fz should be 7,040[psi].

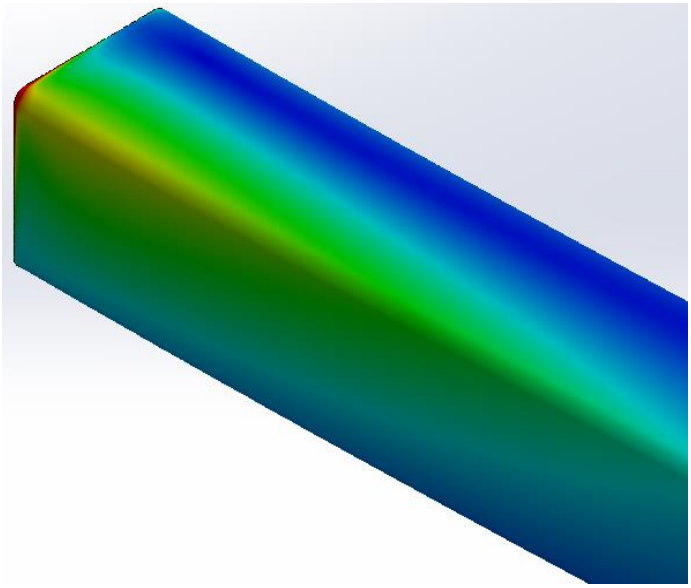

Figure 48: Simplified Beam with Fy & Fz

Utilizing the RMS (root mean squared) stress values on the 0.2[in] line it can be shown that the maximum stress on the radius is 12[%] higher than the additive maximum stresses.

Eq - 22: Maximum Stress on Radius of Arm (+3[%])

$$\sigma_{Max-Radius} = 1.15\left(\sigma_{Max-Fy} + \sigma_{Max-Fz}\right)$$

The construction of the arms for the Glorious Cross present several technical hurdles due to the height, breadth and length of its requirements; not to mention that it is near a large body of salt water. The best method of construction was deemed to be that of an aircraft fuselage.

The classical method of fuselage design is to ignore the skin of the aircraft, however, due to the shear size of the arm it would be inefficient to ignore the skin of the Glorious Cross.

The skin will be textured with a wheel.

Directional Textured with a wheel:
M31 Fine satin: Wheel or belt polishing with aluminum oxide grit of 320 to 400 size, using peripheral wheel speed of 6,000 fpm (30 m/s).

M32 Medium Satin: Wheel or belt polishing with aluminum oxide grit of 180 to 220 size, using peripheral wheel speed of 6,000 fpm (30 m/s).

M33 Coarse Satin: Wheel or belt polishing with aluminum oxide grit of 80 to 100 size, using peripheral wheel speed of 6,000 fpm (30 m/s).

Grit Finish and Estimated RMS and Ra Values

Grit Finish	RMS (Micro-inch)	RMS (Micron)	Ra (Micro-inch)	Ra (Micron)
36	160	4.06	142	3.61
60	98	2.49	87	2.21
80	80	2.03	71	1.8
120	58	1.47	52	1.32
150	47	1.2	42	1.06
USDA Bead Blast	47	1.2	42	1.06
180	34	0.86	30	0.76
220	21	0.53	19	0.48
240	17	0.43	15	0.38
320	14	0.36	12	0.3
400	10	0.25	9	0.23
Mirror	5	0.13	4	0.1

Figure 49: Roughness of Grit/Finish - Maximum

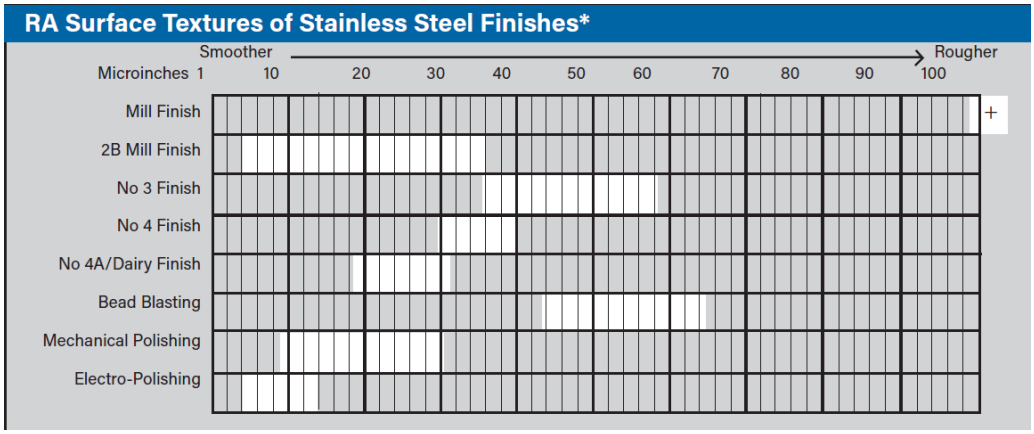

Figure 50: Surface Finish Designation & Roughness

The maximum roughness shown in Figure 49 and their corresponding surface designations in Figure 50 show that the M32 Medium Satin finish is comparable to the #4A stainless steel finish (from Apache Stainless Equipment Corporation) with a maximum roughness of 34[μin].

Texturing will apply scratches to the surface, thereby making some of the material thickness unusable due to stress concentrations caused by the scratches. Medium satin, M32, is widely used in architecture and is acceptable for the Glorious Cross. Therefore, the effective material thickness shall be reduced from (1/16)” or 0.0625[in] to 0.0624[in] or 1.585[mm].

Eq - 23: Glorious Cross Stress-bearing, Mechanical Skin Thickness

$$t_{Effective-(\frac{1}{16})"} = 0.0624[in] = 1.585[mm]$$

To make modeling a bit easier, the skin thickness will be taken as 0.062[in].

Eq - 24: Glorious Cross Stress-bearing, Mechanical Modeling Thickness

$$t_{FEA\ Model-(\frac{1}{16})"} = 0.062[in] = 1.575[mm]$$

Dealing with over 100[m] cantilevered off of the main body presents new challenges. To deal with these, the most effective method is to follow aircraft fuselage construction; keeping the parts aluminum gives a much better strength to weight ratio than steel, plus it is resistant to salt.

To begin, the basic arm structure is further defined:

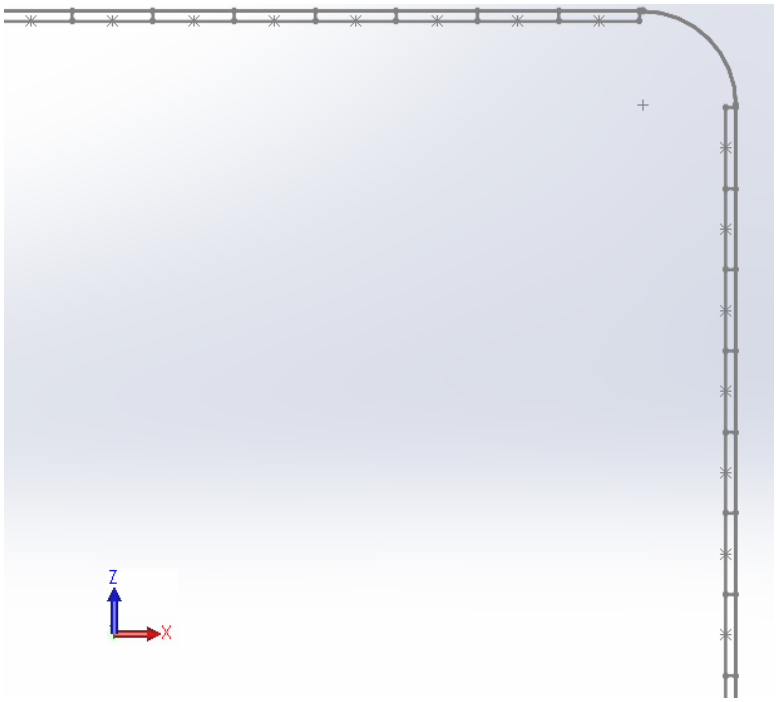

Figure 51: Initial Panel Layout

The center of the arm in noted by the < X, Z > axis. There are (x13)-47.25[in] panels on all sides with (x4) radii of 54.4[in] at each corner. The structure will maintain a central (cg), a center of gravity in the center of the arm.

The basic idea in fuselage stress is to ignore the skin of the aircraft and find the stresses as such:

Eq - 25: Glorious Cross Stress-bearing, Mechanical Skin Thickness

$$\sigma_x{}^i = \frac{Mc_i}{I_y{}^i}$$

Where:
"σ" is the stress
"i" denotes the "i^{th}" element or stiffening member
"M" is the moment

“c” is the maximum distance from “cg”
“I” is the inertia of bending; w/r the stress.

III. Structure, Six-Segments:

The first step taken here will be to find the maximum moments on the arm. The arm is divided into (x6) segments, each of equal length: This is done to minimize weight.

From the loading calculations presented in Table 5: Overall Loading, the following tables were generated:

Table 6: Moment due to Force Acting on the Face

Distance Ratio to Base of Arm	Moment due to Wind @ Face [Lbf-in]
Base @ $(1/6)^{th}$	13,845,384,599
@ $(2/6)^{th}$	11,537,820,499
@ $(3/6)^{th}$	9,230,256,399
@ $(4/6)^{th}$	6,922,692,300
@ $(5/6)^{th}$	4,615,128,200
Endcap @ $(6/6)^{th}$	2,307,564,100

Table 7: Overall Moment on Arm Due to Wind and Gravity

Distance Ratio to Base of Arm	Moment due to Weight [Lbf-in]	Moment due to Wind @ Lateral [Lbf-in]	**Moment due to Gravity & Wind [Lbf-in]**
Base @ $(1/6)^{th}$	998,138,059	2,120,841,529	**3,118,979,588**
@ $(2/6)^{th}$	615,590,970	1,767,367,941	**2,382,958,911**
@ $(3/6)^{th}$	347,351,582	1,413,894,353	**1,761,245,935**
@ $(4/6)^{th}$	174,347,588	1,060,420,765	**1,234,768,353**
@ $(5/6)^{th}$	76,845,937	706,947,176	**783,793,113**
Endcap @ $(6/6)^{th}$	21,922,776	353,473,588	**375,396,364**

Aside: Significant figures will be taken into account at a later time.

Let us consider first supporting the structure using only the beams furthest away from the (cg); about 41[in] inside the skin, making c = 322[in]. Since there are (x13) panels, there will be (x14) ribs or "areas" for structural integrity. Under these conditions, the area for each rib at the base would need to be 75.7[in2]. Now if we add-in the inertia due to the 0.062[in] skin we need only 65.4[in2].

Now to add some background to these calculations:
Referring to Eq - 22 and Table 6.

Eq - 26: Maximum Stress Defined

$$38{,}500\left[\frac{Lbf}{in^2}\right] = 1.15\left(\frac{13.8}{3.12}\sigma_{Max-Fz} + \sigma_{Max-Fz}\right)$$

Therefore, the minimal stresses in the structure will be near 6,200[psi] and the maximum stresses will be near 24,800[psi]; thus the skin stress will be near 38,500[psi]. As such, the design stress for the beams will be 24,800[psi].

In general, the inertia of a beam is:

Eq - 27: Inertia of Beam

$$I_{Total} = I_o + d^2A$$

the arms for the Glorious cross follow aircraft mechanics, where the base inertia is much, much smaller than the cross-sectional area term "d^2A" so the "I_o" value is ignored. Unlike aircraft design, the Glorious cross is so huge that the skin has a significant effect on the values and will not be ignored.

The distance "d" in Eq - 27, or "c" in Eq - 25/Eq - 21 come from this table:

Table 8: Distance for Moments to < CG >

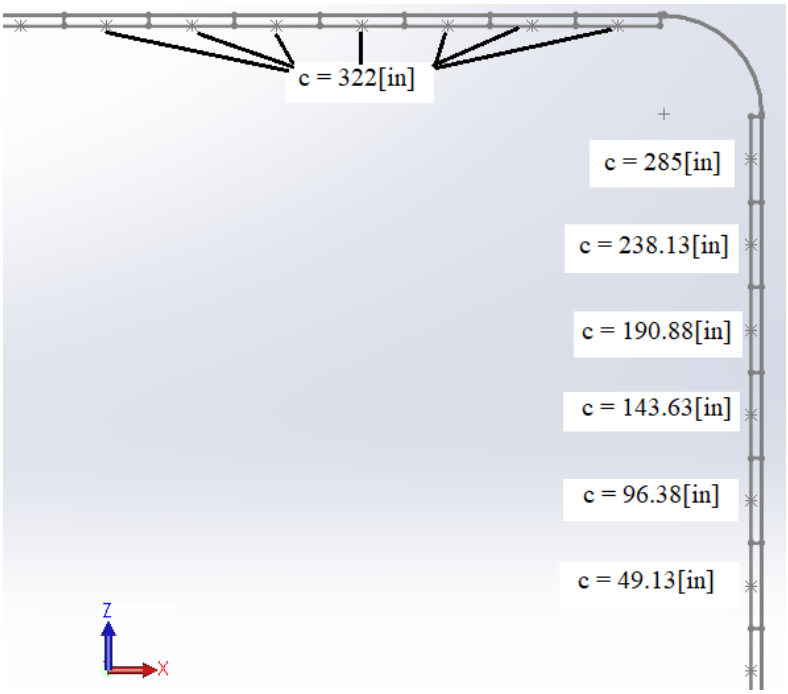

Many methods, beams and various variants there-of were examined for strength, feasibility and construction. The final beam was a formed beam with multi-curls as seen here:

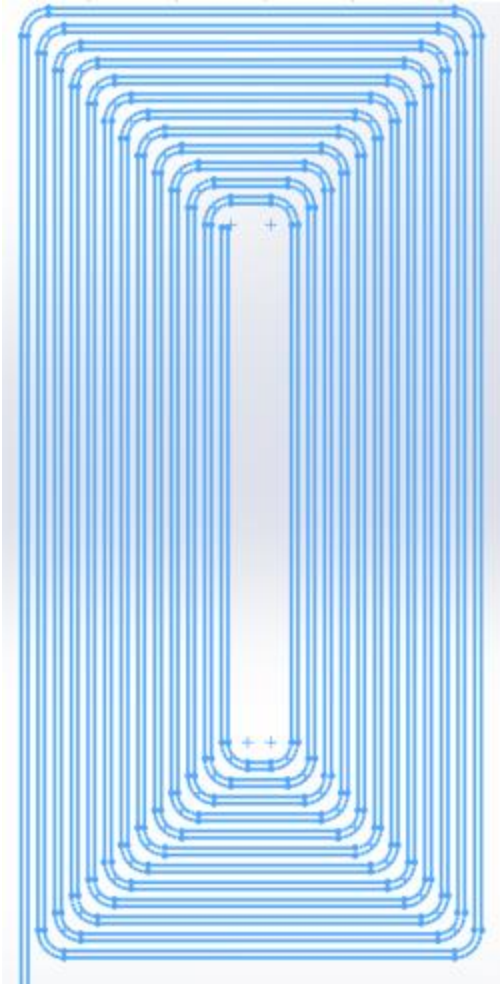

Figure 52: Rib/Beam with Multiple Curls

Continuing to optimize for manufacturing and cost, it can be shown that optimizing a rectangle per its area and perimeter are best when a = b; i.e. both sides are the same (unlike what is shown in Figure 52). Therefore Lxo = Lyo and the following equation is obtained:

Eq - 28: Length of the Multi-curl

$$L_{Total} = (N+1)\left(L_o - N\frac{dL}{2}\right) + N\left(L_o - (N-1)\frac{dL}{2}\right) + NR(\pi - 4)$$

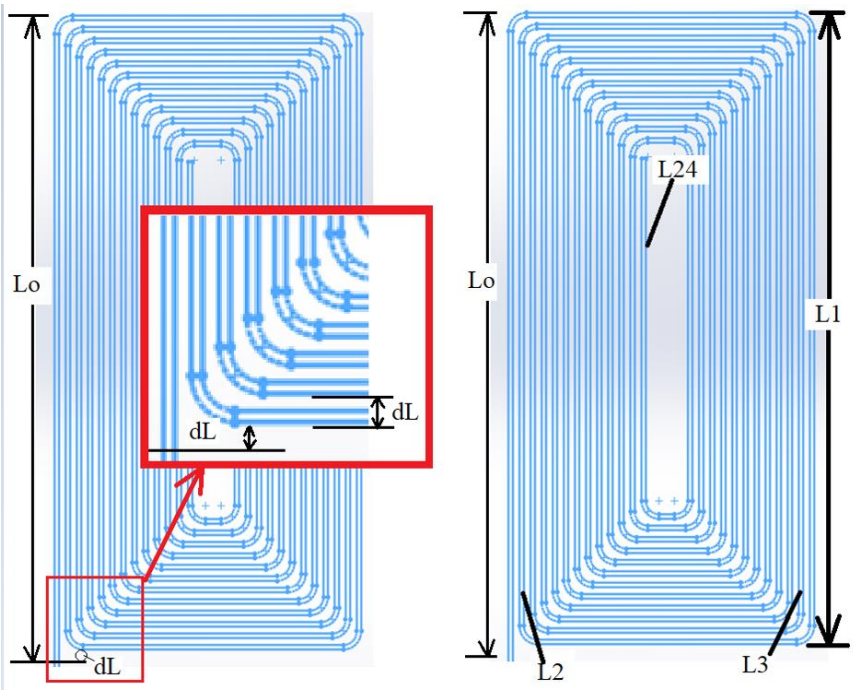

Figure 53: Definition of Length of Multi-curl

Since the high wind requires a 32[in] segment, the curl must be located above the base-rib or minimum rib. The iterations performed were complicated by the series-sum equations which place a step function in the optimization of the rib/s. After a lot of iterations, it can be shown that an L_o of 13[in] is the optimal starting length for the multi-curl segment. The largest multi-curl required for the arm is shown in Table 9.

Table 9: Basic Multi-curl Definition/s

Largest Multi-curl

Lxo = Lyo = Lo =	13.000	[in]
the last "L"	6.250	[in]
N	18	[-]
dL	0.3750	[in]
Radius (mean)	0.438	[in]
L(Total)	353	[in]
Thickness	0.1250	[in]

Table 10: Rib Area, Length and Factor of Safety

Position on Arm	Total Length w/r (1/8)" & (+)15[%] [in]	(+)15[%] of Required Area [in2]	**Final FS w/r Area, Adding "32[in] base" Rib**
at Base	349.63	43.70	**25.5%**
at (5/6)L	290.47	36.31	**27.7%**
at (4/6)L	229.98	28.75	**31.0%**
at (3/6)L	168.38	21.05	**36.9%**
at (2/6)L	101.49	12.69	**51.3%**
at (1/6)L	33.72	4.22	**124.2%**

As seen in Table 10, one rib needs a length of 350[in]. Structurally speaking, it would be best if each rib were from one continuous roll of aluminum. The spacing of (3/8)" shown in Table 9, leaves (1/4)" for the coupling ribbing, between panels: Since the ribbing has a base thickness of (1/8)", there is only (1/16)" per side for any welding. If welding is needed, then the weld must protrude from the surface, have a porosity of less than 2[%] and have a total height of less than (1/16)" per side: And be smooth, no scratches or other imperfections deeper than 0.003[in] are allowed.

To begin the arm analysis, a CFD is performed on the $(6/6)^{th}$ portion, or the Endcap. CFD on the last 6^{th} of the arm (the endcap) at 60.603[m/s], where the temperature is 53.6[F] (with a density of 1.226[kg/m3]). As a comparison, another CFD was performed at 60.603[m/s], where the temperature is 68[F] with a density of 1.18[kg/m3]; which represents a 3.9[%] density difference.

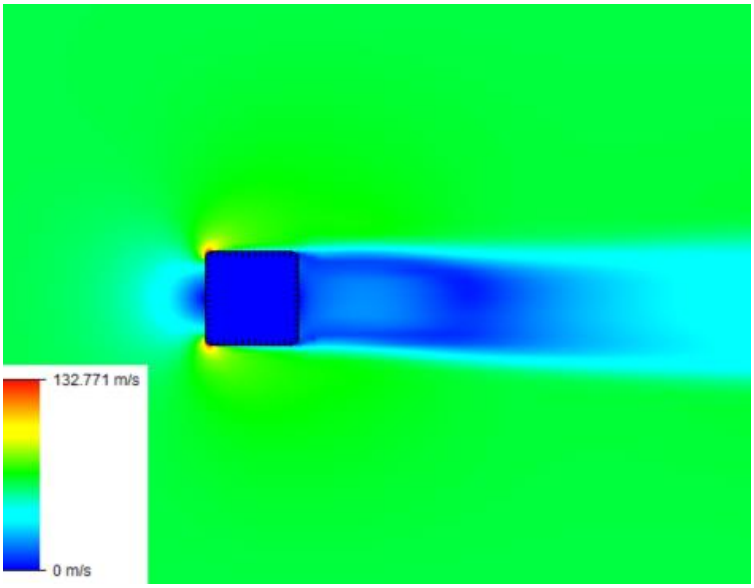

Figure 54: CFD w/ Fine Mesh at Conversion

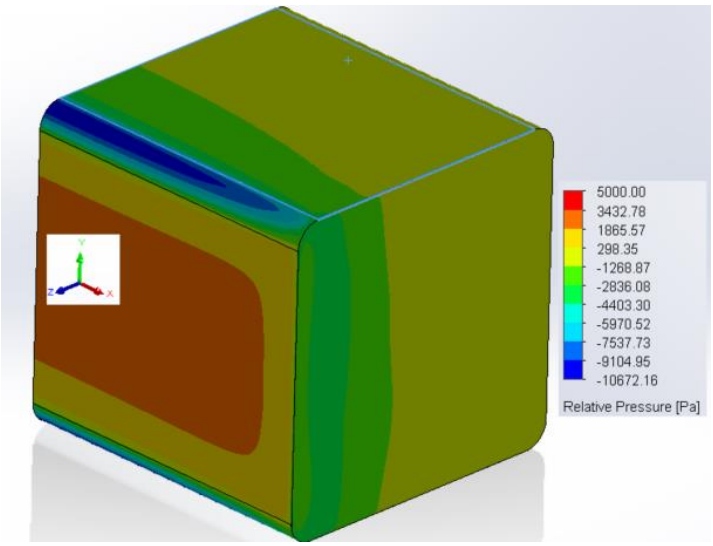

Figure 55: CFD on Endcap Pressure Map

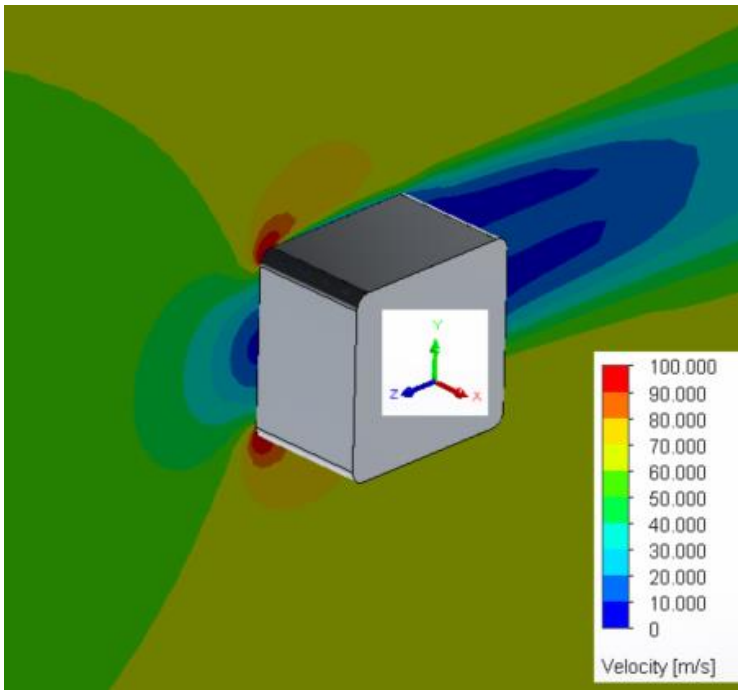

Figure 56: CFD on Endcap, Velocity Map

A. Structure, Six-Segments, Rough-mesh:

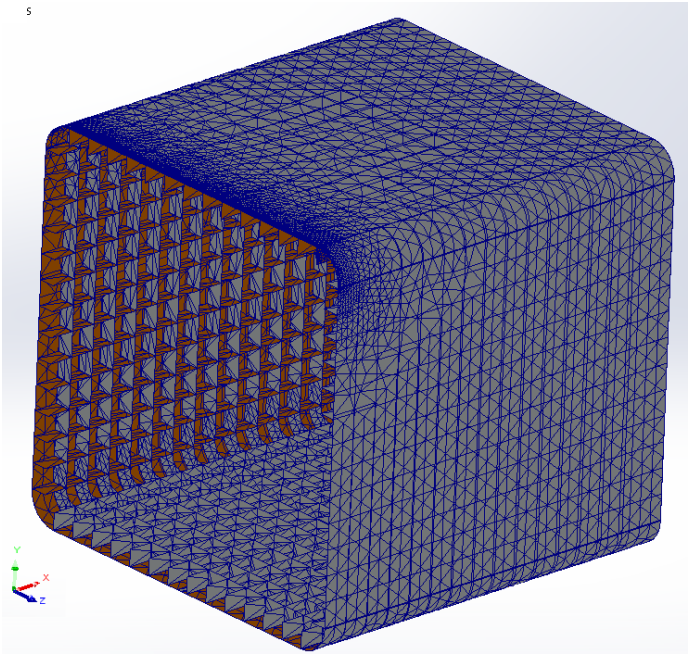

Figure 57: Endcap, Rough Mesh

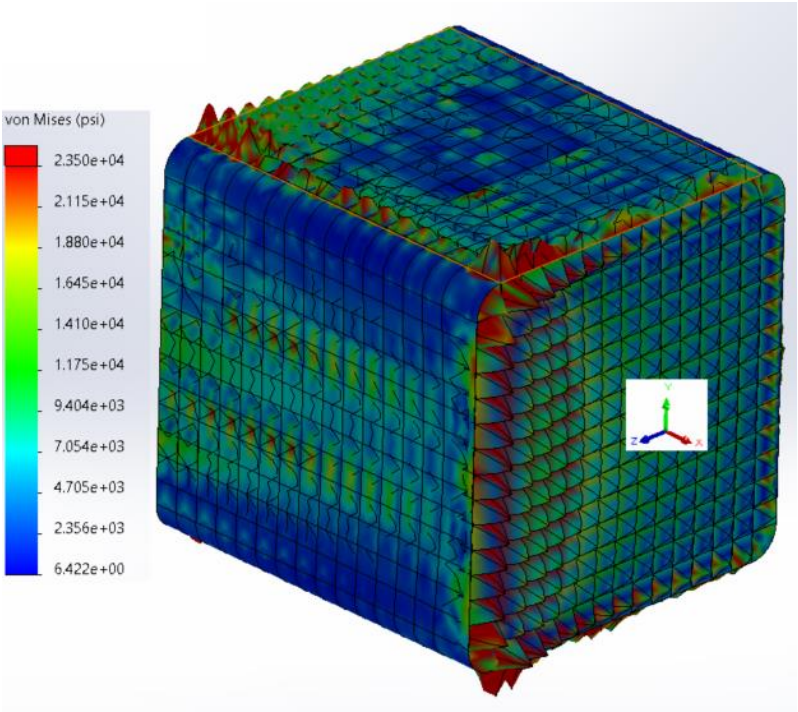

Figure 58: Endcap, Stress w/ Rough Mesh

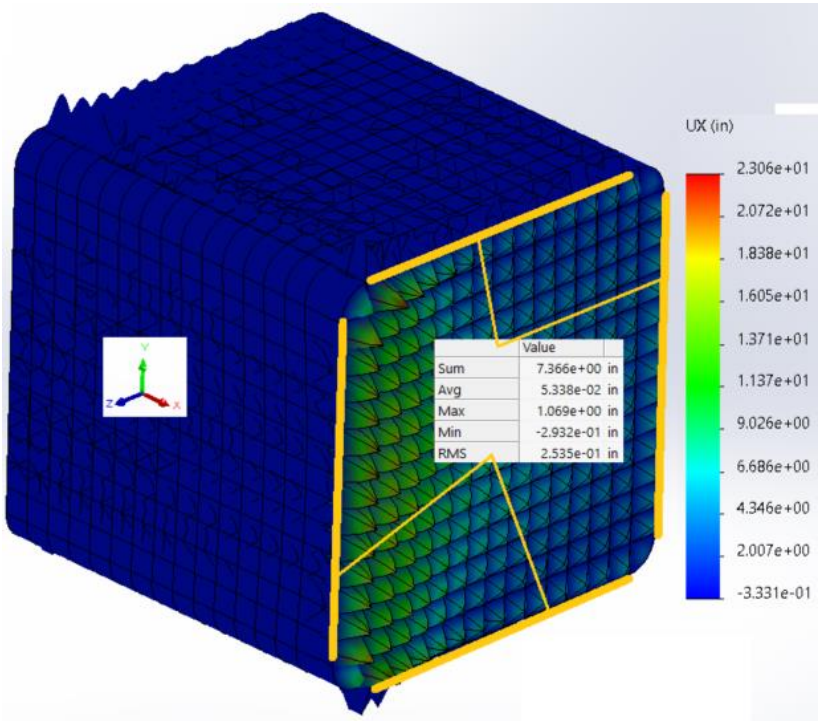

Figure 59: Endcap, Rough Mesh, Deflection "X"

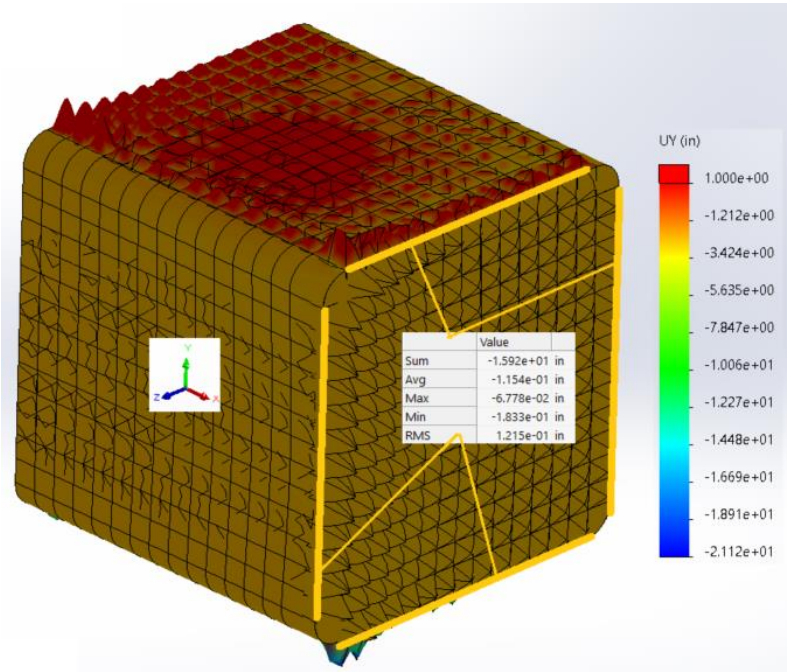

Figure 60: Endcap, Rough Mesh, Deflection "Y"

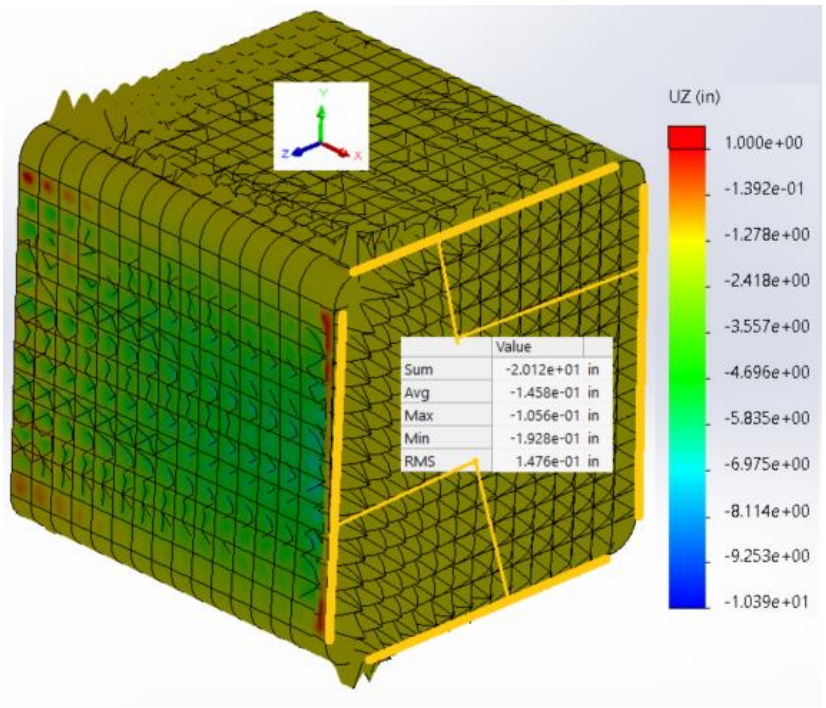

Figure 61: Endcap, Rough Mesh, Deflection "Z"

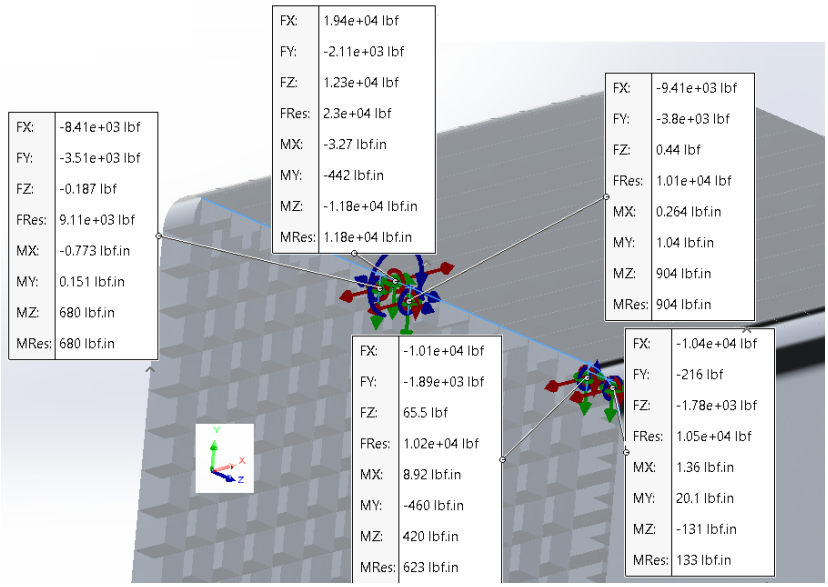

Figure 62: Endcap, Rough Mesh, Reaction Loading w/ / Density 1.18[kg/m3]

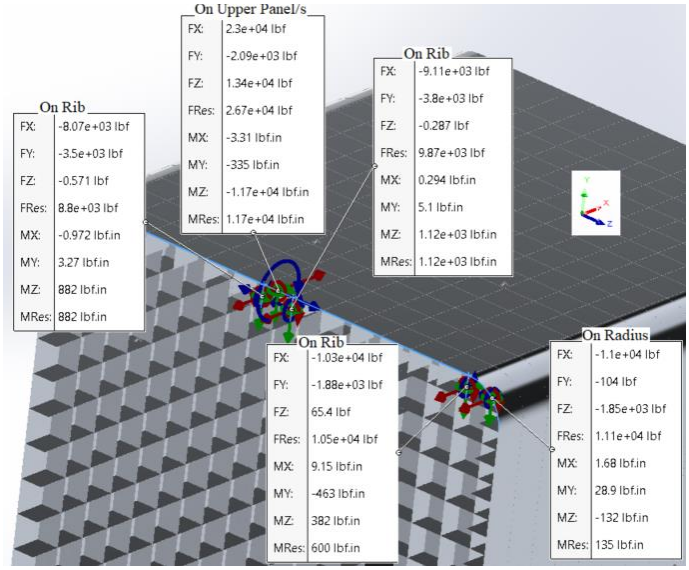

Figure 63: Endcap, Fine Edge Mesh, Reaction Loading w/ Density 1.226[kg/m3]

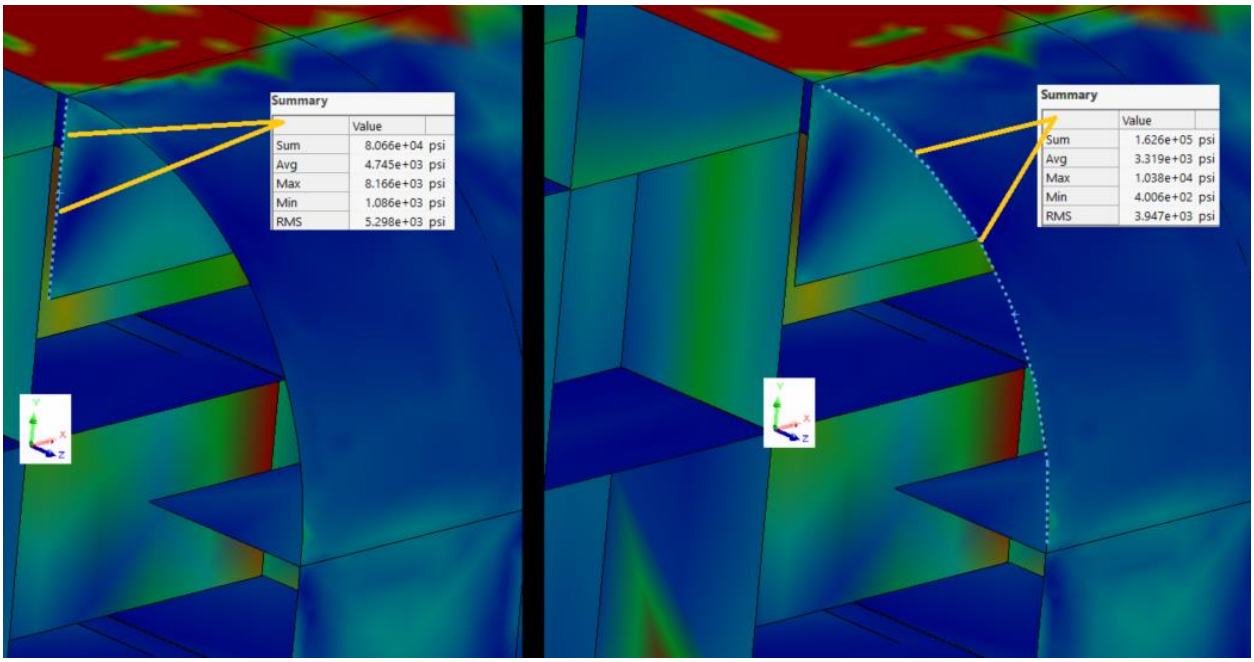

Figure 64: Endcap, Rough Mesh, Critical Member Stress @ 68[F] & 1.18[kg/m3]

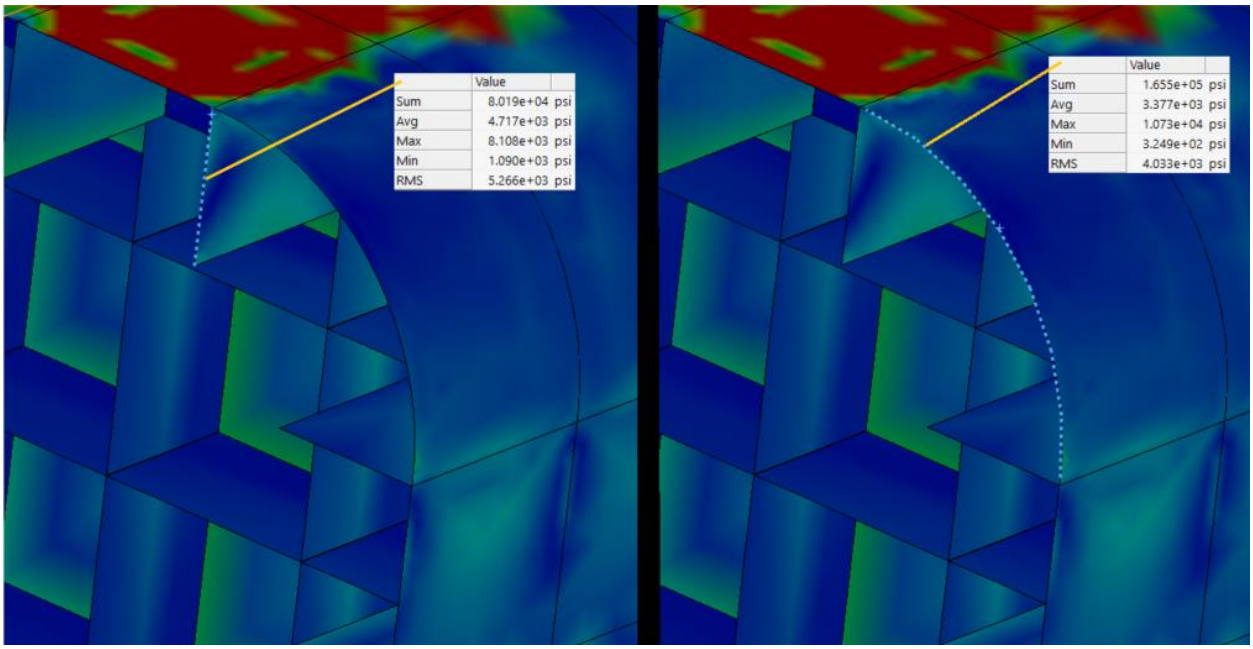

Figure 65: Endcap, Rough Mesh, Critical Member Stress @ 54[F] & 1.226[kg/m3]

B. Structure, Six-Segments, Fine-mesh:

Now a fine mesh is placed on the Endcap and a similar analysis was performed:

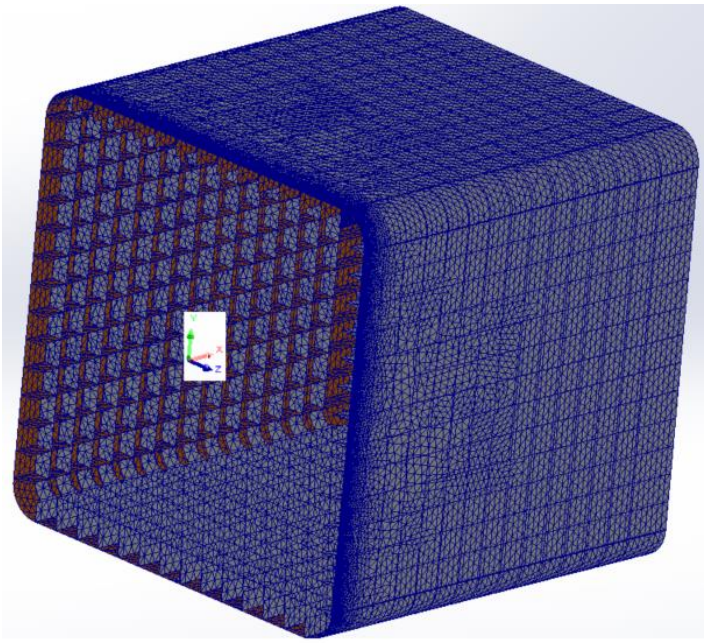

Figure 66: Endcap, Fine Edge Mesh

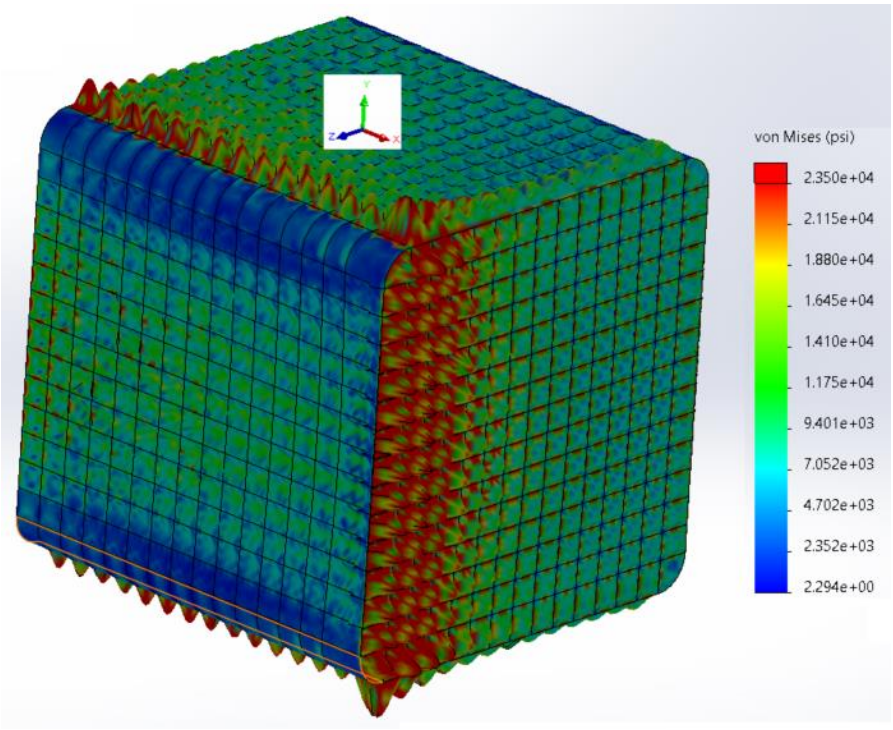

Figure 67: Endcap, Stress w/ Fine Edge Mesh

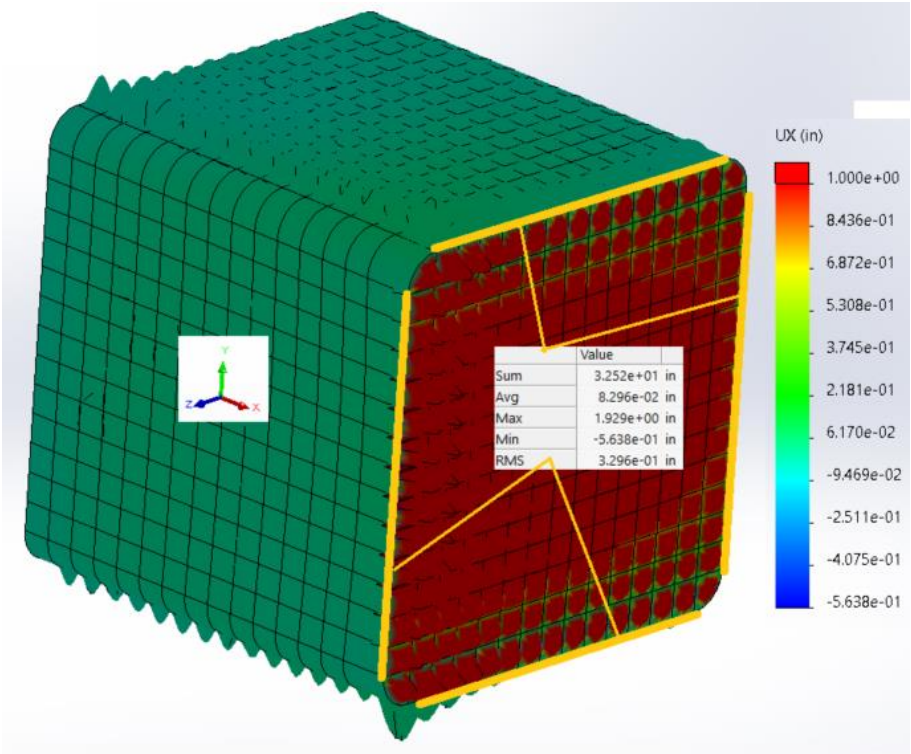

Figure 68: Endcap, w/ Fine Edge Mesh, Deflection "X"

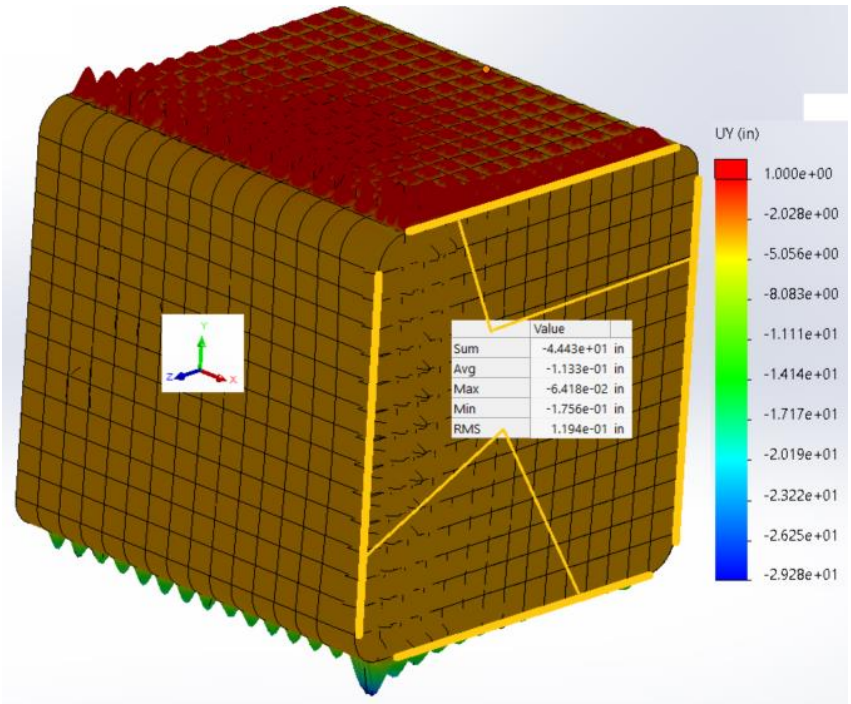

Figure 69: Endcap, w/ Fine Edge Mesh, Deflection "Y"

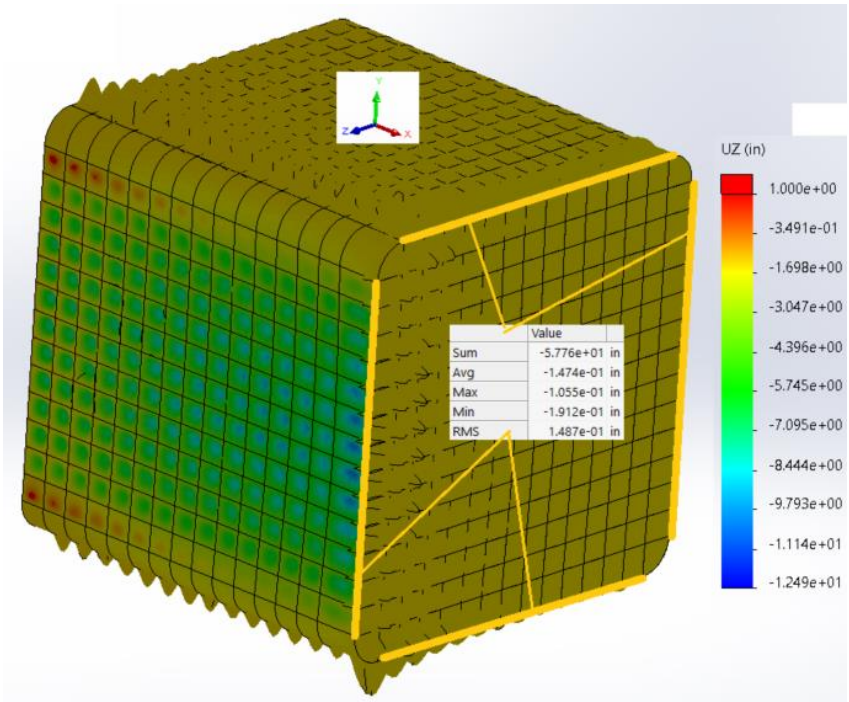

Figure 70: Endcap, Fine Edge Mesh, Deflection "Z"

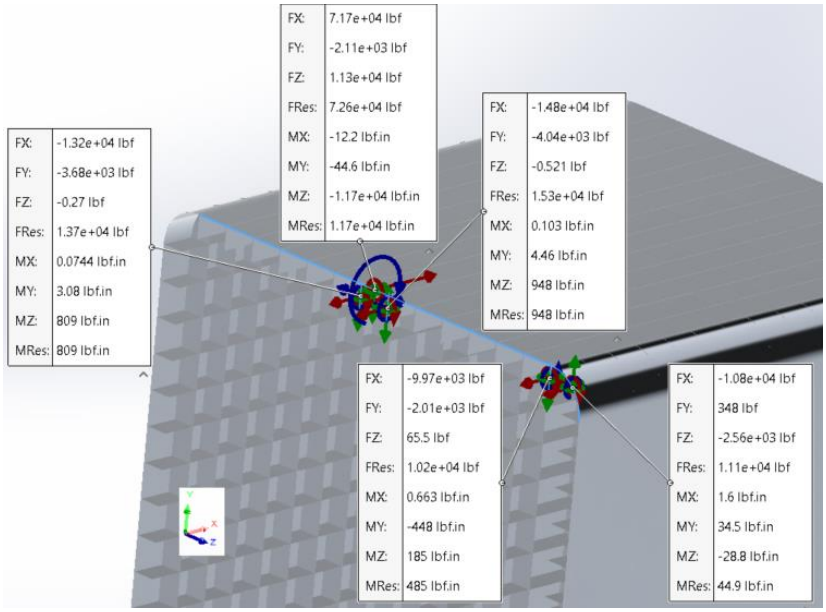

Figure 71: Endcap, Fine Edge Mesh, Reaction Loading w/ Density 1.18[kg/m3]

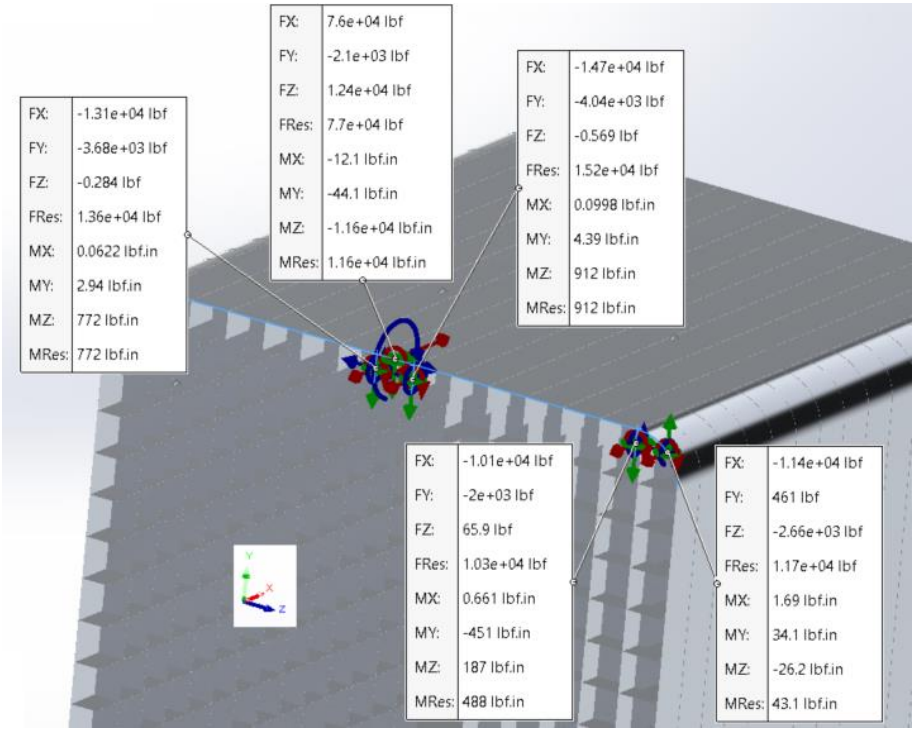

Figure 72: Endcap, Fine Edge Mesh, Reaction Loading w/ Density 1.226[kg/m3]

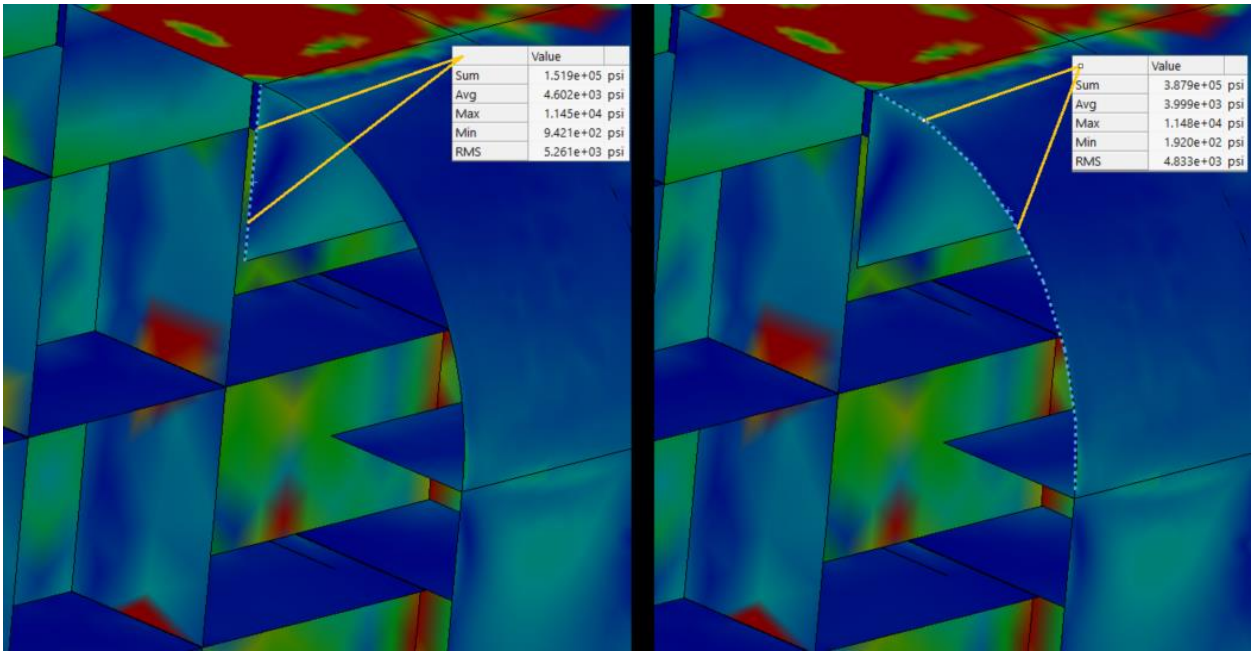

Figure 73: Endcap, Fine Edge Mesh, Critical Member Stress w/ Density 1.18[kg/m3]

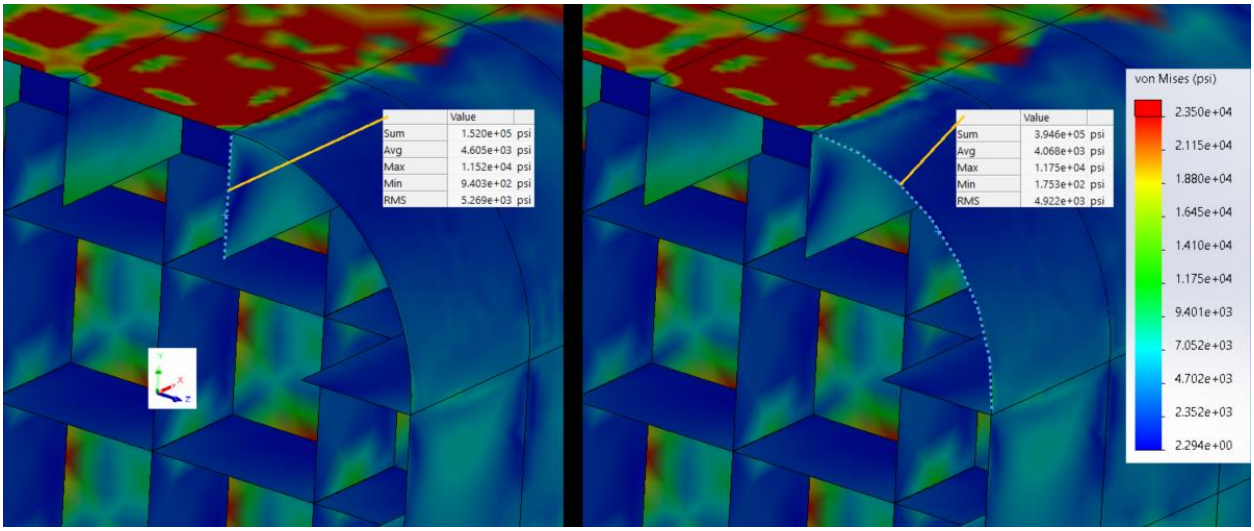

Figure 74: Endcap, Fine Edge Mesh, Critical Member Stress w/ Density 1.226[kg/m3]

The similarities between the rough & fine meshes:

- The Loading
  - Gravity 9.81[m/s2]
  - Wind from CFD at 60.603[m/s]
- Edge Mesh Growth of 1[%]

The mesh differences:

- Rough mesh

    - Divided each panel into (x11) pieces
        - Maximum Size 38.5[in]
        - Minimum Size 12.8[in]
    - Edge Mesh
        - 4.0[in]
        - Growth 1[%]

- Fine-edge mesh
    - Divided each panel into (x24) pieces
        - Maximum Size 15.4[in]
        - Minimum Size 5.13[in]
    - Edge mesh
        - 1.5[in]
        - Growth 1[%]

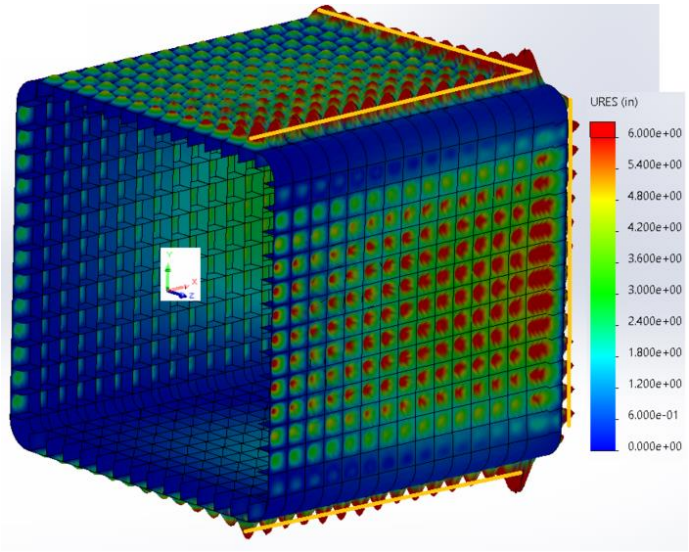

Figure 75: Endcap, Large Deformation Zones

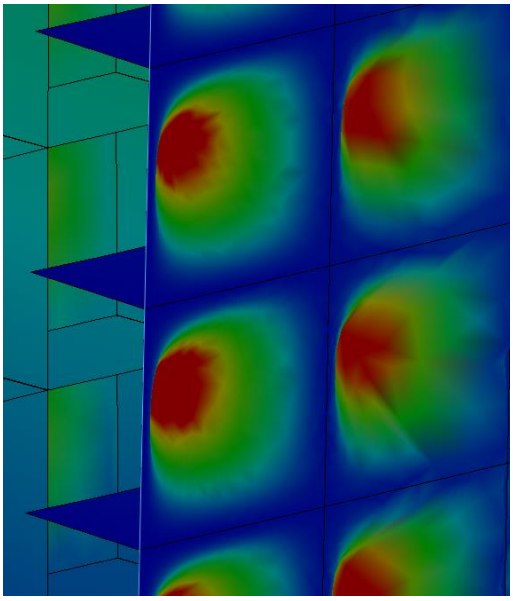

Figure 76: Endcap, Panel Deflections Greater than 6[in]

A graphical item of concern are the large (looking) deformations as noted in Figure 75. The previous analysis (example Figure 26) shows that the panels will not exceed a deflection of more than 0.72[in]. The comparable panel deflections in the fine-edge mesh (on the endcap) are greater than 6[in]: This is due to the number of elements per panel. Therefore, we can ignore the panel deflection/s shown in this segment of the analysis. These high deformation zones do point to large stress regions.

The high deformation regions are in-line with the expected high stress zones. In the calculation of stress and nodal vibrations, the system stiffness is often a point of interest. Note that in Table 11, the overall forces differ by less than 1.6[%] while the moments differ greatly. The ability of the finer mesh to distribute the loading more accurately among the internal members accounts for the discrepancy in the moment values; as seen in Table 12.

Table 11: Reaction Loading, Mesh Comparison @ 1.18[kg/m3], Full Model

Reaction Force [lbf]	Rough Mesh	Fine-edge Mesh	Variance
Component	Entire Model	Entire Model	
Sum X:	-166,450	-166,760	0.19%
Sum Y:	50,486	50,201	-0.56%
Sum Z:	83,516	84,794	1.53%
Resultant:	192,950	193,700	0.39%
Reaction Moment [lbf-in]			
Component	Entire Model	Entire Model	
Sum X:	-615	117	-119%
Sum Y:	17,300	7,505	-56.6%
Sum Z:	-9,387	1,027	-111%
Resultant:	19,692	7,576	-61.5%

Table 12: Member Loading with 1.18[kg/m3], Figure 62 and Figure 71

Reaction Force [lbf]	Rough Mesh	Fine-edge Mesh	Variance
Component			
Sum X:	-18,700	22,986	-223%
Sum Y:	-11,529	-11,503	-0.23%
Sum Z:	10,787	8,892	-17.57%
Resultant:	24,474	27,198	11.13%
Reaction Moment [lbf-in]			
Component			
Sum X:	6	-10	-251%
Sum Y:	-879	-451	-48.7%
Sum Z:	-9,886	-9,764	-1.23%
Resultant:	9,925	9,775	-1.51%

A closer look at ss shows that there is a vacuum force (F_x) due to the end cap of about 167,000[Lbf] or 742,000[N]. This is oversized because there will be a radius on the endcap: Each corner will receive a radius of about 54.4[in]. Due to the missing radius, the F_y component of 50,200[Lbf] (223,300[N]) is also oversized. The missing radius will adjust Fx values by 72.28[%], with a value of 120,500[Lbf] or 536,200[N].

Table 13: Endcap Reaction Forces w/r 1.18[kg/m3], Adjusted

Endcap Last 6th Reaction Force	Fine-edge Mesh	Fine-edge Mesh
Component	Entire Model [Lbf]	Entire Model [N]
Sum X:	-120,537	-536,177
Sum Y:	50,201	223,305
Sum Z:	84,794	377,182
Resultant:	155,690	692,544

The fixed end has an area of 398[in2] with a delta vacuum load of 46,200[Lbf]; which means that the stresses at the fixed end should add 116[psi] with respect to the density of 1.18[kg/m3]. Similarly (w/r 72.28[%]), with respect to the density of 1.226[kg/m3], 104[psi] should be added.

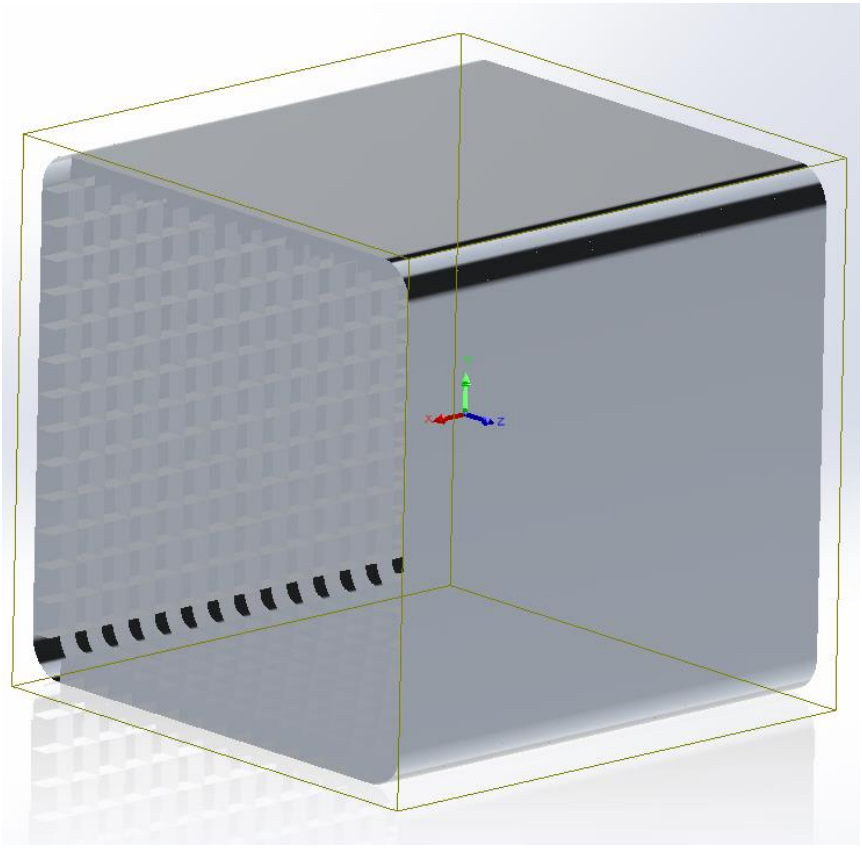

Figure 77: Endcap Mass Properties, (CG) Location

Table 14: Endcap, Mass Properties

	[Lbf]	[N]
Mass:	54,192	241,059
	[in3]	[m3]
Volume:	555,570	9.104
Model Center of Mass (cg)	[in]	[mm]
< X >	438	11,121
< Y >	0.0	0.3
< Z >	0.0	0.0
Overall Center of Mass	[in]	[mm]
< X >	4,473	113,621
< Y >	24,213	615,000
< Z >	0.0	0.0
Reaction Loading Center	[in]	[mm]
< X >	4,035	102,500
< Y >	24,213	615,000
< Z >	0.0	0.0
Inertia, Principle, @ (cg)	[Lbm-in2]	[kg-m2]
Ixx - Twisting	7,898,804,383	2,311,501
Iyy - Bend Fore/Aft	6,982,651,018	2,043,399
Izz - Bend Up/Down	6,982,699,136	2,043,413

Note: Product of Inertias (Ixy, ect) are negligible.

Table 15: Air Density Contribution to Force/Loading

Density Affect	Density @ 1.18[kg/m3]	Density @ 1.226[kg/m3]	ρ(1.18)/ρ(1.226) [%] - Variation
< Fx >	-166,760	-149,390	11.6
< Fy >	50,201	54,017	7.06
< Fz >	84,794	90,934	6.75

Table 16: Air Density Contribution to Stress

Density Affect	Density @ 1.18[kg/m3]	Density @ 1.226[kg/m3]	ρ(1.18)/ρ(1.226) [%] - Variation
Maximum Stress on Rib Fine Mesh [psi]	11,567	11,520	0.4
Maximum Stress on Radius Fine Mesh [psi]	11,597	11,750	1.30

The FEA with a density of 1.18[kg/m3], shows that the maximum stress on the corner rib converges with the maximum stress on the radius. Using the fine-edge mesh and adding 117[psi], the maximum stress on the 32[in] corner rib is 11,567[psi], where-as the maximum stress on the 54.4[in] radius (corner) is 11,597[psi]. By adding 10[%] for safety (calculation/s) a maximum stress of 12,800[psi] or 87.95[MPa]; with 1.18[kg/m3].

The spreadsheet calculations (Table 10) were derived without considering the cross-members with an added safety due to regular beam theory; thus, a safety factor of 3[-] is achieved.

Note: All "factor of safety's" are done with respect to 38,500[psi] unless otherwise specified.

A rather nice method of optimizing the cross-ribs is to examine the stiffness of differing designs. For the endcap with 32[in] cross-ribs, the stiffness matrix is found in Table 17.

Similarly, the maximum stress with respect to the model using 1.226[kg/m3] has a maximum stress of 13,040[psi]; thus, the factor of safety is reduced to 2.95[-]. Therefore, a change in density of about 3.898[%] results in a change in stress and safety factor of 4.74[%].

Table 17: Endcap Stiffness Matrix with Density of 1.18[kg/m3]

Stiffness	Deflection [in]	k [Lbf/in]	k [N/m]
$< k_x >$	0.324	515,328	90,247,612
$< k_y >$	0.064	788,828	138,144,800
$< k_z >$	0.110	772,259	135,243,103

Table 18: Endcap Stiffness Matrix with Density of 1.226[kg/m3]

Stiffness	Deflection [in]	k [Lbf/in]	k [N/m]
$< k_x >$	0.330	453,246	79,375,536
$< k_y >$	0.119	452,404	79,227,961
$< k_z >$	0.149	611,527	107,094,624

Since the structure will not be water tight, a few drains would be advantageous because 1[in] of water is 31.12[%] of the weight of the endcap-model; while 1[in] of ice is about 28.7[%] of the weight of the endcap-model. The endcap itself is about 4[%] of the total weight of the arm: Overall 37.2[%] per of overall weight is added per inch of water and 34.2[%] of weight is added per inch of ice. ***Therefore, the arms should be de-iced and drains need to be within the arms (where the density of water is 62.43[Lbm/ft3] and the density of ice is 57.43[Lbm/ft3]).

An alternative model with 24[in] cross-braces/ribs was made and analyzed; as seen in Figure 78.

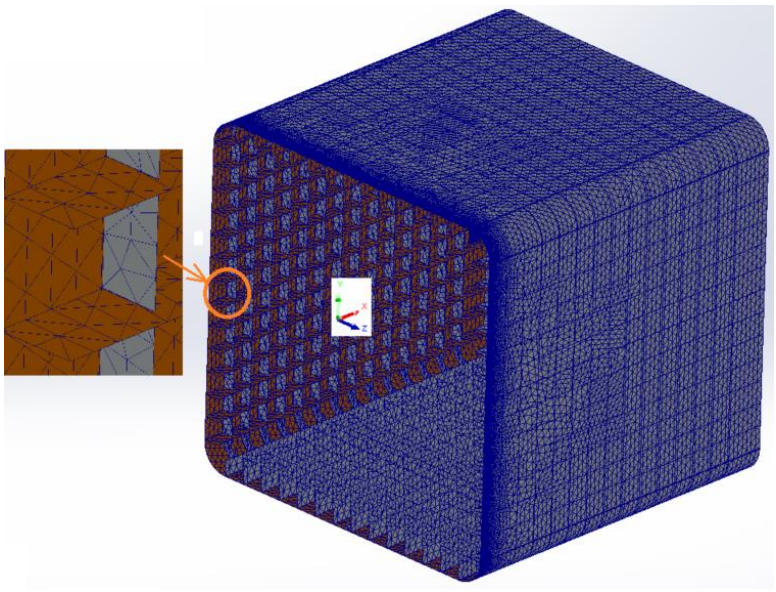

Figure 78: Fine-edge Mesh with 24[in] Cross-ribs

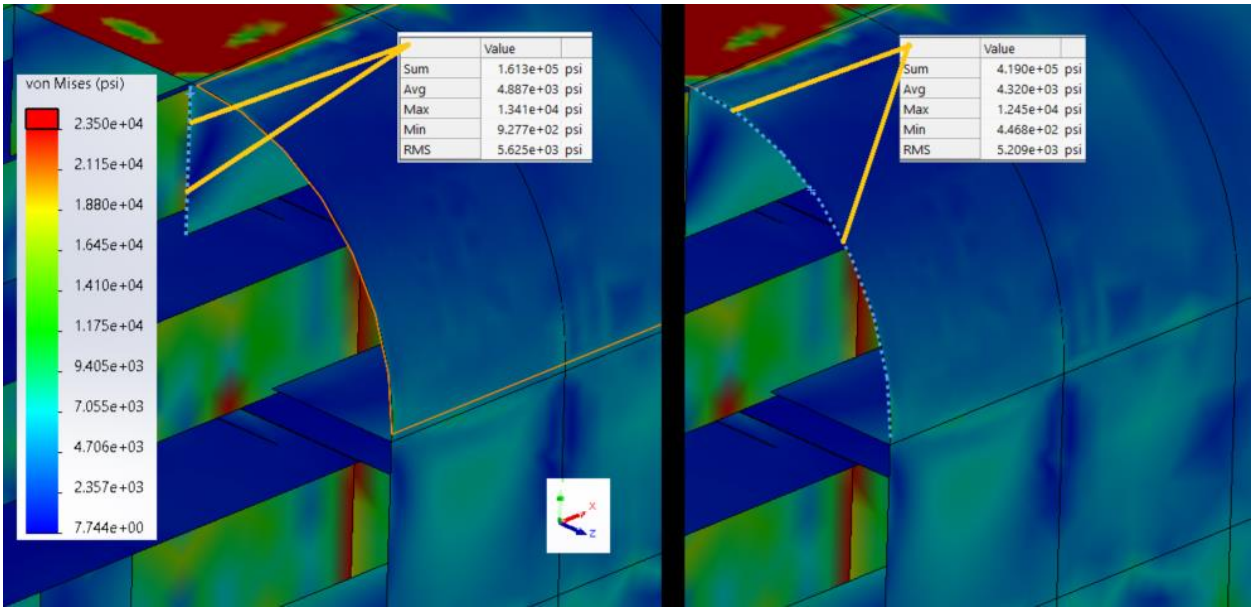

Figure 79: 24[in] Cross-ribs w/ Same Loading & Same Fine Mesh with Density of 1.18[kg/m3], Max-stress

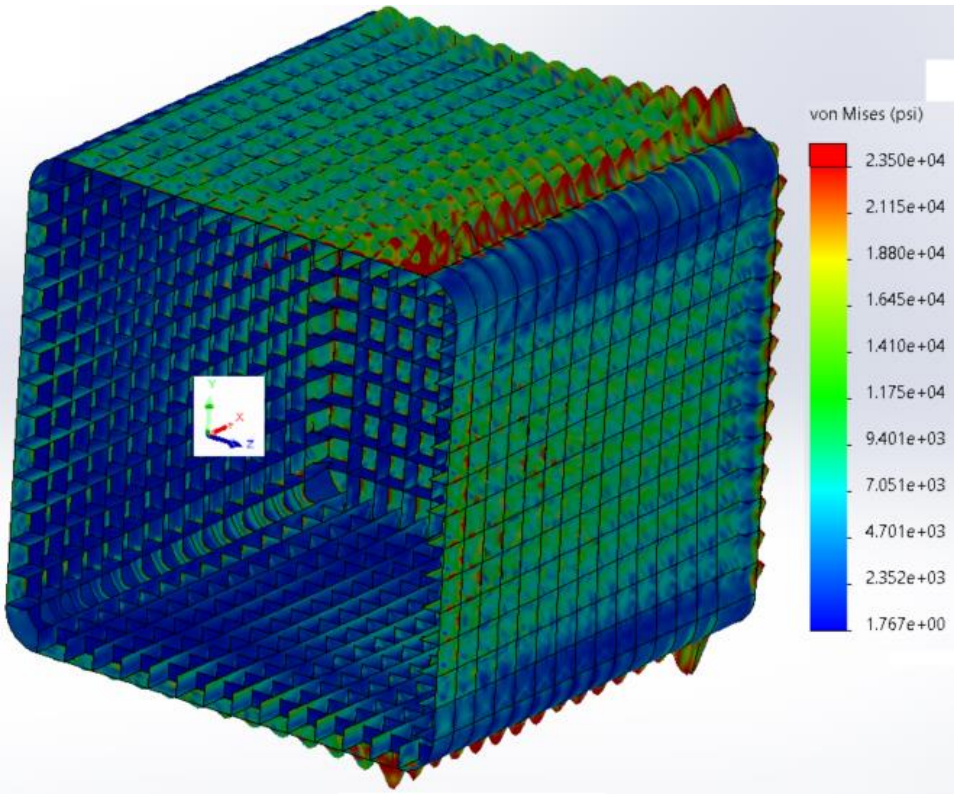

Figure 80: 24[in] Cross-ribs w/ Same Loading & Same Fine Mesh with Density of 1.226[kg/m3], w/ Inside View

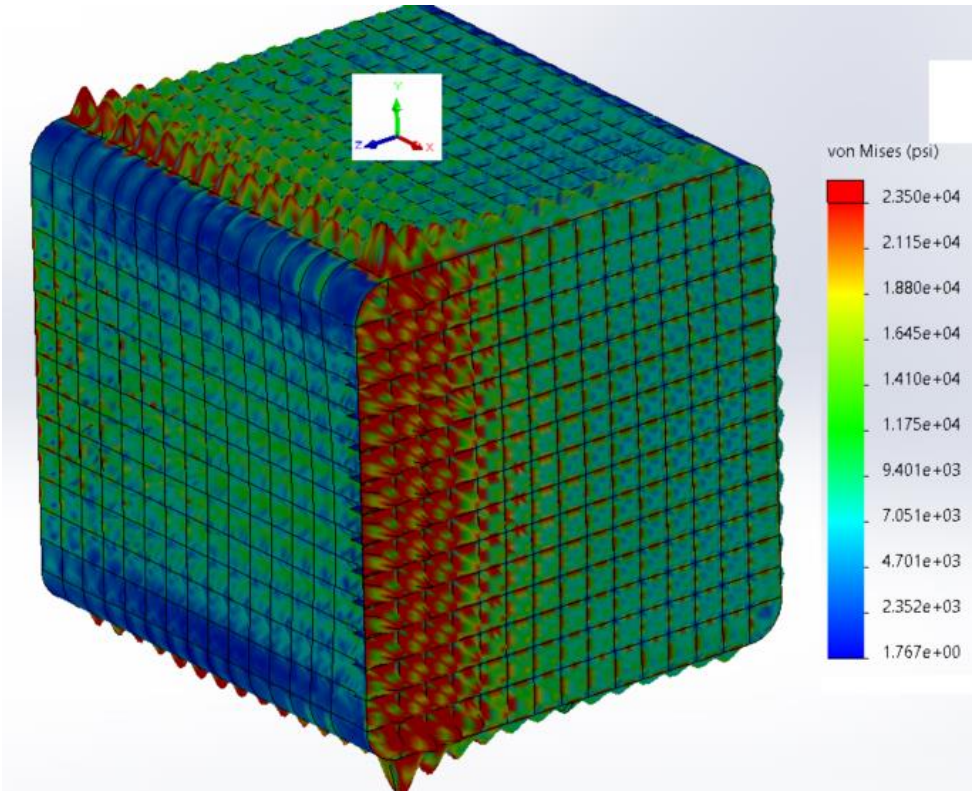

Figure 81: 24[in] Cross-ribs w/ Same Loading & Same Fine Mesh with Density of 1.226[kg/m3], w/ End View

With a 24[in] cross-rib (with a density of 1.18[kg/m3]), the maximum stress is found on the 32[in] longitudinal rib: The radius has a stress of 12,450[psi] while the 32[in] rib has a stress of 13,410[psi]. Adding 10[%] for errors, the maximum stress here is 14,800[psi], resulting in a factor of safety of 2.6[-].

Changing a cross-rib from 32[in] to 24[in], changes the factor of safety from 3.0[-] to 2.6[-]; where the air density is 1.18[kg/m3]. The 24[in] rib brought the weight down by 3,730[Lbf].

Table 19: Endcap Stiffness w/ 24[in] Cross-ribs w/ Density of 1.18[kg/m3]

Stiffness	Deflection [in]	k [Lbf/in]	k [N/m]
$< k_x >$	0.250	667,199	116,844,417
$< k_y >$	0.110	421,315	73,783,432
$< k_z >$	0.155	547,256	95,839,185

Comparing the stiffness of the 32[in] cross-rib assembly with the 24[in] cross-rib assembly, k_x decreased by about 2.31[%], k_y decreased by about 3.88[%] and k_z decreased by 10.3[%].

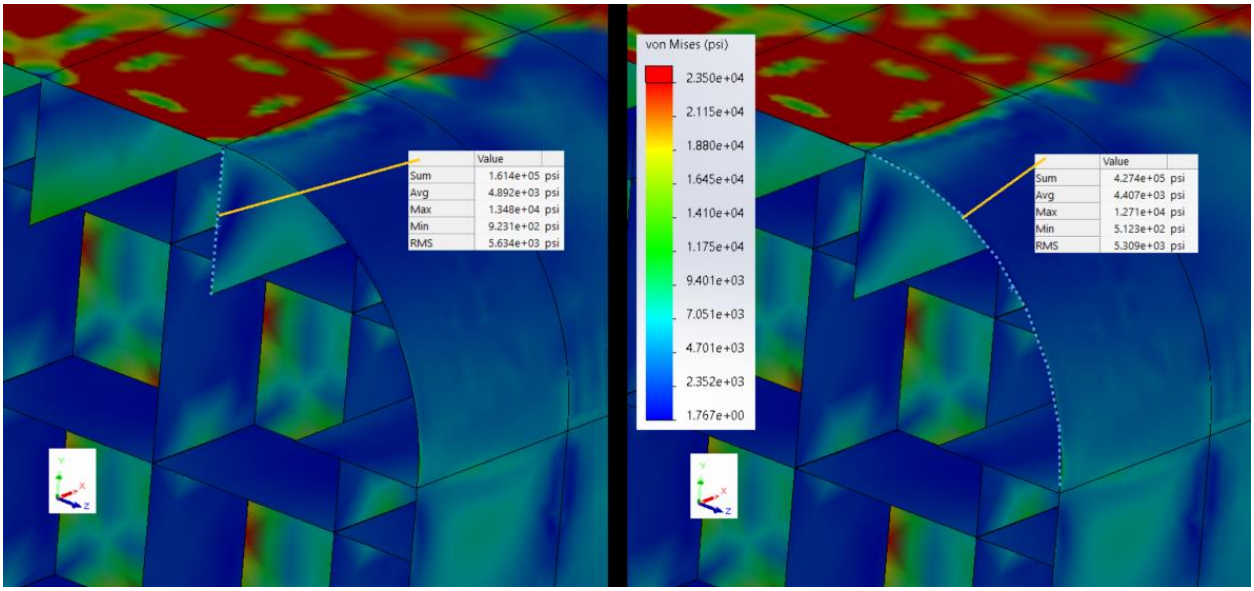

Figure 82: 24[in] Cross-ribs w/ Same Loading & Same Fine Mesh with Density of 1.226[kg/m3], Max-stress

The stress is slightly higher when the density of the air is 1.226[kg/m3]. The 32[in] rib increases less than 100[psi] to 13,480[psi]; and the radii 12,710[psi], an increase of about 260[psi]. The factor of safety remains at 2.6[-] with an air density of 1.18[kg/m3] or 1.226[kg/m3] with the 24[in] cross-rib.

Table 20: Endcap Stiffness w/ 24[in] Cross-ribs w/ Density of 1.226[kg/m3]

Stiffness	Deflection [in]	k [Lbf/in]	k [N/m]
$< k_x >$	0.337	443,145	77,606,588
$< k_y >$	0.115	436,441	76,432,464
$< k_z >$	0.165	552,681	96,789,169

Utilizing linear interpolation, a 27.5[in] cross-rib would decrease k_z stiffness by less than 6[%] and reduce the segment weight by more than 2,000[Lbf]. Proceeding to the next segment to be analyzed, the $(5/6)^{th}$ segment, the primary cross-rib will be 24[in].

For the following mid-segments, the wind speed is 60.603[m/s], the temperature is 12[C], 53.6[F] with a skin a roughness of 3[mm] (3000μm) and an air density of 1.226[kg/m3].

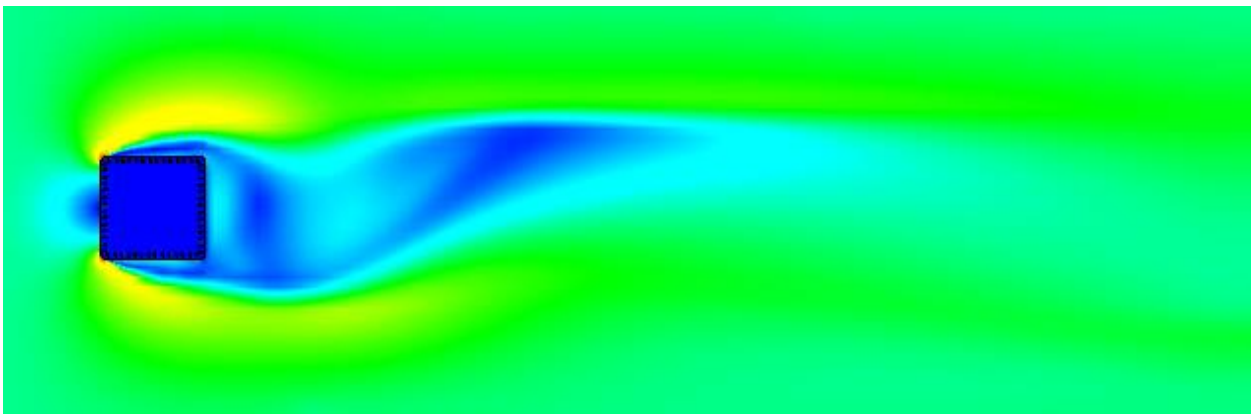

Figure 83: Arm Mid-segment CFD

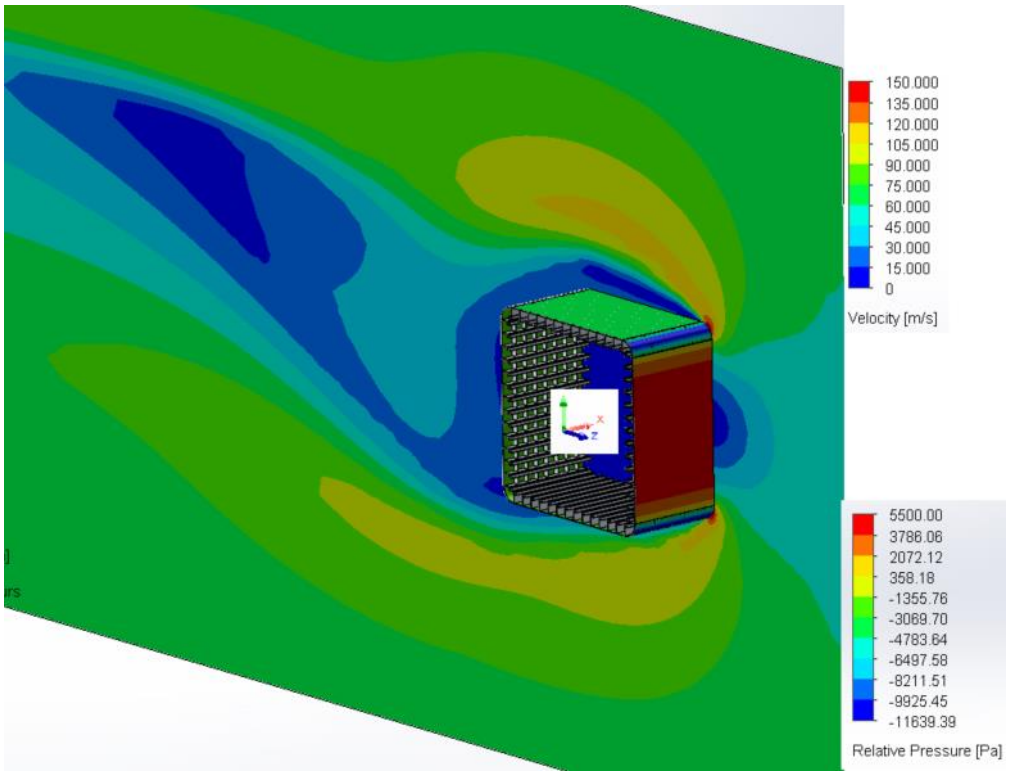

Figure 84: Arm Mid-segment, Velocity & Pressure Maps

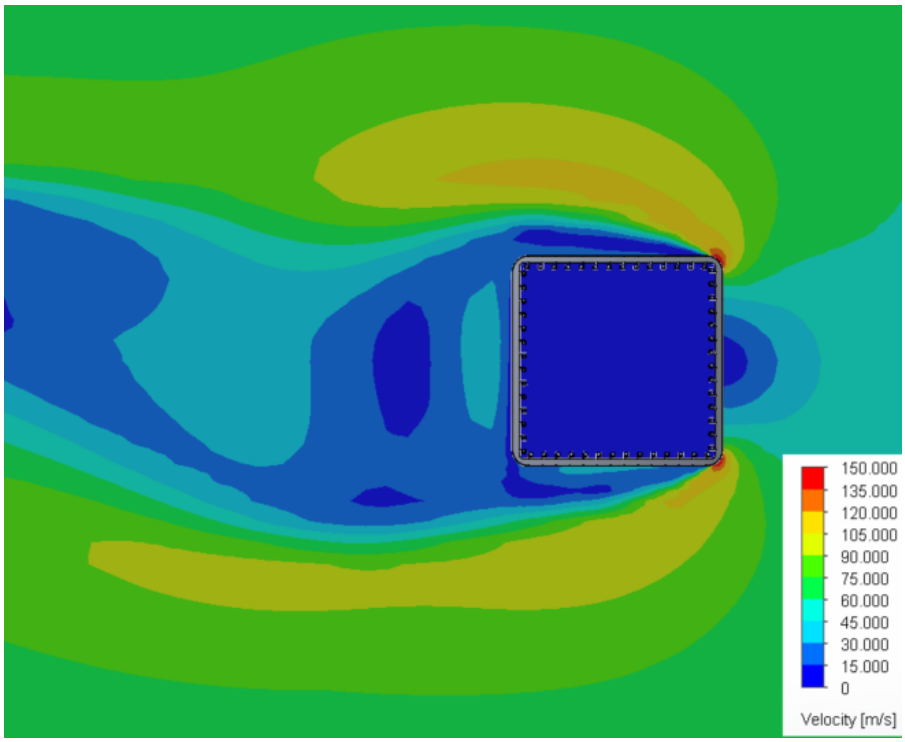

Figure 85: Arm Mid-segment, Velocity Map

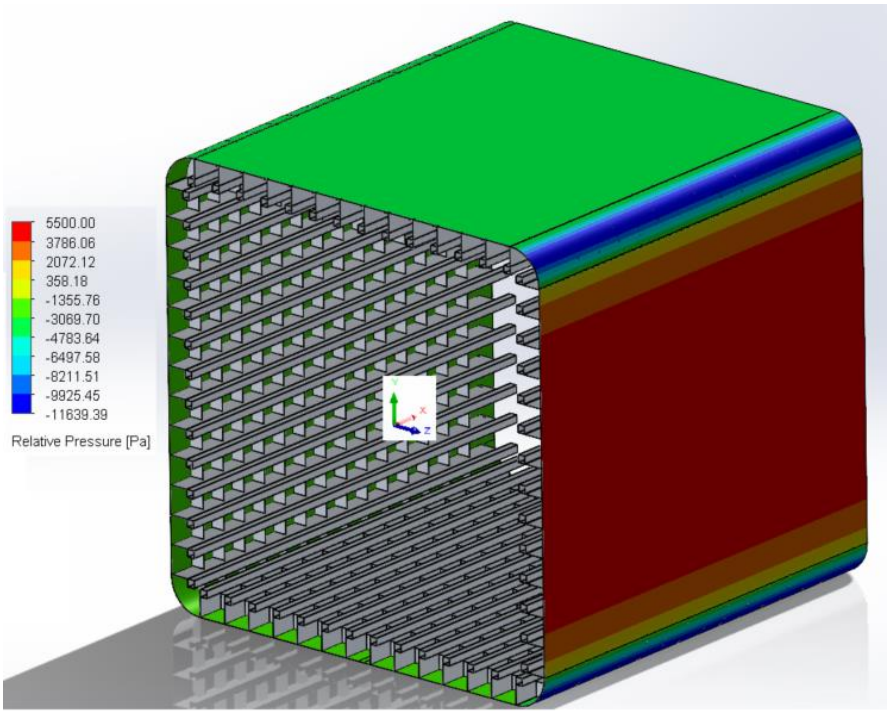

Figure 86: Arm Mid-segment, Pressure Map

Figure 84, Figure 85 and Figure 86 show that there is a vacuum on the radii and a relatively high pressure area in the middle of the front face; the other areas have low pressures. The velocities exceed 150[m/s] as the wind goes around the front-face radii. All this is similar to what is seen in Figure 12 thru Figure 19. This model will be applied to the FEA; similar to what was done in the Endcap analysis.

C. Structure, CFD Transient Analysis:

Prior to continuing with the structural study (FEA), a transient study to investigate harmonics was performed. A transient study is required to calculate the vortex shedding period; should any be present.

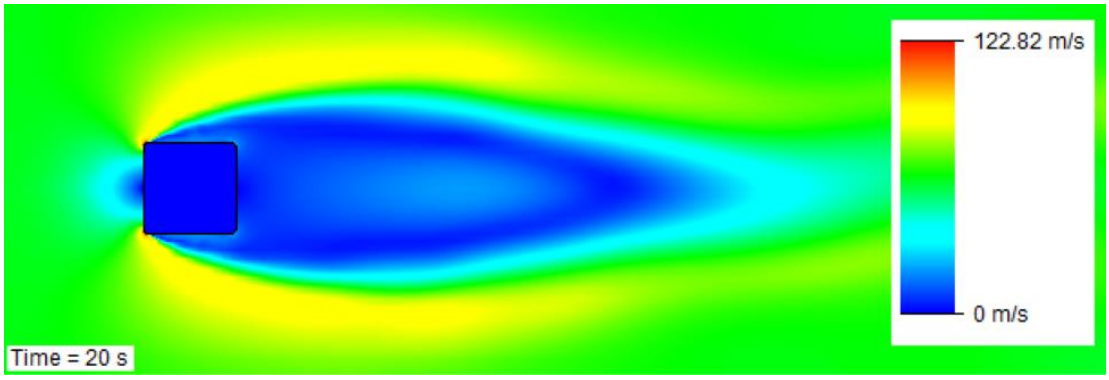

Figure 87: Arm/Body Transient Velocity Flow @ 20[s] w/ dt = 0.0075[s]

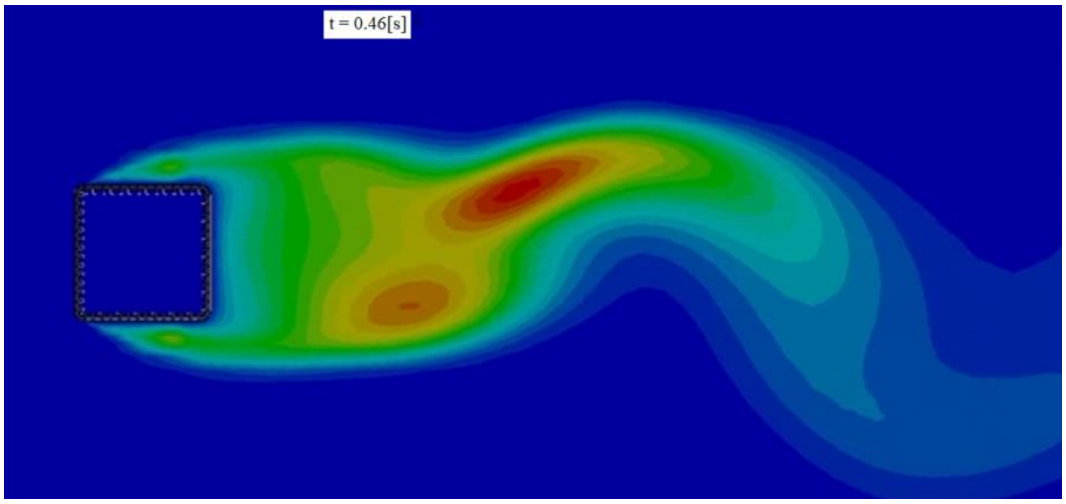

Figure 88: Transient Turbulent Flow on Arm at t = 0.46[s]

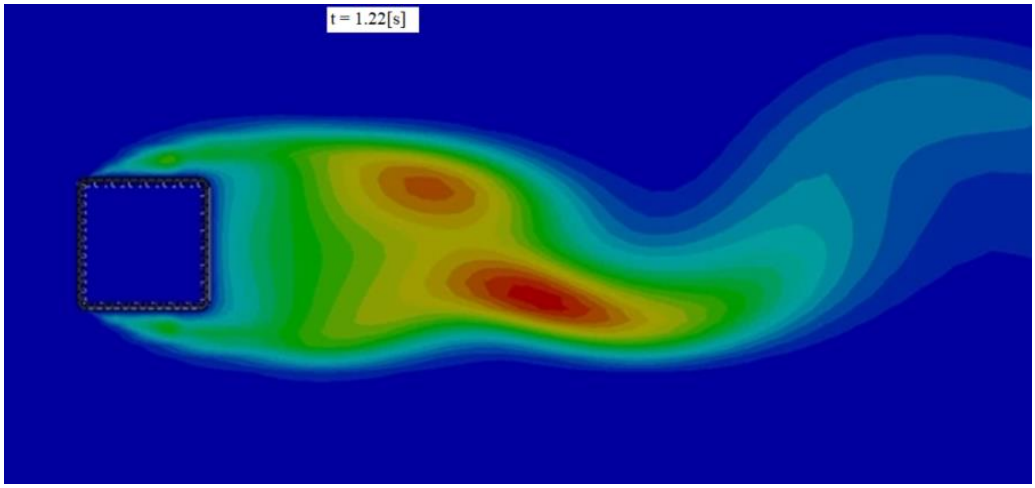

Figure 89: Transient Turbulent Flow on Arm at t = 1.22[s]

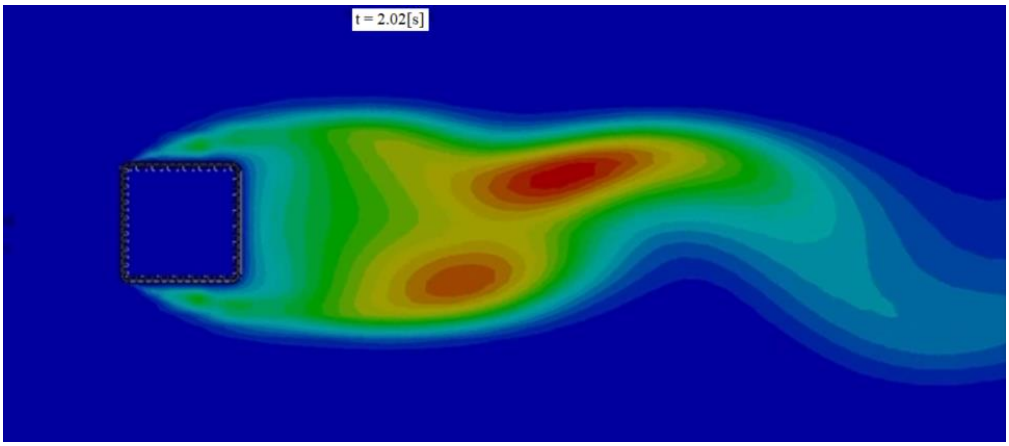

Figure 90: Transient Turbulent Flow on Arm at t = 2.02[s]

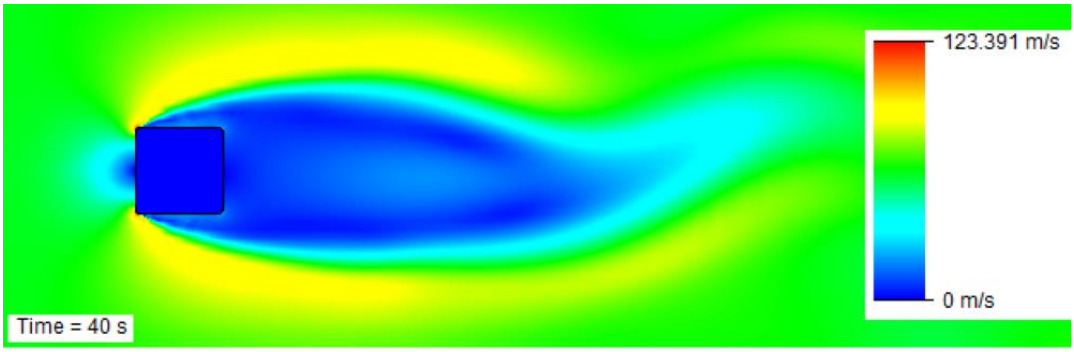

Figure 91: Arm/Body Transient Velocity Flow @ 40[s] w/ dt = 0.01[s]

Vortex Formation dt 0.1[s].avi

Vortex Formation dt 0.075[s].avi

Vortex Formation dt 0.01[s].avi

Velocity dt 0.075[s].avi

Velocity dt 0.01[s].avi

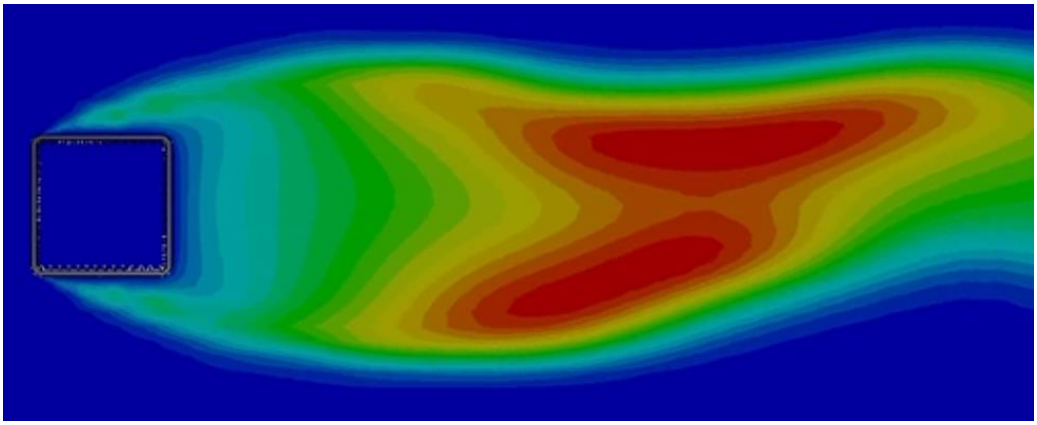

Figure 92: Arm/Body Transient Turbulent Flow @ 21.62[s] w/ dt = 0.01[s]

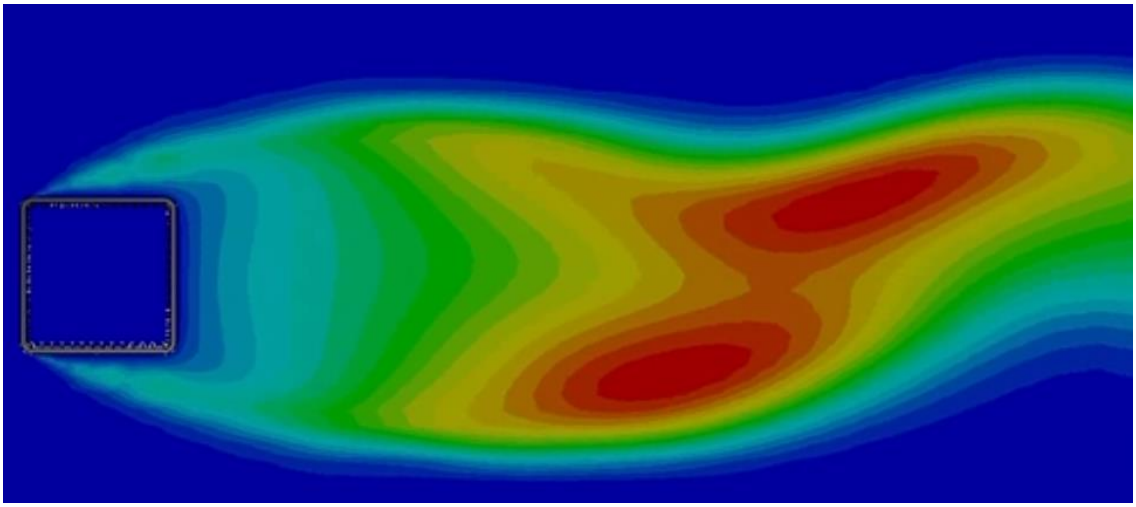

Figure 93: Arm/Body Transient Turbulent Flow @ 39.70[s] w/ dt = 0.01[s]

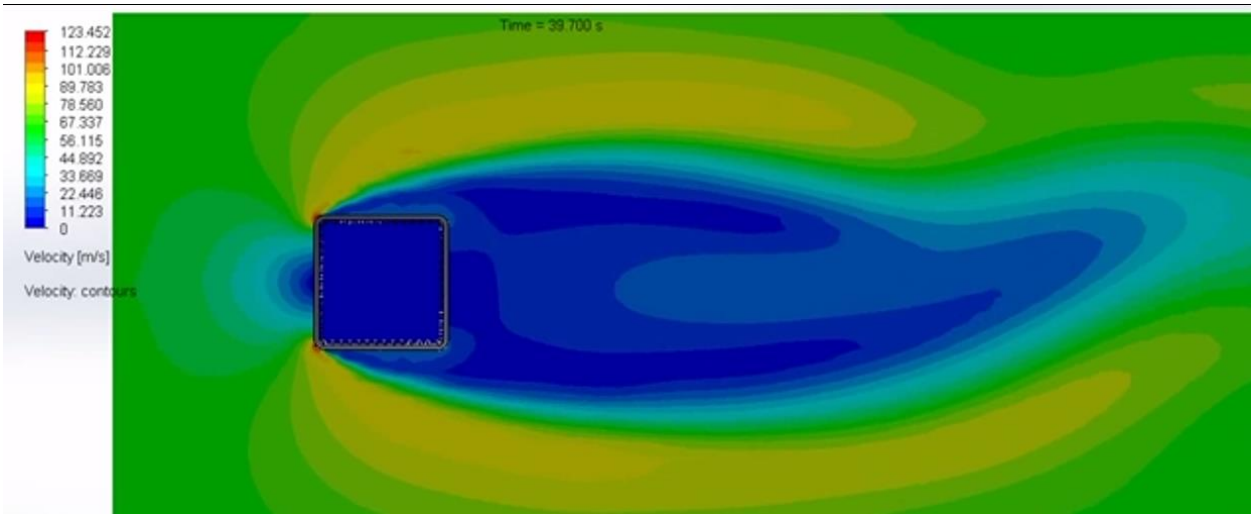

Figure 94: Arm/Body Transient Velocity Flow @ 39.70[s] w/ dt = 0.01[s]

A transient study of a mid-arm segment shows that vortices are produced with a natural period (T_n) of (on average) 2.13[s] (see above videos "Vortex Formation"). There is no vortex shedding. Vortices formed on the top and bottom of the arm move into the flow field every ~1.06[s] and merge between 3-diameters and 5-diameters behind the structure. The stationary vorticity (conglomeration) inhibits boundary layer separation, thus, there is no vortex shedding or significant oscillatory loads are applied to the structure. It is worthwhile to note that these transient studies were performed with a fine mesh on the skin of the structure.

D. Structure, Fine-mesh, 24[in] Cross-ribbing:

Continuing with the structural study Figure 95 and Figure 96 show the fixture and loading for the inner segments of the arm. Note that the 24[in] cross-rib is present.

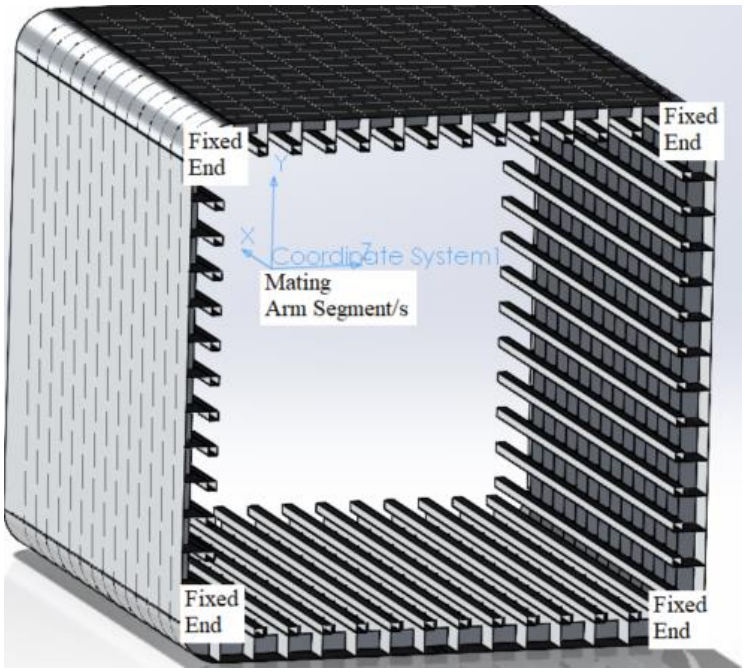

Figure 95: Arm Segment Fixtures/Load-points

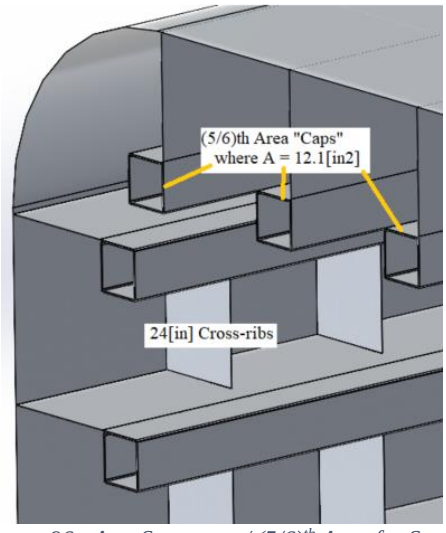

Figure 96: Arm Segment w/ (5/6)th Area for Stress

Table 21: Forces at Mating Arm for Endcap

	Reaction Force [lbf]
Sum X:	-107,946
Sum Y:	50,278
Sum Z:	90,916

Note: The vacuum load is less as a factor of safety (72.28[%]).

Table 22: Moments at Mating Arm for Endcap

	Reaction Moment [lbf-in]
Sum X:	147
Sum Y:	15,216
Sum Z:	472

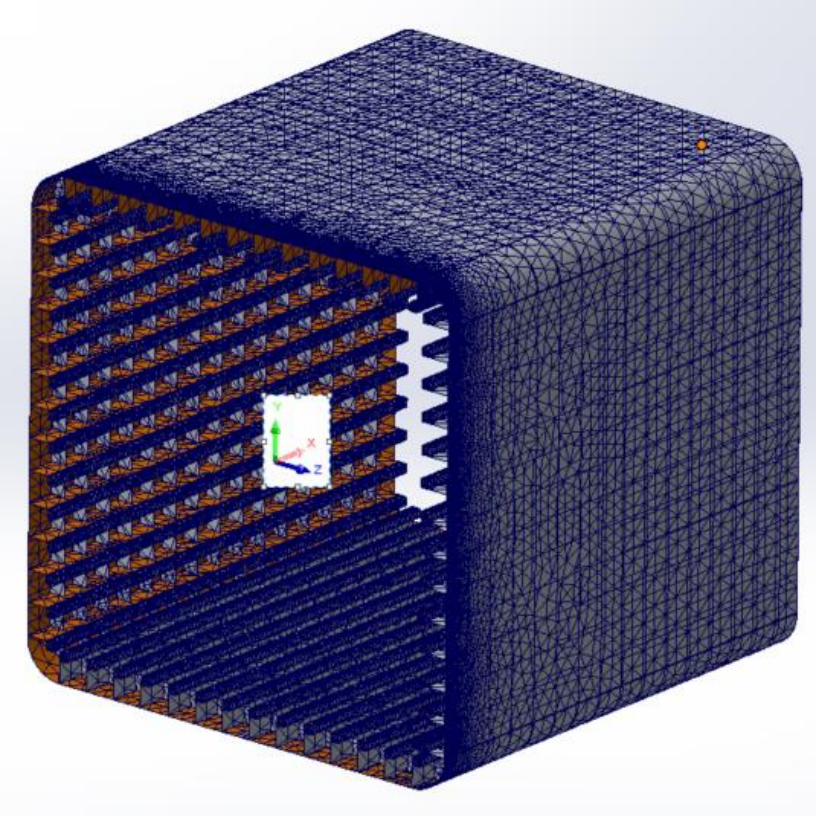

Figure 97: FEA Mesh for (5/6)th Segment

The maximum mesh size for the (5/6)th segment is 24[in], the smallest is 8[in]. The fine mesh has a size of 1.5[in] with a growth rate of 1[%].

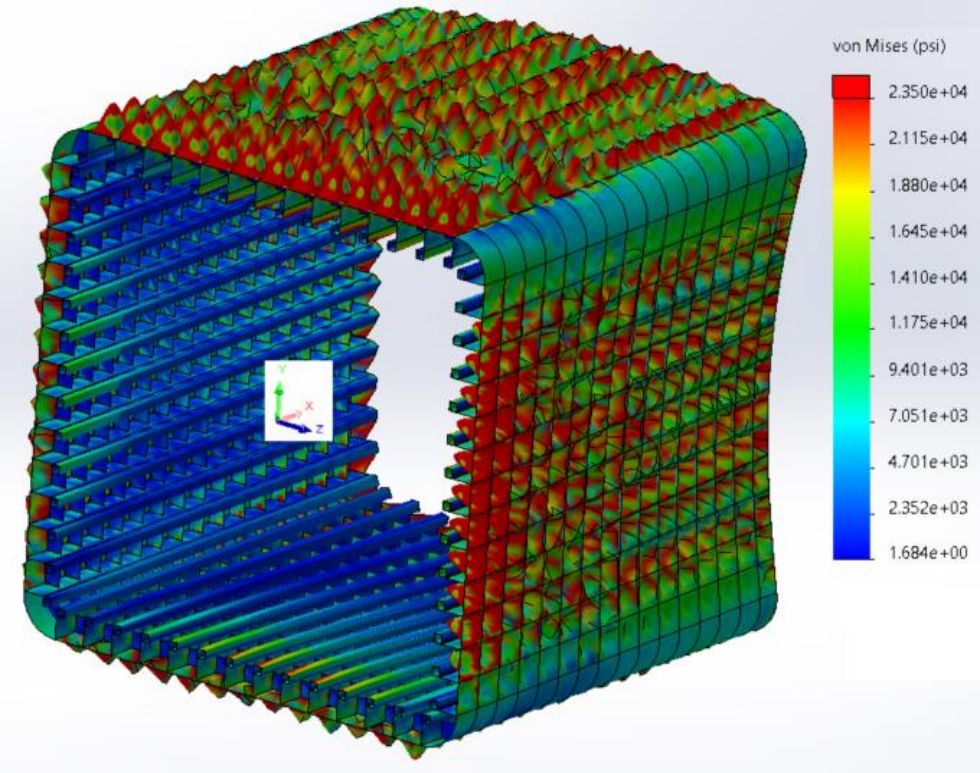

Figure 98: (5/6)th Arm Segment, Stress

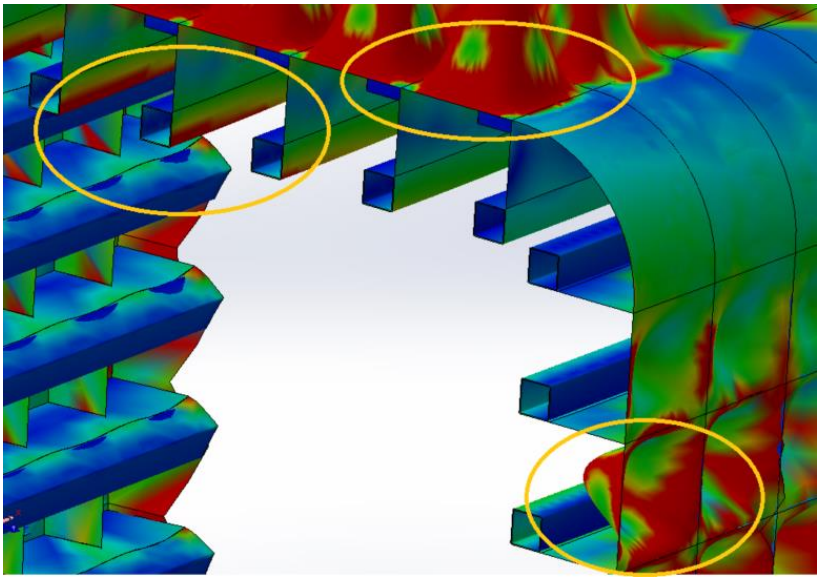

Figure 99: (5/6)th Segment, High Stress w/ Large Elements

The high stress regions noted in Figure 99 either have large/oversized elements or are directly adjacent to panels with high stress and oversized elements. As in the previous analysis, the high stress members are the radius and its adjacent-vertical rib.

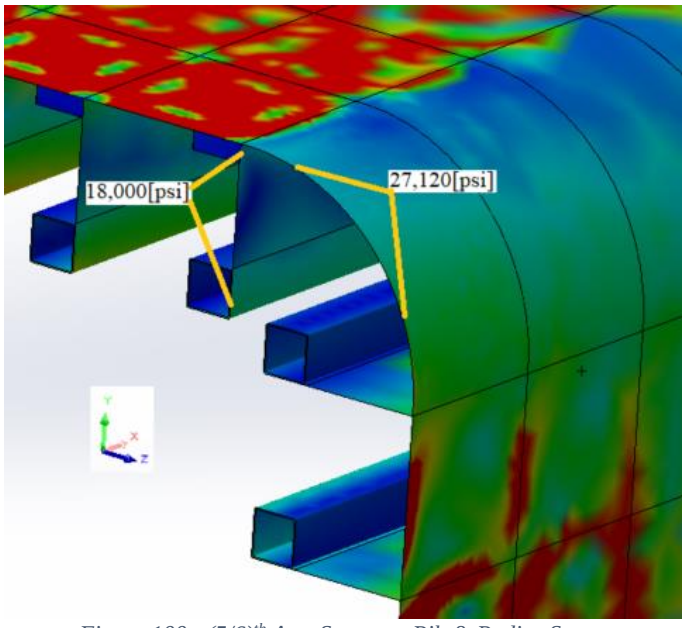

Figure 100: (5/6)th Arm Segment, Rib & Radius Stress

The maximum stress on the rib is 18,000[psi] and the maximum stress on the radius is 27,120[psi]; adding 10[%] to the maximum stress results in 29,832[psi]. Thus, the factor of safety is 1.3[-].

Table 23: Mating Forces for (5/6)th Element onto (4/6)th Segment

Force	Reaction Force [lbf]	Force Applied at Mating Coordinate System [lbf]
Component		
Sum X:	-107,770	107,770
Sum Y:	21,691	-21,691
Sum Z:	458,730	-458,730

Table 24: Mating Moments for (5/6)th Element onto (4/6)th Segment

Moment	Reaction Force [lbf-in]	Force Applied at Mating Coordinate System [lbf-in]
Component		
Sum X:	379	-379
Sum Y:	8,324	-8,324
Sum Z:	-21,336	21,336

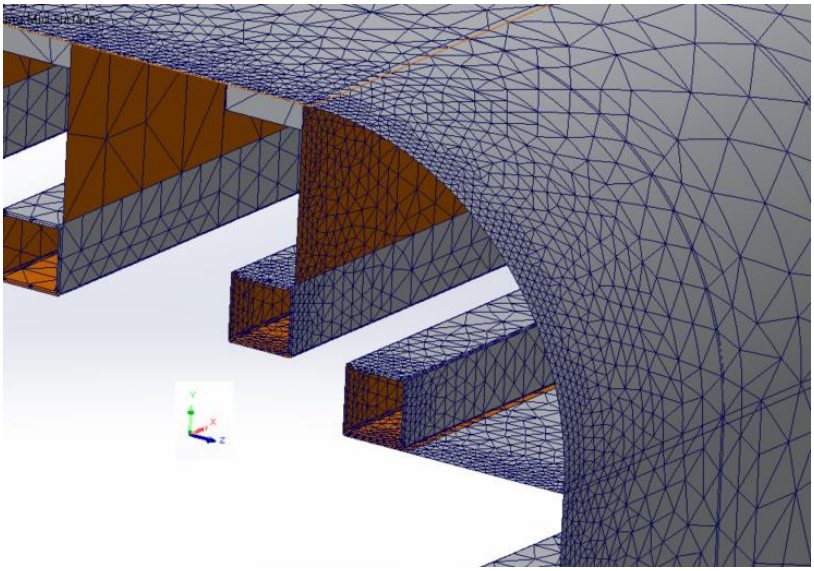

Figure 101: (4/6)th Segment, Fine Mesh

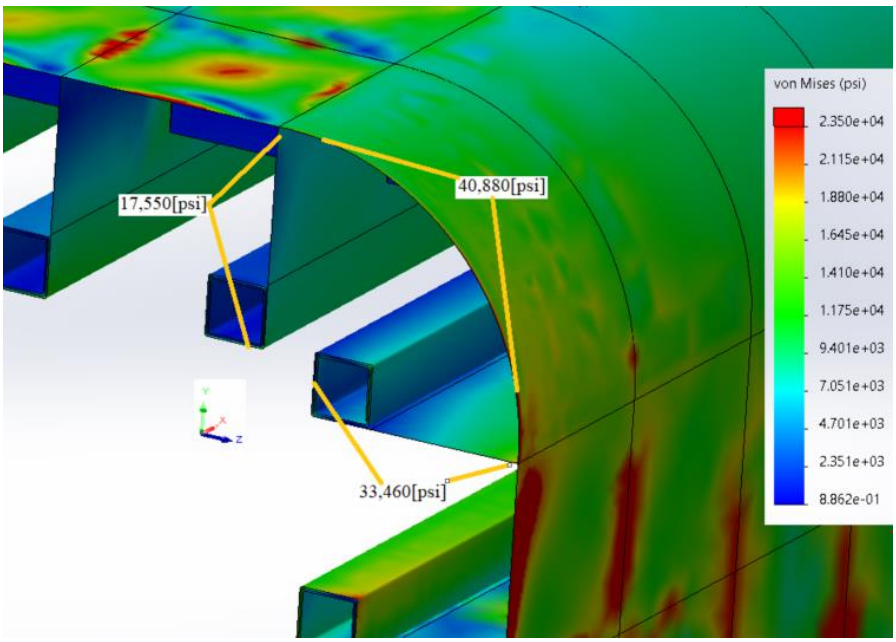

Figure 102: (4/6)th Segment, Critical Stress

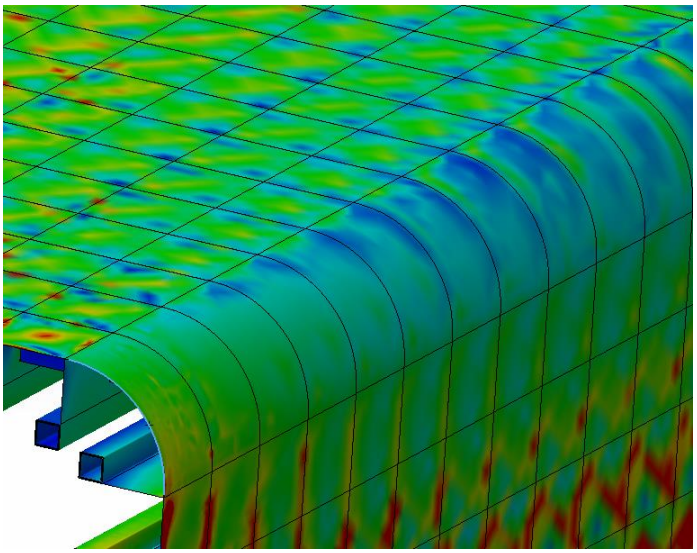

Figure 103: (4/6)th Segment, Low Stress on Cross-rib on Radius

The radial stress on the edge of the part exceeds the elastic stress for the material (AL-T6061-T6). The reported stress of 40,880[psi] can be altered by thickening the segment thru the use of the cross-ribs. In similar locations within Figure 103, the stresses are very low; none the less, the over stress location is noted. The horizontal rib has a stress of 33,460[psi] which has a factor of safety of 14[%]; or 4[%] by adding a calculation safety.

Table 25: Mating Forces for (4/6)th Element onto (3/6)th Segment

Force	Reaction Force [lbf]	Force Applied at Mating Coordinate System [lbf]
Component		
Sum X:	-107,990	107,990
Sum Y:	130,920	-130,920
Sum Z:	680,700	-680,700

Table 26: Mating Moments for (4/6)th Element onto (3/6)th Segment

Moment	Reaction Force [lbf-in]	Force Applied at Mating Coordinate System [lbf-in]
Component		
Sum X:	1,955	-1,955
Sum Y:	-14,556	14,556
Sum Z:	-22,268	22,268

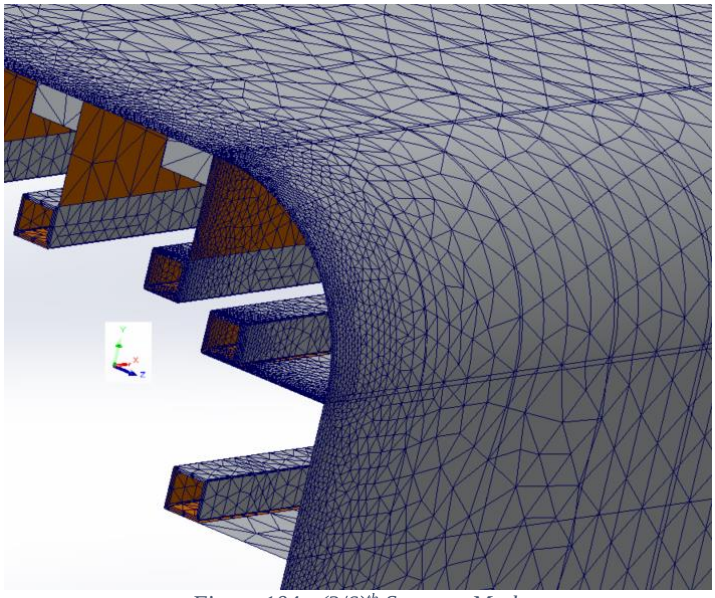

Figure 104: (3/6)th Segment Mesh

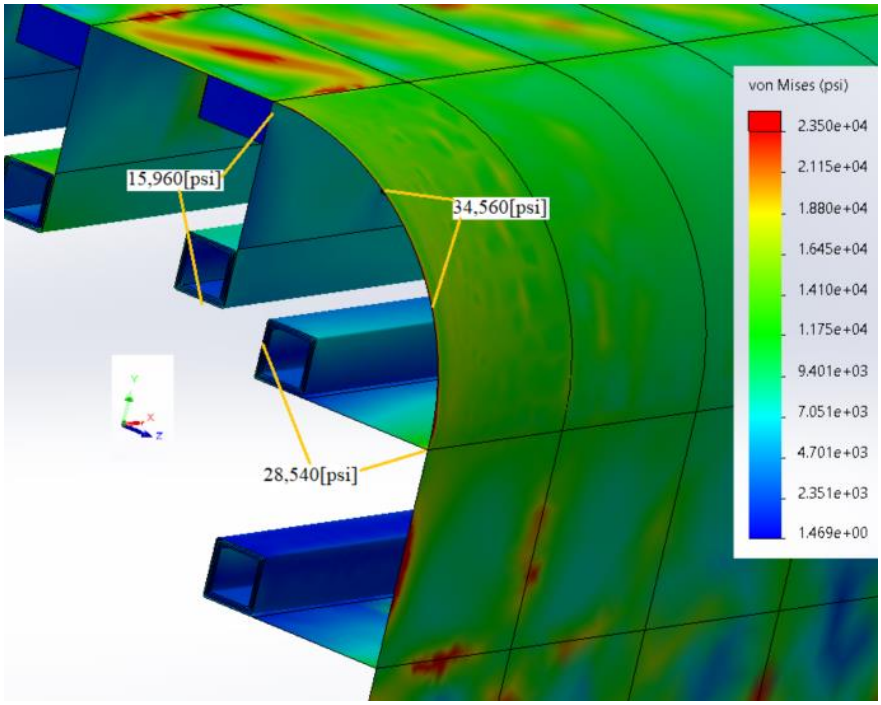

Figure 105: (3/6)th Segment, Critical Stresses

Basic mesh:

- Maximum size = 15.4[in]
- Minimum size = 5.13[in]
- Growth rate 20[%]

Fine mesh - 1: Model Edges

- Maximum size = 1.5[in]
- Growth rate 1.0[%]

Fine mesh - 2: Radius, Horizontal critical rib, Vertical critical rib

- Maximum size = 1.0[in]
- Growth rate 1.0[%]

The maximum stress on the rib is 34,560[psi] which represents a 11[%] factor of safety; and a 1[%] factor of safety if 10[%] is put aside for calculation errors. The resultant force on the high stress rib is 42,302[Lbf]]. The smaller mesh has resulted in lower stress values; this means that the mesh is not optimized.

Table 27: Mating Forces for (3/6)th Element onto (2/6)th Segment

Force	Reaction Force [lbf]	Force Applied at Mating Coordinate System [lbf]
Component		
Sum X:	-107,980	107,980
Sum Y:	273,150	-273,150
Sum Z:	865,780	-865,780

Table 28: Mating Moments for (3/6)th Element onto (2/6)th Segment

Moment	Reaction Force [lbf-in]	Force Applied at Mating Coordinate System [lbf-in]
Component		
Sum X:	1,502	-1,502
Sum Y:	-40,776	40,776
Sum Z:	-33,798	33,798

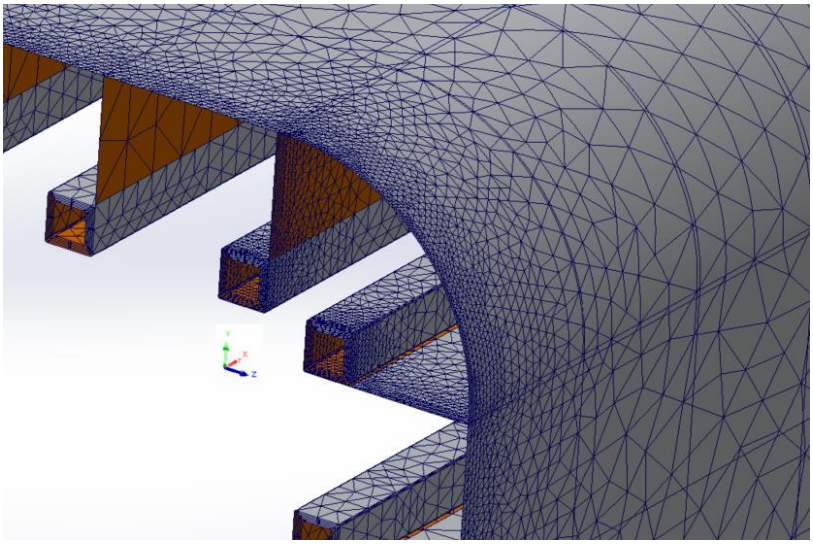

Figure 106: (1/6)th Mesh, same as (2/6)th Mesh

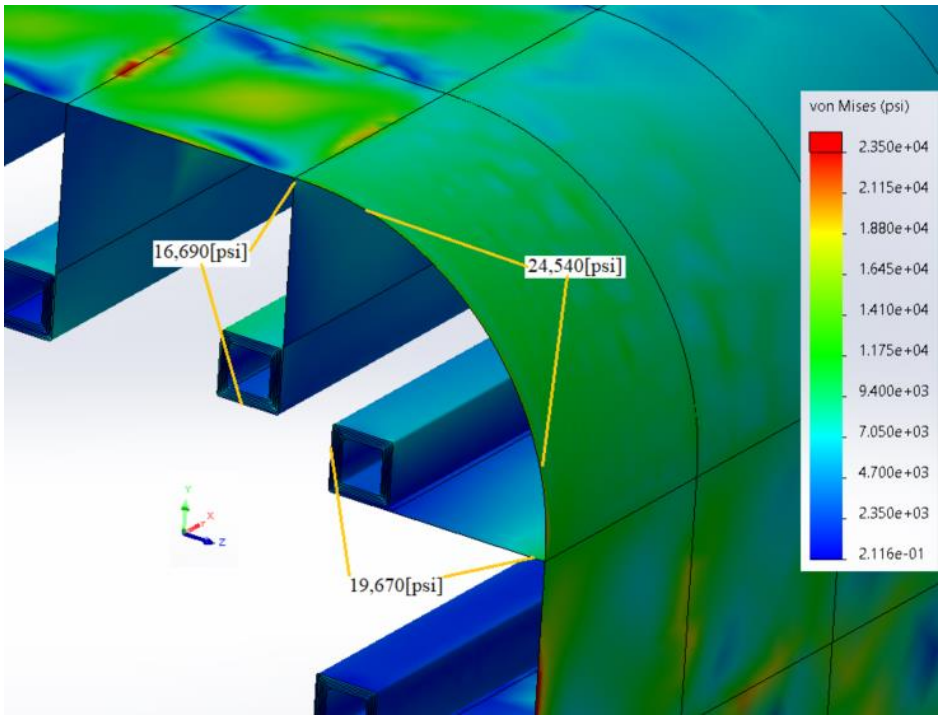

Figure 107: (2/6)th Stress on Critical Components

The maximum stress on the radius is 24,540[psi] which represents a 52[%] factor of safety; and a 42[%] factor of safety if 10[%] is put aside for calculation errors. The resultant force on the high stress rib (of 19,670[psi]) is 36,878[Lbf]].

Table 29: Mating Forces for (2/6)th Element onto (1/6)th Segment

Force	Reaction Force [lbf]	Force Applied at Mating Coordinate System [lbf]
Component		
Sum X:	-107,980	107,980
Sum Y:	454,240	-454,240
Sum Z:	459,020	-459,020

Table 30: Mating Moments for (2/6)th Element onto (1/6)th Segment

Moment	Reaction Force [lbf-in]	Force Applied at Mating Coordinate System [lbf-in]
Component		
Sum X:	702	-702
Sum Y:	-25,797	25,797
Sum Z:	-54,335	54,335

Basic mesh: $(1/6)^{th}$ Segment Main Mesh

- Maximum size = 15.4[in]
- Minimum size = 5.13[in]
- Growth rate 20[%]

Fine mesh - 1: Interior edges on critical ribs (greater than 2)

- Maximum size = 2.1[in]
- Growth rate 20 [%]

Fine mesh - 2: Model Edges and 2^{nd} interior edge on critical ribs

- Maximum size = 1.5[in]
- Growth rate 1.0[%]

Fine mesh - 3: Radius, Horizontal critical rib, Vertical critical rib

- Maximum size = 1.0[in]
- Growth rate 1.0[%]

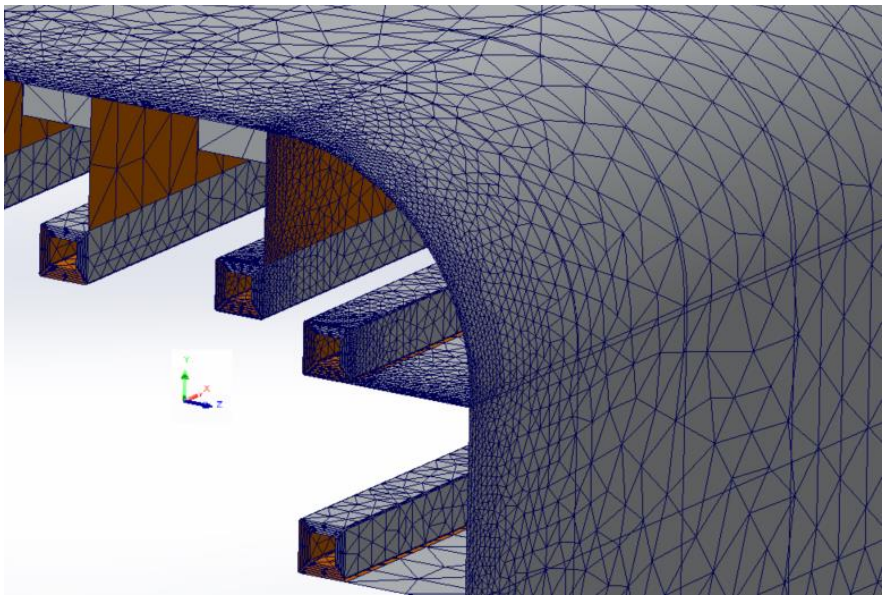

Figure 108: (1/6)th Segment Mesh

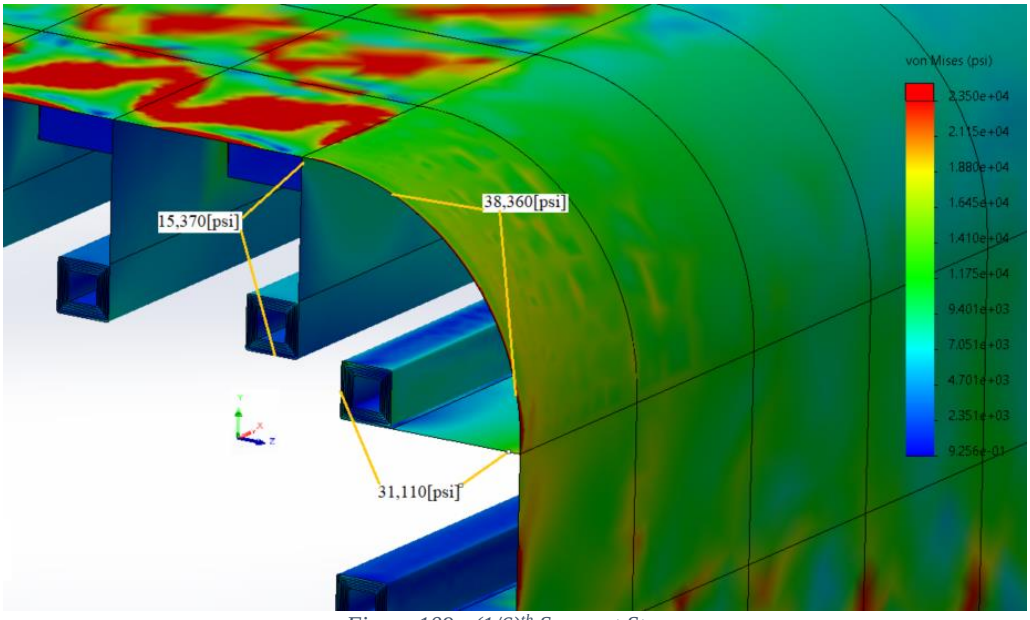

Figure 109: (1/6)th Segment Stress

IV. Structure, Twelve-Segments:

The next portion of the analysis will divide each of the six segments in two; making twelve total segments. The rational for this is two-fold, first, the weight will be dropped by hundreds of tons and lastly a safety factor of (x2) will be applied due to assembly/construction and rain/ice amassing in quantities.

The prior FEA analysis showed that the arm as specified by the hand calculations has a minimum factor of safety of 1.0[-]: Similar calculations were used to specify the rib sizing for the (x2) stronger arm/s.

Table 31: Rib Area per Segment, w/ FS = 2.0[-]

Segment	Area of Rib per Segment [in2]	Area of Rib per Segment [mm2]
1	84.3	2140
2	77.4	1965
3	70.4	1787
4	63.1	1603
5	55.8	1415
6	48.3	1227
7	40.6	1032
8	33	836
9	25.1	638
10	17	432
11	8.8	224
12	4.4	13

Note: The high wind requirement is a 32[in] rib.

The area at the base of the arm went from 44[in2] to 84[in2] for a FS of 2[-].

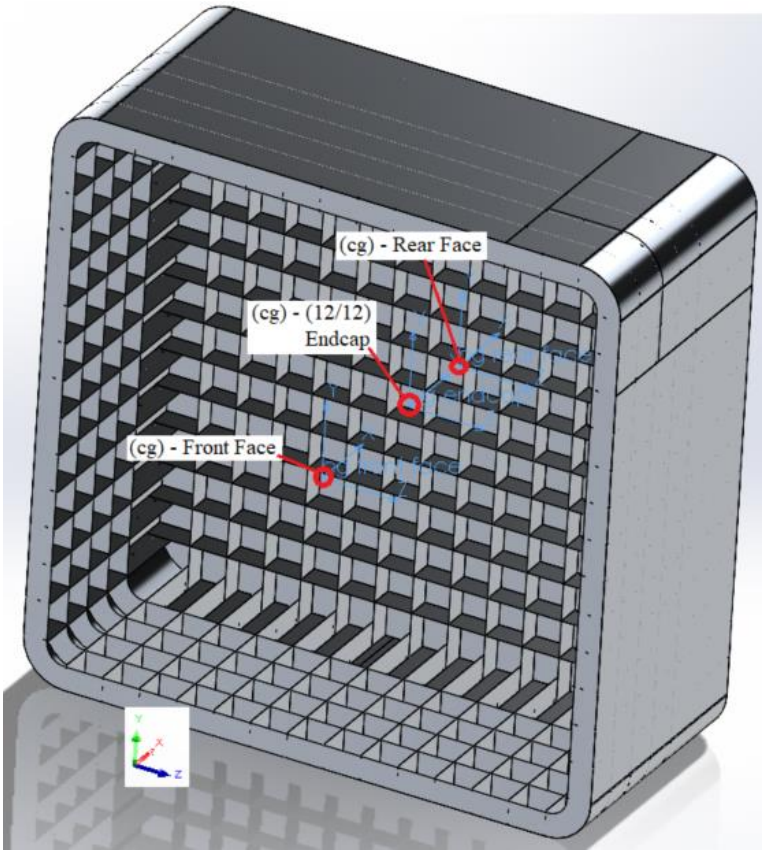

Figure 110: (12/12)th Segment, Endcap

As before, the endcap has no radius to increase the wind loading and model simplification. There are cross-rib members missing, purposely weakening that portion of the structure. The weakened zone is where the endcap radius will occur.

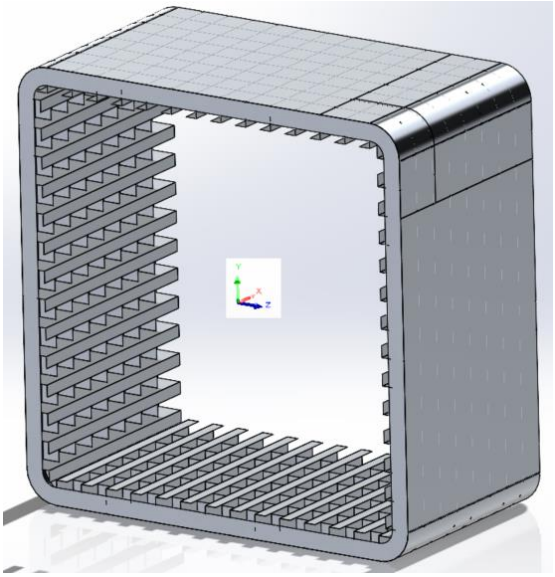

Figure 111: 11th Segment

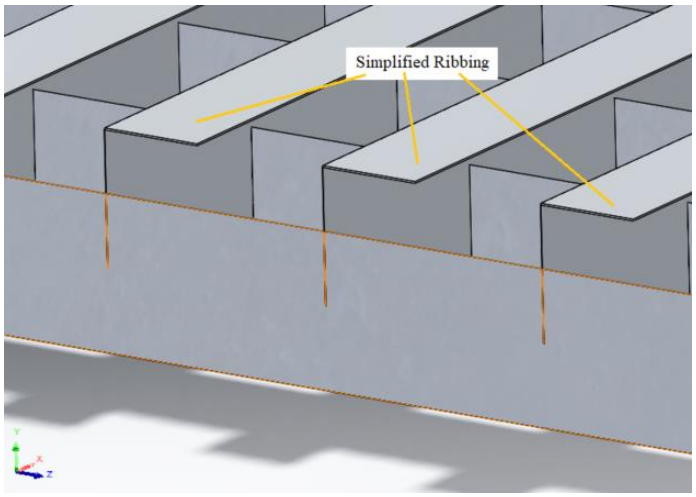

Figure 112: Segment Simplified Ribbing

The simplified ribbing represented in the 11th segment, Figure 112, was made to reduce the mesh size. It's center of gravity and structural area are similar to the original designs represented in the (1/6)th model (where the factor of safety is 1.0[-], as represented in Figure 53). Also, to increase the system strength, all cross-ribs changed from 24[in] to 30[in].

A. Arm, All Twelve-Segments:

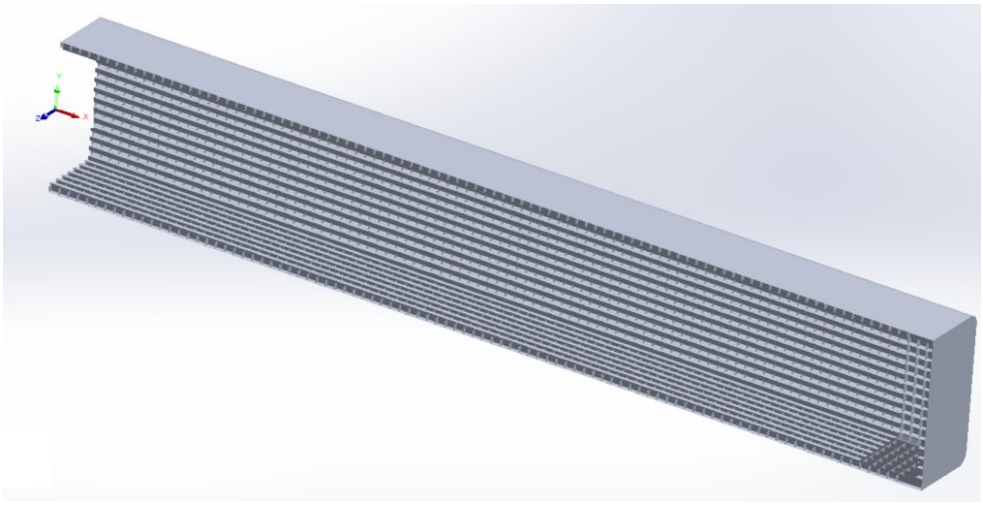

Figure 113: Full Arm, w/o Endcap Radius

The full-arm was brought thru a CFD analysis (as before) where the wind speed was 60.603[m/s], the temperature is 12[C], 53.6[F] with a skin a roughness of 3[mm] (3000μm) and an air density of 1.226[kg/m3]. Note that the flat portion of the arm is 4479[in] or 113.773[m]. This length is 108[in] longer than in Table 2 because the model has no 54.4[in] radius at it base or its endcap.

Table 32: Full Arm Model, Mass & Inertia

	[Lbf]	[N]
Mass (@ 1[g]):	1,357,203	6,037,135
	[in3]	[m3]
Volume:	13,913,800	228.006
Model Center of Mass (cg)	[in]	[mm]
< X >	1,647	41,834
< Y >	0.0	0.0
< Z >	0.0	0.0
Reaction Loading Center	[in]	[mm]
< X >	0	0
< Y >	0	0
< Z >	0	0
Inertia @ Origin	(10^6)-[Lbm-in2]	(10^6)-[kg-m2]
Ixx - Twisting	194,738	57
Iyy - Bend Fore/Aft	5,569,056	1,630
Izz - Bend Up/Down	5,569,056	1,630

The FEA model will add about 2,300[Lbf] for rivets, 14,000[Lbf] for dust/debris, 17,000[Lbf] for water (1" depth) and 40,000[Lbf] for bracketry and other. All of this (plus about 1%) adds about 6.5[%] to the overall weight, therefore the gravity will be 34.25[ft/s2] (411[in/s2]) or 10.44[m/s2].

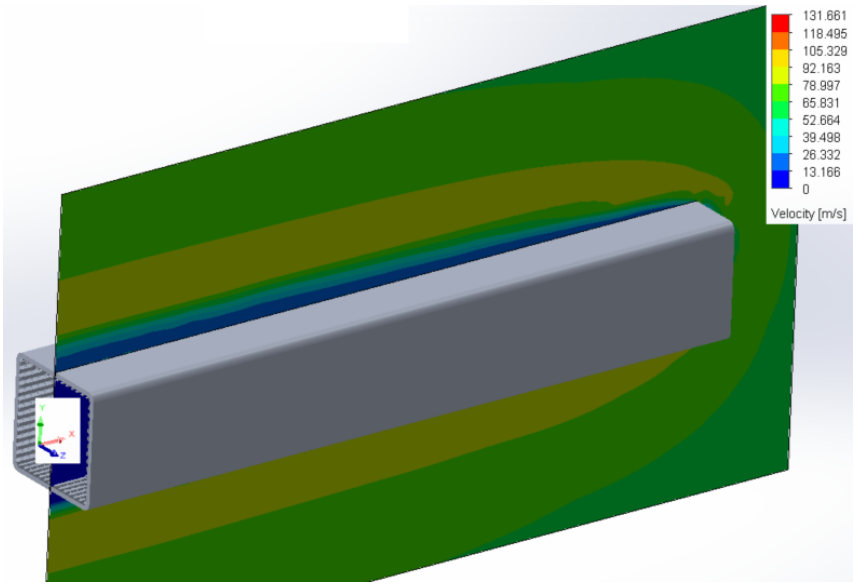

Figure 114: Full Arm Velocity Profile - 1

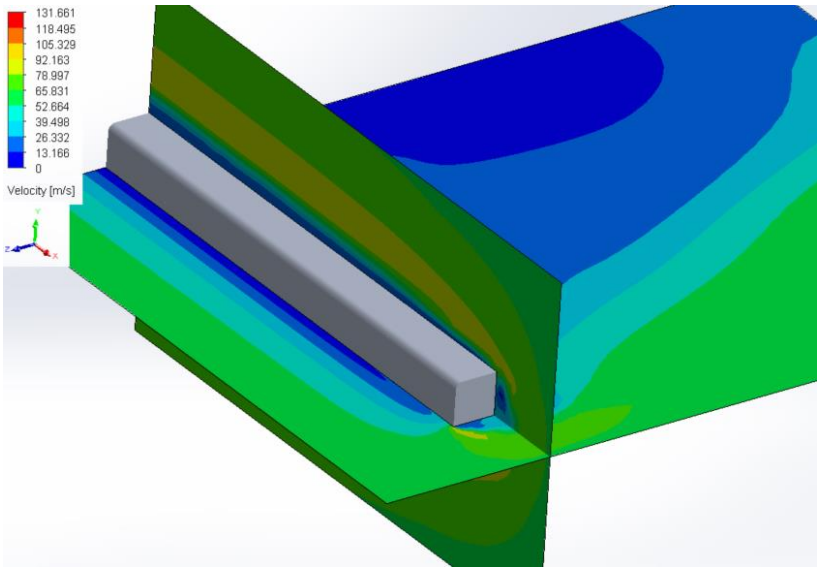

Figure 115: Full Arm Velocity Profile - 2

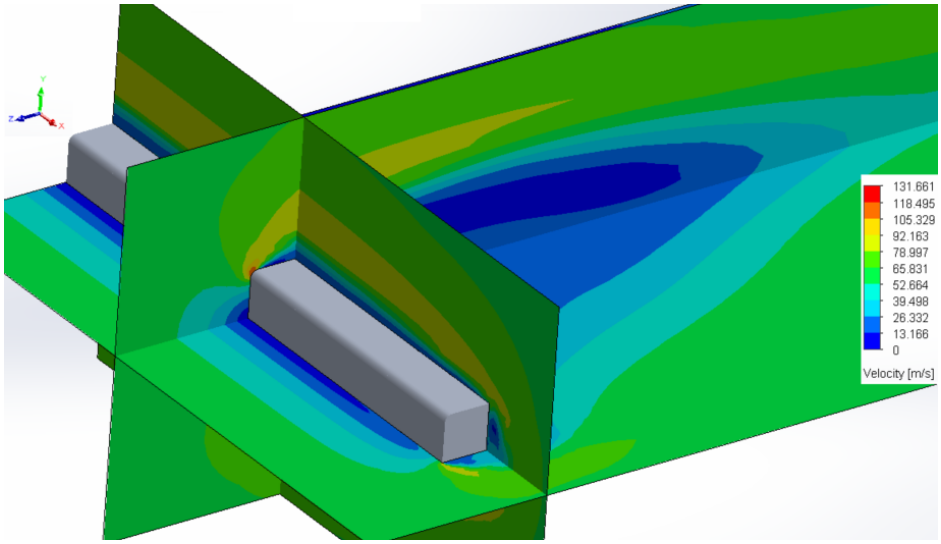

Figure 116: Full Arm Velocity Profile - 3

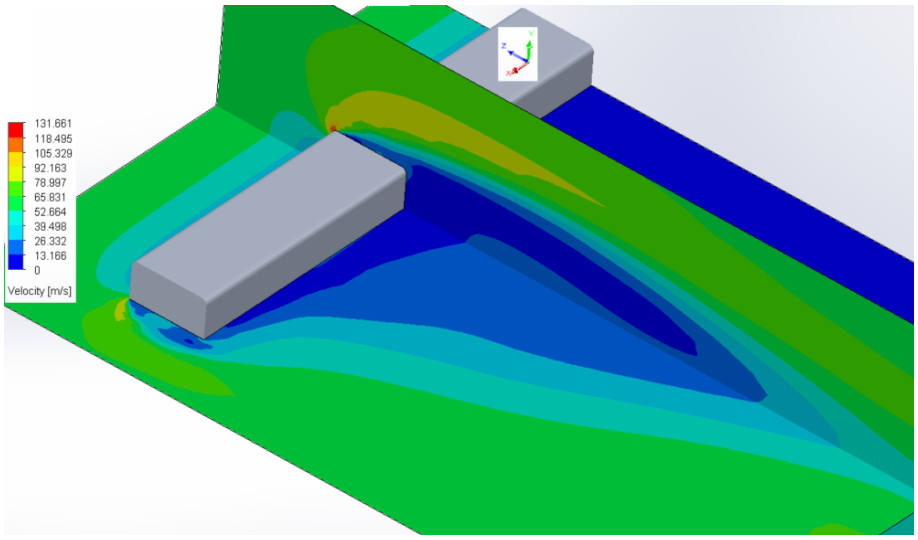

Figure 117: Full Arm Velocity Profile - 4

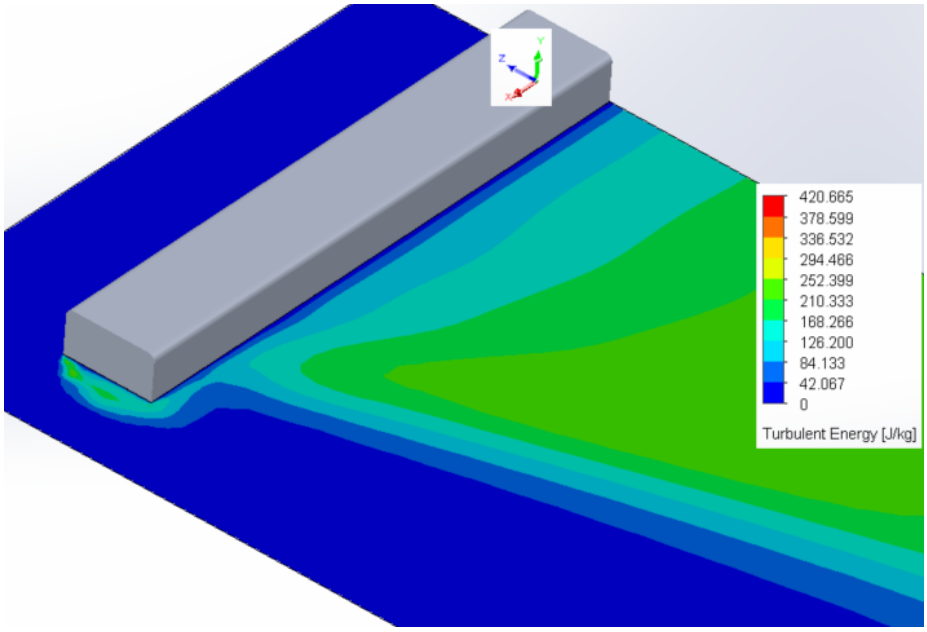

Figure 118: Full Arm, Turbulent Zone/s

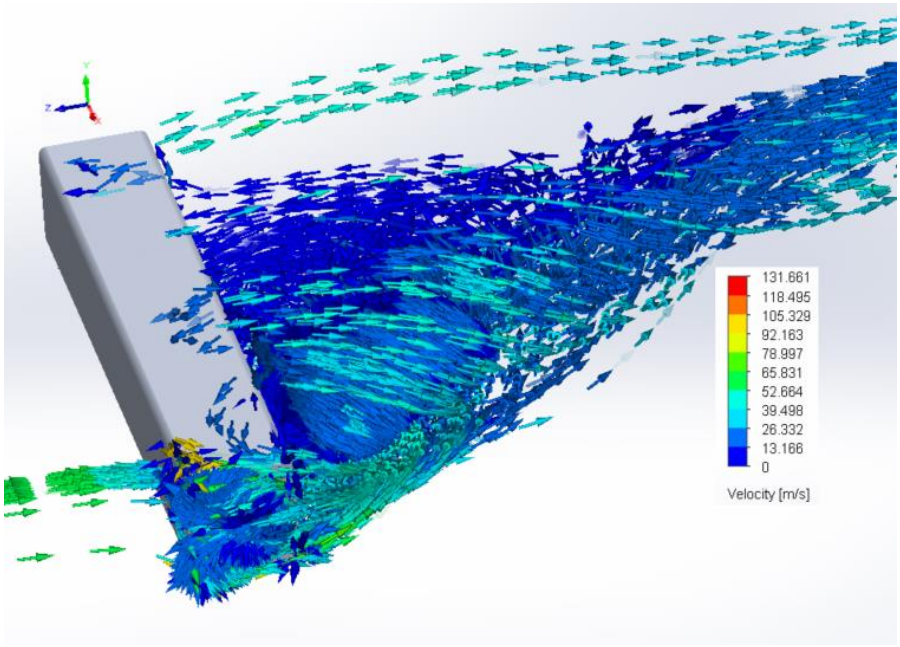

Figure 119: Full Arm, Velocity Streamlines - 1

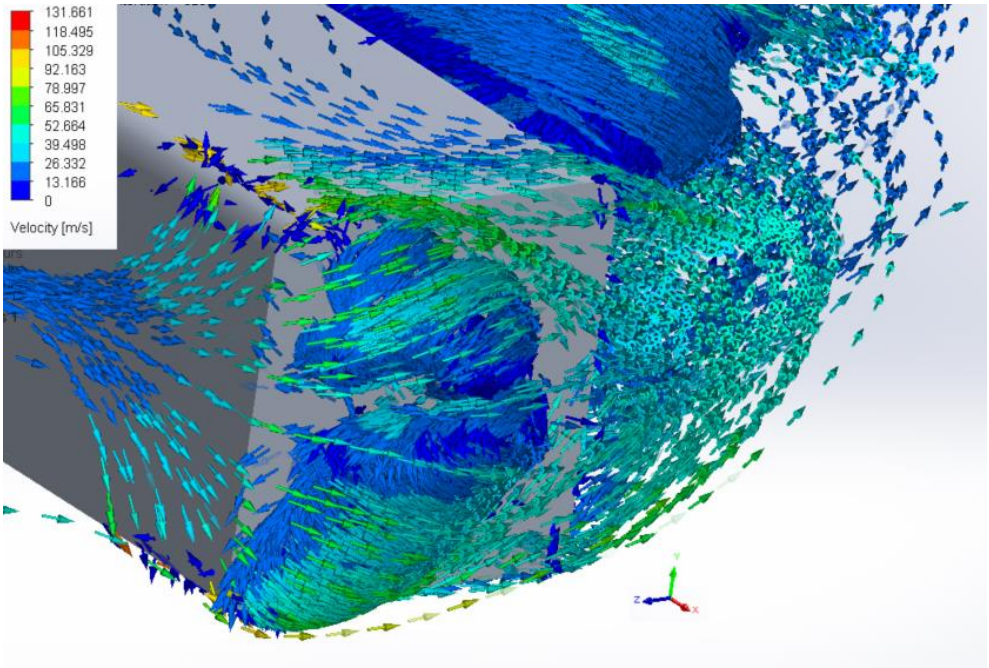

Figure 120: Full Arm, Velocity Streamlines - 2

The full system is too large for available computing power, so it will be broken up into its (x12) segments. The loads from each segment will be brought forward to its mating segment, as in the prior analysis.

This method is valid, recalling Eq - 21:

$$\sigma_{Max}(x) = \frac{M_{Max}(x)}{S} = \frac{M_{Max}(x)}{\frac{I}{c}}$$

The section modulus is body dependent, while the moment is directly related to the center of force and its lever-arm. Since M = F_c x L_{Arm}, the force and the lever-arm define the moment at the mating face. The structures' center of bending plane will have a M = 0: Thus, a symmetric structure will have a M = 0 on its center plane.

B. Segment – 12th, Endcap:

The CFD analysis for the 12th-segment, the endcap, was made with about the same number of fluid cells as the 6th-segment-endcap. Due to the symmetry taken in the analysis, the flow characteristics vary slightly from the full-arm CFD: The skin pressures and shear stresses represent a worse-case scenario, with regards to the front-face forces. Thus, the moment loads due to the wind are maximized.

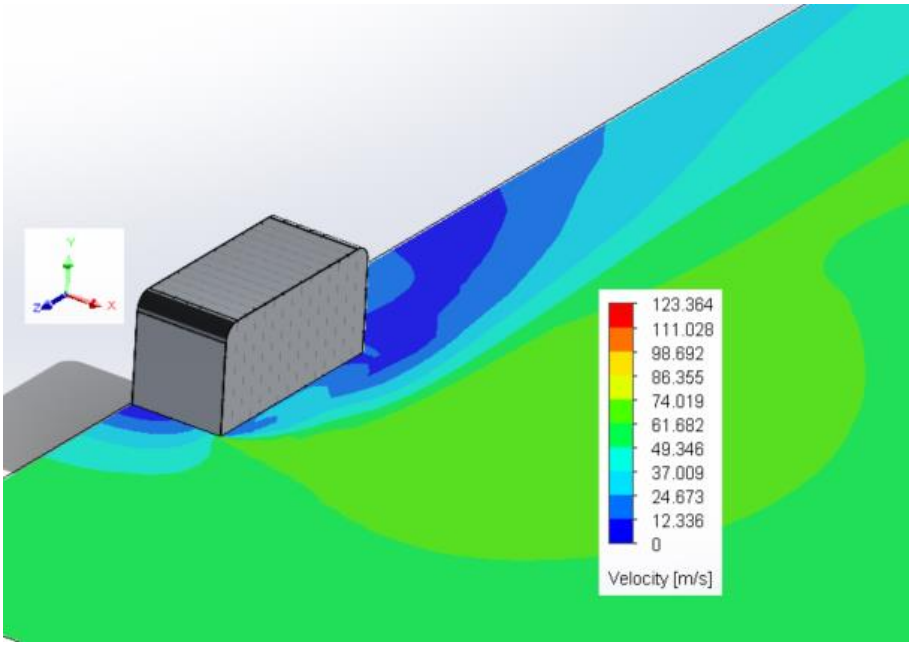

Figure 121: 12th Segment Endcap, Velocity Map

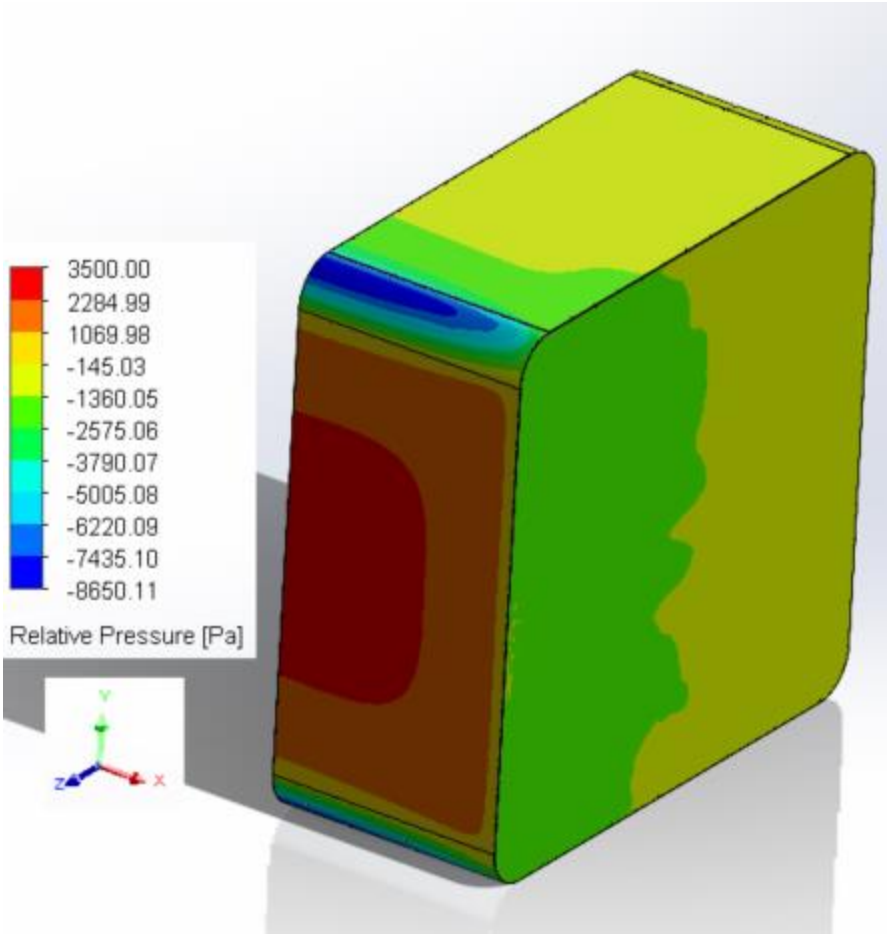

Figure 122: 12th Segment, Relative Pressure

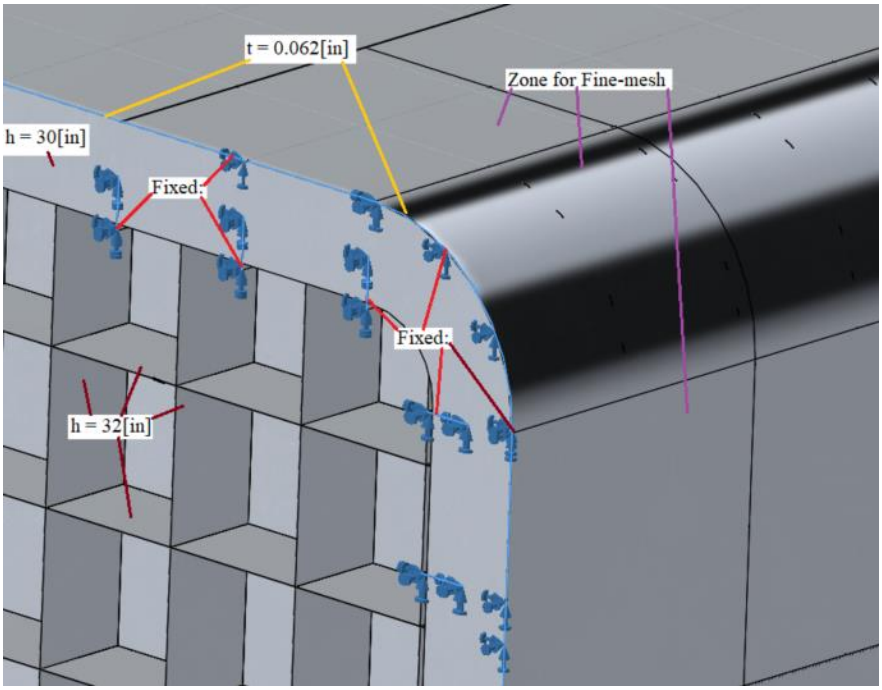

Figure 123: 12th Segment, Typical FEA Set-up

The shell is 0.062[in] thick, the cross-ribs are 0.125[in] thick and 30[in] tall; the fore-aft ribs are 0.125[in] thick and 32[in] tall. The endcap has 32[in] tall ribbing that are 0.125[in] thick.

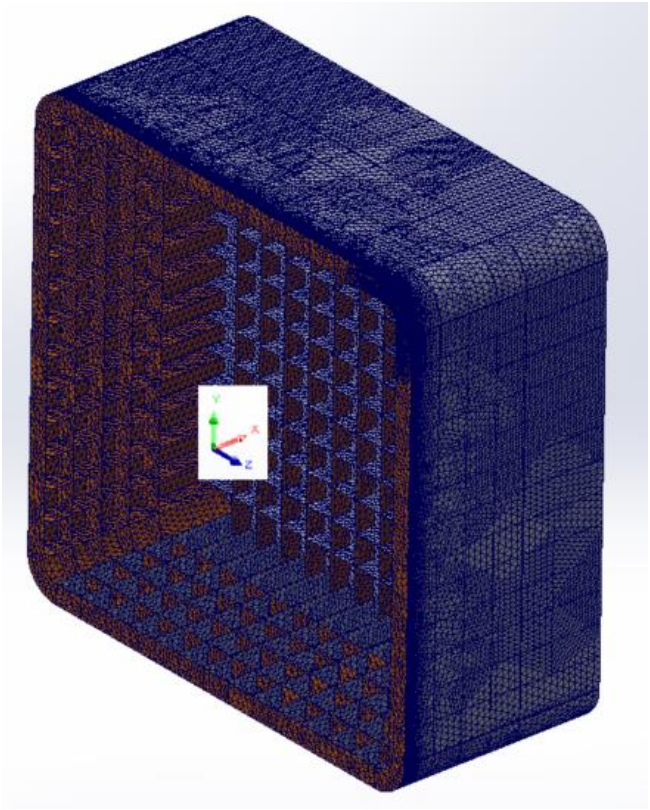

Figure 124: 12th Segment, FEA Mesh

Basic mesh:

- Maximum size = 9.0[in]
- Minimum size = 3.00[in]
- Growth rate 20[%]

Fine mesh - 1: Model Edges and Cross-rib-radii

- Maximum size = 1.5[in]
- Growth rate 5.0[%]

Fine mesh - 2: Shell-Radius, Horizontal critical rib, Vertical critical rib

- Maximum size = 1.0[in]
- Growth rate 5.0[%]

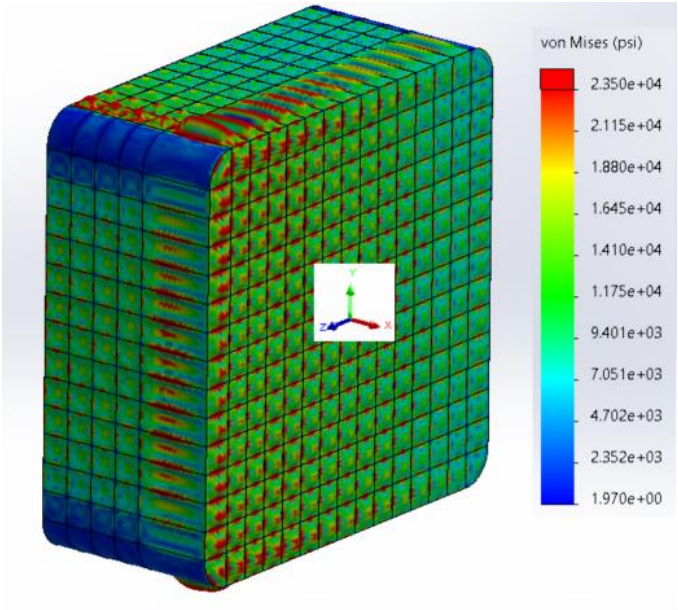

Figure 125: 12th Segment, Overall Stress

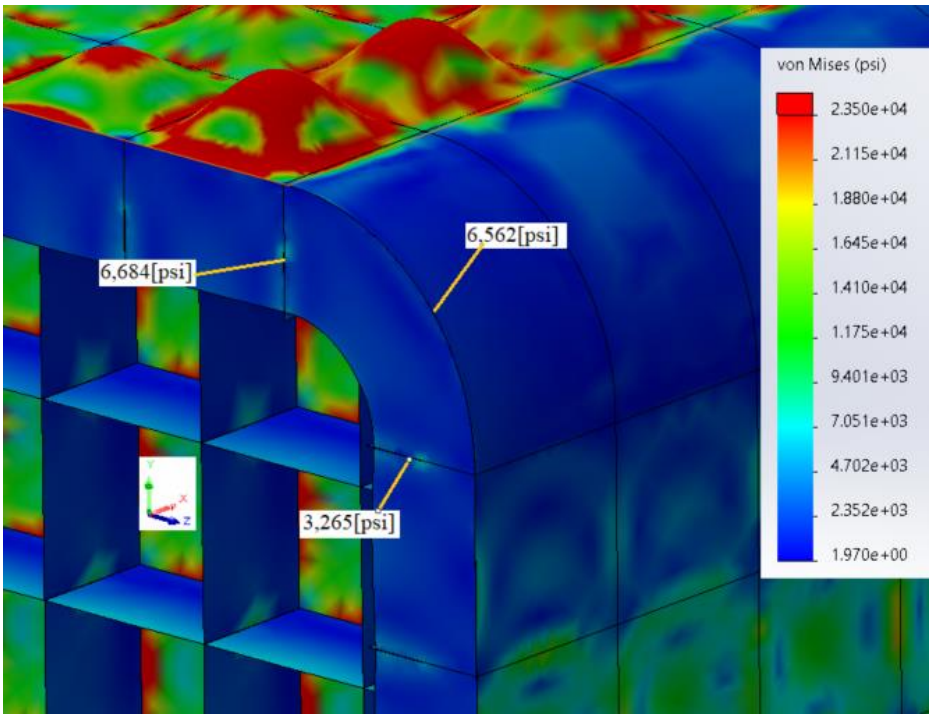

Figure 126: 12th Segment, Critical Member Stress

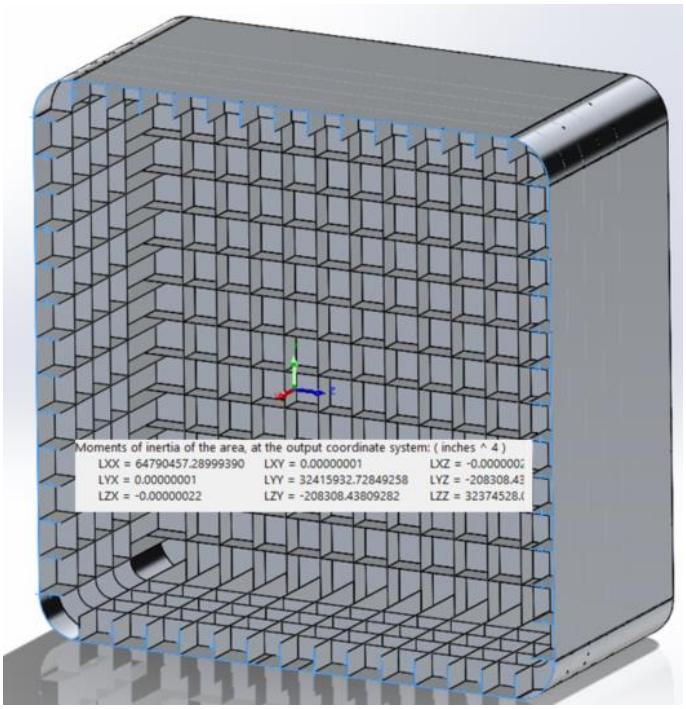

Figure 127: 12th Segment, Mating-face Area of Inertia

Table 33: 12th Segment Geometric Properties

	[Lbf]	[N]
Mass (@ 1[g]):	27,837	123,826

	[in3]	[m3]
Volume:	285,382	4.677

Model Center of Mass (cg)	[in]	[mm]
< X >	205	5,200
< Y >	0.0	0
< Z >	0.0	0

Reaction Loading Center	[in]	[mm]
< X >	0	0
< Y >	0	0
< Z >	0	0

Inertia @ Origin	(10^6)-[Lbm-in2]	(10^6)-[kg-m2]
Ixx - Twisting	3,637	1.0643
Iyy - Bend Fore/Aft	3,316	0.9704
Izz - Bend Up/Down	3,316	0.9704

Area of Inertia @ Origin	(10^3)-[in4]	[m4]
Ixx - Twisting	0	0.00
Iyy - Bend Fore/Aft	32,416	13.49
Izz - Bend Up/Down	32,375	13.48

The maximum stress is on the weight bearing rib, 6,684[psi] with a factor of safety of 5.76[-]: Where the maximum yield stress is 39,500[psi] (this value will be used in the Twelve-segment analysis).

Table 34: 12th Segment Mating Loads

Force	Reaction Force [lbf]	Force Applied at Mating Coordinate System [lbf]
Component		
Sum X:	-136,530	98,687
Sum Y:	29,835	-29,835
Sum Z:	47,310	-47,310

Moment	Reaction Force [lbf-in]	Moment Applied at Mating Coordinate System [lbf-in]
Component		
Sum X:	-24.203	24
Sum Y:	-8,578	8,578
Sum Z:	-2,568	2,568

Note: The vacuum force on the endcap is reduced per the area ratio (0.723[-]).

C. Segment – 11th:

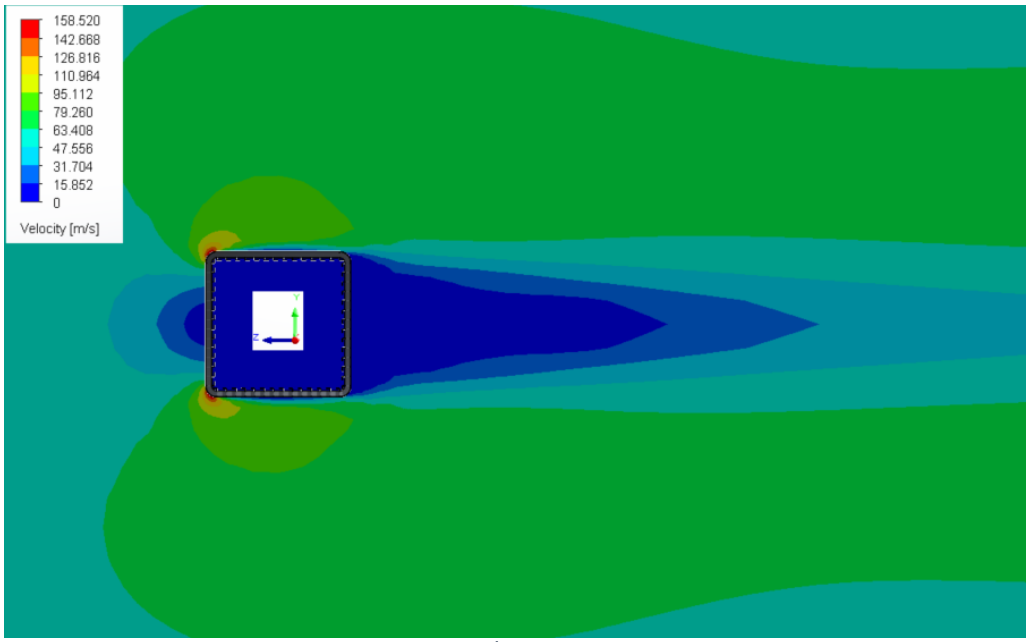

Figure 128: 11th Segment, 2-D CFD

Since the model is half the size of the Sixth-segment model, the CFD mesh is more refined for the Twelfth-segment model. As before, the mating loads will be carried onto the next segment; here, the 11th segment.

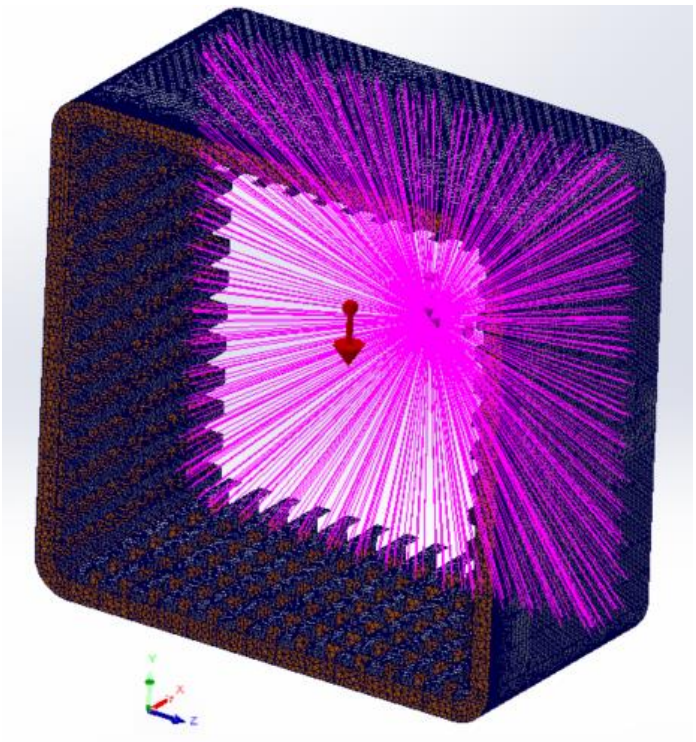

Figure 129: 11th Segment, with Gravity and Mating Load

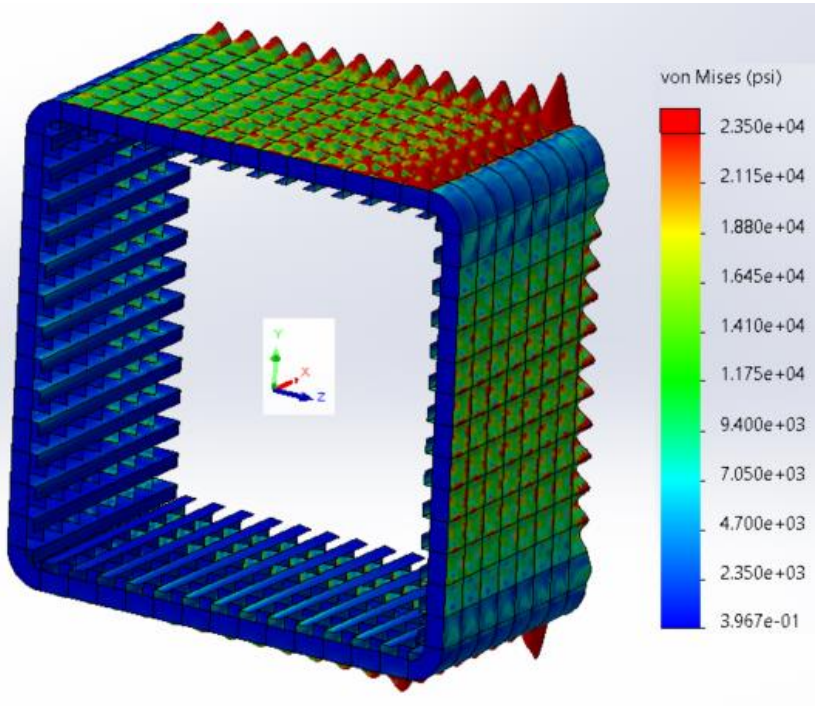

Figure 130: 11th Segment Overall Stresses

Note: The mating-edge is very thin, the wind-loading caused the high deformations; these can be ignored.

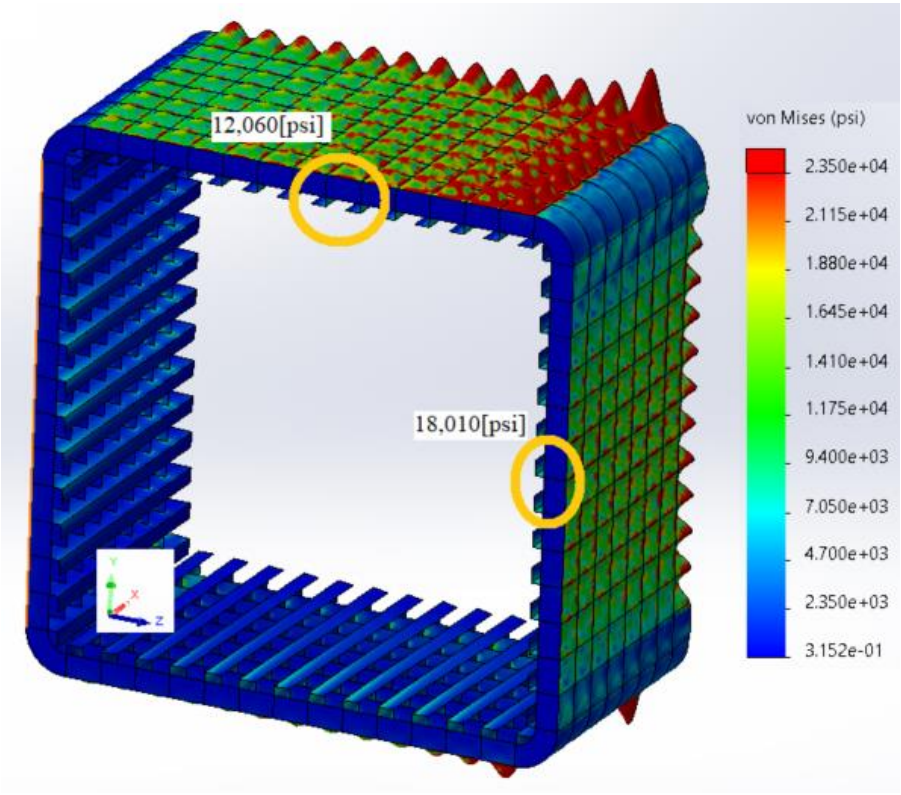

Figure 131: 11th Segment, Critical Stresses

The maximum stress in the 11th segment is on the is in the middle of the "front" face at 18,010[psi]. There is a minimum factor of safety for this segment of 2.19[-].

Table 35: 11th Segment Geometric Properties

	[Lbf]	[N]
Mass (@ 1[g]):	40,744	181,237

	[in3]	[m3]
Volume:	417,698	6.845

Model Center of Mass (cg)	[in]	[mm]
< X >	184	4,684
< Y >	0.0	0
< Z >	0.0	0

Reaction Loading Center	[in]	[mm]
< X >	0	0
< Y >	0	0
< Z >	0	0

Inertia @ Origin	(10^6)-[Lbm-in2]	(10^6)-[kg-m2]
Ixx - Twisting	6,205	1.8159
Iyy - Bend Fore/Aft	4,975	1.4560
Izz - Bend Up/Down	4,975	1.4560

Area of Inertia @ Origin	(10^3)-[in4]	[m4]
Ixx - Twisting	0	0.00
Iyy - Bend Fore/Aft	61,707	25.68
Izz - Bend Up/Down	61,666	25.67

Table 36: 11th Segment Mating Loads

Force	Reaction Force [lbf]	Force Applied at Mating Coordinate System [lbf]
Component		
Sum X:	-98,630	98,630
Sum Y:	72,853	-72,853
Sum Z:	99,955	-99,955

Moment	Reaction Force [lbf-in]	Moment Applied at Mating Coordinate System [lbf-in]
Component		
Sum X:	275.55	-276
Sum Y:	-32,342	32,342
Sum Z:	6,341	-6,341

D. Segment – 10th:

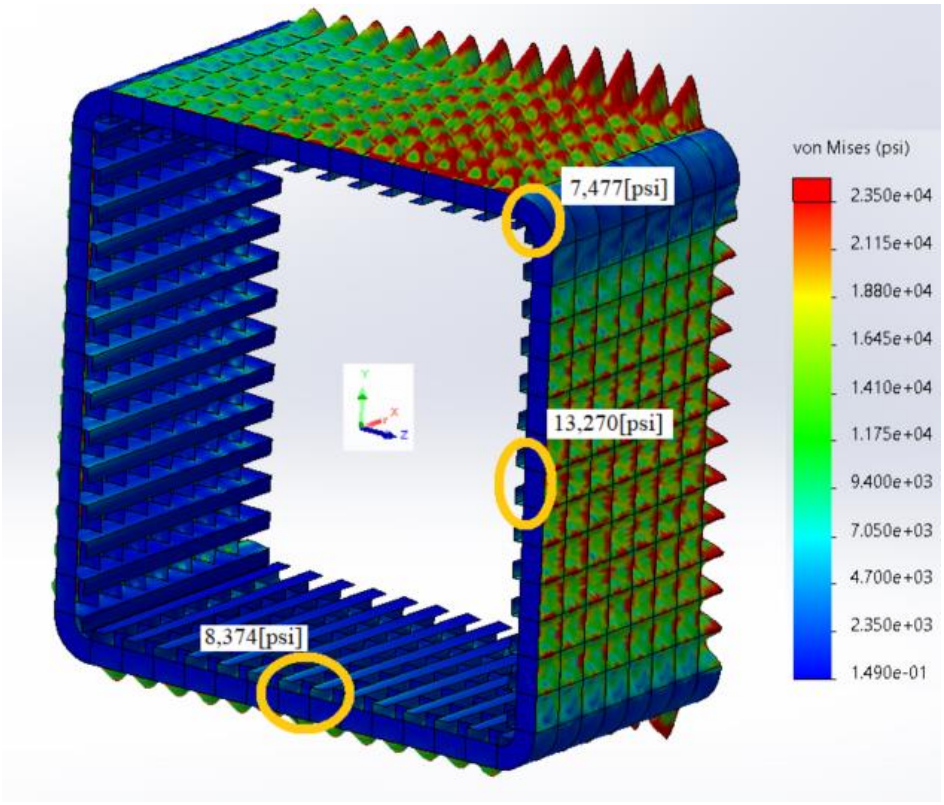

Figure 132: 10th Segment, Critical Stresses

The maximum stress in the 10th segment is on the is in the middle of the "front" face at 13,270[psi]. There is a minimum factor of safety for this segment of 2.98[-].

Table 37: 10th Segment Geometric Properties

	[Lbf]	[N]
Mass (@ 1[g]):	57,679	256,570

	[in3]	[m3]
Volume:	591,318	9.690

Model Center of Mass (cg)	[in]	[mm]
< X >	186	4,718
< Y >	0.0	0
< Z >	0.0	0

Reaction Loading Center	[in]	[mm]
< X >	0	0
< Y >	0	0
< Z >	0	0

Inertia @ Origin	(10^6)-[Lbm-in2]	(10^6)-[kg-m2]
Ixx - Twisting	8,566	2.5068
Iyy - Bend Fore/Aft	6,962	2.0375
Izz - Bend Up/Down	6,962	2.0375

Area of Inertia @ Origin	(10^3)-[in4]	[m4]
Ixx - Twisting	0	0.00
Iyy - Bend Fore/Aft	93,723	39.01
Izz - Bend Up/Down	93,682	38.99

Table 38: 10th Segment Mating Loads

Force	Reaction Force [lbf]	Force Applied at Mating Coordinate System [lbf]
Component		
Sum X:	-98,392	98,392
Sum Y:	93,610	-93,610
Sum Z:	196,380	-196,380

Moment	Reaction Force [lbf-in]	Moment Applied at Mating Coordinate System [lbf-in]
Component		
Sum X:	867.36	-867
Sum Y:	-98,109	98,109
Sum Z:	65,896	-65,896

E. Segment – 9th:

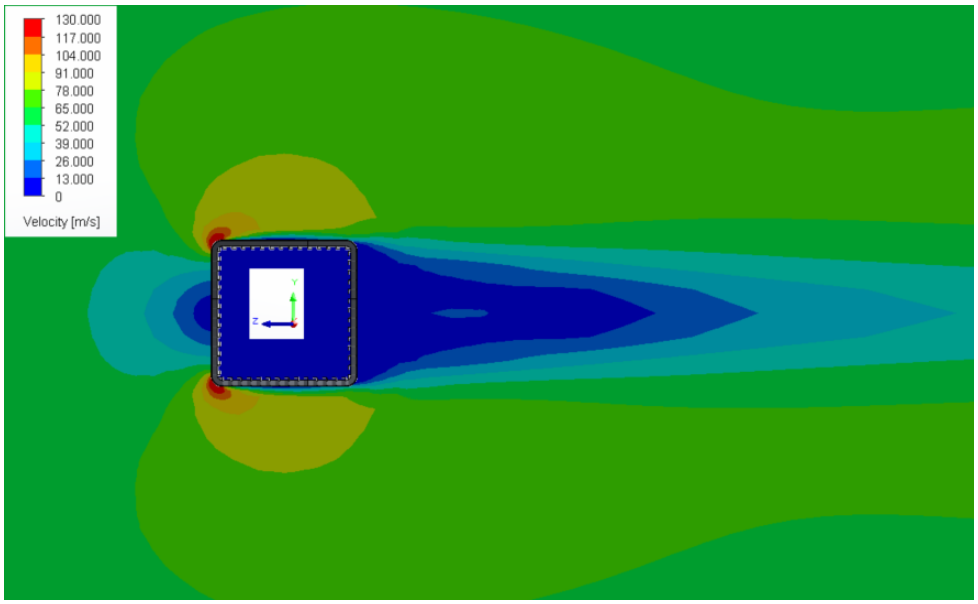

Figure 133: 9th Segment CFD, Same as Figure 128 with Different Scale

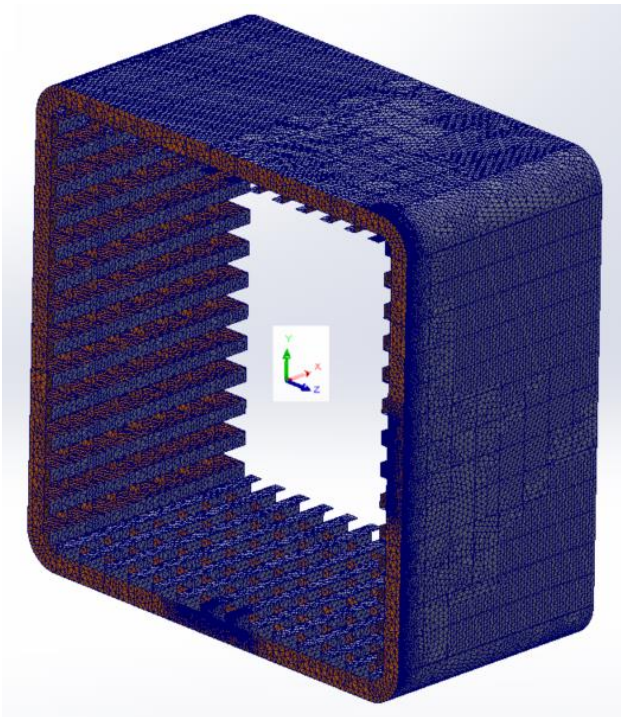

Figure 134: Seg 9 Mesh

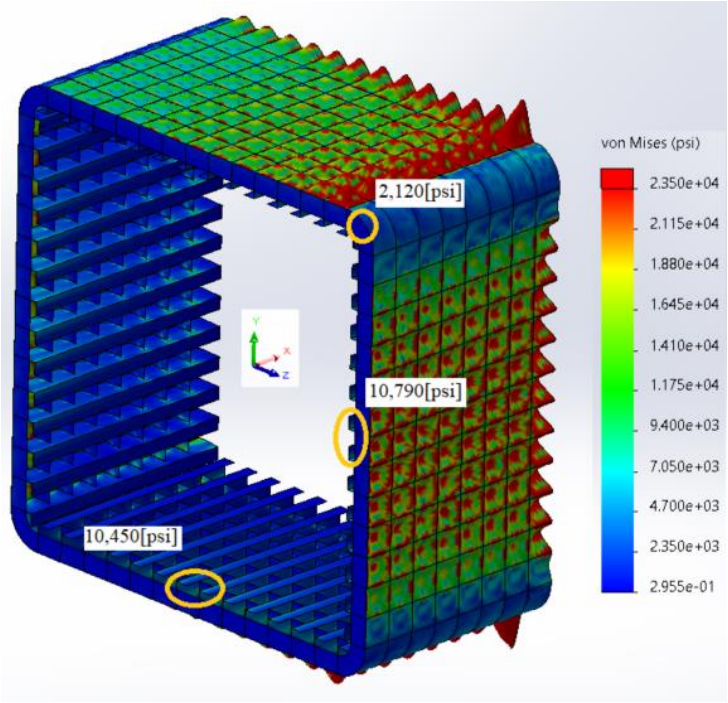

Figure 135: Seg 9 FEA

The maximum stress in the 9th segment is on the is in the middle of the "front" face at 10,790[psi]. There is a minimum factor of safety for this segment of 3.66[-].

Table 39: 9th Segment Geometric Properties

	[Lbf]	[N]
Mass (@ 1[g]):	74,433	331,095

	[in3]	[m3]
Volume:	763,075	12.505

Model Center of Mass (cg)	[in]	[mm]
< X >	186	4,737
< Y >	-0.1	-2
< Z >	0.0	0

Reaction Loading Center	[in]	[mm]
< X >	0	0

< Y >	0	0
< Z >	0	0

Inertia @ Origin	(10^6)-[Lbm-in2]	(10^6)-[kg-m2]
Ixx - Twisting	10,905	3.1912
Iyy - Bend Fore/Aft	8,931	2.6137
Izz - Bend Up/Down	8,928	2.6128

Area of Inertia @ Origin	(10^3)-[in4]	[m4]
Ixx - Twisting	0	0.00
Iyy - Bend Fore/Aft	125,395	52.19
Izz - Bend Up/Down	125,354	52.18

Table 40: 9th Segment Mating Loads

Force	Reaction Force [lbf]	Force Applied at Mating Coordinate System [lbf]
Component		
Sum X:	-98,224	98,224
Sum Y:	173,090	-173,090
Sum Z:	248,820	-248,820

Moment	Reaction Force [lbf-in]	Moment Applied at Mating Coordinate System [lbf-in]
Component		
Sum X:	-1356	1356
Sum Y:	-187,670	187,670
Sum Z:	182,530	-182,530

F. Segment – 8th:

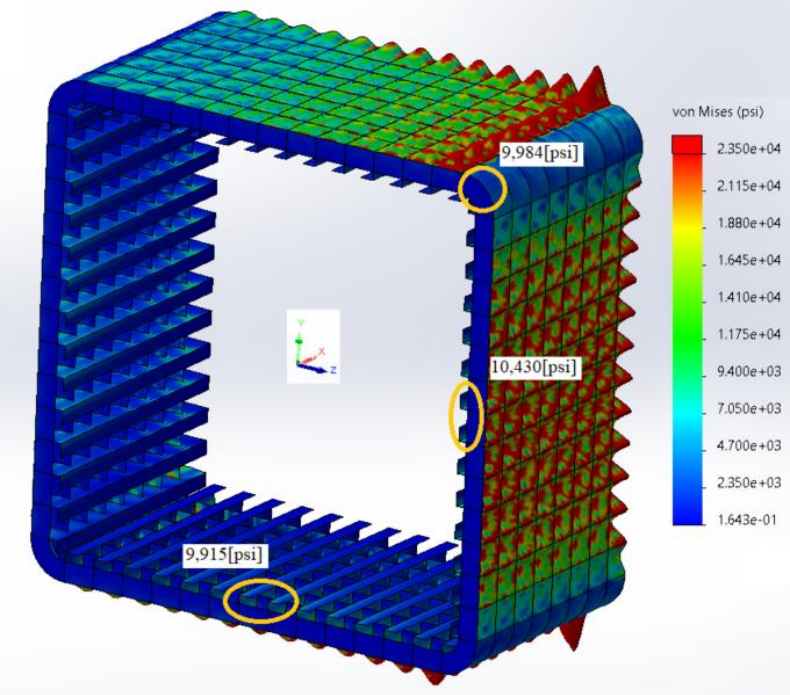

Figure 136: 8th Segment Critical Stresses

The maximum stress in the 8th segment is on the is in the middle of the "front" face at 10,430[psi]. There is a minimum factor of safety for this segment of 3.78[-].

Table 41: 8th Segment Geometric Properties

	[Lbf]	[N]
Mass (@ 1[g]):	90,551	402,791

	[in3]	[m3]
Volume:	928,312	15.212

Model Center of Mass (cg)	[in]	[mm]
< X >	187	4,748
< Y >	0.0	0
< Z >	0.0	0

Reaction Loading Center	[in]	[mm]
< X >	0	0
< Y >	0	0
< Z >	0	0

Inertia @ Origin	(10^6)-[Lbm-in2]	(10^6)-[kg-m2]
Ixx - Twisting	13,149	3.8478
Iyy - Bend Fore/Aft	10,819	3.1662
Izz - Bend Up/Down	10,819	3.1662

Area of Inertia @ Origin	(10^3)-[in4]	[m4]
Ixx - Twisting	0	0.00
Iyy - Bend Fore/Aft	155,865	64.88
Izz - Bend Up/Down	155,824	64.86

Table 42: 8th Segment Mating Loads

Force	Reaction Force [lbf]	Force Applied at Mating Coordinate System [lbf]
Component		
Sum X:	-98,049	98,049
Sum Y:	271,330	-271,330
Sum Z:	301,410	-301,410

Moment	Reaction Force [lbf-in]	Moment Applied at Mating Coordinate System [lbf-in]
Component		
Sum X:	-3589.6	3590
Sum Y:	-306,830	306,830
Sum Z:	315,000	-315,000

G. Segment – 7th:

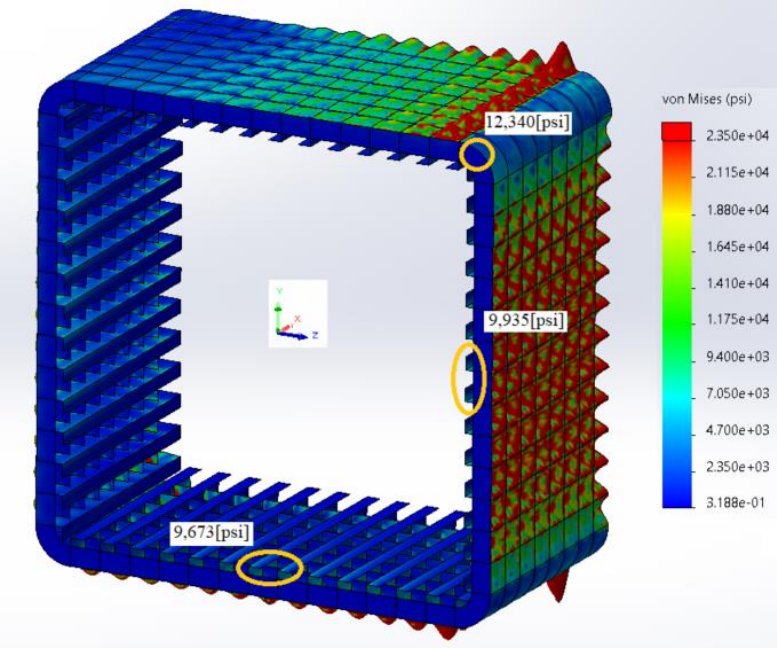

Figure 137: 7th Segment Critical Stresses

The maximum stress in the 7th segment is on the is on the radius at 12,790340psi]. There is a minimum factor of safety for this segment of 3.11[-].

Table 43: 7th Segment Geometric Properties

	[Lbf]	[N]
Mass (@ 1[g]):	106,438	473,458

	[in3]	[m3]
Volume:	1,091,179	17.881

Model Center of Mass (cg)	[in]	[mm]
< X >	187	4,756
< Y >	0.0	0
< Z >	0.0	0

Reaction Loading Center	[in]	[mm]

< X >	0	0
< Y >	0	0
< Z >	0	0

Inertia @ Origin	(10^6)-[Lbm-in2]	(10^6)-[kg-m2]
Ixx - Twisting	15,363	4.4959
Iyy - Bend Fore/Aft	12,683	3.7117
Izz - Bend Up/Down	12,683	3.7117

Area of Inertia @ Origin	(10^3)-[in4]	[m4]
Ixx - Twisting	0	0.00
Iyy - Bend Fore/Aft	185,898	77.38
Izz - Bend Up/Down	185,857	77.36

Table 44: 7th Segment Mating Loads

Force	Reaction Force [lbf]	Force Applied at Mating Coordinate System [lbf]
Component		
Sum X:	-98,000	98,000
Sum Y:	386,370	-386,370
Sum Z:	353,990	-353,990

Moment	Reaction Force [lbf-in]	Moment Applied at Mating Coordinate System [lbf-in]
Component		
Sum X:	-10446	10446
Sum Y:	-479,370	479,370
Sum Z:	509,490	-509,490

H. Segment – 6:

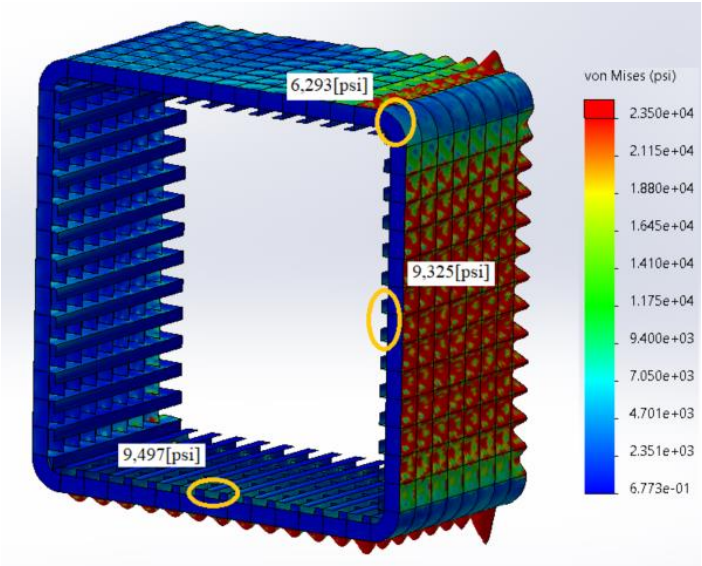

Figure 138: 6th Segment Critical Stresses

The maximum stress in the 6th segment is on the is on the bottom-mid at 9,497[psi]. There is a minimum factor of safety for this segment of 4.05[-].

Table 45: 6th Segment Geometric Properties

	[Lbf]	[N]
Mass (@ 1[g]):	122,279	543,923

	[in3]	[m3]
Volume:	1,253,580	20.542

Model Center of Mass (cg)	[in]	[mm]
< X >	188	4,766
< Y >	0.0	0
< Z >	0.0	0

Reaction Loading Center	[in]	[mm]
< X >	0	0
< Y >	0	0
< Z >	0	0

Inertia @ Origin	(10^6)-[Lbm-in2]	(10^6)-[kg-m2]
Ixx - Twisting	17,572	5.1422
Iyy - Bend Fore/Aft	14,542	4.2556
Izz - Bend Up/Down	14,542	4.2556

Area of Inertia @ Origin	(10^3)-[in4]	[m4]
Ixx - Twisting	0	0.00
Iyy - Bend Fore/Aft	215,846	89.84
Izz - Bend Up/Down	215,804	89.82

Table 46: 6th Segment Mating Loads

Force	Reaction Force [lbf]	Force Applied at Mating Coordinate System [lbf]
Component		
Sum X:	-97,708	97,708
Sum Y:	513,340	-513,340
Sum Z:	406,980	-406,980

Moment	Reaction Force [lbf-in]	Moment Applied at Mating Coordinate System [lbf-in]
Component		
Sum X:	-16187	16187
Sum Y:	-726,960	726,960
Sum Z:	809,420	-809,420

I. Segment – 5:

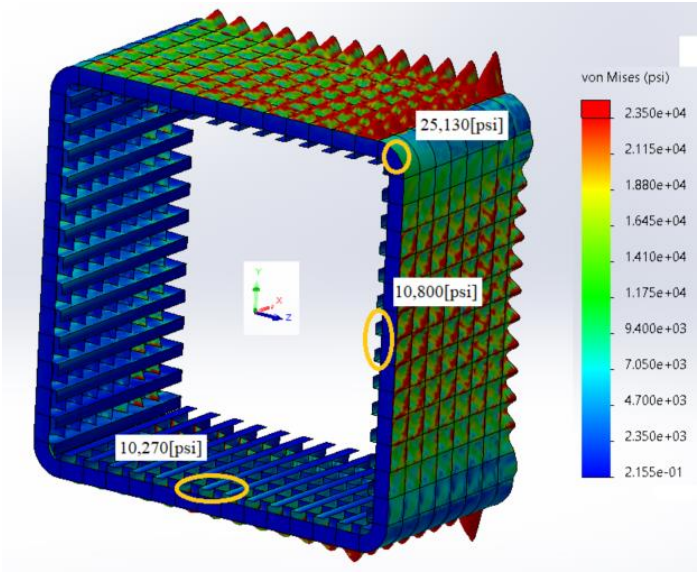

Figure 139: 5th Segment Critical Stresses

The maximum stress in the 5th segment is on the is on the front-face-mid at 10,800[psi]. There is a minimum factor of safety for this segment of 3.65[-]. The support by the radius is insignificant and is not included within the factor of safety.

Table 47: 5th Segment Geometric Properties

	[Lbf]	[N]
Mass (@ 1[g]):	137,637	612,238

	[in3]	[m3]
Volume:	1,411,028	23.123

Model Center of Mass (cg)	[in]	[mm]
< X >	188	4,766
< Y >	0.0	0
< Z >	0.0	0

Reaction Loading Center	[in]	[mm]
< X >	0	0
< Y >	0	0
< Z >	0	0

Inertia @ Origin	(10^6)-[Lbm-in2]	(10^6)-[kg-m2]
Ixx - Twisting	19,713	5.7688
Iyy - Bend Fore/Aft	16,344	4.7829
Izz - Bend Up/Down	16,344	4.7829

Area of Inertia @ Origin	(10^3)-[in4]	[m4]
Ixx - Twisting	0	0.00
Iyy - Bend Fore/Aft	244,880	101.93
Izz - Bend Up/Down	244,838	101.91

Table 48: 5th Segment Mating Loads

Force	Reaction Force [lbf]	Force Applied at Mating Coordinate System [lbf]
Component		
Sum X:	-97,340	97,340
Sum Y:	662,480	-662,480
Sum Z:	460,050	-460,050

Moment	Reaction Force [lbf-in]	Moment Applied at Mating Coordinate System [lbf-in]
Component		
Sum X:	-13666	13666
Sum Y:	-1,073,400	1,073,400
Sum Z:	1,239,500	-1,239,500

J. Segment – 4th:

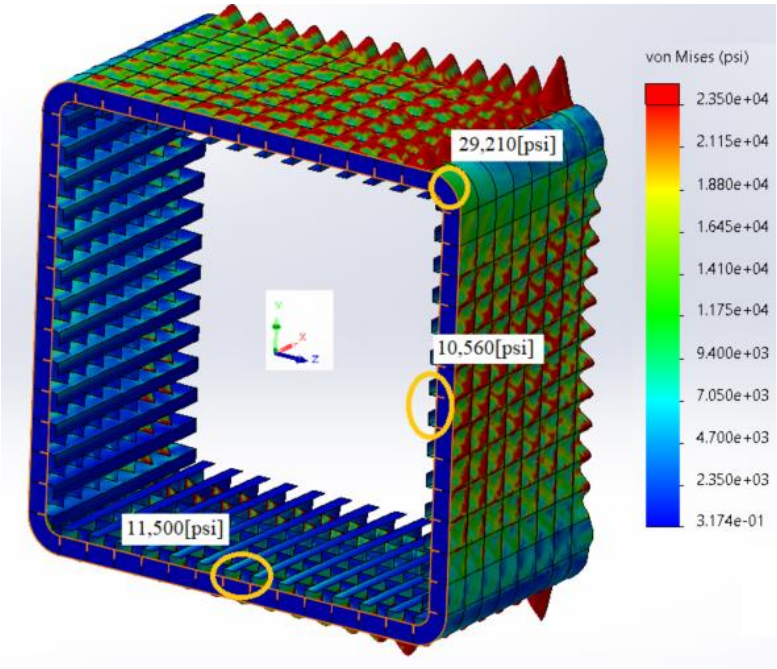

Figure 140: 4th Segment Critical Stresses

The maximum stress in the 4th segment is on the is on the lower-mid at 11,500[psi]. There is a minimum factor of safety for this segment of 3.34[-]. The support by the radius is insignificant and is not included within the factor of safety.

Table 49: 4th Segment Geometric Properties

	[Lbf]	[N]
Mass (@ 1[g]):	152,867	679,985

	[in3]	[m3]
Volume:	1,567,163	25.681

Model Center of Mass (cg)	[in]	[mm]
< X >	188	4,766
< Y >	0.0	0
< Z >	0.0	0

Reaction Loading Center	[in]	[mm]
< X >	0	0
< Y >	0	0
< Z >	0	0

Inertia @ Origin	(10^6)-[Lbm-in2]	(10^6)-[kg-m2]
Ixx - Twisting	21,836	6.3901
Iyy - Bend Fore/Aft	18,131	5.3059
Izz - Bend Up/Down	18,131	5.3059

Area of Inertia @ Origin	(10^3)-[in4]	[m4]
Ixx - Twisting	0	0.00
Iyy - Bend Fore/Aft	273,672	113.91
Izz - Bend Up/Down	273,630	113.89

Table 50: 4th Segment Mating Loads

Force	Reaction Force [lbf]	Force Applied at Mating Coordinate System [lbf]
Component		
Sum X:	-97,451	97,451
Sum Y:	826,850	-826,850
Sum Z:	513,500	-513,500

Moment	Reaction Force [lbf-in]	Moment Applied at Mating Coordinate System [lbf-in]
Component		
Sum X:	-15353	15353
Sum Y:	-1,515,700	1,515,700
Sum Z:	1,913,300	-1,913,300

K. Segment – 3rd:

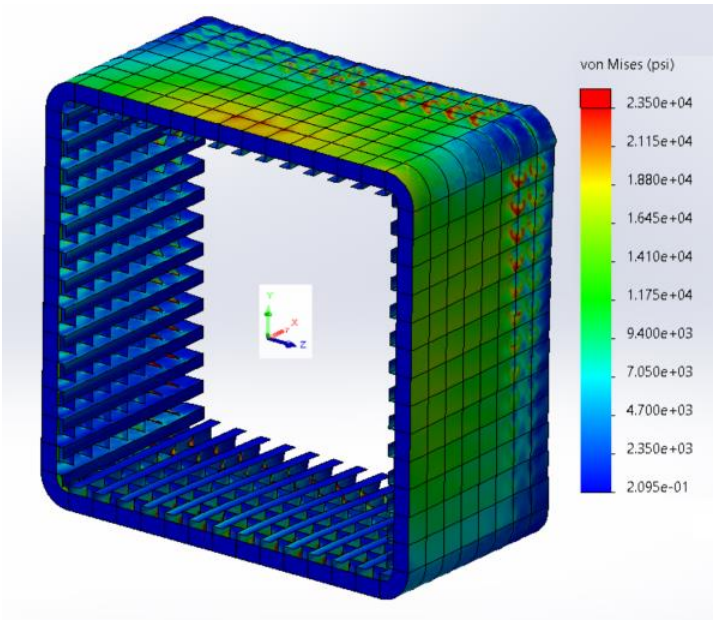

Figure 141: 3rd Segment, Gravity Only

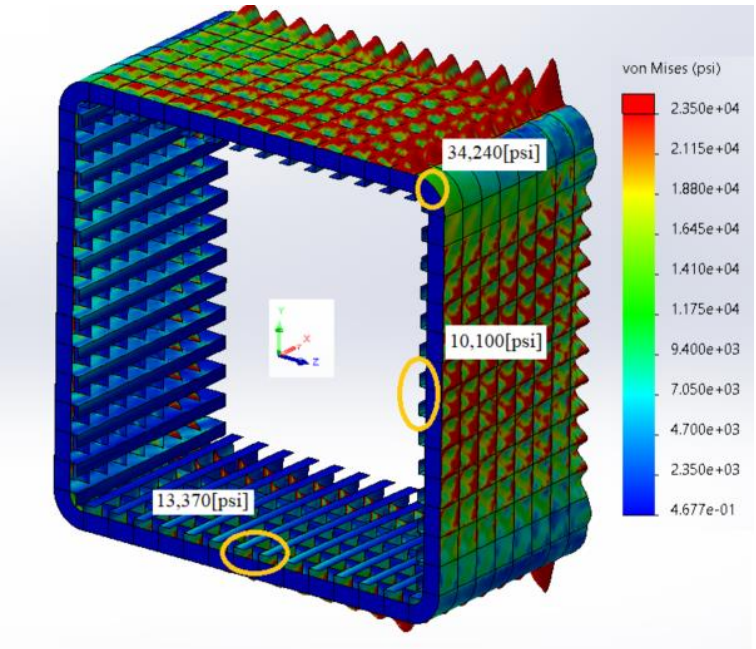

Figure 142: 3rd Segment Critical Stresses

The maximum stress in the 3rd segment is on the is on the lower-mid at 13,370[psi]. There is a minimum factor of safety for this segment of 2.87 [-]. The support by the radius is insignificant and is not included within the factor of safety.

Table 51: 3rd Segment Geometric Properties

	[Lbf]	[N]
Mass (@ 1[g]):	167,849	746,629

	[in3]	[m3]
Volume:	1,720,758	28.198

Model Center of Mass (cg)	[in]	[mm]
< X >	188	4,772
< Y >	0.0	0
< Z >	0.0	0

Reaction Loading Center	[in]	[mm]
< X >	0	0
< Y >	0	0
< Z >	0	0

Inertia @ Origin	(10^6)-[Lbm-in2]	(10^6)-[kg-m2]
Ixx - Twisting	23,925	7.0013
Iyy - Bend Fore/Aft	19,889	5.8203
Izz - Bend Up/Down	19,889	5.8203

Area of Inertia @ Origin	(10^3)-[in4]	[m4]
Ixx - Twisting	0	0.00
Iyy - Bend Fore/Aft	301,995	125.70
Izz - Bend Up/Down	301,954	125.68

Table 52: 3rd Segment Mating Loads

Force	Reaction Force [lbf]	Force Applied at Mating Coordinate System [lbf]
Component		
Sum X:	-97,611	97,611

Sum Y:	1,005,000	-1,005,000
Sum Z:	565,130	-565,130

Moment	Reaction Force [lbf-in]	Moment Applied at Mating Coordinate System [lbf-in]
Component		
Sum X:	-34332	34332
Sum Y:	-2,084,600	2,084,600
Sum Z:	2,870,400	-2,870,400

L. Segment – 2nd:

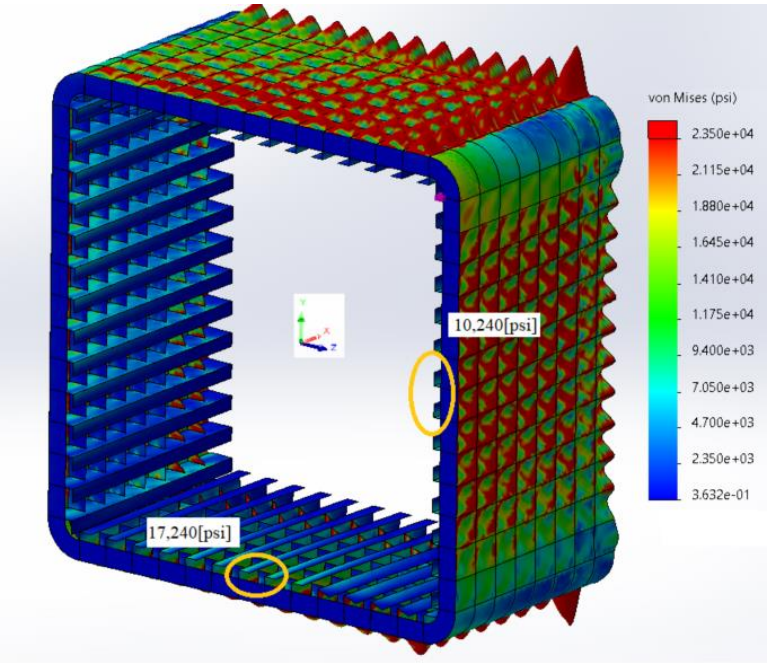

Figure 143: 2nd Segment Critical Stresses

The maximum stress in the 2nd segment is on the is on the lower-mid at 17,240[psi]. There is a minimum factor of safety for this segment of 2.23 [-]. The support by the radius is insignificant and is not included within the factor of safety.

Table 53: 2nd Segment Geometric Properties

	[Lbf]	[N]
Mass (@ 1[g]):	182,315	810,977

	[in3]	[m3]
Volume:	1,869,061	30.628

Model Center of Mass (cg)	[in]	[mm]
< X >	188	4,775
< Y >	0.0	0
< Z >	0.0	0

Reaction Loading Center	[in]	[mm]
< X >	0	0
< Y >	0	0
< Z >	0	0

Inertia @ Origin	(10^6)-[Lbm-in2]	(10^6)-[kg-m2]
Ixx - Twisting	25,941	7.5915
Iyy - Bend Fore/Aft	21,586	6.3170
Izz - Bend Up/Down	21,586	6.3170

Area of Inertia @ Origin	(10^3)-[in4]	[m4]
Ixx - Twisting	0	0.00
Iyy - Bend Fore/Aft	329,343	137.08
Izz - Bend Up/Down	329,302	137.07

Table 54: 2nd Segment Mating Loads

Force	Reaction Force [lbf]	Force Applied at Mating Coordinate System [lbf]
Component		
Sum X:	-97,516	97,516
Sum Y:	1,200,700	-1,200,700

Sum Z:	618,860	-618,860

Moment	Reaction Force [lbf-in]	Moment Applied at Mating Coordinate System [lbf-in]
Component		
Sum X:	-46536	46536
Sum Y:	-2,864,200	2,864,200
Sum Z:	3,512,100	-3,512,100

M. Segment – 1st:

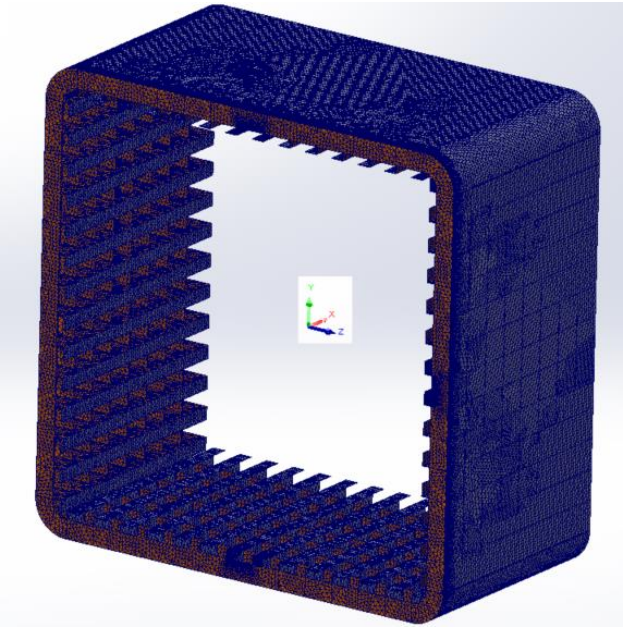

Figure 144: 1st Segment Mesh

Basic mesh:

- Maximum size = 7.0[in]
- Minimum size = 2.33[in]

- Growth rate 20[%]

Fine mesh - 1: Model Edges
- Maximum size = 1.5[in]
- Growth rate 5.0[%]

Fine mesh - 2: Critical Members
- Maximum size = 1.0[in]
- Growth rate 5.0[%]

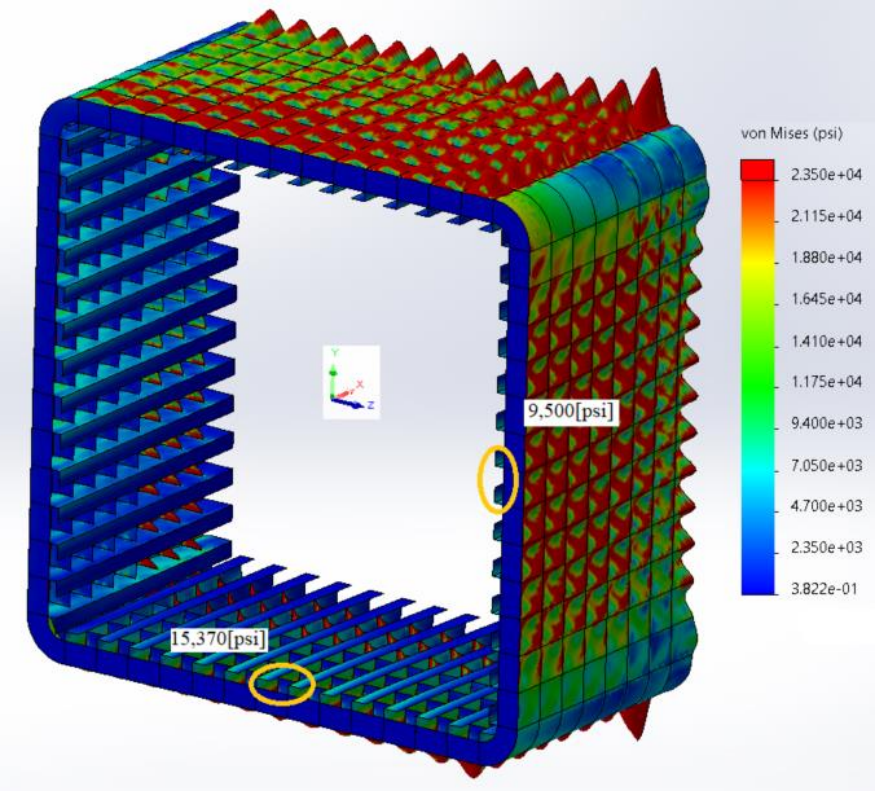

Figure 145: 1st Segment Critical Stress

The maximum stress in the 1st segment is on the is on the lower-mid at 15,370[psi]. There is a minimum factor of safety for this segment of 2.50 [-]. The support by the radius is insignificant and is not included within the factor of safety.

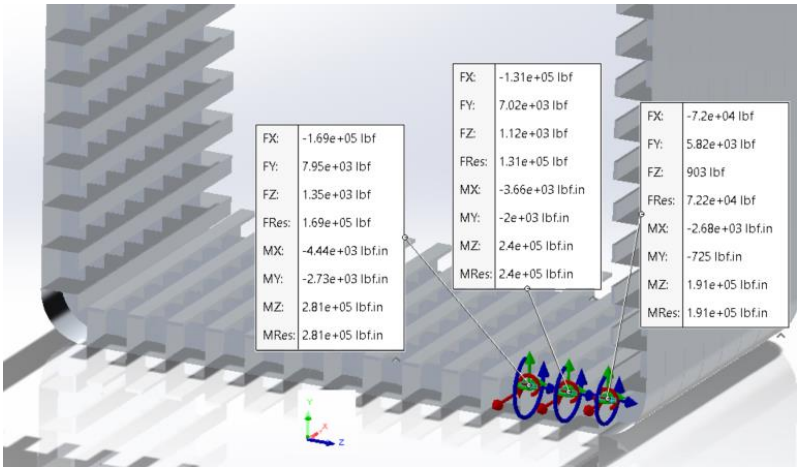

Figure 146: 1st Segment, Frist 3 Beam-loadings, Closest to Front Face

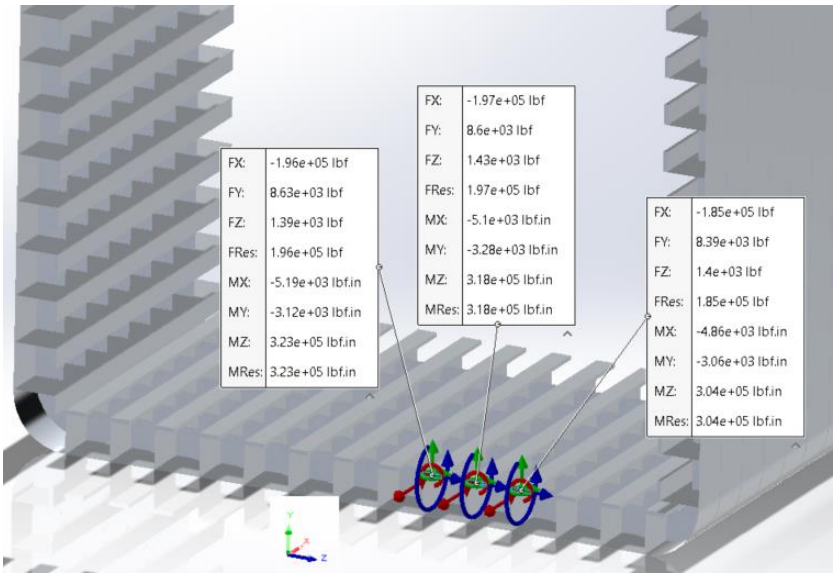

Figure 147: 1st Segment, Beams 4, 5 & 6, Loadings, Closest to Front Face

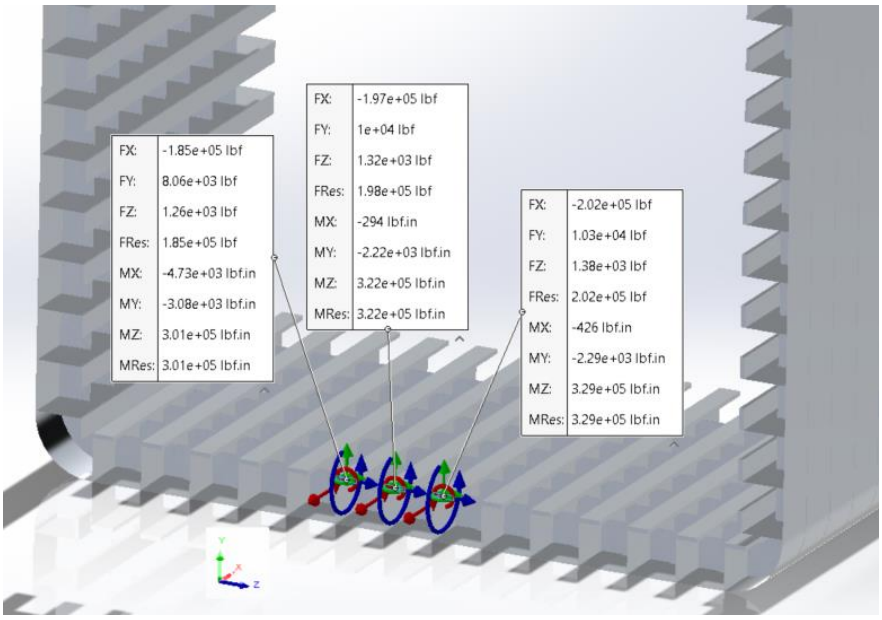

Figure 148: 1st Segment, Beams 7, 8, & 9, Loadings, Closest to Front Face

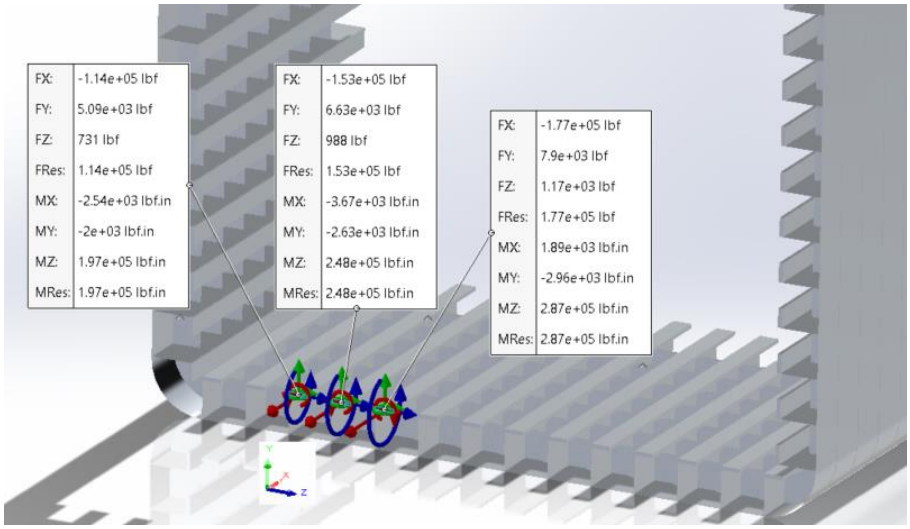

Figure 149: 1st Segment, Beams 10, 11, & 12, Loadings, Closest to Front Face

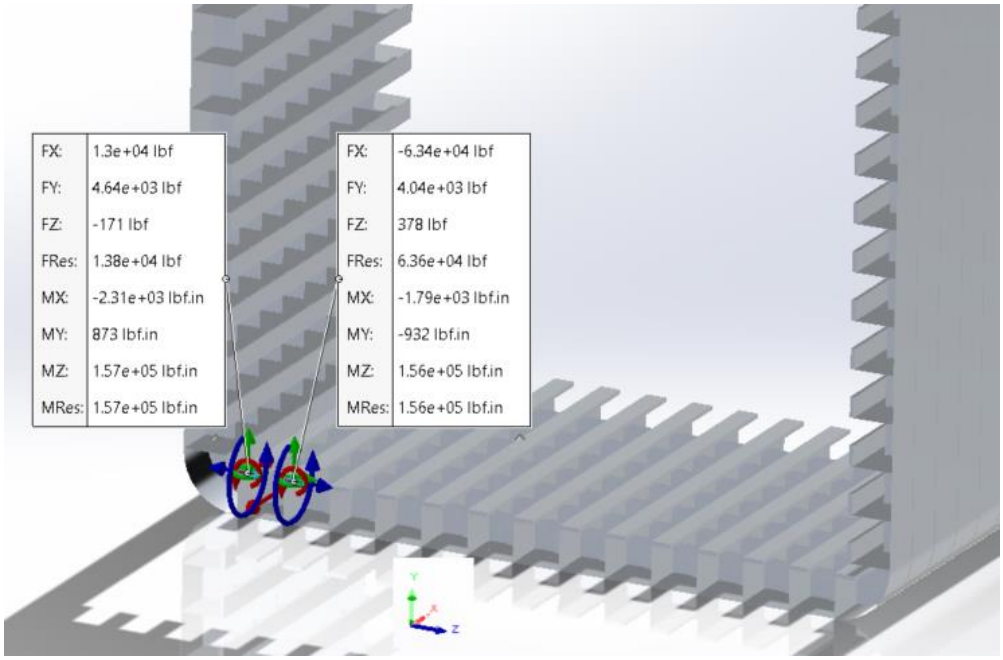

Figure 150: 1st Segment, Beams 13 & 14, Loadings, Closest to Front Face

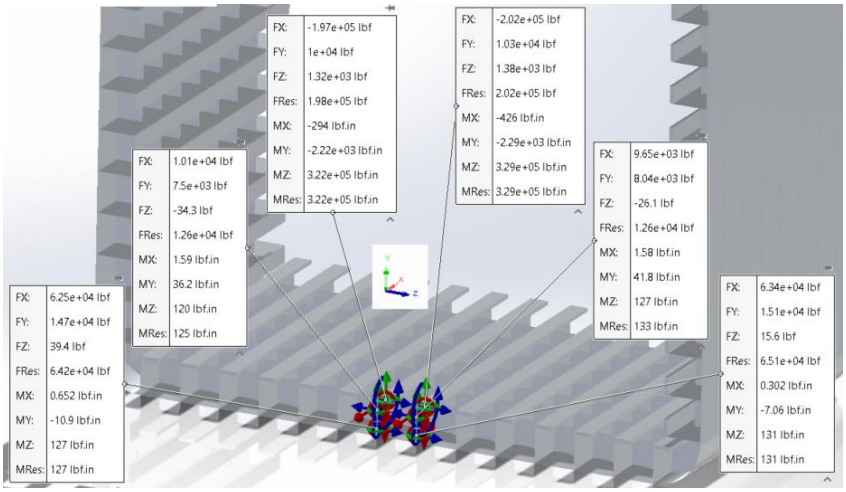

Figure 151: 1st Segment, Beams 7 & 8, Critical Beam Loading/s

Table 55: 1st Segment Geometric Properties

	[Lbf]	[N]
Mass (@ 1[g]):	196,575	874,407

	[in3]	[m3]
Volume:	2,015,247	33.024

Model Center of Mass (cg)	[in]	[mm]
< X >	188	4,776
< Y >	0.0	0
< Z >	0.0	0

Reaction Loading Center	[in]	[mm]
< X >	0	0
< Y >	0	0
< Z >	0	0

Inertia @ Origin	(10^6)-[Lbm-in2]	(10^6)-[kg-m2]
Ixx - Twisting	27,929	8.1732
Iyy - Bend Fore/Aft	23,259	6.8066
Izz - Bend Up/Down	23,259	6.8066

Area of Inertia @ Origin	(10^3)-[in4]	[m4]
Ixx - Twisting	0	0.00
Iyy - Bend Fore/Aft	356,301	148.30
Izz - Bend Up/Down	356,259	148.29

Table 56: 1st Segment Mating Loads

Force	Reaction Force [lbf]	Force Applied at Mating Coordinate System [lbf]
Component		
Sum X:	-97,439	97,439
Sum Y:	1,409,200	-1,409,200
Sum Z:	671,320	-671,320

Moment	Reaction Force [lbf-in]	Moment Applied at Mating Coordinate System [lbf-in]
Component		
Sum X:	-58094	58094
Sum Y:	-3,559,900	3,559,900
Sum Z:	5,893,900	-5,893,900

N. Vibration Model:

Though there is no vortex shedding, it is interesting to know the harmonics frequency range.

Eq - 29: Cantilever Beam Harmonic Frequency[6]:

$$\omega_n = 1.8751^2 \sqrt{\frac{EI}{mL^3}}$$

Eq - 30: Cantilever Beam 1st Natural Period[6]:

$$T_n = \frac{2\pi}{\omega_n} = \frac{2\pi}{1.8751^2} \sqrt{\frac{mL^3}{EI}}$$

Table 57: 12-Segment Part Data - A

Arm Data Segment #	Length [in]	Cross-sectional Area [in2]	Iy Area of Inertia [in4]	Iz Area of Inertia [in4]	Mass [Lbm]	Volume [in3]
Base of Arm - 1	378	4,647	356,300,879	356,259,474	196,575	2,015,247
2	378	4,260	329,343,158	329,301,754	182,315	1,869,061
3	378	3,867	301,995,216	301,953,811	167,849	1,720,758
4	378	3,461	273,671,522	273,630,118	152,867	1,567,163
5	378	3,048	244,879,527	244,838,122	137,637	1,411,028

6	378	2,632	215,845,622	215,804,217	122,279	1,253,580
7	378	2,202	185,898,403	185,856,998	106,438	1,091,179
8	378	1,771	155,865,389	155,823,985	90,551	928,312
9	378	1,334	125,395,259	125,353,854	74,433	763,075
10	378	880	93,722,926	93,681,522	57,679	591,318
11	378	420	61,707,130	61,665,726	40,744	417,698
12	321	396	32,415,933	32,374,528	27,837	285,382
Full Assembly	4,479	2,410	198,086,747	198,045,342	1,357,203	13,913,800

Table 58: 12-Segment Part Data - B

Arm Data Segment #	Center of Gravity from Segment Base "dX"- [in]	Ixx - @ Base of Segment [Lbm-in2]	Iyy - @ Base of Segment [Lbm-in2]	Izz - @ Base of Segment [Lbm-in2]
Base of arm - 1	188	27,929,377,536	23,259,441,840	23,259,441,839
2	188	25,941,434,170	21,586,316,886	21,586,316,885
3	188	23,924,714,626	19,888,969,593	13,963,654,668
4	188	21,836,040,279	18,131,059,275	18,131,059,275
5	188	19,712,831,960	16,344,080,872	16,344,080,872
6	187	17,571,784,453	14,542,085,640	14,542,085,640
7	187	15,363,386,460	12,683,403,021	12,683,403,021
8	187	13,148,661,729	10,819,393,498	10,819,393,498
9	186	10,904,906,505	8,931,455,296	8,928,253,444
10	186	8,566,089,606	6,962,494,915	6,962,494,915
11	184	6,205,148,510	4,975,419,223	4,975,419,223
12	205	3,636,956,049	3,315,971,271	3,315,971,271
Full Assembly	1,647	194,738,128,007	5,569,056,127,624	5,569,056,127,623

Table 59: Estimated Natural Frequency

Arm Data Segment #	Natural Frequency ω_n [1/s]	Natural Period T_n [s]
Base of Arm - 1	1,278	0.0049
2	1,276	0.0049
3	1,273	0.0049
4	1,270	0.0049
5	1,266	0.0050
6	1,261	0.0050
7	1,255	0.0050
8	1,246	0.0050
9	1,232	0.0051
10	1,210	0.0052
11	1,168	0.0054
12	1,307	0.0048
Full Assembly	8.89	0.7067

The vortex shedding analysis determined there was no vortex shedding and the above frequency analysis shows that the arms' natural period is (x3 = 2.13/0.7067) smaller. The 2nd nodal period is approximately 0.113[s] for the assembly. If there was vortex shedding, no special design modifications would be necessary.

The analysis shows a minimum factor of safety of 2.19[-] in the 11th segment. The structure has a safety variance from about 2.2[-] to 5.7[-]; with a standard deviation of 0.97[-]. The optimization is not very good because the wind is perpendicular to the gravity and the weight estimation in the hand calculations have cushion. In any case, two viable systems have been shown to withstand the environmental stresses.

It is clear from this analysis that in order to optimize the structural area, the actual wind-loadings should be refined. The main parts of the wind-loading are the arms and the head of the cross.

V. Wind Loadings:

A. The arms of the Glorious Cross:

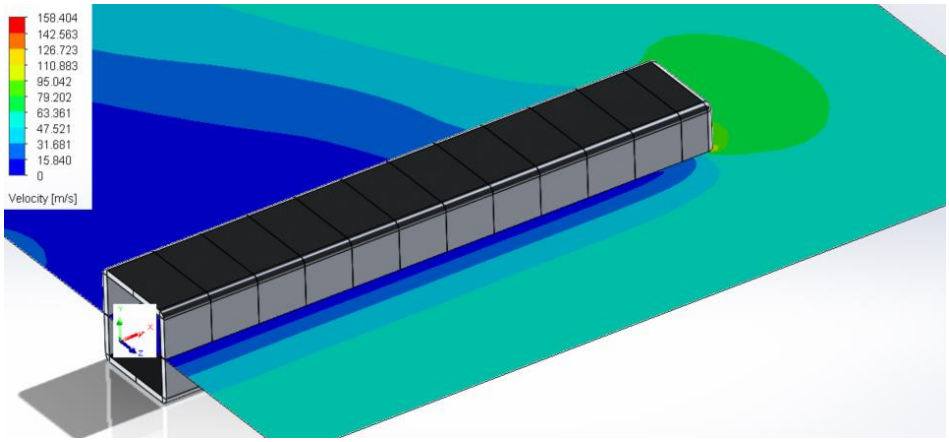

Figure 152: 12-Segmented Arm CFD @ 60.603[m/s] & 1.226[kg/m3]

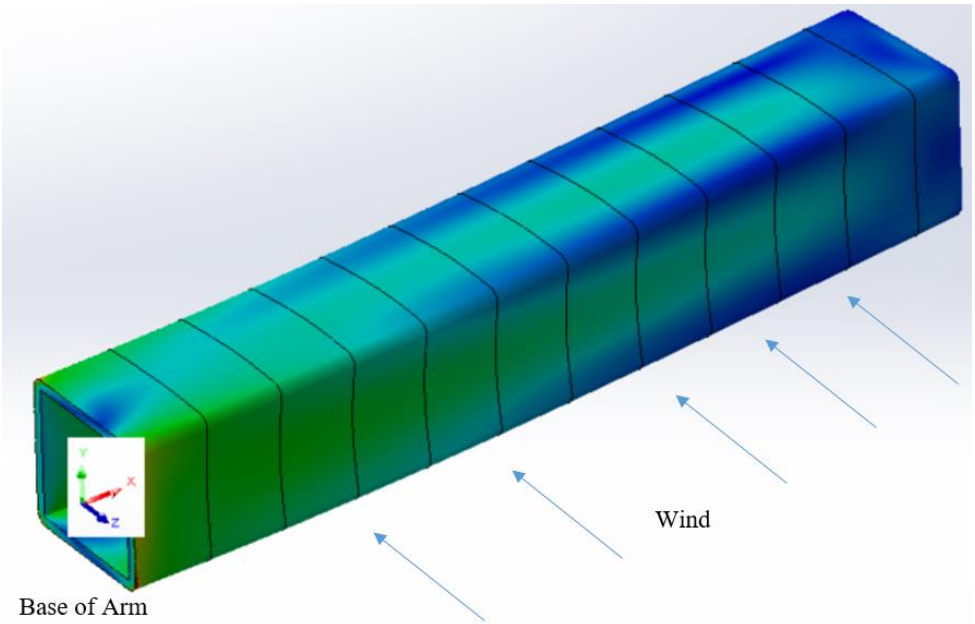

Figure 153: 12-Segment FEA Stress Due to Wind

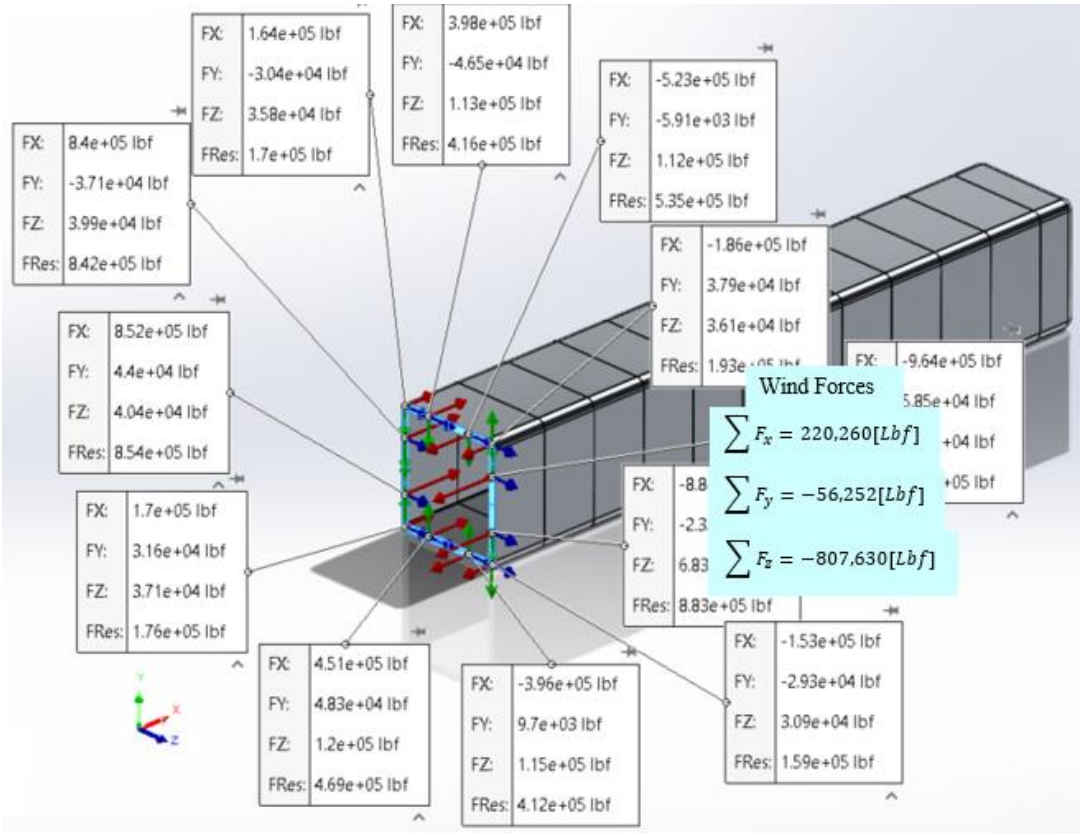

Figure 154: Arm, Maximum Wind Forces

In Figure 154 the maximum wind forces acting on the arm are shown. The vacuum force is 220,200[Lbf]. The lift force in this equilibrium state acts with gravity, adding 56,225[Lbf] to the weight (with unequal distribution). The wind impinges on the face of the cross with 807,830[Lbf].

Table 60: Maximum Forces and Lever-arms Acting on an Arm

Forces of Action	[Lbf]	[N]	Distance (dX) from Intersection [in]	Distance (dX) from Intersection [mm]
Fx	220,260	979,764	na	na
Fy	-56,252	-250,221	2,094	53,188
Fz	-807,630	-3,592,514	2,648	67,270

Note: "F_y" is acting on the 5th segment and "F_z" is acting on the 6th segment.

Table 61: Maximum Shear forces Acting on an Arm

Average Shear Forces of Action	[Lbf]	[N]
Back of Arm (f_y)	-428,221	-1,904,819
Front of Arm (f_y)	30,598	136,107
Bottom of Arm (f_z)	440,740	1,960,508
Top of Arm (f_y)	-18,075	-80,401

Note: The roughness was exaggerated at 3[mm].

The calculation of M_x:

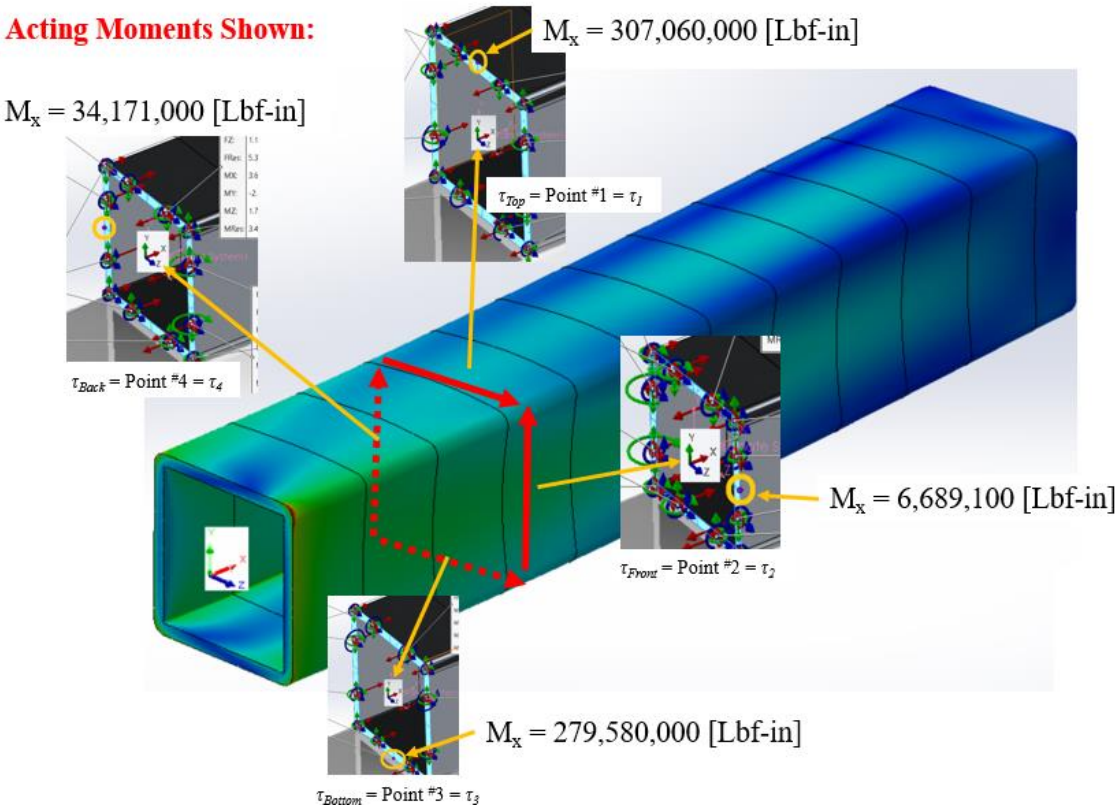

Figure 155: Calculation of Twisting Moment - 1

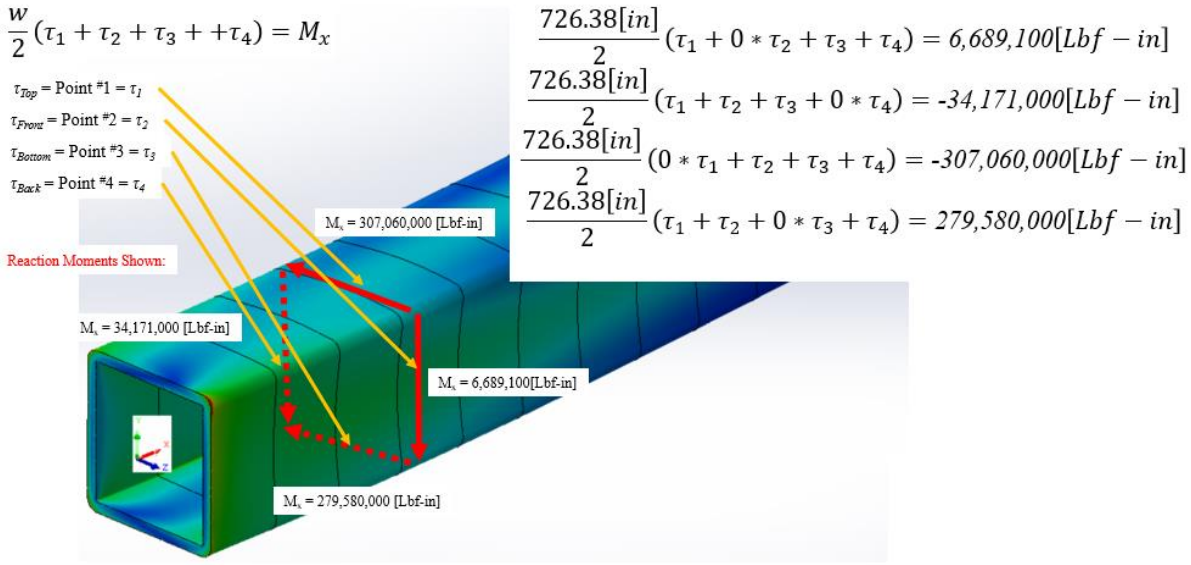

Figure 156: Calculation of Twisting Moment - 2

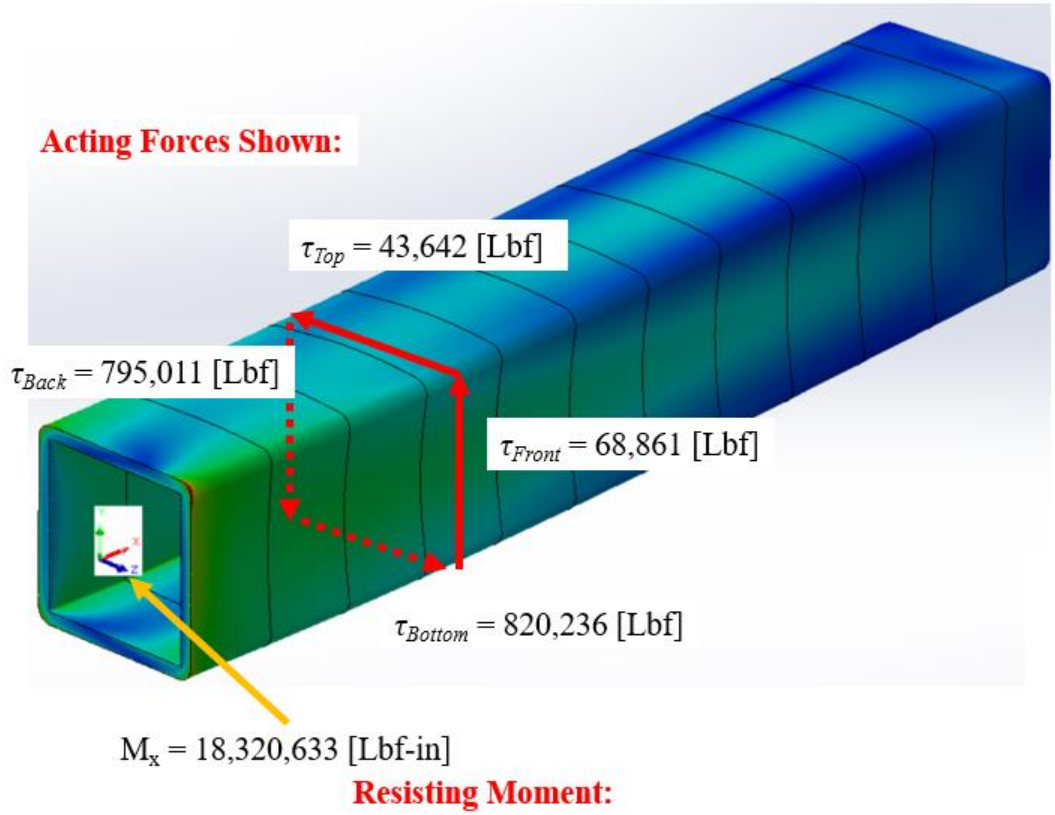

Figure 157: Calculation of Twisting Moment - 3

Solving the system of equations (Figure 156), the twisting moment is found.

Table 62: Maximum Moments Acting on an Arm

Moments of Action	[Lbf-in]	[N-m]
M_x	-18,320,633	-2,069,952
M_y	1,801,700,000	203,564,600
M_z	-94,303,000	-10,654,800

Note: Moments about the centroid of the arms' base.

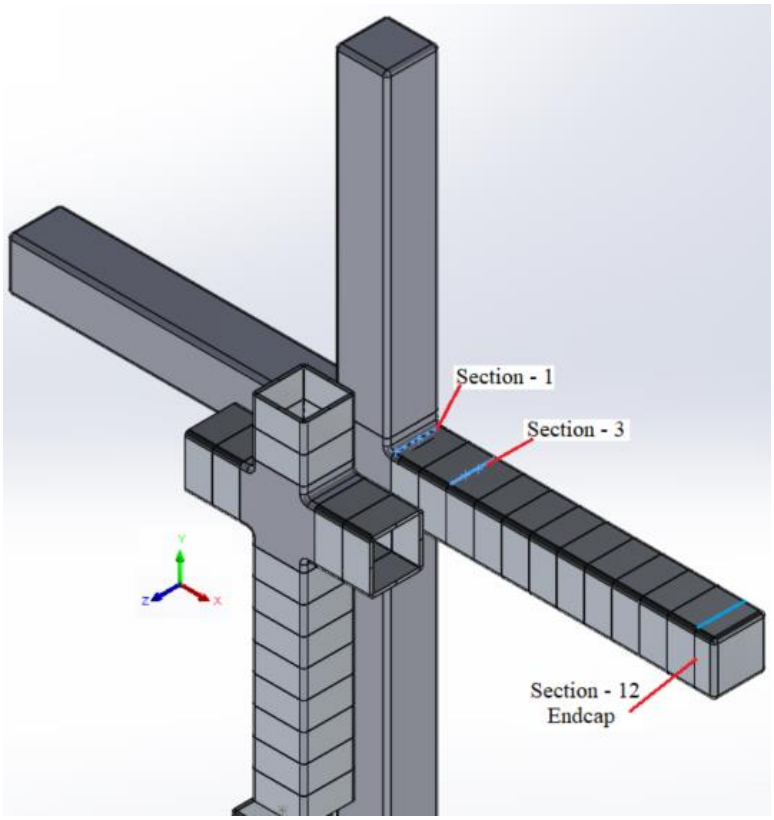

Figure 158: Arm Loading In-Body-Position

Table 63: Arm Loading, Sections 1 - 3

	Section - 1		Section - 2		Section - 3	
	[Lbf]	[N]	[Lbf]	[N]	[Lbf]	[N]
Fx	220,260	979,764	220,050	978,830	219,900	978,163

Fy	-56,252	-250,221	-62,425	-277,680	-65,387	-290,856
Fz	-807,630	-3,592,514	-720,980	-3,207,076	-644,930	-2,868,789

	[Lbf-in]	[N-m]	[Lbf-in]	[N-m]	[Lbf-in]	[N-m]
Mx	-18,320,633	-2,069,952	-20,919,167	-2,363,547	-21,384,300	-2,416,100
My	1,801,700,000	203,564,600	1,512,100,000	170,844,221	1,254,700,000	141,761,949
Mz	-94,303,000	-10,654,800	-72,396,000	-8,179,643	-47,591,000	-5,377,057

Note: The 3rd section was used in the "Intersection" segment.

Table 64: Arm Loading, Sections 4 - 6

	Section - 4		Section - 5		Section - 6	
	[Lbf]	[N]	[Lbf]	[N]	[Lbf]	[N]
Fx	219,760	977,540	219,680	977,185	219,550	976,606
Fy	-62,618	-278,539	-47,759	-212,442	-15,234	-67,764
Fz	-581,290	-2,585,705	-516,460	-2,297,327	-447,680	-1,991,378

	[Lbf-in]	[N-m]	[Lbf-in]	[N-m]	[Lbf-in]	[N-m]
Mx	-19,905,133	-2,248,976	-15,777,567	-1,782,624	-6,659,383	-752,409
My	1,023,000,000	115,583,386	815,390,000	92,126,625	633,050,000	71,524,988
Mz	-23,349,000	-2,638,081	-1,837,500	-207,609	10,454,000	1,181,142

Table 65: Arm Loading, Sections 7 - 9

	Section - 7		Section - 8		Section - 9	
	[Lbf]	[N]	[Lbf]	[N]	[Lbf]	[N]
Fx	219,410	975,984	219,420	976,028	219,410	975,984
Fy	1,084	4,820	9,178	40,825	11,238	49,989
Fz	-387,560	-1,723,951	-332,340	-1,478,321	-278,410	-1,238,428

	[Lbf-in]	[N-m]	[Lbf-in]	[N-m]	[Lbf-in]	[N-m]
Mx	-6,659,383	-752,409	-367,367	-41,507	-47,800	-5,401
My	475,320,000	53,703,905	339,190,000	38,323,293	223,660,000	25,270,166
Mz	12,442,000	1,405,756	10,373,000	1,171,991	6,275,500	709,036

Table 66: Arm Loading, Sections 10 - 12

	Section - 10		Section - 11		Section - 12	
	[Lbf]	[N]	[Lbf]	[N]	[Lbf]	[N]
Fx	219,390	975,895	219,260	975,316	219,220	975,138
Fy	7,445	33,115	3,367	14,979	1,644	7,311
Fz	-222,940	-991,686	-156,510	-696,191	-56,889	-253,055

	[Lbf-in]	[N-m]	[Lbf-in]	[N-m]	[Lbf-in]	[N-m]
Mx	319,867	36,140	288,733	32,622	289,807	32,744
My	128,660,000	14,536,616	56,168,000	6,346,127	14,695,000	1,660,311
Mz	2,640,700	298,359	691,390	78,117	-189,500	-21,411

Since Mz and My are perpendicular to one-another, only My will be considered for use in determining the area of inertia.

Since M_x is significant, torsional stress must be considered.

Eq - 31: Classical Mechanics, Bending Beam

$$\sigma_y = \frac{M_y c}{I} \approx \frac{M_y(c_{min})}{Ad^2} = \frac{M_y(363.2 - 54.4)}{A(363.2 - 54.4)^2}$$

Note: This equation considers the front and back: Does not include the top and bottom.
Where the yield stress (S_y) for T6061-T6 aluminum is 39,500[psi].

Eq - 32: Torsion Mechanics

$$\tau = G\theta = \frac{(T)(r)}{J} \approx \frac{M_x(\bar{c}_{min})}{I_y + I_z}$$

Where:
G = Shear Modulus
θ = Shear strain
T = Torsion
R = Lever-arm
J = Polar moment of inertia
M_x = Arm torsion, moment
$I_y = I_z$ = Inertia

Eq - 33: Torsion Mechanics, Maximum Shear Stress Theory

$$\tau_{Max} = \frac{\sigma_{ut}}{2} \approx \frac{M_x(\bar{c}_{min})}{I_y + I_z} = \frac{M_x(363.2 - 54.4)}{2A(363.2 - 54.4)^2}$$

Where the ultimate stress (S_{ut}) for T6061-T6 aluminum is 44,900[psi].

Eq - 34: Torsion Mechanics, Thin-walled Shells

$$\tau = \frac{\sigma_{ut}}{2} \approx \frac{T}{2At}$$

Eq - 35: Torsion Mechanics, Shear Flow

$$q = \tau t = \frac{T}{2A}$$

Utilizing the thin-wall mechanics of torsion, it becomes clear that the shell cannot hold the stresses at the base of the arm, so all of the stress must be held by the internal skeleton. As seen in Eq - 36, the minimum shell thickness required is 4.6 [in].

Eq - 36: Example of Thickness at Arm-base

$$t = \frac{T}{\sigma_{ut}At} = \frac{18{,}339{,}000[Lbf - in]}{44{,}900\left[\frac{Lbf}{in^2}\right]174.3[in^2]} = 2.343[in]$$

Eq - 37: Area Required to Resist Wind Loading w/o Correction Factor

$$A_{Wind} = \frac{1}{c}\left(\frac{M_y}{\sigma_y} + \frac{M_x}{\sigma_{ut}}\right) + \frac{F_x}{\sigma_y}$$

The body of the arm is very large and its stress distribution varies. Upon examining the nodal values across the front face of the arm it was found that the maximum stress was about 7.88[%] above the average stress; therefore 13[%] (8[%]+5[%]) will be added to the area calculation.

Eq - 38: Area Required to Resist Wind Loading with Correction Factor

$$Area_{Minimum-Wind\ for\ Arm} = 1.13\left(\left(\frac{M_y}{\sigma_y} + \frac{M_x}{\sigma_{ut}}\right)\frac{1}{c} + \frac{F_x}{\sigma_y}\right)$$

Table 67: Minimum Area Required to Resist Wind Loading

	Mx [Lbf-in]	My [Lbf-in]	Area Required due to Wind [in2]	Area per Support (x14)-per Side [in2]
Base (#1)	18,320,633	1,801,700,000	175	12.5
Segment 2	20,919,167	1,512,100,000	148	10.6
Segment 3	21,384,300	1,254,700,000	124	8.9
Segment 4	19,905,133	1,023,000,000	103	7.3
Segment 5	15,777,567	815,390,000	83	5.9
Segment 6	6,659,383	633,050,000	66	4.68
Segment 7	6,659,383	475,320,000	50.9	3.64
Segment 8	367,367	339,190,000	37.8	2.70
Segment 9	47,800	223,660,000	27.0	1.93
Segment 10	319,867	128,660,000	18.3	1.30
Segment 11	288,733	56,168,000	11.5	0.82
Segment 12	289,807	14,695,000	7.69	0.55
Maximum	21,384,300	1,801,700,000	175	12.5

Note: F_x was taken as a constant 220,260[Lbf].

Looking back to the previous hand calculations, about 33.6[in2] would achieve a factor of safety ~1.0[-]; this implies that about 21[in2] is used to resist the weight of the arm. Thus, approximately 60[%] of the area is used (at the base of the arm) to resist its weight: Therefore, minimizing the weight will greatly optimize the structure.

Though a further optimization may be made by separating the front-back with the top-bottom, this may cause manufacturing errors so it will be avoided. Here, all of the ribbing in a segment/section will have the same area.

B. The Head of the Glorious Cross

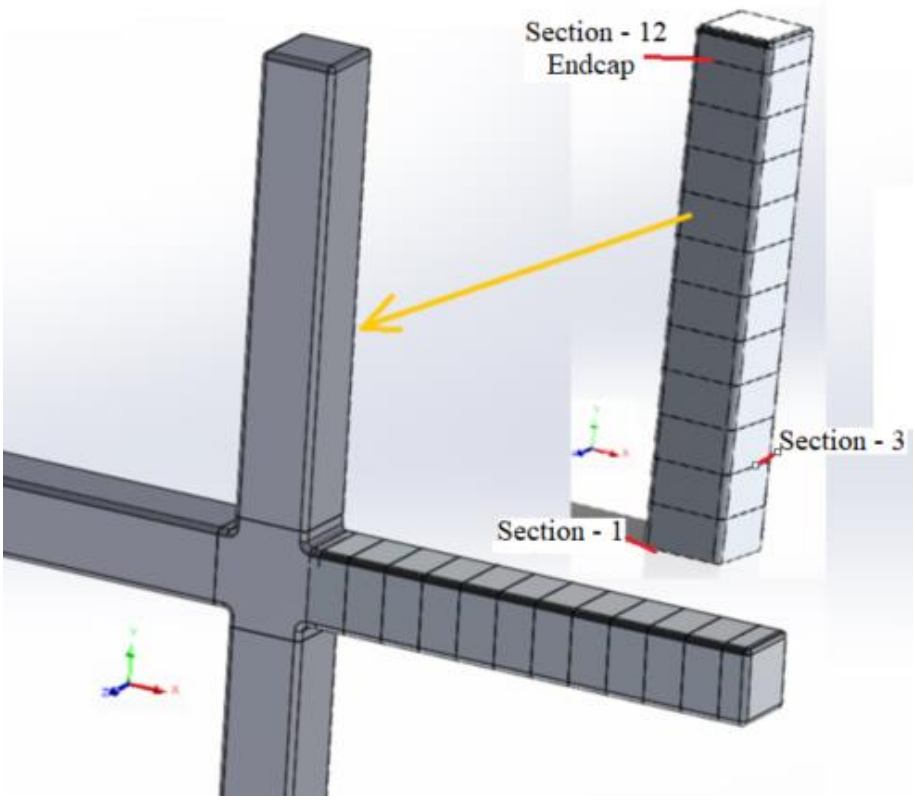

Figure 159: Head of the Glorious Cross

The flow pattern for the head of the Glorious Cross is similar to what was found on the arms; with an axis change (Fx goes to Fy). The CFD for the head was done at 12[C] with an air density of 1.226[kg/m3] and a speed of 61.33[m/s]. Section #1 is at the base, just after the radius; just as in the arm (Figure 158).

Table 68: Heads' Forces at its Base

Forces of Action	[Lbf]	[N]	Distance (dY) from Intersection [in]	Distance (dY) from Intersection [mm]
Fx	-86,585	-385,149	1,507	38,280
Fy	230,110	1,023,579	na	na
Fz	-925,420	-4,116,470	2,647	67,246

Table 69: Heads' Moments at its Base

Moments of Action	[Lbf-in]	[N-m]
Mx	-18,320,633	-2,069,952
My	1,801,700,000	203,564,600
Mz	-94,303,000	-10,654,800

Table 70: Head of Glorious Cross Loading, Sections 1 - 3

	Section - 1		Section - 2		Section - 3	
	[Lbf]	[N]	[Lbf]	[N]	[Lbf]	[N]
Fx	-86,585	-385,149	-63,267	-281,425	-38,892	-173,000
Fy	230,110	1,023,579	229,910	1,022,690	229,870	1,022,512
Fz	-925,420	-4,116,470	-852,020	-3,789,971	-771,760	-3,432,957

	[Lbf-in]	[N-m]	[Lbf-in]	[N-m]	[Lbf-in]	[N-m]
Mx	-2,063,600,000	-233,155,303	1,726,800,000	195,102,044	-1,419,800,000	-160,415,729
My	17,967,667	2,030,072	11,114,667	1,255,788	7,792,667	880,452
Mz	94,333,000	10,658,189	65,540,000	7,405,020	47,118,000	5,323,615

Note: The 3rd section was used in the "Intersection" segment.

Table 71: Head of Glorious Cross Loading, Sections 4 - 6

	Section - 4		Section - 5		Section - 6	
	[Lbf]	[N]	[Lbf]	[N]	[Lbf]	[N]
Fx	-33,889	-150,746	-39,032	-173,623	-35,556	-158,161
Fy	229,910	1,022,690	229,910	1,022,690	229,820	1,022,289
Fz	-689,880	-3,068,737	-598,320	-2,661,458	-508,430	-2,261,607

	[Lbf-in]	[N-m]	[Lbf-in]	[N-m]	[Lbf-in]	[N-m]
Mx	-1,143,800,000	-129,231,942	-899,600,000	-101,641,069	-690,980,000	-78,070,193
My	8,661,167	978,580	10,852,167	1,226,129	10,737,467	1,213,170
Mz	33,318,000	3,764,425	19,383,000	2,189,983	4,428,400	500,342

Table 72: Head of Glorious Cross Loading, Sections 7 - 9

	Section - 7		Section - 8		Section - 9	
	[Lbf]	[N]	[Lbf]	[N]	[Lbf]	[N]
Fx	-20,292	-90,263	-4,928	-21,919	12,104	53,841
Fy	229,590	1,021,266	229,490	1,020,822	229,490	1,020,822
Fz	-435,840	-1,938,711	-367,110	-1,632,985	-298,470	-1,327,660

	[Lbf-in]	[N-m]	[Lbf-in]	[N-m]	[Lbf-in]	[N-m]
Mx	-512,880,000	-57,947,612	-360,790,000	-40,763,763	-235,080,000	-26,560,452
My	7,525,533	850,270	4,672,500	527,921	598,367	67,606
Mz	-5,930,400	-670,045	-11,260,000	-1,272,208	-9,288,300	-1,049,436

Table 73: Head of Glorious Cross Loading, Sections 10 - 12

	Section - 10		Section - 11		Section - 12	
	[Lbf]	[N]	[Lbf]	[N]	[Lbf]	[N]
Fx	11,232	49,962	6,924	30,797	3,585	15,947
Fy	229,410	1,020,466	229,240	1,019,709	229,180	1,019,443
Fz	-234,890	-1,044,842	-163,610	-727,773	-59,732	-265,701

	[Lbf-in]	[N-m]	[Lbf-in]	[N-m]	[Lbf-in]	[N-m]
Mx	-134,160,000	-15,158,032	-58,121,000	-6,566,786	-14,750,000	-1,666,525
My	-739,067	-83,503	-616,033	-69,602	-694,837	-78,506
Mz	-4,585,600	-518,103	-1,175,800	-132,847	729,160	82,384

Eq - 39: Area Required to Resist Wind Loading with Correction Factor

$$Area_{Minimum-Wind\ for\ Head} = 1.13\left(\left(\frac{M_y}{\sigma_{ut}} + \frac{M_x}{\sigma_y}\right)\frac{1}{c} + \frac{F_x}{\sigma_y}\right)$$

Table 74: Minimum Area Required for Head of Glorious Cross

	My [Lbf-in]	Mx [Lbf-in]	Area Required due to Wind [in2]	Area per Support (x14)-per Side [in2]
Base (#1)	2,063,600,000	17,967,667	199.35	14.24
Segment 2	1,726,800,000	11,114,667	167.57	11.97
Segment 3	1,419,800,000	7,792,667	138.84	9.92
Segment 4	1,143,800,000	8,661,167	113.32	8.09
Segment 5	899,600,000	10,852,167	90.86	6.49
Segment 6	690,980,000	10,737,467	71.51	5.11
Segment 7	512,880,000	7,525,533	54.74	3.91
Segment 8	360,790,000	4,672,500	40.41	2.89
Segment 9	235,080,000	598,367	28.42	2.03
Segment 10	134,160,000	739,067	19.08	1.36
Segment 11	58,121,000	616,033	12.02	0.86
Segment 12	14,750,000	694,837	8.01	0.57
Maximum	2,063,600,000	17,967,667	199.35	14.24

Note: F_y was taken as a constant 230,110[Lbf].

C. The Intersection of the Glorious Cross:

The intersection of the arms and head will be considered for the next portion of analysis of the forces and moments. The CFD for the intersection was done at 12[C] with an air density of 1.226[kg/m3] and a speed of 60.74[m/s]. The velocity is the maximum (worst-case) velocity encountered in this segment.

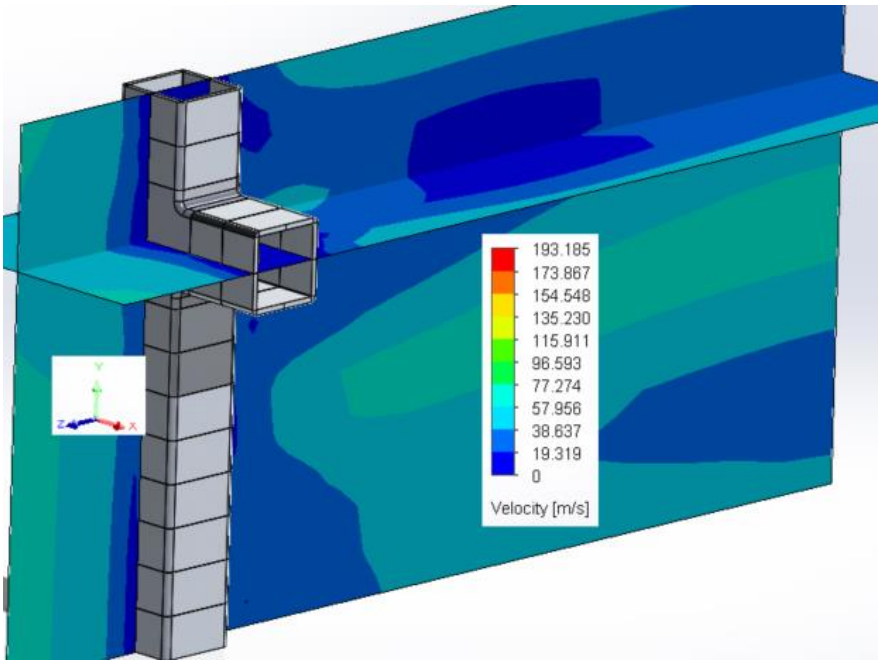

Figure 160: Intersection Segment, Velocity Profile

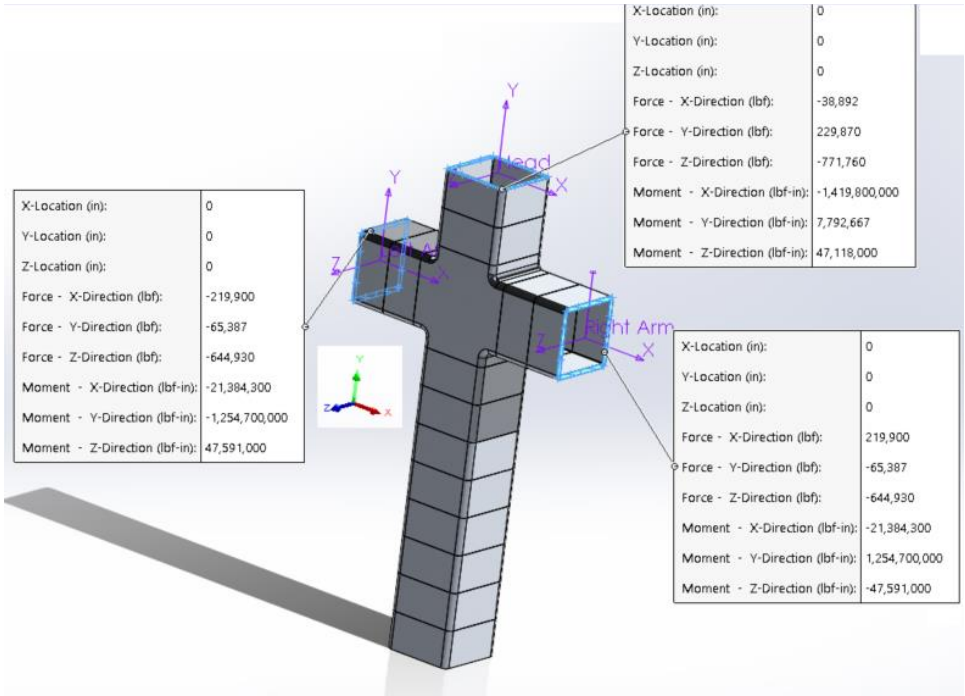

Figure 161: Intersection Segment, Loading Distribution, Modified for Worst-case

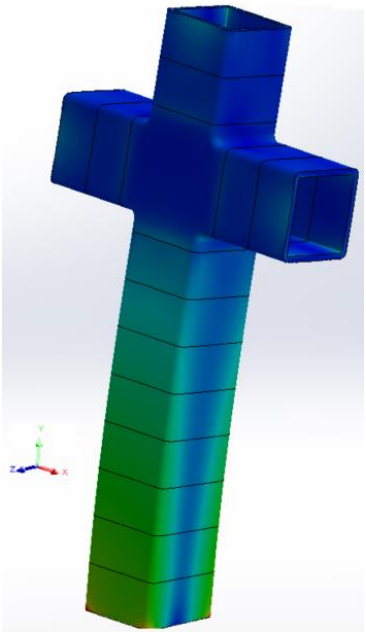

Figure 162: Intersection Segment Stress Color-map

The loadings represented here were modified to obtain the worst-case conditions. The M_x was modified so that both arms twist rearward.

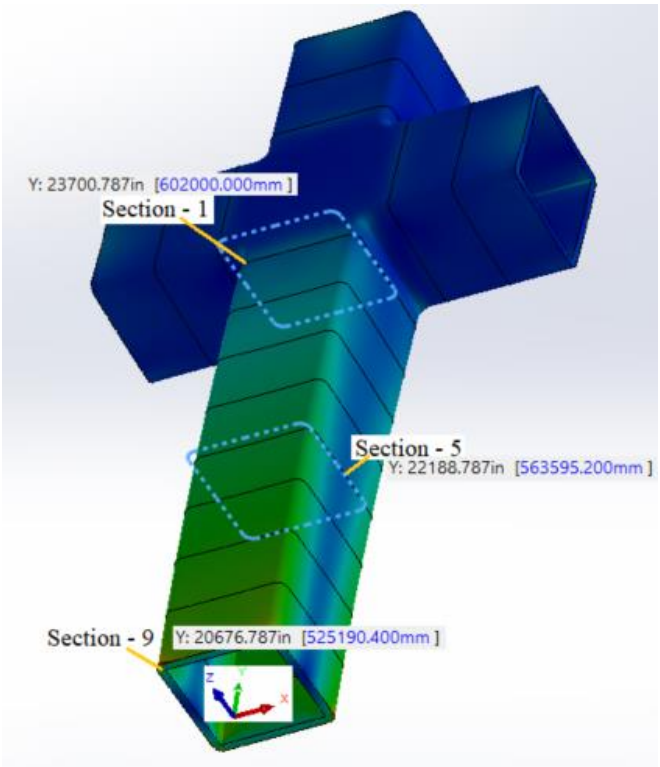

Figure 163: Segment-1 for the Intersection-Model

Table 75: Intersection Loading, Sections 1 - 3

	Section - 1		Section - 2		Section - 3	
	[Lbf]	[N]	[Lbf]	[N]	[Lbf]	[N]
Fx	-44,790	-199,236	-48,706	-216,655	-51,452	-228,870
Fy	113,650	505,540	111,830	497,444	110,180	490,105
Fz	-4,466,700	-19,868,855	-4,680,800	-20,821,219	-4,905,800	-21,822,068

	[Lbf-in]	[N-m]	[Lbf-in]	[N-m]	[Lbf-in]	[N-m]
Mx	-5,180,100,000	-585,272,235	-6,911,700,000	-780,916,606	-8,723,800,000	-985,656,247
My	-4,865,333	-549,708	-4,948,000	-559,048	-4,544,333	-513,440
Mz	131,260,000	14,830,377	148,980,000	16,832,466	167,820,000	18,961,099

Table 76: Intersection Loading, Sections 4 - 6

	Section - 4		Section - 5		Section - 6	
	[Lbf]	[N]	[Lbf]	[N]	[Lbf]	[N]
Fx	-53,699	-238,865	-57,915	-257,619	-63,027	-280,358
Fy	108,970	484,722	108,540	482,810	107,990	480,363
Fz	-5,118,400	-22,767,759	-5,308,600	-23,613,810	-5,479,200	-24,372,676

	[Lbf-in]	[N-m]	[Lbf-in]	[N-m]	[Lbf-in]	[N-m]
Mx	-10,620,000,000	-1,199,897,906	-12,591,000,000	-1,422,590,822	-14,632,000,000	-1,653,192,670
My	-4,473,000	-505,381	-4,419,000	-499,280	-4,943,667	-558,559
Mz	187,800,000	21,218,534	208,860,000	23,597,992	231,750,000	26,184,213

Table 77: Intersection Loading, Sections 7 - 9

	Section - 7		Section - 8		Section - 9	
	[Lbf]	[N]	[Lbf]	[N]	[Lbf]	[N]
Fx	-66,411	-295,411	-68,563	-304,983	-71,397	-317,589
Fy	107,630	478,762	107,700	479,073	107,870	479,829
Fz	-5,627,300	-25,031,457	-5,779,300	-25,707,586	-5,927,300	-26,365,922

	[Lbf-in]	[N-m]	[Lbf-in]	[N-m]	[Lbf-in]	[N-m]
Mx	-16,731,000,000	-1,890,347,632	-18,888,000,000	-2,134,055,710	-21,106,000,000	-2,384,655,856
My	-4,592,000	-518,826	-3,724,667	-420,830	-2,988,333	-337,636
Mz	256,070,000	28,932,002	281,450,000	31,799,554	307,940,000	34,792,520

Note: The 9th section was used in the "Middle" segment.

Table 78: Intersection Minimum Required Area

	My [Lbf-in]	Mx [Lbf-in]	Area Required due to Wind [in2]	Area per Support (x14)-per Side [in2]
Base (#1)	5,180,100,000	4,865,333	484	34.6
Segment 2	6,911,700,000	4,948,000	644	46.0
Segment 3	8,723,800,000	4,544,333	812	58.0
Segment 4	10,620,000,000	4,473,000	988	70.6
Segment 5	12,591,000,000	4,419,000	1,171	83.6
Segment 6	14,632,000,000	4,943,667	1,360	97.1
Segment 7	16,731,000,000	4,592,000	1,555	111
Segment 8	18,888,000,000	3,724,667	1,754	125
Segment 9	21,106,000,000	2,988,333	1,960	140
Maximum	21,106,000,000	4,948,000	1,960	140

D. Middle of Main Member of the Glorious Cross:

The CFD for the intersection was done at 12[C] with an air density of 1.226[kg/m3] and a speed of 59.90[m/s]. The velocity is the maximum (worst-case) velocity encountered in this segment.

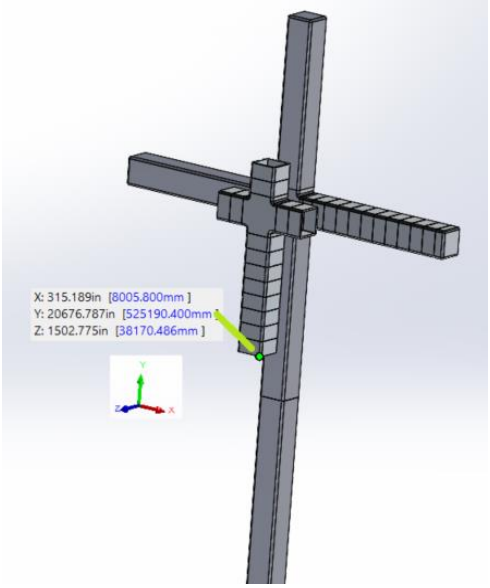

Figure 164: Middle of Main Member, Top Dimension

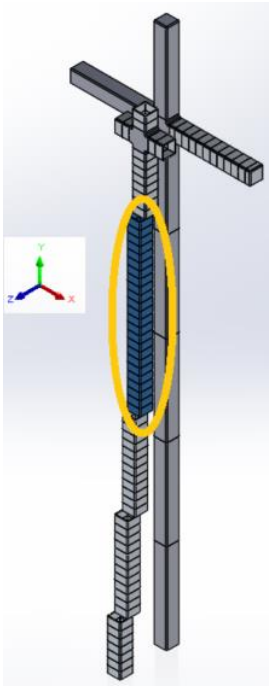

Figure 165: Middle of Main Member, Location

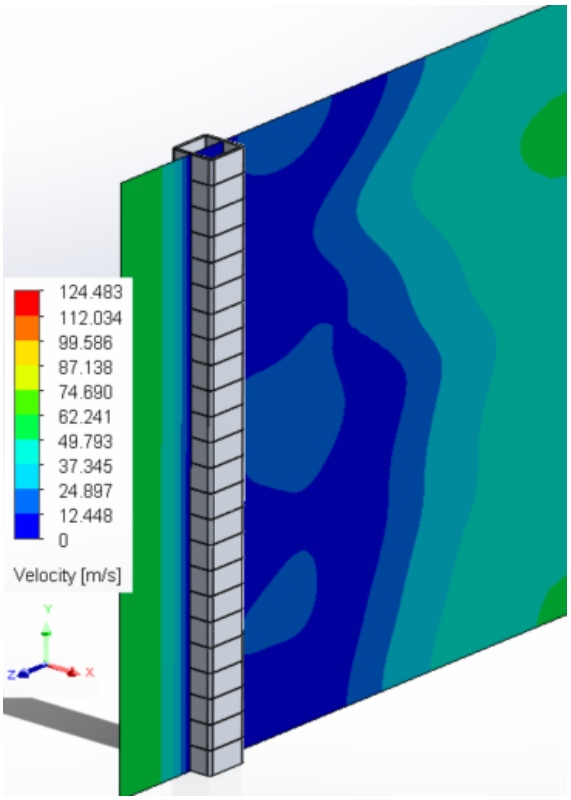

Figure 166: Velocity Profile-A of Middle-Main Member

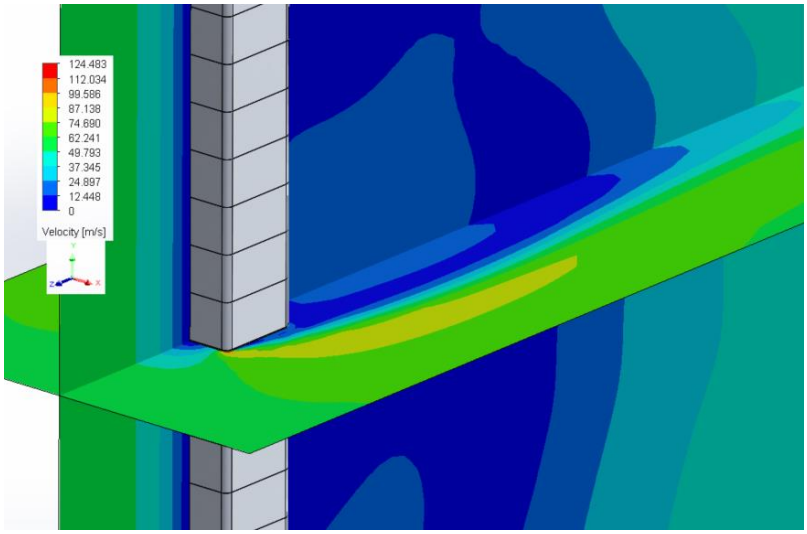

Figure 167: Velocity Profile-B of Middle-Main Member

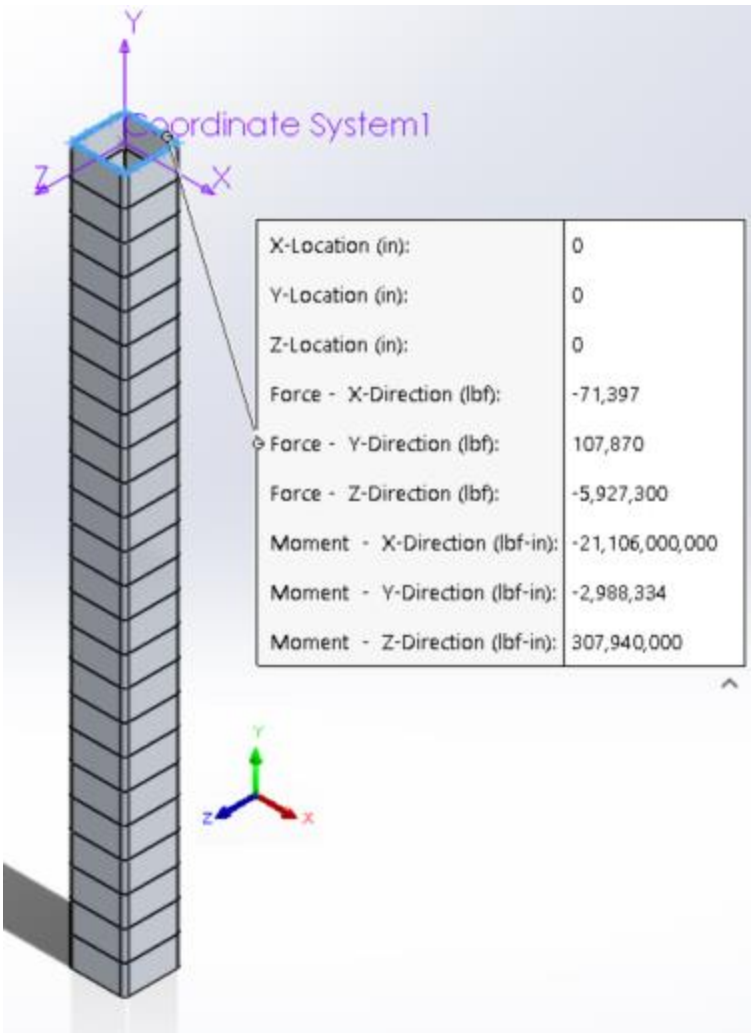

Figure 168: Upper Segment Loading of Middle-Main Member

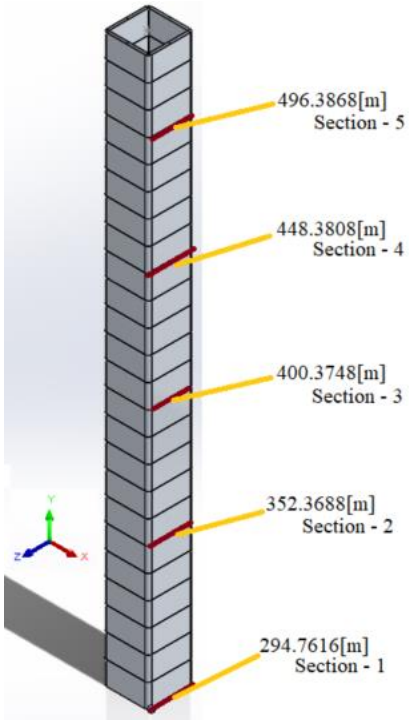

Figure 169: Segment Numbering of Middle-Main Member

Table 79: Middle-Main-Member, Loading, Sections 1 - 3

	Section - 1		Section - 2		Section - 3	
	[Lbf]	[N]	[Lbf]	[N]	[Lbf]	[N]
Fx	-259,160	-1,152,800	-198,820	-884,395	-123,570	-549,666
Fy	106,150	472,178	106,990	475,915	103,960	462,437
Fz	-8,378,300	-37,268,505	-7,750,600	-34,476,358	-7,248,200	-32,241,574

	[Lbf-in]	[N-m]	[Lbf-in]	[N-m]	[Lbf-in]	[N-m]
Mx	-85,990,000,000	-9,715,557,523	-67,683,000,000	-7,647,145,945	-53,508,000,000	-6,045,587,300
My	67,344,000	7,608,844	47,674,333	5,386,472	23,476,667	2,652,505
Mz	1,433,700,000	161,986,217	877,570,000	99,152,016	578,730,000	65,387,657

Note: The 1st section was used in the "290[m]" segment.

Table 80: Middle-Main-Member, Loading, Sections 4 - 5

	Section - 4		Section - 5		Section - 6	
	[Lbf]	[N]	[Lbf]	[N]	[Lbf]	[N]
Fx	-11,381	-50,625	-78,344	-348,491	na	na
Fy	103,830	461,858	104,930	466,752	na	na
Fz	-6,751,900	-30,033,923	-6,230,500	-27,714,622	na	na

	[Lbf-in]	[N-m]	[Lbf-in]	[N-m]	[Lbf-in]	[N-m]
Mx	-40,265,000,000	-4,549,330,430	-27,991,000,000	-3,162,555,770	na	na
My	2,739,633	309,537	8,944,000	1,010,535	na	na
Mz	459,600,000	51,927,785	395,860,000	44,726,138	na	na

Table 81: Middle-Main-Member Required Areas

	Mx [Lbf-in]	My [Lbf-in]	Area Required due to Wind [in2]	Area per Support (x14)-per Side [in2]
Base (#1)	85,990,000,000	67,344,000	7,980	570
Segment 2	67,683,000,000	47,674,333	6,281	449
Segment 3	53,508,000,000	23,476,667	4,965	355
Segment 4	40,265,000,000	2,739,633	3,736	267
Segment 5	27,991,000,000	8,944,000	2,599	186
Maximum	85,990,000,000	67,344,000	7,980	570

E. Mid-Lower I, @ 290[m]

The CFD for the intersection was done at 12[C] with an air density of 1.226[kg/m3] and a speed of 57.60[m/s]. The velocity is the maximum (worst-case) velocity encountered in this segment.

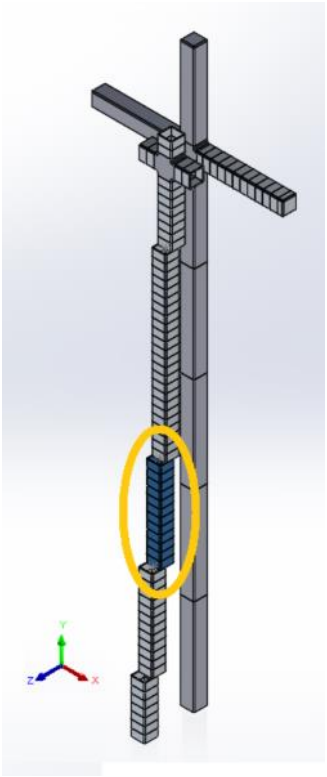

Figure 170: Mid-Lower Assembly Location - 1

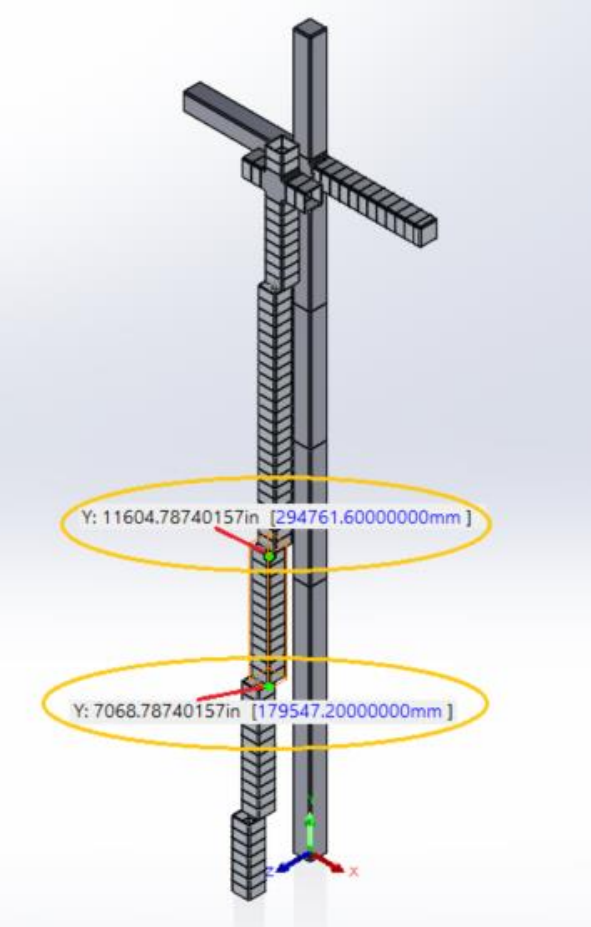

Figure 171: Mid-Lower Assembly Location - 2

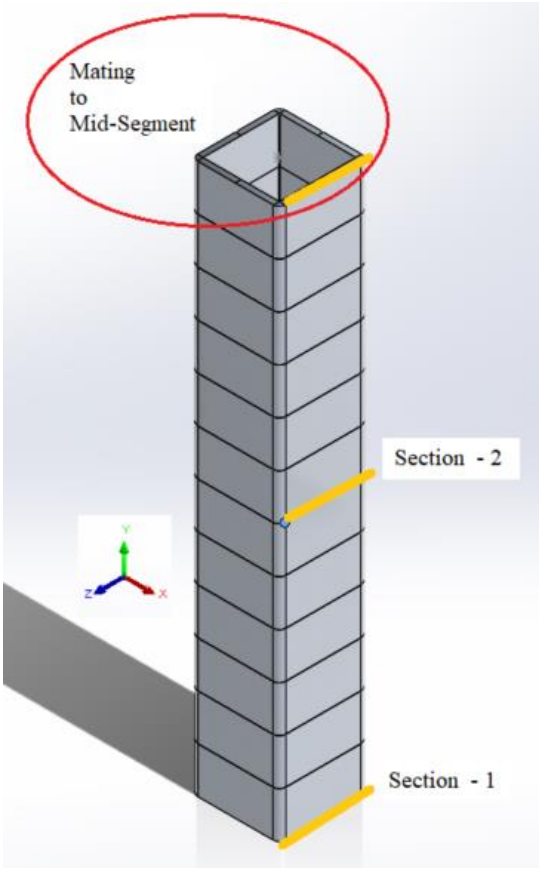

Figure 172: Mid-Lower Assembly Section Location/s

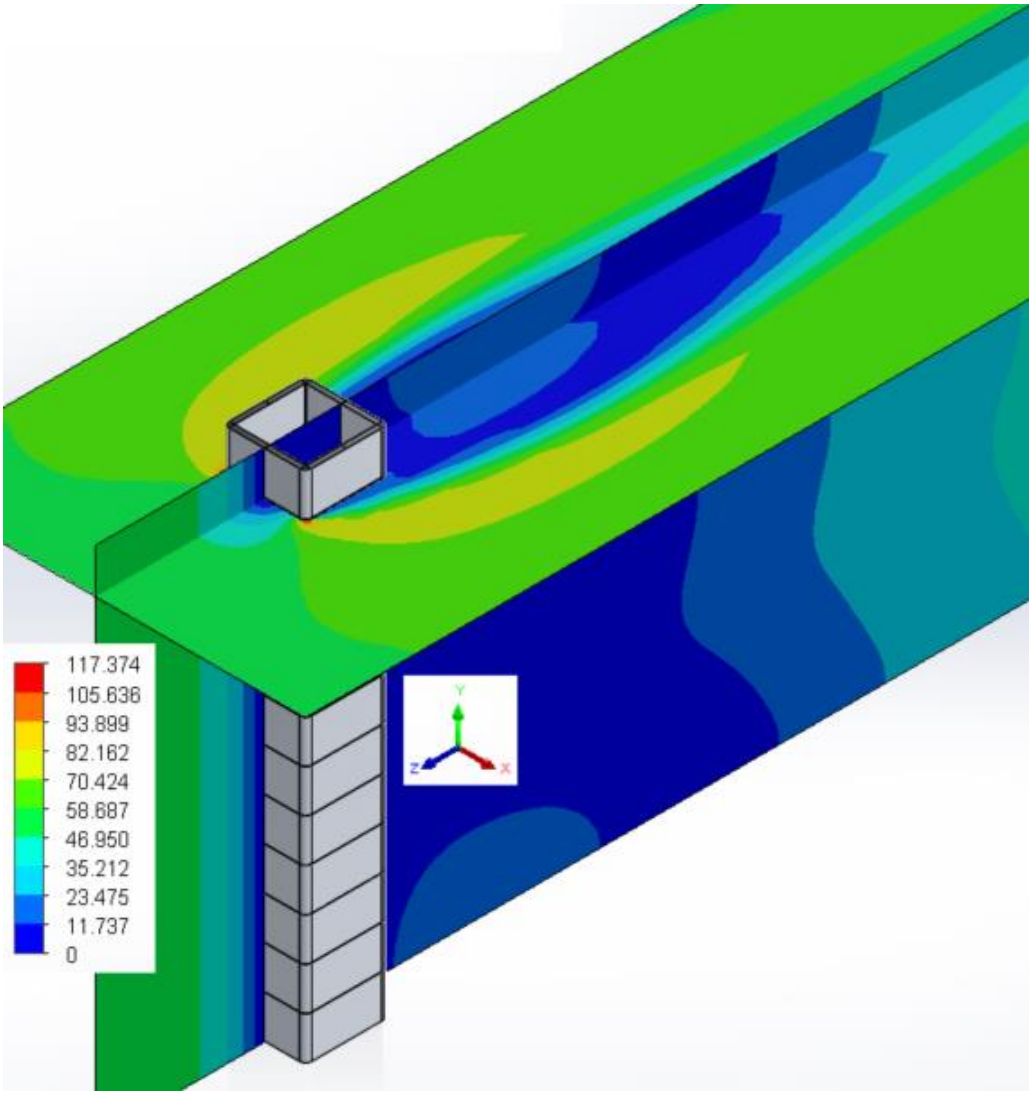

Figure 173: Mid-Lower Assembly CFD

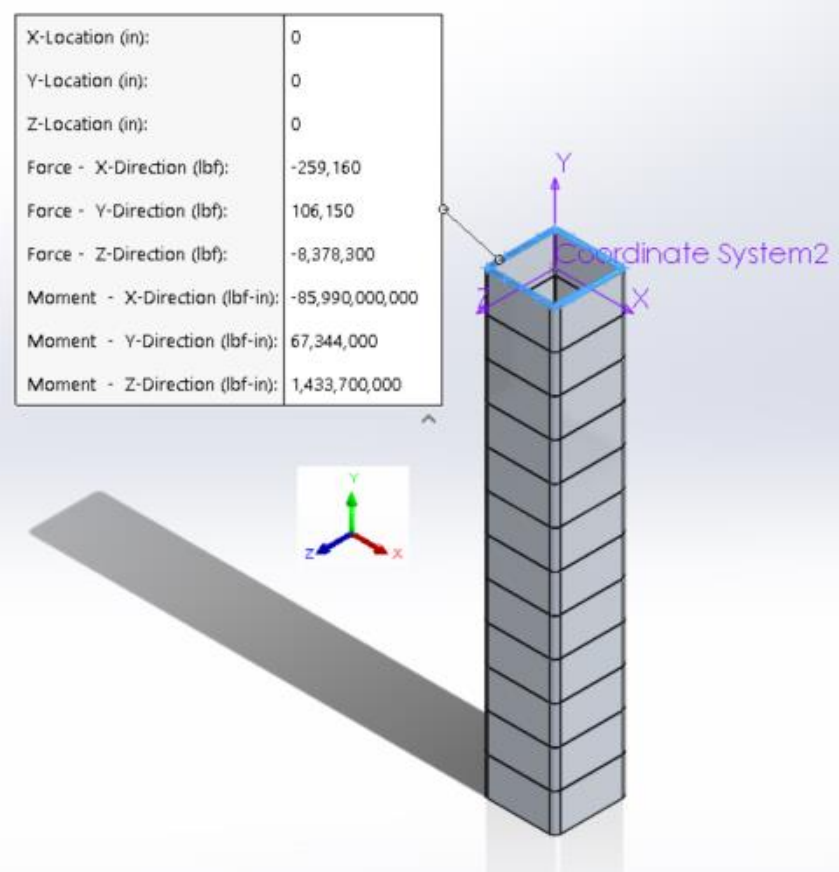

Figure 174: Mid-Lower Assembly, FEA Loading

Table 82: Middle-Lower I, Loading, Sections 1 & 2

	Section - 1		Section - 2		Section - 3	
	[Lbf]	[N]	[Lbf]	[N]	[Lbf]	[N]
Fx	-185,280	-824,166	-228,220	-1,015,172	na	na
Fy	108,660	483,343	103,260	459,323	na	na
Fz	-9,488,100	-42,205,137	-8,927,300	-39,710,576	na	na

	[Lbf-in]	[N-m]	[Lbf-in]	[N-m]	[Lbf-in]	[N-m]
Mx	-126,500,000,000	-14,292,569,213	-105,580,000,000	-11,928,928,518	na	na
My	-102,084,133	-11,533,949	-95,874,667	-10,832,374	na	na
Mz	2,471,300,000	279,219,180	2,023,100,000	228,579,421	na	na

Note: The 1st section was used in the "Mid-Lower II" segment.

Table 83: Middle-Lower I, Minimum Area Required

	My [Lbf-in]	Mx [Lbf-in]	Area Required due to Wind [in2]	Area per Support (x14)-per Side [in2]
Base (#1)	296,021,333	126,520,000,000	11,756	839.7
Segment 2	198,901,667	105,610,000,000	9,809	700.7

F. Mid-Lower II,

The CFD for the intersection was done at 12[C] with an air density of 1.226[kg/m3] and a speed of 55.52[m/s]. The velocity is the maximum (worst-case) velocity encountered in this segment.

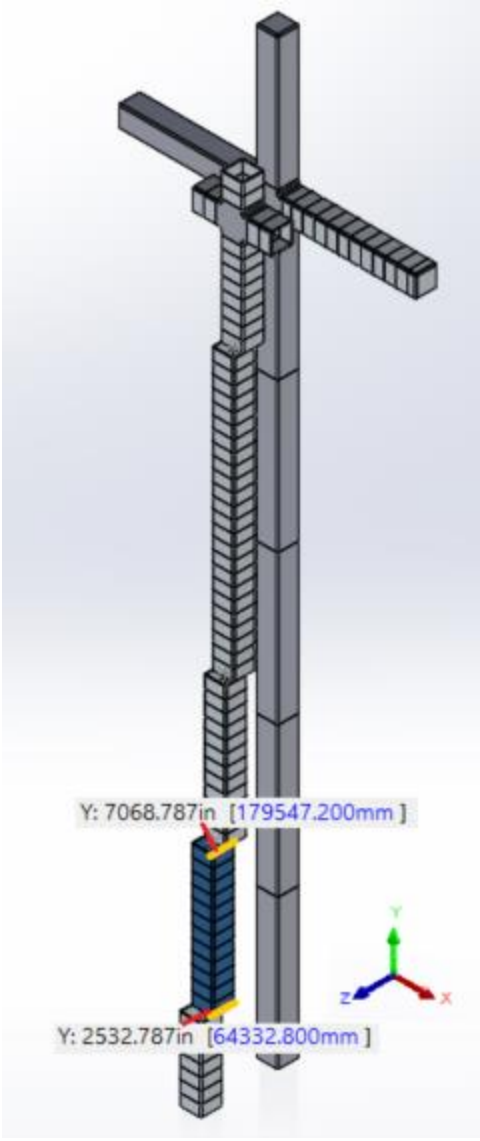

Figure 175: Mid-Lower II, Height

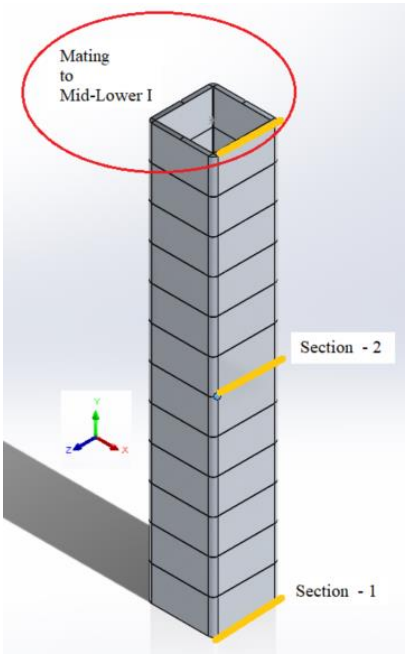

Figure 176: Mid-Lower II, Section Definition

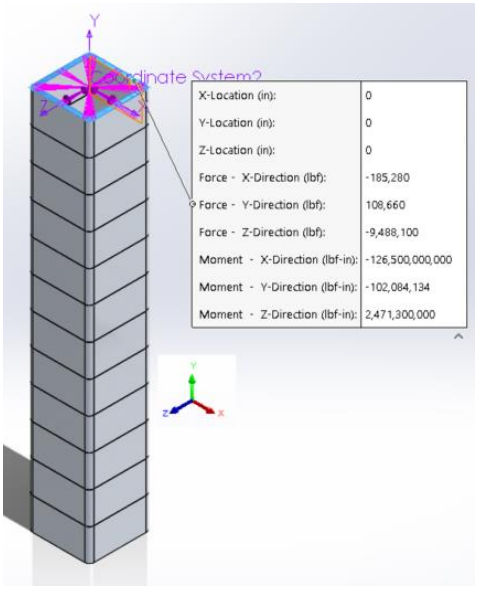

Figure 177: Mid-Lower II, Loading

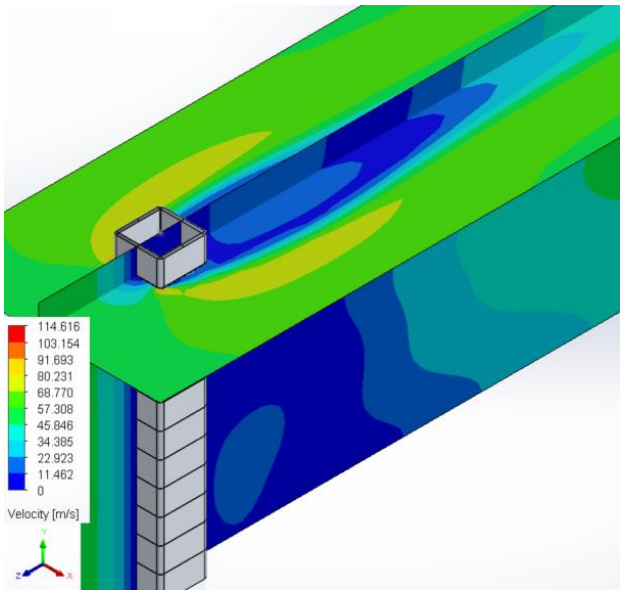

Figure 178: Mid-Lower II, Velocity Map

Table 84: Mid-Lower II, Section Action Loading

	Section - 1		Section - 2		Section - 3	
	[Lbf]	[N]	[Lbf]	[N]	[Lbf]	[N]
Fx	-185,280	-824,166	-228,220	-1,015,172	na	na
Fy	108,660	483,343	103,260	459,323	na	na
Fz	-9,488,100	-42,205,137	-8,927,300	-39,710,576	na	na

	[Lbf-in]	[N-m]	[Lbf-in]	[N-m]	[Lbf-in]	[N-m]
Mx	-126,500,000,000	-14,292,569,213	-105,580,000,000	-11,928,928,518	na	na
My	-102,084,133	-11,533,949	-95,874,667	-10,832,374	na	na
Mz	2,471,300,000	279,219,180	2,023,100,000	228,579,421	na	na

Note: The 1st section was used in the "Base" segment.

Table 85: Mid-Lower II, Minimum Area

	Mx [Lbf-in]	My [Lbf-in]	Area Required due to Wind [in2]	Area per Support (x14)-per Side [in2]
Base (#1)	126,500,000,000	102,084,133	11,738	838
Segment 2	105,580,000,000	95,874,667	9,798	700
Maximum	126,500,000,000	102,084,133	11,738	838

G. Mid-Lower III, The Base

The CFD for the intersection was done at 12[C] with an air density of 1.226[kg/m3] and a speed of 51.94[m/s]. The velocity is the maximum (worst-case) velocity encountered in this segment.

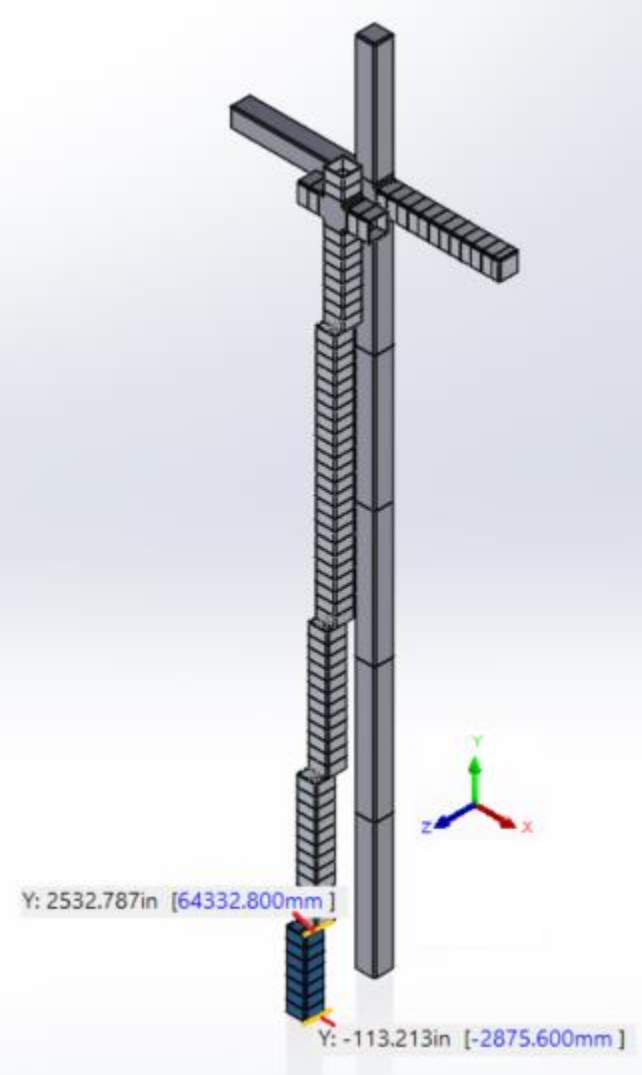

Figure 179: Base Segment Height

Note: The Model is about 9[ft] or 2.9[m] below ground Level.
Note: The CFD model did not account for ground affects; applying more load to the model.

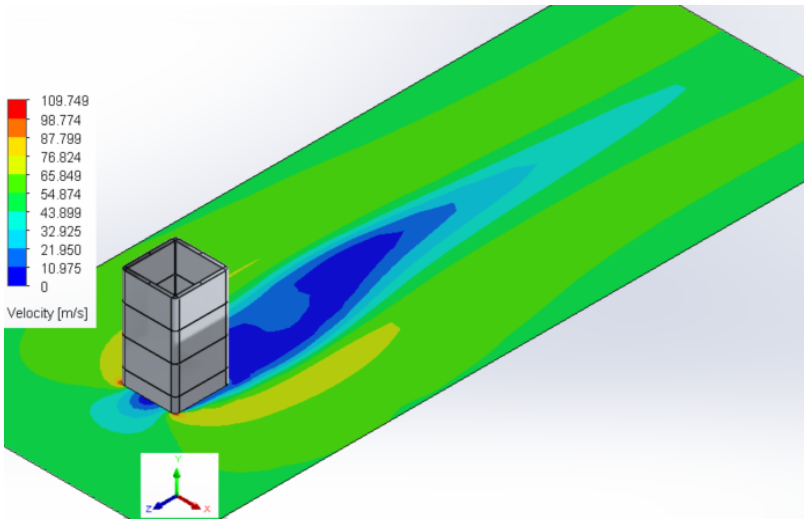

Figure 180: Base Segment Velocity Map - 1

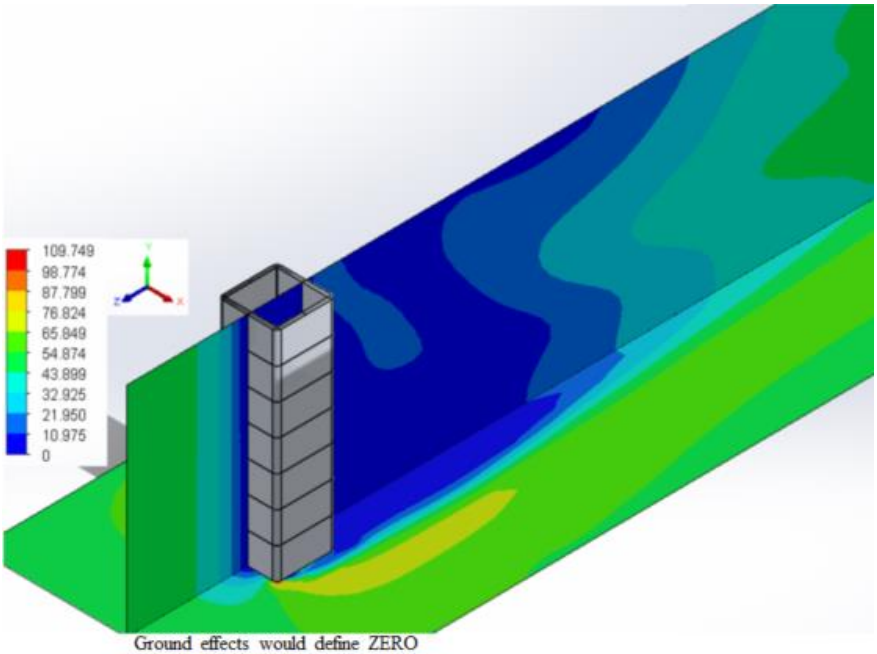

Ground effects would define ZERO velocity at ground level: Here, the velocity profile is constant.

Figure 181: Base Segment Velocity Map - 2

Table 86: Wind Loading at the Base of the Glorious Cross via CFD

	BASE of the Glorious Cross - V_z	
Wind "-Z"	[Lbf]	[N]
Fx	-197,880	-880,213
Fy	107,670	478,940
Fz	-11,070,000	-49,241,773

	[Lbf-in]	[N-m]
Mx	-200,520,000,000	-22,655,699,436
My	-200,915,000	-22,700,328
Mz	3,923,300,000	443,273,018

	[Lbf-ft]
Mx	-16,710,000,000
My	-16,742,917
Mz	326,941,667

Table 87: Base Ribbing Area Required

	Mx [Lbf-in]	My [Lbf-in]	Area Required due to Wind [in2]	Area per Support (x14)-per Side [in2]
Base (#1)	200,520,000,000	200,915,000	18,611	1,329

(for comparison purposes only)

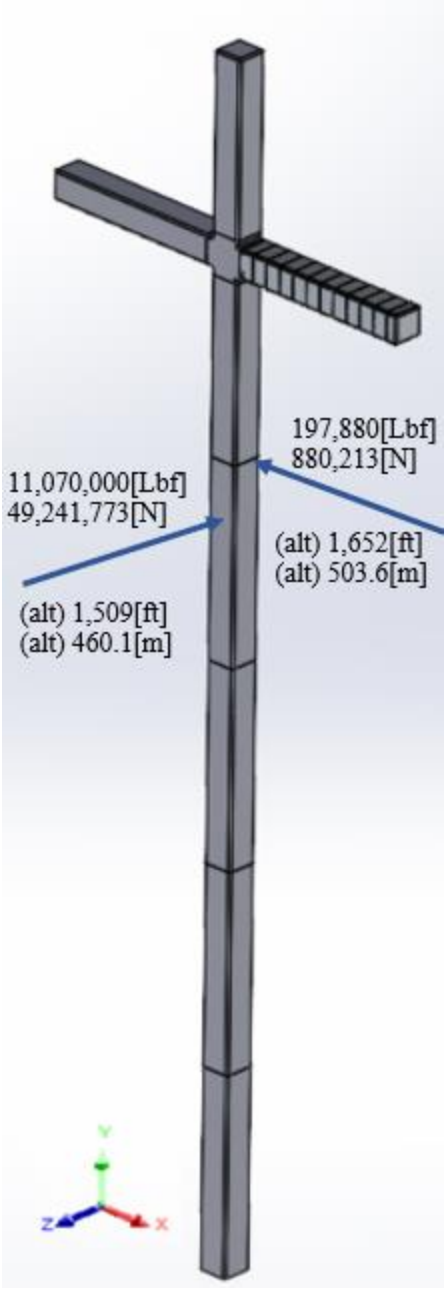

Figure 182: Main Forces and Lever-arms for Maximum Wind, with Velocity in "-Z"

The hand calculations represented in Table 5 are (x4) times greater than these CFD results. Since these CFD results comprise a 3-D model, (verses the 2-D model of the hand calculations) these CFD results will be used in the final design. Though the twisting moment, M_y, is $1/1000^{th}$ M_x or $1/20^{th}$ M_z, it will be carried forward as well.

The next case to consider is the maximum wind loading perpendicular to "Z." Utilizing the data in the previous case (wind in "-Z") and subtracting the arm-loadings, as worst-case conditions, the base loadings were obtained; for the maximum velocity in the "-X" direction (V_x).

To obtain the base loading with V_x (the previous has been w/r V_z) another CFD analysis was performed with the arm and Vx = -60.603[m/s] (density = 1.226[kg/m3]).

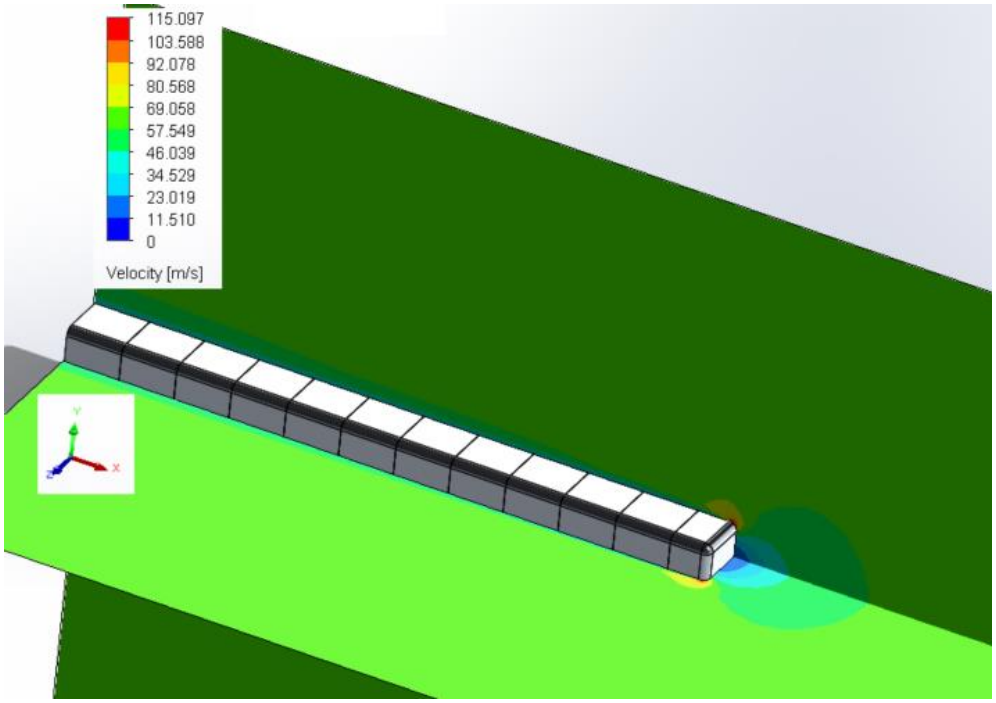

Figure 183: V_x = -60.603[m/s] on Arm

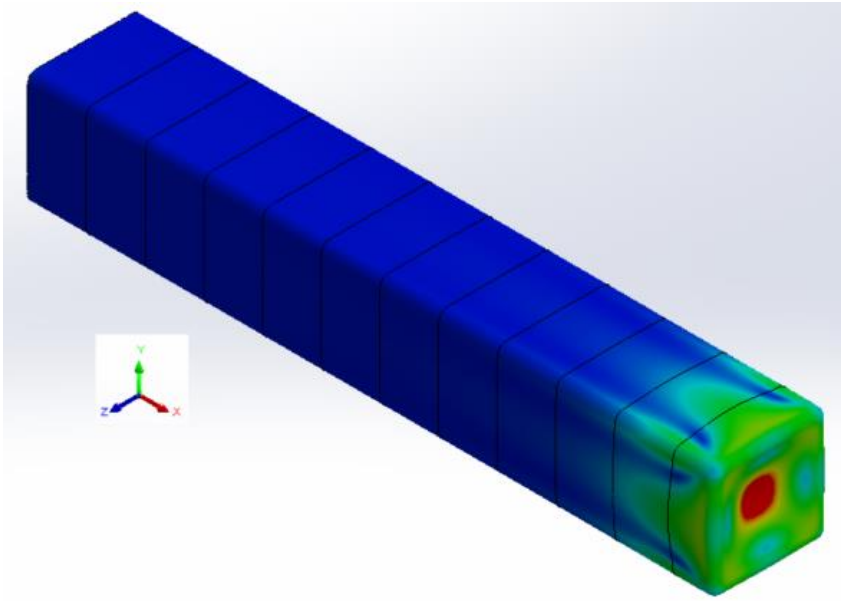

Figure 184: V_x Stress w/r Wind Loading

Table 88: Arms' Forces & Moments at its Base for V_x

	Section - 1	
	[Lbf]	[N]
Fx	-35,439	-157,640
Fy	-71	-316
Fz	410	1,824

	[Lbf-in]	[N-m]
Mx	6,467	731
My	-1,632,900	-184,493
Mz	-377,250	-42,623

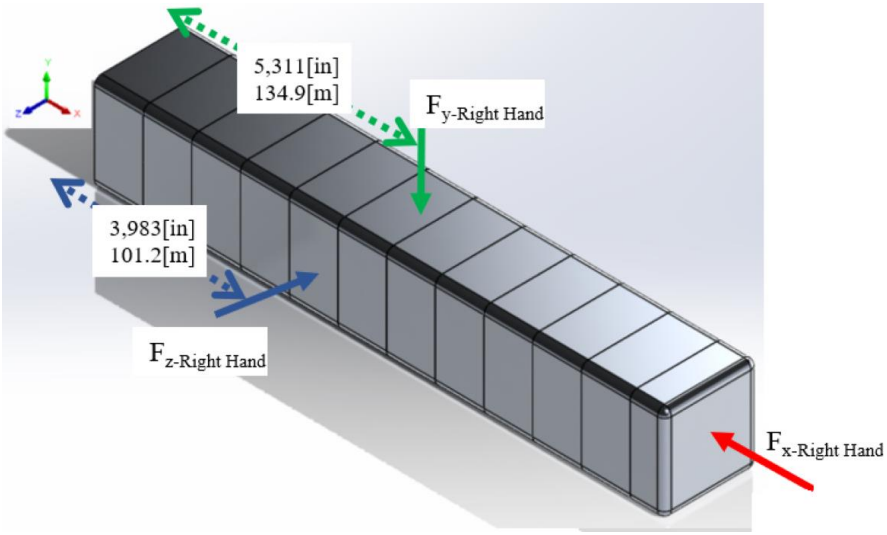

Figure 185: V_x Arm Loading Profile, Pictorial

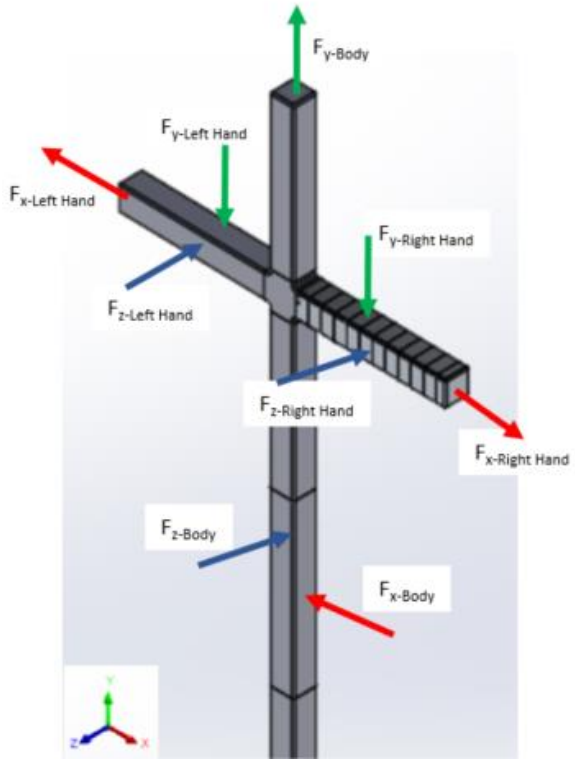

Figure 186: V_z Body & Arm Loading Profile

A manipulation of loadings was performed to obtain the loadings when the velocity in in the "-X" direction (V_x). Note that the arm force Fx and the moments My and Mz cancel-out with respect to the body loadings. After re-mapping the forces and moments from each condition, the V_x direction base loadings were obtained as seen in Table 89.

Table 89: Base Loadings with Velocity in "-X" (Vx) Direction

	BASE of the Glorious Cross - V_x	
Wind "-X"	[Lbf}	[N]
Fx	-9,490,179	-42,214,385
Fy	220,316	980,014
Fz	-198,700	-883,860

	[Lbf-in]	[N-m]
Mx	3,923,312,933	443,274,479
My	-204,180,800	-23,069,314
Mz	-161,409,603,768	-18,236,821,609

	[Lbf-ft]
Mx	326,942,744
My	-17,015,067
Mz	-13,450,800,314

dY - w/r Fz	19,745	[in]
dY - w/r Fx	17,008	[in]

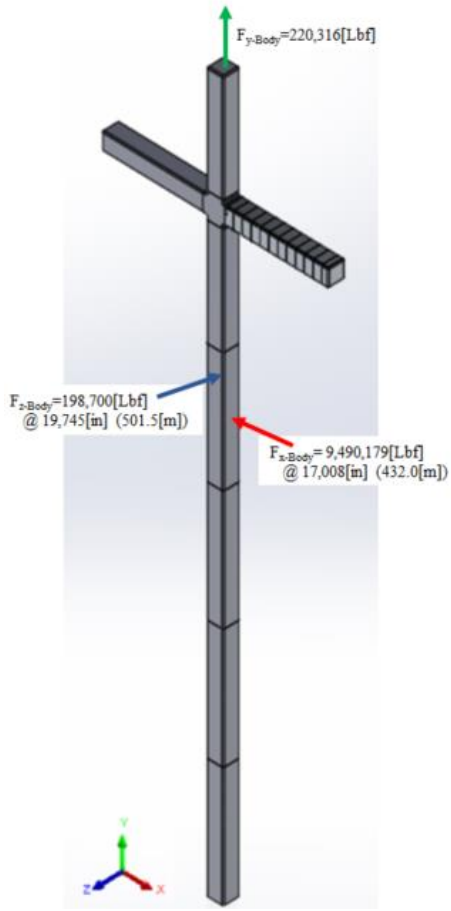

Figure 187: Main Forces and Lever-arms for Maximum Wind, with Velocity in "-X"

The worst-case conditions for wind in "-X" direction included carrying over higher than expected values from the previous case (wind in "-Z" direction) and adding forces together when appropriate; to achieve a higher absolute force ($|F_x| = |-f_{x\text{-}Case(A)}| + |f_{x\text{-}Case(B)}|$; then normal sign conventions were applied. The structural difference between the two cases is about 20[%]. Putting these conditions together, V_z and V_x, the design for the base of the Glorious Cross may commence.

VI. Design of Arm:

Since the basic design and its associated loadings have been determined, the drafting may commence. The 123[m] long arms are the most challenging portion of the design and is an excellent place to begin the design of the Glorious Cross.

The factor of safety (FS) is integral to the design and is determined from the endurance stress; this will be its minimum stress value. The next factor of 8[%] comes from the stress distribution over the arm due to the wind. Then 30[%] will be taken for calculation and manufacturing inconsistencies. Overall, 13,913[psi], represents a FS of 2.875[-] from the Sy (yield stress) of T6061-T6 aluminum. Carrying this safety factor to the rivets, the main rivet to be used will be a (3/8)" Mil-spec Brazier-head, made with 5056-H32 aluminum. Its design pull-out force is 653[Lbf] (2907[N]) and it design shear force is 1,152[Lbf] (5126[N]); and as seen in Figure 28, this rivet will be sufficient for the main panels.

The standard panel will be 47.125[in] square. The standard radiused panel will be 54.4[in] (radius). There will be 24[-] rivets with equal separation, approximately 1.966[in] on a straight length. The 54.4[in] radius will have 2.476[in] flat on both sides with the same spacing as the 47" square panels: The radius will have a spacing of about 1.965 [in].

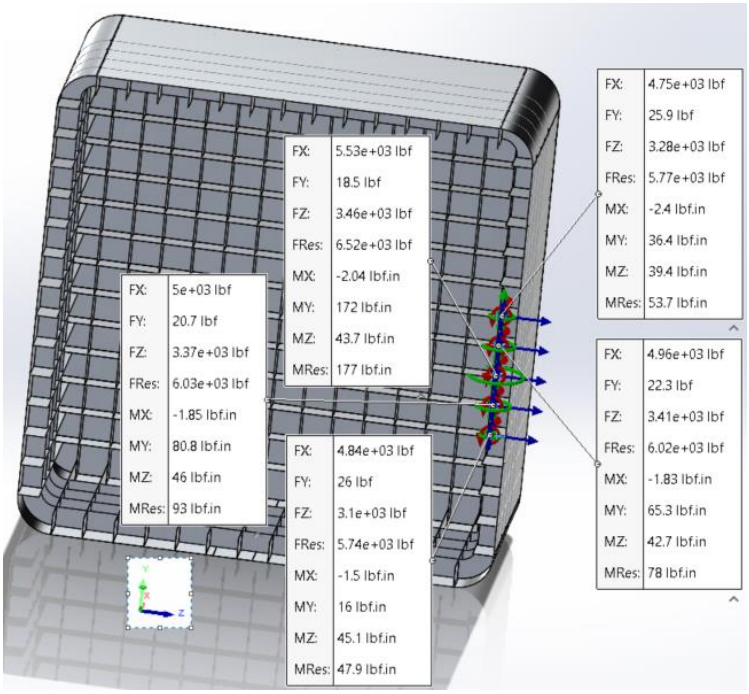

Figure 188: Endcap Maximum Member/Ribbing Load

The maximum shear loading is about 6,520[Lbf] (the simulated maximum stress was 12,200[psi]), requiring 6[-] rivets to meet the factor of safety. The pull-out force is about 31[Lbf] which is much less than 653[Lbf] and is covered by the 6 rivets for shear.

The FEA Endcap model was 321[in] in length and the CFD model was 212.6[in] in length. The flat length of the actual arms' Endcap will be 218.6[in] in length. Since the FEA model was larger than the actual arm, no load compensations are necessary. To calculate the required area with respect to the CFD model,6.18[%] will be added to loadings.

The drains will take into account the surface tension of a water droplet. It has been shown that the minimum capillary radius is less than the capillary length of 2.7[mm] or 0.106[in][4]. The wire mesh on the screens should be wider than 0.106[in].

Eq - 40: Minimum Capillary Radius/Length

$$R \ll L_C = \sqrt{\frac{72\left[\frac{J-m}{m^2}\right]}{\rho g}}$$

A. 12th Segment, Endcap, for Design:

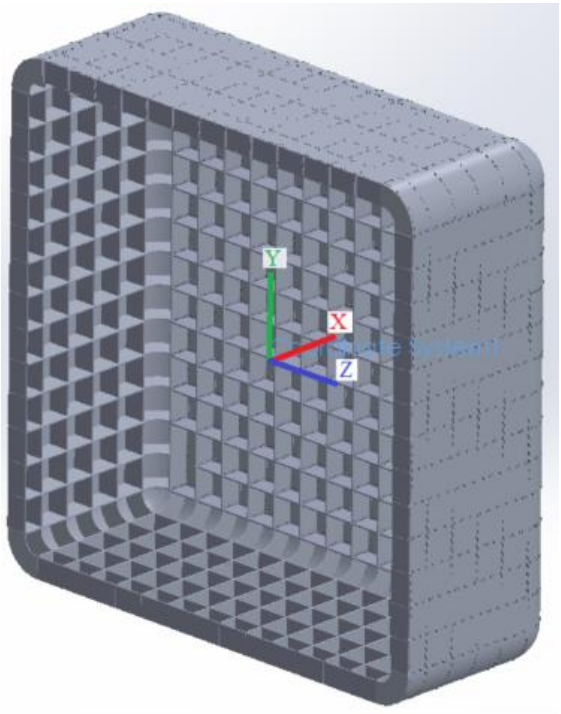

Figure 189: Endcap Design Model (12th Segment)

Table 90: 12th Segment, Endcap, Design Information

Total Weight	37,823	[Lbf]
	17,156	[kg]
CG from Centroid of Mating Surface/Plane		
X	181.9	[in]
Y	-1.3	[in]
Z	1.1	[in]

[Lbm-in2]	[kg-m2]

Ix - Twisting	4,571,761,649	1,337,879
Iy - Resist Wind in "Z"	3,849,007,224	1,126,372
Iz - Resist Weight	3,863,919,750	1,130,736

Riveted Ribbing (w/o Shell)

Ix - Twisting	33,247,020	[in4]
Iy - Resist Wind in "Z"	16,623,409	[in4]
Iz - Resist Weight	16,623,611	[in4]

Shell (w/o Riveted Ribbing)

Ix - Twisting	30,316,753	[in4]
Iy - Resist Wind in "Z"	15,158,376	[in4]
Iz - Resist Weight	15,158,376	[in4]

Table 91: 12th Segment, Endcap, Design Loading

	Wind Load	Gravity	TOTAL
	[Lbf]	[Lbf]	[Lbf]
Fx	232,678	0	232,678
Fy	1,744	46,423	48,167
Fz	-60,381	0	60,381
		[Lbf-in]	[Lbf-in]
Mx	307,598	0	307,598
My	15,597,119	0	15,597,119
Mz	-201,133	-8,443,658	8,644,792

Note: 8,600[Lbf] was added for construction equipment weight.

Table 92: 12th Segment, Endcap, Maximum Stresses

Ribbing Stress - w/o Shell/skin		
Stress due to Axial Load	1,099	[psi]
Sx - Twisting Stress	5	[psi]
Sy - Stress due to Wind	341	[psi]
Sz - Stress due to Gravity	189	[psi]
Total Stress	1,703	[psi]
Shell Stress - w/o Ribbing		

Stress due to Axial Load	1,324	[psi]
Sx - Twisting Stress	5	[psi]
Sy - Stress due to Wind	374	[psi]
Sz - Stress due to Gravity	207	[psi]
Total Stress	1,986	[psi]
Factor of Safety - FS	19.9	[-]

Since the FS is greater than 2.875[-] the design is accepted.

Eq - 41: Stress to Resist Axial Loading

$$\sigma_{Axial} = \frac{F_x}{A}$$

Eq - 42: Stress to Resist Torsion

$$\sigma_{x-Torsion} = \frac{(T)(r)}{J} = \frac{M_x(c\sqrt{2})}{I_y + I_z} = \frac{M_x(c\sqrt{2})}{I_x}$$

Note: Half the body width, c = 0.5*18.45[m] = 363[in].

Eq - 43: Stress to Resist the Wind

$$\sigma_{y-Wind} = \frac{M_y c}{I_y}$$

Eq - 44: Stress to Resist the Gravity

$$\sigma_{z-Gravity} = \frac{M_z c}{I_z}$$

Eq - 45: Maximum Stress on "Face"

$$\sigma_{Wind} = 1.08\big(Max[\sigma_{x-Torsion}] + Max[\sigma_{y-Wind}]\big) + \sigma_{Axial}$$

Eq - 46: Maximum Stress on "Upper/Lower"

$$\sigma_{Gravity} = 1.08\big(Max[\sigma_{x-Torsion}] + Max[\sigma_{z-Gravity}]\big) + \sigma_{Axial}$$

Eq - 47: Maximum Possible Stress: Total Stress

$$\sigma_{Total} = 1.13\left(Max[\sigma_{x-Torsion}] + Max[\sigma_{y-Wind}] + Max[\sigma_{z-Gravity}]\right) + \sigma_{Axial}$$

B. 11th Segment for Design:

The difference between the CFD mating surface and the design surface is about 7[in] so about 2[%] will be added to the loading.

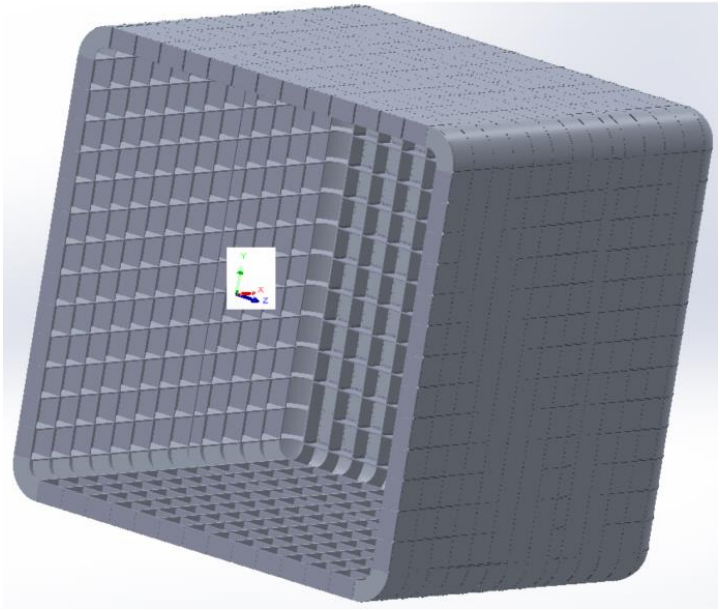

Figure 190: 11th & 12th Segment Design

Table 93: 11th Segment Design Information

Total Weight	67,238	[Lbf]
	30,499	[kg]
CG from Centroid of Mating Surface/Plane		
X	392.5	[in]
Y	-0.7	[in]
Z	0.4	[in]

	[Lbm-in2]	[kg-m2]
Ix - Twisting	9,303,933,272	2,722,701
Iy - Resist Wind in "Z"	18,066,088,119	5,286,855
Iz - Resist Weight	18,080,998,516	5,291,219

Riveted Ribbing (w/o Shell)

Ix - Twisting	33,247,020	[in4]
Iy - Resist Wind in "Z"	16,623,409	[in4]
Iz - Resist Weight	16,623,611	[in4]

Shell (w/o Riveted Ribbing)

Ix - Twisting	30,316,753	[in4]
Iy - Resist Wind in "Z"	15,158,376	[in4]
Iz - Resist Weight	15,158,376	[in4]

Table 94: 11th Segment, Design Loading

	Wind Load	Gravity	TOTAL
	[Lbf]	[Lbf]	[Lbf]
Fx	224,271	0	224,271
Fy	3,444	75,838	79,283
Fz	-160,087	0	160,087
	[Lbf-in]	[Lbf-in]	[Lbf-in]
Mx	295,332	0	295,332
My	57,451,561	0	57,451,561
Mz	707,190	-29,765,787	30,472,977

Note: 8,600[Lbf] was added for construction equipment weight.

Table 95: 11th Segment, Maximum Stresses

Ribbing Stress - w/o Shell/skin		
Stress due to Axial Load	1,059	[psi]
Sx - Twisting Stress	5	[psi]
Sy - Stress due to Wind	1,255	[psi]
Sz - Stress due to Gravity	666	[psi]
Total Stress	3,235	[psi]
Shell Stress - w/o Ribbing		
Stress due to Axial Load	1,276	[psi]
Sx - Twisting Stress	5	[psi]
Sy - Stress due to Wind	1,377	[psi]
Sz - Stress due to Gravity	730	[psi]
Total Stress	3,662	[psi]
Factor of Safety - FS	10.8	[-]

C. 10th Segment for Design:

The difference between the CFD mating surface and the design surface is about 5[in] so about 1.3[%] will be added to the loading.

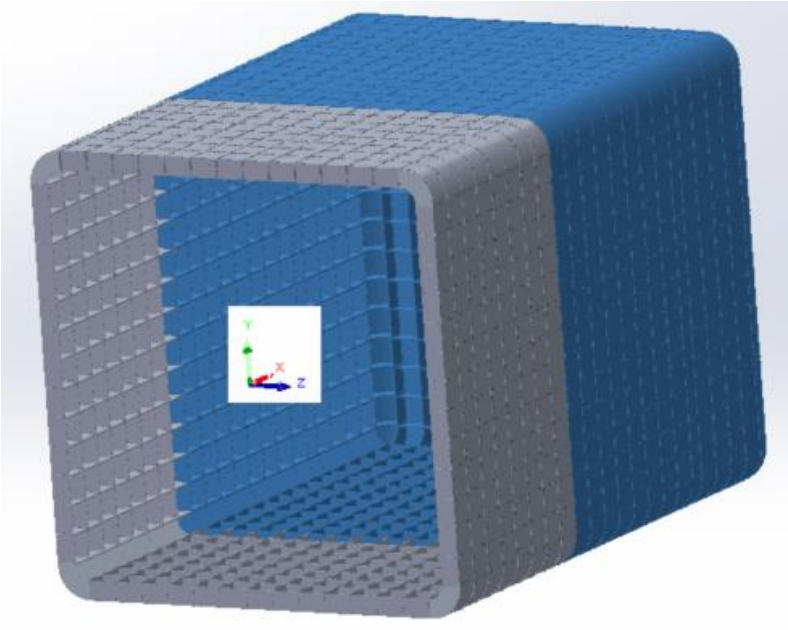

Figure 191: 10th Segment for Design

Table 96: 10th Segment Design Information

Total Weight	96,654	[Lbf]
	43,841	[kg]
CG from Centroid of Mating Surface/Plane		
X	589.6	[in]
Y	-0.5	[in]
Z	0.2	[in]

	[Lbm-in2]	[kg-m2]
Ix - Twisting	14,036,104,894	4,107,522
Iy - Resist Wind in "Z"	51,175,217,922	14,975,902
Iz - Resist Weight	51,190,126,191	14,980,265

Riveted Ribbing (w/o Shell)

Ix - Twisting	33,247,020	[in4]

Iy - Resist Wind in "Z"	16,623,409	[in4]
Iz - Resist Weight	16,623,611	[in4]

Shell (w/o Riveted Ribbing)

Ix - Twisting	30,316,753	[in4]
Iy - Resist Wind in "Z"	15,158,376	[in4]
Iz - Resist Weight	15,158,376	[in4]

Table 97: 10th Segment, Design Loading

	Wind Load	Gravity	TOTAL
	[Lbf]	[Lbf]	[Lbf]
Fx	222,141	0	222,141
Fy	7,538	105,254	112,792
Fz	-225,736	0	225,736
	[Lbf-in]	[Lbf-in]	[Lbf-in]
Mx	323,878	0	323,878
My	130,273,477	0	130,273,477
Mz	2,673,816	-62,061,876	64,735,692

Table 98: 10th Segment, Maximum Stresses

Ribbing Stress - w/o Shell/skin		
Stress due to Axial Load	1,049	[psi]
Sx - Twisting Stress	5	[psi]
Sy - Stress due to Wind	2,846	[psi]
Sz - Stress due to Gravity	1,414	[psi]
Total Stress	5,869	[psi]
Shell Stress - w/o Ribbing		
Stress due to Axial Load	1,264	[psi]
Sx - Twisting Stress	5	[psi]
Sy - Stress due to Wind	3,121	[psi]
Sz - Stress due to Gravity	1,551	[psi]
Total Stress	6,550	[psi]
Factor of Safety - FS	6.0	[-]

D. 9th Segment for Design:

The difference between the CFD mating surface and the design surface is about 5[in] so about 1.0[%] will be added to the loading.

Table 99: 9th Segment for Design

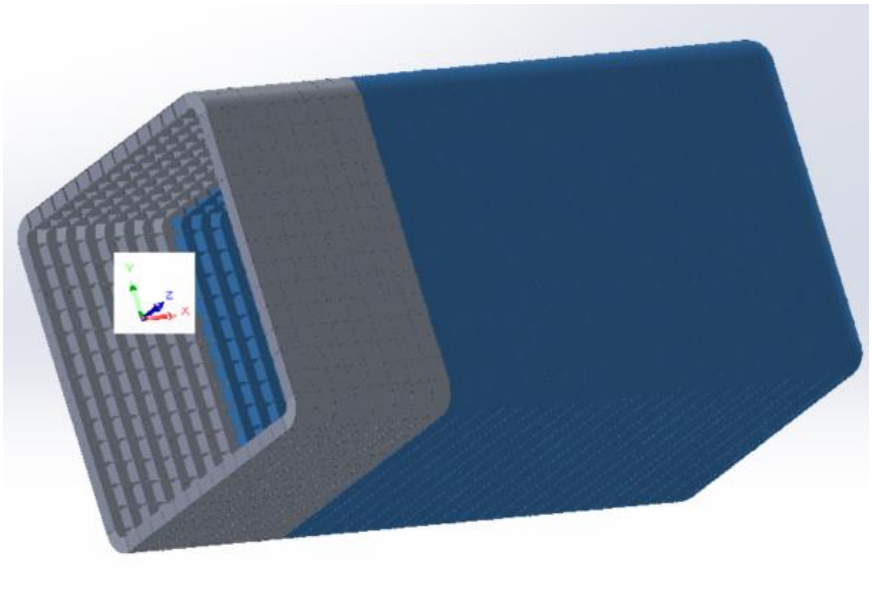

Table 100: 9th Segment Design Information

Total Weight	126,069	[Lbf]
	57,184	[kg]
CG from Centroid of Mating Surface/Plane		
X	782.8	[in]
Y	-0.4	[in]
Z	0.1	[in]

	[Lbm-in2]	[kg-m2]
Ix - Twisting	18,768,276,516	5,492,343
Iy - Resist Wind in "Z"	111,538,004,795	32,640,452
Iz - Resist Weight	111,552,910,936	32,644,814

Riveted Ribbing (w/o Shell)

Ix - Twisting	33,247,020	[in4]
Iy - Resist Wind in "Z"	16,623,409	[in4]
Iz - Resist Weight	16,623,611	[in4]

Shell (w/o Riveted Ribbing)

Ix - Twisting	30,316,753	[in4]
Iy - Resist Wind in "Z"	15,158,376	[in4]
Iz - Resist Weight	15,158,376	[in4]

Table 101: 9th Segment for Design Loading

	Wind Load	Gravity	TOTAL
	[Lbf]	[Lbf]	[Lbf]
Fx	221,112	0	221,112
Fy	11,325	134,669	145,995
Fz	-280,570	0	280,570
	[Lbf-in]	[Lbf-in]	[Lbf-in]
Mx	-48,171	0	48,171
My	225,394,952	0	225,394,952
Mz	6,324,180	-105,412,917	111,737,096

Table 102: 9th Segment Maximum Stresses

Ribbing Stress - w/o Shell/skin		
Stress due to Axial Load	1,044	[psi]
Sx - Twisting Stress	1	[psi]
Sy - Stress due to Wind	4,925	[psi]
Sz - Stress due to Gravity	2,441	[psi]
Total Stress	9,368	[psi]
Shell Stress - w/o Ribbing		
Stress due to Axial Load	1,258	[psi]
Sx - Twisting Stress	1	[psi]
Sy - Stress due to Wind	5,401	[psi]
Sz - Stress due to Gravity	2,677	[psi]
Total Stress	10,387	[psi]
Factor of Safety - FS	3.8	[-]

E. 8th Segment for Design:

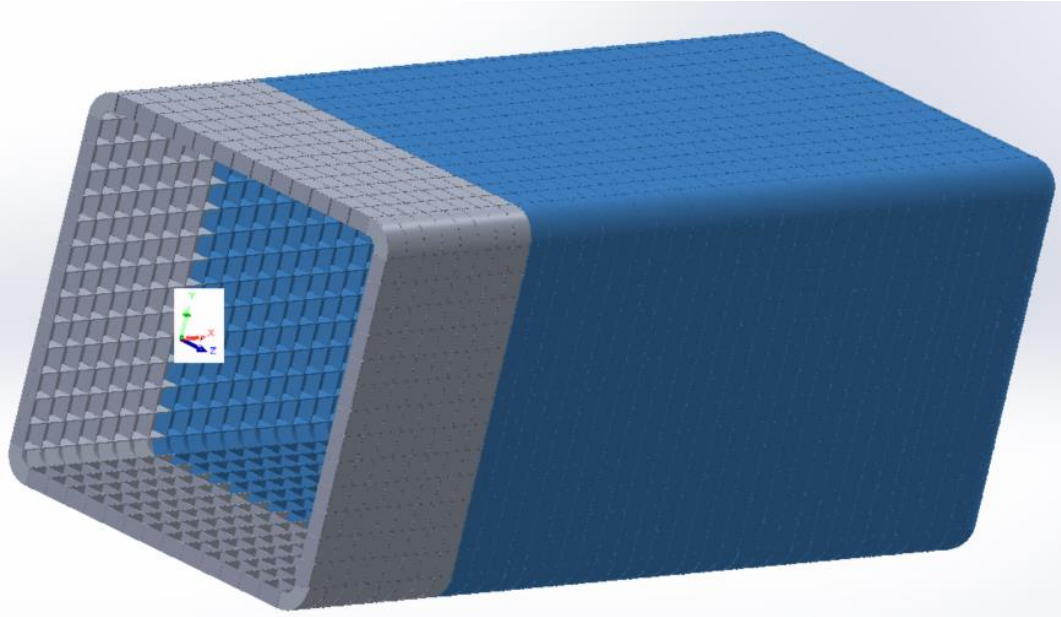

Figure 192: 8th Segment for Design

Table 103: 8th Segment Design Information

Total Weight	155,485	[Lbf]
	53,791	[kg]
CG from Centroid of Mating Surface/Plane		
X	974.1	[in]
Y	-0.8	[in]
Z	-0.1	[in]

	[Lbm-in2]	[kg-m2]
Ix - Twisting	18,359,665,016	5,372,768
Iy - Resist Wind in "Z"	156,728,084,961	45,864,865
Iz - Resist Weight	156,738,513,199	45,867,917

Structure

Ix - Twisting	63,563,773	[in4]
Iy - Resist Wind in "Z"	31,781,786	[in4]
Iz - Resist Weight	31,781,987	[in4]

Table 104: 8th Segment for Design Loading

	Wind Load	Gravity	TOTAL
	[Lbf]	[Lbf]	[Lbf]
Fx	220,762	0	220,762
Fy	9,234	164,085	173,319
Fz	-334,373	0	334,373
	[Lbf-in]	[Lbf-in]	[Lbf-in]
Mx	-369,614	0	369,614
My	341,264,941	0	341,264,941
Mz	10,436,455	-159,838,612	170,275,067

Table 105: 8th Segment Maximum Stresses

Maximum Structural Stress		
Stress due to Axial Load	570	[psi]
Sx - Twisting Stress	3	[psi]
Sy - Stress due to Wind	3,900	[psi]
Sz - Stress due to Gravity	1,946	[psi]
Total Stress	7,179	[psi]
Factor of Safety - FS	5.5	[-]

F. 7th Segment for Design:

The 7th segment must resist higher loads, so the point-area method for aircraft design will be employed. The coil-beam will be used to minimize costs and maximize shear-flow. One item of note with respect to the coil-beam, seen in Figure 193 with an inline applied load, the flange bends-in upon itself; not away. Thus, the main loading/s will cause the coil-beam to bend inward: This means the mating coil-beams should wrap around the standard panel coil beams.

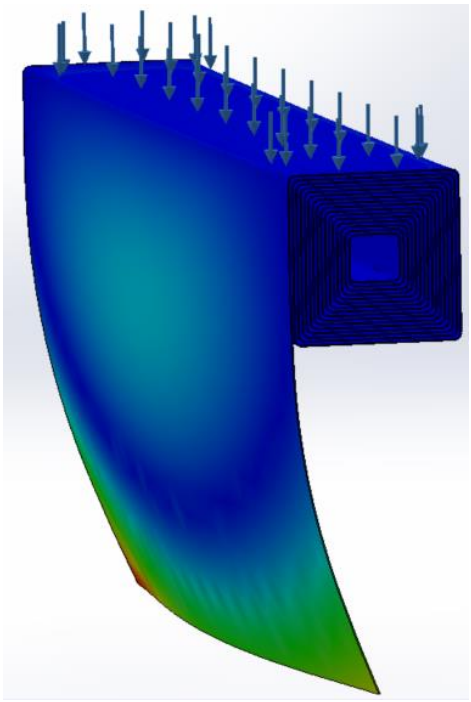

Figure 193: Coil-beam, Flange Inward Bend w/ Parallel Loading

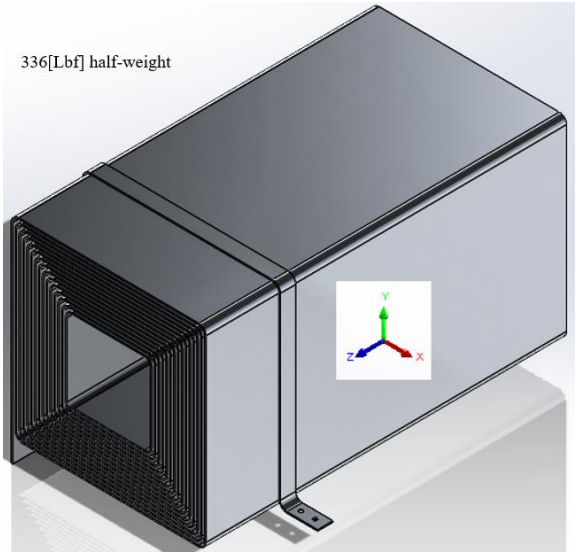

Figure 194: Coil-beam Simulated Full Weight on Bracket

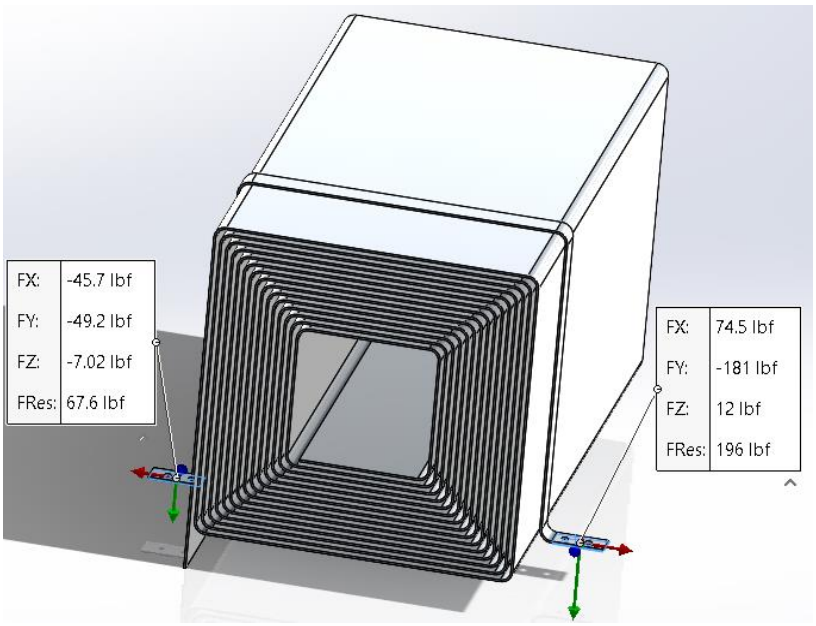

Figure 195: Bracket Reaction Loading with 10[%] Gravity (425[in/s2])

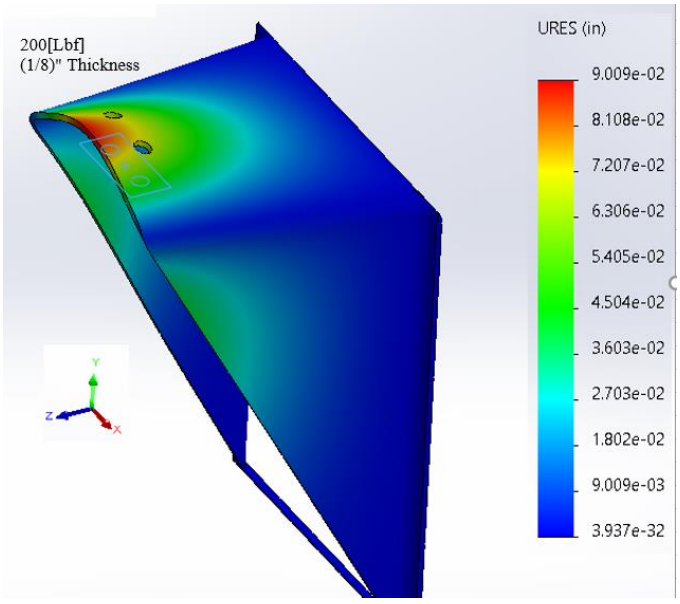

Figure 196: Deflection of Rib-supports for Coil-beam

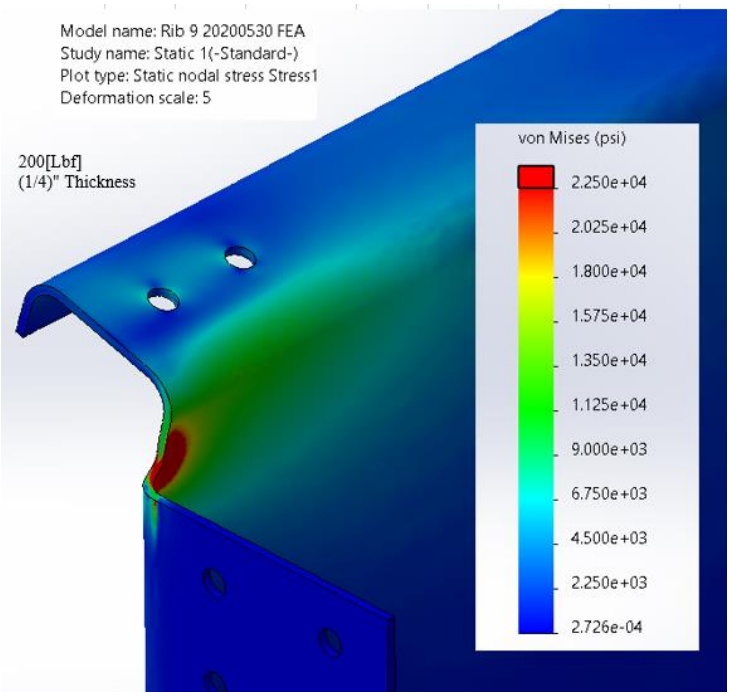

Figure 197: Stress on Panel-ribs Due to Coil-beam Weight

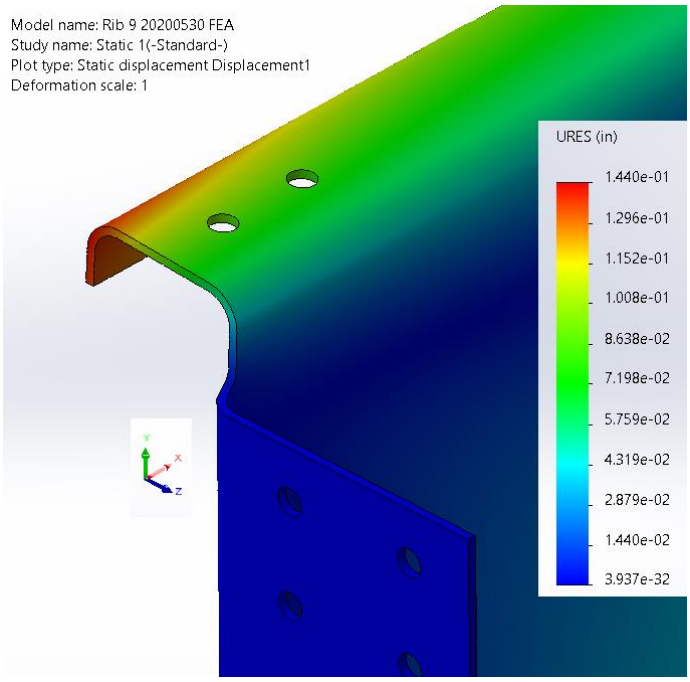

Figure 198: Panel-rib Deflection Due to Coil-beam Weight

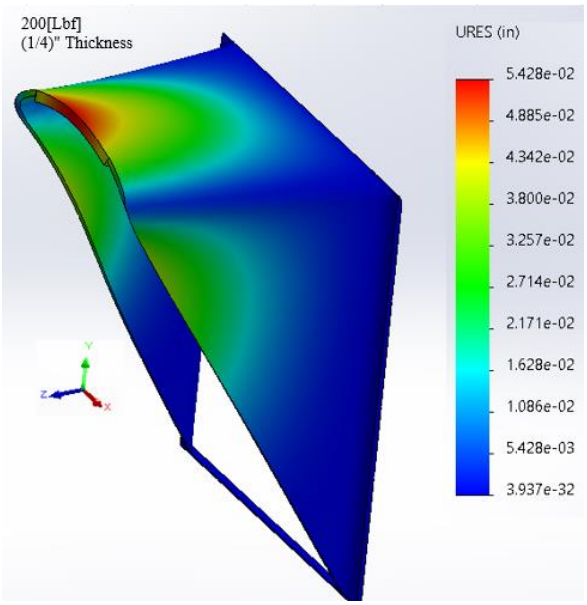

Figure 199: Deflection w/ (1/4)" thick, on Radial-rib Support Due to the Coil-beam Weight

The average maximum deflection on the panel-rib, due to the weight of the coil is about 0.09[in]; this corresponds to the maximum deflection of the radial-rib. Adding a (1/8)" support to the radial rib will reduce the deflection by about 0.035[in]: However, the panel-rib deflection with the added support remains about 0.09[in] so the support will not be added at this time.

When the coil-beam (x1) weight reaches 205[Lbf] supports will be added. The stresses with the brackets under maximum loading are represented in Figure 200, Figure 201 and Figure 202.

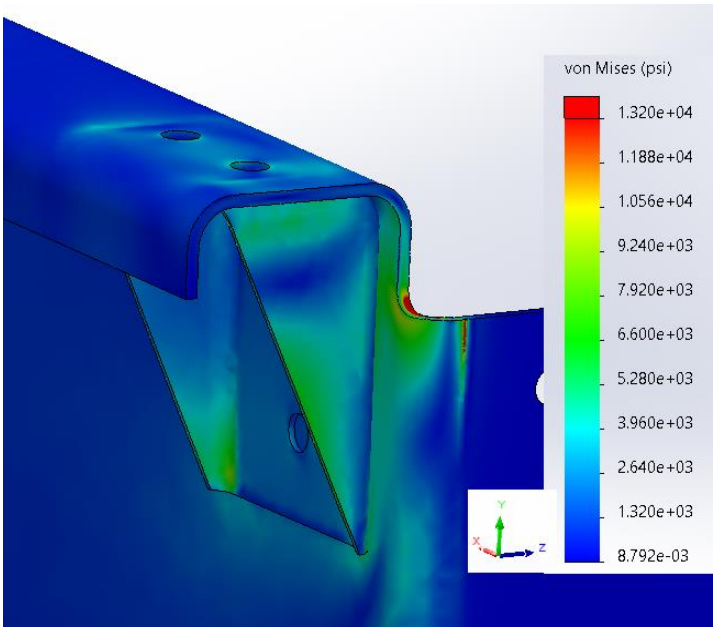

Figure 200: Stress of Cross-rib with Edge Bracket, with Maximum Loading

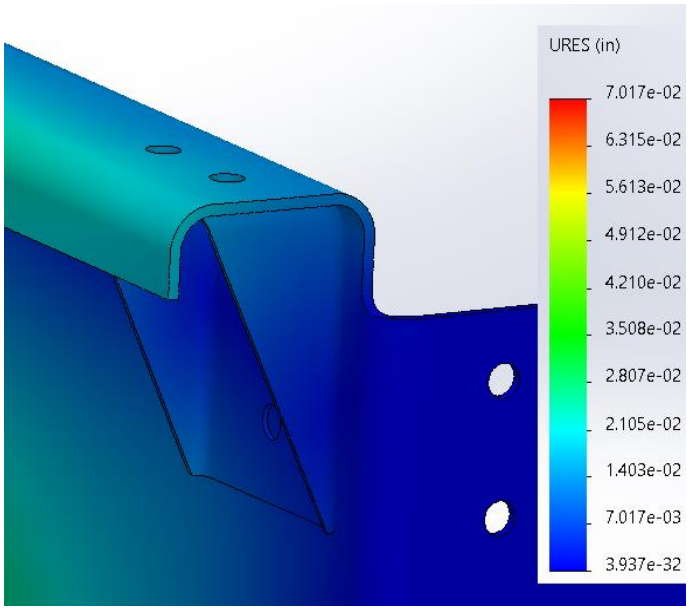

Figure 201: Deflection of Cross-rib with Edge Bracket, with Maximum Loading

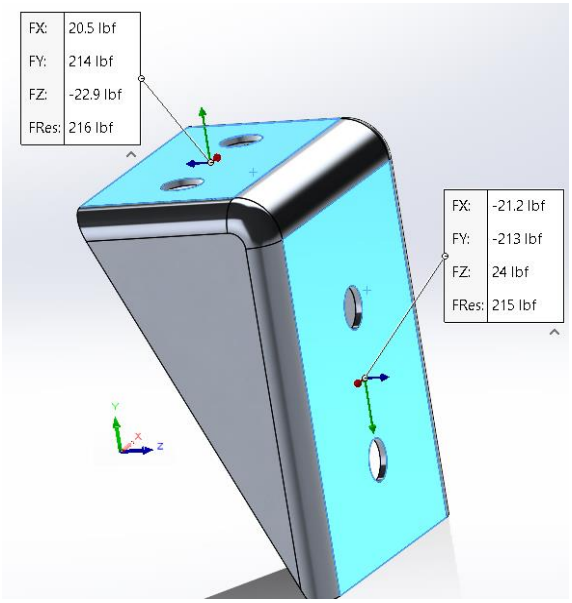

Figure 202: Bracket for Cross-rib with Coil-beam Weight at Maximum Loading

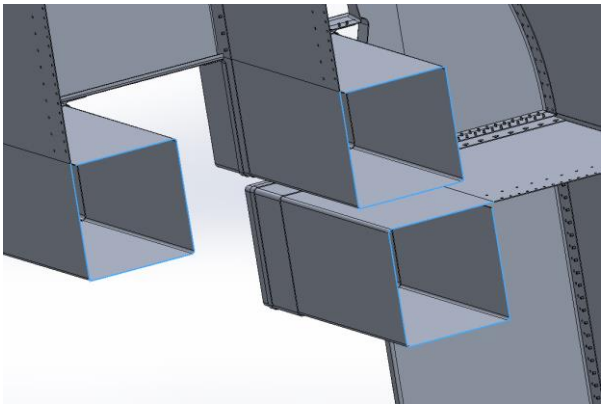

Figure 203: 7th Segment, Coil-beam Area of Inertia

For segment 7, the area of inertia was taken with respect to the coil-beams alone, as seen in Figure 203. This method will be duplicated for all coil-beam segments. One coil-beam segment weight with respect to rivet/retention is 64[Lbf]: The coil-beam itself weighs 41.2[Lbf] and the connect-coil-beam weighs 22.6[Lbf]. Since this is under 205[Lbf] no reinforcements are needed.

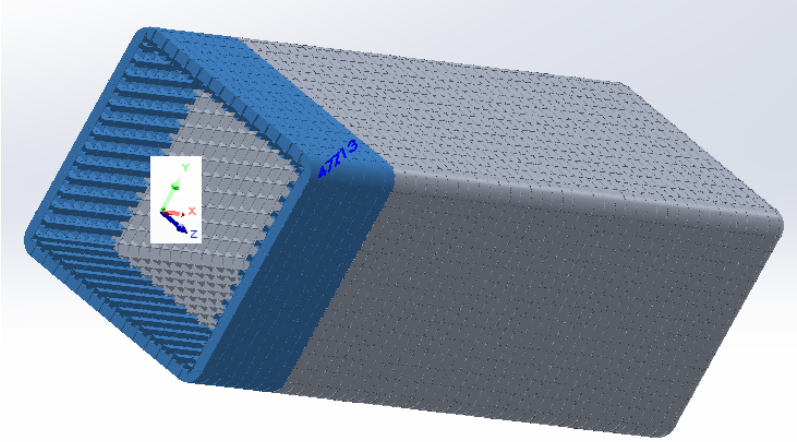

Figure 204: 7th Segment

Table 106: 7th Segment Design Information

Total Weight	212,681	[Lbf]
	96,471	[kg]
CG from Centroid of Mating Surface/Plane		
X	1,034	[in]
Y	-0.2	[in]
Z	-0.2	[in]

	[Lbm-in2]	[kg-m2]
Ix - Twisting	32,145,847,633	9,407,152
Iy - Resist Wind in "Z"	350,466,187,363	102,560,333
Iz - Resist Weight	350,480,639,147	102,564,562

Coil-beam/s

Ix - Twisting	70,223,197	[in4]
Iy - Resist Wind in "Z"	36,230,970	[in4]
Iz - Resist Weight	36,221,943	[in4]

Table 107: 7th Segment for Design Loading

	Wind Load	Gravity	TOTAL
	[Lbf]	[Lbf]	[Lbf]
Fx	220,112	0	220,112
Fy	1,087	221,678	222,765
Fz	-388,800	0	388,800
	[Lbf-in]	[Lbf-in]	[Lbf-in]
Mx	-6,680,683	0	6,680,683
My	476,840,264	0	476,840,264
Mz	12,481,795	-229,208,561	241,690,356

Table 108: 7th Segment Maximum Stresses

Maximum Structural Stress		
Stress due to Axial Load	438	[psi]
Sx - Twisting Stress	49	[psi]
Sy - Stress due to Wind	4,932	[psi]
Sz - Stress due to Gravity	2,500	[psi]
Total Stress	8,892	[psi]
Factor of Safety - FS	4.4	[-]

G. 6th Segment for Design:

Segment 6 utilizes the same coil-beam as segment 7 because the loadings yield a factor of safety of more than 2.875[-].

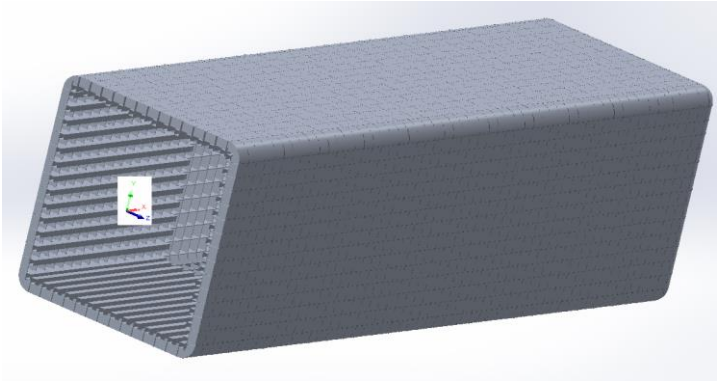

Figure 205: Segments 6 – 12, Center of Mating Face

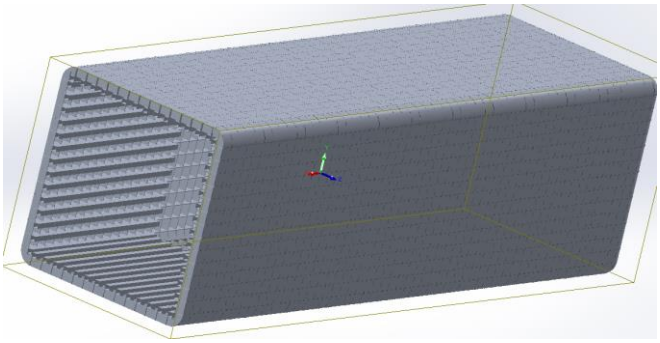

Figure 206: Segments 6 - 12 CG Location

Table 109: 6th Segment Design Information

Total Weight	272,041	[Lbf]
	123,396	[kg]
CG from Centroid of Mating Surface/Plane		
X	1,142	[in]
Y	-0.2	[in]
Z	-0.3	[in]

	[Lbm-in2]	[kg-m2]
Ix - Twisting	41,092,833,310	12,025,396
Iy - Resist Wind in "Z"	553,574,433,797	161,997,876
Iz - Resist Weight	553,588,393,431	162,001,961

Coil-beam/s

Ix - Twisting	70,223,197	[in4]
Iy - Resist Wind in "Z"	36,230,970	[in4]
Iz - Resist Weight	36,221,943	[in4]

Table 110: 6th Segment Loading

	Wind Load	Gravity	TOTAL
	[Lbf]	[Lbf]	[Lbf]
Fx	219,975	0	219,975
Fy	-15,263	281,148	296,412
Fz	-448,546	0	448,546
	[Lbf-in]	[Lbf-in]	[Lbf-in]
Mx	-6,672,269	0	6,672,269
My	634,274,958	0	634,274,958
Mz	10,474,229	-321,079,603	331,553,832

Table 111: 6th Segment Maximum Stresses

Maximum Structural Stress		
Stress due to Axial Load	1,750	[psi]
Sx - Twisting Stress	49	[psi]
Sy - Stress due to Wind	6,560	[psi]
Sz - Stress due to Gravity	3,430	[psi]
Total Stress	13,095	[psi]
Factor of Safety - FS	3.0	[-]

H. 5th Segment for Design

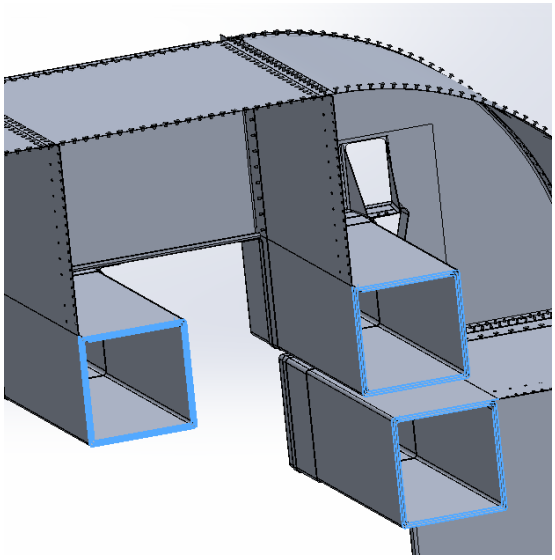

Figure 207: 5th Segment has (x3) Wraps for Coil-beams

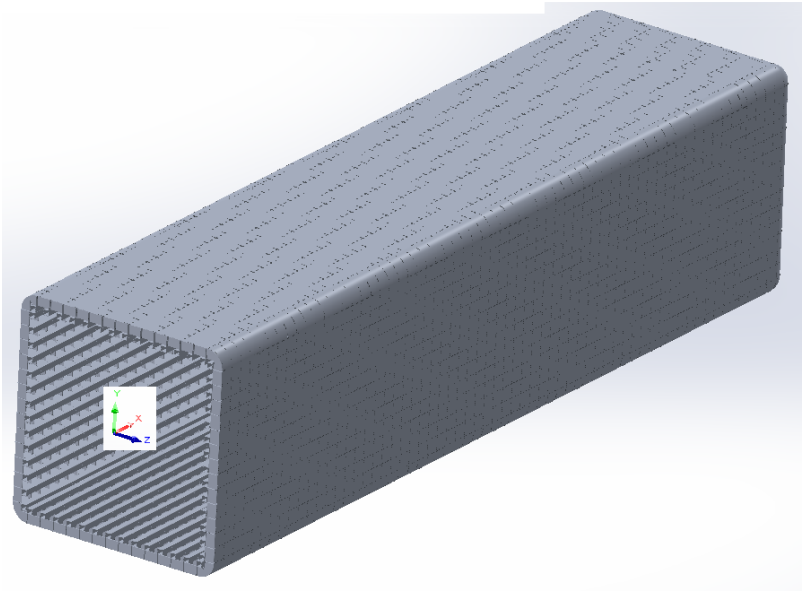

Figure 208: 5th Segment Mating Face

Table 112: 5th Segment Design Information

Total Weight	375,433	[Lbf]
	170,294	[kg]
CG from Centroid of Mating Surface/Plane		
X	1,150	[in]
Y	-0.1	[in]
Z	-0.4	[in]

	[Lbm-in2]	[kg-m2]
Ix - Twisting	56,191,099,715	16,443,749
Iy - Resist Wind in "Z"	838,644,652,473	245,420,750
Iz - Resist Weight	838,657,330,078	245,424,460

Coil-beam/s

Ix - Twisting	202,237,110	[in4]
Iy - Resist Wind in "Z"	104,342,197	[in4]
Iz - Resist Weight	104,316,242	[in4]

Table 113: 5th Segment Loading

	Wind Load	Gravity	TOTAL
	[Lbf]	[Lbf]	[Lbf]
Fx	219,899	0	219,899
Fy	-47,807	384,733	432,540
Fz	-516,976	0	516,976
	[Lbf-in]	[Lbf-in]	[Lbf-in]
Mx	-15,793,320	0	15,793,320
My	816,204,144	0	816,204,144
Mz	-1,839,335	-442,609,316	444,448,651

Table 114: 5th Segment Maximum Stresses

Maximum Structural Stress		
Stress due to Axial Load	608	[psi]
Sx - Twisting Stress	40	[psi]
Sy - Stress due to Wind	2,931	[psi]
Sz - Stress due to Gravity	1,597	[psi]
Total Stress	5,769	[psi]
Factor of Safety - FS	6.8	[-]

I. 4th Segment for Design

Utilizing the same coil-beam as in the 5th segment, the 4th segment factor of safety is 5.5[-].

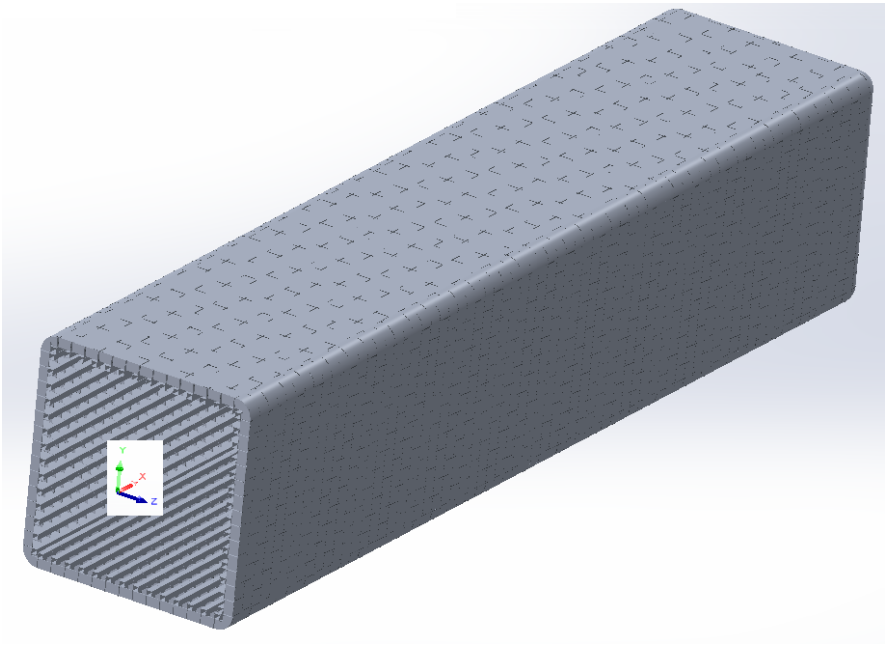

Figure 209: 4th Segment for Design, Mating Plane

Table 115: 4th Segment Design Information

Total Weight	478,825	[Lbf]
	217,191	[kg]
CG from Centroid of Mating Surface/Plane		
X	1,237	[in]
Y	-0.1	[in]
Z	-0.5	[in]

	[Lbm-in2]	[kg-m2]
Ix - Twisting	71,289,366,119	20,862,101
Iy - Resist Wind in "Z"	1,229,818,298,557	359,893,702
Iz - Resist Weight	1,229,829,694,134	359,897,037

Coil-beam/s

Ix - Twisting	202,237,110	[in4]
Iy - Resist Wind in "Z"	104,342,197	[in4]
Iz - Resist Weight	104,316,242	[in4]

Table 116: 4th Segment Loading

	Wind Load	Gravity	TOTAL
	[Lbf]	[Lbf]	[Lbf]
Fx	219,821	0	219,821
Fy	-62,635	488,318	550,953
Fz	-581,451	0	581,451
	[Lbf-in]	[Lbf-in]	[Lbf-in]
Mx	-19,910,637	0	19,910,637
My	1,023,282,832	0	1,023,282,832
Mz	-23,355,455	-603,859,402	627,214,857

Table 117: 4th Segment Maximum Stresses

Maximum Structural Stress		
Stress due to Axial Load	607	[psi]
Sx - Twisting Stress	51	[psi]
Sy - Stress due to Wind	3,675	[psi]
Sz - Stress due to Gravity	2,253	[psi]
Total Stress	7,363	[psi]
Factor of Safety - FS	5.4	[-]

J. 3rd Segment for Design

The 4th segment design is copied for the 3rd segment, leading to a factor of safety of 4.4[-].

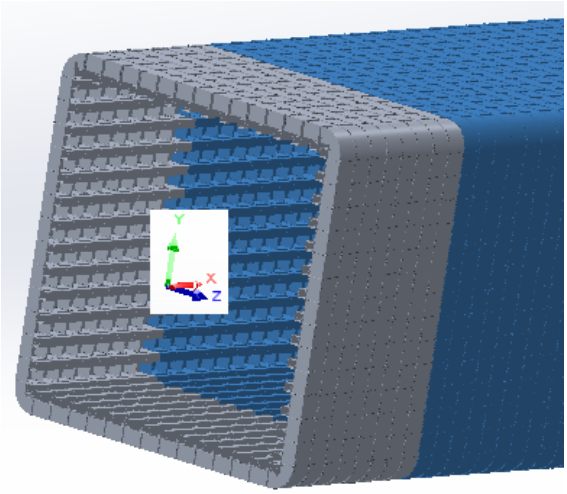

Figure 210: 3rd Segment Mating Face

Table 118: 3rd Segment Design Information

Total Weight	582,217	[Lbf]
	264,089	[kg]
CG from Centroid of Mating Surface/Plane		
X	1,359	[in]
Y	-0.1	[in]
Z	-0.6	[in]

	[Lbm-in2]	[kg-m2]
Ix - Twisting	86,387,632,524	25,280,454
Iy - Resist Wind in "Z"	1,241,971,893,755	363,450,327
Iz - Resist Weight	1,241,982,007,303	363,453,287

Coil-beam/s

Ix - Twisting	202,237,110	[in4]
Iy - Resist Wind in "Z"	104,342,197	[in4]
Iz - Resist Weight	104,316,242	[in4]

Table 119: 3rd Segment Loading for Design

	Wind Load	Gravity	TOTAL
	[Lbf]	[Lbf]	[Lbf]
Fx	219,900	0	219,900
Fy	-65,387	591,903	657,290
Fz	-644,930	0	644,930
	[Lbf-in]	[Lbf-in]	[Lbf-in]
Mx	-21,384,300	0	21,384,300
My	1,254,700,000	0	1,254,700,000
Mz	-47,591,000	-804,473,517	852,064,517

Table 120: 3rd Segment Maximum Stresses

Maximum Structural Stress		
Stress due to Axial Load	608	[psi]
Sx - Twisting Stress	54	[psi]
Sy - Stress due to Wind	4,506	[psi]
Sz - Stress due to Gravity	3,061	[psi]
Total Stress	9,220	[psi]
Factor of Safety - FS	4.3	[-]

K. 2nd Segment for Design

The 3rd segment design is copied for the 2nd segment, leading to a factor of safety of 3.6[-].

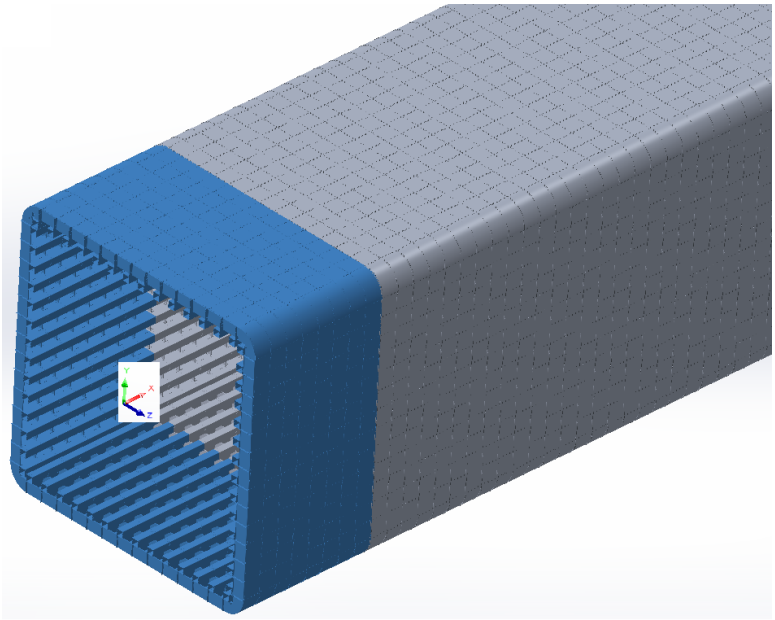

Figure 211: 2nd Segment for Design

Table 121: 2nd Segment Design Information

Total Weight	685,609	[Lbf]
	310,987	[kg]
CG from Centroid of Mating Surface/Plane		
X	1,502	[in]
Y	0.0	[in]
Z	-0.6	[in]

	[Lbm-in2]	[kg-m2]
Ix - Twisting	101,485,898,928	29,698,807
Iy - Resist Wind in "Z"	1,254,125,488,952	367,006,952
Iz - Resist Weight	1,254,134,320,472	367,009,536

Coil-beam/s

Ix - Twisting	202,237,110	[in4]
Iy - Resist Wind in "Z"	104,342,197	[in4]
Iz - Resist Weight	104,316,242	[in4]

Table 122: 2nd Segment Loading for Design

	Wind Load	Gravity	TOTAL
	[Lbf]	[Lbf]	[Lbf]
Fx	220,050	0	220,050
Fy	-62,425	695,488	757,913
Fz	-720,980	0	720,980
	[Lbi-in]	[Lbf-in]	[Lbf-in]
Mx	-20,919,167	0	20,919,167
My	1,512,100,000	0	1,512,100,000
Mz	-72,396,000	-1,044,310,268	1,116,706,268

Table 123: 2nd Segment Maximum Stresses

Maximum Structural Stress		
Stress due to Axial Load	608	[psi]
Sx - Twisting Stress	53	[psi]
Sy - Stress due to Wind	5,431	[psi]
Sz - Stress due to Gravity	4,012	[psi]
Total Stress	11,338	[psi]
Factor of Safety - FS	3.5	[-]

L. 1st Segment for Design

If the same coil-beams used in the previous four segments were utilized here, the factor of safety would be 2.96[-]. However, connections and other hardware would likely bring this value below 2.875[-]; therefore, a new coil-beam will be used with the first segment.

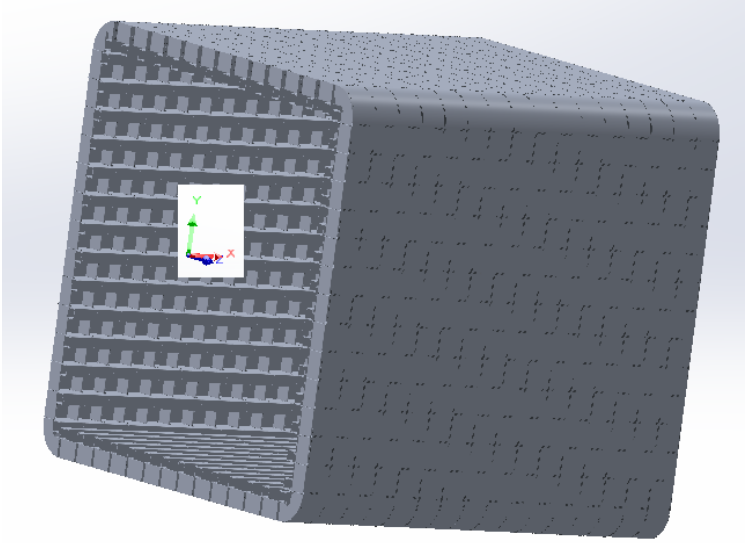

Figure 212: 1st & 2nd Segments for Design

Table 124: 1st Segment Design Information

Total Weight	809,601	[Lbf]
	367,228	[kg]
CG from Centroid of Mating Surface/Plane		
X	1,619	[in]
Y	0.0	[in]
Z	-0.6	[in]

	[Lbm-in2]	[kg-m2]
Ix - Twisting	119,461,609,019	34,959,214
Iy - Resist Wind in "Z"	1,268,656,409,115	371,259,277
Iz - Resist Weight	1,268,663,587,660	371,261,377

Coil-beam/s

Ix - Twisting	263,838,073	[in4]
Iy - Resist Wind in "Z"	136,124,671	[in4]
Iz - Resist Weight	136,090,816	[in4]

Table 125: 1st Segment Loading for Design

	Wind Load	Gravity	TOTAL
	[Lbf]	[Lbf]	[Lbf]
Fx	220,260	0	220,260
Fy	-56,252	819,711	875,963
Fz	-807,630	0	807,630
	[Lbl-in]	[Lbf-in]	[Lbf-in]
Mx	-18,320,633	0	18,320,633
My	1,801,700,000	0	1,801,700,000
Mz	-94,303,000	-1,326,766,446	1,421,069,446

Table 126: 1st Segment Maximum Stresses

Maximum Structural Stress		
Stress due to Axial Load	466	[psi]
Sx - Twisting Stress	36	[psi]
Sy - Stress due to Wind	4,960	[psi]
Sz - Stress due to Gravity	3,913	[psi]
Total Stress	10,533	[psi]
Factor of Safety - FS	3.750	[-]

The (x4) wraps of the coil-beam bring the factor of safety to 3.86[-]. The addition of the supporting beams, connecting the arms to the main structure will provide a FS greater than 2.875[-].

M. Natural Frequency:

Utilizing the information for each section, the 1st harmonic, natural frequency is less than 0.72[s]. Any/all modifications to the design (hence-forth) will increase the system/structural stiffness, reducing its harmonics. Thus, as in Table 59 (the prior estimate) even if there were vorticity shedding, no modifications would be necessary because the vortices are generated with a period of 2.13[s], (FS = 2.98[-]).

Table 127: Arm Natural Frequency & Period, Actual

Arm Segment #	Natural Frequency ω_n [1/s]	Natural Period T_n [s]	2nd Nodal T_n [s]	2nd Nodal ω_n [1/s]
Base of Arm - 1	1,095	0.0057	0.0009	6,864
2	1,081	0.0058	0.0009	6,773
3	1,081	0.0058	0.0009	6,773
4	1,081	0.0058	0.0009	6,773
5	1,081	0.0058	0.0009	6,773
6	1,012	0.0062	0.0010	6,341
7	1,031	0.0061	0.0010	6,460
8	991	0.0063	0.0010	6,209
9	991	0.0063	0.0010	6,209
10	991	0.0063	0.0010	6,209

11	991	0.0063	0.0010	6,209
12	2,083	0.0030	0.0005	13,057
Endcap	32,424	0.0002	0.0000	203,198
Assembly	8.79	0.715	0.114	55

VII. Fixing the Arm to the Main Structure:

Assembling the arm to the main structure is a critical phase in the construction of the Glorious Cross. Somewhat similar to fixing a wing to an aircraft body; fuselage. To ensure minimal stress several iterations were performed to achieve the following result/s.

A. Connection Beams:

The lateral/parallel beam of choice is 18" x 1.5". Due to computational limits, the FEA for this analysis was divided into two problems/scenarios. Thus, the beam array, as seen in Figure 213, is divided into two arrays for analysis. Scenario 1 concerns gravity, Fx and Fy due to the wind along with the half of the twisting moment (½)Mx. Scenario 2 concerns Fx and Fz due to the wind with (½)Mx.

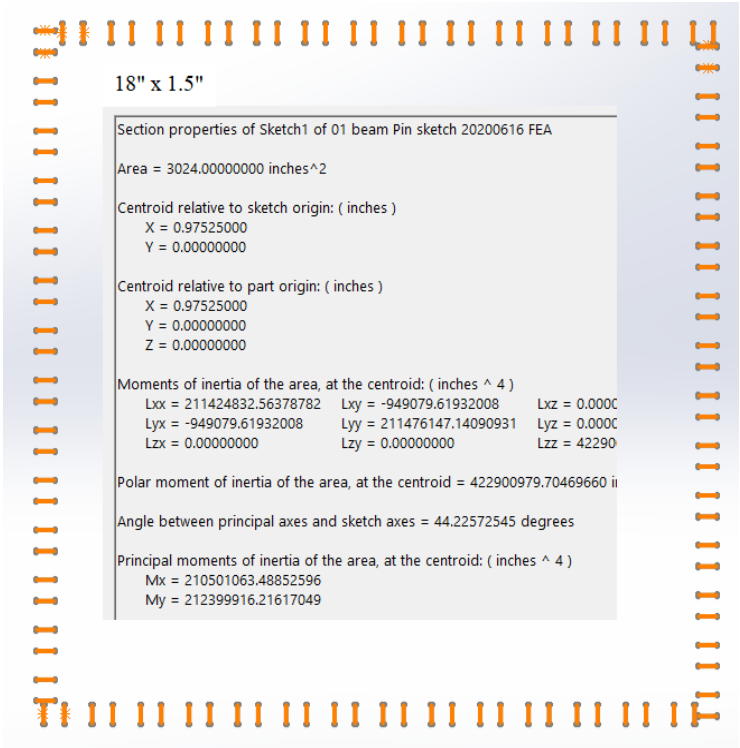

Figure 213: Lateral/Parallel Connection Beam Array

The resulting area of inertia is 211,476,100[in4] which is about 60[%] larger than the coil-beam area of inertia. Comparing a 12" x 1.5" beam to the 18" x 1.5" beam, the deflection over 10[ft] is reduced from 2[in] to 0.2[in]. Note that without the coil-beam, the beams are not very resistant to the twisting moment, Mx.

Table 128: Coordinates for Arm Loads

Arm Center of Gravity from Arms' Base Coil-beam Plane of Segment 1		
< X >	1,619	[in]
< Y >	-0.04	[in]
< Z >	-0.65	[in]

CG from Fy - Wind		
< X >	1,677	[in]

CG from Fz - Wind		
< X >	2,231	[in]

Table 129: Arm Loading for Scenario - 1

Scenario - 1		
Fx (wind)	220,260	[Lbf] on (cg)
Fy (gravity)	-819,712	[Lbf] on (cg)
Fy (wind)	-56,252	[Lbf] on (cg of Fy wind)

Mx	-9160317	[Lbf-in]

Table 130: Arm Loading for Scenario - 2

Scenario - 2		
Fx (wind)	220,260	[Lbf] on (cg of Fz wind)
Fz (wind)	-807,630	[Lbf] on (cg of wind)

Mx	-9,160,317	[Lbf-in]

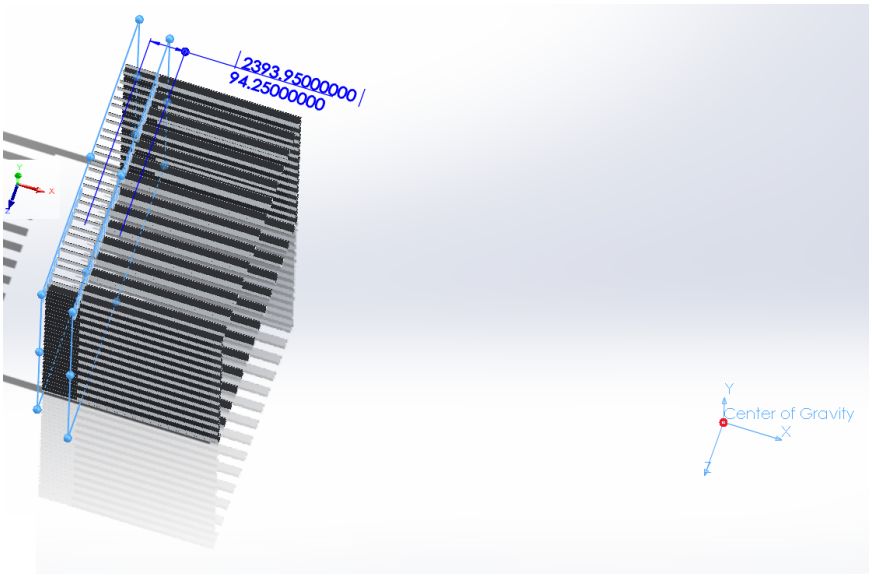

Figure 214: CG, Gravity Center is 94.25" + 1677" in < X > from Connection Plane

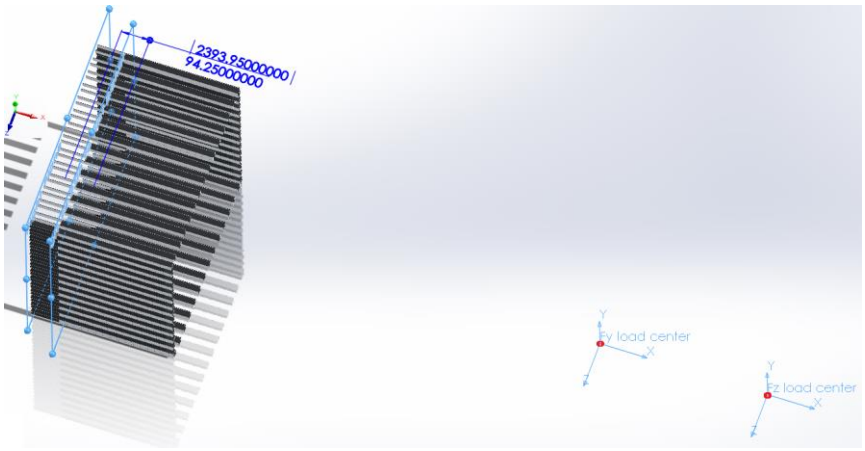

Figure 215: Wind Centers are 94.25" + 1677"/2231" in < X > from Connection Plane

As seen in Table 125, the moment due to the wind is greater than the loadings for gravity. FEA analysis confirms that the beams in Scenario 2 receive the greatest loading. The previous FEA analysis over-estimated the weight of the arm so the calculations are a bit askew.

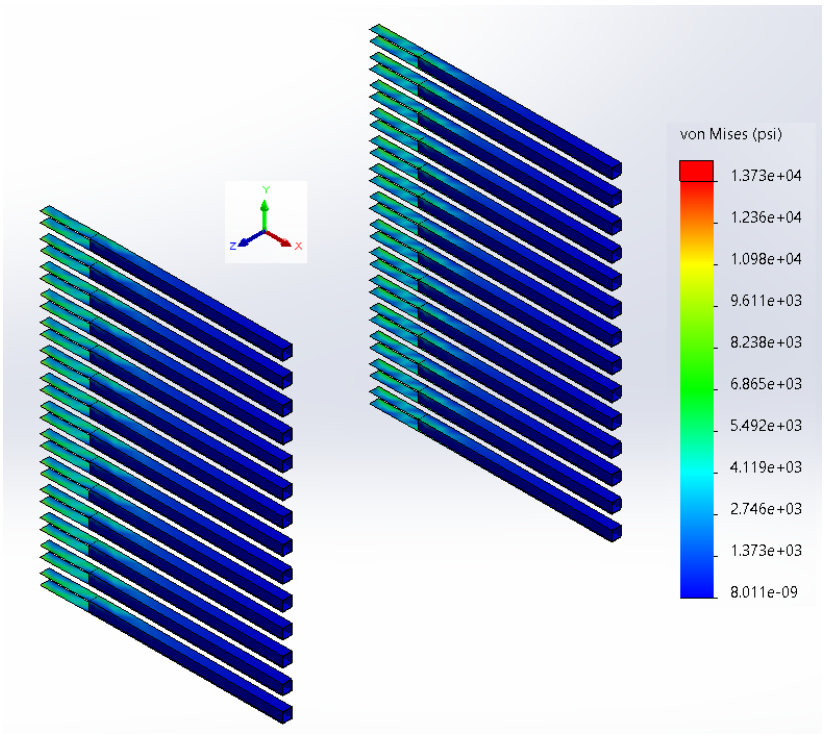

Figure 216: Stress of Wind-loaded beams

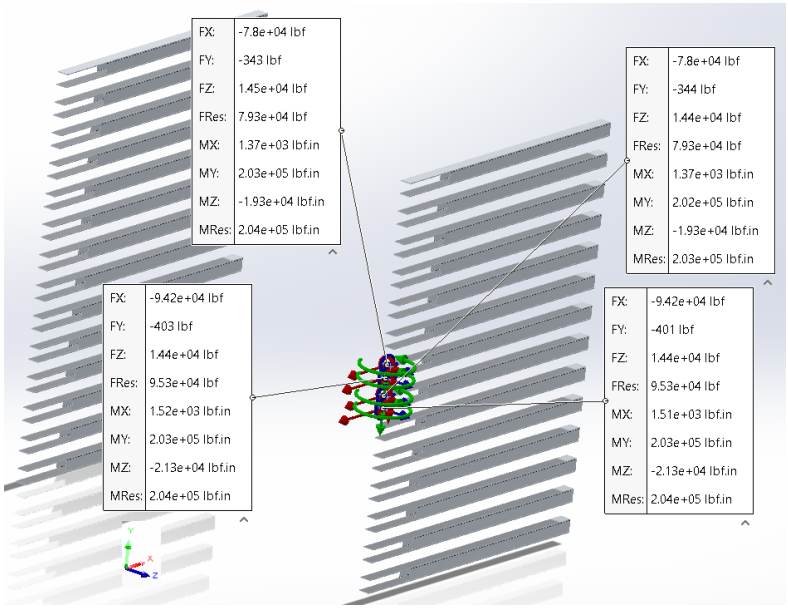

Figure 217: Wind-loading with Distributed Connection/s

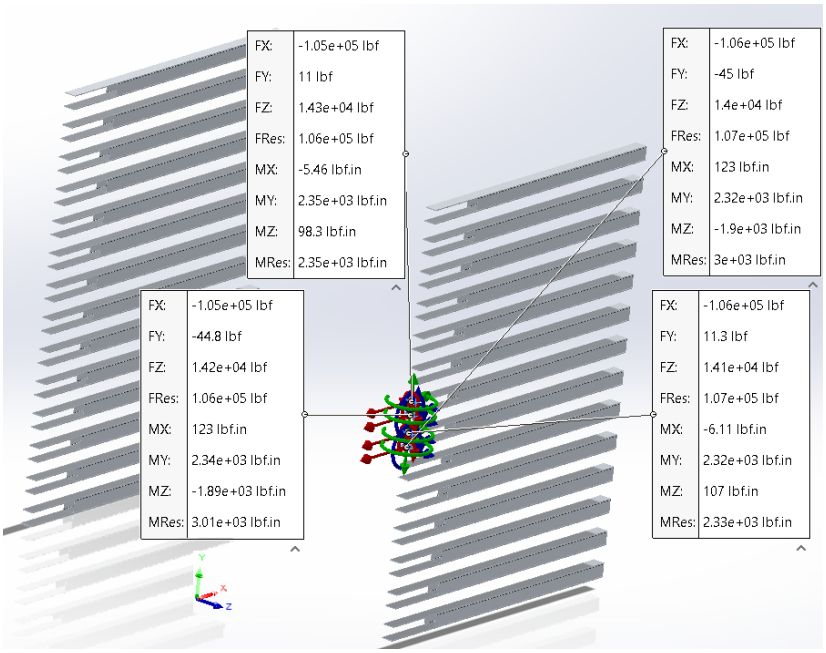

Figure 218: Wind-loading with Ridged Connections

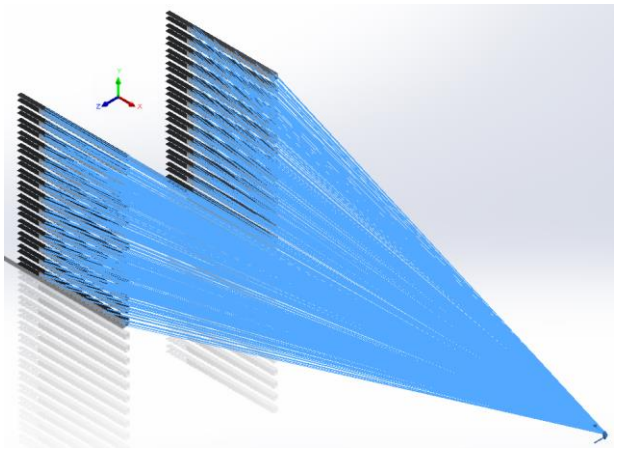

Figure 219: Wind-loading Connection Lines ***to Coil-beam/s***

To connect the remote loadings without adding the enormous amount of detail that is in the model of the arm, connections are utilized. The ridged connection is used when a structure has a "solid" or a well-defined structure between the load/s and the point/s of contact. The distributed load is a soft type of connection, distributing the load in a constant fashion or as defined by the user. The distributed load often removes "hot-spots" from a ridged connection. Both types of connections were compared in this analysis (as seen in Figure 217 and Figure 218). The reaction forces/moments with respect to the distributed loadings were relatively constant and did not comport well with prior FEA analysis or hand calculations. The ridged connection did comport well with prior FEA analysis and hand calculations.

Thus, the ridged connection/s analysis will be utilized for the loading connections; and as seen in Figure 216 the stresses comport well with a FS of 2.875[-].

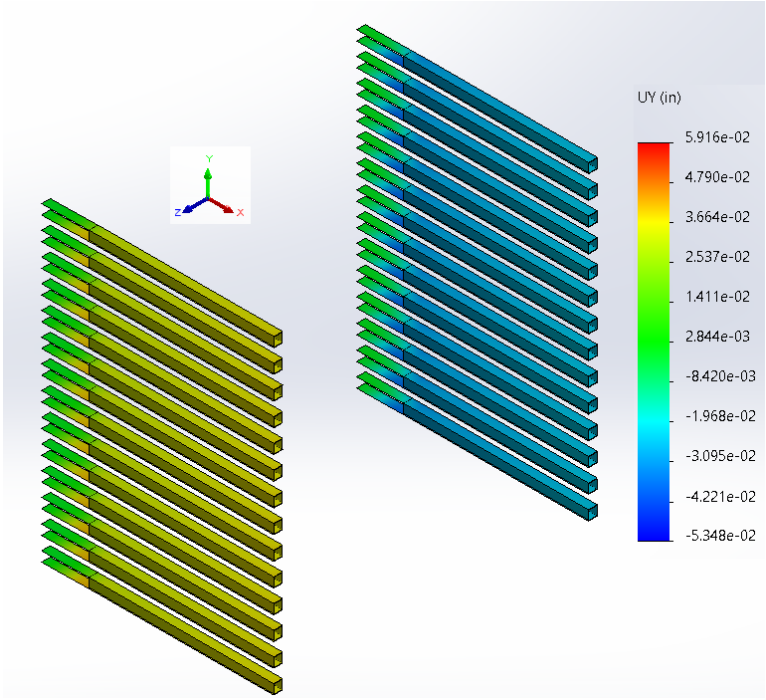

Figure 220: dY, Maximum Deflection due to M_x @ End of 1st Segment

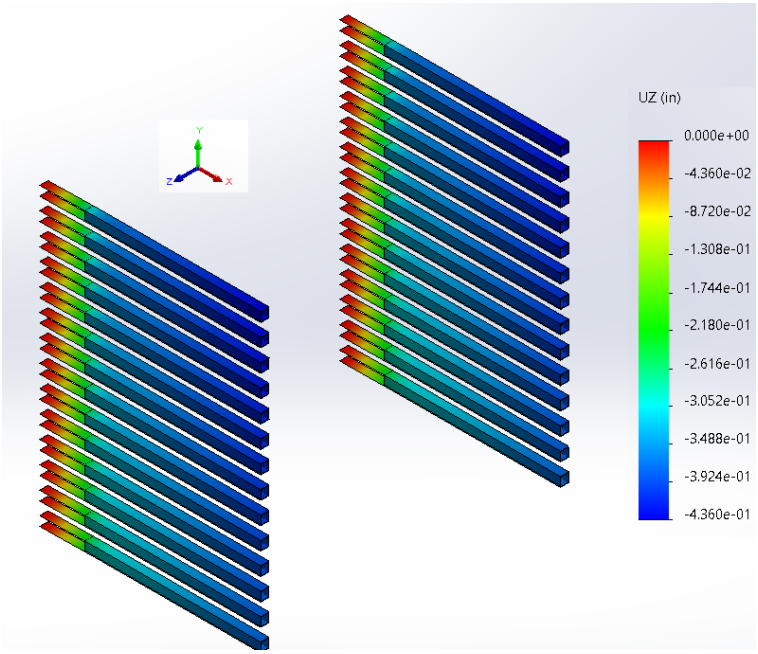

Figure 221: dZ, Maximum Deflection due to Wind @ End of 1st Segment

The maximum deflection due to the wind is about 0.432[in] at a length of 471[in]: This represents a slope of less than 0.1[%]. Since the simplified slope of deflection is less than 0.56[%] (by a factor of {x6}) the arm will appear ridged/sound.

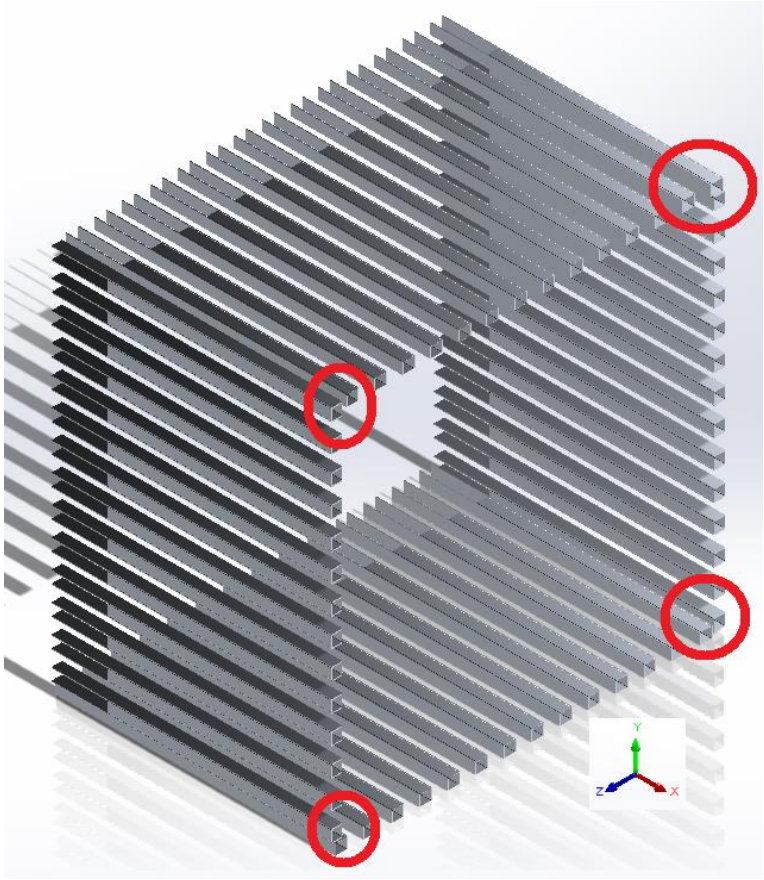

Figure 222: Arm Connection Beams, Corner Beams

Since each scenario is modified to fit the specific loading condition, the reaction loads will not be exact. The corner beams will apply significant stiffness to resist its neighbors load, therefore, the loading distribution will be similar to the previous FEA. Thus, the average loading will be multiplied by 1.08 to obtain the maximum loading for the structure. Plus, the maximum load will appear in the center of the arms' face.

Utilizing the loading information along with the afore mentioned studies, the maximum shear loading of 233,000[Lbf] (with the moment and (x2) pins), in Table 132, comports well with FEA results and expected values.

Table 131: Maximum Reaction Forces at Connection-plane

Maximum Reaction Loading Per Coil-beam (+8[%])		
Fx	175,004	[Lbf] - Gravity Beams

Fx	220,741	[Lbf] - Wind Beams
Fy	34,888	[Lbf] - Gravity Beams
Fz	32,252	[Lbf] - Wind Beams

Note: Absolute values are represented.

Table 132: Maximum Shear Loading at Connection-plane

Shear Load - 1	178,448	[Lbf] - Gravity
Shear Load - 2	223,084	[Lbf] - Wind
Maximum Shear Force	230,000	[Lbf] – w/o Moment

Note: Absolute values are represented.

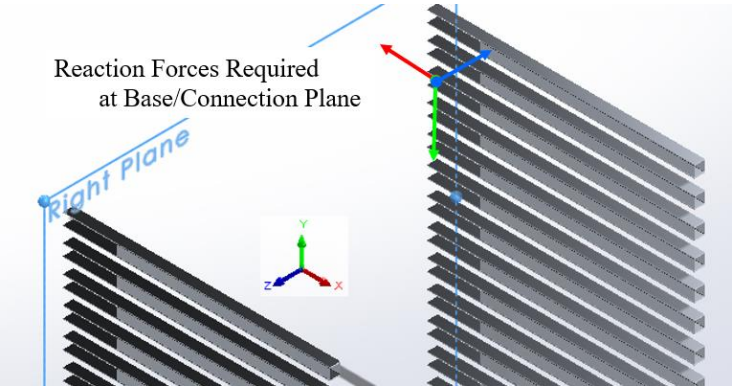

Figure 223: Depiction of Attachment Loading/s

Table 133: Coil-beam to Main Structure Design Loading/s

Coil-beam Attachment Loadings		
{Absolute Value, for Design}		
Fx	230,000	[Lbf]
Fy	35,000	[Lbf]
Fz	33,000	[Lbf]
Mx	200	[Lbf-in]
My	5,100	[Lbf-in]
Mz	2,100	[Lbf-in]

Note: This Loading is applied to (x2) – 18” x 1.5” attachment/connection-beams.

The FEA shows that there is less than a 1[%] variance in the acting loads between each 18[in] beam, therefore, the maximum loading depicted in Table 133, may be cut in half for each beam design. However, the maximum moments may be experienced by either beam.

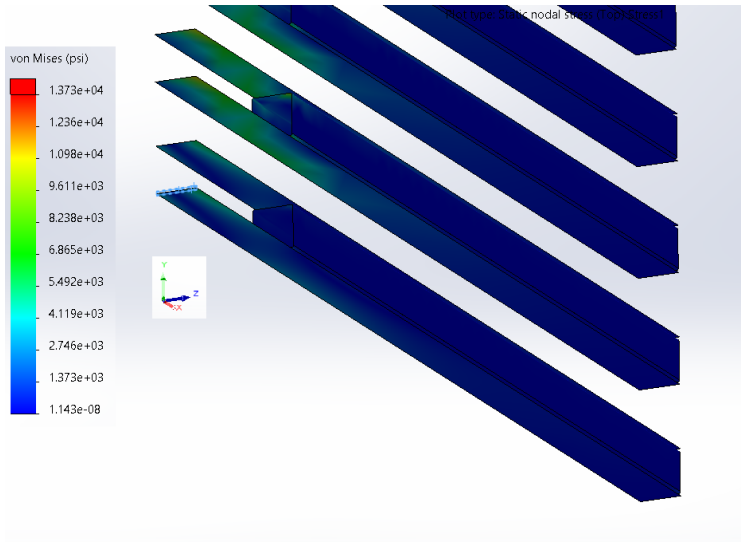

Figure 224: Connection-beam Maximum Stress, w/Fine Mesh on Max-loaded Beam

As seen in Figure 224, the maximum stresses (after adding 10[%] for calculation error) are less than 9,000[psi]. Hand calculations for the Von Mises stress for the beams is 8,974[psi]. The calculations show that a 12[in] beam would suffice; however, the greater factor of safety is welcome due to the various connection points that will be required. After the 1st segment a 12[in] x 1.5[in] beam may be utilized.

Table 134: Pin/s & Diameter/s Required per Segment Length of 377"

N - Pins	Diameter
2	4.000
3	3.250
4	2.750
5	2.500
6	**2.250**
7	2.125
8	2.000

Choosing (x6) pins over (x3) panels yields a pin diameter of 2.25[in] and a FS of 3.16[-]; where a stress concentration factor of 4 was used for the circular holes. Therefore, every coil-beam will receive (x2) – 2.25[in] aluminum T6061-T6 pins.

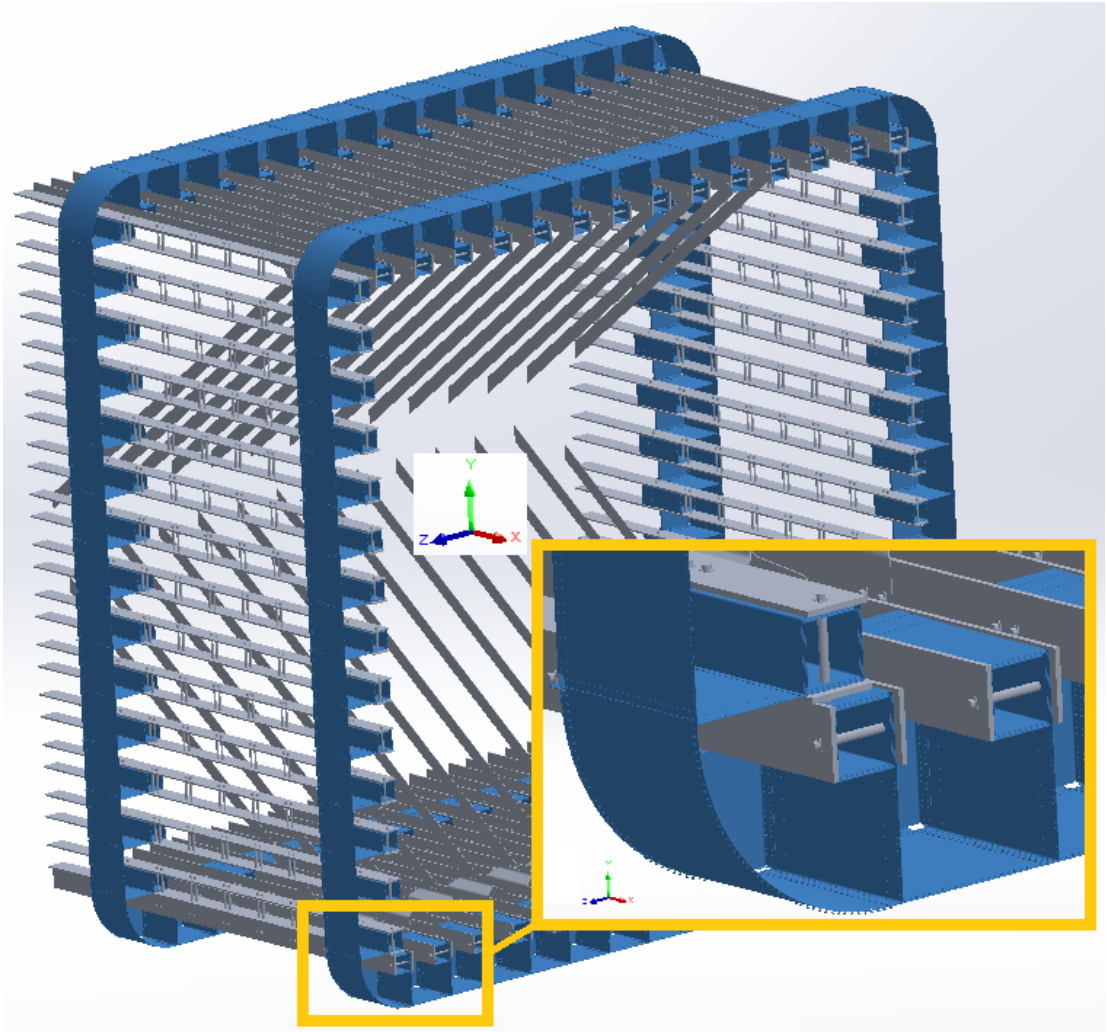

Figure 225: 2.25" Aluminum Pins in Connection-beams & Coil-beam/s

The connection-beams will be fixed to the main structure via connection plates. The main-body-beams originate at the base of the structure, resisting the maximum loadings the Glorious Cross will experience.

B. Main/Body Structure:

The structure must resist a moment of < 201, 0.201, 3.92 $>10^9$ [Lbf-in] at the base; more commonly known notation < 16.7, 0.017, 0.327 $>10^9$ [Lbf-ft] or < 22.7, 0.023, 0.443 $>10^9$ [N-m]. The extremely

large loads cause an engineer to say “wow!” Since these loads are caused by the wind, making a wider or larger base would increase the loads proportionally; plus, vortex shedding will occur with certain body ratios. These factors and others caused a design freeze and the project proceeded to the design of the foundation.

The beam layout was finalized based upon the maximum body stress; which included bending stress, beam weight, body weight and force loading/s. The overall layout was based off of the arms’ connection beams; however, the overall layout was dictated from the stress requirements.

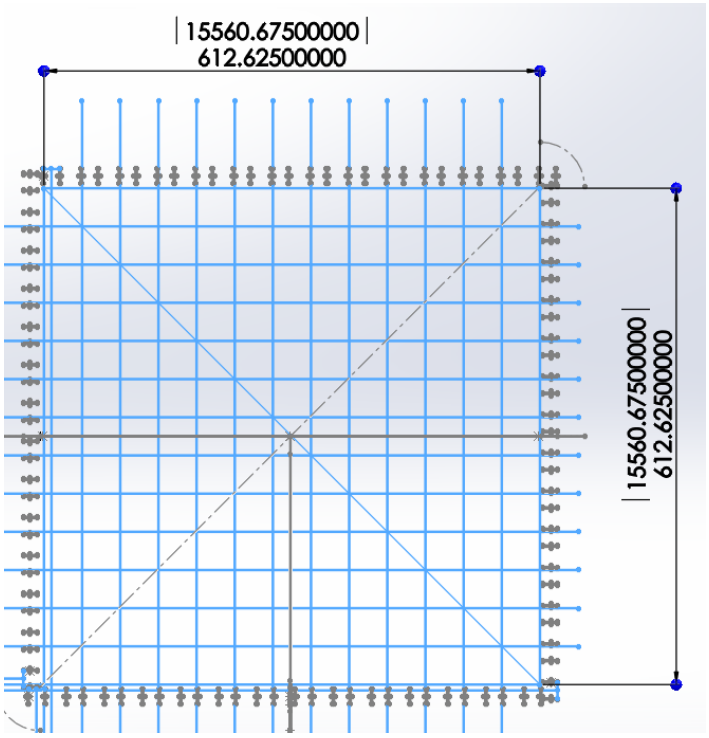

Figure 226: Connection-beam Layout

The connection-beam layout is an off-center square of 612[in], with beams every 47.25[in].

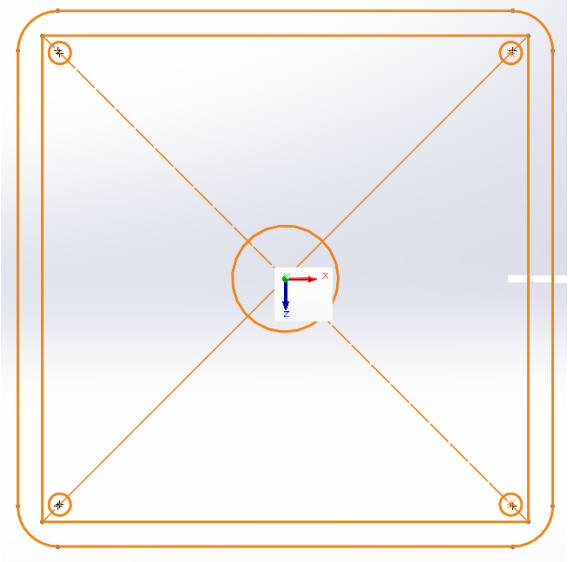

Figure 227: Foundation-beam Layout, 659.75[in] - Square

The foundation beams encompass the perimeter defined by the connection-beams; as shown by Figure 226 and Figure 227. To verify the beam loading per the acting forces, scaled FEA's were performed. A loading "bump" was found for a continuous array of beams.

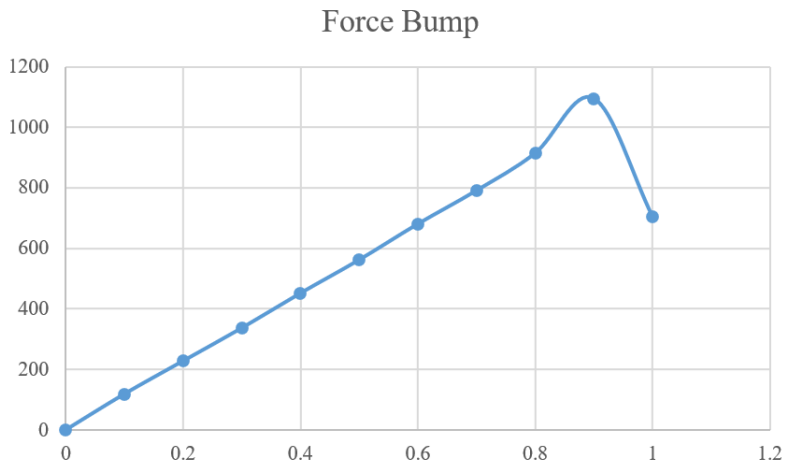

Figure 228: Beam Force/Loading "Bump" for Continuous Array

Figure 228, shows there is a loading "bump" due to a force/moment acting on the structure. The "bump" is about 6.5[%] from the average (typical) slope. This "bump" does not occur without a continuous array: Where "0" is the center of the structure.

Table 135: Foundation-beam Inertia Values

Beam Row	dY [in]	Inertia - (i)th Beam [in4]	Total Inertia (Both Sides) [in4]
1	329.9	15,057,688	722,769,027
2	301.2	12,554,880	602,634,251
3	272.5	10,279,600	493,420,818
4	243.8	8,231,848	395,128,728
5	215.1	6,411,625	307,757,981
6	186.5	4,818,929	231,308,578
7	157.8	3,453,761	165,780,518
8	129.1	2,316,121	111,173,801
9	100.4	1,406,009	67,488,428
10	71.7	723,425	34,724,398

Table 136: Foundation-beam Axial Forces for Wind in < Z >

Beam Row	Theoretical Slope F(i) = m*F(i+1) [-]	Force Distance @ Beam - "i" [in]	Force per Row [Lbf]	Force "Bump" from FEA
1	1.095	329.875	72,373,729	
2	1.105	275.000	66,080,361	70,705,986
3	1.118	225.113	59,786,993	
4	1.133	180.215	53,493,626	
5	1.154	140.306	47,200,258	
6	1.182	105.385	40,906,890	
7	1.222	75.453	34,613,523	
8	1.286	50.510	28,320,155	
9	1.400	30.556	22,026,787	
10	1.667	15.590	15,733,419	

The W14x665, A913-04 Grade 50 (0.12[%] carbon), beam fits the design criterion and was used to generate the foundational beam loadings and stresses. The force-bump noted from the FEA is smaller than the theoretical slope at the outer most beam; noted in Table 135 and Table 136. Thus, the maximum axial design load/s where taken from the theoretical beam loadings “Force per Row” as in Table 136. Since no appreciable contribution to the reduction of stress came from beams beyond row 9,

the calculations ceased at row 9. The A913-04 low carbon beam was chosen due to its conductivity in salt-water and its close relation to aluminum; thereby reducing corrosion.

Table 137: Number of 2" - Grade 8 - Bolts Required/Row

Beam Row	Force per Beam [Lbf]	2" (Gr 8) Bolts Required [-]
1	3,015,572	10.2
2	1,376,674	4.6
3	1,245,562	4.2
4	1,114,451	3.8
5	983,339	3.3
6	852,227	2.9
7	721,115	2.4
8	590,003	2.0
9	458,891	1.5

Table 137 shows that the outer two rows require 12[-] (2" grade 8) bolts and the next four rows require 6[-] bolts; while 4[-] bolts may be used on the inner beams. A minimum of four bolts is used for stability; the shear-force of $11.1(10)^6$[Lbf] requires less than (x1) – 2" bolt per beam.

When the maximum wind conditions are in the < X > direction, only (x5) beams are required to meet the design specifications. The maximum axial load on a particular beam is about $3.0(10)^6$[Lbf] so the wind conditions for the < Z > direction will be used for the foundation-beam design.

Table 138: Foundation-beam Loadings for Wind in < X >

Beam Row	dY [in]	Inertia $(i)^{th}$ Beam [in4]	Total Inertia (Both Sides) [in4]	Theoretical Slope F(i) = m*F(i+1) [-]	Force Distance @ Beam - "i" [in]	Force per Row [Lbf]
1	329.9	15,057,688	722,769,027	1.095	329.875	58,055,014
2	301.2	12,554,880	602,634,251	1.105	275.000	53,006,752
3	272.5	10,279,600	493,420,818	1.118	225.113	47,958,490
4	243.8	8,231,848	395,128,728	1.133	180.215	42,910,228
5	215.1	6,411,625	307,757,981	1.154	140.306	37,861,966
6	186.5	4,818,929	231,308,578	1.182	105.385	32,813,704

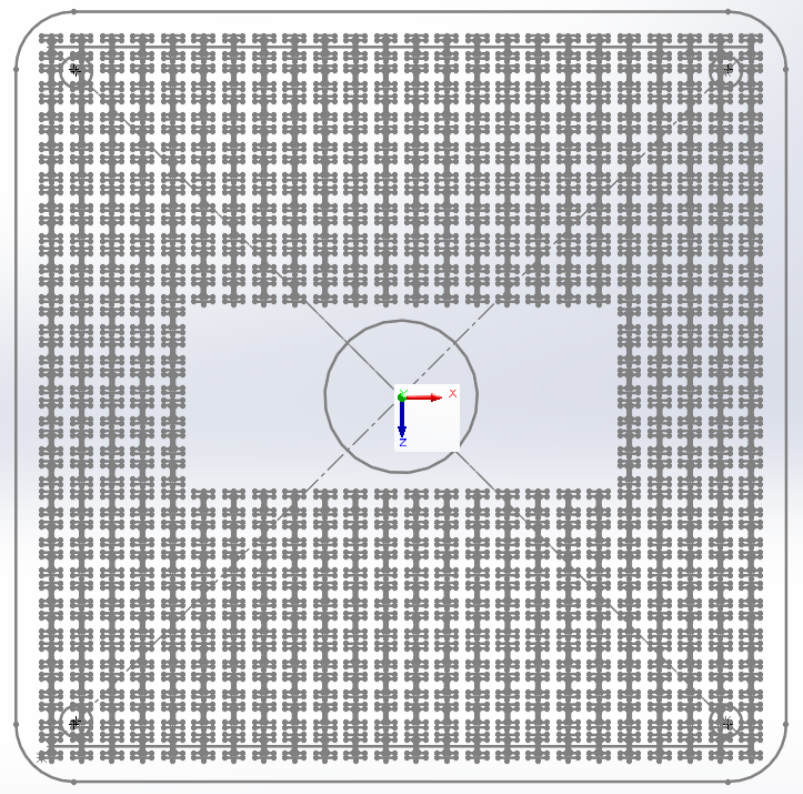

Figure 229: Initial Foundation-beam Array/Lay-out

Thus, the foundation of the Glorious Cross requires 492[-] columns of beams to meet the design stress. The foundation was designed with the endurance factor plus 15[%], allowing for a FS of 1.77[-]$^{+}$ from the yield stress. As the structure increases in height, fewer beams are required: About 600[m] above the foundation, only a portion of the outer (1st) array is needed to maintain structural integrity. Thus, the beam-array will change with altitude.

Each arm will have a compression zone on one side of the face. The beams need to be connected with enough "meat" so that they will withstand the compression without buckling. The connecting plate to withstand the loads and contain a FS of 2.875 was determined to be 12[in] x 2[in].

At the arm elevation the W14x193 beam will be used. To simplify the FEA, an equivalent rectangular beam was used. The rectangular beam was found to have a height of 14.6578[in] and a width of 9.1358[in]; yielding inertial values slightly less than the W14x193 beam. As seen in Figure 230, the stresses were minor; where steel with a yield stress of 50[ksi] was used.

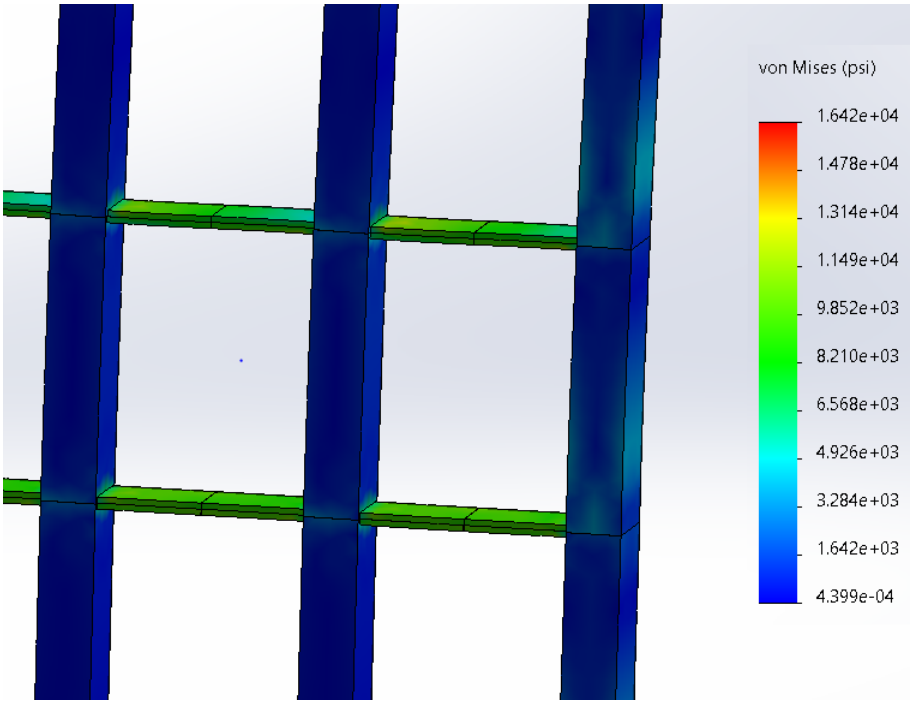

Figure 230: Arm Intersection Stresses, Face

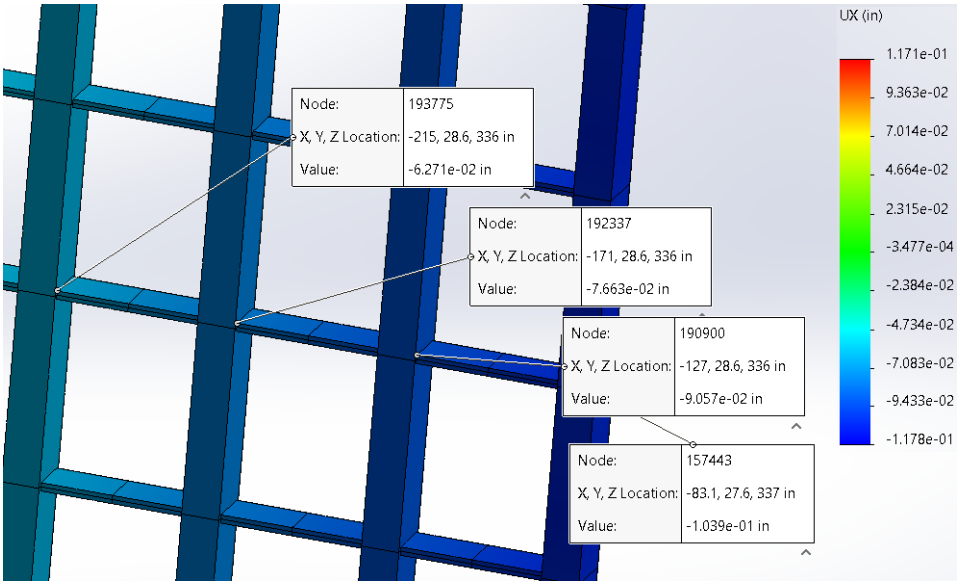

Figure 231: Arm Intersection Lateral Deflection

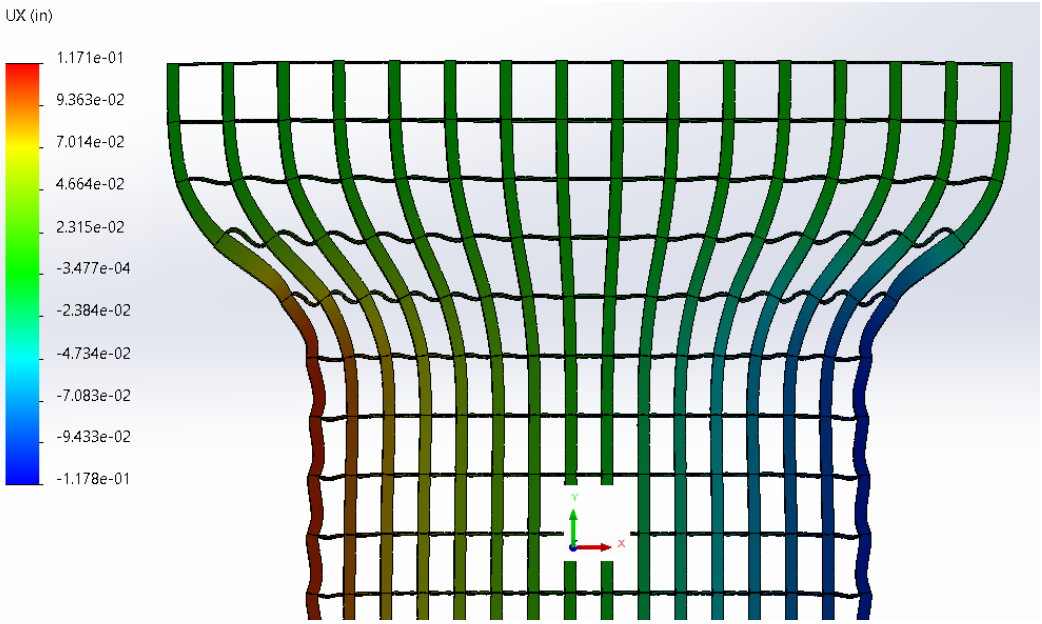

Figure 232: Arm Intersection, (x1,000) Deflection Map

As seen in Figure 231, the lateral or < X > deflection in the structure is less than 0.12[in]. It is also seen that much of the bending occurs within the first or outer (x3) columns. Due to the advantageous affects of (x3) columns on the inertial values of the structure and the limited benefit of having more than (x3)-deep columns, maintaining (x4) columns to this altitude will not be considered (at this time).

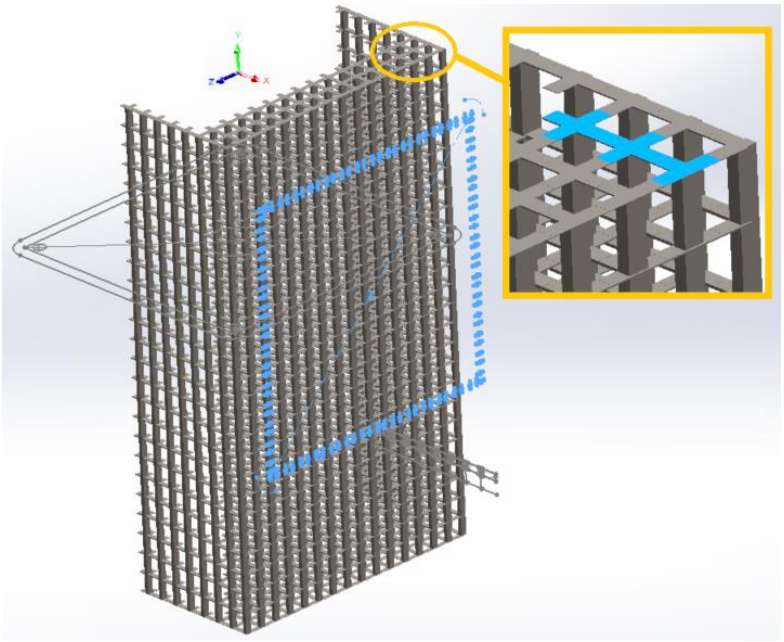

Figure 233: Arm Intersection Set-up w/(x3)-Beams

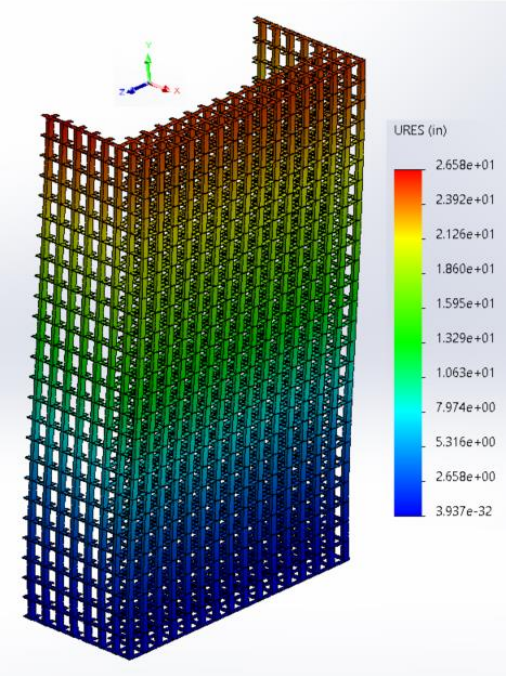

Figure 234: Deflection at Arm Intersection w/(x3)-Column/Beams

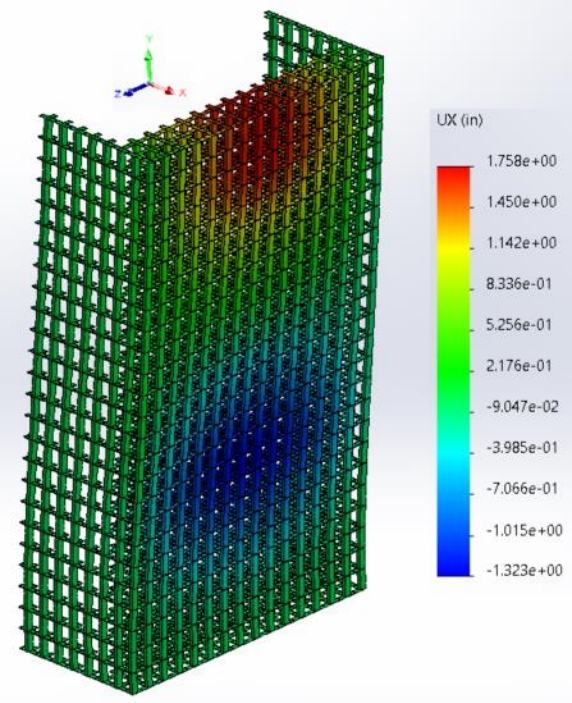

Figure 235: "dX" - Deflection at Arm Intersection w/(x3)-Column/Beams

Figure 235 shows the < *dX* > deflection with (x3) columns supporting the arm-loads. The arm-loads were exaggerated because the model was simplified. The purpose of the model is to confirm the

thickness of the perpendicular members and the number of columns which will suffice for the overall design.

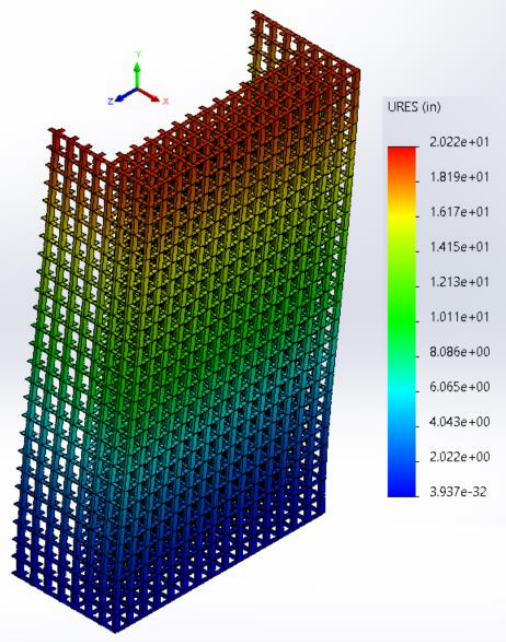

Figure 236: Deflection at Arm Intersection w/(x4)-Column/Beams

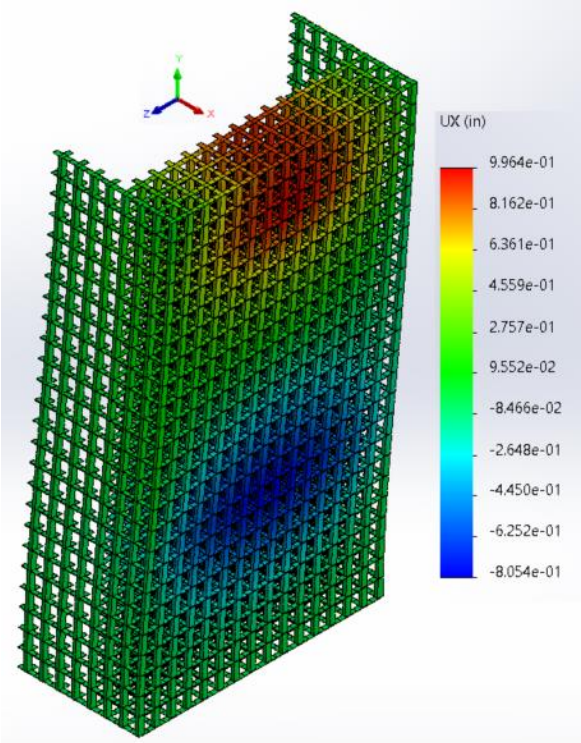

Figure 237: "dX" - Deflection at Arm Intersection w/(x4)-Column/Beams

There was a 76[%] decrease in the "*dX*" direction by adding the 4th beam. The deflection can be minimized two ways:

1) Carrying (x5) beams to above the arms
2) Traverse beams from one arm to the opposing arm

Note: At this time, the arm connection/design will be updated to examine any changes in deflection/s.

C. Coupling of Arm to Main Body:

The coupling connecting the beams to the main structure is crucial in obtaining a stable structure. The design of the coupling was done to achieve deflections on the order of 0.04[in]; a tenth of the deflections in the beam-array FEA (Figure 221).

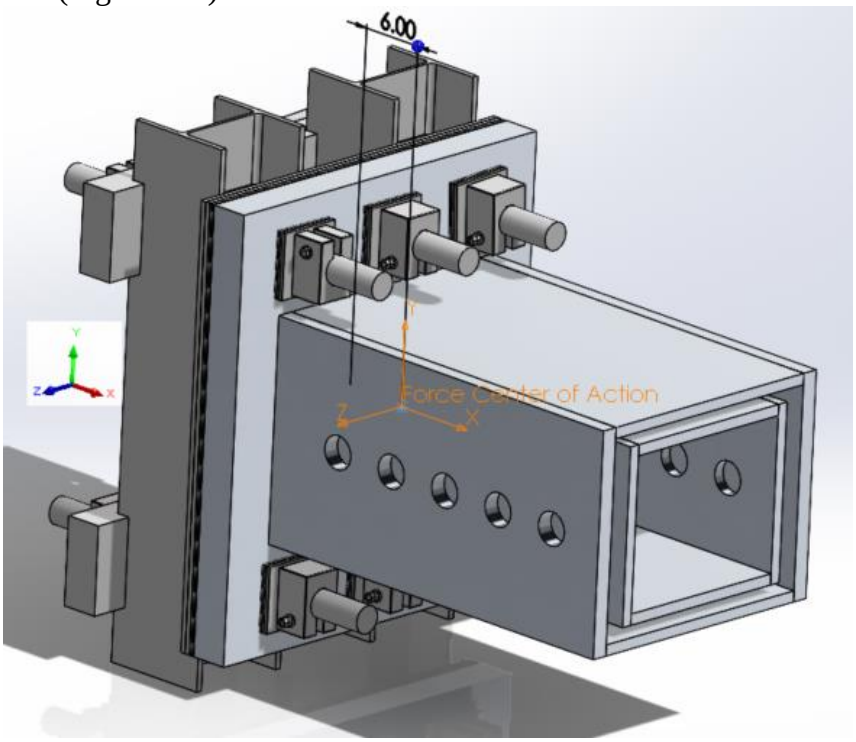

Figure 238: Loading for Arm to Main Structure Coupling

The loads were slightly exaggerated (w/r Table 133) as seen in Table 139; and placed on the pin-holes.

Table 139: Coupling Loadings for FEA

per Coil-beam	ABSOLUTE VALUES	
Fx - for FEA	230,000	[Lbf]
Fy - for FEA	35,000	[Lbf]
Fz - for FEA	35,000	[Lbf]
Forces @	6	[in]

Mx - for FEA	0	[Lbf-in]
My - for FEA	210,000	[Lbf-in]
Mz - for FEA	210,000	[Lbf-in]

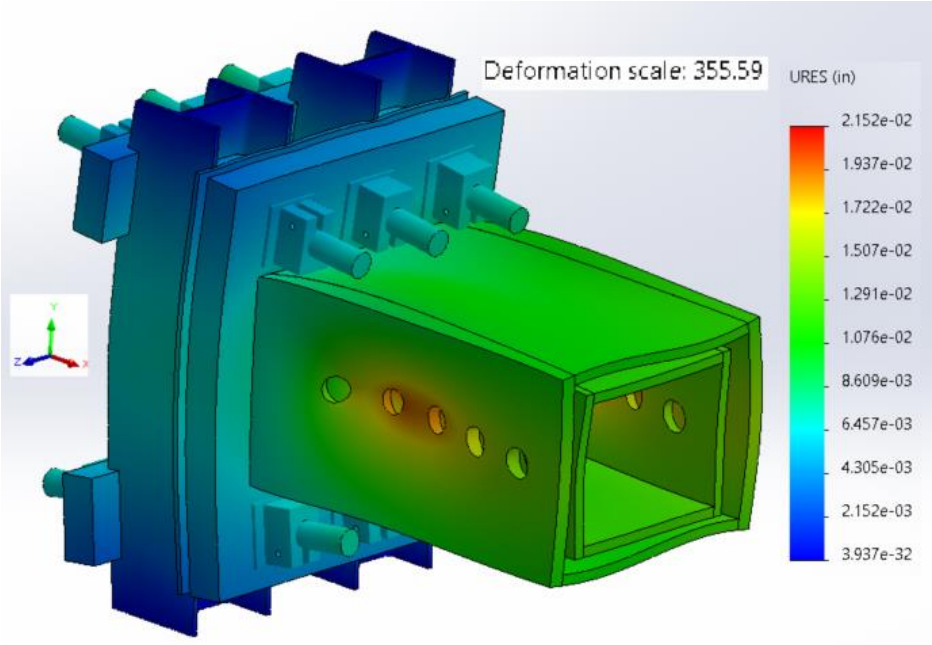

Figure 239: Deformation of Arm to Main Structure Coupling

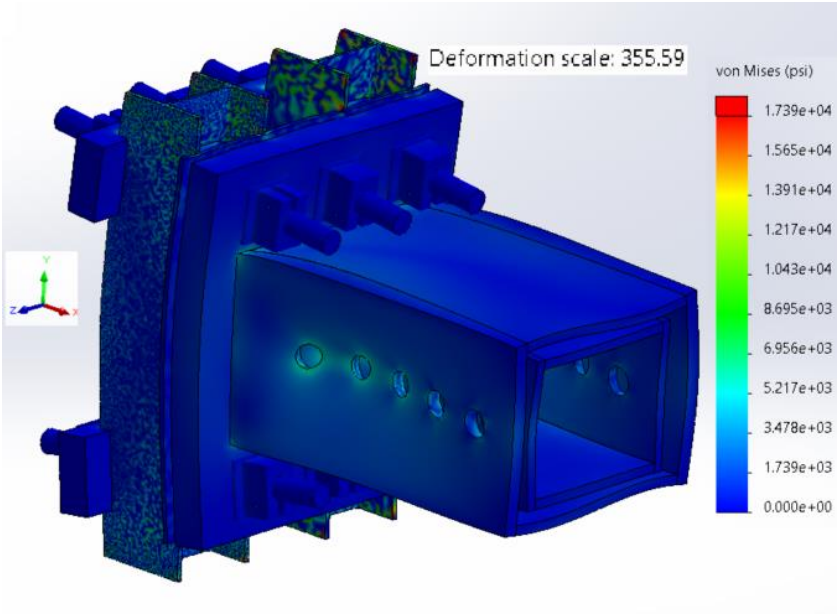

Figure 240: Stress of Arm to Main Structure Coupling

When the main force is pushing into the structure, the targeted maximum deflection was surpassed by the design. Under these conditions, the coupling has a factor of safety over 4.5[-]; with oversized moments.

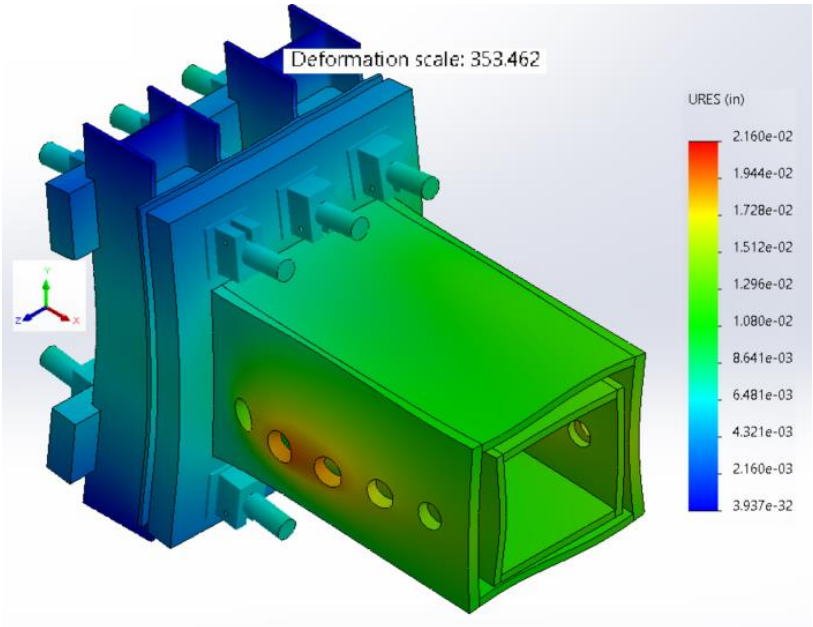

Figure 241: Deflection with Pull-loading on Coupling

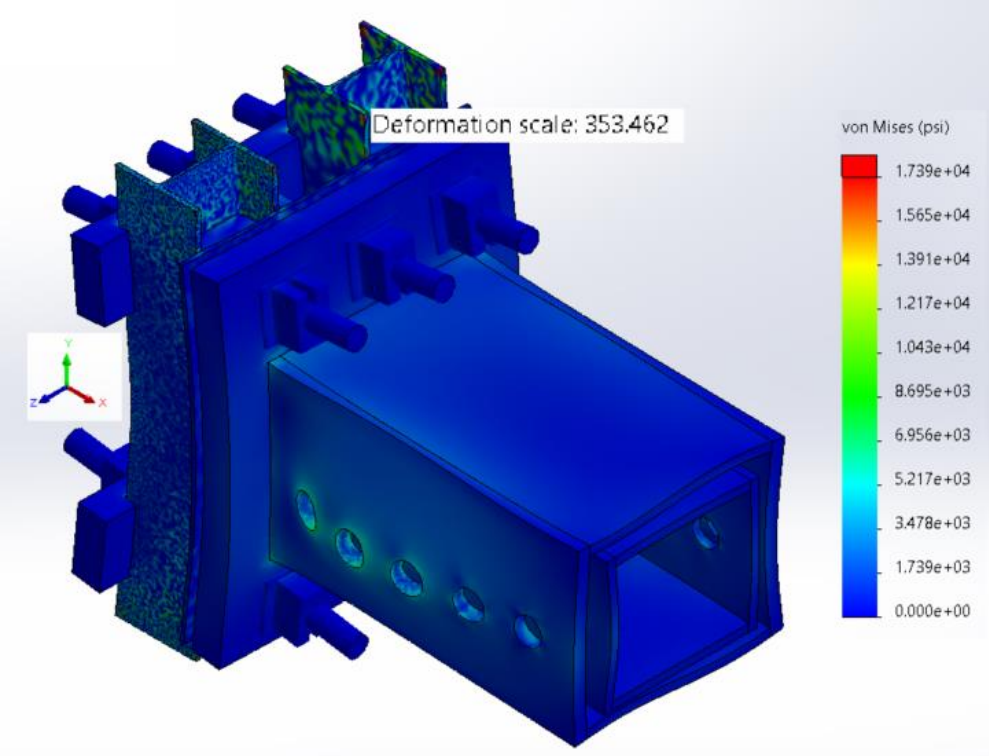

Figure 242: Stress of Arm to Main Structure Coupling with Pull-Loading

Figure 239 thru Figure 242 represent stresses for the main body of the coupling. The pin loadings and relevant members require a separate analysis. For the following analysis an axial load of 38,400[Lbf] (230,000/6) was applied and the maximum pin stress surpassed 17,390[psi]. The connecting cross-member does meet the 2.875[-] safety requirement; however, the diameter of the pin will have to go to 3[in].

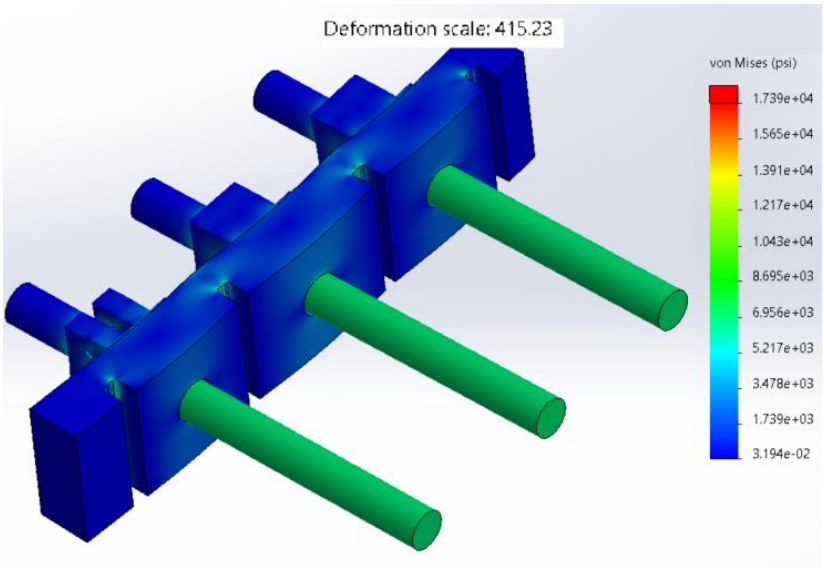

Figure 243: Stress (I) for Pin Assembly on Arm-Coupling Assembly

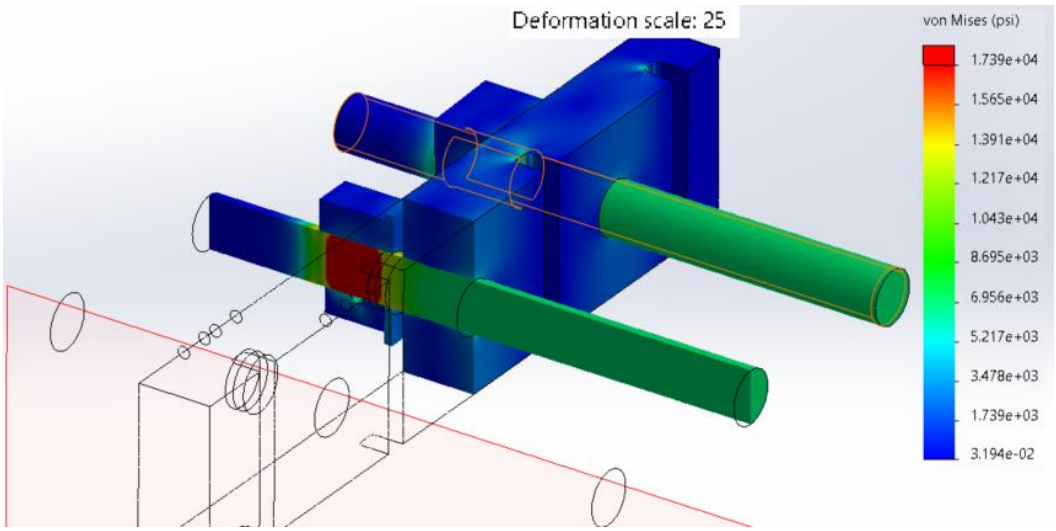

Figure 244: Stress (II) for Pin Assembly on Arm-Coupling Assembly

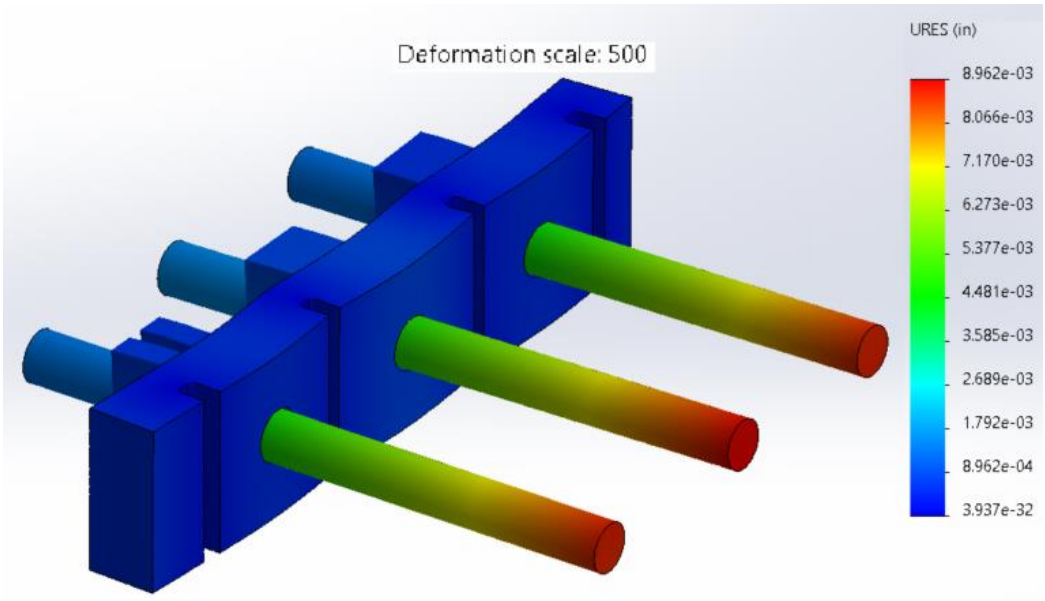

Figure 245: Deflection of the Pin Assembly on Arm-Coupling Assembly

Note: The deflection is largely due to the stretching of the pins.

After some optimization efforts, it was found that the clevis, the pin-clip/s, width (thickness) could be reduced and its inner gap increased without affecting the system performance. The clip width was reduced from 3.24[in] (as in Figure 245) to 3.0[in] (as in Figure 246). An inner gap of 1.132[in] (Figure 245) gives a relatively equivalent mating area from clevis to pin: Where the pin mating area is 3.3136[in2] and the adjoining clevis mating area is 3.051[in2].

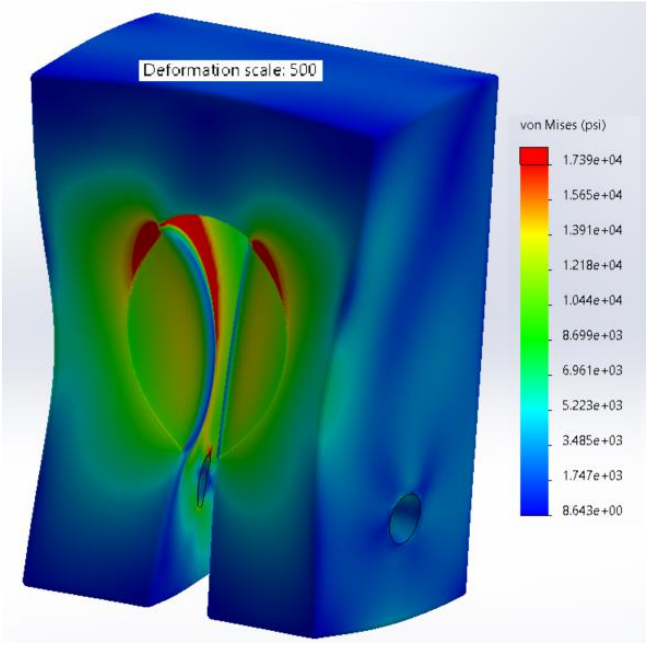

Figure 246: Stress of Clevis for Pin/s with 3.0[in] Width/Thickness

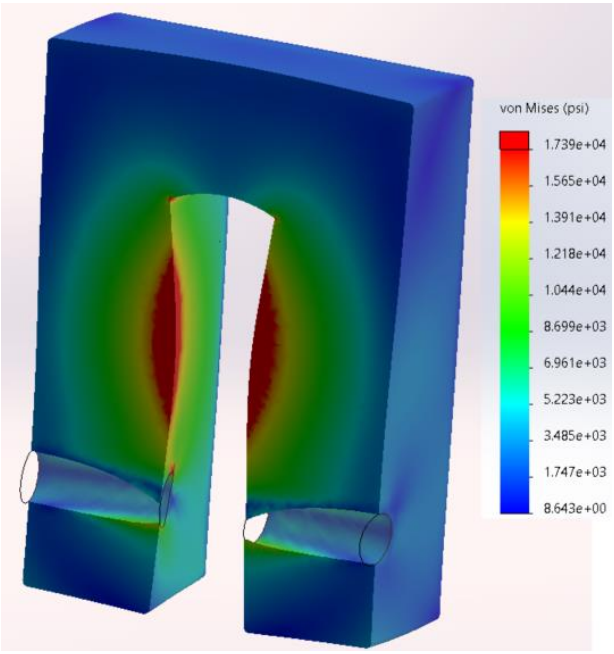

Figure 247: Mid-Stress for Clevis for Pin/s

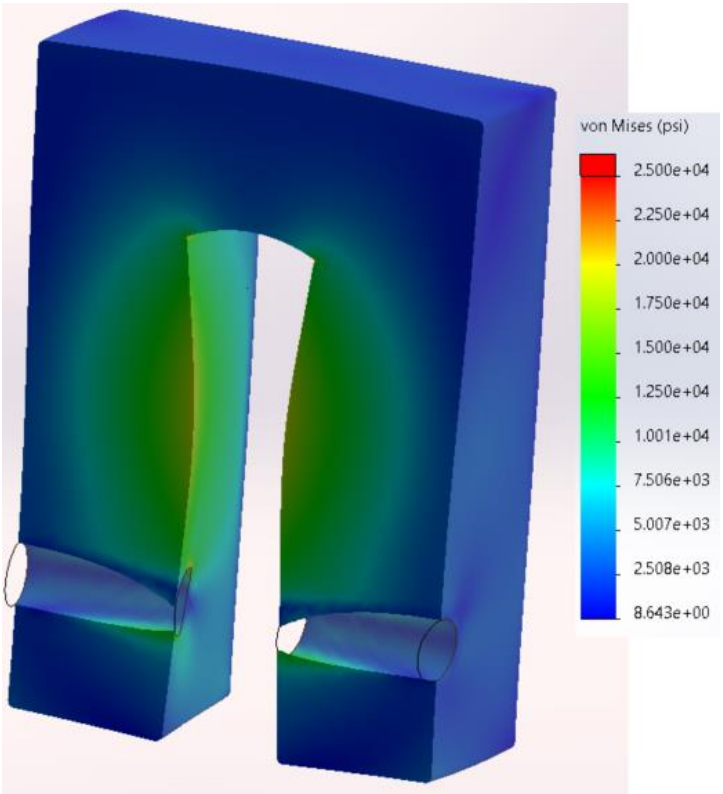

Figure 248: Mid-Stress for Clevis for Pin/s, Endurance Stress (Se) is Not Attained

Though the stresses of some elements exceed 17,390[psi], no elements exceed the endurance stress (Se) of 25ksi]; as seen in Figure 248.

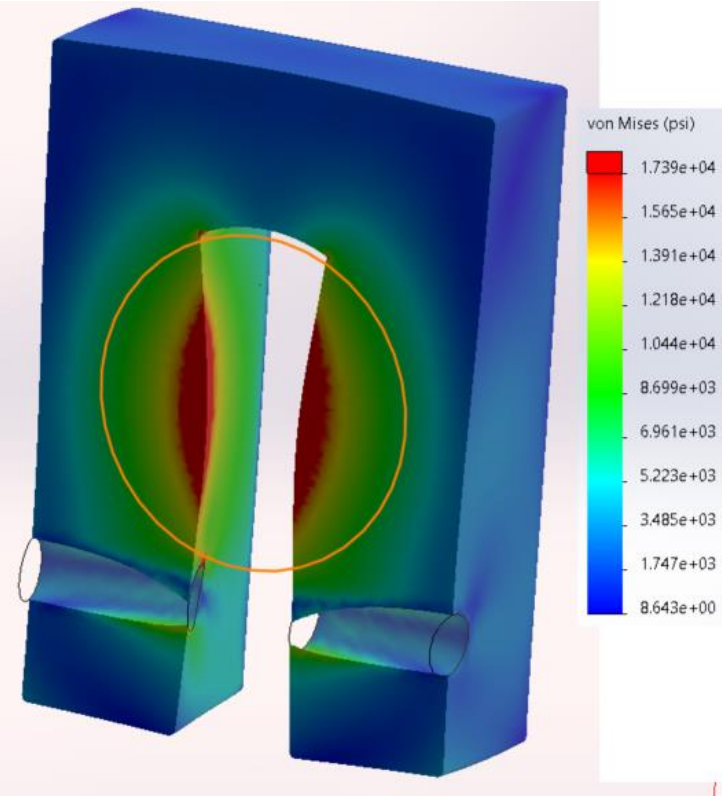

Figure 249: Mid-Stress for Clevis for Pin/s with 3[in] Pin-line

As seen in Figure 249, the zone over 17,390[psi] is a corner segment that penetrates into the clevis about 0.33[in]; with a radius of encroachment/penetration of 0.98[in]. The stress analysis shows that the clevis pin with a thickness/width of 3[in] and a separation of 1.3[in] + 0.005[in] (0.0025[in] on each side) will maintain a FS of 2.875[-]. Note also, that the magnitude-vector deformations (Figure 250) are less than 0.002[in].

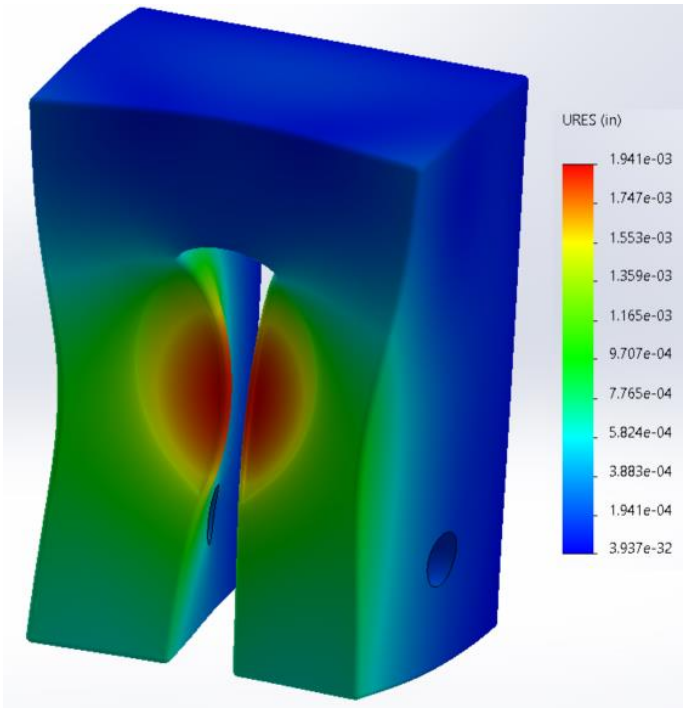

Figure 250: Deformations of Clevis for Pin/s

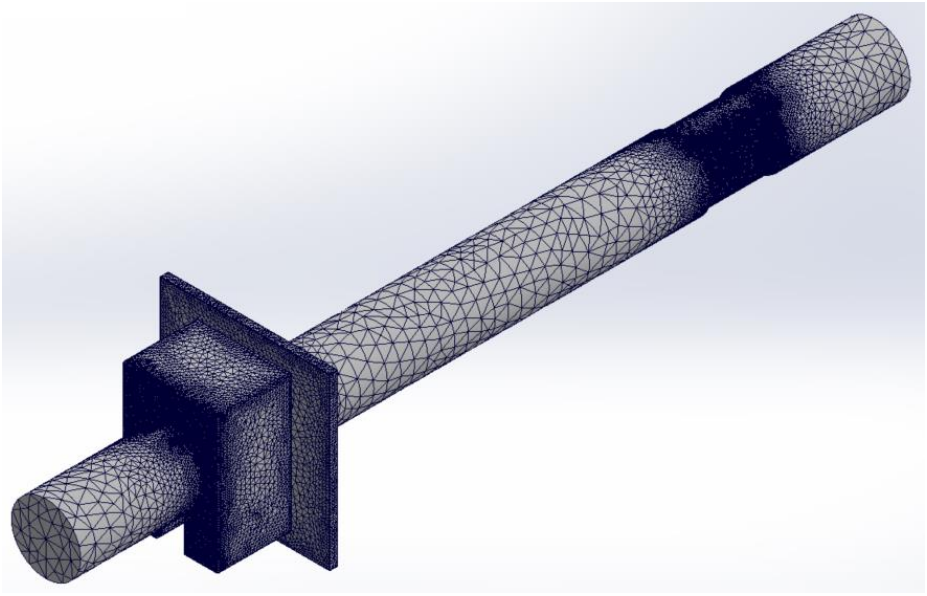

Figure 251: Main Coupling-Arm Pin with Fine Mesh

Note: The single pin was overloaded with an axial load of 39,300[Lbf].

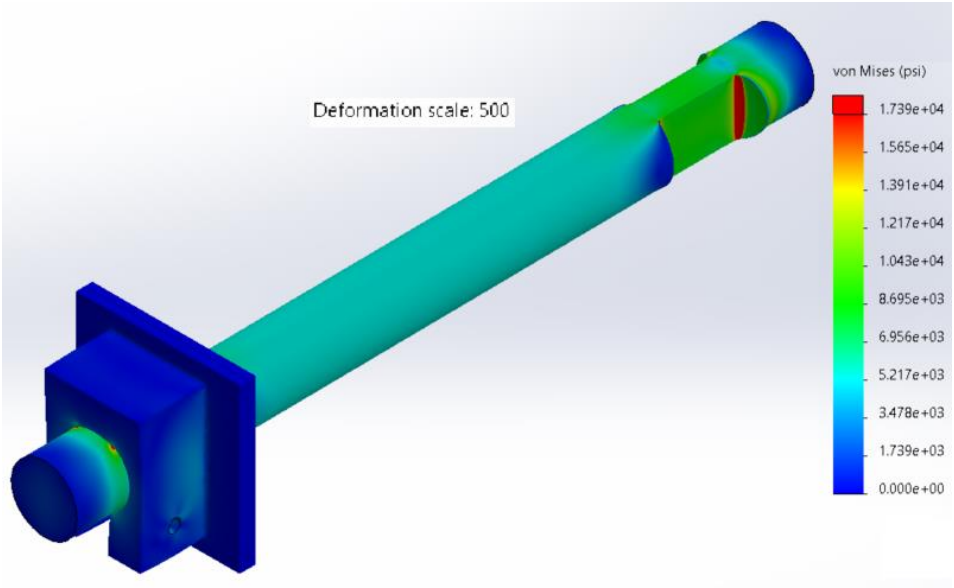

Figure 252; Overall Stress of Main Coupling-Arm Pin

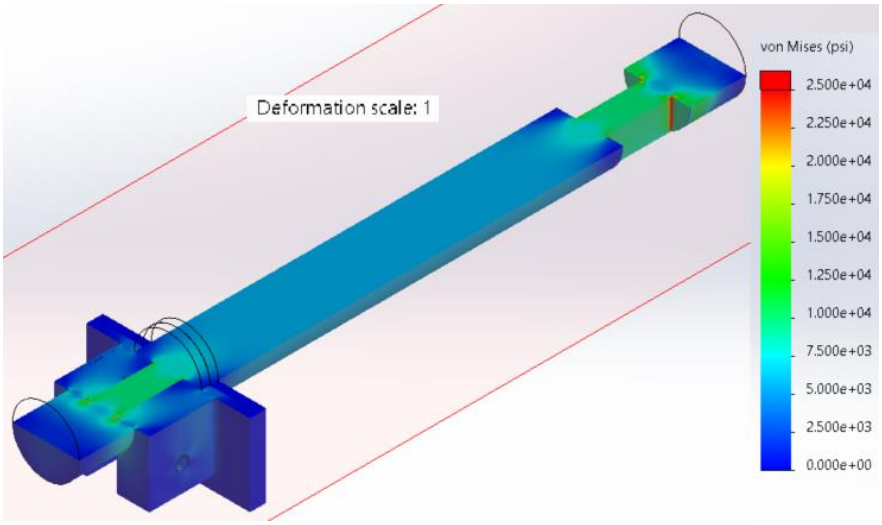

Figure 253: Mid-section Stress of Main Coupling-Arm Pin

Note: The clevis, the pin-clips, have less stress in the assembly.

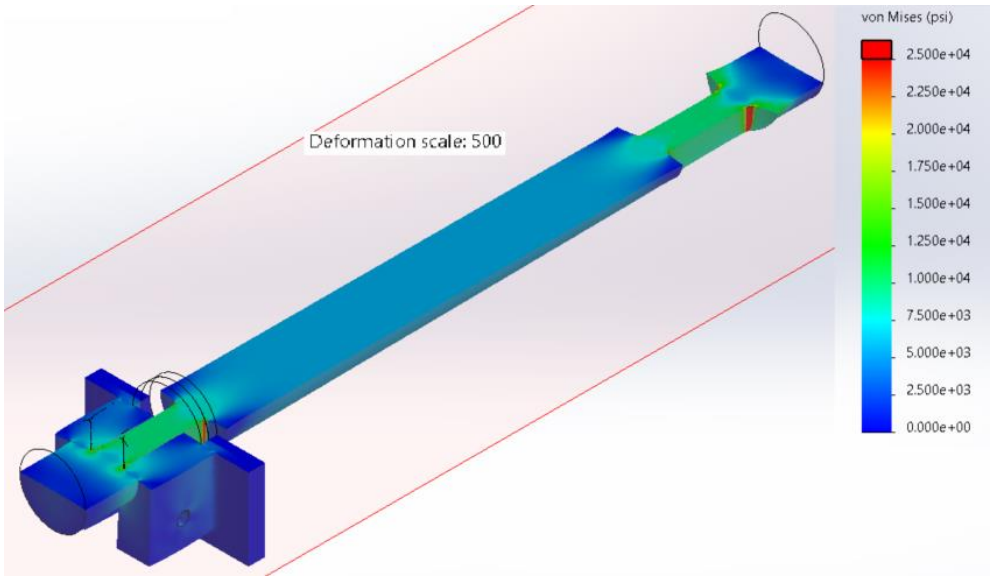

Figure 254: Mid-section Stress of Main Coupling-Arm Pin (Scale 500)

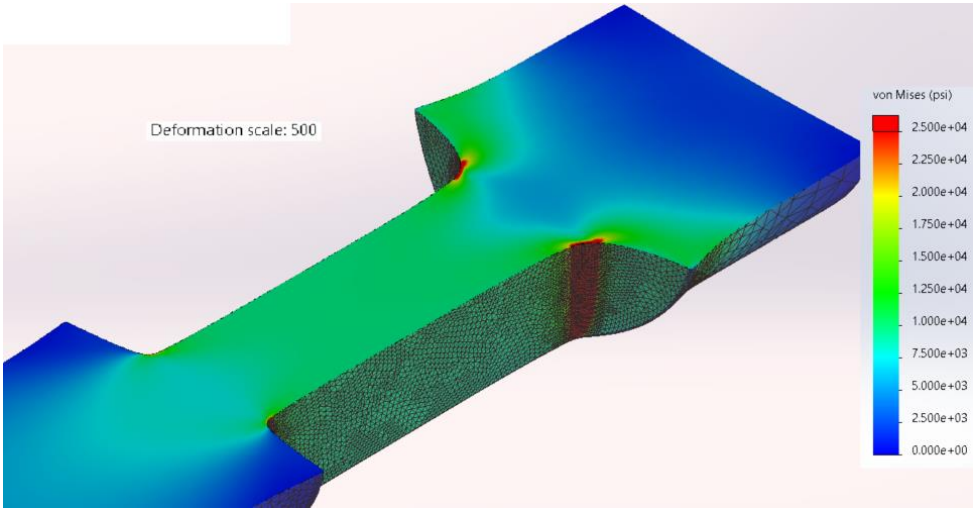

Figure 255: Clevis Stress of Main Coupling-Arm Pin, Ingress 0.15"

Note: No full-elements yield. Minor surface (2D) yielding occurs.
Note: The mesh size is on the order of 0.02[in], more than (x5) elements per radius).

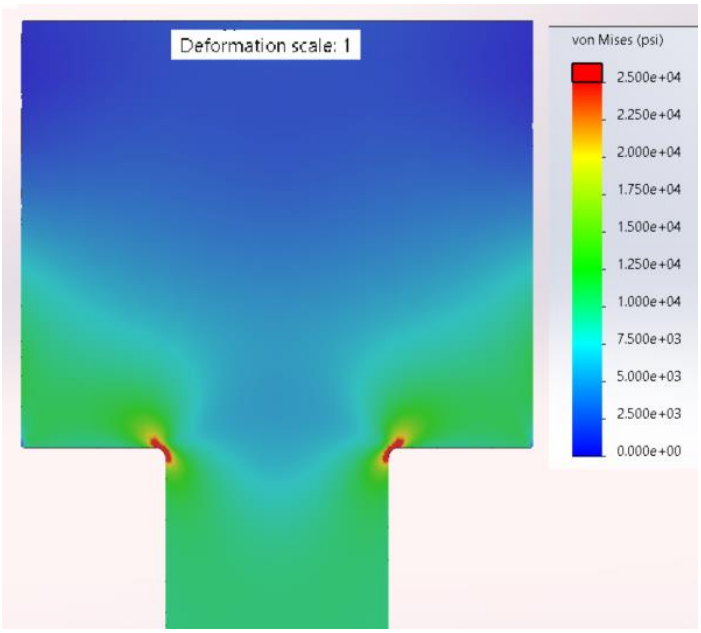

Figure 256: Pin-corner S_e of 25[ksi] Envelope, Penetrates/Ingress 0.06[in]

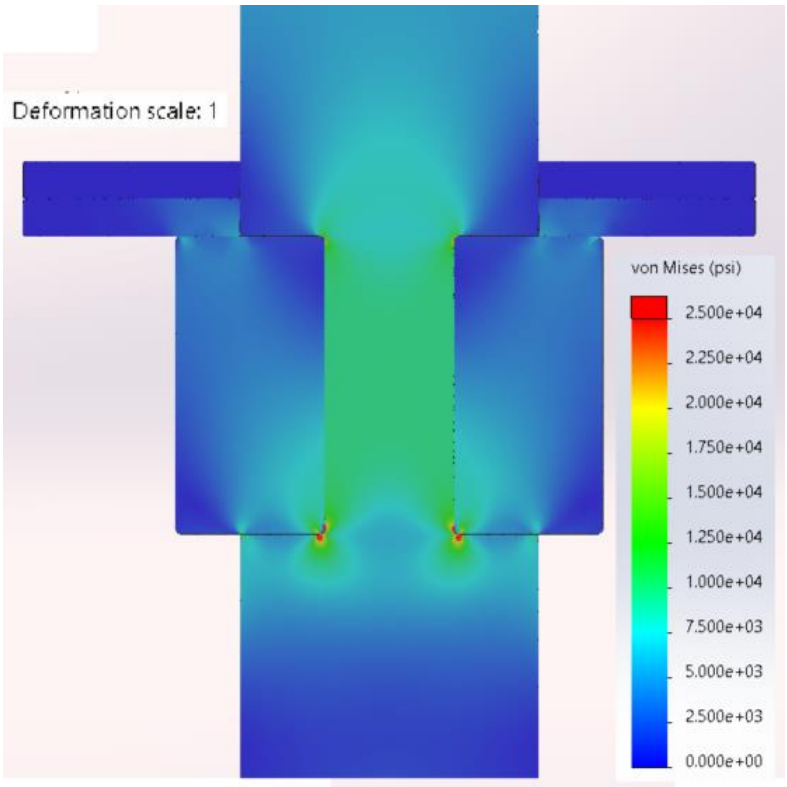

Figure 257: S_e Stress of Pin-Coupling Assembly Side

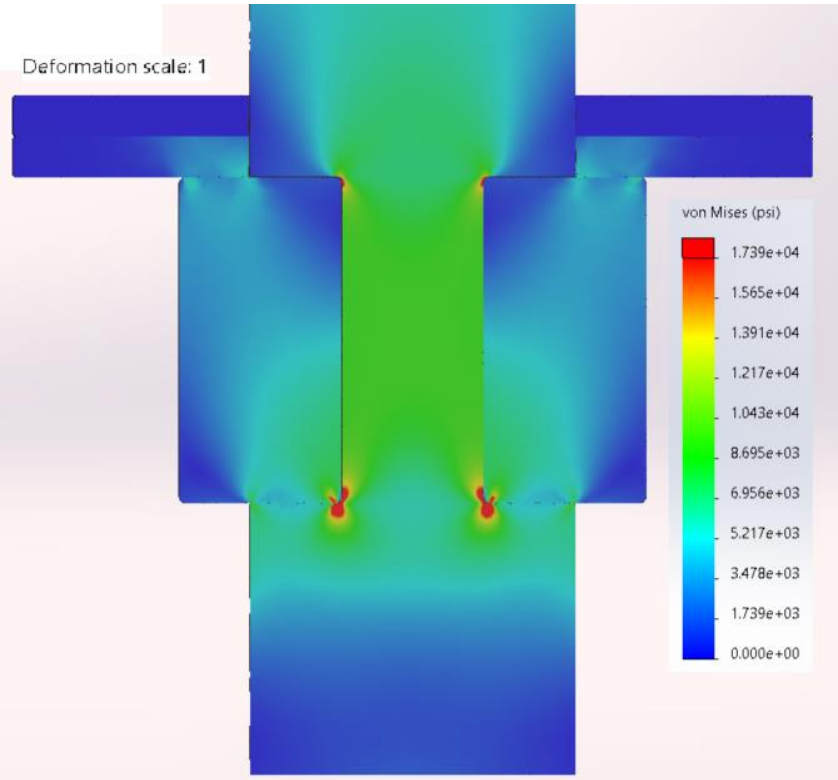

Figure 258: Limiting Stress (17390[psi]) of Pin-Coupling Assembly Side

The high-stress region of ingress, due to the radius, is about 0.15[in]. The endurance stress ingress is about 0.06[in]. The ratio of ingress of S_e with respect to the width of the shaft is 0.06/1.3/2 = 10.8[-]: Since the ingress is insignificant with respect to the supporting structure the pin assembly maintains a FS of 2.875[-].

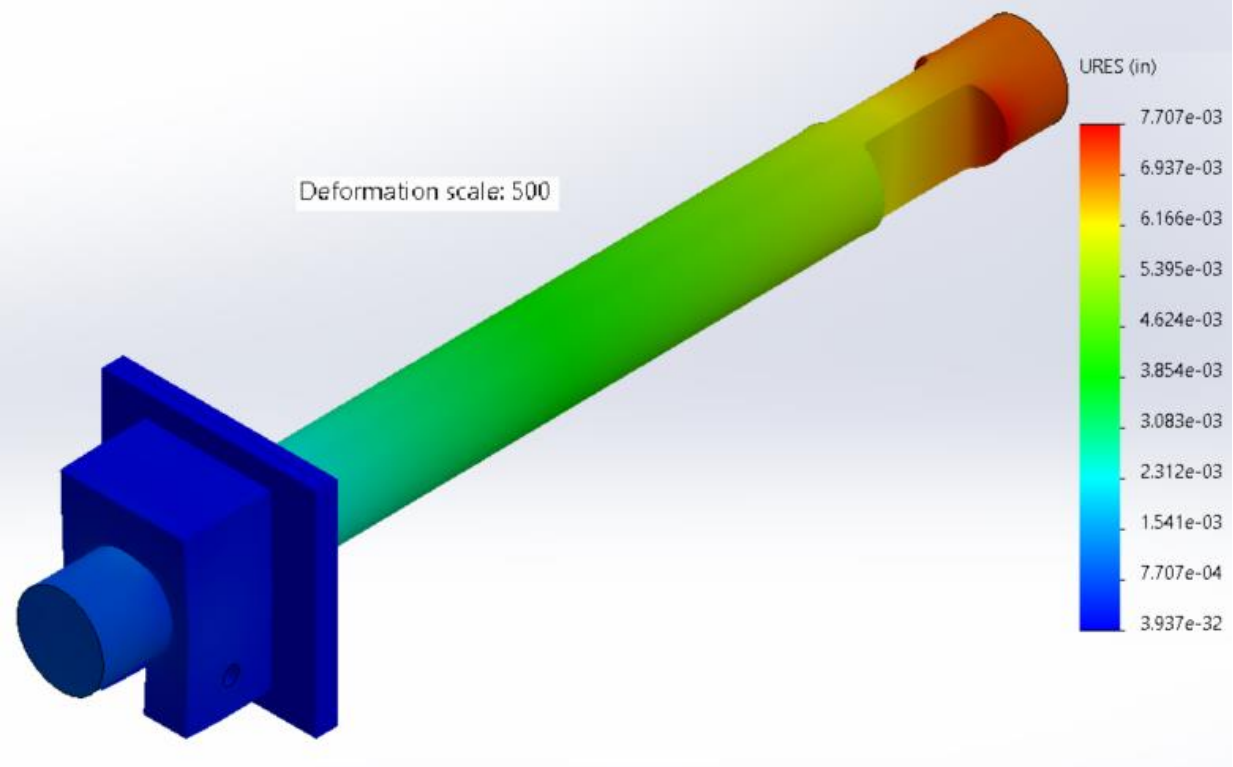

Figure 259: Deformation of Coupling Pin Assembly, 0.008[in] (0.198[mm])

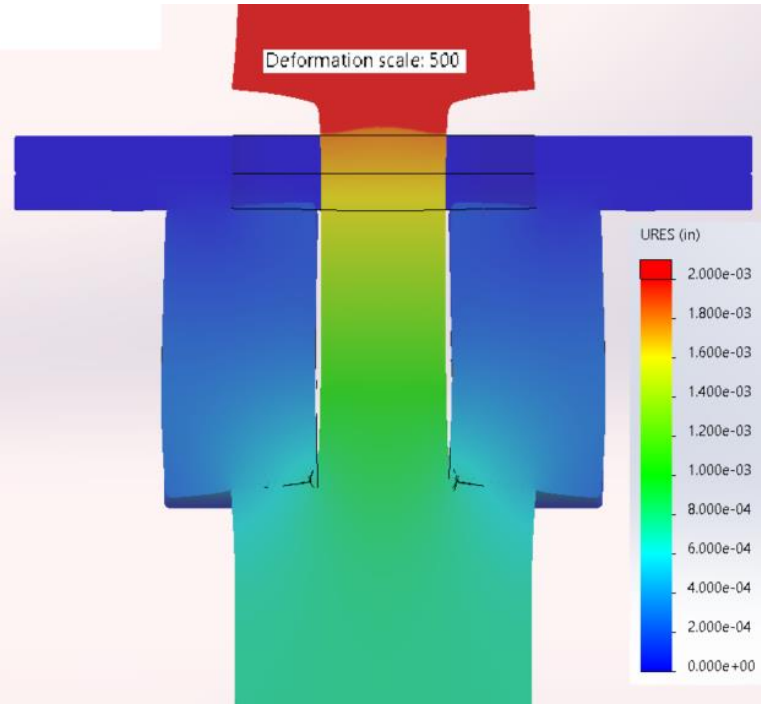

Figure 260: Deformation Near Clevis is less than 0.002[in]

After a short interlude, the pin designs were improved and the arm-base structure was re-designed. Each support (above) is a bit over designed. The pins below will have reduced stress and utilize more of its available material.

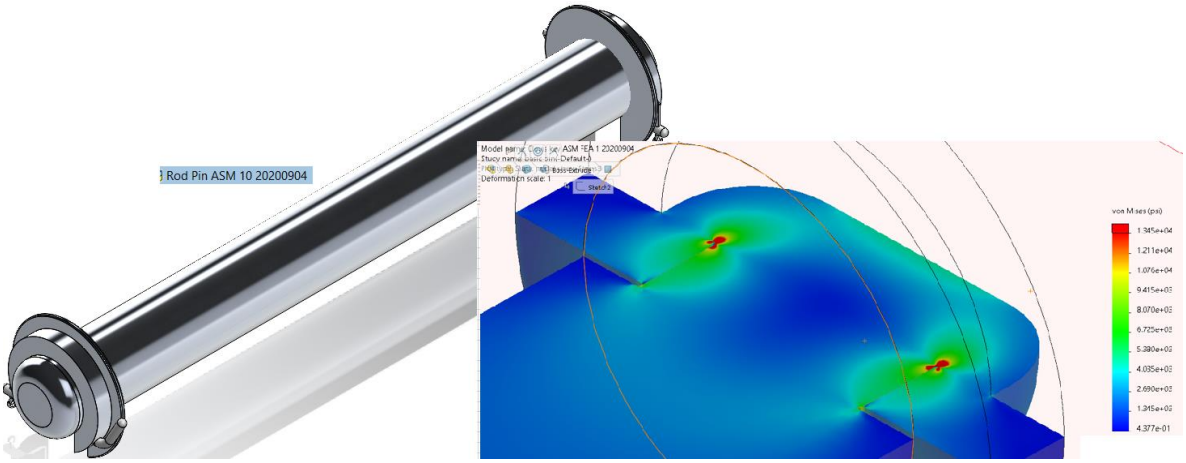

Figure 261: Standard Rod-Clevis Assembly

The standard rod-clevis assembly undergoes minor axial stresses on the order of 6,700[Lbf] and a shear load on the order of 0[Lbf]. As mentioned earlier, Table 134, this is accomplished with a 2.25[in] rod-clevis assembly. This rod-clevis/pin assembly is found in segments 2 thru 7.

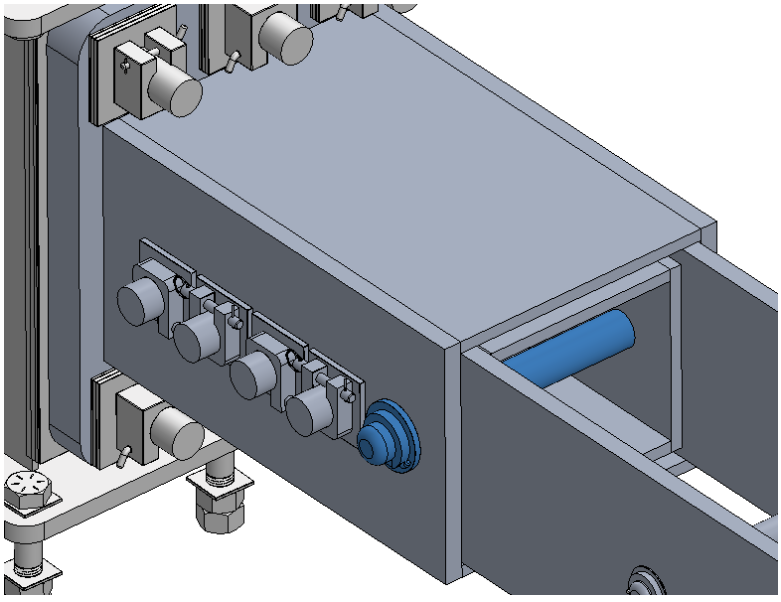

Figure 262: Main (x5) Pin Assembly Design Change

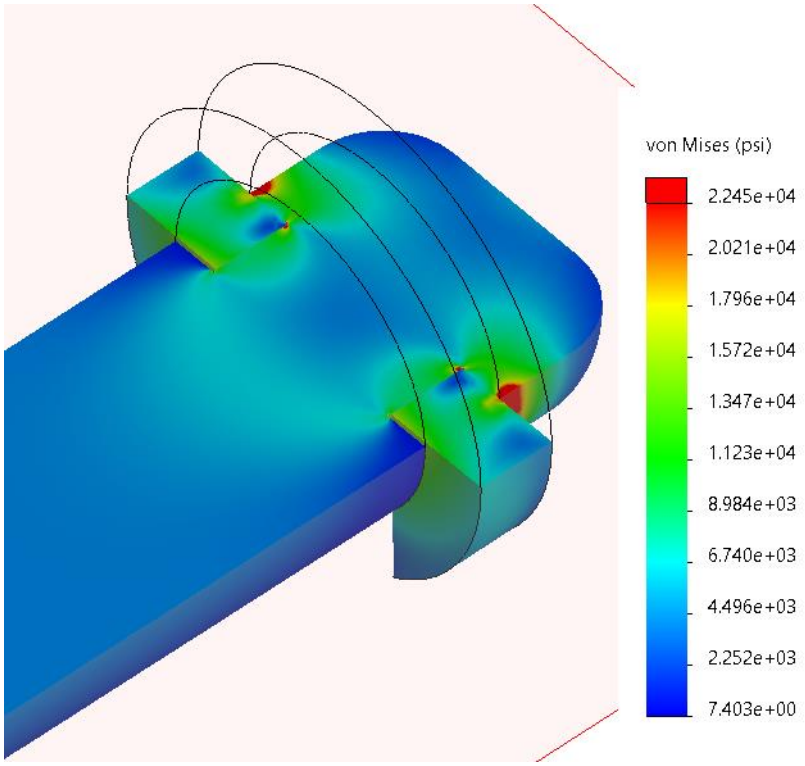

Figure 263: Endurance Stress on Main (x5)-Pin Assembly

The two main components of this redesign are less length or less weight and a compact design. It will be slightly more difficult to assembly, however, there will be slightly more space/room to work-with.

The loading point of action (from the previous analysis) is about 5” rearward of the first pin; on the brace-coupling to the main structure. Note that the previous design had a 3[in] back-plate. An attempt will be made to decrease the weight and the foot-print of the standard brace-coupling, to the main structure (from the arm/s).

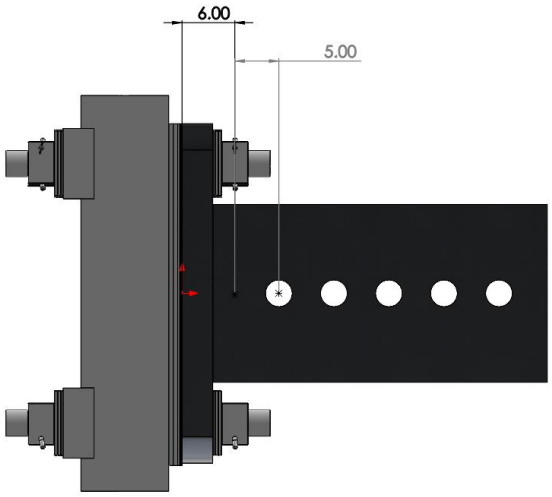

Figure 264: Previous Design with 3" Back-plate

An evaluation of a lighter, more compact Arm-to-Base joint was performed. The findings from that evaluation show that the upper left joint, back-plate, experiences the greatest amount of deflection; as-is (seen in Figure 265, on the order of 0.5"). The back-plate was reduced to 2" and only the outer most pins were "fixed." Also, the loadings (as noted from Table 139 to Table 140 & Table 141) were applied to achieve the worst-case bending; not and actual case.

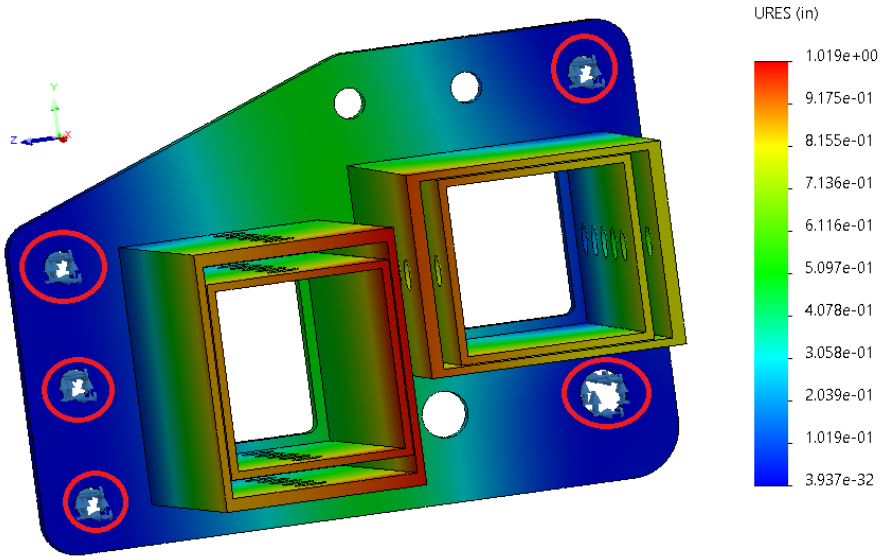

Figure 265: Upper-left Corner Arm-to-Base Joint/Coupling

Table 140: Left Member Loading in Figure 265

Fx	-230,000	[Lbf]
Fy	35,000	[Lbf]
Fz	-35,000	[Lbf]
Mx	-5,100	[Lbf-in]
My	5,100	[Lbf-in]
Mz	5,100	[Lbf-in]

Table 141: Right Member Loading in Figure 265

Fx	-230,000	[Lbf]
Fy	35,000	[Lbf]
Fz	35,000	[Lbf]
Mx	5,100	[Lbf-in]
My	-5,100	[Lbf-in]

Mz	5,100	[Lbf-in]

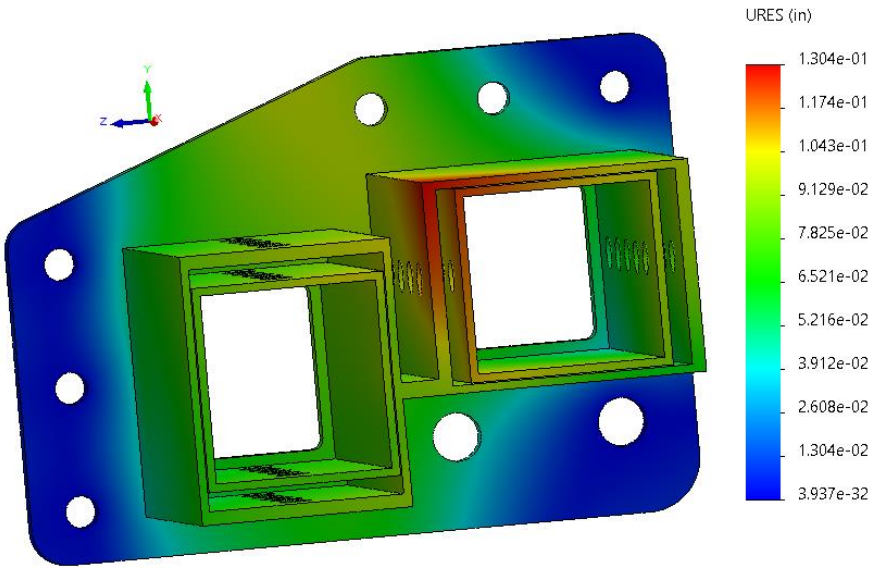

Figure 266: Upper-left Corner Arm-to-Base Joint/Coupling w/Joining-member

As seen in Figure 266, the addition of a joining or coupling member between the right and left beams reduces the plate deflection by almost a factor of 10; to 0.065[in]. The addition of a center-beam would reduce this deflection further.

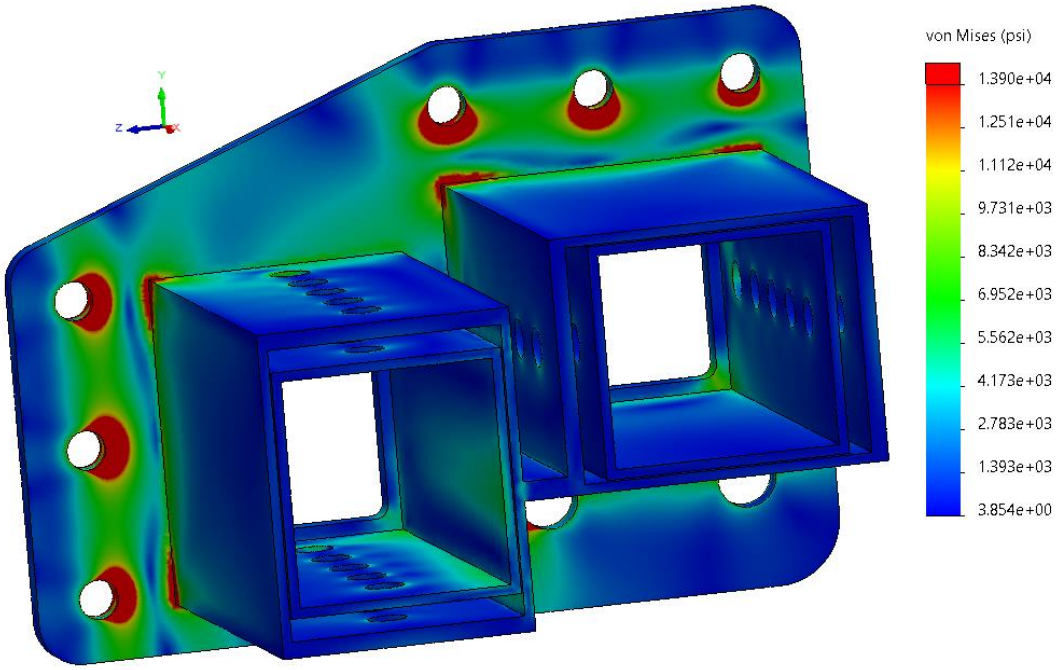

Figure 267: Stress of Upper-left Corner Arm-to-Base Joint/Coupling w/All Fixed Pins

Since the upper-left corner brace is the largest, it will experience the greatest amount of bending stress. The FEA shows that the maximum deflection of its support plate is less than 0.04[in]; under the worst-case (improbable) condition.

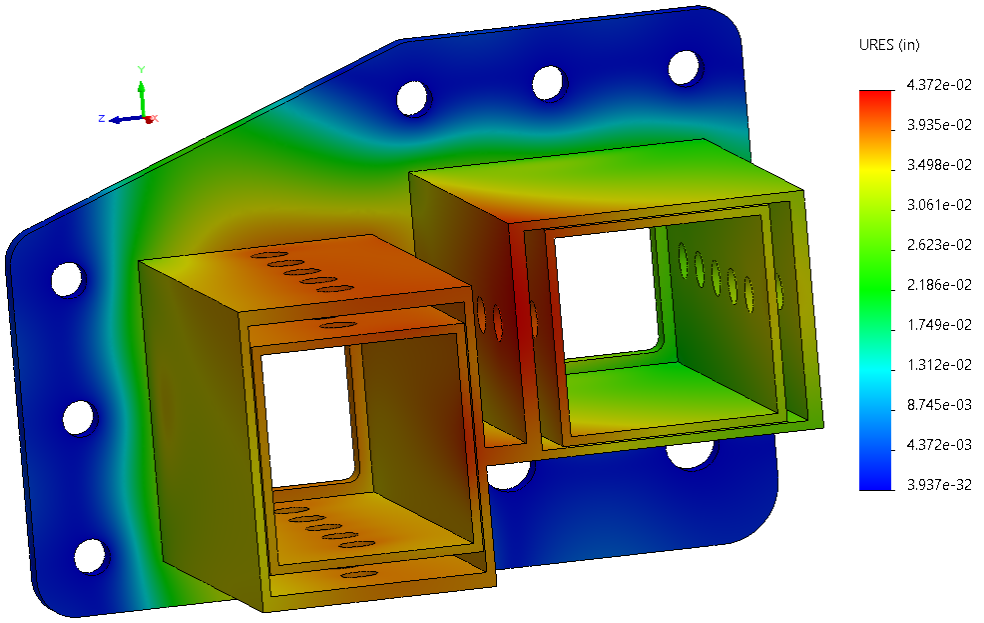

Figure 268: Deflection of Upper-left Corner Arm-to-Base Joint/Coupling w/All Fixed Pins

A deflection on the order of 0.04[in] can be expected in the upper-left corner back-plate. As seen in Figure 269, the maximum loading on the 4.5" pin is < 119050, 7877, 27380 >[Lbf]. Adding 10[%] to these values yields an axial load of 131,000[Lbf] and a shear load of 31,200[Lbf]. Adding 10[%] to the 3[in] pins yields an axial load of 67,310[Lbf] and a shear load of 43,600[Lbf].

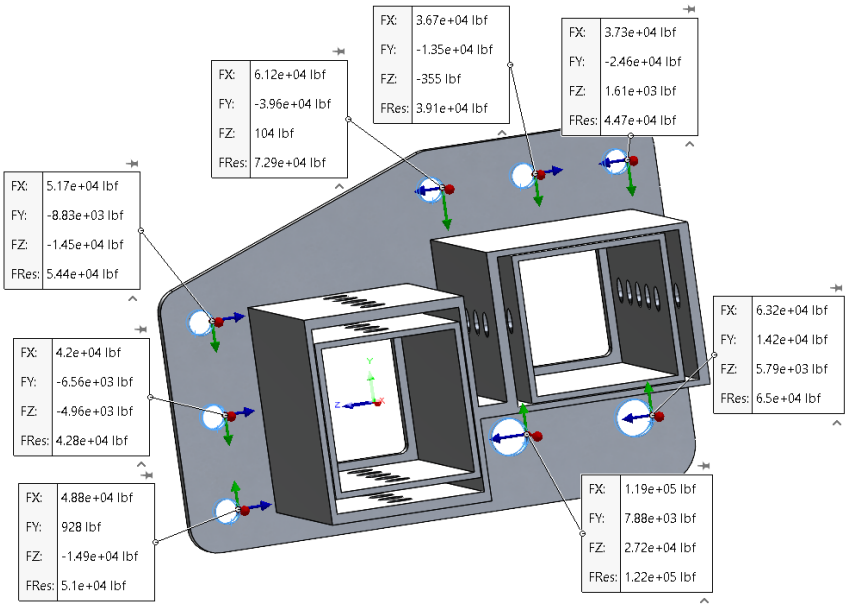

Figure 269: Reaction Forces at Pin Locations, Upper Left Coupling

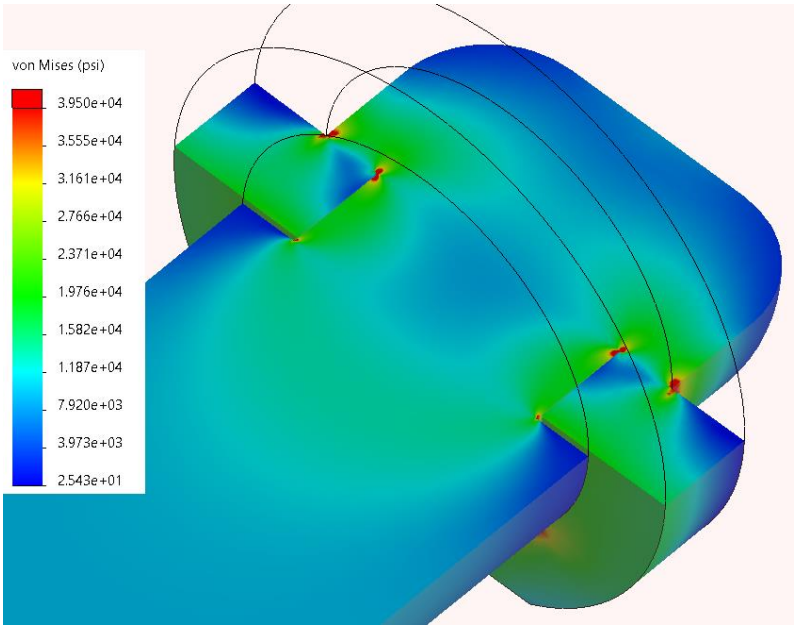

Figure 270: Yield Stress on 3" Pin on Upper Left Back-plate

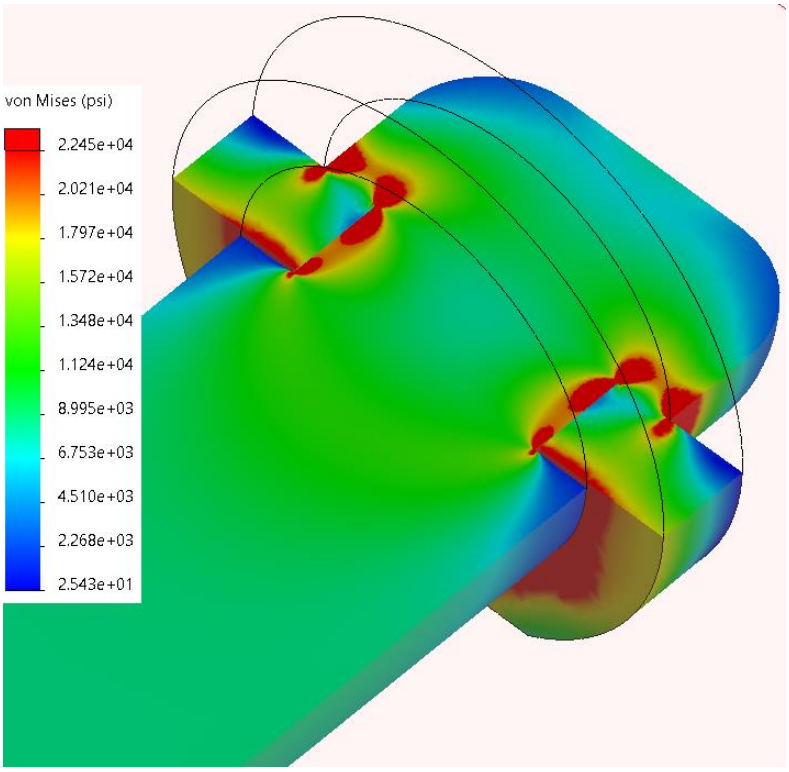

Figure 271: Endurance Stress on 3" Pin on Upper Left Back-plate

As seen in Figure 270, the 3[in] pin will not yield. If the part undergoes many cycles, it may experience some deformation; as seen in Figure 271. By itself, the pin does not satisfy the FS of 2.875[-]. The reasons to keep this 3[in] pin (with a 2.1[in] clevis diameter) are:

1) That the maximum loading conditions less than 1 in 50[years]; thus, the event may occur once in 100[years] or more.

2) Under the maximum load the pin will not yield.

3) Endurance stress deformations are minimal; should they form.

4) There are many other pins holding the corner-coupling in-place.

Note: The inner structure should be examined annually and after a major event

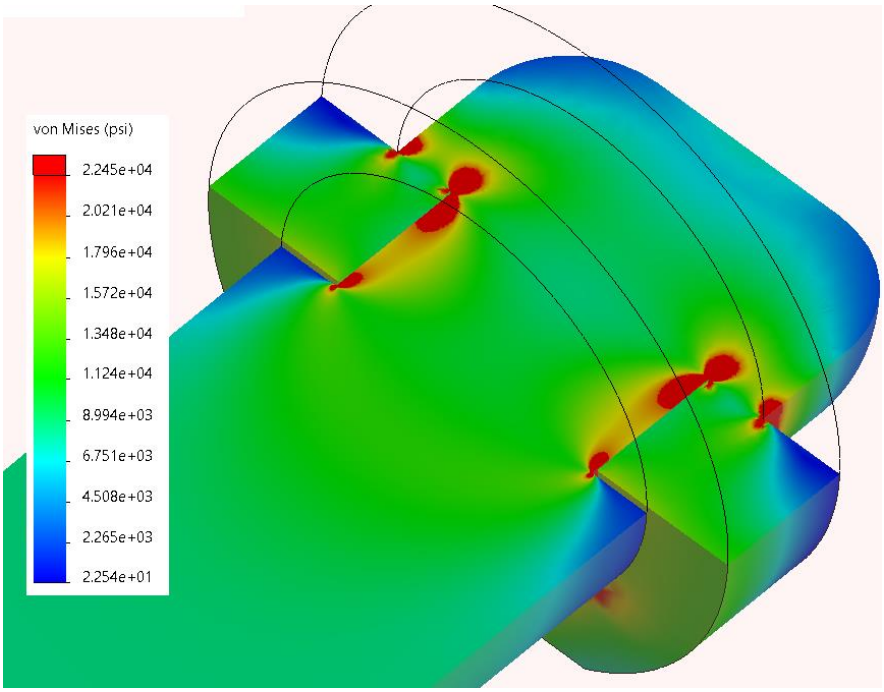

Figure 272: Figure 271, with 1" Thick Clevis

As seen in Figure 272, increasing the clevis from 0.75” to 1.0” eliminate deformation due to endurance. Therefore, the 3” backplate-pins will have 1” thick clevises.

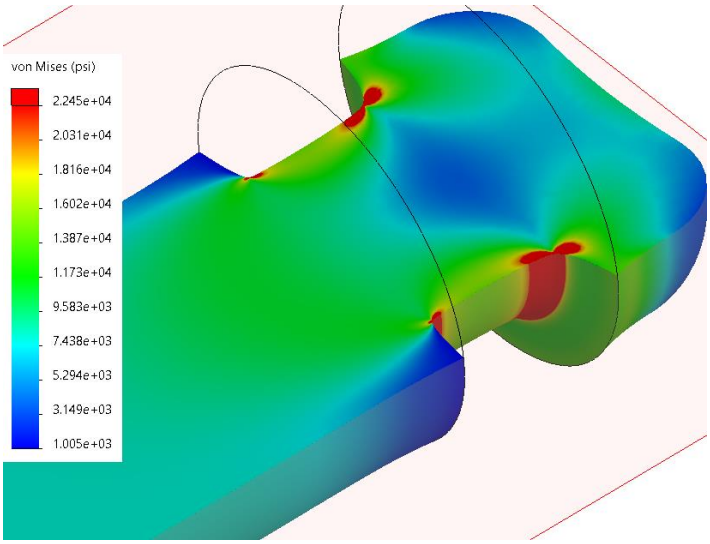

Figure 273: Endurance Stress on the 4.5[in] Pin with 131,000[Lbf] and 1.25[in] Clevis

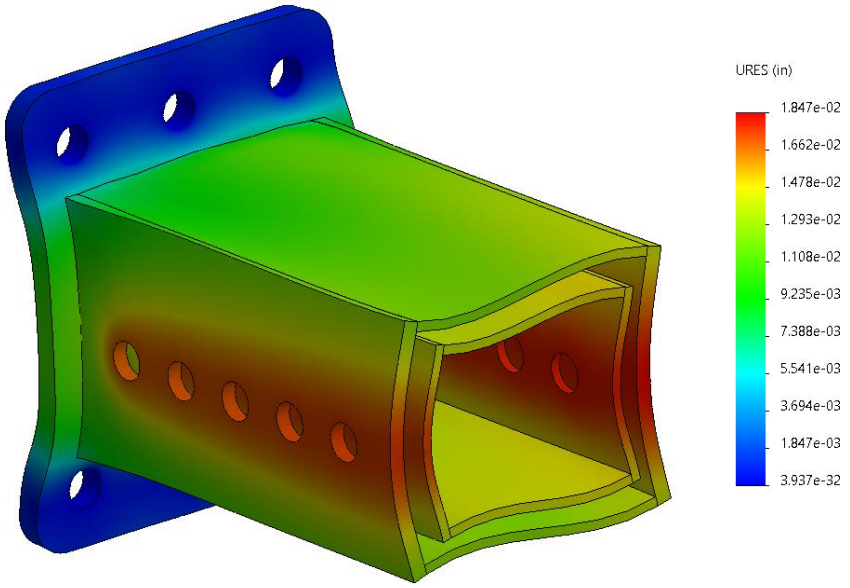

Figure 274: Deflection of Standard Coupling of Arm to Main Structure w/2" Backplate w/ Pull-loading

The standard couplings change to a 2[in] backplate with about 0.012[in] of deflection. The pin areas will experience deflections on the order of 0.02[in]. Since the acting stresses are low, this structure has a FS of 2.875[-]. Similar results appear when a "pushing" load is applied.

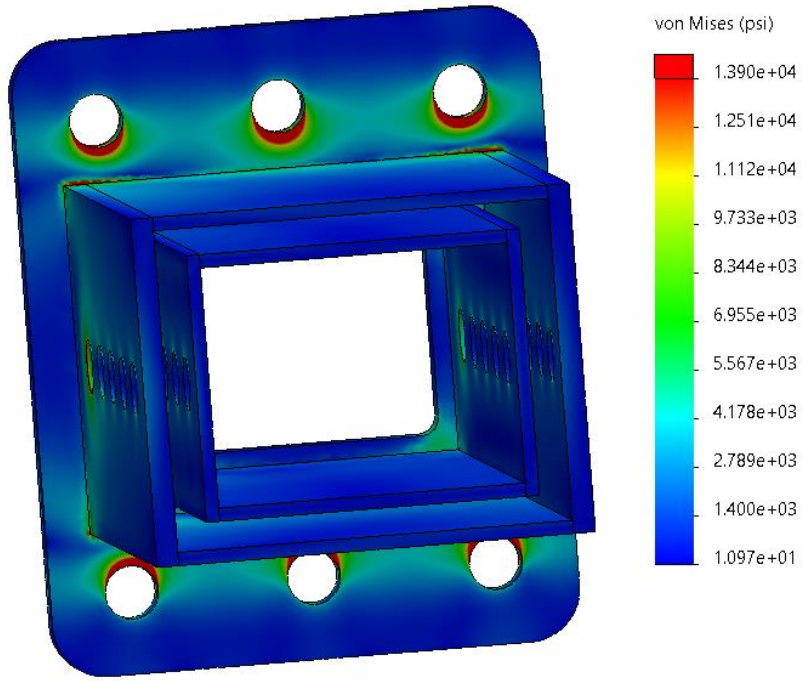

Figure 275: FS of 2.875[-] of Standard Coupling of Arm to Main Structure w/2" Backplate

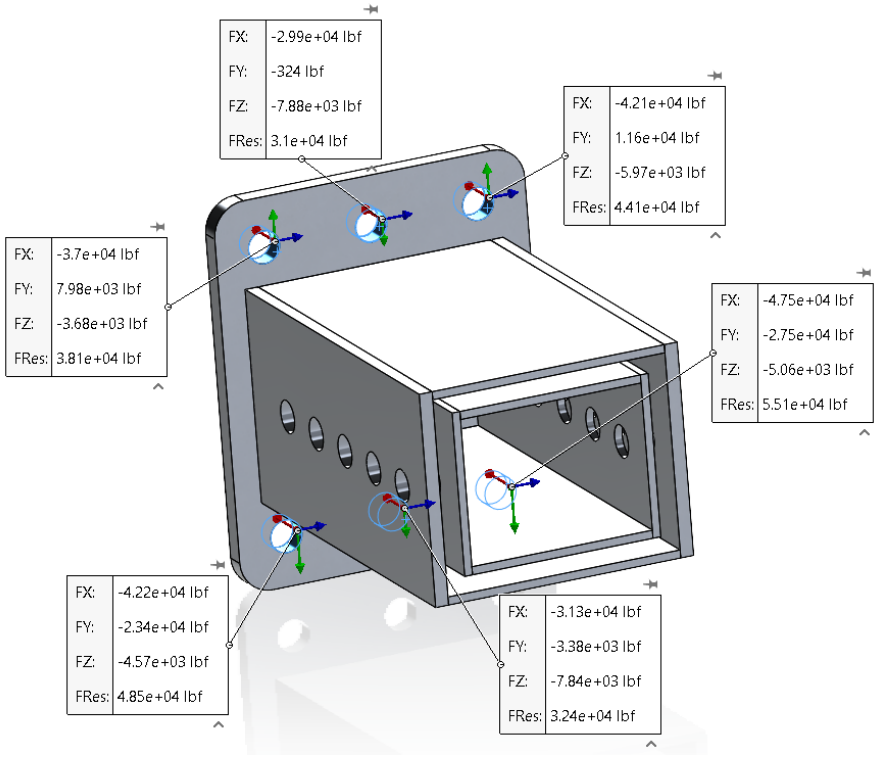

Figure 276: Maximum Axial Pin Loading of 47,460[Lbf]

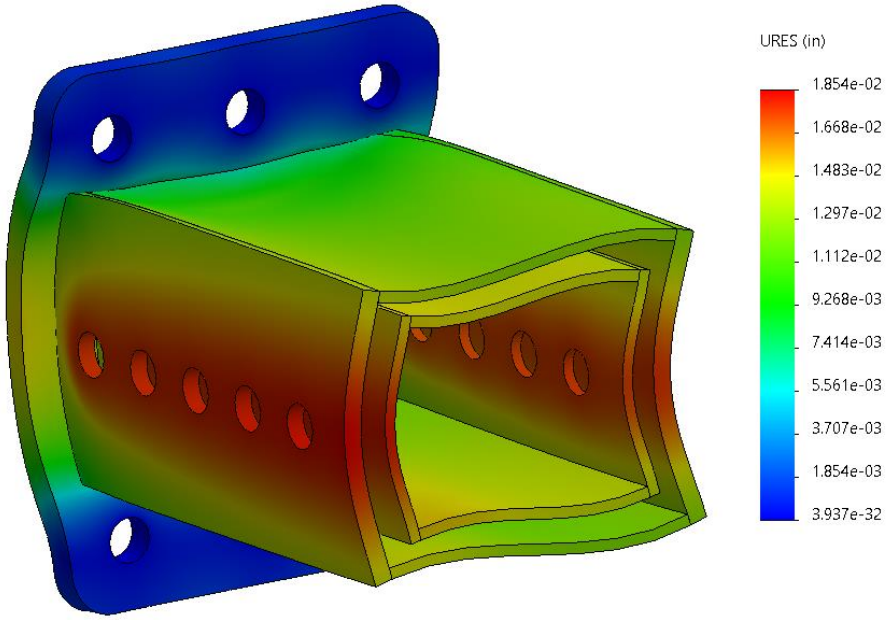

Figure 277: Deflection of Standard Coupling of Arm to Main Structure w/2" Backplate w/ ***Pushing****-loading*

The main arm-to-main structure couplings/support (Figure 274, Figure 275, Figure 276 and Figure 277) maximum stresses and deflections are relatively small; therefore its expected life is greater than 100[years]. The coupling-pins do have high concentrated loads, therefore, after a major event (such as high winds) the couplings-to-pin areas should be examined for gaps and other deformities.

After placing the necessary structure together, the joining of the arm/s to the main structure is achieved with approximately 500[tons] of metals (steel and aluminum). As seen in Figure 278, only (x2) rows of W14x193 main column structural beams are shown: This is done because these beams are directly attached to the arms' main structure. This figure shows the structure of the first segment, of the arm.

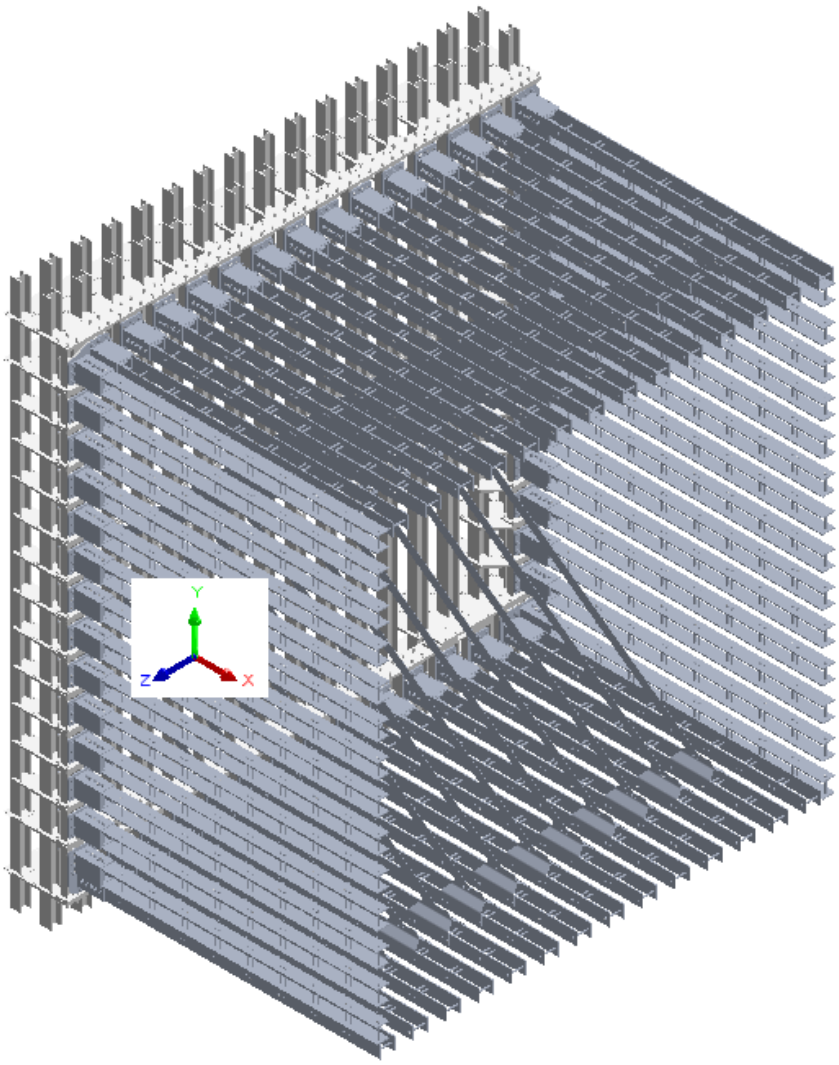

Figure 278: Arm Structure to Main Body

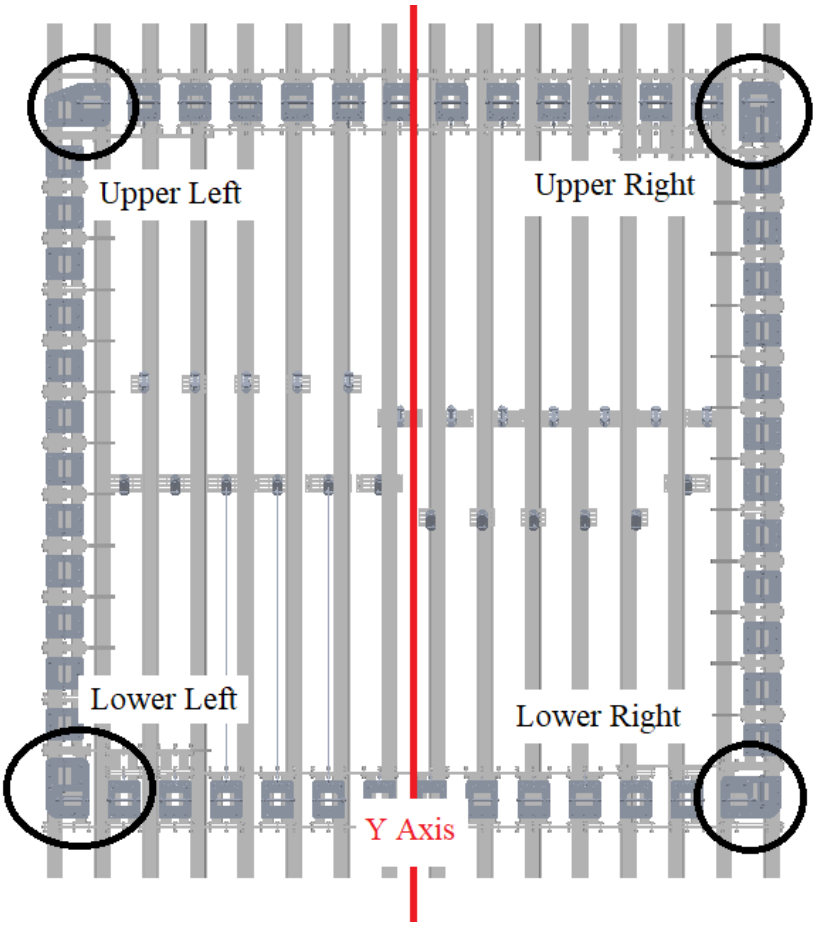

Figure 279: Arm Main Connecting Structure, End View of Positive "X" Arm

Some typical definitions are noted in Figure 279, utilizing the arm extending in the positive "X" direction. To generate the arm extending in the negative "X" direction, the system is rotated about the "Y" axis.

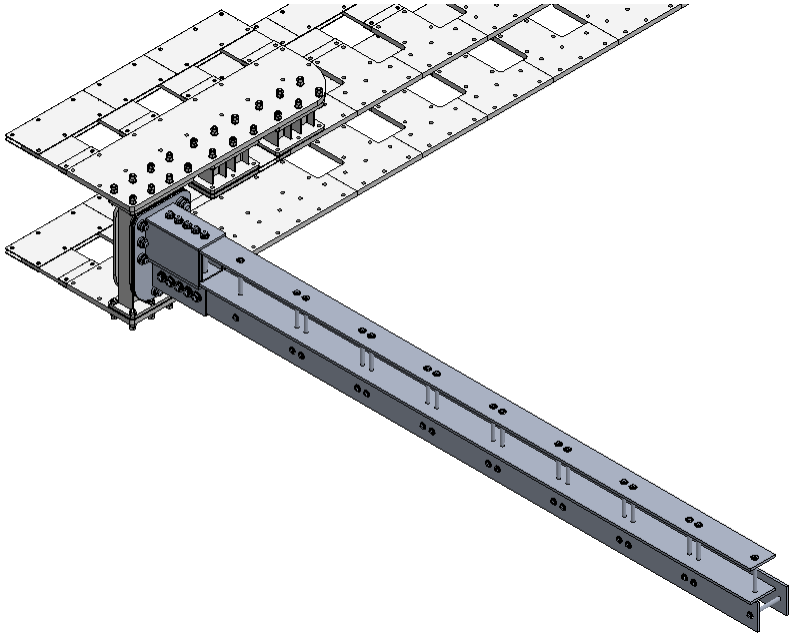

Figure 280: Arm-to-Main Structure, Lower Left

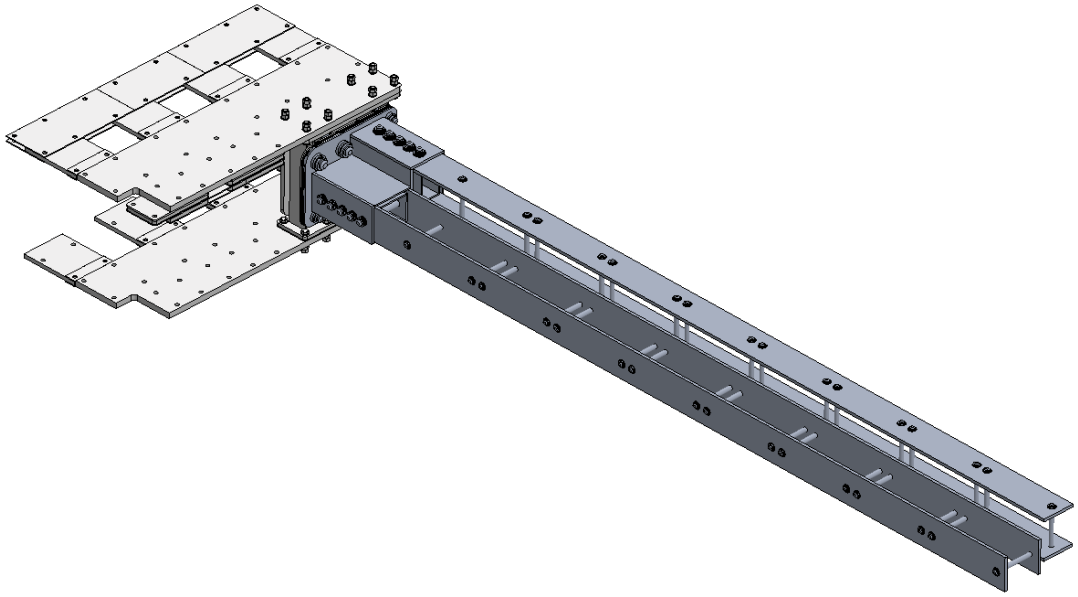

Figure 281: Arm-to-Main Structure, Lower Right

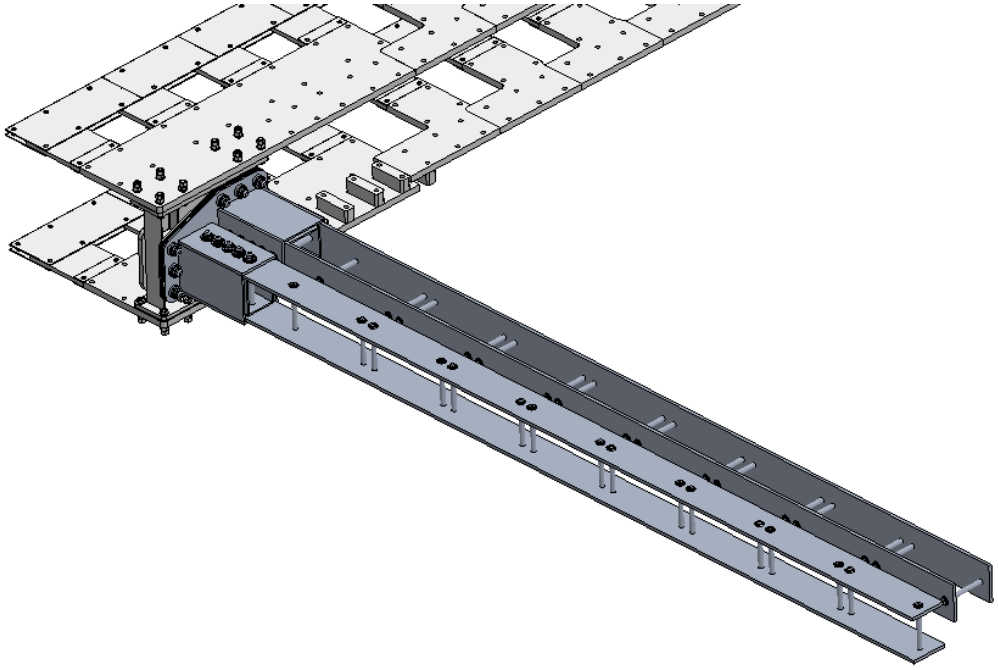

Figure 282: Arm-to-Main Structure, Upper Left

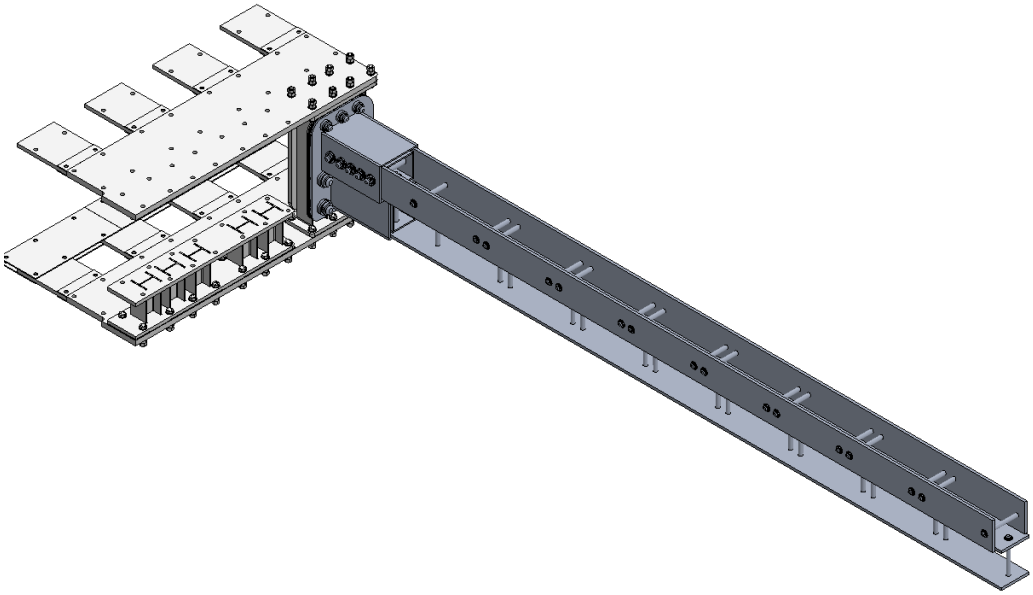

Figure 283: Arm-to-Main Structure, Upper Right

Figure 284: Arm-to-Main, Typical Side Structure

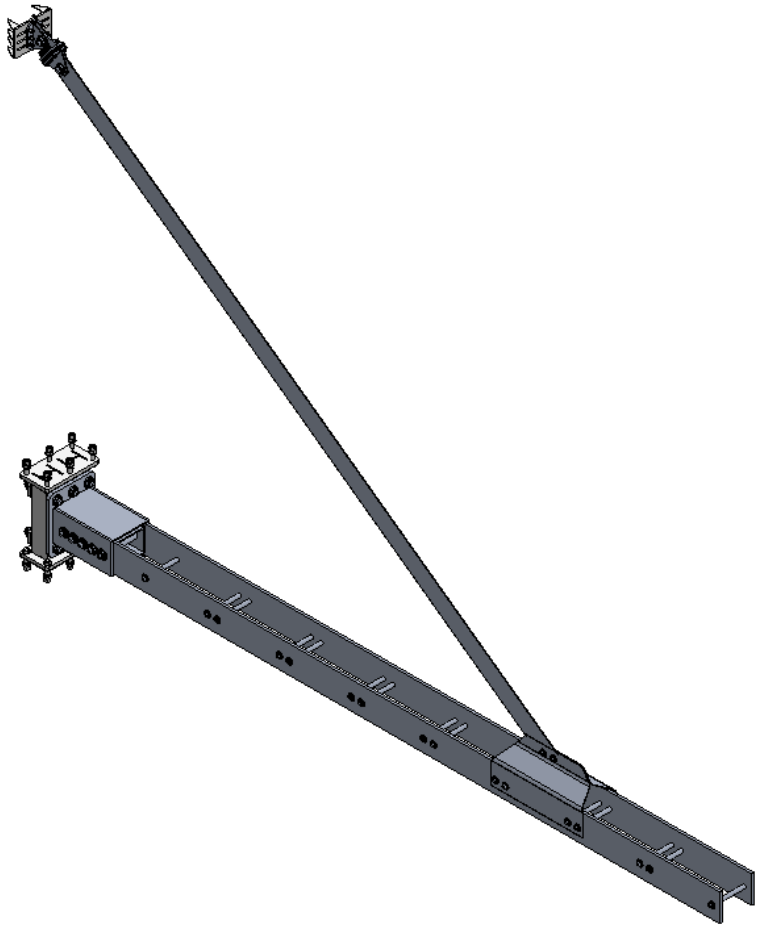

Figure 285: Arm-to-Main, Typical Top/Bottom Structure

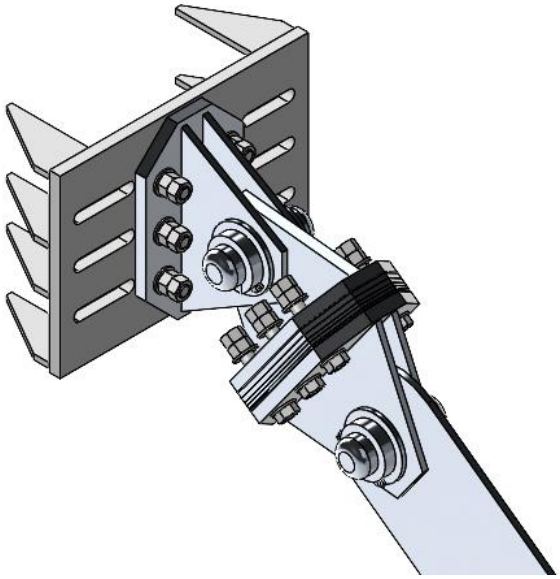

Figure 286: Angled Connection Plate to 1st Structural Beam

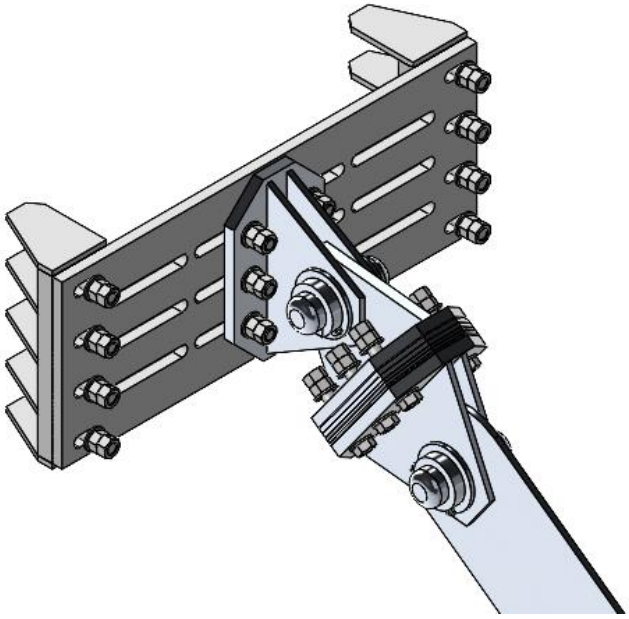

Figure 287: Angled Connection Plate to 2nd Structural Beam

The arms' structure that attaches to the 2nd structural beam as seen in Figure 287, is found within Figure 285. Though, structurally they are not needed, these angled beam-connections will assist in resisting gravity and reduce the arm deflection.

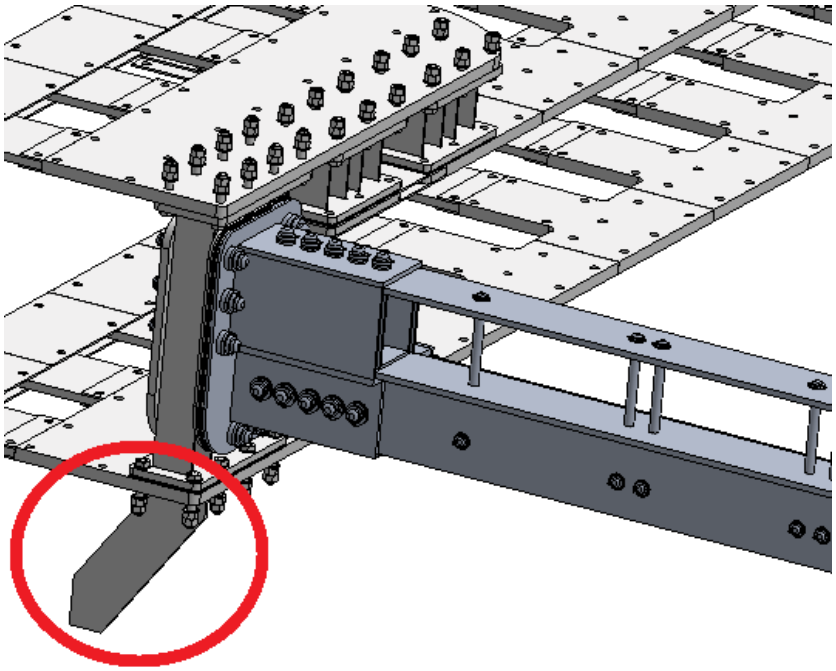

Figure 288: Arm Support to Main Structure, 55[deg] Support

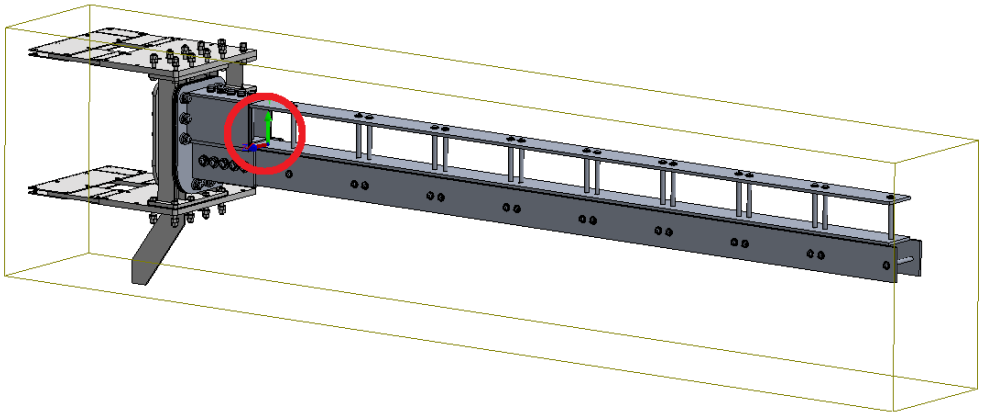

Figure 289: Arm Support to Main Structure, 55[deg] Support - Cg

The actual mass and cg shown in Figure 289, is 19,811]Lbf] at 37.15[in] from the front face of the main coupling (lower left-hand shown). Without the 55[deg] brace and under these conditions, the lower plate deflection is about 0.132[in] (max). At 123[ksi] the maximum deflection (without the 55[deg] support) is about 0.82[in].

Under an estimated worst-case condition, the maximum load per-55[deg] support/brace will be about 123,300[Lbf]. With a 1[in] support/brace, the maximum stress in the beam will be less than 10,000[psi]; thus, it passes. Utilizing the maximum load conditions, the 1[in] x 55[deg] brace is expected to compress less than 0.022[in], with a dy-deflection of less than 0.018[in]. After some design changes, the standard support brace grew a bit wider and its angle changed to 60[deg]; both of these actions increased variability in the model and reduced stress in the part.

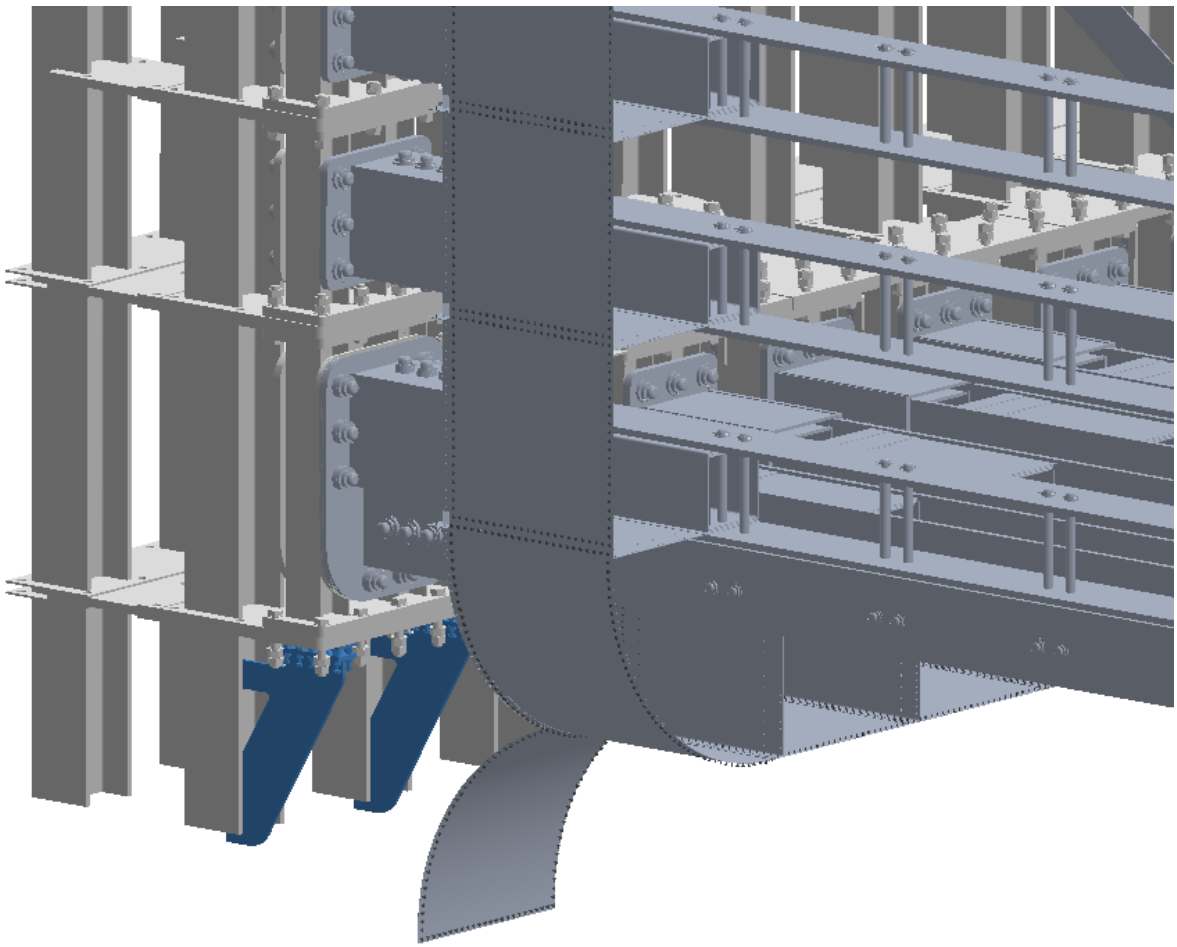

Figure 290: Arm Support to Main Structure, 60[deg] Support

The final design for supporting the main arm-couplings is a 1[in] plate at about 60[deg]. Where weight is the only consideration, the expected deflection of the lower 3[in] plate is less than 0.01[in].

D. Panels for Arm to Main Body

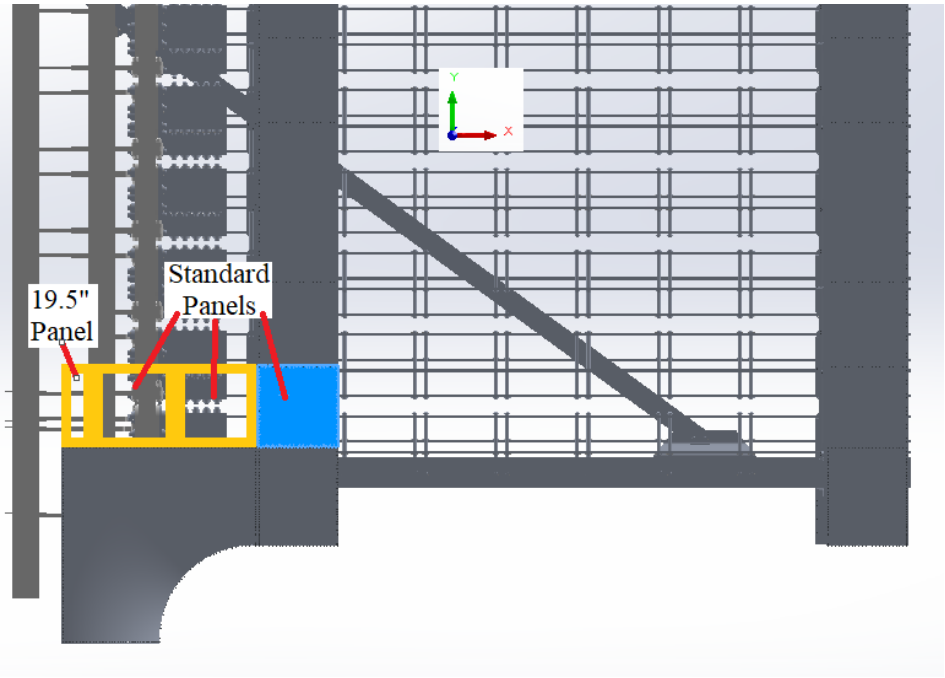

Figure 291: Panel Transition from Arm to Main/Standard Panel Layout

Maintaining an outer-skin radius of 54.4[in], a corner structure must be employed to support the transition panels. The (x3) transition panels and the standard (main-structure) panels are supported by two edges, rather than all four (as found in the arm structure). This is done to optimize the structure and reduce assembly/maintenance costs.

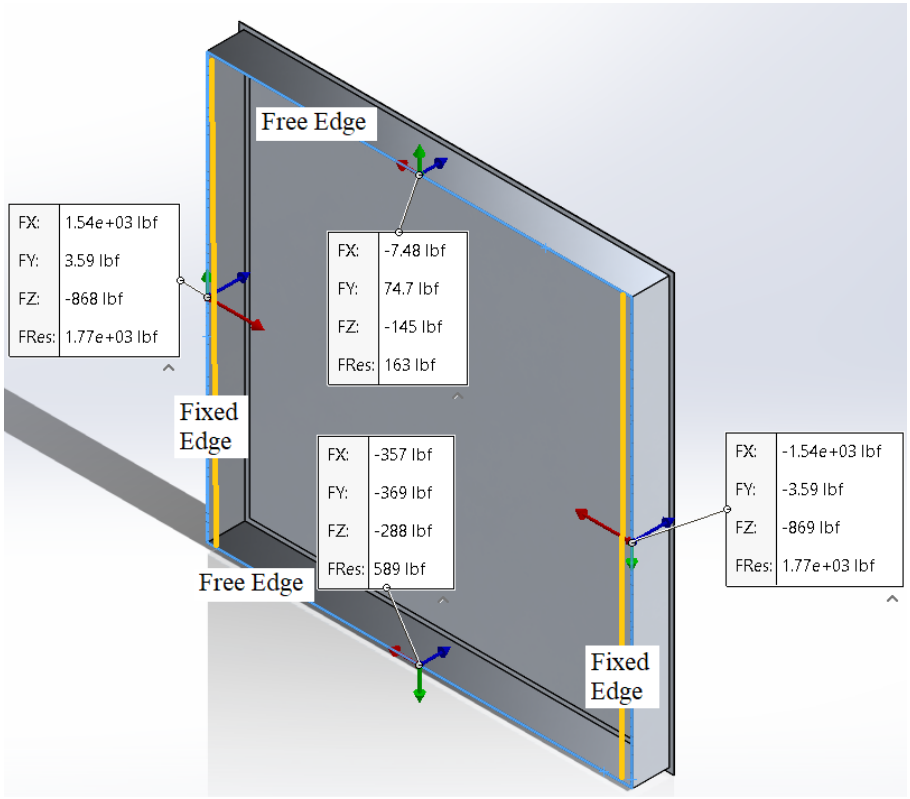

Figure 292: Standard Panel, 47.125", w/Two Edges Supported

With a maximum loading pressure of 0.782[psi] or 5392[Pa] (representing 16% safety) the fixed edges have a compression load of about 870[Lbf], a twisting/lateral load of 1,540[Lb] and an axial load of about 5[Lbf]. The twisting or lateral load is negated by the adjacent panel, thus, the only significant load that remains is the compression load of 870[Lbf]. Therefore, the "free" edges must support a distributed load of no less than 870[Lbf] with minimal deflection/s.

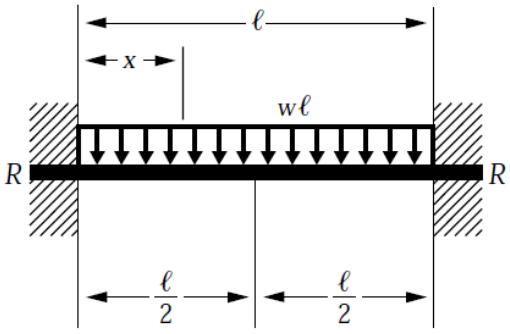

Figure 293: Model of a Beam with Distributed Load

As seen in Figure 22, the maximum deflection of the panel (alone) is on the order of 0.5[in]. Utilizing $1/10^{th}$ the maximum deflection of the panel as one condition and the FS of 2.875[-] as the secondary condition the supporting beam may be characterized/defined. It may be demonstrated that the secondary condition (where the FS is 2.875) is the limiting condition; using AL-T6061-T6. A simple rectangular section of 0.125" x 3.44" allows both conditions to be met (or exceeded); for one panel. Since each panel is surrounded by other panels, each support will be required to resist twice the load. Thus, the minimum acceptable support beam would have an inertia similar to the rectangular cross-section of 0.125" x 4.86"; or a bending inertial value of 1.193[in4] (or a section modulus of 0.492[in3]); with a maximum deflection on the order of 0.014[in].

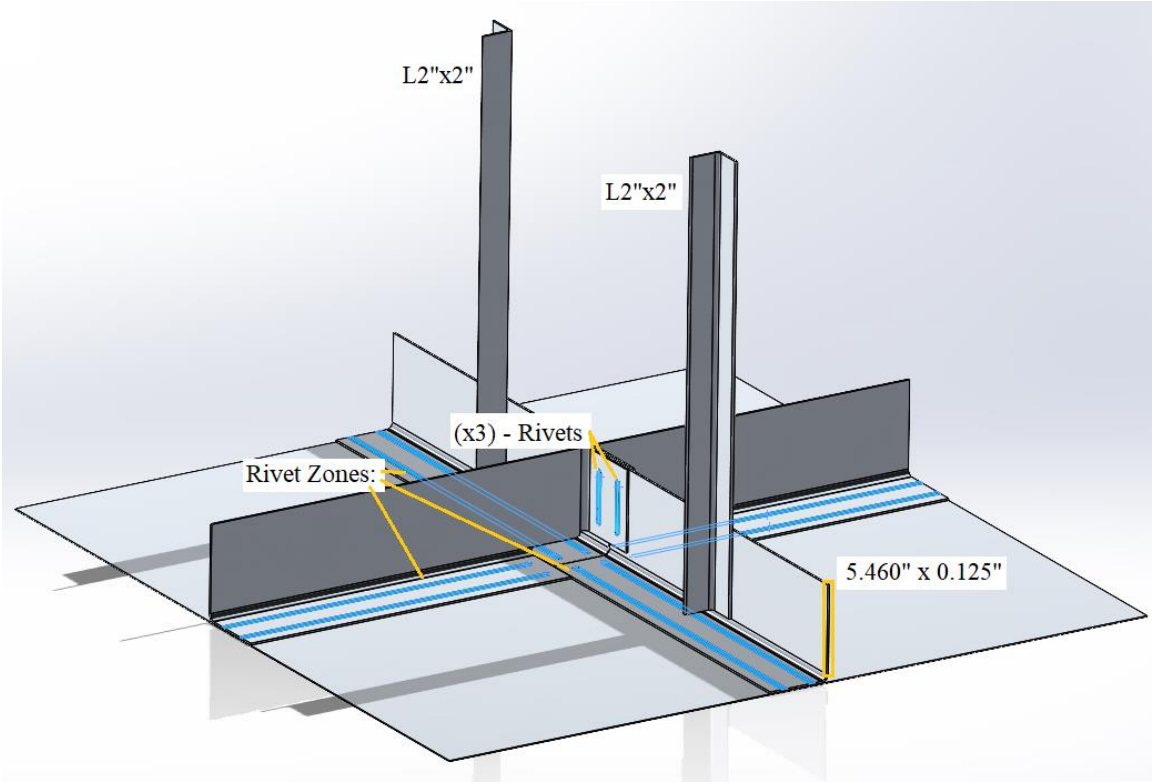

Figure 294: Standard Panel Support Configuration on Main Body

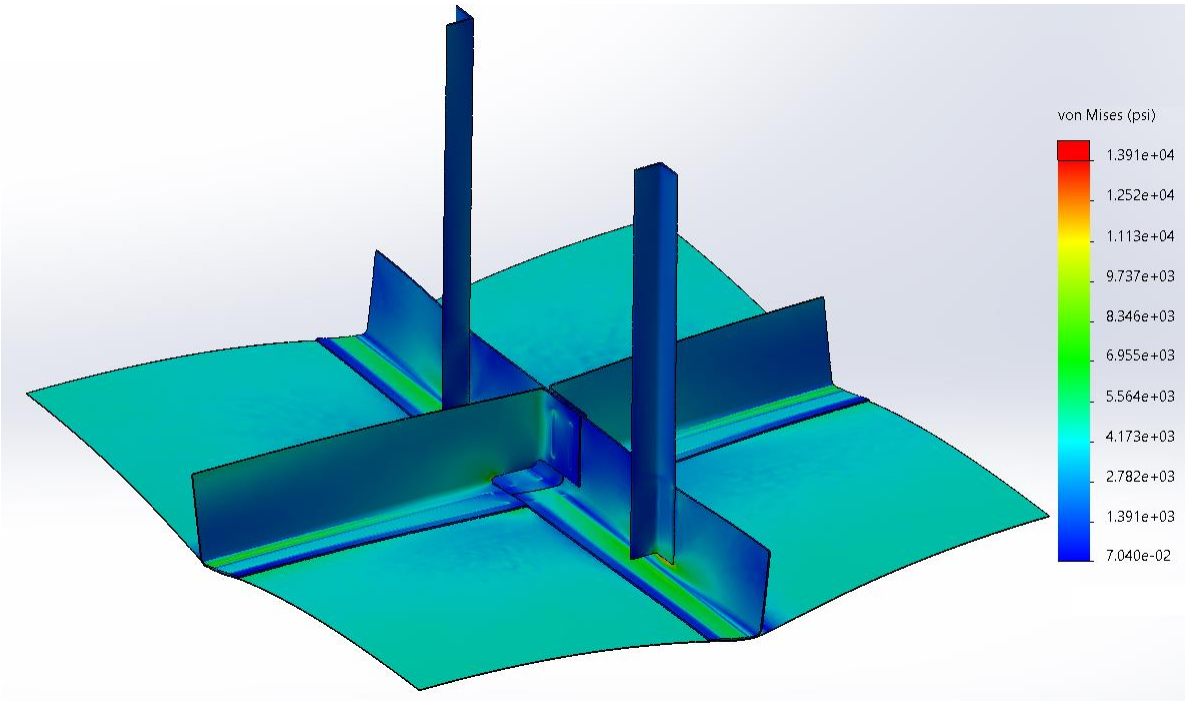

Figure 295: Stress on Main Body Panels, The Intersection of (x4) Standard Panels

Note: Recall, each standard panel is 47.125[in] square.

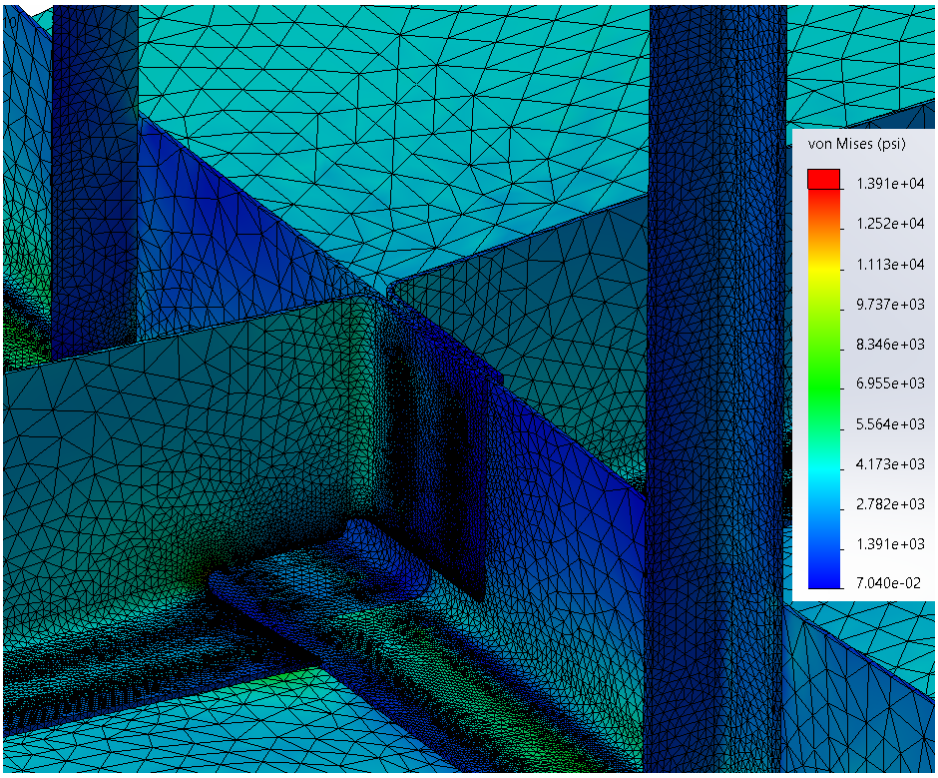

Figure 296: Intersection Zone of Standard Panels w/ Fine Mesh

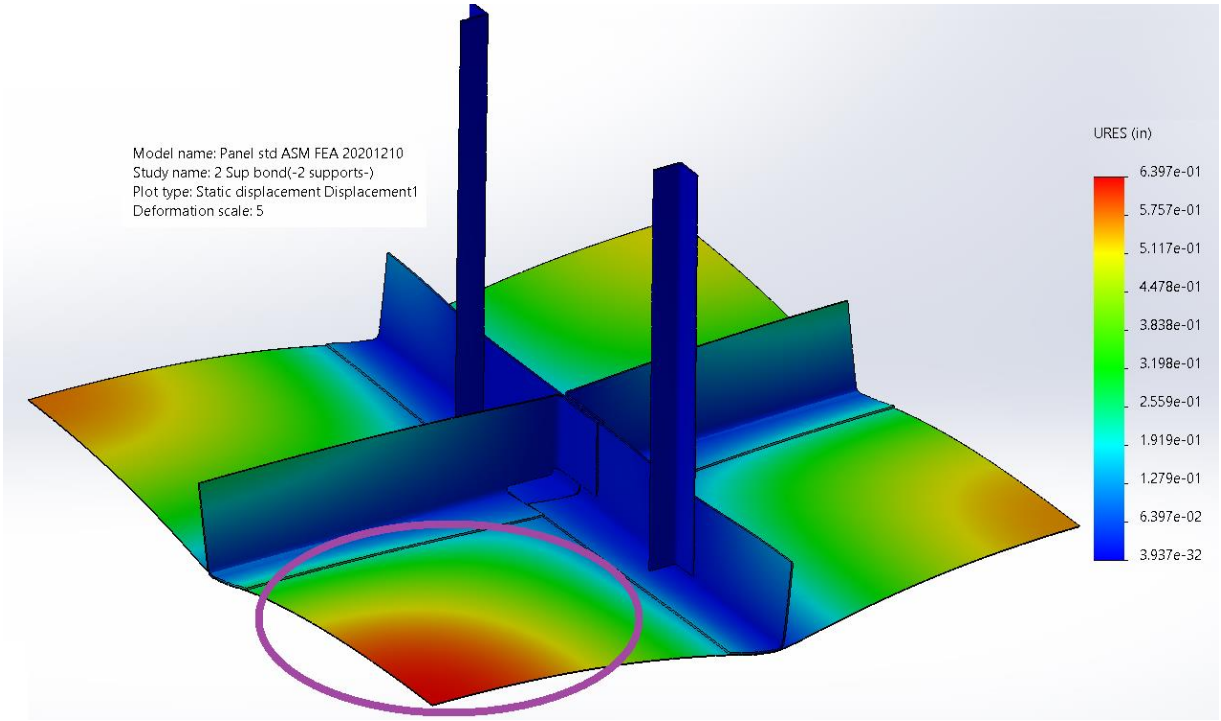

Figure 297: Deflection of Standard Panels on Main Body

Note: Worst-case condition due to asymmetrical ribbing.

In an effort to support the standard panels on the main body of the cross (x2) – L2" x 2" x (1/8)" are utilized, attached with (x3) rivets (each). Due to the eccentricity of the loading, angles are used to avoid buckling. The asymmetrical layout of the supports cause one panel to deflect about 0.64" (max) while the opposite panel deflects only 0.12". Note that the maximum and minimum deflection experienced on the arms will be slightly less; because its structure is much stiffer. In this short study, the end-faces of the L2's were the only "fixed" features. Also, the L2's are 23.5625" apart, in the above figures; or 11.781[in] (calculated from 47.125/4) off of center-panel.

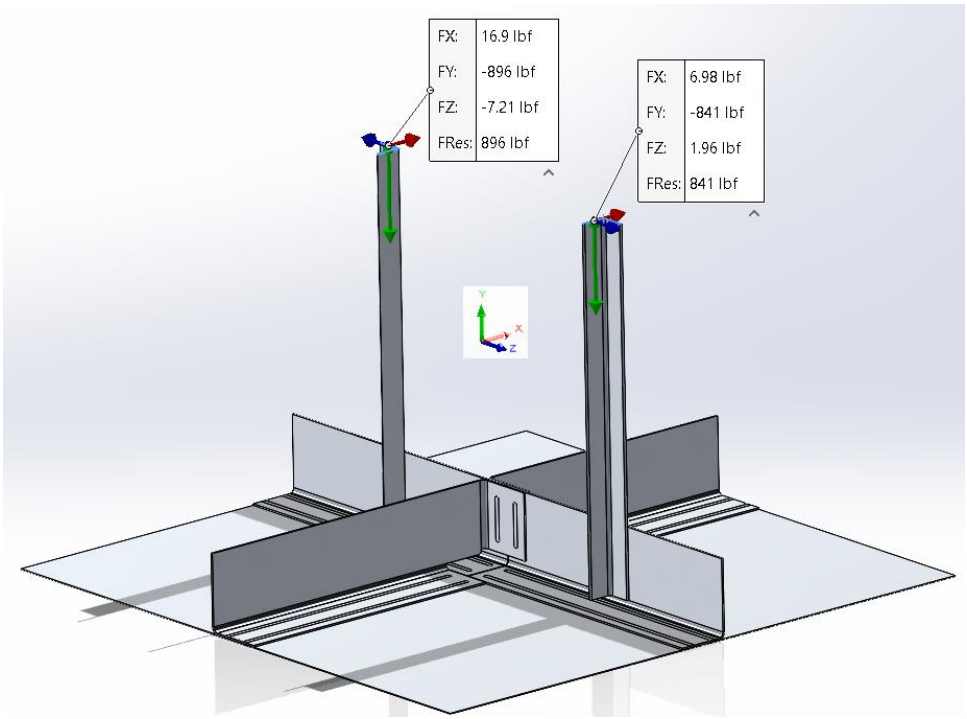

Figure 298: Main Body, Standard Panel Support Load

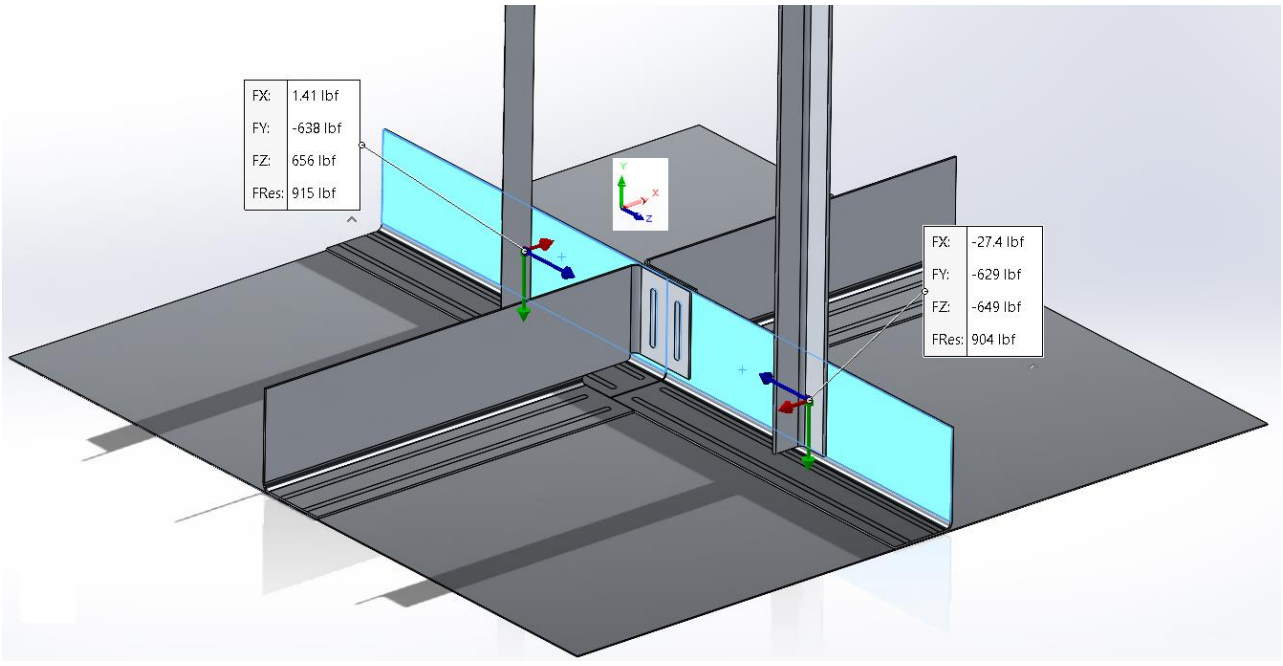

Figure 299: Main Body, Standard Panel Rib Free-body Loads w/r L2's

The maximum shear load for the rivets, with respect to the L2's, is about 920[Lbf] and the pull-out load is about 30[Lbf]; thus, the maximum stress on one rivet would be less than 8,500[psi]. Therefore, (x1) – (3/8)" rivet will be able to hold the structure together.

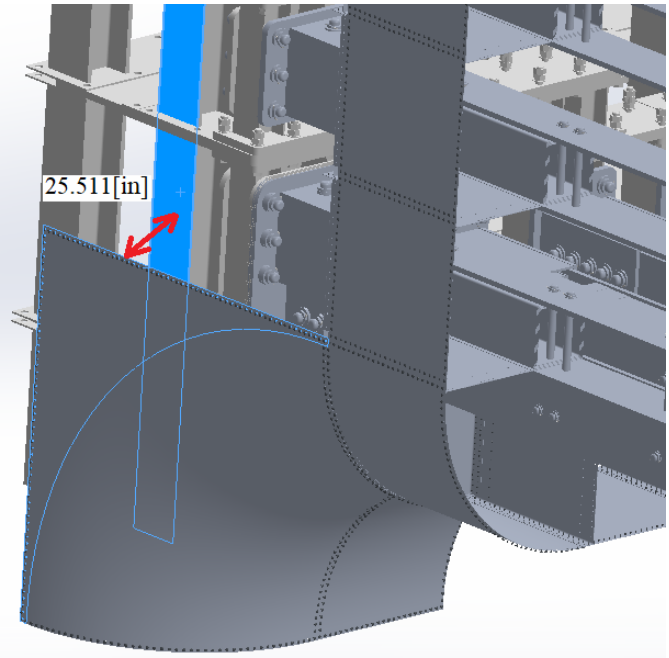

Figure 300: Distance from Beam to Skin w/r Main Body

The maximum lever-arm for the (x4) supports for each square 47.125" panel is 25.511[in]. When assembled every (x2) supports will be required to support about 30[Lbf] at (about) 25.511[in] from its base.

The assembly of the panels to the main structure is performed with tolerances; nothing is perfect; thus, it is likely that a lower panel-support/s will have to support at least part of the weight of the above/adjoining panel. From the assembly variances three cases are obtained: 1) Each support resists 15[Lbf], 2) Each support resists 150[Lbf], (x10) panels, and 3) Each support resists 1,500[Lbf].

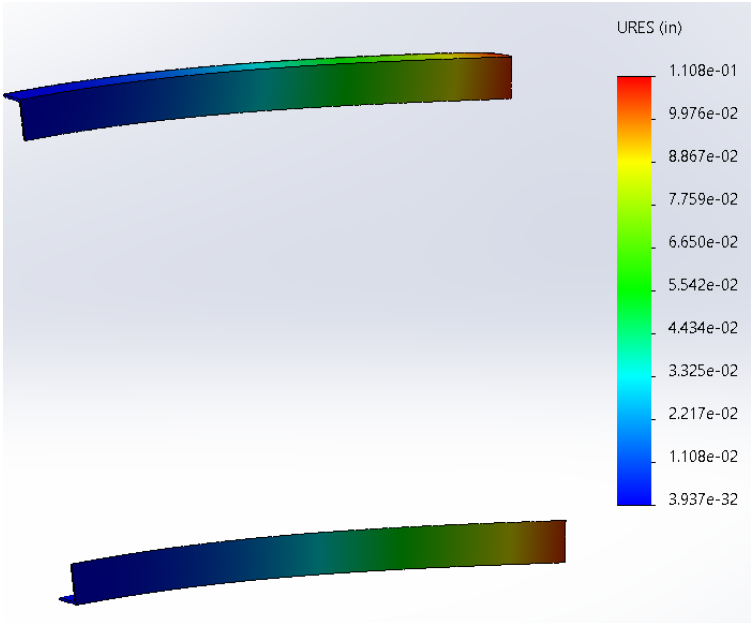

Figure 301: Deflection of Panel Supports with (x1) - Panel, 15[Lbf]-ea

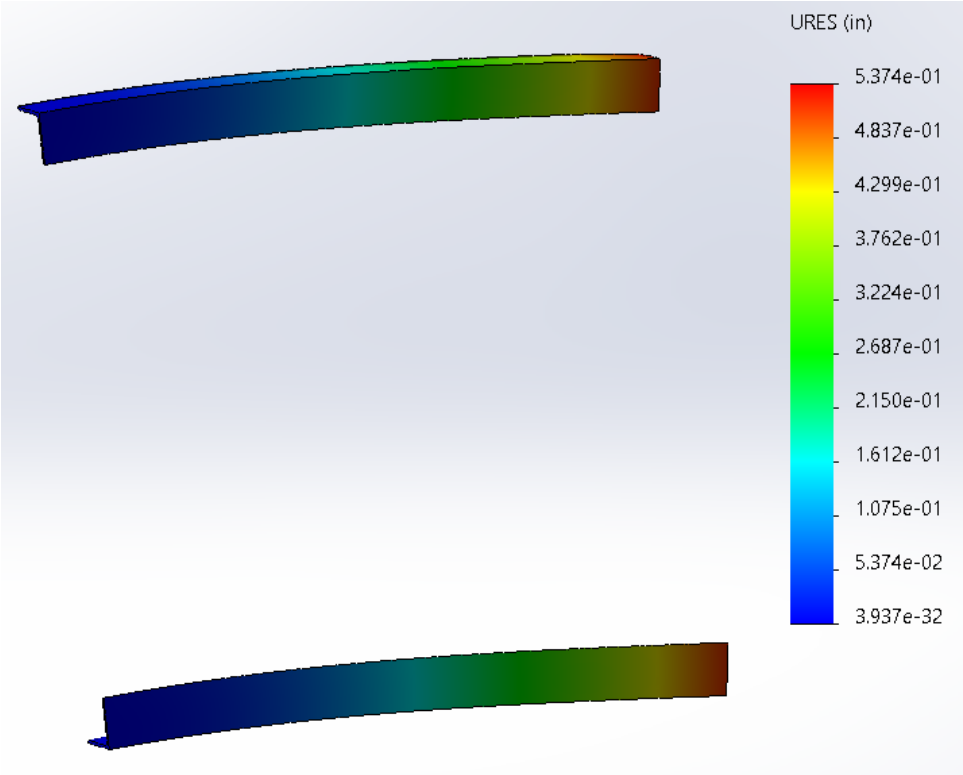

Figure 302: Deflection of Panel Supports with (x10) - Panels, 150[Lbf]-ea

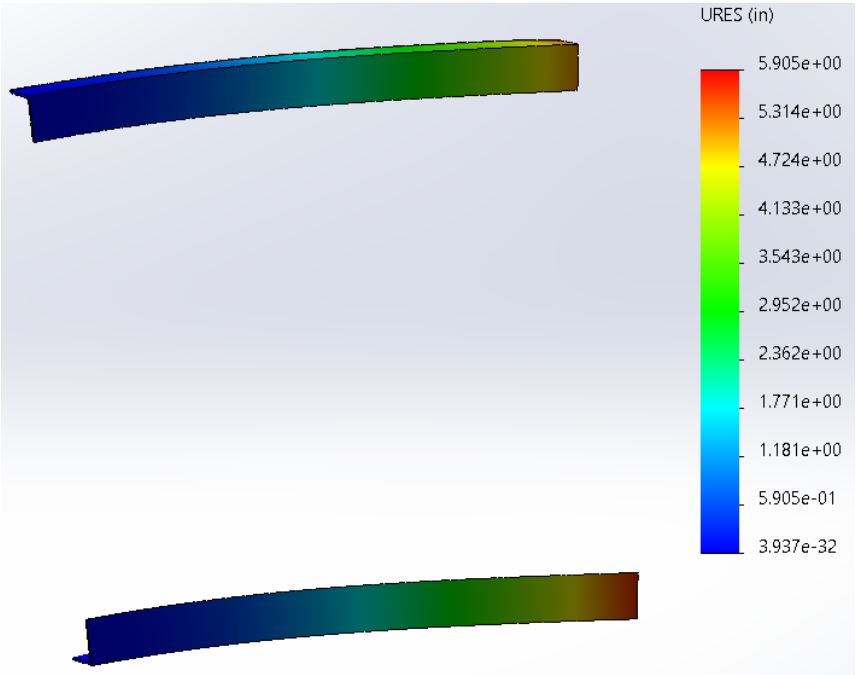

Figure 303: Deflection of Panel Supports with (x100) - Panels, 1,500[Lbf]-ea

When the supports are subjected to (x1) panel weight, the deflection is on the order of 0.11[in]. When the supports are subjected to (x10) panels weight, the deflection is on the order of 0.54[in]; and the stresses exceed 13,910[psi] (the members do not yield). When the supports are subjected to (x100) panels weight, the deflection is on the order of 6[in]; and the supports fail (yield). Since the tolerance around the bolts and rivets is on the order of (1/32)[in] and (1/16)[in], the total number of panels that probably (most likely) would be supported by a lower structure is less than three.

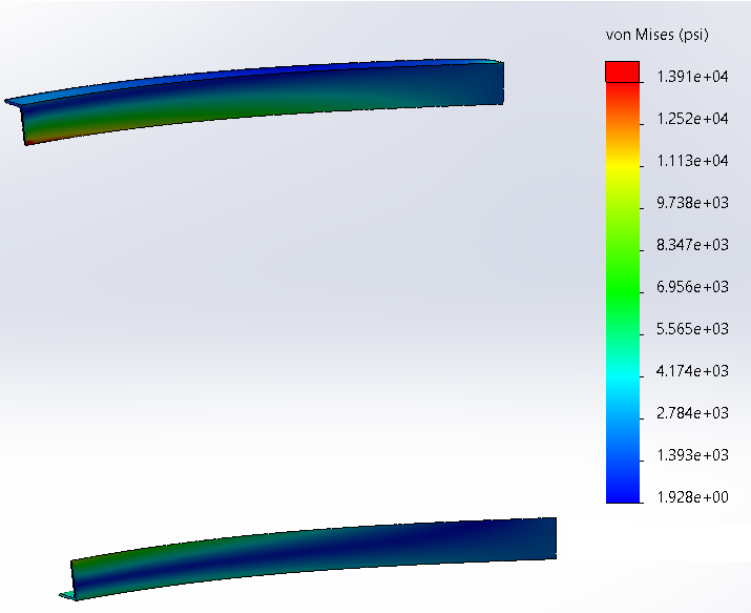

Figure 304: Stress of Panel Supports with (x3) - Panel, 45[Lbf]-ea

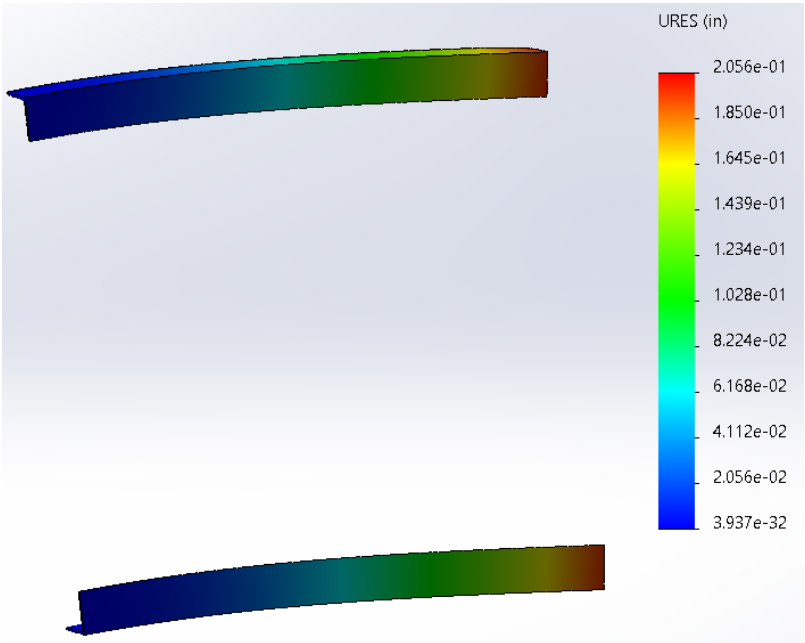

Figure 305: Deflection of Panel Supports with (x3) - Panel, 45[Lbf]-ea

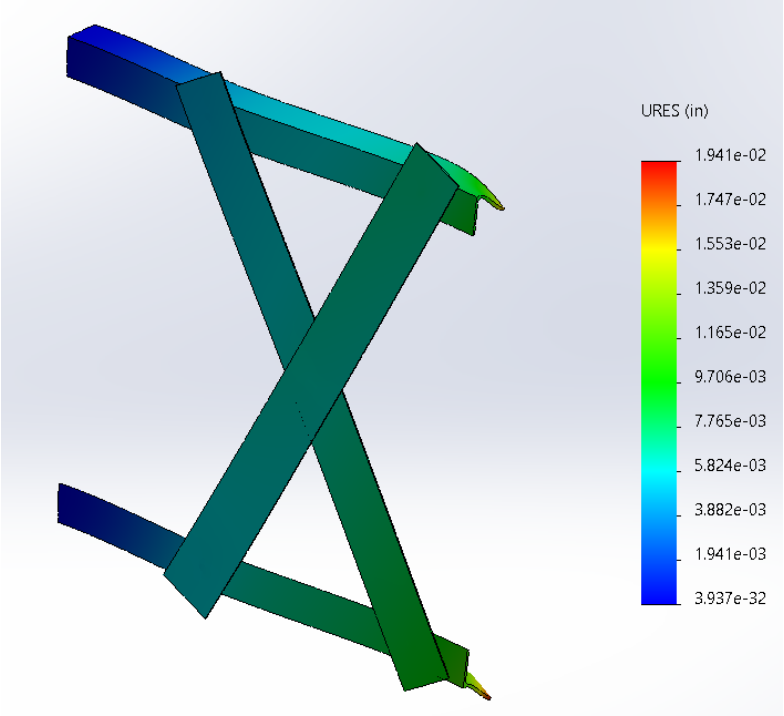

Figure 306: Panel Supports w/ Cross-members w/ (x3) Panel Weight

Note: The "X-member" is riveted at its intersection.

The addition of cross-members to the structure reduces the deflection from 0.21[in] to 0.019[in]. The stresses are reduced as well. The cross-members are 3" x (1/16)" aluminum metal. The (x10) reduction in deflection makes the addition of the cross-members worth their weight; thus, they will be added to the support structure.

Moving to a more accurate models of the standard panels, the fixtures and loading were the same in both models (Figure 307 and Figure 308); they difference are the "X-Supports." Initial calculations were performed with all edges as "symmetric" (Figure 309); thus, the only accurate panel is the center panel. Stresses and deflections outside the center panel are not accurate. The effect of gravity and (x3) panels was modeled by utilizing only side-symmetric edges; as in Figure 310.

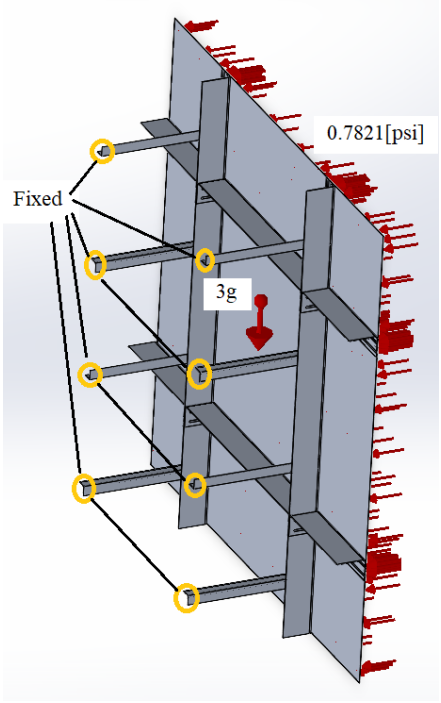

Figure 307: Main-body Standard Panel w/o X-Supports

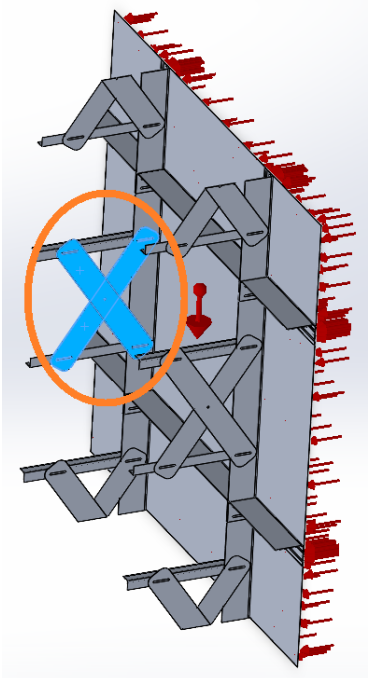

Figure 308: Main-body Standard Panel w/ X-Supports

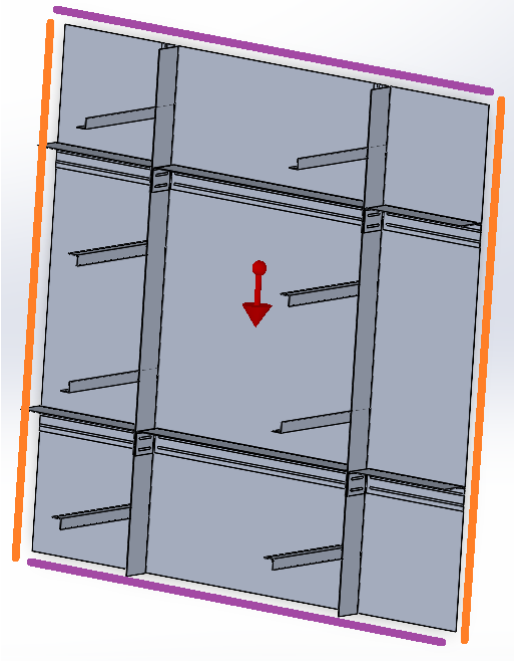

Figure 309: Initial Model w/ Symmetric Edges

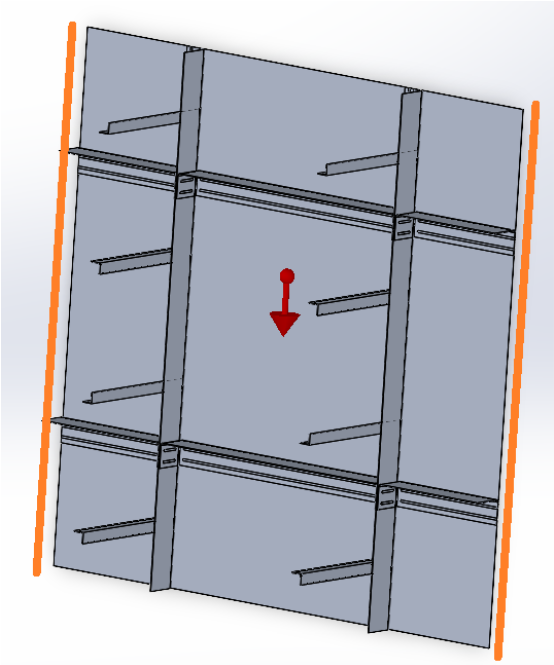

Figure 310: Effect of Gravity on Standard Panels, Side-symmetric

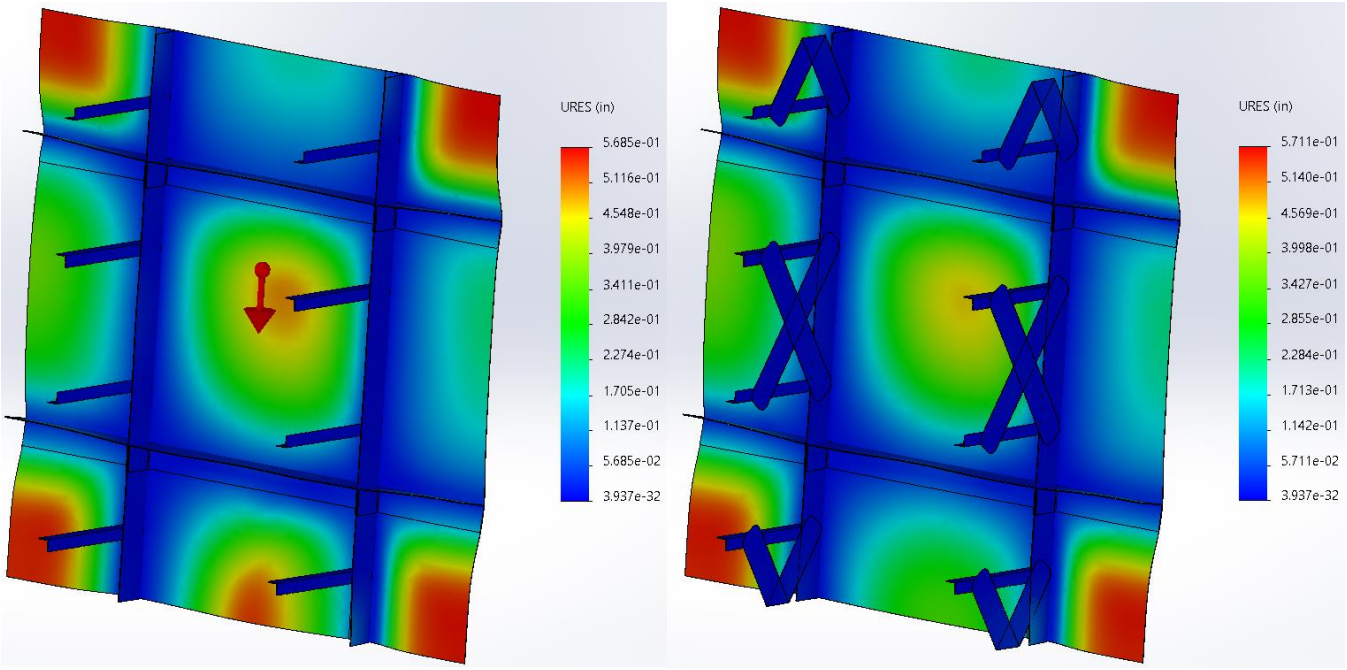

Figure 311: Standard Panel Deflection w/ All Sides Symmetrical

Where all side have a symmetric condition (Figure 309), the maximum deflection of the center panel w/o X-supports is 0.50[in]; and the maximum deflection of the center panel w/ X-supports is 0.47[in]. Where-as with only the side-symmetrical condition, the FEA panel deflections increase to 0.68[in].

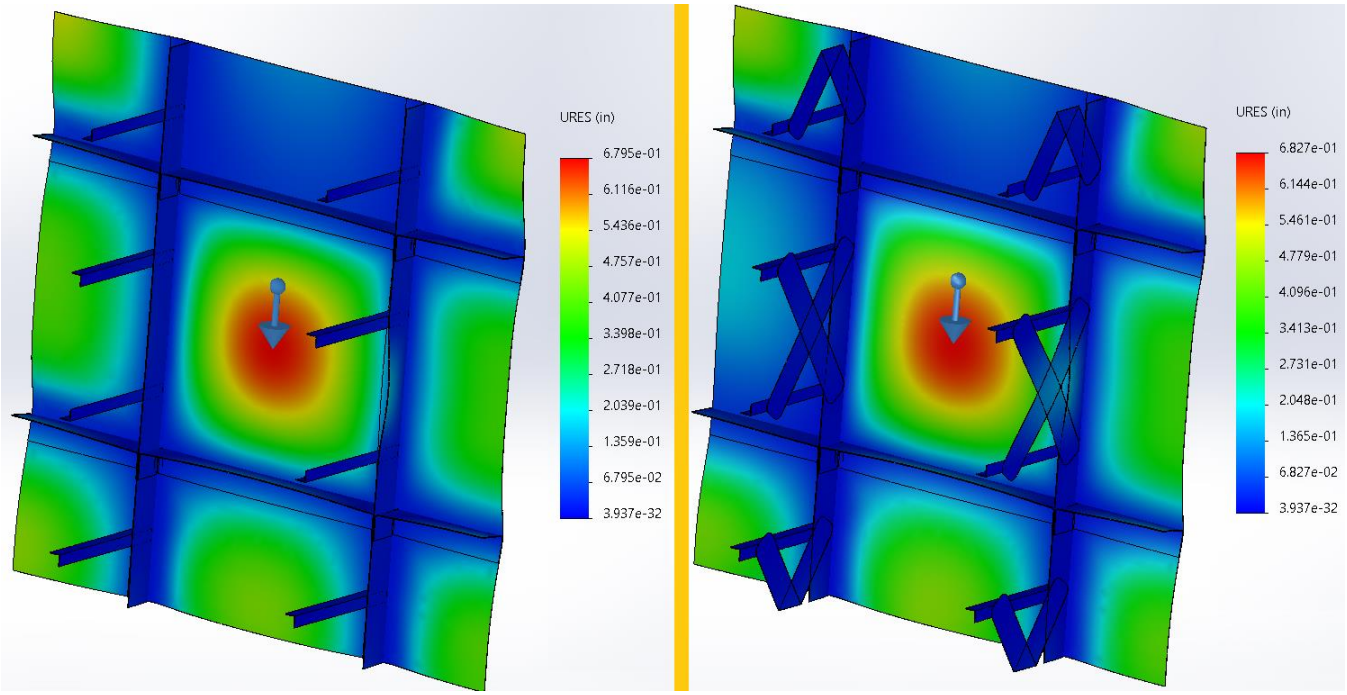

Figure 312: Standard Panel Deflection w/ Left & Right Sides Symmetrical (Figure 310)

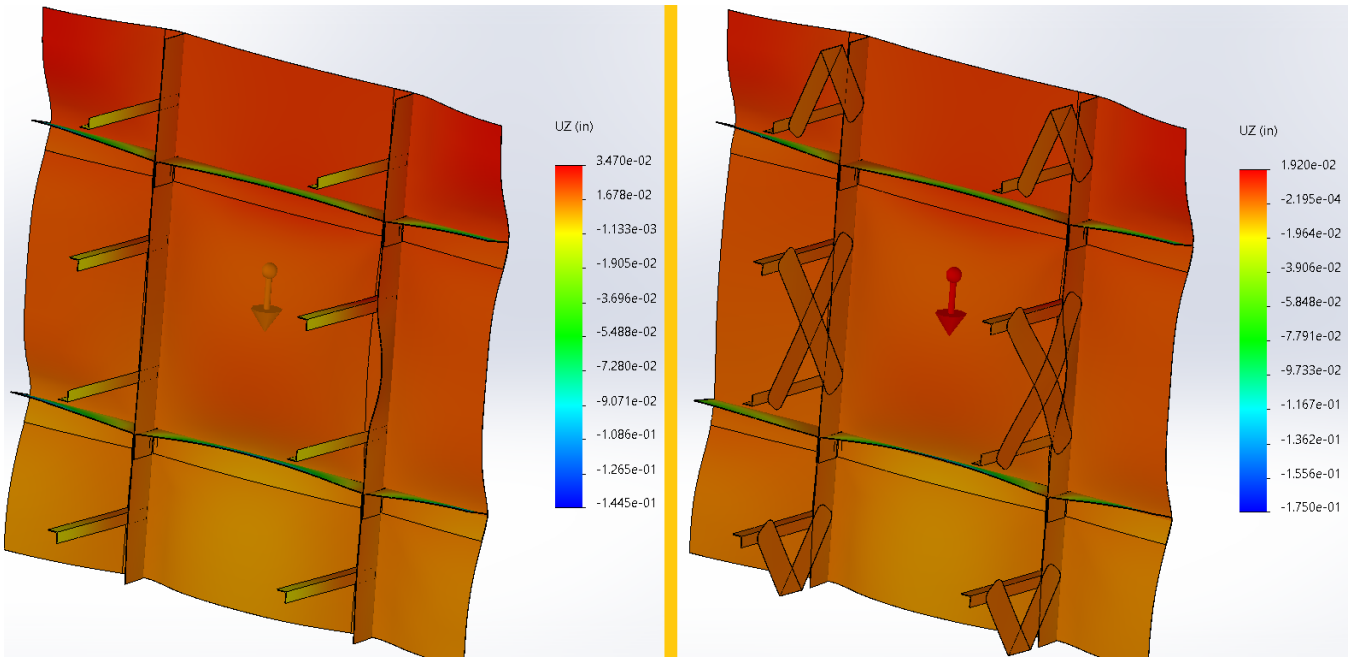

Figure 313: Standard Panel "dY-Deflection" w/ Left & Right Sides Symmetrical (Figure 308)

The item of interest, the deflection due to gravity (change in "Y" or "dY") is noticeable in Figure 313. The main panel supports (the L2's), without the support of the "X" members experience a maximum deflection of 0.024[in], and the L2's with the "X" members experience a maximum deflection of 0.007[in]; thus, the resistance to gravity is increase by a factor of 3.4[-] with the "X-member" supports.

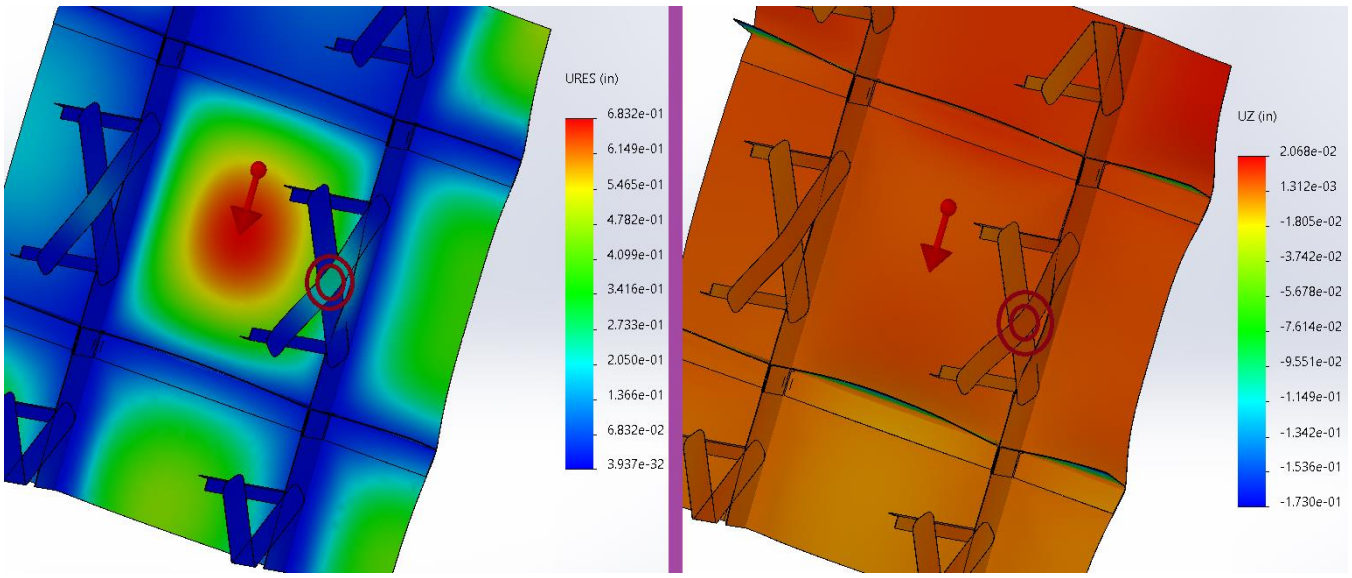

Figure 314: Standard Panel "dY-Deflection" w/ Left & Right Sides Symmetrical, w/o Center-rivet/s

Figure 314 shows the panels with X-supports (as in Figure 313), without center-rivets. The L2's have a maximum deflection on the order of 0.009[in]; which represents a panel that is (x2.5) greater than the system without X-supports. Thus, the center rivets stiffen the part/s by 33[%]; with respect to the panel/s with center-rivets. Since the deflection of 0.009[in] is less than the general tolerancing (in this area), the panels will be constructed with X-supports, without center-rivets.

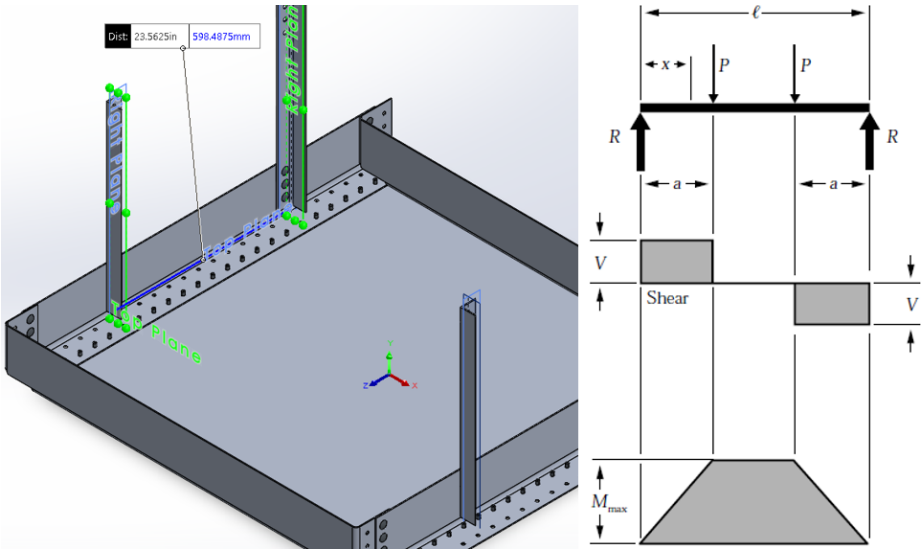

Figure 315: L2 Connection Member w/r Beam Mechanics

To maintain a deflection of one cross-beam (connecting the L2's) to the order of 0.005[in], the beam would have to maintain an inertia of 9.73[in^4]. This minimum inertia value can be archived by utilizing an L6"x3.5"x(5/16)" angle. This 6" cross-beam/angle and the other components within Figure 315 are aluminum. Due to the utilization of rivets, the L6 angle will have square ends.

Note: Recall, only one rivet per L2 brace is needed.

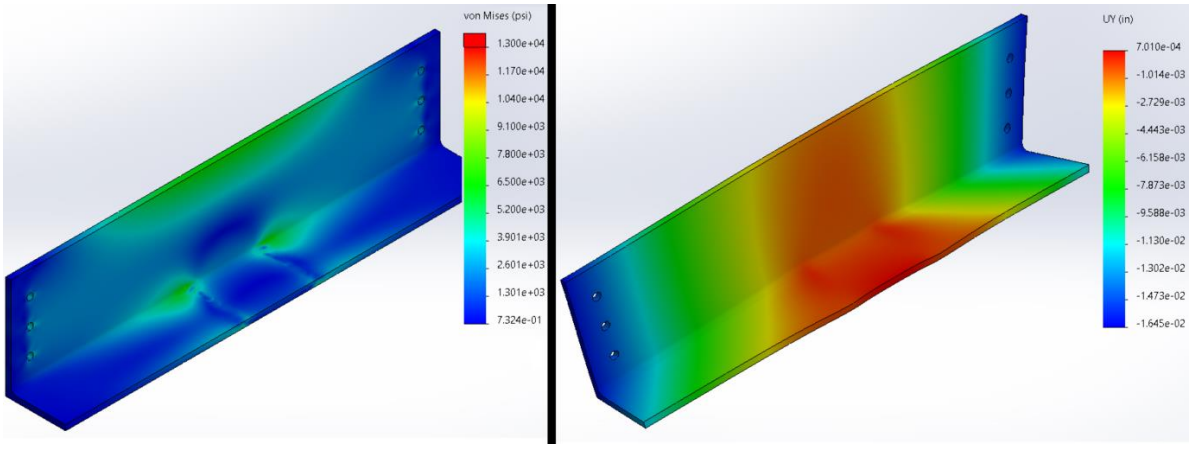

Figure 316: LS6 Angle Support with 4" Wide Fixed Center

As seen/interpolated in Figure 316, with a 4" wide support, the deflection in "Y" is on the order of 0.015[in]. An 8[in] wide center-support the deflection is on the order of 0.10[in]. In either case, the minimum factor of safety (yield and shear) is 10.4[-].

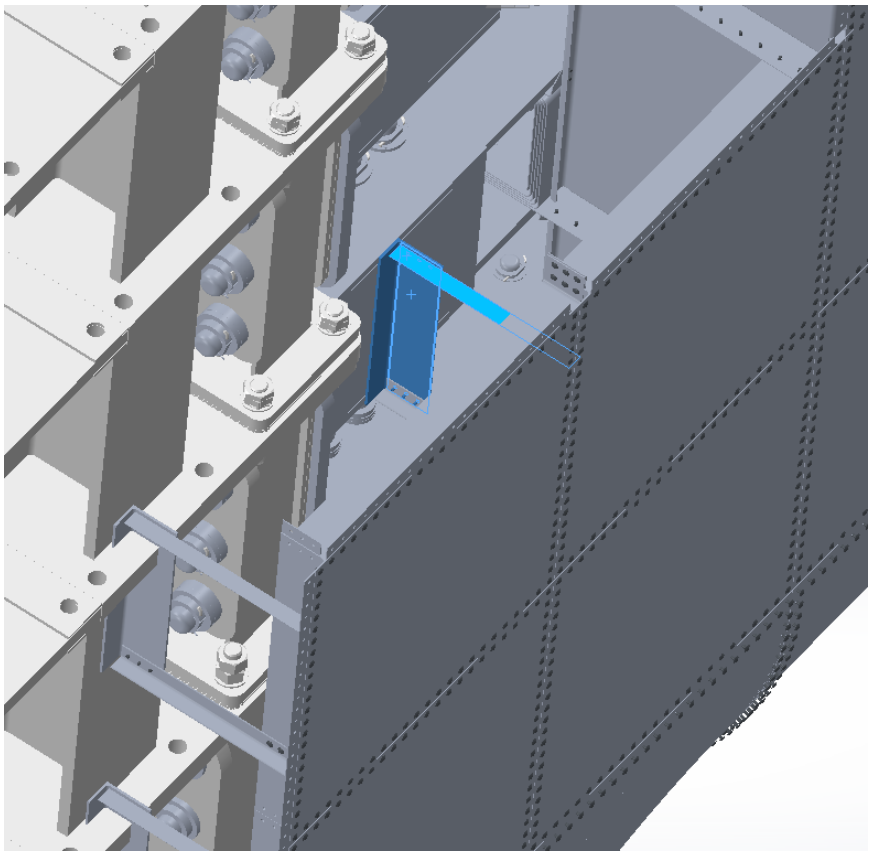

Figure 317: One Unsupported Brace, Requires Cantilever Beam

During the radial transition to the main body, one panel support/brace (highlighted in Figure 317) is not supported: To maintain support of the panels, this transition zone will require special consideration. The support/brace, being less than 45.6[in] away from the main body's structural beam-center, lends itself to a cantilever type of support. Using the beam bending equations for a fixed end (cantilever) beam with a concentrated load, the W6x15 will maintain a FS of 6[-] and have a deflection on the order of 0.08[in] (2[mm]).

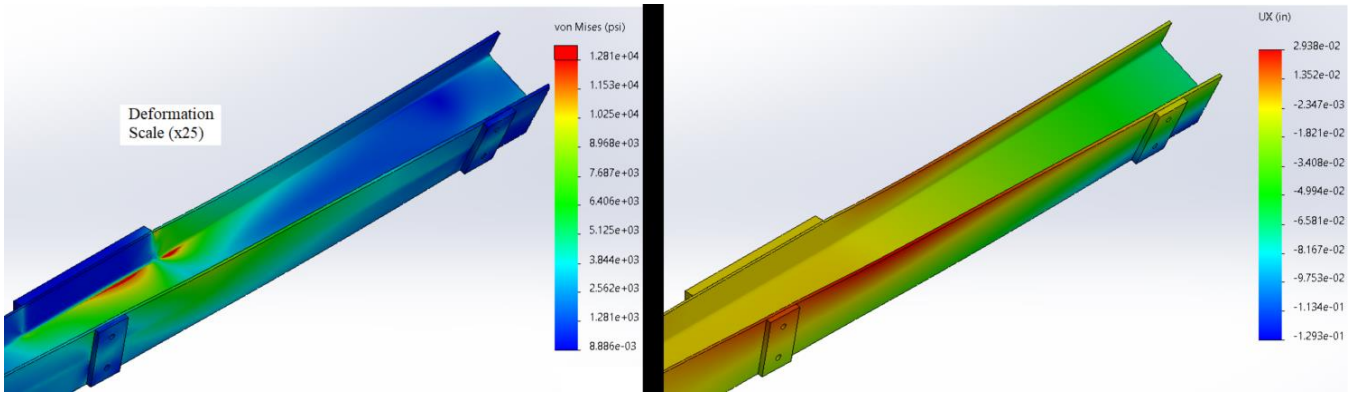

Figure 318: W6 Panel Transition Beam w/o Side Plates for Anti-Rotation

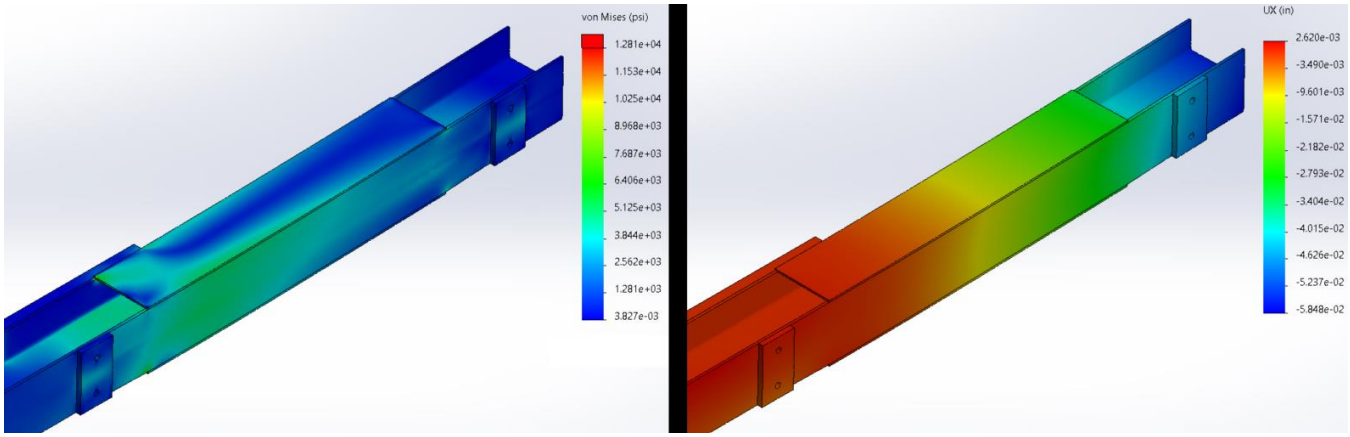

Figure 319: W6 Panel Transition Beam w/ Side Plates for Anti-Rotation

Note: Transition to Steel, AISI 1045 Cold-drawn with Sy = 76.8[ksi]

Adding side plates to the W6 beam, supporting the main panels, cuts the twisting by almost a factor of (x3). The FEA model had a panel loading force (fore/aft) of 1,972[Lbf] and a (x3) panel weight of 230[Lbf]; for each set of bolt holes. The bending up/down goes from 0.123[in] to 0.009[in] and the bending fore/aft goes from 0.065[in] to 0.046[in]. The increased resistance to twist brings the minimum safety factor to 5.0[-].

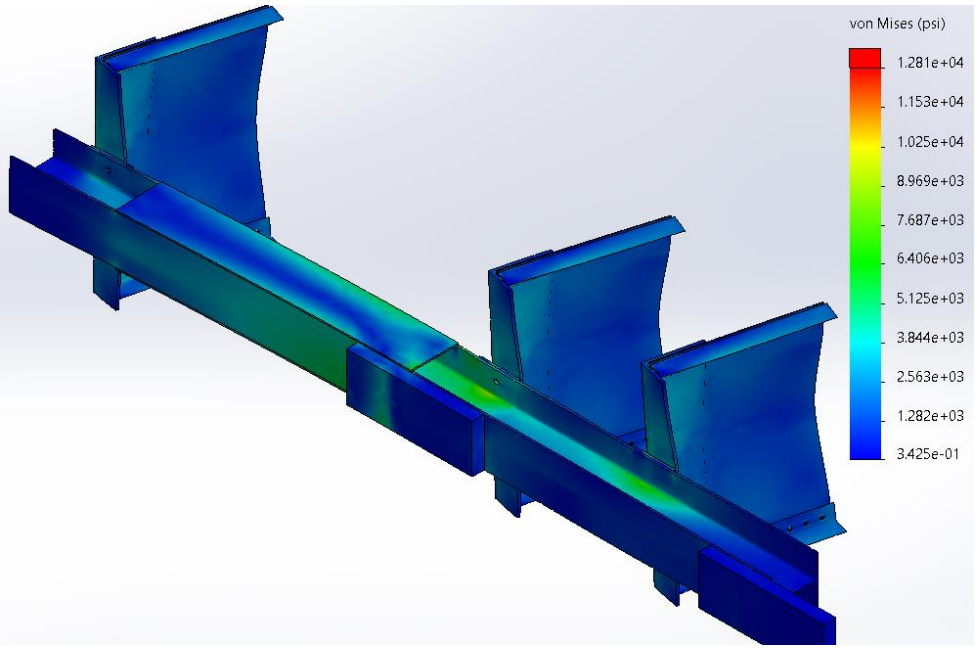

Figure 320: Representative W6 Panel Transition Beam w/ Side Plates for Anti-Rotation

The final FEA representative model shows a FS of 6.0[-]; as seen in Figure 320. The dZ (fore/aft) beam deflection is on the order of 0.05[in] and a dY (up/down) on the order of 0.01[in]; with an overall displacement vector on the order of 0.05[in]. The panels' edge will experience an added fore/aft deflection on the order of 0.07[in]. The completed design of the radial transition zone from the main body to the arm is depicted in Figure 321.

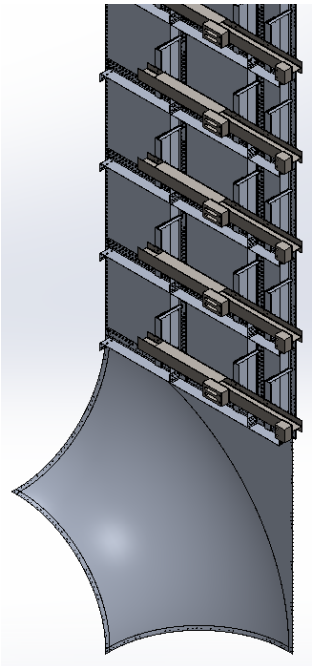

Figure 321: Main to Arm Radial Transition

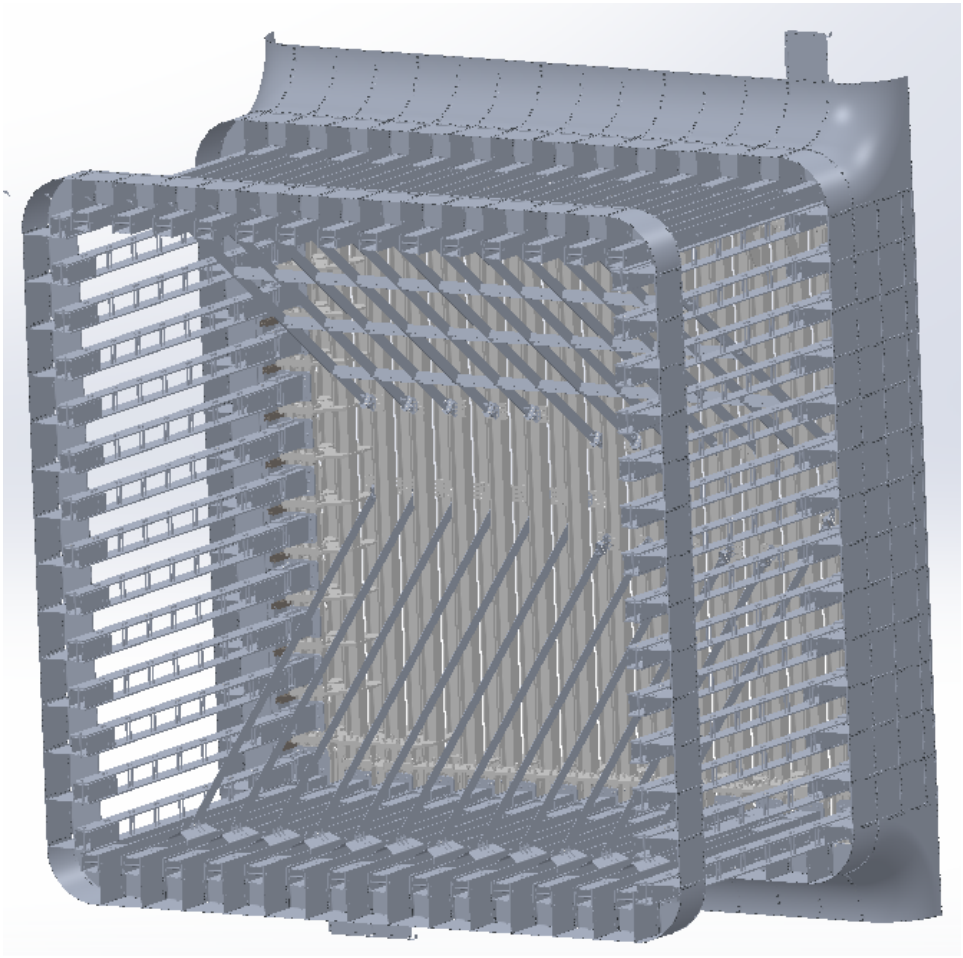

Figure 322: Arm 1st Segment to Main Structure w/o Main-beam Detail/s

VIII. Foundation:

Now that the arms, along with their coupling to the main body, the foundation can be defined. To do this, the loading of weight and wind are applied to the base. Through various modeling efforts (switching the direction of the wind), it was found that the loading represented in Table 142 and Table 143 yield the highest stresses on the beams of the foundation. A change in the direction of the wind varied the maximum stresses by less than 3[%].

Table 142: Weight Loading w/r Base

	Arm Weight	Arm Coupling	Shell Weight
Total [Lbf]	-1,639,419	-1,269,058	-4,390,189
(1/2) Model [Lbf]	**-819,709**	**-634,529**	**-2,195,095**
< X > [in]	1,619	355	0
< Y > [in]	24,213	24,213	14,528
< Z > [in]	-0.64	-2.6	0
		*Arm to Main Body	*Main Body

used in FEA

Total [Lbf]	**-1,639,420**	**-1,269,060**	**-4,390,190**
< X > [in]	0	0	0
< Y > [in]	24,213	24,214	14,550
< Z > [in]	-0.64	-2.6	0
(1/2) Model [Lbf]	**-819,710**	**-634,530**	**-2,195,095**
half < X > [in]	1,650	355	0
half < Y > [in]	24,213	24,214	14,550
half < Z > [in]	-0.64	-2.6	0

Note: Weight occurs in ($-F_y$) direction.

Table 143: Wind Loading w/r Base

	Wind F_x	Wind F_y	Wind F_z	M_y (Twist)
Total [Lbf]	197,880	-107,670	-11,070,000	-200,915,000
(1/2) Model[Lbf]	**98,940**	**-53,835**	**-5,535,000**	**-100,457,500**
< X > [in]	363	0	0	0
< Y > [in]	19,827	29,055	18,114	0
< Z > [in]	0	0	363	0

*Fy is a Lifting Force

used in FEA

Total [Lbf]	**197,880**	**0**	**-11,070,000**	**200,915,000**
< X > [in]	363	0	0	0
< Y > [in]	19,827	29,055	18,114	0
< Z > [in]	0	0	363	0
(1/2) Model [Lbf]	**98,940**	**0**	**-5,535,000**	**100,457,500**
half < X > [in]	363	0	0	0
half < Y > [in]	19,827	29,055	18,114	0
half < Z > [in]	0	0	363	0

Note: F_y is a lifting force, this will be left out as an added factor of safety.

A. Foundation Array/s:

One additional loading was applied, that of the beam weight, with supporting/connecting structure. Due to the height of the structure, the foundation beams must carry an inordinate (not typical) amount of weight. The model held 200 beams, each having to support 1,534,760[Lbf]; thus, the models had a point load of 306,952,000[Lbf] at "y = 14550[in]" or 369.6[m]. The long rows (in dX) contained 20[-] beams and the short rows (in dZ) contained 5[-] beams per half-model; for a total of 200[-] beams separated by 34.72[in].

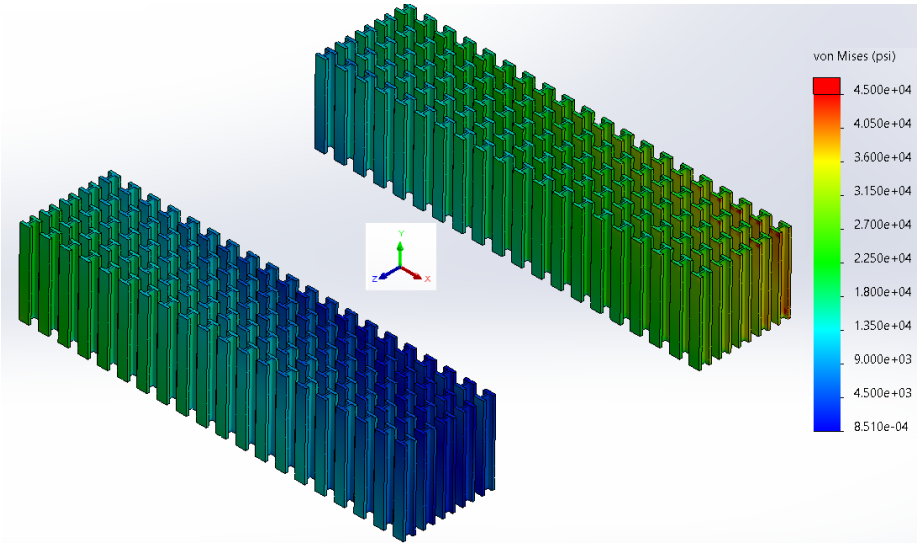

Figure 323: Foundation Beam Maximum Stress

Note: The maximum Stressed Beam is in the corner, < -329.875, 0, -329.875 >[in].

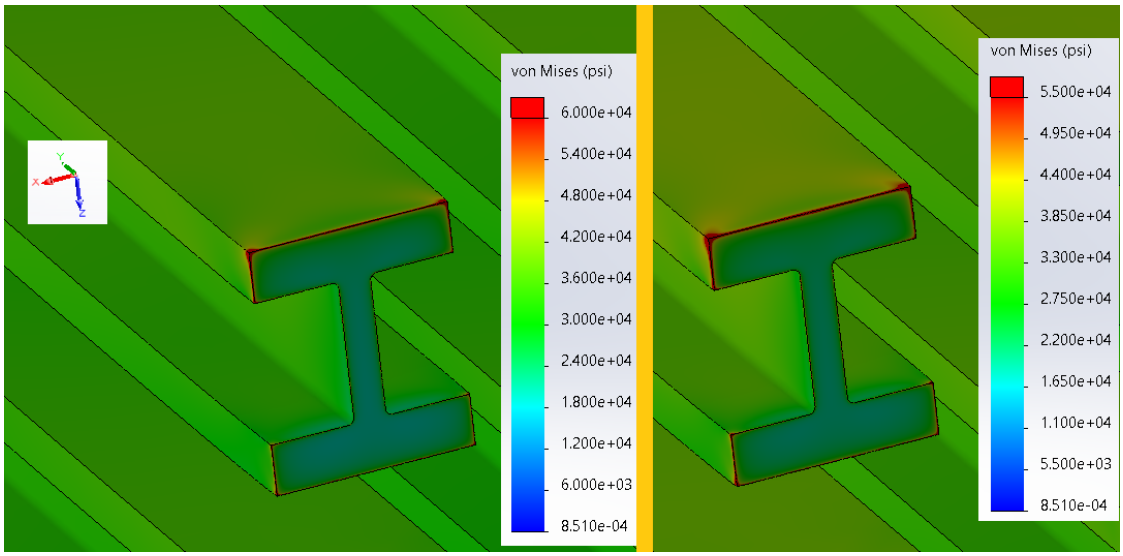

Figure 324: Maximum Stressed W14x665 Beam w/r 60[ksi] & 55[ksi]

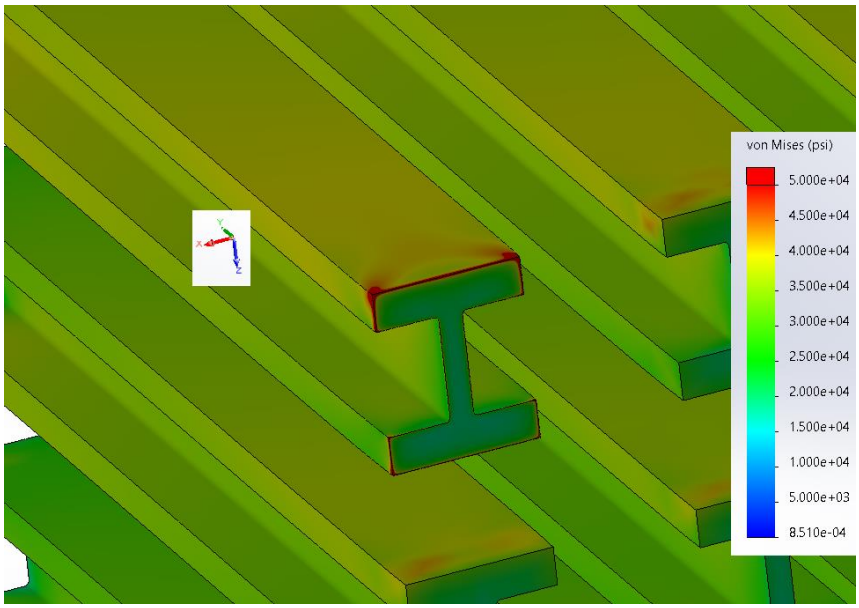

Figure 325: Maximum Stressed W14x665 Beam w/r 50[ksi]

As noted in ss, the maximum stress of the beams are less than 60[ksi]; however less than 0.8[in] from the mating edge, the stresses exceed 70[ksi]. These high stresses are likely due to the corner of the beam (a 90[deg] edge) and the mating surface). The RMS maximum stress is on the order of 53,600[psi]. A 65[ksi] beam will not yield under these conditions. Beams of 55[ksi] and below are not recommended. The choice for this design is the ASTM 913 G65 (65[ksi]) beam with ASTM galvanizing G100 (min 2.3[oz/ft2]). The factor of safety of 2.875 is not realized within the foundation beams. Averaging the (x6) corner beams, the RMS stress is 47,400[psi]; a FS of 1.37[-].

It is important to note that the FEA model beams are 118[in] long and the wind loading was surmised at 113[in] below ground. Therefore, with (x20) beams per row in dX and (x5) rows in dZ the 2.875[-] factor of safety is not realized with respect to maximum stresses. However, the thickness of the W14x665 beam has a lot of meat on it and only the outer web-membrane contains high stresses. When taking the cross-sectional area of the beam into account, the FS goes from 1.37[-] to 2.06[-].

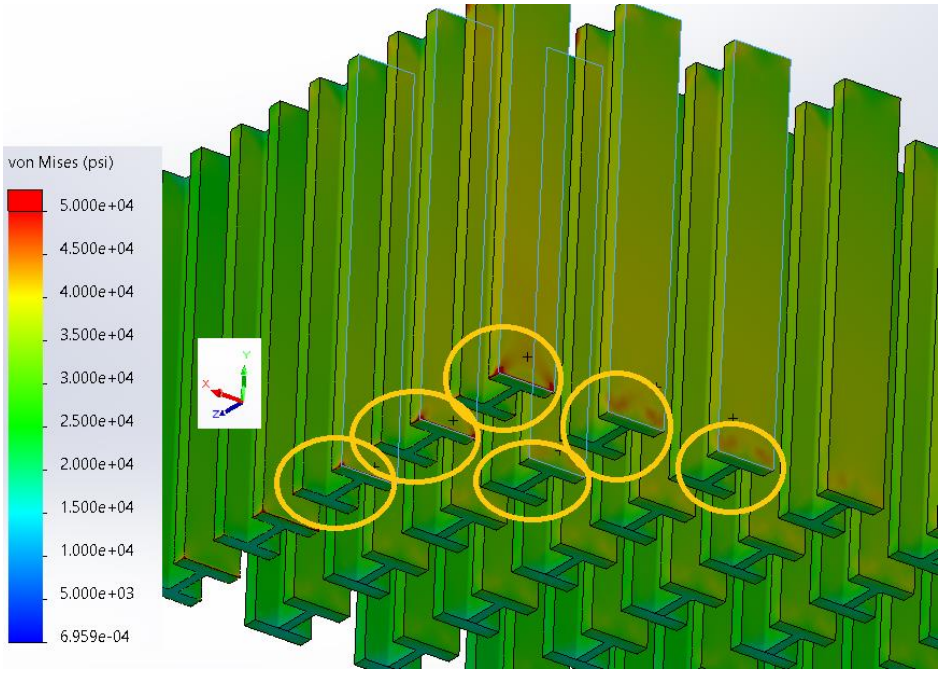

Figure 326: (x6) High Stressed Corner Beams

The question arises, how many high-stress states will the Glorious Cross experience? The answer is unknown. A best-guess can be made by referring to the bible, Matthew 1:17 whereby (x3) lots of 14 generations pass to the birth of Christ. Taking data from https://ourworldindata.org/life-expectancy it is possible to decern the 6th age of 14 generations begins around the 1500's. In 1531 there was a visitation by Our Mother (Our Lady of Guadalupe) to Juan Diego who's sum is 6 (from Latin to Hebrew). Taking the averages of the data, the earliest (and using 120[years] as a maximum age, as referenced in the bible) the 14th generation will occur/end is around 2658. Thus, a bell-curve or gaussian curve may be generated, as in Figure 327. From this curve, there is a 0.3[%] chance that the 14th generation will end around the year 2283 and a 99.7[%] that the 14th generation will pass around the year 3032. Since the high wind event/s are expected to occur once every 50[years] (mean, @ 0.02[%/y]) there will be no more than 21 high-stress (cyclic) events prior to the year 3032.

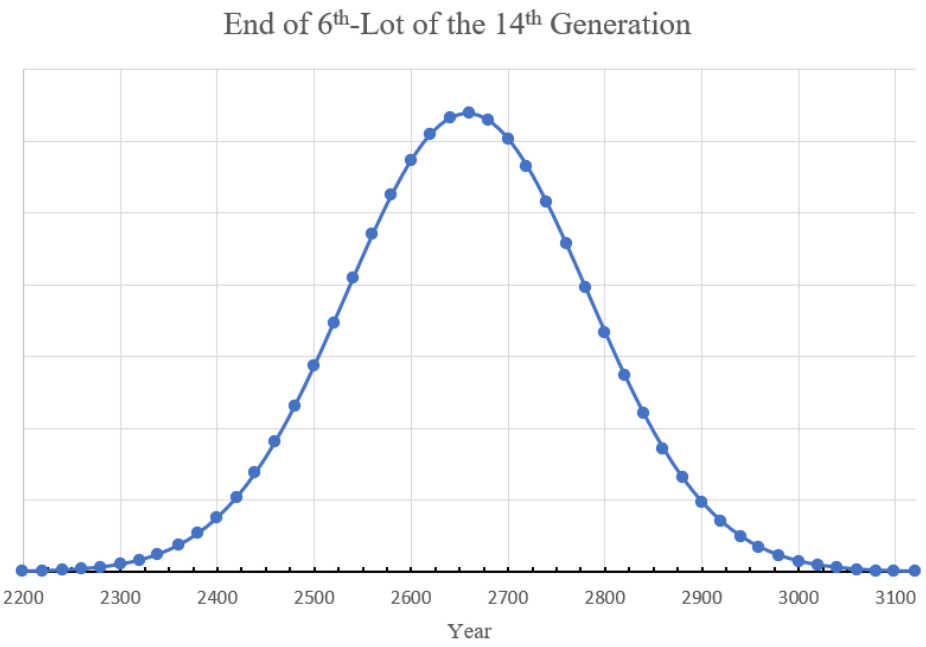

Figure 327: Bell/Gaussian Curve for the Probability of the End of the 14th Generation

Note: Several presumptions were made as a best-guess to generate this curve.

The beam grade ASTM 913 specification has a toughness requirement for seismic resistance. Data exists to show its advantage over hot rolled steels and others, such as A36; "Steels for Seismic Applications: ASTM A913 GRADE 50 AND GRADE 65" by G. Axmann. Therefore, the endurance stress or surface factor K_a is greater than the hot-rolled curve on "Mechanical Engineering Design" 3rd edition by J. E. Shigley, 1977. The ultimate stress of G65 steel is about 80[ksi], yielding a K_a greater than 0.61[-]. Thus, the endurance stress (S_e) is about (0.61*80) 48.4 [ksi]. Using the alternating stress equations from Soderberg, the Soderberg Line, the factor of safety is 1.17[-], where the minimum stress is zero. Using the Goodman Line, the factor of safety is 1.27[-]. The final factor of safety will be determined when the foundation design is defined.

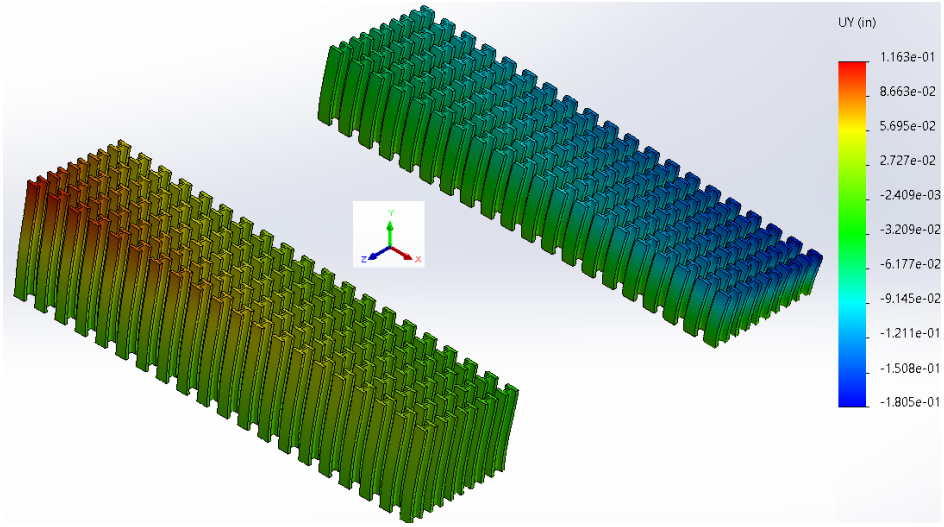

Figure 328: Up/Down "dY" Maximum Deflection +0.12" to -0.18"

Table 144: Foundation Deflection Vectors over a 118" Beam

	X [in]	Y [in]	Z [in]	|v| [in]	Angle [deg]
Beam Vector	0.000	118.000	0.000	118.0	0.0
Deflection Vector 1	0.013	118.116	0.003	118.1	0.006
Deflection Vector 2	-0.004	117.820	-0.053	117.8	0.026

In examining the deflections, opposite corners of the base panels can expect to be lifted/pushed no more than 0.72[in] off and into the ground during a maximum wind event. The highest angle of deflection occurs at the high-stress (compression) beam; with a value of 0.026[deg] over 118[in].

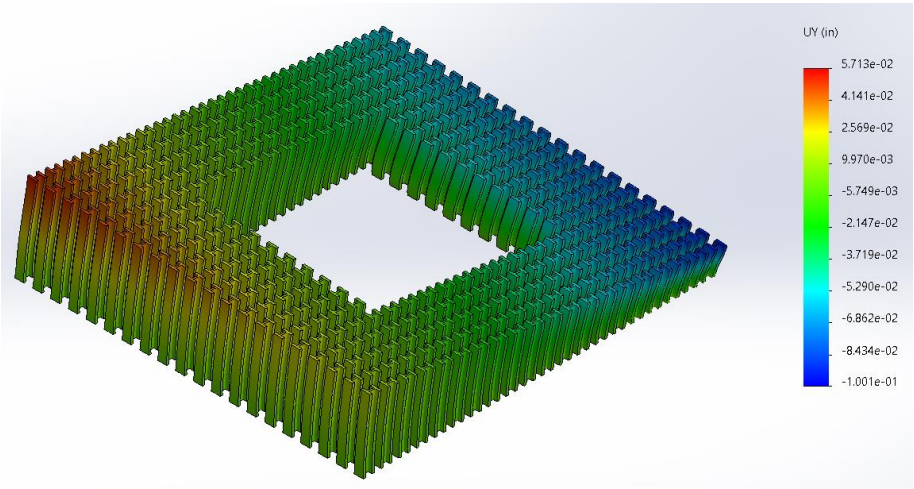

Figure 329: Full Foundation w/r (x20) Beams per Row

Table 145: Deflection w/r Full Foundation at (x20) Beams per Row

	X [in]	Y [in]	Z [in]	|v| [in]	Angle [deg]
Beam Vector	0.000	118.000	0.000	118.0	0.0
Deflection Vector 1	0.008	118.082	0.002	118.1	0.004
Deflection Vector 2	-0.003	117.855	-0.041	117.9	0.020

Adding the center beams for wind in the "X" direction, affects the total deflection. The deflection in Table 144 is reduced by 37[%] when all beams are present; as seen in Table 145. The maximum RMS stress is reduced to 41,290[psi]; far below the required 54[ksi] (FS = 131).

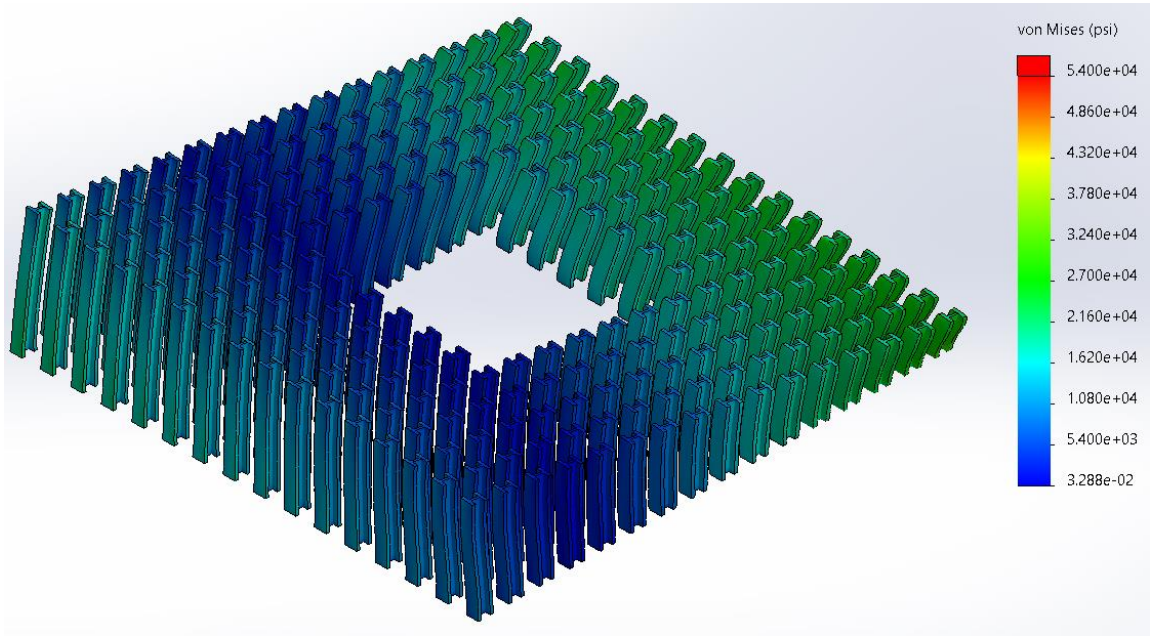

Figure 330: Foundation of (x16) Array

Table 146: Deflection of (x16) Foundation Array

	X [in]	Y [in]	Z [in]	|v| [in]	Angle [deg]
Beam Vector	0.000	118.000	0.000	118.0	0.0

Deflection Vector 1	0.086	118.067	0.041	118.1	0.046
Deflection Vector 2	-0.076	117.867	-0.121	117.9	0.070

The (x16) array has a beam weight of -344,466,030 [Lbf] representing 220 beams and plates; while the other loadings remain the same. The maximum stress is on the order of 39,200[psi]. The deflection of the corner beam w/r (x20) beams per row is on the order of 0.123[in/in] with an angle of deflection of 0.020[deg]. The deflection of the corner beam w/r (x16) beams per row is on the order of 0.113[in/in] with an angle of deflection of 0.070[deg]. Though the angle of the (x16)-foundation is (x3.5) that of the (x20) array, their dY deflections are similar; with a variance of less than 10[%]. The web stress decreased due to the decrease in the estimated fixturing; fewer beams lead to fewer plates/fixtures.

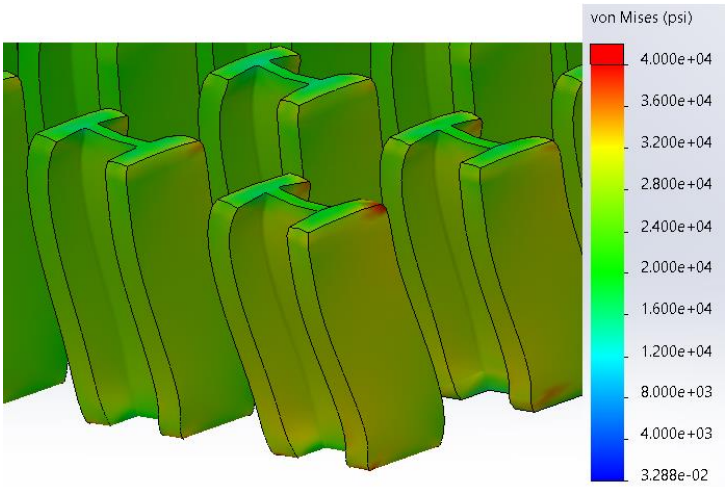

Figure 331: High Stress Corner Beam in (x16) Array

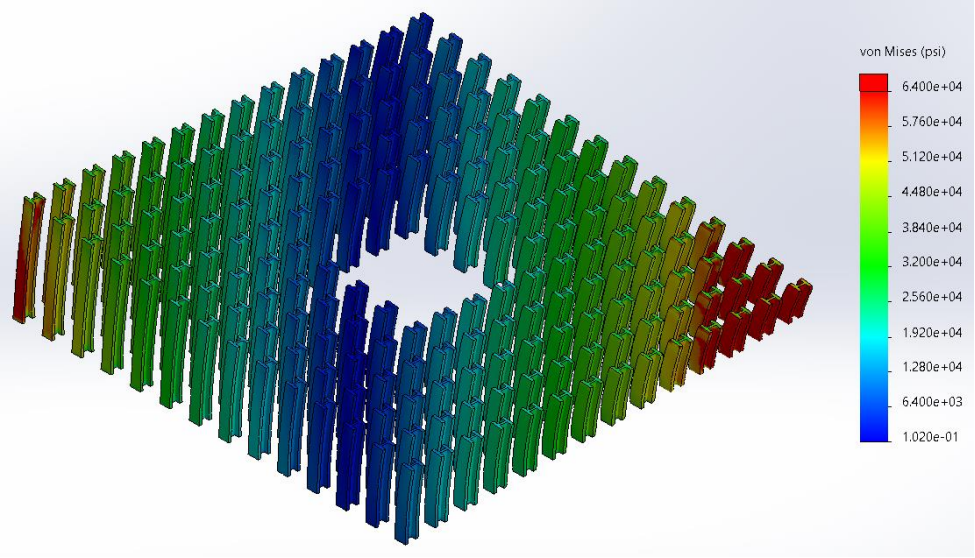

Figure 332: (x14) Foundation Array, Yielding Occurs

Table 147: Deflection Vectors for (x14) Foundation Array

	X [in]	Y [in]	Z [in]	|v| [in]	Angle [deg]
Beam Vector	0.000	118.000	0.000	118.0	0.0
Deflection Vector 1	0.054	118.272	0.007	118.3	0.027
Deflection Vector 2	-0.007	117.660	-0.080	117.7	0.039

As seen in Figure 332, a typical (x14) array, yielding occurs in several beams. It is interesting to note that the deflection in "Y" (dY) almost triples. Due to the yielding conditions of this array, it will not be considered.

The (x16) array matches the desired configuration for the arm-intersection beams and it has a reasonably low stress; enduring over time. Therefore, the (x16) foundation array will be the standard.

B. The (x16) Foundation Array:

Since the previous foundation models were general, a more detailed model was made to flush-out possible improvements and/or note areas of concern. The beams' connection plates are the driver of the load distribution throughout the structure. Thus, an effort will be made to distribute the loads/stresses in an effective manner; recalling that W14x665 beams will not be needed higher-up.

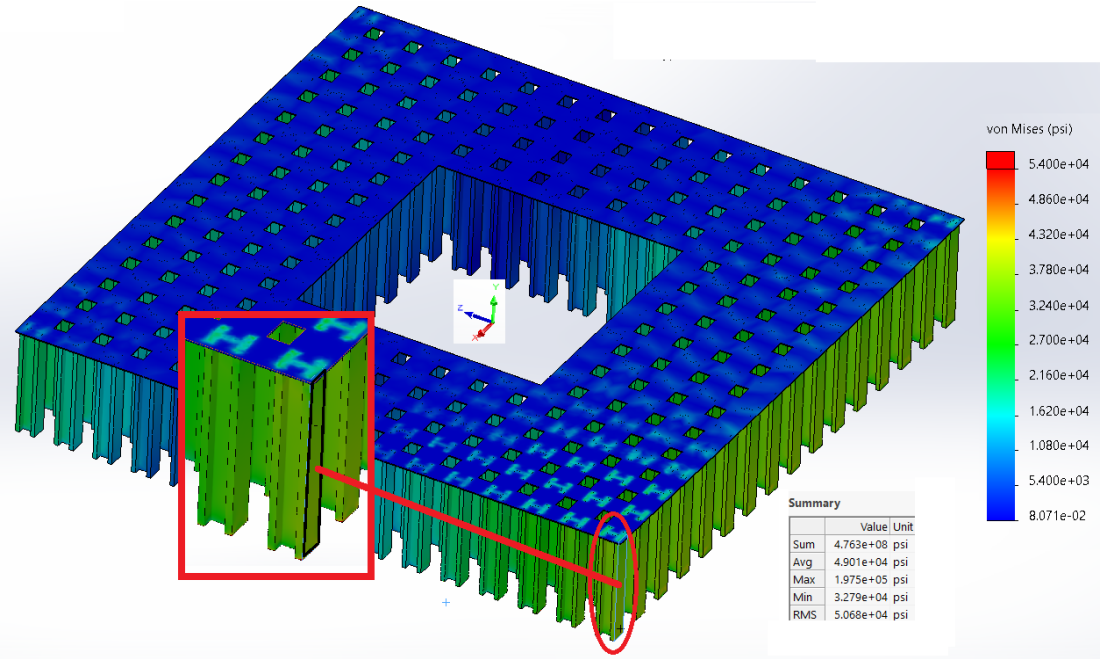

Figure 333: (x16) Foundation Array w/ 1" Connection Plates

As noted in Figure 333, the maximum web-stress is on the order of 51[ksi] with a series of 1[in] connection plates; connecting each beam. Also, the worst-case conditions make the < x, 0, -z > corner beam the highest stressed beam. From Table 148 the maximum movement at the base is on the order of 0.7[in]; using (x10) panels w/r dY. Also, the maximum offset angle is on the order of 0.026[deg].

Table 148: (x16) Foundation Array Maximum Displacement w/ 1" Connection Plates

	X [in]	Y [in]	Z [in]	|v| [in]	Angle [deg]
Beam Vector	0.000	118	0.000	118	0.0
Deflection Vector 1	0.006	118.105	0.003	118.1	0.003
Deflection Vector 2	-0.005	117.830	-0.053	117.8	0.026

Note: Deflection Vector 1 is the corner beam at < -x, 0, z >.
Note: Deflection Vector 2 is the corner beam at < x, 0, -z >.

It is seen in the above, that the corner beam reaches a stress of 50,680[psi]. This is above the acceptable limits of both the Soderberg and Goodman Lines (diagrams for fatigue loading); thus, the factor of safety is less than 1.0[-].

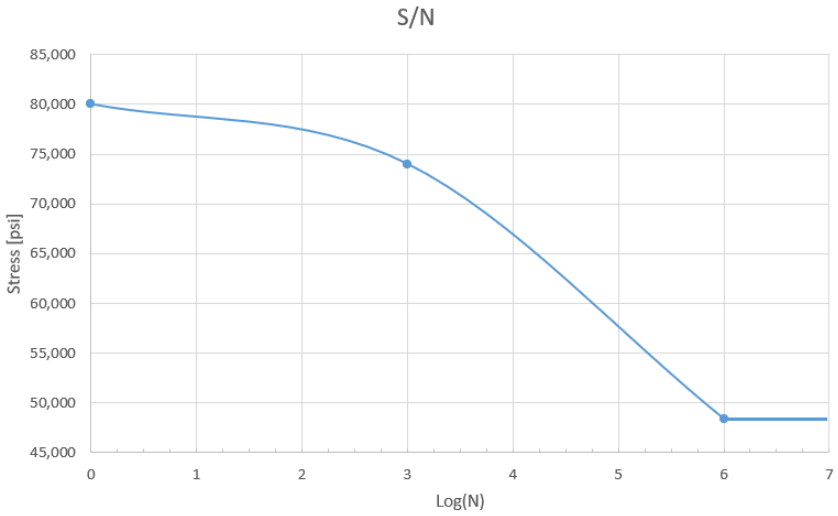

Figure 334: S/N Curve for A913 G65 Steel

The endurance curve suggests that the corner beam will last 540,548[cycles] without failing (0[psi] to 50,680[psi]). It is worth recalling that the wind loads are 16^{+}[%] higher than the curve seen in Figure 10 and that the maximum stress is 6.9[%] higher than the endurance stress: Though it is unlikely that these stresses will be seen in the corner beam, it is a point of concern. The wind speed at 5[m] in height (from Table 1) for the analysis is noted at 38.72[m/s], therefore, the critical velocity to count as (x1) cycle is attained the velocity reaches 37.8[m/s] (at a height of 5[m]). Thus, the structure will retain its integrity far past the 6-sigma (3-sigma past mean, Gaussian distribution) year noted in Figure 327; with a factor of safety well over 100[-] (per cyclic event).

Table 149: High Stressed Foundation Beams

Stress [psi]	Stress [psi]	Stress [psi]	Stress [psi]	Stress [psi]
41,600	41,800	41,820	**50,190**	**50,690**
	37,450	37,330	**45,440**	**45,470**
			33,200	40,640

Note: The "blue-highlighted" value is the stress/location of the high-stress corner beam as in Figure 333.

As seen in Table 149, only the two corner beams located at < 285.892, 0, -329.875 >[in] and < 329.875, 0, -329.875 >[in] exceed the endurance stress (S_e) of 48,400[psi]. It is recommended that at the 4 corner beams (in bold-print, Table 149) receive a visual check after each major event; where the velocity at a height of 5[m] reaches/exceeds 37.8[m/s].

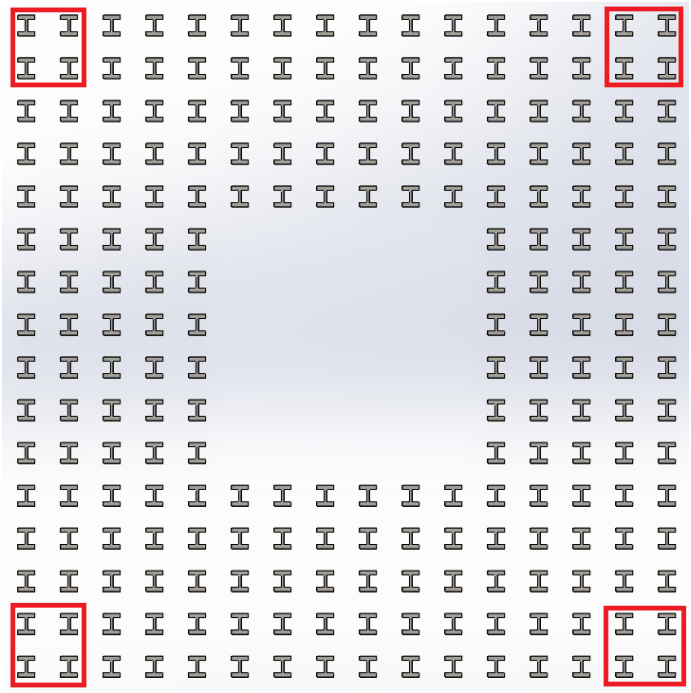

Figure 335: Critical Beams for Visual Check, Wind Greater than 37.8[m/s] @5[m]

The foundation models thus far have been calculated with in-house data. The foundation models do not show any yielding of the material; therefore, the model deflections and stresses are accurate. Though the material data and modeling are very close to the actual beam data, the stress data could change (a bit).

C. Foundation Model Accuracy:

The foundation models thus far do not show any yielding however, in order to achieve higher accuracy in the stress data from the FEA models, a foundation beam model will be made with high accuracy beam material definition/s. Documents published on the web present with respect to "Steel grades according to American standards - A36, A572, A588, A709, A913, A992." The beam material is A913 G65, where the yield of the material is 65[ksi]. In published data, the average percent-percent elongation is noted as 16[%-%]. Using the offset Young's Modulus from A36 steel, the Youngs Modulus of A913 is calculated at 34,800[ksi].

Example calculation of Youngs Modulus:
A36: Published data on Matweb (www.matweb.com "a36 flange")
S_y = 36.3[ksi]
ε = 20.5[%-%]
E = 29,000[ksi]

Calculation 1) E(calc) = Sy/ ε = 36.3/20.5 = 17,707,307[psi]
Calculation 2) γ = E(actual)/E(calc) = 1.64[-]

A913: Published data
S_u = 80[ksi]
S_y = 65[ksi]
ε = 16[%-%]
E = ???[ksi]
Calculation 1) E(calc) = S_y/ ε = 65/16 = 20,312,500[psi]
Calculation 2) E(actual) = γ *E(calc) = 1.64*65 = 33,200,000[psi]

Add-in a 10[%] factor of safety and the Young's Modulus used in the following calculations (for the foundation beams) is defined as **29,900[ksi]**. After a recalculation of stresses, the high stress beam went from 50,680[psi] to 50,510[psi] in the new model. The less than 0.5[%] difference can be attributed to the new model and calculations there-in.

Note that the main effect the Young's Modulus has on a "member" is with respect to its deflection/elongation/compression. Though the Young's Modulus is not present in the theoretical equations for pure bending, it is present in torsion (the shear modulus is related to the Young's Modulus via the Poisson's ratio).

The new model contains foundation beam lengths of 36[in] rather than 118[in]; so, the S(RMS) stress should've increased more than a few-percent. Instead, the stress decreased by less than 0.5[%]. This result implies that the torsional loadings are insignificant with respect to the other loads.

The reduction in stress leads to an increase in survivability. The foundation cycle life of about 4.7[%] to 565,922[cycles]; from 0 – 51,510[psi]. The maximum wind velocity (to count as one cycle) increases to 37.9[m/s] or 84.78[mph]; at a height of 5[m].

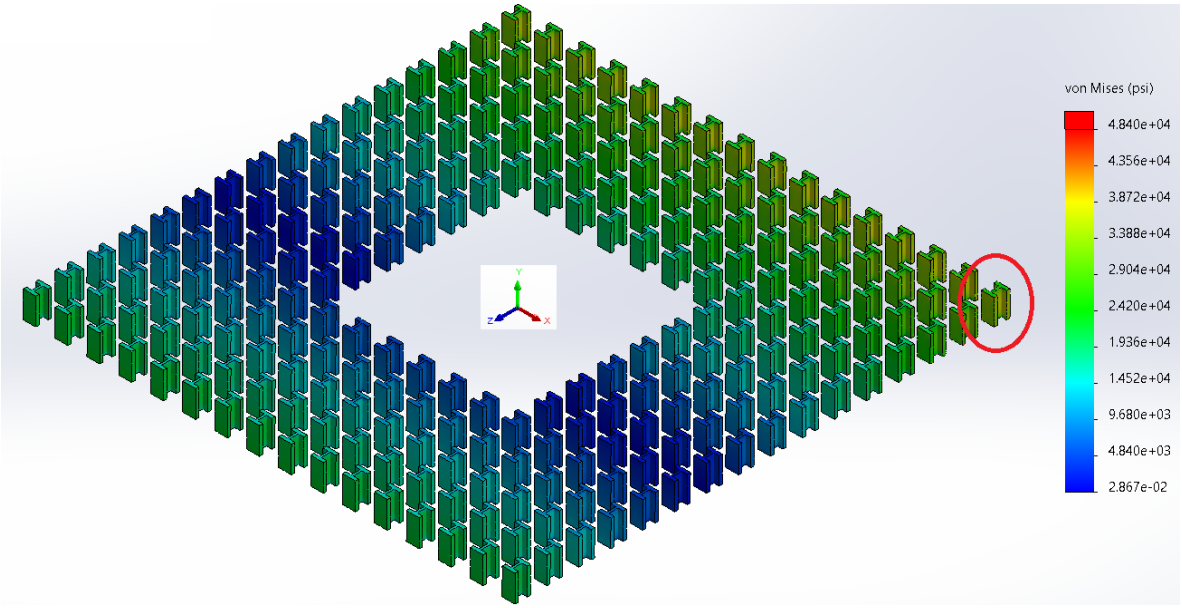

Figure 336: Von Mises Stresses @ H=0[m] with L(beam) = 36[in]

Note: CFD results are at 113[in] below H=0[m].

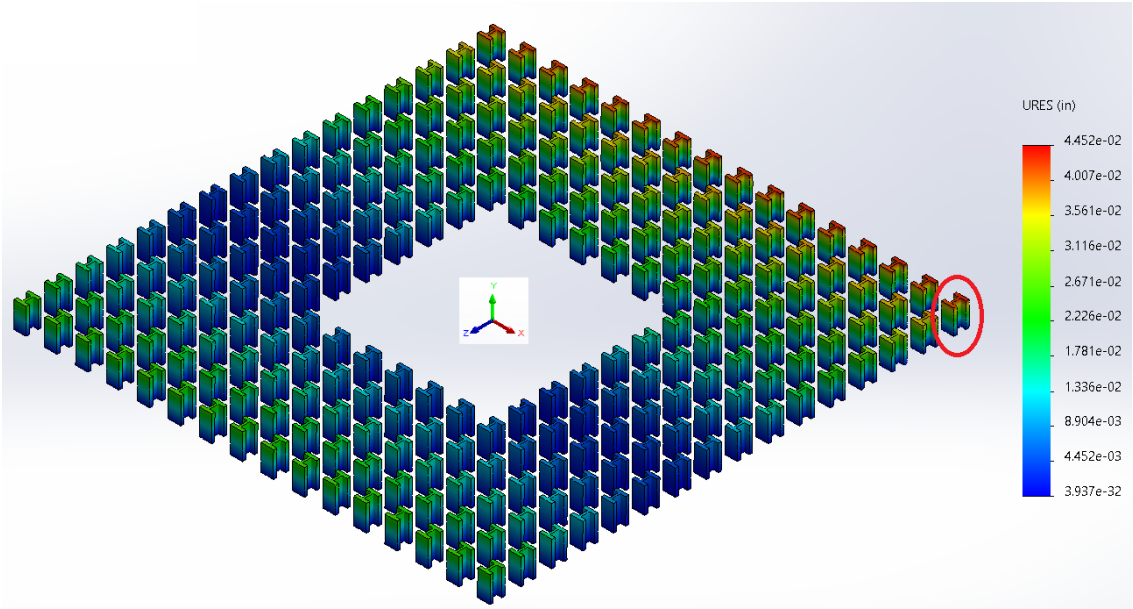

Figure 337: Deflection @ H=0[m] with L(beam) = 36[in]

Note: CFD results are at 113[in] below H=0[m].

Table 150: Deflection-vector of High-stress Corner Beam (Figure 337)

	X [in]	Y [in]	Z [in]	|v| [in]	Angle [deg]
Beam Vector	0.000	36.000	0.000	36.0	0.0
Deflection Vector 1	0.001	35.960	-0.004	35.96	0.006
Deflection Vector 2	-0.001	35.957	-0.005	35.96	0.008
Deflection Vector RMS	0.000	36.042	0.004	36.04	0.007

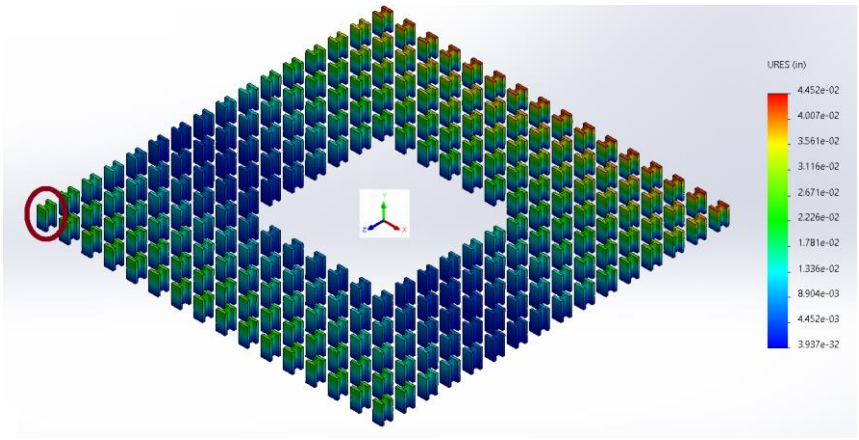

Figure 338: Opposite/Diagonal Corner Beam

Table 151: Deflection-vector of Opposite/Diagonal Corner Beam

	X [in]	Y [in]	Z [in]	|v| [in]	Angle [deg]
Beam Vector	0.000	36.000	0.000	36.0	0.0
Deflection Vector 1	0.001	36.027	-0.004	36.03	0.006
Deflection Vector 2	0.000	36.024	-0.005	36.02	0.007
Deflection Vector RMS	0.000	36.026	0.004	36.03	0.007

The deflection data of the two opposite beams (Table 150 and Table 151), the maximum change in beam length is 0.121[%]; or 0.00121[in/in]. The greatest angular deflection is found in the high-stressed corner beam; with an (RMS) angle of 0.007[deg]. This data also suggests that 21[%] of the deflection is due to the weight (total mass) of the Glorious Cross; with respect to the foundation (with no other loads applied).

D. Supporting Structure Lay-out Defined:

Now that the base/foundation is well defined, other factors will be checked and optimized and/or reduced. The wind coming from the "X" direction (side-force/wind) applies less load than noted in Table 152. Also, the beam-type with respect to height will be further defined.

Table 152: Loads w/r Velocity from < X >

	Wind in V_x - < V, 0, 0 >		
	Wind F_x [Lbf]	Wind F_z [Lbf]	M_y (Twist) [Lbf-in]
[*]	9,490,179	-198,700	204,180,800
< X > - [in]	-363	0	0
< Y > - [in]	17,026	19,763	0
< Z > - [in]	0	363	0

Note: These loads represent worst-case; the calculated loading from CFD is less.

An FEA with the loading described in Table 152, applies a stress of 41,970[psi] to the corner beam; the same corner beam as noted in Figure 336. Since the stresses are within the Goodman line, no further investigation of the V_x loading will occur.

Table 153: Beam Type/Designation w/r Height

Altitude [m]	Beam Designation	Maximum Axial Pull-out Load [Lbf]	Maximum Axial Compression Load [Lbf]	Maximum Shear Load [Lbf]
0	W14x665	4,924,000	8,063,200	52,525
130	W14x550	3,148,900	6,123,800	51,941
185	W14x455	2,501,700	5,210,000	51,635
240	W14x370	1,858,400	4,299,000	51,284
295	W14x283	1,216,700	3,392,600	50,805
360	W14x193	462,550	2,339,200	51,255

Table 154: 4" Beam-to-Bolt Classifications/Specifications

Altitude [m]	Beam Designation	Defined Bolt Diameter [in]	Defined N-bolts [-]	Resultant Proof Stress [psi/bolt]
0	W14x665	4.00	6	69,154
130	W14x550	3.25	6	67,227
185	W14x455	2.75	6	73,791
240	W14x370	2.50	6	67,072
295	W14x283	2.00	6	68,438
360	W14x193	2.00	4	50,188

Note: The maximum stress on a bolt is w/r the W14x455 beam; at 73,791[psi].

The extremely high loads dictate that the bolts must be heavy duty; A563 DH. To resist the salt air, they must also be galvanized. The proof load of these bolts/nuts is 150[ksi].

Eq - 48: Resultant Proof Stress

$$\overrightarrow{Stress}_{Proof} = \sqrt{(\sigma_{Normal})^2 + 3(\sigma_{Shear})^2} = \sqrt{\left(\frac{F_{Axial}}{N_{Bolts}\frac{\pi}{4}Dia_{Bolt}^2}\right)^2 + \left(\sqrt{3}\frac{F_{Shear}}{N_{Bolts}}\right)^2}$$

Note: The $(3)^{(-0.5)}$ comes from the shear energy equations.

Eq - 49: Hebrant Ultimate Stress[7]

$$Stress_{Ultimate} = \sqrt{(\sigma_{Normal})^2 + 1.5(\sigma_{Shear})^2} = \sqrt{\left(\frac{F_{Axial}}{N_{Bolts}\frac{\pi}{4}Dia_{Bolt}^2}\right)^2 + 1.5\left(\frac{F_{Shear}}{N_{Bolts}}\right)^2}$$

In this project, Eq - 48 is 1[%] to 2[%] more stringent than Eq - 49; up to the 360[m] mark. When W14x193 beam is used at a height of 360[m], Eq - 48 becomes 7[%] more stringent; thus, it can be considered to be over-cautious.

Table 155: Bolt Safety per Beam Designation

Altitude [m]	Beam Designation	Factor of Safety w/r Hebrant Eq. [-]	Elliptical Equation w/o Shear thru Threads [-]	Elliptical Equation with Shear thru Threads [-]
0	W14x665	75.9%	0.425	0.585
130	W14x550	81.5%	0.408	0.565
185	W14x455	63.6%	0.446	0.602
240	W14x370	82.0%	0.401	0.554
295	W14x283	77.9%	0.405	0.556
360	W14x193	212.0%	0.284	0.437

Note: The criteria for the elliptical equations are less-than/equal to (<=) 1.0.

The elliptical equations come from the specifications for bolts/nuts. Their dimensional specifications are from ASME B18.2.1 & B18.2.2. Washers or spacers should follow ASTM F436.

Eq - 50: Chession Elliptical Equation with Stress passing thru Bolt-shaft[8]

$$\sqrt{\left(\frac{\frac{\sigma_{Shear}}{\sigma_{UT}}}{0.83}\right)^2+\left(\frac{\sigma_{Tension}}{\sigma_{UT}}\right)^2}=\sqrt{\left(\frac{\frac{\sigma_{Shear}}{150[ksi]}}{0.83}\right)^2+\left(\frac{\sigma_{Axial}}{150[ksi]}\right)^2}$$

Note: Elliptical equations for A325 bolts transferred here-in.

Where:
S_{shear} is the shear stress.
S_{ut} is the ultimate stress.
$S_{tension}$ is the tensile or axial stress.

Eq - 51: Chession Elliptical Equation with Stress passing thru Threads[8]

$$\sqrt{\left(\frac{\frac{\sigma_{Shear}}{\sigma_{UT}}}{0.64}\right)^2+\left(\frac{\sigma_{Tension}}{\sigma_{UT}}\right)^2}=\sqrt{\left(\frac{\frac{\sigma_{Shear}}{150[ksi]}}{0.64}\right)^2+\left(\frac{\sigma_{Axial}}{150[ksi]}\right)^2}$$

Note: Elliptical equations for A325 bolts transferred here-in.

The base criteria for the bolt size and number (amount) required was the longevity; 1[mil] cycles. The S_{ut} of the bolt was taken as 150[ksi]; and per standard/accepted equations/procedures the S_e was taken as

$0.5S_{ut}$; for this material. Thus, the endurance stress to achieve 1[mil] cycles is 75[ksi]. The result of applying this criterion to the structure is noted in Table 154 & Table 155.

Table 156: 3.5" Beam-to-Bolt Classifications/Specifications

Altitude [m]	Beam Designation	**Defined Bolt Diameter [in]**	**Defined N-bolts [-]**	Resultant Proof Stress [psi/bolt]
0	W14x665	**3.50**	**8**	66,209
130	W14x550	**2.75**	**8**	68,430
185	W14x455	**2.50**	**8**	65,950
240	W14x370	**2.25**	**8**	60,864
295	W14x283	**1.75**	**8**	65,491
360	W14x193	**2.00**	**4**	50,188

Changing the bolt specification to the 3.5" classification as in Table 156, the resultant stresses are reduced and the base-plate becomes about 0.76" smaller. This configuration utilizes (x8) bolts in the lower members, creating a more ridged base for the lower beams; while maintaining a cyclic longevity of over 1[mil] cycles.

Table 157: Beam Base-plate Thickness Classifications/Specifications

Altitude [m]	Beam Designation	Beam Perimeter [in]	**Weld Width at Base [in]**	Weld Stress [psi]
0	W14x665	103.42	**3.50**	22,276
130	W14x550	99.72	**2.50**	24,564
185	W14x455	96.55	**2.25**	23,983
240	W14x370	93.63	**2.00**	22,957
295	W14x283	90.54	**1.50**	24,980
360	W14x193	87.22	**1.25**	21,456

Note: The perimeter of the beam did not include the radii.

The base-plate thickness per beam is defined by the necessary weld stress for survivability. The minimum yield stress in the calculations were taken as 62,500[psi], this was also taken to be the ultimate stress. The endurance stress for 1[mil] cycles was estimated at 31,250[psi]. A 40[%] factor of safety gives a target stress of 25,775[psi]; which is about 20[%] beneath the endurance stress.

Eq - 52: Minimum Plate/Weld Width

$$Plate|Weld_{Minumum\ Thickness} = \frac{F_{Proof|Load}}{P_{Beam}} \frac{(FS)\sqrt{3}}{\sigma_{Weld}} = \frac{F_{Proof|Load}}{P_{Beam}} \frac{(1.4)\sqrt{3}}{62{,}500[psi]}$$

Note: P_{Beam} is the beam perimeter w/r its cross-sectional area.

Eq - 53: Proof Load

$$F_{Proof|Load} = \sqrt{(F_{Axial})^2 + 3(F_{Shear})^2}$$

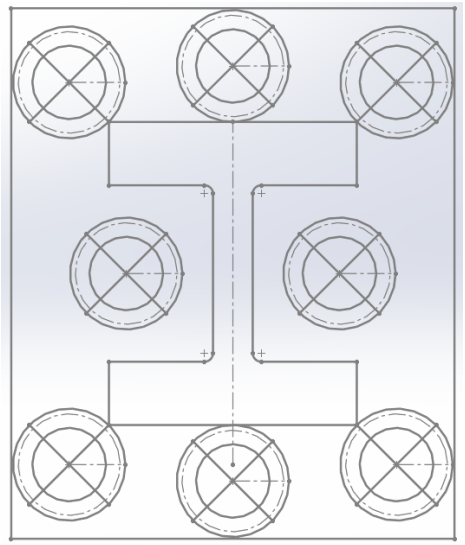

Figure 339: Base-plate Plan-view for the W665 Beam

A final note in regards to the loading on the structure, the main beams: The wind load contained a 16[%] safety factor and the added 113" adds another precent to the safety factor (deflections are 2[%] larger). Thus, the overall loading factor of safety is 17^{+}[%]. This is enough to bring all stresses below S_e: Allowing the structure to survive over 1[mil] cyclic loads (0 – 48,400[psi]). Each base-plate will be approximately 31.56" x 37.89"; with their respective thicknesses as defined in Table 157.

E. Base Segments:

The analysis shows the basic construct of each segment; including the initial, ground, segments. Each segment at and below the arms of the Cross will have (x220) beams in a (16x16) array. Since the maximum length of I-beams is set at 20[ft], the length of each segment will be (x5) panels tall; just under 20[ft].

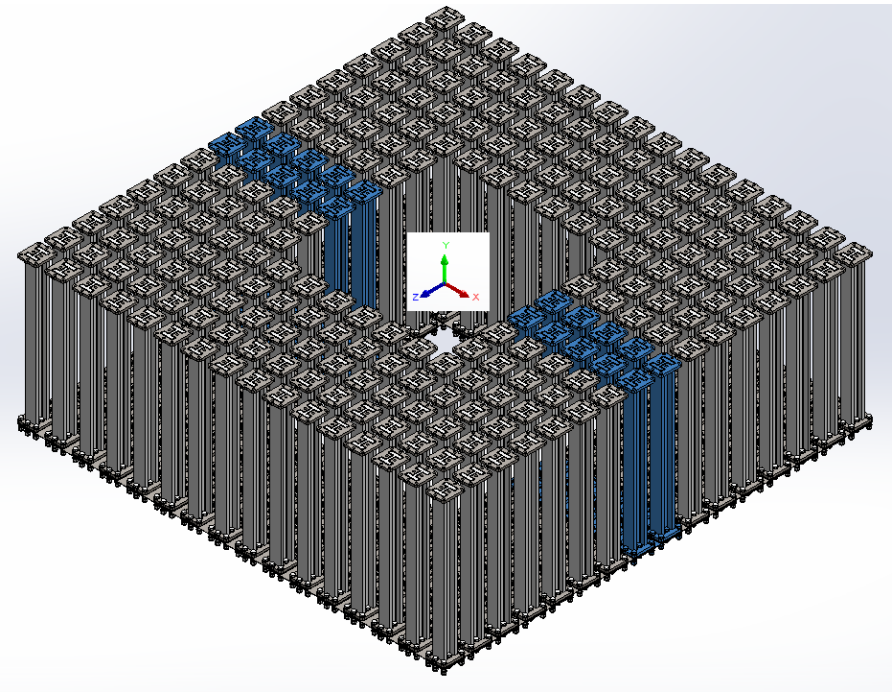

Figure 340: W14x665 Base Beam Array

The weight of the forest of beams is near 1,800[tons] and will support the maximum load conditions described here-in. Each beam requires galvanization and welding, prior to arrival at the construction site.

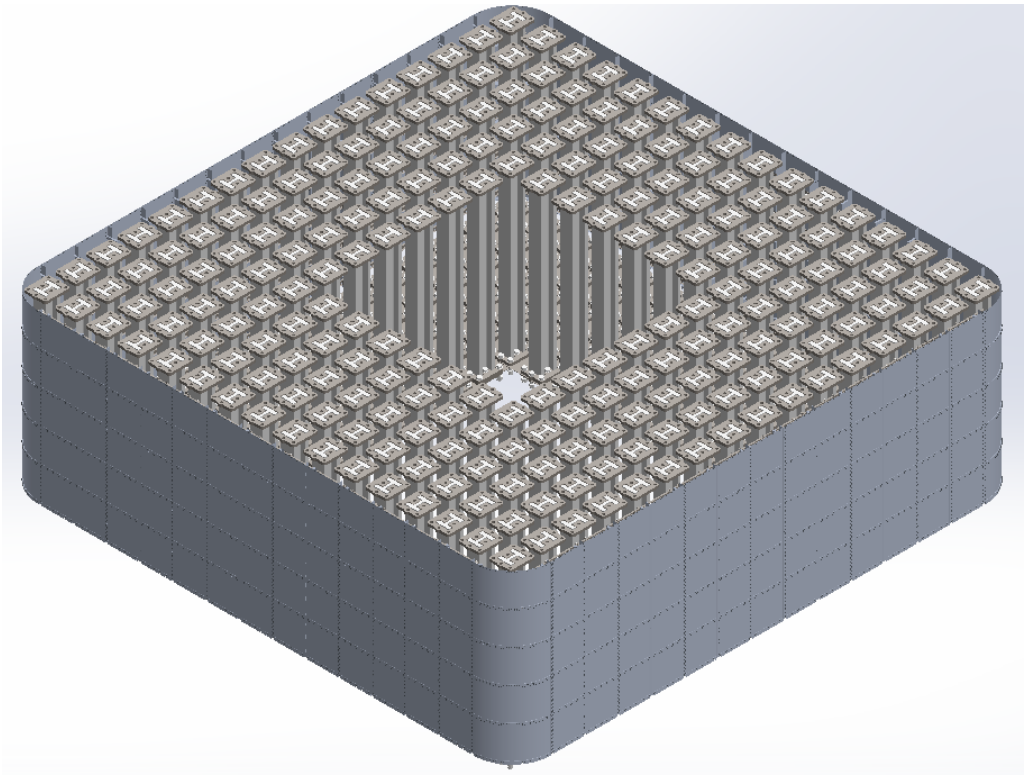

Figure 341: Segment 1 of Base Structure

Each W14x665 segment, with galvanization, welding and shim-plates weighs about 1,810[tons]. The weight will decrease as the beam changes; with altitude. The W14x665 beams will be utilized for the foundation.

F. Base Radial Panel:

The configuration of the radial panel, on the main body, has not been determined. It has been noted that a radial panel with R = 54.4[in] and t = (1/16)[in] will withstand a direct wind load with 61.3[m/s]; of Vx = Vz = 43.37[m/s].

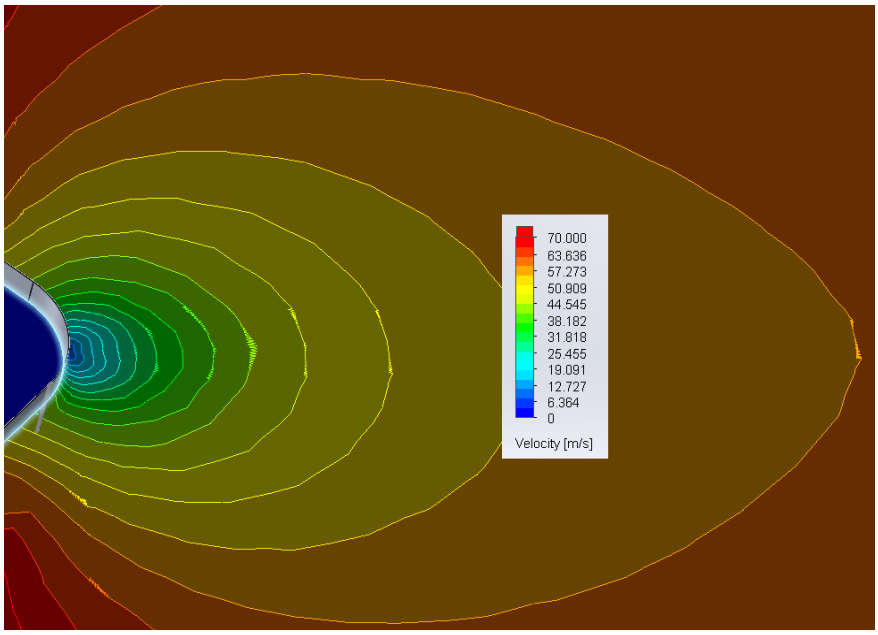

Figure 342: Wind @ $V_x = V_z = 43.37$[m/s]

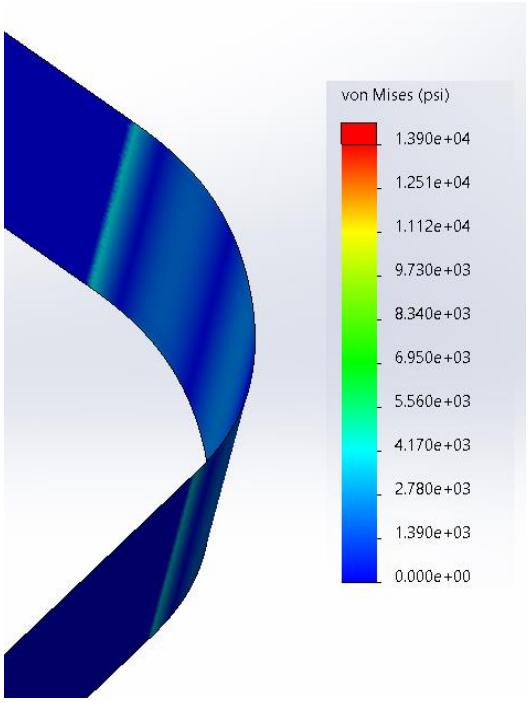

Figure 343: Stress of (1/16)" Radius Panel w/r Figure 342

However, there may be a state where the wind is directed at the "face" of the panel; and the radial design fails. This occurs when V_x or V_z is 61.34[m/s]. In this case, the radial rib requires reinforcement.

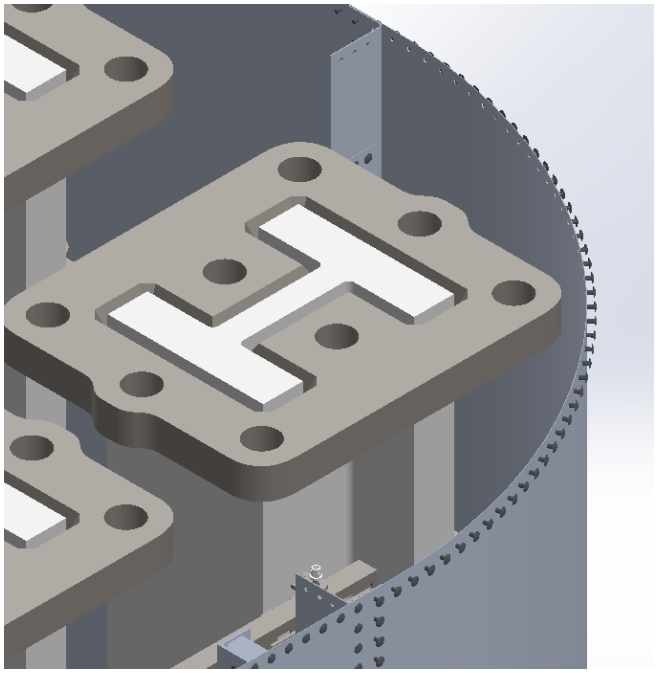

Figure 344: Clearance w/o Rib about 2[in]

The beam-array has a minimum clearance of about 2[in] to the inside of the (1/16)" panel. Support ribbing must allow for clearance while maintaining structural integrity.

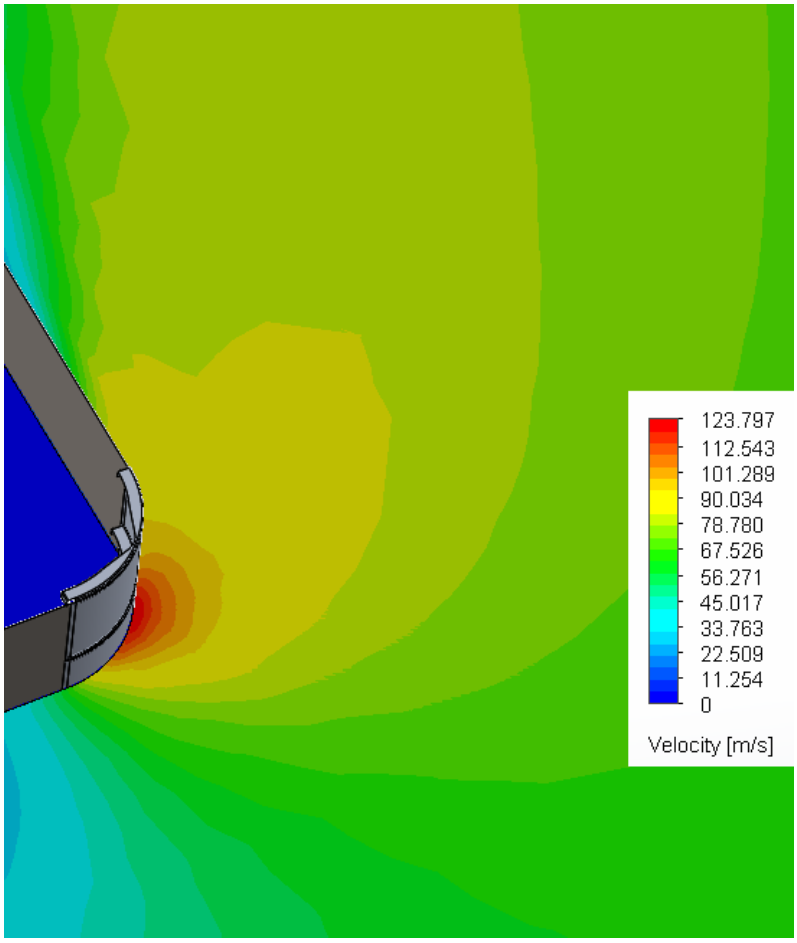

Figure 345: V_z = 61.34[m/s] on Radius

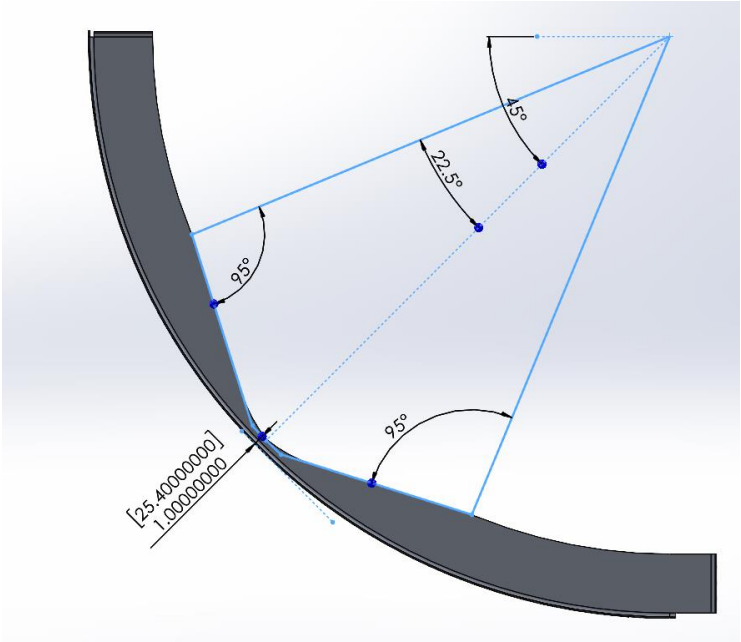

Figure 346: Radial Rib on Main Structure

After several design modifications, the radial rib in Figure 346, having a center arch of 45[deg], provides enough strength for the structure to maintain a FS of 2.875[-]. As a side note, an arch of 60[deg] does not provide enough safety to meet the prescribed criterion.

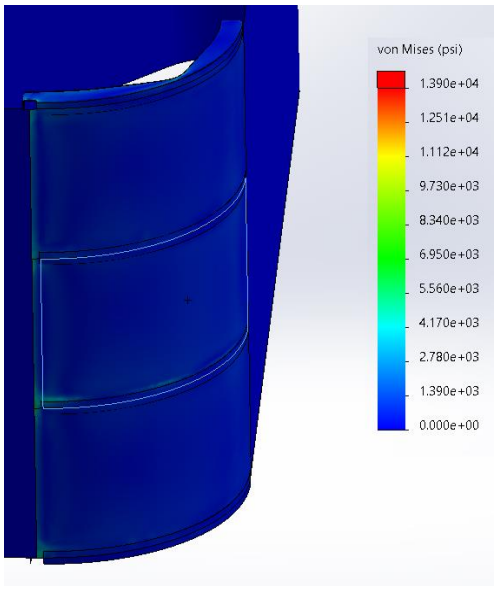

Figure 347: Stress with V_z = 61.34[m/s], Center Radial Panel Only

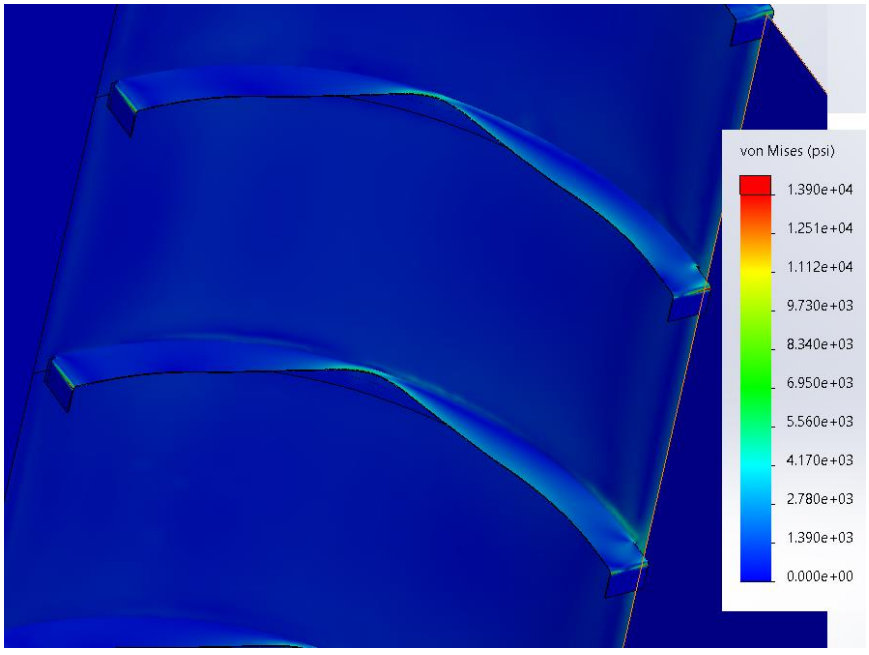

Figure 348: Rib Stress with V_z = 61.34[m/s], Center Radial Panel Only

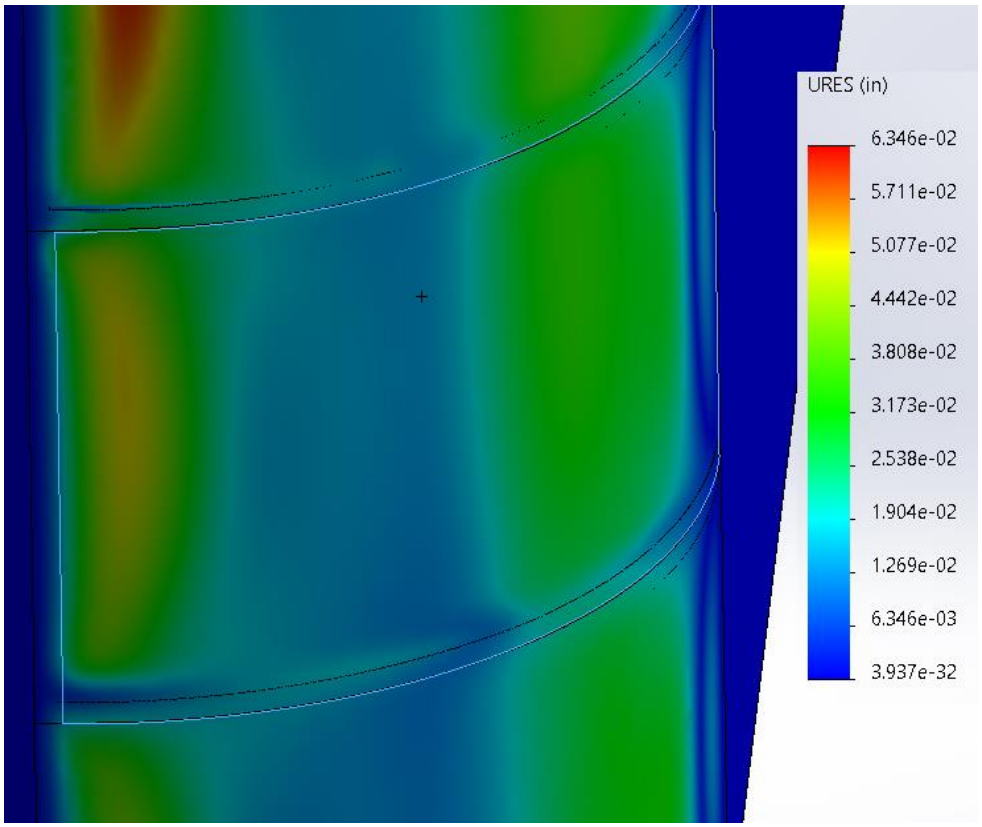

Figure 349: Deflection with V_z = 61.34[m/s], Center Radial Panel Only

The deflections in the FEA-accurate, center, panel are on the order of $(1/1000)^{th}$ the radius of the panel. The minimum clearance to the beam-plate is on the order of (1/2)[in]; as seen in Figure 350.

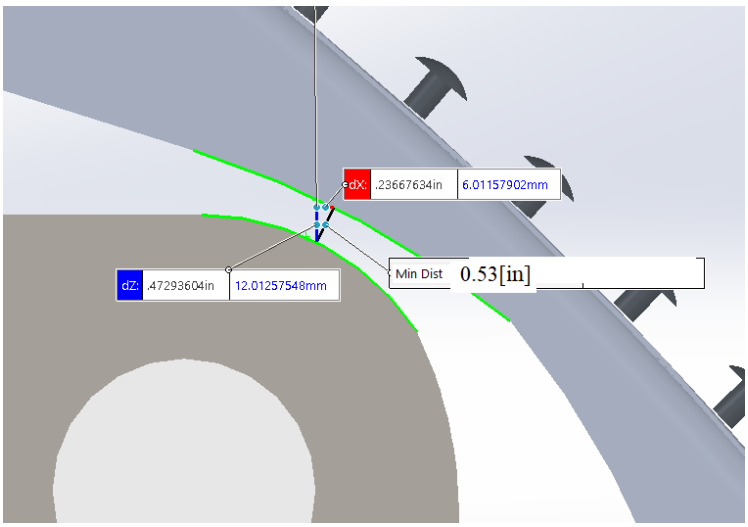

Figure 350: Beam Clearance to Rib Radius at Base

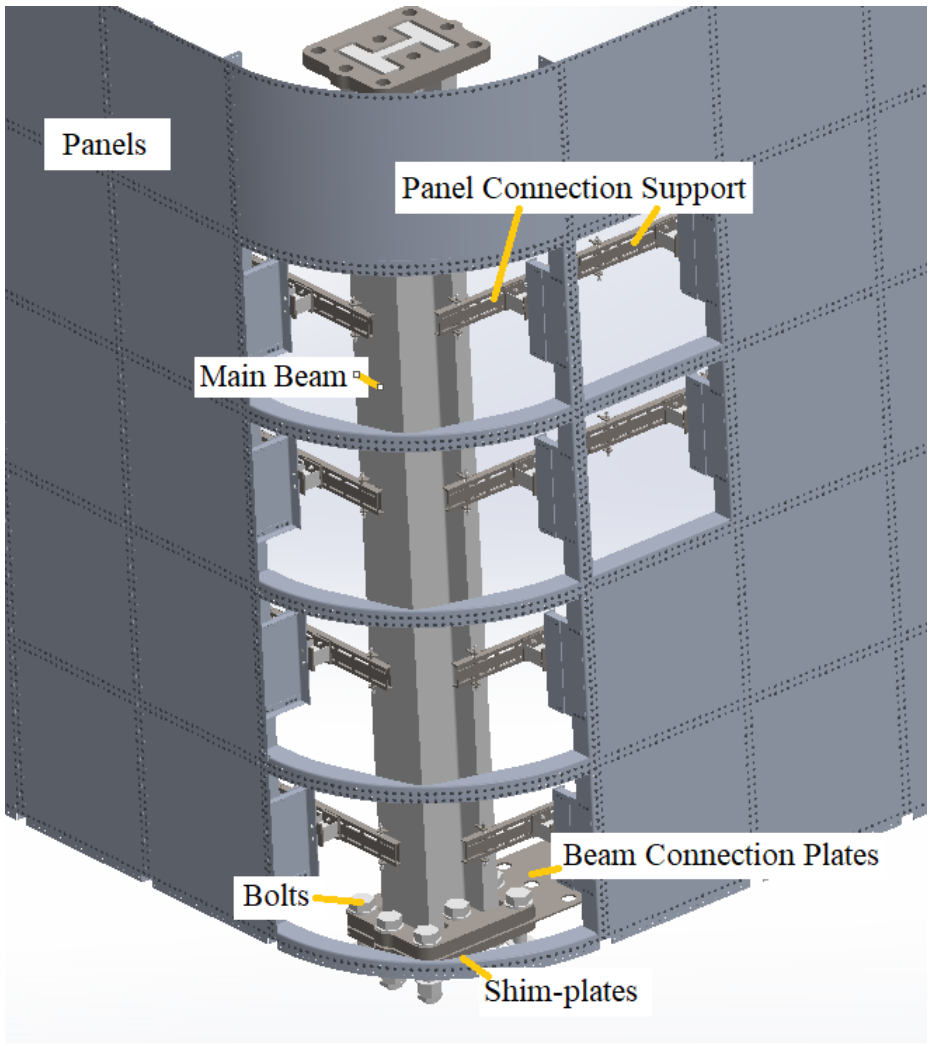

Figure 351: Base Segment Construction

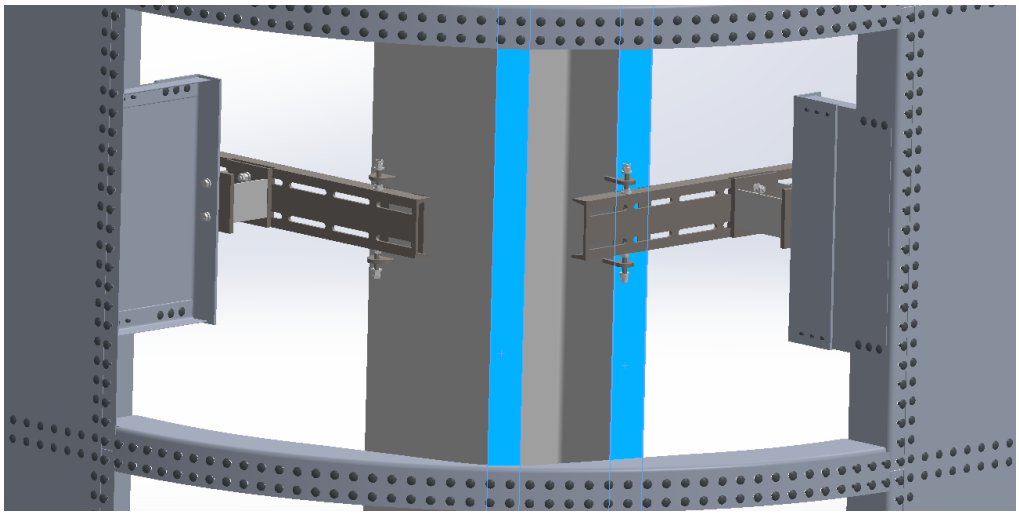

Figure 352: Example of Panel Support, Front & Side

The modeling of the main-body segments will vary with height per Table 156; as the structural beams change. The only items that are affected are the main-body beams and the panel support I-beam.

G. Foundation on Bedrock:

Due to the glorious size of the structure, it will rest on bedrock. Examining mine data from Ref. 10 the bedrock where the Glorious Cross rests is marble; reference Figure 353 & Figure 354. Elevation data shows the height of the site near 110[m] or 360[ft]. The foundation is constructed per American standard in reference 9. To reduce costs and verify hand calculations, FEA simulations showed that the design will maintain structural integrity.

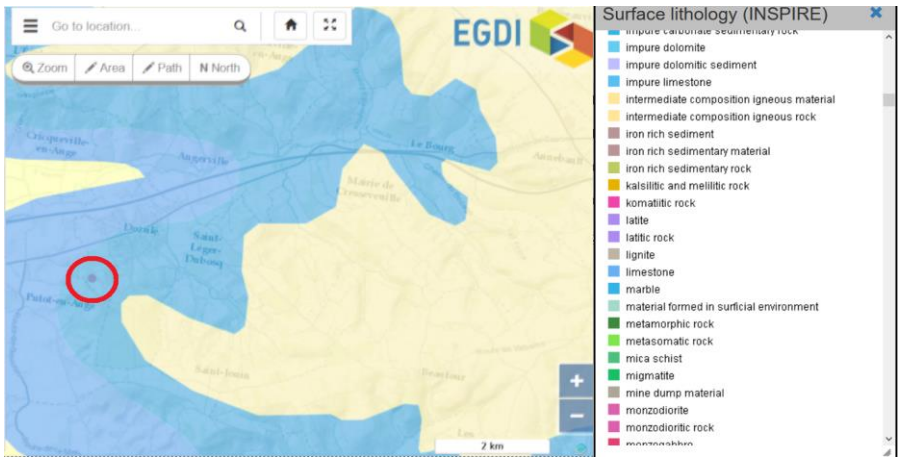

Figure 353: Bedrock, Dozule France

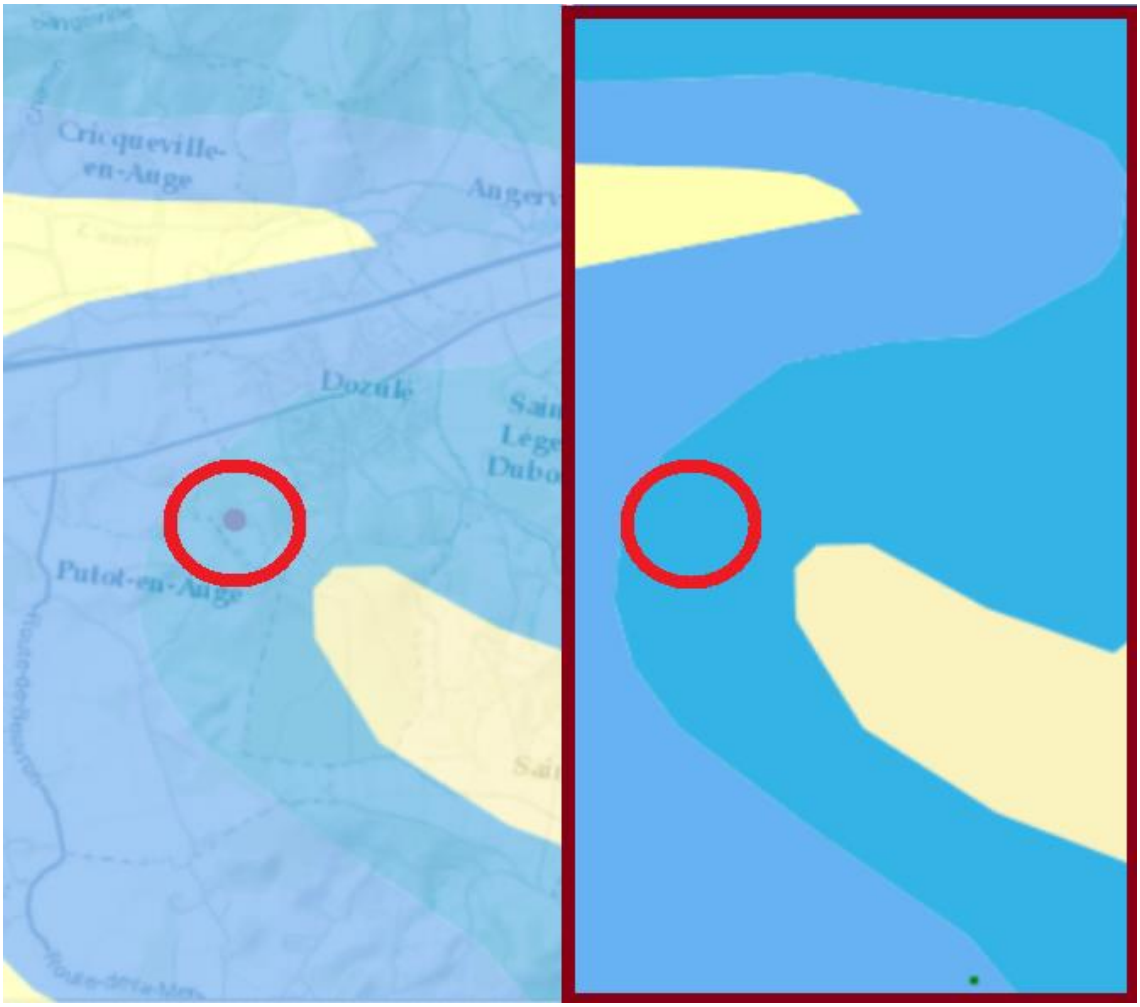

Figure 354: Overlay of Map & Bedrock, Dozule, France

Note: Dark-blue (red circle) is marble, light-blue is limestone, inner (to right of circle) light-yellow is clay.

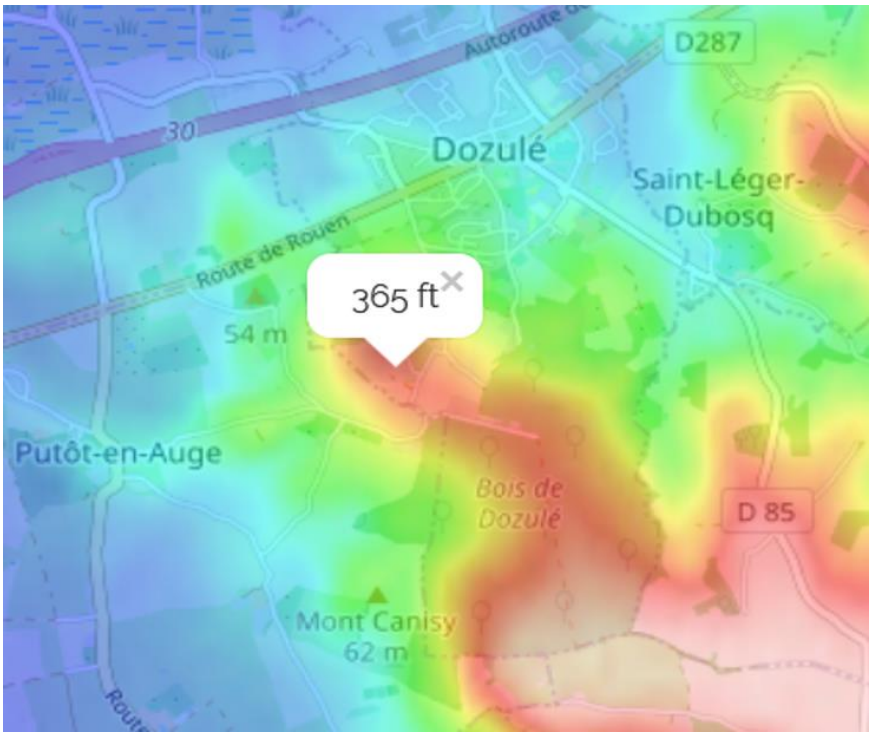

*Figure 355: Elevation Map-II of Dozule, France (**Figure 3**)*

The use of 5,000[psi] concrete was set as the design standard for the construction. Per Ref. 11, the endurance factor for concrete is 4[-] from fc, compression strength (5,000[psi]). Thus, any compression loads will be under 1,250[psi]. The tensile equation comes from Ref. 9, equation 48.7.

Eq - 54: Yield Strength of Concrete (US-units)

$$f_r = 7.5\lambda\sqrt{f_c'} = 7.5(1 * 0.85)\sqrt{5000}$$

Note: Factor of Safety of 15[%] was taken.

Eq - 55: Yield Strength of Concrete (SI-units)

$$f_r = 0.62\lambda\sqrt{f_c'}$$

Table 158: Lambda - λ - Factors for Weight of Concrete[9]

Normal Weight	1.0
Sand Lightweight	*0.85*
Lightweight	0.75

Utilizing Roark's equation for the relationship between the Elastic Modulus (E) and the Shear Modulus (G, eq. 2.2-7), Table 159is obtained. The concrete weight was calculated to be 144[Lbm/ft3] with an estimate Poisson's ratio of 0.20[-] from Ref. 11.

Table 159: Properties of Concrete

	[psi]	[Mpa]
E - Elastic Modulus	4,030,509	27,789
G - Shear Modulus	1,679,379	11,579
fc - Compressive Strength	5,000	34.5
fr - Rupture Strength	451	3.11

Hand calculations from several section of Ref. 9 lead to an initial design of the foundation. The design was further optimized with the use of FEA.

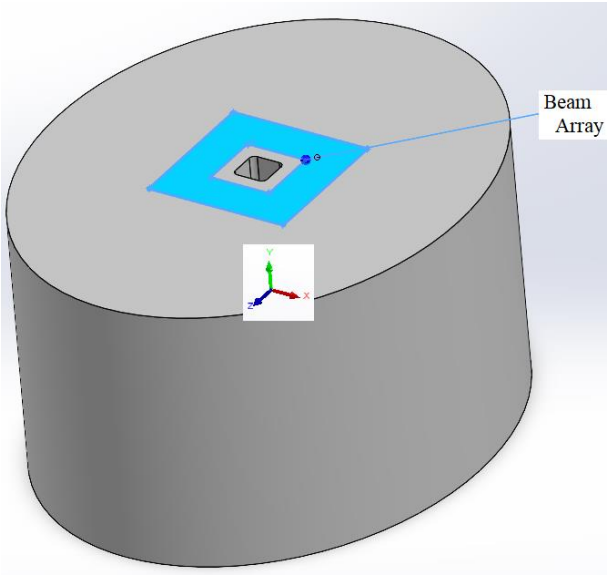

Figure 356: Foundation/Concrete Base Design

The foundation is elliptical with a major axis of 2,400[in] or 60.96[m] and a minor axis of 1,950[in] or 49.53[m]. The weight of the concrete is 183,700[tons], with a center of gravity located 605.5[in] or 15.38[m] below grade. The resultant moment to resist is 200.76[GLbf-in] and the resistive moment by the concrete is 225.5[GLbf-in]; yielding a factor of safety with respect to the moment is 1.10[-]; or 10[%].

The depth was defined by the “minimum thickness for deflection control” calculation standard of $(1/24)^{th}$, found in table 51.1 of Ref. 9 for reinforced concrete slabs; where one end is supported with a continuous load. The depth is then determined to be 738[m]/24 = 30.75[m] or 1,211[in]; recalling that 738[m] is the total height of the structure.

The FEA loadings added gravity to the loadings in Figure 337. Without reinforcement, the concrete weight withstands the maximum loading case. The ratio of the ellipse was taken to be the same as the ratio between the loading cases of V_x and V_z; where the wind was coming from the side (V_x) and the front (V_z). The loading ratio between the maximum front-loading and side-loading is 1.242[-].

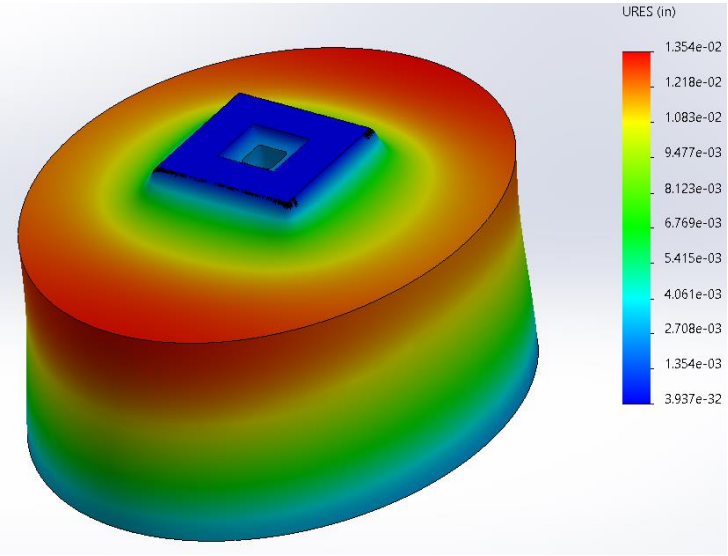

Figure 357: Overall Deflection of Concrete-base

The overall deflections noted in ss are misleading; they have a deformation scale of 18,000[-] and most of the deflection comes from moving in < X > and < Z >. The zone where the structural beams reside remains relatively flat. As seen in Figure 358, the center remains flat while the outer edges sink due to gravity.

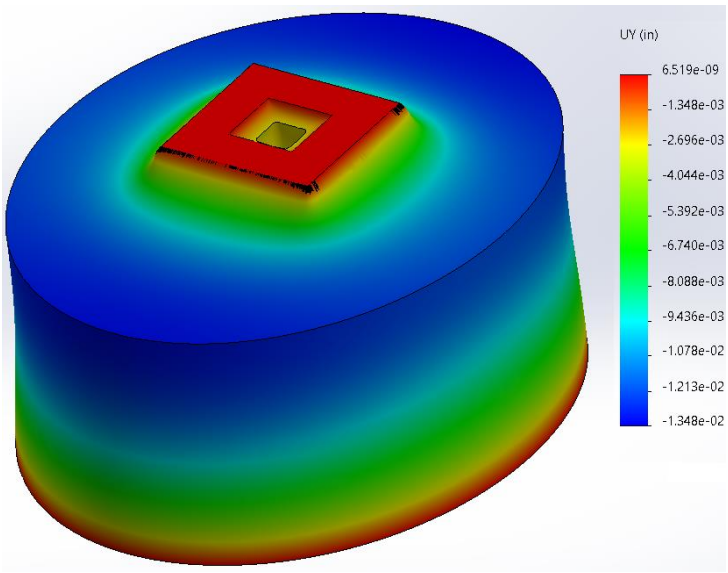

Figure 358: dY-Up/Down Deflection of Concrete-base

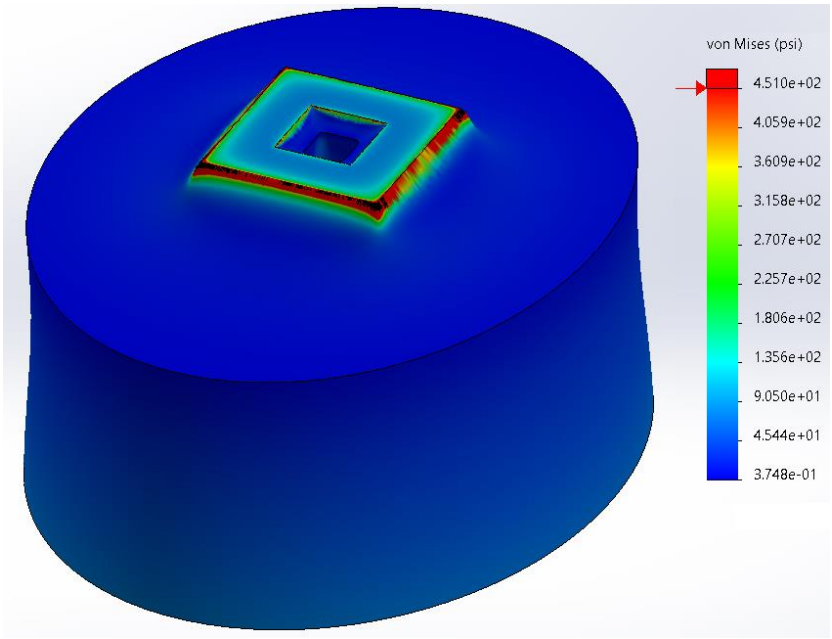

Figure 359: Von Mises Stress of Concrete Foundation

The Von Mises map in Figure 359 is similar to the maximum strain map; where the outer edge elements enter yielding. This is likely due to the simplified model that was employed; where one segment was used to simulate all 220 beams running to a depth of 30.75[m] (1,211[in). Since the "red" area is not present elsewhere in the model and the general stresses are on the order of 50[psi] ($1/100^{th}$ f_c) the foundation will support the loadings of the main structure. It is worth noting that the principal stresses jump sharply as they near the element/boundary-line of the main-beam zone.

To avoid structural damage to the concrete, it will be reinforced per Ref. 9 & ACI 318 the steel area ratio is 0.0018[-] for steel with fy = 60[kips]. From section 55.4 of Ref. 9, the maximum spacing is 18[in] if the depth of the slab is greater than 18[in]; therefore, the area of the steel will be defined by this definition rather than the equations. The results were also verified "ok" by reference 12; the isolated footing worksheet.

After much research, an estimated depth to the bedrock was found to be near 13[m]; as presented by reference 13. This distance alters the design of the foundation. A redesign of the foundation will consider a free depth to bedrock of 12.7[m] (500[in]).

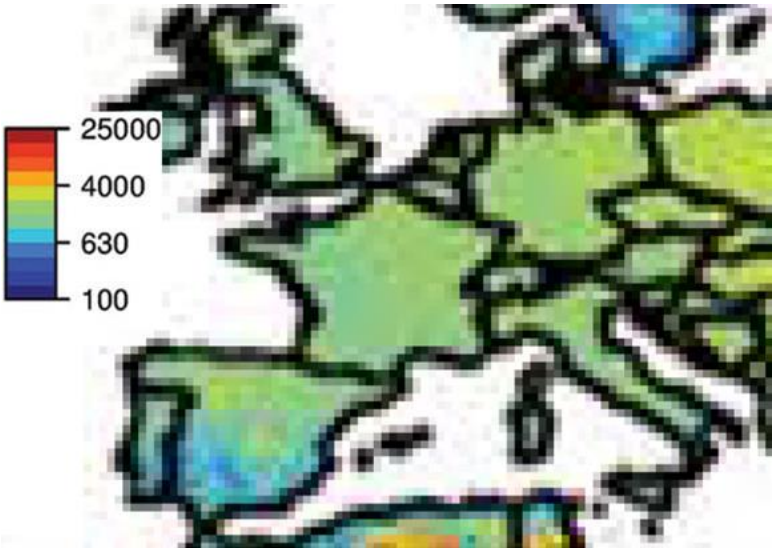

Figure 360: Absolute Distance to Bedrock [cm][13]

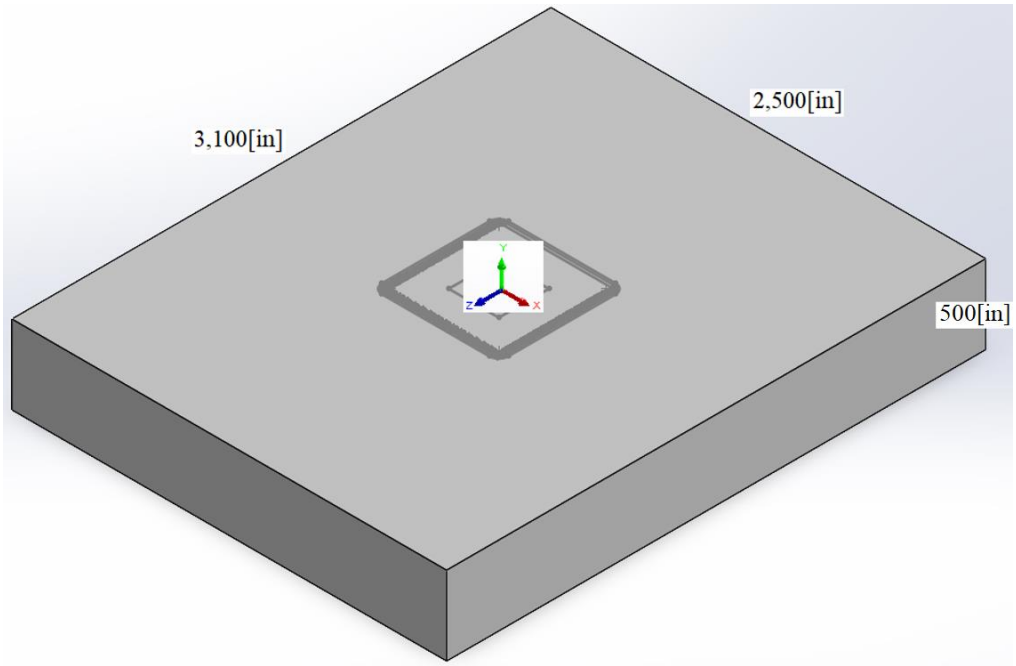

Figure 361: Foundation Pad with Bedrock Depth Greater than 12.7[m]

Note: Pad Dimension are 78.74[m] x 63.5[m] x 12.7[m].

The foundation pad or footing represented in Figure 361 has a 10[%] FS with respect to the two-way shear loading; at maximum wind conditions. Should a depth of 12.7[m] be unattainable, the foundation design should be re-examined.

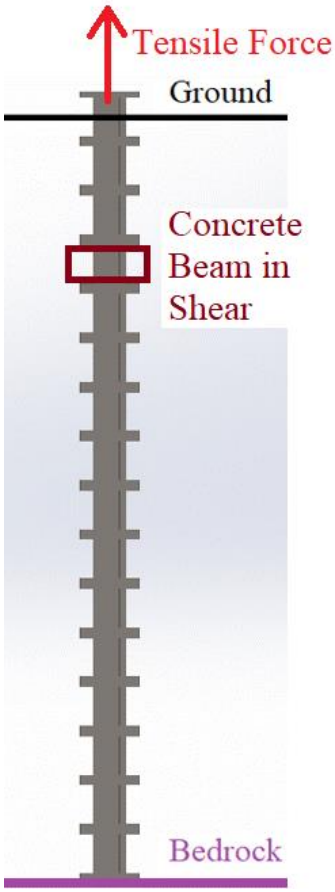

Figure 362: Rebar Loading - Size Determination

The predominate load is either 4.92(10^6)[Lbf] in tension or 8.06(10^6)[Lbf] in compression, with a shear of no more than 52.53[ksi]. Since the fc (compression loading limit) of the concrete is 5,000[psi] and the fr (rupture {or tensile} loading limit) is 482[psi], the tensile loading condition is the worst-case for the design of the foundation stress and strain. The pressure-contact-area for the foundation plate is on the order of 1,019[in2]: Thus, the number of plates needed on the tensile side is 7[-] while the number of plates required on the tensile side is 12[-].

As seen in Figure 362, the number of "beams" is 15[-] and the number of fully loaded plates is 16[-]. Then, utilizing Hooke's law (F*L = d*A*E) the force in the concrete (Fc) is equal to 0.724Fs (force in the steel beam). Under the stable conditions of Eq - 56, the strain is 0.0005[-].

Eq - 56: Concrete Force w/r Steel-beam Force

$$\frac{F_c}{F_s} = \frac{\frac{\delta AE}{L}|_c}{\frac{\delta AE}{L}|_s} = \frac{\epsilon_c(1019)\left(4.03(10^6)\right)}{\epsilon_s(195.5)\left(29(10^6)\right)} = 0.724[-]$$

Note: Since the lengths are the same, the strains are equal; under stable conditions.

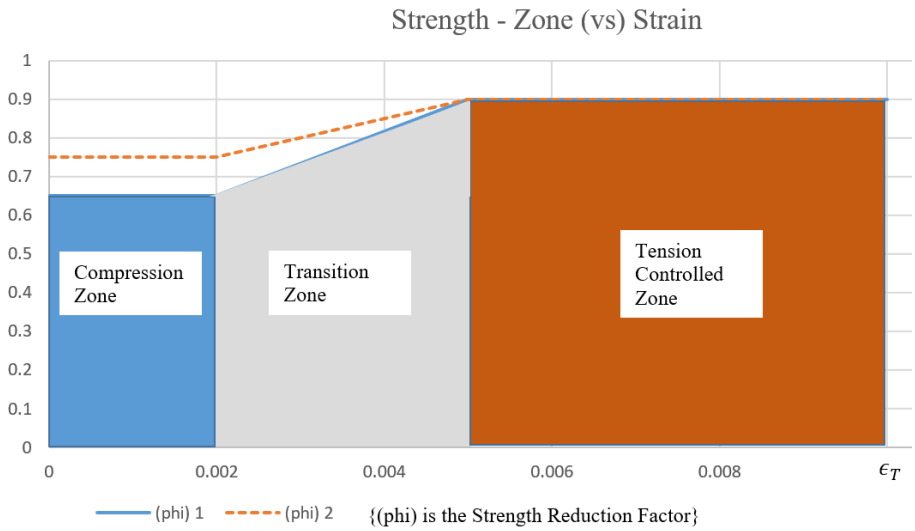

Figure 363: Variation of Concrete Strength Factor with Tensile Strain[9]

Note: Section 50 of ref. 9.

As seen in Figure 363, the compression zone for concrete includes all strains below 0.002[-]. Since 0.0005 < 0.002 (by a factor of 10) the concrete is fully within the compression zone.

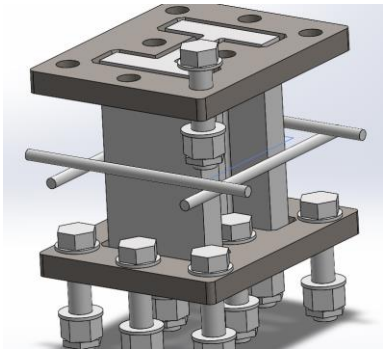

Figure 364: Rebar Positioned Mid-Plane

Following the equations for concrete beams, A_s, the minimum steel area is 0.63[in^2]; for one segment of four (pictured in Figure 362). The maximum steel area is 5.04[in^2]. The maximum shear load is on the order of 8.06(10^6)[Lbf], with b_w = 7.04[in] and d = 25.25[in] (where c = 0.5*d). To resist the shear load, an area of 4.1[in^2] is necessary (which is less than 5.04[in^2]).

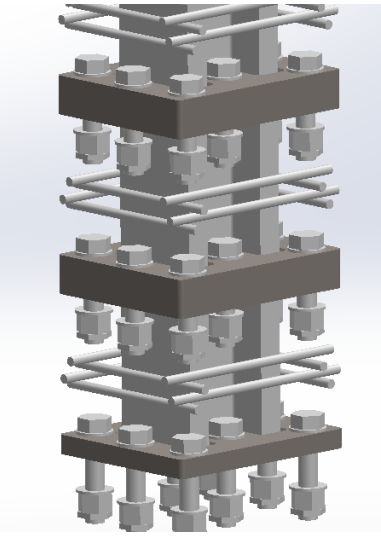

Figure 365: Rebar Reinforcement for Concrete Foundation w/r Beams

The final reinforcement per beam, depicted in Figure 365, contains slightly off-center #14 Rebar (1.693[in] in diameter with f_y – 60[ksi]). The total factor of safety is slightly over 3.0[-]. This configuration acts (and was modeled) as if there are (x4) reinforced concrete beams surrounding each 32.25[in] plate/beam/plate.

An FEA was performed on a foundation segment for compression, as seen in Figure 366, Figure 367 and Figure 368. The tensile load was 377,600[Lbf]; which is 15[%] higher than the design load. The shear load was maximized at (+10[%]) to a value of 58,000[Lbf]. The rebar endpoints were fixed. The highest strain was on the order of 0.0001[-], occurring in the steel: The overall volumetric strain (iso-surface) over 0.00005[-] is insignificant (less than 0.15[%]). The total deflection per segment is on the order of 0.001[in]; over 15 segments, the overall deflection would be on the order of 0.015[in] (maximum). The results confirmed the hand calculations.

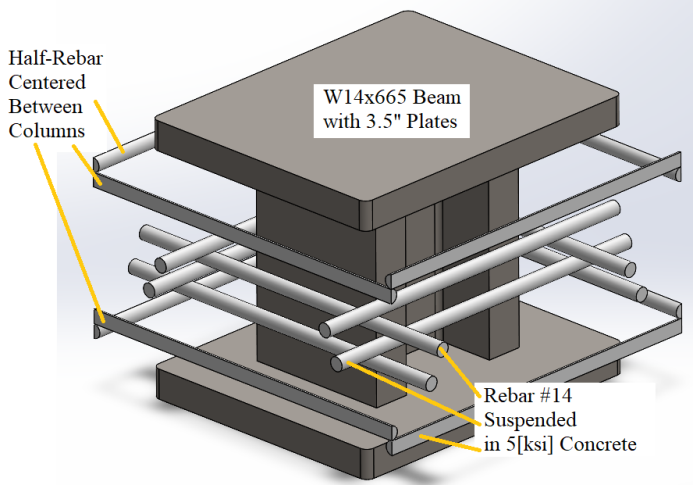

Figure 366: Typical FEA Foundation Segment, w/o Concrete

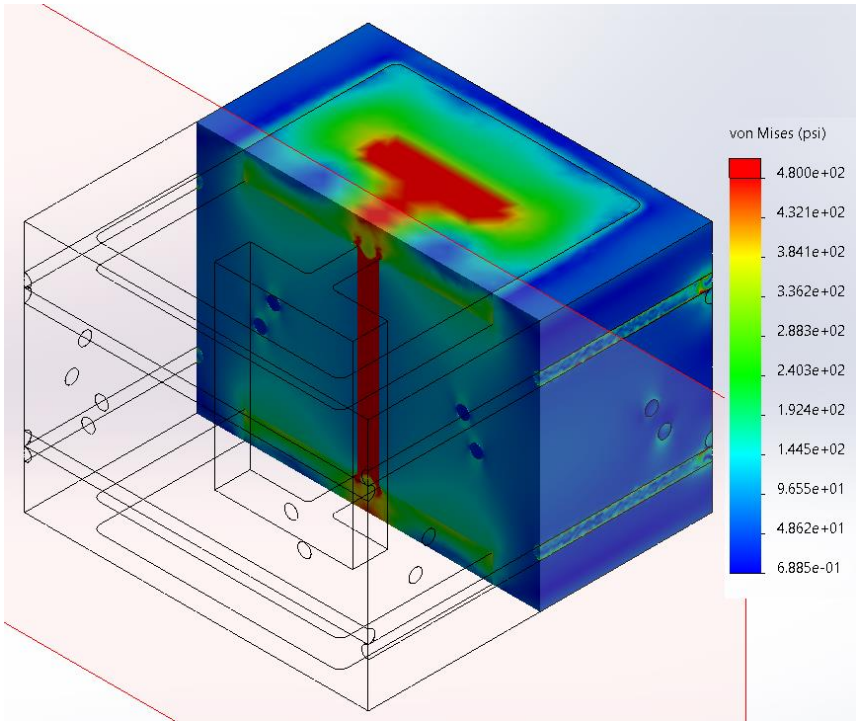

Figure 367: Stress in Tension Loaded Foundation Segment

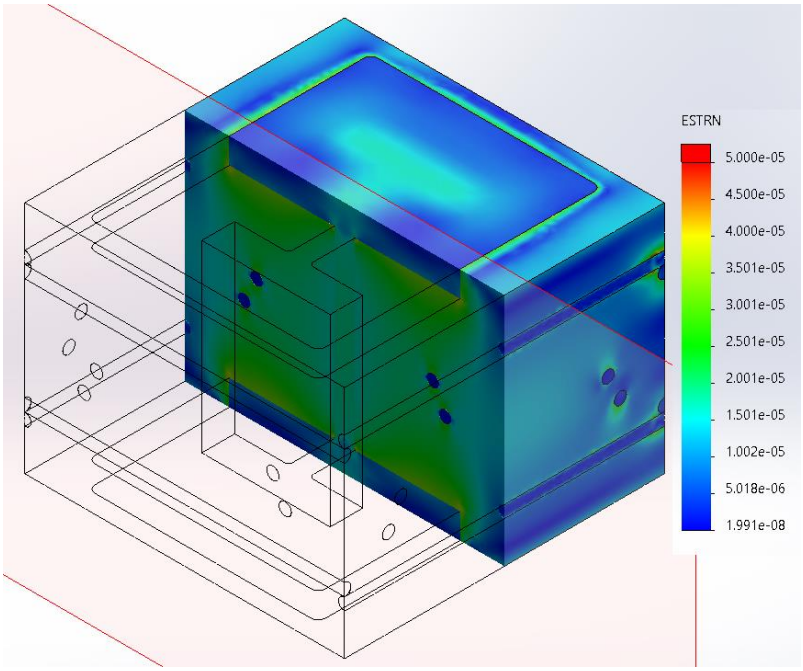

Figure 368: Strain in Tension Loaded Foundation Segment

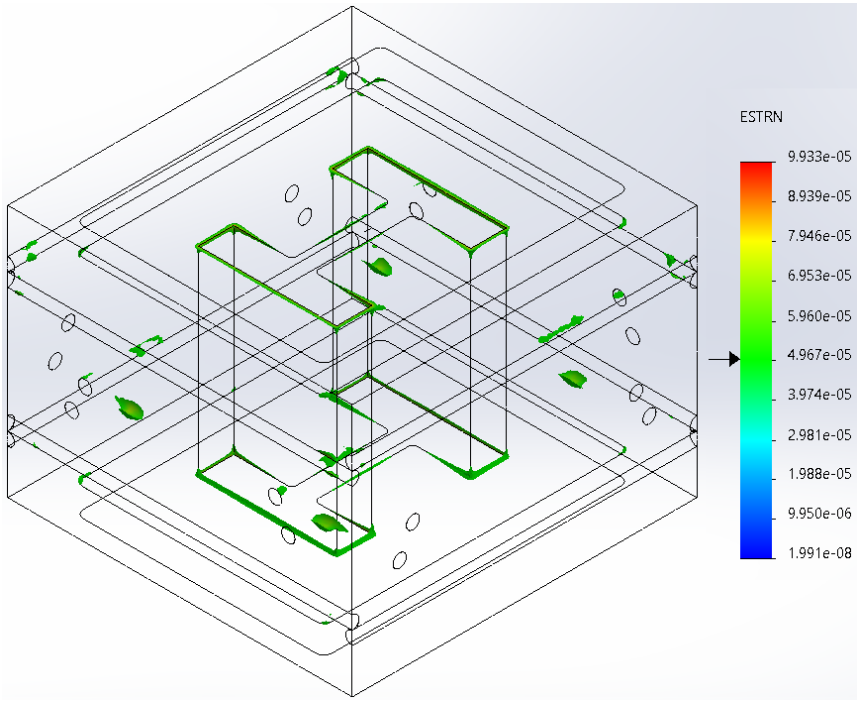

Figure 369: Tension Volumetric Strain Over 0.00005[-] is less than 0.13[%] by Volume

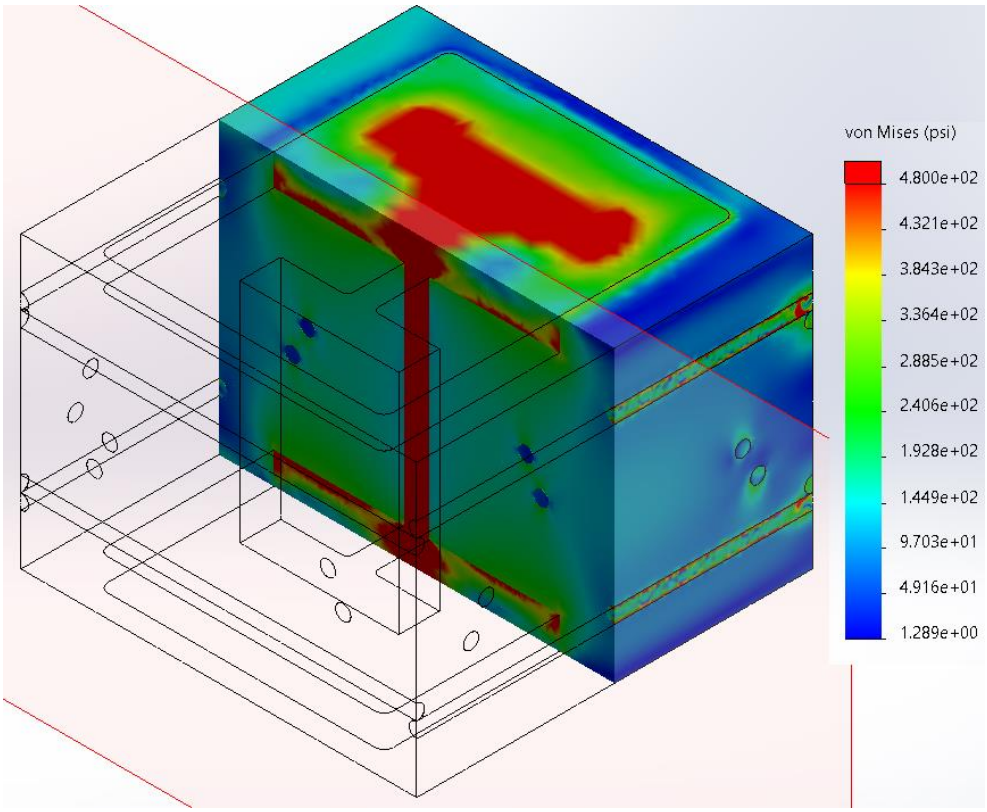

Figure 370: Stress in Compression Loaded Foundation Segment

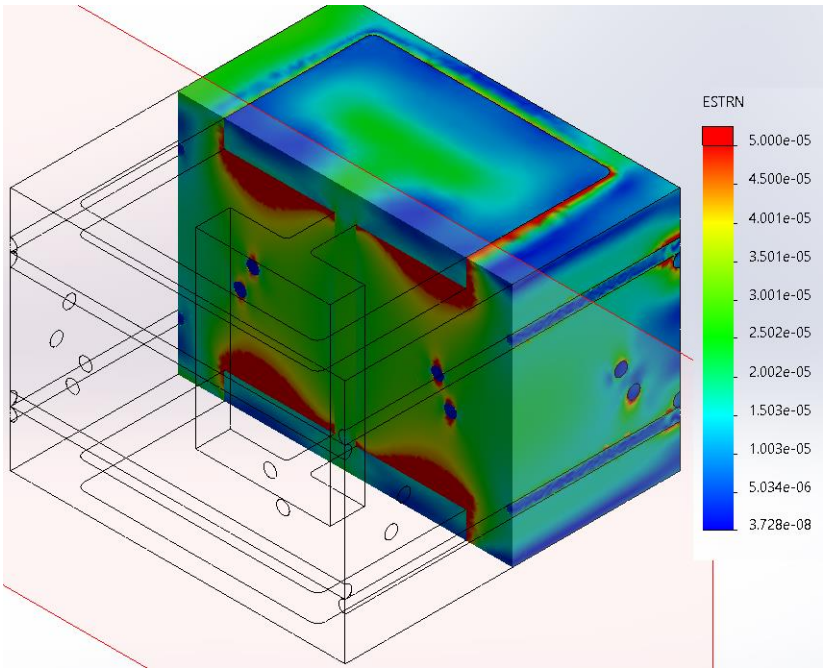

Figure 371: Strain in Compression Loaded Foundation Segment

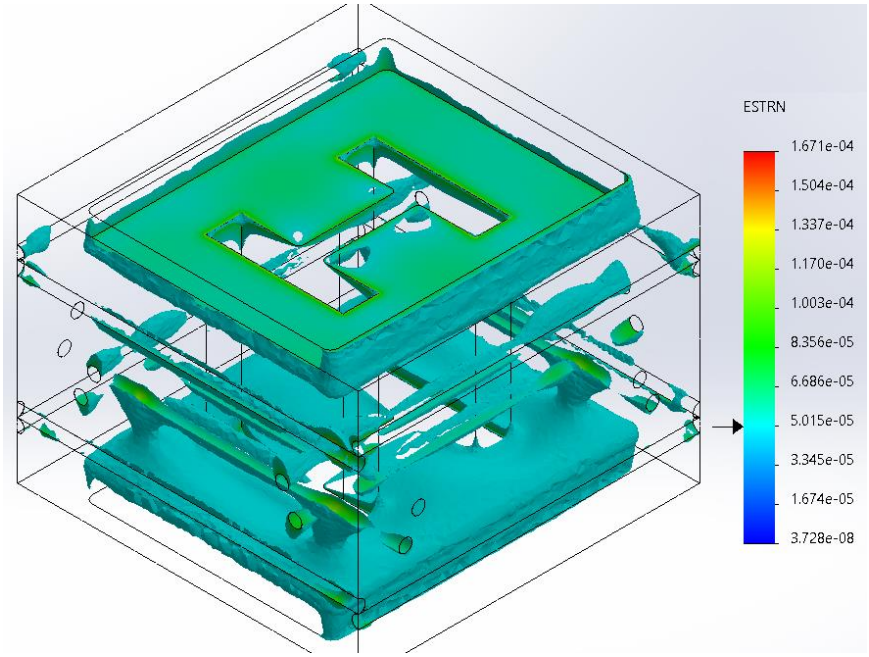

Figure 372: Compression Volumetric Strain Over 0.00005[-] is less than 12[%] by Volume

In compression, Figure 370 and Figure 371, the axial loading was 618,200[Lbf]; also 15[%] greater than the design-segment. The shear loading was maximized at (+10[%]) - 58,000[Lbf]. The maximum stresses in the concrete are on the order of 300[psi], more than (x10) less than its f_c (yield compressive value). The segment's maximum deflection is on the order of 0.0017[in]; thus, the entire foundation column (under maximum loading) could be expected to sink about 0.026[in]. The conclusion/summary

of the analysis of the foundation is that it will support the Glorious Cross; with a factor of safety about 3[-].

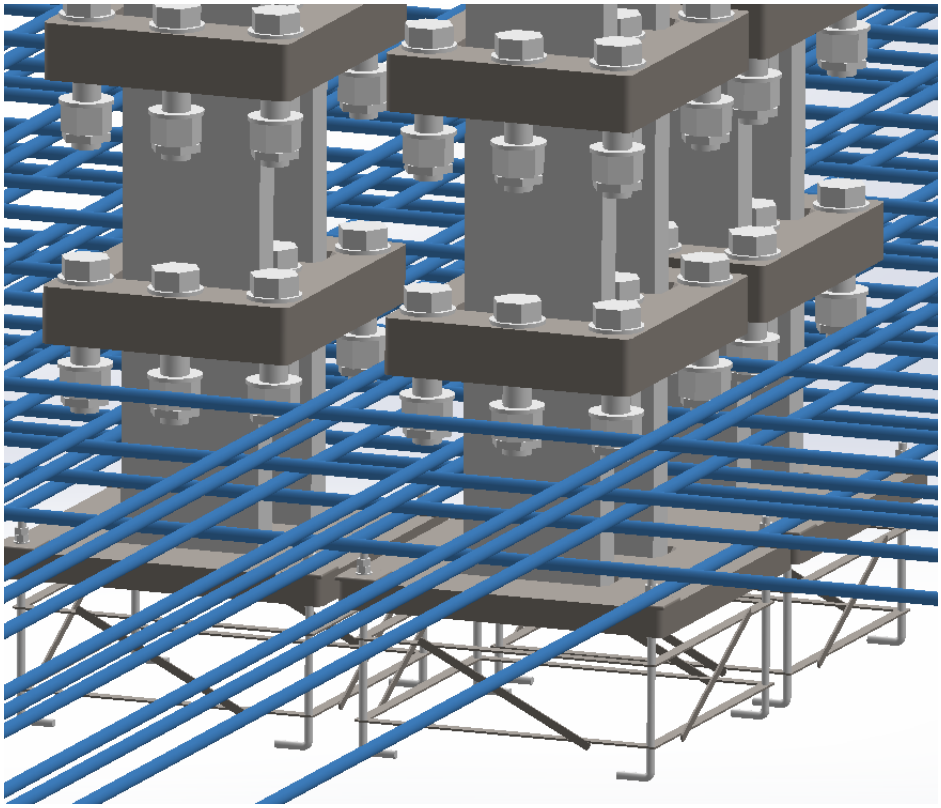

Figure 373: Foundation with Rebar w/o Concrete

Note: Each 32” segment receives the rebar-array.

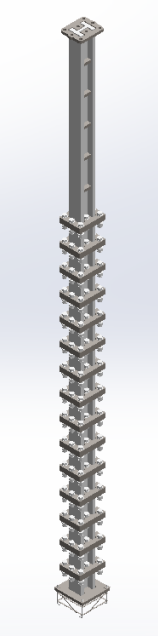

Figure 374: Foundation Beams to Main Support Transition Beam

Note: The weight of one column (above) is on the order of 40[tons]; and there are 220[-] of them.

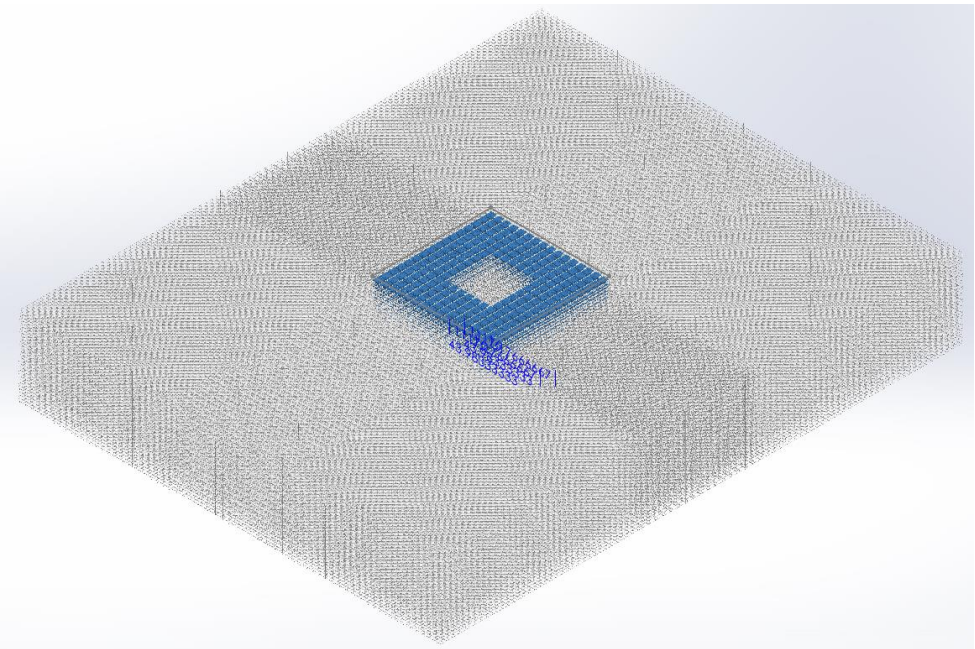

Figure 375: Foundation Beams with Rebar-array

The material usage consists of about 18.4(10^6)[Lbf] of #14 rebar, about 2,700[Lbf] of #3 rebar and about 8,500[Lbf] of #4 rebar. The 5[ksi] concrete volume is about 65,600[m3] or 2.32(10^6)[ft^3]; weighing approximately 333.5(10^6)[Lbf]. The finished weight of the foundation is on the order of 176,000[tons].

The intersection of the Glorious Cross consists of beam/s C125 thru C140. Column (in < Y >) C141 is the beginning of the “head” of the Glorious Cross.

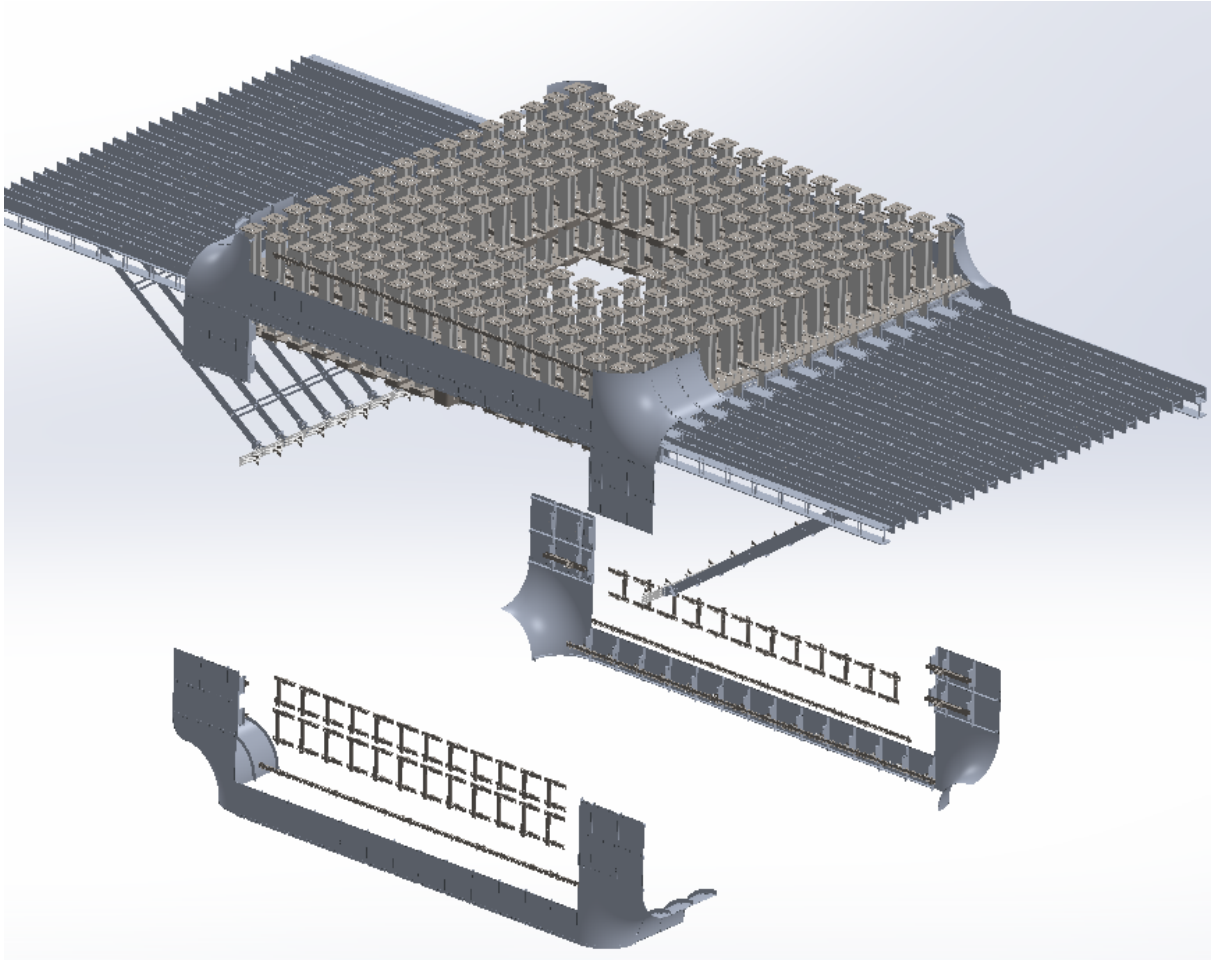

Figure 376: Intersection Beam Array/s C139 & C140

IX. Prints & Summary:

The structural stability of the Glorious Cross has been insured by utilizing international specifications and best practices with respect to construction: Lasting 1,000[year/s] will be possible with minor maintenance. The current design uses higher than expected loadings, to insure it will maintain its shape over hundreds of years: No fatigue, or drooping of the arms should occur. Overall, the two main challenges in the design, the wind and the arm length, were overcome by bringing current materials near their yield point: The third difficulty, the corrosive salt-air environment, can be controlled thru minimal maintenance. By no means, mechanism or mode was the design easy.

The 171 prints cover the construction and tolerancing involved. Though the tolerancing is considered high-precision, the objective/s can be met.

Table 160: LIST OF PRINTS

PRINTS		
A001	OVERALL ASSEMBLY	OVERALL VIEW
A002	OVERALL LOADING	GENERAL NOTES AND LOADING
B001	INITIAL ALINGMENT	INITIAL ALIGNMENT WITH 4-CORNERS
B002	FOUNDATION ROW 1	BEAM ALIGNMENT ARRAY
B003	FOUNDATION BEAM WITH LASER GUIDE	LEVELING OF BEAM/S
B004	FOUNDATION BEAM 1	BASE-BEAM, 1ST FOUNDATION BEAM
B005	FOUNDATION PLATE VISUAL PLACEMENT	VIEW OF FOUNDATION PLATE PLACEMENT NOT ASSEMBLED
B006	HOLE-CENTERING FIXTURE 1	FIXTURE FOR FIELD LEVELING GAUGE
B007	LEVELING GAUGE 1	THE LEVELING GAUGE FOR FIELD
B008	REBAR ORIENTATION 1	REBAR W/R BEAM/S
B009	FOUNDATION BEAM FOR TRANSITION	BEAM THAT TRANSITIONS FROM CONCRETE TO PANEL
B010	ASM FOUNDATION BEAM TO TRANSITION	SINGLE FOUNDATION BEAM ASSEMBLY WITH COLUMN/BEAM DESIGNATION
B011	REBAR ASSEMBLY 1	GENERAL REBAR ARRAY ASSEMBLY
B012	FOUNDATION BEAM ARRAY (x220)	FULL ARRAY OF FOUNDATION BEAMS

B013	SHELL/SKIN BASE ASSEMBLY - 1	CORNER COLUMN WITH 1ST & 2ND PANEL ROWS
C001	PANEL/SKIN P41	41" STANDARD PANEL, 1ST ROW ONLY
C002	RIB - PANEL/SKIN - 1 TOP/BOTTOM TYPICAL	RIB FOR ALL PANEL ROWS, 1ST RIB
C003	RIB - PANEL/SKIN - 2 LOWER ONLY	RIB FOR FIRST PANEL ROW, 2ND RIB
C004	RIB - PANEL/SKIN - 3	RIB FOR FIRST PANEL ROW, 3RD RIB
C005	ANGLE LS6x3.5x0.3 - 1	LS-ANGLE, FIRST L6
C006	ANGLE L2x2x(1/8) - 1	L-ANGLE, FIRST L2
C007	I - BEAM ASM - 1	I-BEAM OR W-BEAM ASSEBLY FOR FRONT AND SIDE
C008	RIB-FRONT & SIDE ASM - 1	RIB ASSEMBLY FOR FRONT/BACK AND SIDE/SIDE
C009	PANEL ASM - 1 PR41	PANEL/SKIN ASSEMBLY FOR FIRST ROW
C010	RADIAL RIB - 1 RIB - 4	FIRST RADIAL RIB, 4TH OVERALL RIB
C011	RADIAL PANEL/SKIN - 1	FIRST RADIAL PANEL WITH RIB
C012	PR-1 ASSEMBLY	ASSEMBLY OF FIRST PANEL ROW
C013	C6 - CHANNEL SUP FRONT AND SIDE - 1	C6 CHANNEL SUPPORT
C014	C6 - SUPPORT ASM FOR PR-1, C16	FRIST COLUMN C6 SUPPORT ARRAY
D001	PANEL/SKIN P47	47.125" STANDARD PANEL, MOST COMMON
D002	RIB - PANEL/SKIN - 5 SIDE/SIDE - TYPICAL	TYPICAL SIDE/SIDE RIB FOR 47.125" PANEL
D003	PANEL/SKIN ASM - 2 P47	PANEL/SKIN ASSEMBLY FOR STANDARD PANEL P47
D004	RADIAL RIB - 2 RIB - 6	2ND RADIAL RIB, STD
D005	RADIAL PANEL/SKIN - 2	2ND RADIAL PANEL WITH RIB
D006	PR-2 ASSEMBLY STD	ASSEMBLY OF FIRST PANEL ROW
D007	CAM-LEVER - 1 ACCESS PANEL	CAM-LEVER HANDLE FOR ACCESS PANEL

D008	ACCESS PNL - 1 47"x47"	STANDARD ACCESS PANEL
E001	W14x665 STD SEG ASM FOR MAIN BODY	MAIN BODY STANDARD SEGMENT ASSEMBLY FOR W14x665
E002	PLATE, STD, W14x665	STANDARD PLATE FOR W14x665, ALSO FOUND IN B009
E003	PLATES CONNECT/SHIM - 1	STANDARD CONNECING AND SHIM/SPACER PLATES
E004	CONNECT-PLATE ARRAY W14x665	STANDARD CONNECING-PLATE ARRAY FOR W14x665
E005	W14x665 STD BEAM ASM	STANDARD BEAM ASSEMBLY FOR W14x665
E006	C6 CHNL ORIENTATION W/R STD W14x665	C6 CHANNEL ORIENTATION FOR STANDARD W14x665
E007	W14x665 - C37 TRANSITION BEAM	BEAM #C37, TRANSITION BEAM FROM 665 TO 550
F001	W14x550 STD SEG ASM FOR MAIN BODY	MAIN BODY STANDARD SEGMENT ASSEMBLY FOR W14x665
F002	PANEL/SKIN ASM - 3 PR111 - PR155	PANEL/SKIN ASSEMBLY FOR STANDARD PANEL P111
F003	W14x550 STD BEAM ASM	STANDARD BEAM FOR W550 SEGMENT
F004	PLATES CONNECT/SHIM - 2	STANDARD CONNECING AND SHIM/SPACER PLATES FOR W14X550
F005	W14x550 - C46 TRANSITION BEAM	BEAM #C46, TRANSITION BEAM FROM 550 TO 455
G001	W14x455 STD SEG ASM FOR MAIN BODY	MAIN BODY STANDARD SEGMENT ASSEMBLY FOR W14x455
G002	PANEL/SKIN ASM - 4 PR156 - 205	PANEL/SKIN ASSEMBLY FOR STANDARD PANEL PR156
G003	W14x455 STD BEAM ASM	STANDARD BEAM FOR W455 SEGMENT
G004	PLATES CONNECT/SHIM - 3	STANDARD CONNECING AND SHIM/SPACER PLATES FOR W14X455

G005	W14x455 CONNECTION PLATE ARRAY	CONNECTION PLATE ARRAY FOR W14x455
G006	C6 - CHANNEL SUP FRONT AND SIDE - 2	C6 CHANNEL SUPPORT
G007	W14x455 - C56 TRANSITION BEAM	BEAM #C56, TRANSITION BEAM FROM 455 TO 370
H001	W14x370 STD SEG ASM FOR MAIN BODY	MAIN BODY STANDARD SEGMENT ASSEMBLY FOR W14x370
H002	PANEL/SKIN ASM - 4 PR206 - 250	PANEL/SKIN ASSEMBLY FOR STANDARD PANEL PR206
H003	W14x370 STD BEAM ASM	STANDARD BEAM FOR W370 SEGMENT
H004	PLATES CONNECT/SHIM - 4	STANDARD CONNECING AND SHIM/SPACER PLATES FOR W14X370
H005	W14x370 CONNECTION PLATE ARRAY	CONNECTION PLATE ARRAY FOR W14x370
H006	W14x370 - C65 TRANSITION BEAM	BEAM #C65, TRANSITION BEAM FROM 370 TO 283
I001	NA	NA
J001	W14x283 STD SEG ASM FOR MAIN BODY	MAIN BODY STANDARD SEGMENT ASSEMBLY FOR W14x283
J002	PANEL/SKIN ASM - 5 PR251 - 305	PANEL/SKIN ASSEMBLY FOR STANDARD PANEL PR251
J003	W14x283 STD BEAM ASM	STANDARD BEAM FOR W283 SEGMENT
J004	PLATES CONNECT/SHIM - 5	STANDARD CONNECING AND SHIM/SPACER PLATES FOR W14X283
J005	W14x283 CONNECTION PLATE ARRAY	CONNECTION PLATE ARRAY FOR W14x283
J006	W14x283 - C76 TRANSITION BEAM	BEAM #C76, TRANSITION BEAM FROM 283 TO 193
K001	W14x193 STD SEG ASM FOR MAIN BODY	MAIN BODY STANDARD SEGMENT ASSEMBLY FOR W14x193
K002	PANEL/SKIN ASM - 6 PR306 - 495	PANEL/SKIN ASSEMBLY FOR STANDARD PANEL PR306

K003	W14x193 STD BEAM ASM	STANDARD BEAM FOR W193 SEGMENT
K004	PLATES CONNECT/SHIM - 6	STANDARD CONNECING AND SHIM/SPACER PLATES FOR W14X193
K005	W14x193 CONNECTION PLATE ARRAY - 1	CONNECTION PLATE ARRAY FOR W14x193 FOR MAIN STRUCTURE
K006	C6 - CHANNEL SUP FRONT AND SIDE - 3	C6 CHANNEL SUPPORT
L001	W14x193-S1 STD SEG ASM FOR MAIN BODY	MAIN BODY SEGMENT ASSEMBLY FOR W14x193-S1, ABOVE AND BELOW ARM INTERSECTION
L002	W14x193-S1 STD BEAM ASM	STANDARD BEAM FOR W193-S1 SEGMENT
L003	PLATES CONNECT/SHIM - 6	STANDARD CONNECING AND SHIM/SPACER PLATES FOR W14X193
L004	W14x193 CONNECTION PLATE ARRAY - 2	CONNECTION PLATE ARRAY FOR W14x193-S1
M001	INT - PANEL CONNECTION - 01	OVERVIEW OF INTERSECTION PANEL CONNECTION/S ARRAY - 1
M002	INT - C6 PANEL CONNECTION - 1	C6 PANEL CONNECT ASM2, C127
M003	INT - C6 PANEL CONNECTION - 2	C6 PANEL CONNECT ASM3, FRONT C128 - C139
M004	INT - C6 PANEL CONNECTION - 3	C6 PANEL CONNECT ASM1, ALL REAR ROWS
M005	INT - BEAM ARRAY - 1	MAIN INTERSECTION BEAM ARRAY
M006	INT - C125 ARRAY	FRIST COLUMN/ROW OF THE INTERSECTION
M007	INT - C125 BEAM	STD BEAM FOR C125
M008	INT - C125 LOWER ARM BRACE	BRACE FOR LOWER ARM
M009	INT - C126 LOWER ARM W/LOWER ARM-BEAM/S	C126 INTERSECTION BEAM AND ARM ARRAY
M010	INT - C126 PLATE ARRAY W/TRANS-PLATE/S	C126 PLATE ARRAY WITH ARM TRANSITION PLATES

M011	INT - C126 BEAM ARRAY	C126 INTERSECTION BEAM ARRAY
M012	INT - C126 LOWER LEFT CORNER ARM-BEAM/S	LOWER LEFT CORNER ARM-BEAM
M013	INT - C126 LOWER LEFT BASE/BRACE - 1	LOWER LEFT CORNER ARM-BASE
M014	INT - C126 LOWER LEFT SHIMPACK	LOWER LEFT CORNER SHIMPACK
M015	INT - C126 LOWER LEFT BASE/PLATE	LOWER LEFT CORNER BASE PLATE
M016	INT - C126 BASE/BRACE ARM-PINS - 1	STD ARM PINS FOR ARM/BRACE/S
M017	INT - C126 W10 ASM LOWER LEFT - 1	W10x49 BEAM ASM FOR LOWER LEFT CORNER
M018	INT - STD ARM/BEAM PANEL SUPPORT/BRACE	INT - STD ARM/BEAM PANEL SUPPORT/BRACE
M019	INT - ARM/BEAM PANEL SUPPORT/BRACE - 2	INT - ARM/BEAM PANEL SUPPORT/BRACE - 2 LOWER SUPPORT/BEAM/S
M020	INT - ANGLE/BRACE FOR SUPPORT - 2	ANGLED BRACE FOR SUPPORT/BRACE - 2
M021	INT - LOWER BRACKET ANGLE/ARM/BRACE	LOWER BRACKET FOR ANGLED BRACE
M022	INT - C126 BASE/BRACE ARM-PINS - 2	PIN/S FOR ANGLED SUPPORT/BRACE
M023	INT - C126 UPPER BRACE/BRACKET - 1	UPPER BRACKETS AND SHIM-PACK FOR BOTTOM ANGLE/SUPPORT
M024	INT - C126/C131 BRACE SUPPORT/ANGLE	BRACE WELDED TO C131 FOR BEAM/S C126
M025	INT - STD MID-ARM SUPPORT/BRACE	STD ARM SUPPORT/BRACE FOR ARM - TO - MAIN STRUCTURE
M026	INT - C126 LOWER RIGHT CORNER ARM-BEAM/S	LOWER RIGHT CORNER ASSEMBLY
M027	INT - C126 LOWER RIGHT CORNER BASE/BRACE	BASE/BRACE FOR LOWER RIGHT CORNER
M028	INT - C127 BEAM/BRACE ASM	OVERALL VEIW OF C127
M029	INT - C127 CONNECT PLATE ARRAY	PLATE ARRAY - CONNECTION PLATES
M030	INT - C127 BEAM ARRAY	BEAM ARRAY FOR C127

M031	INT - C127 FRONT/SIDE BEAM SUPPORT	FRONT/SIDE BEAM BRACE/SPPORT
M032	INT - C127 REAR/SIDE BEAM SUPPORT	REAR/SIDE BEAM BRACE/SPPORT
M033	INT - C128 THRU 137 BEAM/BRACE ASM	OVERALL VEIW OF C128 THRU 137
M034	INT - C128/37 BEAM/S AND PLATE/S ARRAY/S	BEAM & PLATE ARRAY - CONNECTION PLATES
M035	INT - 11.974[IN] CORNER TRANSITION BEAM/S	CORNER TRANSITION BEAM/S FOR C128 THRU C137
M036	INT - C128 THRU 137 FRONT/BACK BEAM SUPPORT	FRONT/SIDE BEAM BRACE/SPPORT FOR C128 THRU 137
M037	INT - C138 BEAM/BRACE ASM	OVERALL VEIW OF C138
M038	INT - C138 BEAM/S AND PLATE/S ARRAY/S	C138 BEAM & PLATE ARRAY - CONNECTION PLATES
M039	INT - C138 FRONT/BACK BEAM SUPPORT	FRONT/SIDE BEAM BRACE/SPPORT FOR C138
M040	INT - C139 BEAM/BRACE ASM	OVERALL VEIW OF C139
M041	INT - C139 BEAM/S AND PLATE/S ARRAY/S	C139 BEAM & PLATE ARRAY - CONNECTION PLATES, UPPER AND LOWER PLATES
M042	INT - C139 UPPER LEFT CORNER BASE/BRACE	BASE/BRACE FOR UPPER LEFT CORNER
M043	INT - C139 UPPER LEFT CORNER BASE PLATE	BASE-PLATE FOR UPPER LEFT CORNER
M044	INT - C139 UPPER RIGHT CORNER BASE/BRACE	BASE/BRACE FOR UPPER RIGHT CORNER
M045	INT - C139 UPPER LEFT CORNER BASE PLATE	BASE-PLATE FOR UPPER LEFT CORNER
M046	INT - C139 UPPER-MID BEAM ANGLE/BRACES	OVERALL ASSEMBLY OF UPPER ANGLE/BRACE/BEAMS
M047	INT - C139 UPPER-MID BASE BRACE	BRACE FOR BEAM/S UPPER-MID
M048	INT - C139 CONNECTION PLATES, UPPER/LOWER	CONNECTION PLATES FOR C139
M049	INT - C140 BEAM ARRAY	BEAM ARRAY FOR UPPER/LAST ROW FOR INTERSECTION
M050	INT - PANEL/SKIN ARRAY/ASM	PANEL/SKIN ARRAY/ASM FOR INTERSECTION

M051	INT - PANEL/SKIN P19, PR359, ASM - 7	PANEL/SKIN ASSEMBLY FOR STANDARD PANEL PR359
M052	INT - PANEL/SKIN P19, PR360, ASM - 8	PANEL/SKIN ASSEMBLY FOR STANDARD PANEL PR360
M053	INT - CORNER RADIUS SKIN PR357/374, ASM - 9	LOWER LEFT CORNER RADIUS OF ARM
M054	INT - CORNER RADIUS SKIN PR357/374, ASM - 10	UPPER RIGHT CORNER RADIUS OF ARM
M055	INT - MID-RADIUS SKIN PR357/374, ASM - 11	RADIUS PANEL ABOVE/BELOW ARM/S
M056	INT - W6 PANEL SUPPORTASM, PR360-371	W6 PANEL SUPPORT ATTACHED TO W14x193
M057	INT - W6/C6 PANEL WELDING/POSITIONS	WELDING/POSITIONS FOR PANEL SUPPORTS TO W14x193 BEAMS REF M001
N001	ARM - FIRST SEGMENT PANEL ARRAY	FIRST SEGMENT OF THE ARM, ATTACHED DIRECTLY TO THE MAIN STRUCTURE
N002	ARM - FLAT PANEL ASM SEGMENT - 1	STANDARD FLAT PANEL FOR SEGMENT 1
N003	ARM - dX RIB W/ SEG-1 COIL-BEAM	dX RIB WITH SEGMENT 1 COIL-BEAM
N004	ARM - dX COIL-CONNECT W/R SEG-1	CONNECTION-COIL BRACE FOR PANEL INTERFACE
N005	ARM - dZ RIB W/R SEG-1 CONFIGURATION	dZ RIB W/R SEG-1 CONFIGURATION
N006	ARM - LWR RIGHT/LEFT RADIAL PANEL/RIB ASM	TYPICAL RADIAL RIB FOR LOWE RIGHT/LEFT
N007	ARM - UPPER RIGHT RADIAL PANEL/RIB ASM	TYPICAL RADIAL RIB FOR UPPER LEFT
N008	ARM - UPPER LEFT RADIAL PANEL/RIB ASM	TYPICAL RADIAL RIB FOR UPPER LEFT
N009	ARM - 2ND SEGMENT PANEL ARRAY	2ND SEGMENT OF THE ARM, ATTACHED TO 1ST SEGMENT
N010	ARM - 6TH SEGMENT PANEL ARRAY	6TH SEGMENT OF THE ARM, ATTACHED TO 5TH SEGMENT
N011	ARM - 6/7TH SEGMENT TRANSITION ARRAY	16TH SUB-ASSEMBLY, TRANSITION ARRAY TO 8TH SEGMENT

N012	ARM - 7TH SEG, < dX > TRANSITION RIB	RIB FOR TRANSITION SEGMENT, 8TH SUB-ASM IN SEGMENT 7
N013	ARM - 8TH SEGMENT PANEL ARRAY	8TH THRU 11TH SEGMENT OF THE ARM, ATTACHED TO 7TH TRANSITIONAL SUB-ASM
N014	ARM - RIB/S dX AND dZ FOR 8TH SEGMENT	RIBBING FOR 8TH THRU 11 SEGMENTS
N015	ARM - RADIAL RIB-1 LWR RIGHT, 8TH SEG	RADIAL RIB-1 LOWER RIGHT, FOR 8TH SEGMENT
N016	ARM - RADIAL RIB-2 UP RIGHT, 8TH SEG	RADIAL RIB-2 UPPER RIGHT, FOR 8TH SEGMENT
N017	ARM - RADIAL RIB-2 UP LEFT, 8TH SEG	RADIAL RIB-2 UPPER LEFT, FOR 8TH SEGMENT
N018	ARM - ENDCAP 30[IN] PANEL ASM, P30	30[IN] PANEL ASM
N019	ARM - ENDCAP 30[IN] LWR R, RADIUS PNL ASM	LOWER RIGHT, 30[IN] RADIUS PANEL ASM
N020	ARM - ENDCAP 30[IN] UP R, RADIUS PNL ASM	UPPER RIGHT, 30[IN] RADIUS PANEL ASM
N021	ARM - ENDCAP 30[IN] UP L, RADIUS PNL ASM	UPPER LEFT, 30[IN] RADIUS PANEL ASM
N022	ARM - ENDCAP CORNER RADIUS	CORNER RADIUS ON ENDCAP
N023	ARM - ENDCAP UPPER/LOWER RADIUS PANEL	LOWER ROW, RADIUS PANEL FOR ENDCAP
N024	ARM - ENDCAP RH CORNER, REAR RADIUS PANEL	RIGHT HAND, REAR SIDE, CORNER RADIUS PANEL FOR ENDCAP
N025	ARM - ENDCAP LH, FRT CORNER RADIUS PANEL	LEFT HAND, FRONT SIDE, CORNER RADIUS PANEL FOR ENDCAP
N026	ARM - DRAIN PANEL	DRAIN PANELS FOR ARM, ENDCAP
N027	ARM - 12TH SEGMENT, ENDCAP ASM	12TH SEGMENT, ENDCAP OF ARM
O001	NA	NA
P001	HEAD - ABOVE INTER, C141 THRU C150	(x10) SEGMENTS JUST ABOVE THE INTERSECTION
P002	HEAD - C151 THRU C160	NEXT (x10) FULL BEAM ARRAYS

P003	W14x90 BEAM ASM C151-160	STD BEAM ASM FOR W14x190, C151 THRU C160 PR-425-474
P004	C6 PANEL CONNECTION FOR W14x90	C6 PANEL CONNECTION BEAM FOR W14x90
P005	PANEL ASM FOR W14x90, W6 BEAM	W6 BEAM CHANGE ON PANEL ASM, FOR W14x90
P006	HEAD - C161 BEAM ARRAY W/ PLATFORM/S	C161 NO LONGER FULL BEAM ARRAY, LIFT-BUCKET AND LIFT-PLATFORM, PR-475-479
P007	HEAD - C162 THRU C171 BEAM ARRAY/S	BEAM ARRAY/S C162-C171 PR-480-529
P008	HEAD - CONNECTION PLATE/S, C162 THRU C172	CONNECTION PLATE/S, C162 THRU C172
P009	HEAD - C172 TOP BEAM ARRAY, TO ENDCAP	FINAL BEAM ARRAY ON HEAD, C172

Final thoughts:
There are too many flukes, too many numbers that line-up, for this to be a mistake; for a soul is indescribably beautiful and oh-so innocent.

Appendix:

Ref – 1: Geography, http://www.map-france.com/Dozule-14430/

Ref – 2: Eurocode calculations: https://www.eurocodeapplied.com/design/en1991/wind-peak-velocity-pressure-uk

Ref – 3: wind: https://www.windfinder.com/windstatistics/deauville

Ref – 4: http://www.cns.gatech.edu/ | Chapter 5 of physics course 4421-13, http://www.cns.gatech.edu/~predrag/courses/PHYS-4421-13/Lautrup/ "surface.pdf"

Ref – 5: DuckDuckgo-maps, Mapquest, Google-maps for maps

Ref – 6: "Mechanical Engineering Reverence Manual," 13th Edition, by M. Lindeburg

Ref – 7: "Tests on Assemblies with Stretched Bolts or Rivets" by F. Hebrant, L. Demol & Ch. Massonnet, 17th Volume of International Association for Bridge and Structural Engineering, 1957

Ref – 8: "Static Strength of High-strength Bolts under Combined Tension and Shear" by E. Chesson JR, N Faustino & W. Munse, Dept. of Civil Engineering University of Illinois, Urbana Illinois, 1964

Ref – 9: "PE Civil Reference Manual," 16th Ed. by M. Lindeburg

Ref – 10: http://www.europe-geology.eu/promine/ for bedrock, soil definition

Ref – 11: "Roark's Formulas for Stress and Strain 8th Ed" by W. Young, R. Budynas & A. Sadegh

Ref – 12: https://skyciv.com/concrete-footing-calculator/

Ref – 13: "Mapping the global depth to bedrock for land surface modeling" in the Journal of Advances in Modeling Earth Systems, Article 10.1002/2016MS000686; https://agupubs.onlinelibrary.wiley.com/doi/pdf/10.1002/2016MS000686

Computer 1) Dell 7520, Xeon E3-1535M v6 3.10GHz, Win10 64-bit, 32Gb RAM, Hynix 16Gb HMA82GS7AFR8N (ECC).